Recent tectonic evolution of the Alboran Ridge and Yusuf regions

Evolución tectónica reciente de la Cresta de Alboran y la región de Yusuf

Instituto Andaluz de Ciencias de la Tierra

ugr Universidad de Granada

CSIC
Consejo Superior de Investigaciones Científicas

Pedro Martínez-García

Tesis Doctoral 2012

Programa de Doctorado Ciencias de la Tierra

Instituto Andaluz de Ciencias de la Tierra (CSIC-UGR)

Tesis Doctoral

Recent tectonic evolution of the Alboran Ridge and Yusuf regions

Evolución tectónica reciente de la Cresta de Alboran y la región de Yusuf

Pedro Martínez-García

El doctorando

Granada, junio de 2012 — Pedro Martínez-García

Vº Bº de los directores

Juan Ignacio Soto Hermoso — Menchu Comas Minondo

Programa de doctorado Ciencias de la Tierra (UGR)
2012

Editor: Editorial de la Universidad de Granada
Autor: Pedro Martínez García
D.L.: GR 373-2013
ISBN: 978-84-9028-332-5

Esta Tesis Doctoral ha sido desarrollada dentro y con objetivos de los proyectos REN2001-3868-CO3-01-MAR: "*Estudios geológicos y geofísicos integrados en márgenes y cuencas sedimentarias del sur de Iberia: Relación entre Procesos Superficiales y Profundos en el Mar de Alborán y su Conexión con el Atlántico* (MARSIBAL), CTM2005-08071-C03-01/MAR: *"El Sistema del Arco de Gibraltar: procesos geodinámicos activos de los márgenes sud-ibéricos* (SAGAS*)* y CTM2009-07715: *"El Sistema del Arco de Gibraltar: Mejora y validación de investigaciones sobre casos geológicos notables en la Cuenca de Alborán"* (GASALB), financiados por el Plan Nacional de I+D de la Secretaría de Estado de Investigación, Desarrollo e Innovación (MINECO, actual). También en el seno del Grupo RNM215 del Plan Andaluz de Investigación-PAI (Junta de Andalucía). Las campañas marinas TECALB (2000) y MARSIBAL 1-06 (2006) realizadas a bordo del BIO *HÉSPERIDES*, fueron financiadas adicionalmente por el Plan Nacional de I+D en el marco de proyectos, y suministraron los perfiles de sísmica de reflexión de multicanal y perfiles TOPAS originales que constituyen el eje de la base de datos utilizada para la realización de esta Tesis. Se hace constar la colaboración del programa *Training-Through-Research*-TTR (IOC-UNESCO y Universidad Estatal de Moscú) para el desarrollo de las Campañas TTR-12 (2002) y TTR-14 (2004) que adquirieron datos geofísicos originales utilizados en esta Tesis. Asimismo esta tesis ha estado adscrita a los *Collaborative Research Projects* (CRP) españoles del Programa EUROCORES de la *European Science Foundation* (ESF) REN2002-12095-E/MAR (WESTMED) y CGL2008-03474-E/BTE (TOPOMED) y al proyecto Consolider-Ingenio CSD2006-00041 (TOPOIBERIA) todos ellos financiados por el Plan Nacional de I+D+I (Secretaría de Estado de Investigación, Desarrollo e Innovación, MINECO). Financiación complementaria para los proyectos mencionados mas arriba ha sido a cargo del Fondo Europeo de Desarrollo Regional (FEDER).

El trabajo de investigación del doctorando ha sido financiado por una beca-contrato de investigación predoctoral del programa I3P (01/2006-12/2009) concedida por el Consejo Superior de Investigaciones Científicas (CSIC) y por un Contrato de Investigación (02/2010-01/2011) en la Universidad de Granada a cargo del Grupo RNM215 (PAI, Junta de Andalucía); financiación adicional ha sido a cargo del Proyecto CSD2006-00041 (TOPOIBERIA). Las estancias breves en el extranjero del doctorando (4 meses en 2008 y 2 meses en 2009), realizadas en el *Departament of Earth Science and Ingineering,* del *Imperial College London,* han sido financiadas por el Consejo Superior de Investigaciones Científicas. El trabajo de investigación ha sido desarrollado íntegramente en el Instituto Andaluz de Ciencias de la Tierra (IACT) del Consejo Superior de Investigaciones Científicas (CSIC y Universidad de Granada), en Granada.

El doctorando, Pedro Martínez García y los directores de la tesis, Juan Ignacio Soto Hermoso y M. Carmen Comas Minondo, garantizamos, al firmar esta tesis doctoral, que el trabajo ha sido realizado por el doctorando bajo la dirección de los directores de la tesis y hasta donde nuestro conocimiento alcanza, en la realización del trabajo, se han respetado los derechos de otros autores a ser citados, cuando se han utilizado sus resultados o publicaciones.

Granada, 13 junio de 2012

El doctorando

Fdo.: Pedro Martínez García

Los directores de la tesis

Fdo.: Juan Ignacio Soto

M. Carmen Comas Minondo

Los directores de esta tesis doctoral garantizamos que los artículos y manuscritos que componen este volumen no han sido presentados en otras tesis doctorales y renunciamos a presentarlos en el futuro como parte de otras tesis. También garantizamos la conformidad a este respecto de los coautores: Lidia Lonergan (Reader in Geotectonics, Imperial College London) y Anthony B. Watts (Professor of Marine Geology and Geophysics, University of Oxford).

Granada, 13 junio de 2012

Los directores de la tesis

Fdo.: Juan Ignacio Soto M. Carmen Comas Minondo

Acknowledgments

This research is supported by the Projects CTM2009-057715/MAR (GASALB), CGL2008-03474-E/BTE (TOPOMED), Consolider-Ingenio 2010 CSD2006-00041 (TOPO-IBERIA), TRA2009_0205, from R&D Plan MICINN and FEDER Funds and Research Groups RNM-215 and RNM-376 (PAI Junta de Andalucía, Spain). I was supported by a fellowship and a contract from the Spanish program *Itinerario Integrado de Inserción Profesional* (I3P form CSIC).

Thanks to Juan Ignacio Soto and Menchu Comas as supervisors of this thesis. Thanks also to the Departamento de Geodinámica for allowing me to use their resources and especially to Fernando Simancas and Antonio Azor for supporting me at critical moments. Thanks also go to the *Programa de Doctorado en Ciencias de la Tierra* and to Antonio Gracía Casco for his courage. Thanks to the Imperial College London for hosting me for part of this work and to the Spanish program of s*hort stays in foreign institutions* from CSIC for funding my stays in the UK. My best regards to Lidia Lonergan, who supervised my work in London. Thanks also to Tony Watts, from Oxford University, for supplying complementary data for my thesis and for his constructive suggestions and ideas.

Moreover, I wish to thank the various technical staff, scientific parties, and crews of the RSS Charles Darwin, R/V Robert D. Conrad and the BIO Hespérides for their work during data collection. Thanks also go to Marcel·lí Farran for helping me to collect old analogue data. Thanks to Seismic Micro Technology for providing the Kingdom Suite® software through a research license. Part of this thesis, corresponding with published and accepted papers, benefited from the comprehensive reviews of J. Bourgois, K. Reicherter and A. Maldonado and other anonymous reviewers and constructive comments by the different journal editors, who are acknowledged.

Preamble

During the last decades, the Alboran Sea Basin has promoted a significant interest, not only by the scientific community, but also on social and economical aspects. Since the late 1980's successive research projects from the Spanish *"Plan Nacional de I+D+I"* have been focussed in the study of this region. Simultaneously, international projects were developed implicating European researchers from the United Kingdom, France and Holland, for example. The scientific problem concerning the origin and evolution of this basin was included into international scientific programs as the "*Deep Sea Drilling Project"* (DSDP) and the subsequent *"Ocean Drilling Program"* (ODP) or the EUROCORES-EUROMARGINS and TOPOMED from the *"European Science foundation"* (ESF). The *"Program to Investigate Convective Alboran Sea System Overturn"* (PICASSO) from the "*National Science Foundation"* (NSF) is currently another international project devoted to this region, which is also explored by large European programs as EUROARRAY and TOPOEUROPE. Different companies have also performed oil and gas exploration surveys since the 1970's. Abundant single and multichannel seismic profiles were acquired and several wells were drilled. Deep seismic sounding experiments were also performed in the Alboran Sea supplying crustal profiles from both, seismic reflection and refraction records. In addition, these marine surveys acquired bathymetric and side-scan sonar mosaics, sub-bottom parametric profiles and bottom sampling by means of drags and gravity cores. Other geophysical data acquired during these researches include for example heat flow measurements, gravimetric and magnetic data. This large amount of data and scientific activity has resulted in numerous scientific publications concerning mainly to the seafloor morphology, stratigraphy of the sedimentary infill, nature and evolution of the underlying basement, crustal structure, distribution of deformations and seismicity and particularly debated the origin and tectonic evolution of the region. These results have incremented the knowledge about the Alboran Sea Basin, which at present arouses interest to many research groups working in very different disciplines.

Index

Abstract 17

Resumen 19

1. Introduction 23

1.1 Geological setting 25

1.1.1 The Gibraltar Arc System 25

1.1.2 The Alboran Sea Basin 29

1.1.3 Tectonic evolution of the Alboran Sea Basin 34

1.1.4 Seismicity and actual plate motions 37

1.1. 5 Geodynamic models 40

1.2 The scientific target 43

1.3 Objectives 45

1.4 Thesis outline 47

2. Data and methodology 49

2.1 Swath bathymetry 51

2.2 Sub-bottom parametric profiles 53

2.3 Seismic reflection profiles 56

2.4 Wells 66

2.5 Seismic interpretation and gridding 73

2.6 Interval velocities and depth conversions 77

3. Seafloor morphology and Recent tectonics 79

Abstract 81

3.1 Introduction 82

3.2 Materials and methods 84

3.3 Results 85

3.4 Discussion and conclusions 100

Influence of sedimentary processes on seafloor morphology 100

Active tectonic structures 101

4. Plio-Quaternary stratigraphy and tectonic evolution 109

Abstract 95

4.1 Introduction 110

4.2 Regional setting and background 110

4.3 Data and methodology 113

4.4 Plio-Quaternary seismic stratigraphy 113

M reflector 115
Pliocene Sequences 118
Quaternary Sequences 118
Sediment accumulation rates 109

4.5 Post-Messinian structure 123

4.6 Timing of deformation 129

4.7 Discussion 133

Plio-Quaternary tectonic evolution 133
Implications for the Messinian salinity crisis and reflooding of the Mediterranean 134
Plio-Quaternary Basin Evolution 136

4.8 Conclusions 138

5. Submarine instability processes 139

Abstract 141

5.1 Introduction 142

5.2 Geological setting 142

5.3 Dataset and Methodology 144

5.4 Plio-Quaternary seismic stratigraphy 147

5.5 Evidences of slide and Mass Transport Deposits 147

5.6 Discussion 151

Age of slides 151
Submarine instability processes and active tectonics 154

5.7 Conclusions 157

6. Tectonic inversion and geodynamic implications 159

Abstract 161

6.1 Introduction 162

6.2 Geological setting 164

6.3 Data and methodology 166

6.4 Key reflectors and main seismic units 168

Acoustic basement 168
Miocene Sequence 168
M reflector 170
Plio-Quaternary sequence 173
Isopach maps 173

6.5 Fault structure 175

Miocene structures 176
Plio-Quaternary structures 181
Active structures 198

6.6 Discussion 190

Miocene rifting in the Alboran Sea Basin 190
Plio-Quaternary partial basin inversion 194
Active deformations along the present-day Africa-Eurasia plate boundary in the western Mediterranean 199

6.7 Discussion 200

7. Conclusions 203

7. Conclusiones 215

8. References 223

9. Appendixes 225

Abstract

A comprehensive dataset consisting of single and multichannel seismic profiles, bio-stratigraphic and log information from nearby DSDP, ODP and commercial wells, multibeam bathymetry data, high-resolution acoustic profiles (TOPAS), hypocenter distribution of seismicity and focal mechanisms, have been used to constrain the Late Miocene to present basin evolution of the central and southeastern parts of the Alboran Sea Basin. It is documented the evolution from a Miocene extensional basin to complex, compartmentalized sub-basins dominated by strike-slip and reverse faulting during the Plio-Quaternary. This study determines that ongoing deformation of the basin is heterogeneously distributed in space and time. Miocene NE-SW High-angle normal faults, tilted basement blocks and growth wedges indicate that rifting in the study area was predominatingly NW-SE oriented and it promoted a reduced amount of extension, which formed Miocene depocentres with maximum thickness of about 2.5-3 km. During the Messinian salinity crisis, intense erosion and local subsidence resulted in small, isolated, basins with shallow marine and lacustrine sedimentation, comparable to the isolated marginal basins of the Betics. Throughout the Plio-Quaternary, the Alboran Sea Basin experienced complex interplay between sediment supply from the surrounding Betic and Rif mountains, tectonics and inherited previous Miocene structures and magmatic intrusions. Plio-Quaternary NW-SE shortening, resulting from convergence between the African and Eurasian plates, coexisted with thermal subsidence and reactivated some extensional structures as reverse faults and folds. Three major shortening phases have affected the basin during the Early Pliocene (~5.33 to 4.57 Ma), the Late Pliocene (~3.28 to 2.45 Ma) and the early Pleistocene (~1.81 to 1.19 Ma). The SW-NE Alboran Ridge, which is the most prominent feature in the Alboran Sea (>130 km in length), accommodated most of shortening. Its main uplift occurred during the Late Pliocene, coinciding with a rotation of the Eurasian/African plate convergence vector from NW-SE to WNW-ESE. This phase also caused transtension between some overlapping fault segments along the WNW-ENE Yusuf fault zone, which is sub parallel to the plate convergence vector at that time. Tectonic inversion occurred in the Alboran Sea Basin mainly during the Plio-Quaternary. This process was partial, affecting only to some of the Miocene NE-SW faults, which had favourable orientation respect to the Recent NW-

SE convergence between the African and Eurasian plates. Positive tectonic inversion occurred, for example, along the western Alboran Ridge. Simultaneously other new south-dipping reverse faults were formed along the northeastern slope of the ridge, where previous Miocene magmatic intrusions formed rheological anisotropies and favoured focussing of deformations.

At present-day, both, the Alboran Ridge and the Yusuf faults disturb the seafloor of the Alboran Sea. These two fault zones are connected, constituting a wide zone of deformation of tens of kilometres in width and showing a complex geometry including different active fault segments and in-relay folds. Reverse faults and associated folds are SW-NE along the Alboran Ridge and they shift progressively to WNW–ESE trend towards the Yusuf Escarpment. Present-day right-lateral transtensive deformation induces faulting and subsidence in the Yusuf pull-apart basin. The entire band of deformation has scattered associated seismicity including some moderate earthquakes (M_w > 4). The Al-Idiris fault zone has been identified as a narrow SSW–NNE band with folding and reverse faulting, which cuts across the western end of the Alboran Ridge. This structure concentrates most of the upper crustal seismicity in the region defining a seismogenic, left-lateral fault zone that connects to the south with the Al Hoceima seismic swarm, and represents a potential seismic hazard. In the Djibouti High, there are other active faults that form two conjugate strike-slip fault systems and locate at the southwestern termination of the Carboneras fault. One system is NNE-SSW trending and has a dominant left-lateral movement, similarly to the Al-Idrisi fault. The other system comprises NW-SE faults with a dominant right-lateral component.

Detected buried and Recent slides along the Alboran Ridge and the Yusuf Escarpment are clear signs of submarine instabilities in these seismically active fault zones. Some Mass Transport Deposits (MTD) are composed internally by several superposed lobes of chaotic sediments and they are separated by layers of draping hemipelagic sediments. These observations collectively suggest that instability processes are recurrent throughout the Plio-Quaternary and were probably triggered by earthquakes, occurring during tectonic pulses of faults that were active, at least, since Pliocene times.

The present-day distribution of deformation in the study area resembles to those along the Algerian margin. The entire region comprises different NE-SW trending segments, with lengths between 125 and 180 km, which are displaced by a number of NW-SE to WNW-ESE right-lateral, strike-slip transfer faults zones between the compressive segments. These structures are long-lived zones of weakness formed during the Miocene opening of the Algerian and Alboran Sea basins that were later reactivated and locally inverted. The inherited structures and basin geometry from pre-Messinian times has resulted in a partitioning of the subsequent deformation and the resulting subsidence and uplift in the Pliocene to recent basins. Towards the west, the inherited structures are cut by the Al-Idrisi fault zone, which is a more recent structure. It was formed during the Pliocene and continued being active until present-day. This structure contributes to partition present-day deformation and its left-lateral strike-slip kinematics of promotes the lateral escape of the frontal part of the Gibraltar Arc towards the southwest.

Resumen

Para caracterizar la evolución de los sectores central y suroriental de la Cuenca del Mar de Alboran se ha usado una extensa base de datos que consiste en perfiles sísmicos monocanal y multicanal, información bioestratigráfica y diagrafías procedentes de pozos cercanos perforados por DSDP, ODP y comerciales. También se han empleado datos de batimetría multihaz, perfiles acústicos de alta resolución (TOPAS), distribución de la sismicidad y mecanismos focales. Se ha documentado la evolución desde una cuenca extensional miocena hasta formar complejas sub-cuencas compartimentadas dominadas por fallas de salto en dirección e inversas durante el Plio-Cuaternario. Este estudio determina que la deformación continua de la cuenca se distribuye heterogéneamente en el espacio y el tiempo. Las fallas normales miocenas de alto ángulo de orientación NE-SO, los bloques basculados de basamento y las geometrías de crecimiento en sedimentos formado cuñas indican que el rifting en el área de estudio ocurrió predominantemente en dirección NO-SE y dio lugar a una cantidad de extensión reducida que formó depocentros miocenos con espesores máximos de unos 2.5 a 3 km. Durante la crisis de salinidad messiniense, una intensa erosión y subsidencia local dieron lugar a la formación de pequeñas cuencas con sedimentación marina somera y lacustre. Estas cuencas son comparables a las cuencas marginales aisladas durante la misma época que han sido estudiadas en las Béticas. A lo largo del Plio-Cuaternario, la cuenca del Mar de Alborán experimentó una compleja interacción entre el aporte sedimentario desde las montañas Béticas y Rif que la rodean, la tectónica y las estructuras previas e intrusiones magmáticas miocenas que fueron heredadas. El acortamiento Plio-Cuaternario de dirección NO-SE, que resultó de la convergencia entre las placas Africana y Euroasiática, coexistió con la subsidencia térmica y reactivó algunas de las estructuras extensionales produciendo fallas inversas y pliegues. Tres fases principales de acortamiento han afectado a esta cuenca durante el Plioceno Inferior (~5.33 a 4.57 Ma), el Plioceno Superior (~3.28 a 2.45 Ma) y el Pleistoceno más temprano (~1.81 a 1.19 Ma). La Cresta de Alborán de orientación SO-NE, que es el rasgo más prominente en el Mar de Alborán (>130 km de longitud), acomodó la mayor parte del acortamiento. La mayoría del levantamiento de este relieve ocurrió durante el Plioceno Superior, coincidiendo con una rotación del vector de convergencia de placas entre Eurasia y África

que cambió de NO-SE a ONO-ESE. Esta fase también causó transtensión entre algunos segmentos de fallas solapantes a lo largo de la zona de falla de Yusuf, de orientación ONO-ENE, que es sub-paralela al vector de convergencia de placas durante esa época. En la Cuenca del Mar de Alborán ocurrió una inversión tectónica de edad fundamentalmente Plio-Cuaternaria. Este proceso fue parcial y afectó sólo a algunas de fallas miocenas de dirección NE-SO que tenían la orientación adecuada respecto al convergencia reciente NO-SE entre las placas Africana y Euroasiática. Por ejemplo, una inversión tectónica positiva ocurrió a lo largo del sector occidental de la cresta de Alborán. Al mismo tiempo, se generaron otras fallas inversas nuevas y buzantes al sur en el talud nororiental de la cresta, donde las intrusiones magmáticas previas (miocenas) constituyeron zonas de anisotropía reológica, favoreciendo que las deformaciones se concentraran allí.

En la actualidad, las zonas de falla de la Cresta de Alborán y Yusuf deforma el fondo marino del Mar de Alborán. Estas dos zonas de falla están conectadas, formando una ancha zona de deformación de decenas de kilómetros de anchura que muestra una geometría compleja con distintos segmentos de falla activos y pliegues en relevo. Las fallas inversas y los pliegues asociados tienen orientación SO-NE a lo largo de la cresta de Alborán y cambian progresivamente de orientación hasta adquirir dirección ONO-ESE hacia el Escarpe de Yusuf. Las deformaciones transtrensivas dextras actuales producen fallamiento y subsidencia en la cuenca pull-apart de Yusuf. Toda esta banda de deformación tiene asociada una sismicidad dispersa incluyendo algunos terremotos de magnitud moderada (M_w > 4). La zona de falla de Al-Idrisi se ha identificado como una banda estrecha de orientación SSO-NNE con pliegues y fallas inversas, que corta el extremo occidental de la Cresta de Alborán. Esta estructura concentra la mayor parte de la sismicidad de la corteza superior en la región, definiendo una zona de falla sismogénica con movimiento sinistro, que conecta hacia el sur con el enjambre sísmico de Alhucemas y representa un potencial riesgo sísmico. En el Alto de Djibouti existen otras fallas activas que forman dos sistemas de fallas conjugados localizados en la terminación suroccidental de la falla de Carboneras. Un sistema tiene orientación NNE-SSO y movimiento predominantemente izquierdo, similarmente a la falla de Al-Idrisi. El otro sistema comprende fallas de orientación NO-SE con una componente dextra dominante.

Los deslizamientos enterrados y recientes que han sido encontrados a lo largo de la Cresta de Alborán y el Escarpe de Yusuf son signos claros de inestabilidades submarinas en estas zonas de falla sísmicamente activas. Algunos depósitos transportados en masa (Mass Transport Deposits, MTD) están compuestos internamente por varios lóbulos de facies caóticas superpuestos y separados por capas de sedimentos hemipelágicos que los recubren. Estas observaciones indican conjuntamente que los procesos de inestabilidad son recurrentes a lo largo del Plio-Cuaternario y fueron probablemente desencadenados por terremotos ligados a pulsos tectónicos de fallas activas, al menos desde el Plioceno.

La distribución actual de la deformación en el área de estudio se asemeja a aquella existente a lo largo del margen argelino. Toda la región comprende diferentes segmentos de orientación NE-SO, con longitudes entre 125 y 180 km, que son desplazados por varias fallas transfer de salto en dirección dextras y orientación NO-SE a ONO-ESE y que se localizan entre los distintos segmentos compresivos. Estas estructuras son zonas de debilidad con una larga historia que se formaron durante la apertura miocena de las cuencas Argelina y de Alborán y que después fueron reactivadas

y localmente invertidas. La estructuras y la geometría de las cuencas heredadas de épocas pre-messinienses ha dado lugar a una partición de la deformación posterior y ha controlado la subsidencia y el levantamiento en las cuencas desde el Plioceno a la actualidad. Hacia el Oeste, las estructuras heredadas son cortadas por la falla de Al-Idrisi que es más reciente. Esta falla se formó durante el Plioceno y continuó siendo activa hasta la actualidad. La falla de Al-Idrisi contribuye a particionar la deformación actual y su cinemática de salto en dirección izquierda favorece el escape lateral de la parte frontal del Arco de Gibraltar hacia el Suroeste.

1. Introduction

1.1 Geological setting

1.1.1 The Gibraltar Arc System

The Gibraltar Arc System is the western termination of the Alpine orogen in the Mediterranean (Figure 1-1). It comprises a strongly arcuate and thickened orogenic belt integrated the Betics and Rif cordilleras accompanied by a frontal sedimentary wedge in the Gulf of Cadiz and a thick sedimentary basin floored by thinned continental crust in the inner part: the Alboran Sea Basin, which connects to the east with the Algerian Basin. Several works have established that this orogen was originated in the Early Miocene by thrusting and shortening of the peripheral mountain belt coeval with crustal extension in the basin within a general setting of convergence between the African and Eurasian plates (*e.g.* Platt and Vissers 1989; Comas *et al*., 1992, 1999; García-Dueñas *et al*., 1992; Maldonado *et al*., 1992; Watts *et al*., 1993; Jolivet and Faccenna, 2000; Rosenbaum *et al*., 2000). The Alpine orogen was originally located to east of its present-day position, approximately next to the current location of the Algerian Basin and the whole system moved westward by 100-250 km (*e.g.* Andrieux *et al*., 1971; Platt *et al*., 2003). Simultaneously the whole region experienced about 200 km of roughly north-south convergence between the Mid Oligocene an Late Miocene followed by about 50 km of northwest-southeast convergence from the latest Tortonian (9-8 Ma) to Present (*e.g.* Dewey *et al*., 1989).

The Gibraltar Arc involves three pre-Neogene crustal domains: (1) the Subbetic, Prebetic and Maghrebian covers of passive continental margins; (2) the Flysch Trough Units; and (3) the Alboran Domain. Moreover, large amounts of Neogene-to-Quaternary sediments are distributed along a number of basins located in different structural positions within the orogen (Figure 1-2).

The Subbetic, Prebetic and Maghrebian covers are Mesozoic and Tertiary sedimentary series laying over the Variscan basement of the Iberian Massif and the Moroccan Meseta and Atlas (Figure

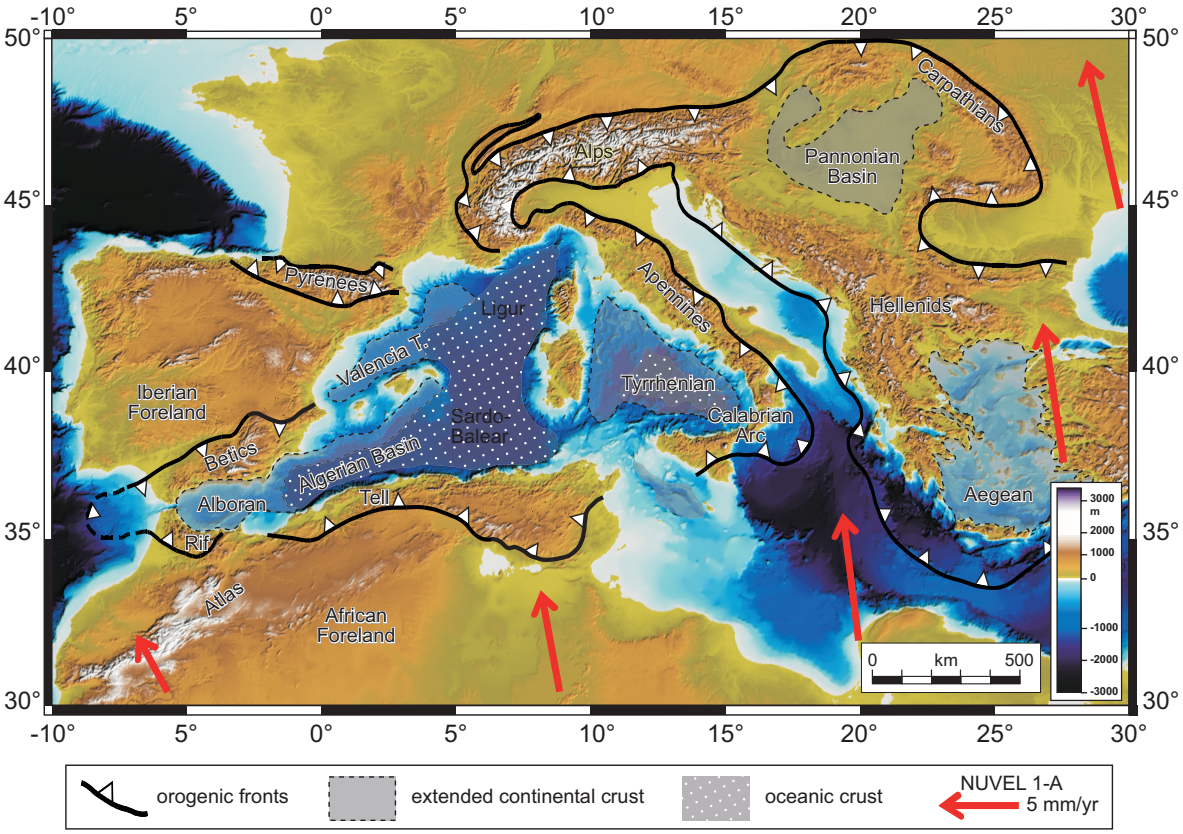

Figure 1-1. Tectonic sketch of the Mediterranean Sea showing Neogene extensional basins and external fronts of surrounding Alpine thrust belts (modified from Comas *et al*., 1999). Red arrows indicate plate convergence vectors according to NUVEL-1A model (DeMets *et al*. 1994).

1-2). These rocks form the External Zones of the Betics and Rif and were deformed by fold and thrust systems imbricated in a "thin-skinned" tectonic style, detached from the Variscan basement (*e.g.* Flinch, 1996; Vera, 2001; Zizi, 2002; Crespo-Blanc and Frizon de Lamotte, 2006; Chalouan *et al*., 2008). This domain is interpreted as the passive continental paleomargins of Iberia and North Africa and it is commonly subdivided in different domains according to the sedimentary facies and paleogreographical setting. In the northern branch of the orogen, the Prebetics comprises shallow facies representing shelf environments, while the Subbetics is dominated by pelagic facies indicating basinal realms (*e.g.* García-Hernández *et al*., 1980; Vera, 1983). The Maghrebian cover is divided into the Prerif, Mesorif and Intrarif from the outer to the inner part of the arc (Durand-Delga *et al*., 1962; Wildi, 1983). Sedimentary facies indicate a progressively increase of paleobathymetry from the Prerif to the Intrarif. Generally, in both the Betics and Rif, these sedimentary covers are non-metamorphic, but some units in Rif record low grade metamorphism (*e.g.* Frizon de Lamotte, 1985).

The Flysch Trough Units are Early Cretaceous to Early Miocene napes of sedimentary rocks with dominance of turbiditic facies are mainly represented in the Rif and Tell regions (Figure 1-2). These units are deformed forming a frontal wedge, which thrusts the Subbetic and Maghrebian Domains (*e.g.* Balanyá and García-Dueñas, 1988; Crespo-Blanc and Campos, 2001; Frizon de Lamotte *et al*., 2004). The deep-water flysches were originally deposited in an ancient basin or trough over oceanic or very thin continental crust located between the two paleomargins (*e.g.* Durand-Delga and Fontboté, 1980; Durand-Delga *et al*. 2000).

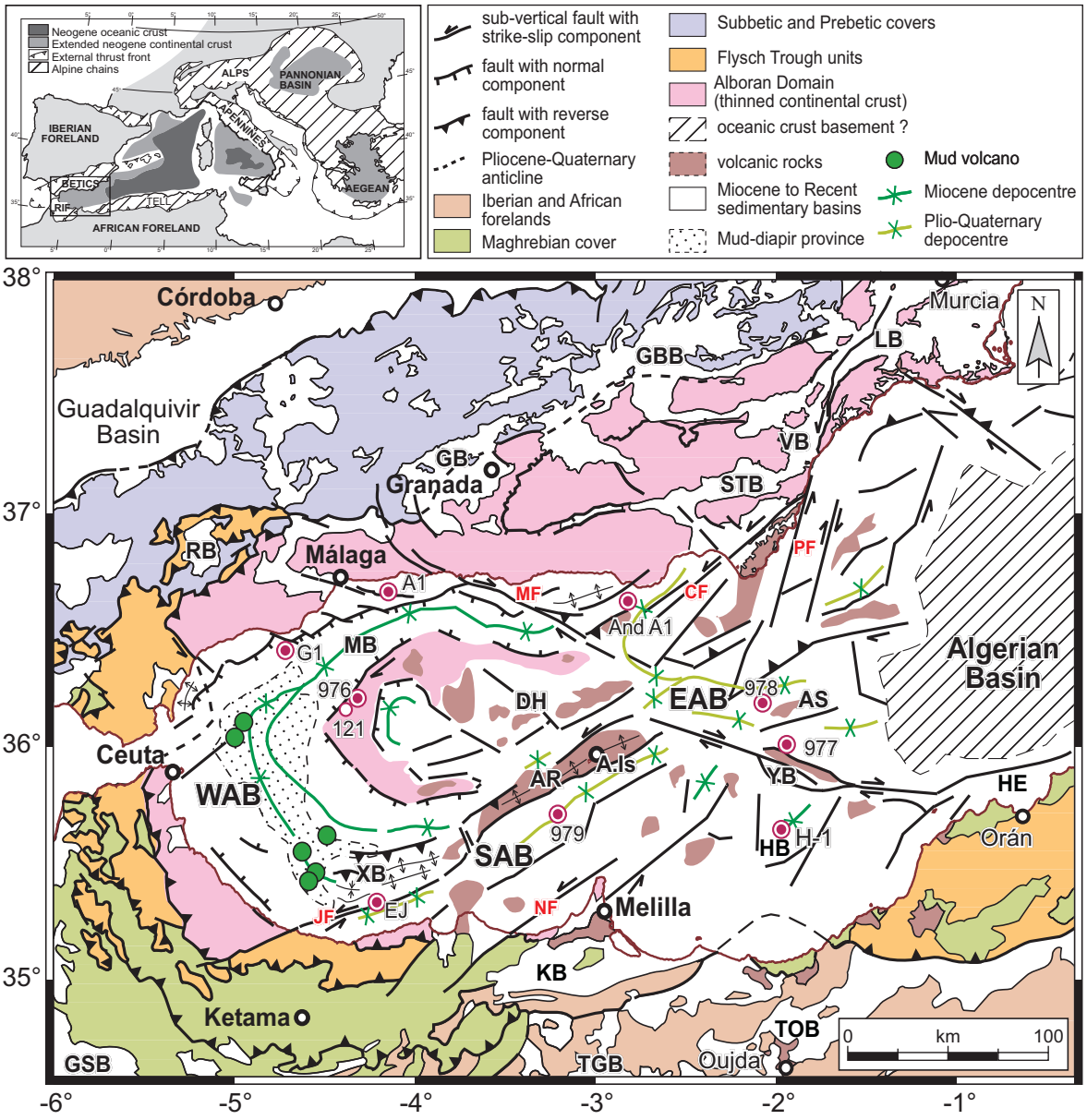

Figure 1-2. Structural map of the Alboran Sea Basin and surrounding areas showing main geological domains of the Gibraltar Arc System and major tectonic features (from Comas *et al*., 1999). Circles show location of ODP Leg 161 sites (976 to 979), DSDP site 121 and commercial boreholes offshore (G1, Andalucía-G1; A1, Alboran-A1; And-A1, Andalucía-A1; EJ, El-Jebha; H-1, Habibas-1). Inset map is a tectonic sketch of the Mediterranean Sea, showing the Neogene extensional basins and the fronts of the surrounding Alpine thrust belts (from Comas *et al*., 1999). Abbreviations: A. Is, Alboran Island; AR, Alboran Ridge; AS, Al-Mansour Seamount, CF, Carboneras Fault; DH, Djibouti High; EAB, East Alboran Basin; GB, Granada Basin; GBB, Guadix-Baza Basin; GSB, Gharb-Saïss Basin; HB, Habibas Basin; HE, Habibas Escarpment; JF, Jebha Fault; KB, Kert Basin; LB, Lorca Basin; MB, Málaga Basin; MF, Maro-Nerja Fault; NF, Nekor Fault; PF, Palomares Fault; RB, Ronda Basin; SAB, South Alboran Basin; STB, Sorbas-Tabernas Basin; TGB, Taza-Guercif Basin; TOB, Taourirt-Oujda Basin; VB, Vera Basin; XB, Xauen Bank; YB, Yusuf Basin and WAB, West Alboran Basin.

The Alboran Domain comprises the Internal Zones of Betics and Rif, which are formed by a thrust stack of three nappe complexes Paleozoic and Mesozoic metamorphic rocks (Balanyá and García-Dueñas, 1988; García-Dueñas *et al*., 1992). From top to bottom, the different metamorphic complexes are: (1) the Maláguide equivalent of the Ghomáride in the Rif; (2) the Alpujárride

analogous to the Sébtide Complex in the Rif and (3) the Nevado-Filábride. The Maláguide Complex is formed by rocks with very low metamorphic grade or non metamorphosed rocks (Martín Algarra, 1987; Chalouan and Michard, 1990). Both the Nevado-Filábride and Alpujárride complexes show an extensive Alpine ductile deformation and metamorphic conditions evolving from high pressure/ low temperature to low pressure and moderate to locally high temperature (*e.g.* Bakker *et al*., 1989; Goffé *et al*., 1989; De Jong, 1991; Tubía and Gil Ibarguchi, 1991; Azañón *et al*., 1998; Soto and Platt, 1999; Puga *et al*., 2000). In addition, the Dorsal and Predorsal are complexes, which also belong to the Alboran Domain and are formed by Triassic to Early Neogene sedimentary rocks. These units probably correspond with the original sedimentary cover of the Maláguide or Alpujárride complexes (Wildi *et al*., 1977; Balanyá and García-Dueñas, 1988).

The original contractional structures bounding the different complexes of the Alboran Domain were later modified by extensional episodes and appear reactivated or cut by Miocene low-angle normal faults (García-Dueñas *et al*., 1988, 1992; Galindo-Zaldívar *et al*., 1989; Platt and Vissers, 1989; Jabaloy *et al*., 1993; Lonergan and Platt, 1995; Martínez-Martínez *et al*., 1997).

Neogene Basins

According to their structural position and tectonic evolution, three major Neogene basins can be distinguished in the Gibraltar Arc System: (1) the Guadalquivir and Gharb-Saïss foreland basins; (2) the intramontane basins of the Betics and Rif; and (3) the Alboran Sea Basin, located at the centre of the orogen, that will be extensively depicted in further sections.

The Guadalquivir and Gharb-Saïss basins are located between the External Zones and the Iberian and North African Variscan forelands, respectively (Figure 1-2). These basins have sediments from Early Miocene to present-day and correspond with the foreland basins formed by flexure of the Variscan crust under the orogenic wedge (*e.g.* Flinch, 1996; García-Castellanos *et al*., 2002; Zizi, 2002; Zouhri, 2002; Crespo-Blanc and Frizon de Lamotte, 2006).

The Guadalquivir Basin is an elongated basin with ENE-WSW trend, which is bounded to the south by the Prebetic and Subbetic domains, to the north by the Iberian Massif and to the west by the Atlantic Ocean. This basin has a total volume of sediments of approximately 20 500 km^3 and their deposits form an asymmetric depocentre with maximum thickness next to the boundary with the External Zones (Berástegui *et al*., 1998, Iribarren *et al*, 2003). In the southern margin of this basin lies an olistostromic unit containing polymictic rocks, dropped from the orogenic front and are embedded in a sedimentary matrix of Triassic age (*e.g.* Martínez del Olmo *et al*., 1984; Sierro *et al*., 1996). Generalized sedimentation in this basin began in the late Langhian, when this domain was a marine realm connecting the Atlantic Ocean with the Mediterranean forming the North Betic Strait (Berástegui *et al*., 1998; Vera, 2000).

The Gharb-Saïss Basin, in North Africa, is bounded to the north and east by the Pre-Rif, to the south by the Moroccan Meseta, and to the west by the Atlantic Ocean. The Gharb-Saïss Basin contains also significant volumes of polymictic rocks embedded in a shale matrix, similarly to the olitostromic unit of the Guadalquivir Basin. The alloctonous blocks in the Gharb-Saïss Basin have different ages and came from the different units of the Maghrebian Domain. The basement of the Gharb-Saïss Basin

is structured with several horsts and grabens and the sedimentary cover sequence starts with Triassic and Jurassic series that correspond to clays, evaporites and carbonates deformed by normal faults of the Triassic-Jurassic rifting. (*e.g.* Zizi, 2002; Zouhri, 2004). The Neogene foreland Gharb-Saïss Basin opened in the Late Miocene as a marine basin dominated by sedimentation of blue marls and constituted another marine passageway connecting the Atlantic Ocean and the Mediterranean Sea. During the Early Pliocene marine sandy turbidites were deposited. The basin become continental during the Late Pliocene, when lacustrine sedimentation was predominant. The most recent deposits (Late Pliocene to Quaternary) consist on terrestrial conglomerates and interbeded lacustrine marls and limestones evidencing that the Rifian Corridor was closed at this time (*e.g.* Benson *et al*., 1991; Krijgsman *et al*., 1999).

In addition to the foreland basins, other emerged Neogene basins are located over the different orogenic domains. These basins are filled by both marine and continental sediments. Main basins in the Betics are: Granada, Guadix-Baza, Lorca, Ronda, Sorbas-Tabernas and Vera. Other comparable basins in the Rif are the Kert, Taza-Guercif and Taourirt-Oujda basins (Figure 1-2). The average sedimentary thickness in these basins is about 800-900 m and they all together comprise a total volume of sediments of approximately 10 000 km^3. The oldest deposits in these basins are Early to Middle Miocene marine sediments and these sequences are lithostratigraphically similar to that found in the Alboran Sea Basin. However, the Plio-Quaternary sequences in the Neogene emerged basins are mainly continental. This suggests that all these basins were originally integrated into a single marine basin during the Miocene, which was compartmentalised during the Late Miocene and finally, the onshore basin were progressively isolated and emerged from the Early Pliocene to the Quaternary (Comas *et al*., 1992; Sanz de Galdeano and Vera, 1992; Rodríguez-Fernández and Sanz de Galdeano, 1992, 2006). The presence of Miocene marine sediments at height of more than 1000 m in some of these basins documents their fast recent uplift. This is the case, for example, of the Guadix-Baza Basin, where marine sediments lie at 1600 m above the present-day sea level (Braga *et al*., 2003).

1.1.2 The Alboran Sea Basin

Sedimentary infill

The Alboran Sea Basin is the largest Neogene basin (~54 000 km^2) in the Gibraltar Arc System and locates in the inner part of the orogen. Clay mineral assemblages in these sediments indicate that their source area corresponds mainly with the different metamorphic complexes outcropping in the surrounding Betics and Rif mountains (Marsaglia *et al*., 1999). Sedimentation in the Alboran Sea Basin was synchronous with tectonic processes and it resulted in significant thickness variations of the sedimentary infill and basin compartmentalization into several sub-basins, being the largest: the West Alboran Basin (WAB), East Alboran Basin (EAB) and South Alboran Basin (SAB) (Figure 1-2). The total volume of sediments in the Alboran Sea Basin is ~120 000 km^3 and maximum thicknesses locate in the WAB, where the sedimentary pile is up to 8 km thick and displays a curved depocentre that mimics the orogenic front of the Gibraltar Arc System (Comas *et al*., 1992; Soto *et al*., 1996; Chalouan *et al*., 1997; Iribarren *et al*, 2003). This major depocentre is N-S trending along the WAB

and its orientation changes to E-W direction along the northern margin of the Alboran Sea forming the Málaga and Motril basins (Alonso and Maldonado, 1992; Campillo *et al*., 1992; Ercilla *et al*., 1992; Soto *et al*., 1996). Towards the East, the thickness of the sedimentary filling decreases to 2-3 km in the EAB, at the transition towards the Algerian Basin, and in the SAB maximum sediment accumulation reaches up to 3 km (Comas *et al*., 1995; Booth-Rea *et al*., 2007; Mauffret *et al*., 2007).

Six seismostratigraphic units have been recognized within the sedimentary infill of the Alboran Sea Basin (Units I to VI, labelled from top to bottom) (Comas *et al*., 1992; Jurado and Comas, 1992). These units are comparable to those identified by Chalouan *et al*. (1997) for the SW margin of the basin and they are bounded by regional unconformities or discontinuities according to lithologic and chronostratigraphic information derived from several wells drilled during commercial oil exploration and scientific drilling programs (DSDP and ODP). The sedimentary sequences are predominantly dominated by marine sediments with variable lithologies and facies and their ages range from Aquitanian-Burdigalian to Holocene (Figure 1-3). This acoustic basement underlaying these sedimentary sequences is an irregular surface formed by the interference between fault planes with high and low angle, folds and possible paleo-reliefs (de la Linde *et al*., 1996).

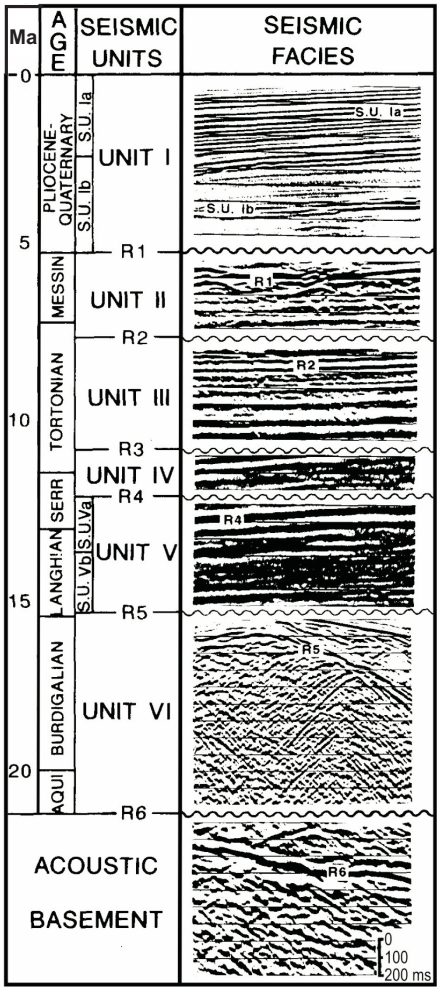

Figure 1-3. Representative seismic facies for all seismic units forming the sedimentary infill of the Alboran Sea Basin (modified from Jurado and Comas, 1992). Vertical scale is time. The main unconformities that constitute the boundaries of the seismic units are represented by wavy lines.

Unit I is Pliocene to Quaternary and is mainly composed by pelagic marls, muddy turbidites, hemipelagic clays and rare silty sand turbidites (Alonso *et al*., 1999). Sediments from Unit II (Messinian) consist of marine and lacustrine sandy turbidites interbedded with fine-laminated sediments and shallow carbonate facies, with occasional volcanoclastic layers and some gypsum and thin anhydrite intervals (Jurado and Comas, 1992; Iaccarino and Bossio, 1999). The Tortonian aged Unit III comprises sandstone intervals with claystone and silty clay beds with turbiditic facies. Unit IV is Serravallian to early Tortonian and is formed by graded sand-silt-clay turbidites and turbiditic muds. Unit V is subdivided in two subunits: subunit Va, which is late Langhian to Serravallian and has similar lithostratigraphy to the overlying Unit IV; and subunit Vb, which has Langhian age and is constituted by undercompacted shales with interbedded sandy and sandy-pebbly intervals. The lowermost deposits in the basin are late Aquitanian to Burdigalian (Sautkin *et al*., 2003) and correspond with Unit VI. This unit is formed by marine olistoliths and rock breccia embedded into an undercompacted shale matrix and. These undercompacted materials at the base of the lithostratigraphic sequence are the origin of well-known diapirism processes in this basin (Comas *et al*., 1992, 1999; Jurado and Comas, 1992; Watts *et al*., 1993; Chalouan *et al*., 1997; Pérez-Belzuz *et al*., 1997; Talukder, 2003; Talukder *et al*., 2003). Diapiric ascent occurs along an elongated province comprising an approximate total volume of 1800 km^3. This area, which is known as *"the diapiric province"*, coincides with the maximum depocentre of the WAB (Figure 1-2). Locally some diapirs pierce the whole sedimentary sequence forming active mud volcanoes in the seafloor (Woodside *et al*., 2000; Comas *et al*., 2003; Talukder *et al*., 2003).

The Messinian salinity crisis

A strong erosional unconformity marks the boundary between the Plio-Quaternary and Messinian sequence. This event is a prominent seismic marker known as the M-reflector and is recognized throughout the Mediterranean as a strong and positive high amplitude reflector (*e.g.* Hsü *et al*., 1973; Ryan *et al*., 1973). This unconformity is interpreted as having formed because of deep desiccation and erosion during the Messinian salinity crisis, at about 5.6-5.5 Ma, and the subsequent Zanclean flooding (*e.g.* Clauzon *et al*., 1996; Krijgsman *et al*., 1999; Blanc, 2002; Sprovieri *et al*., 2008; Bache *et al*., 2009, 2011; García-Castellanos *et al*., 2009; Estrada *et al*., 2011; Just *et al*., 2011). This event resulted from the closure of marine passages between the Atlantic Ocean and the Mediterranean Sea, which existed during the Late Miocene in southern Spain and northern Morocco and known as the Betic and Rifian Corridors (Benson *et al*., 1991; Esteban *et al*., 1996; Krijgsman *et al*., 1999b; Gelati *et al*., 2000).

The local sea level change in the Mediterranean during the Messinian salinity crisis has estimated to be between 1300 and 1500 m (*e.g.* Field and Gradner, 1991; Bache *et al.*, 2009; Urgeles *et al.*, 2011). Nevertheless, there is not still general consensus about the mechanisms responsible of the closure of the marine corridors, which connected the Atlantic Ocean and the Mediterranean. Some authors have proposed a global eustatic change with a sea level drop of ~60 m (*e.g.* Adams *et al*., 1977; Hodell *et al*., 1986, 2001) and others consider that it was triggered by a tectonic uplift event in the Gibraltar Arc (*e.g.* Clauzon *et al*., 1996; Krijgsman *et al*., 1999a; Duggen *et al*., 2003; Jolivet *et al*., 2006). In any case, there is consensus that this desiccation episode was not caused directly

by a climatic change (*e.g.* Vidal *et al*., 2002; Fauquette *et al*., 2006). The opening of the Gibraltar Strait at the end of the Messinian caused the reflooding of the Mediterranean (*e.g.* Krijgsman *et al*., 1999; Blanc, 2002; Loget *et al*., 2005). This transgression re-established marine sedimentation in the Alboran Sea Basin, similarly to other Mediterranean basins, and thus hemipelagic and turbiditic facies were deposited from Early Pliocene to Present.

Basement and crustal structure

The continental crustal basement underlaying the sedimentary cover of the Alboran Sea Basin has is predominantly formed by metamorphic rocks belonging to the metamorphic complexes of the Alboran Domain (Platt *et al*., 1996, 1998; Comas *et al*., 1999; Soto and Platt, 1999). This metamorphic basement has been penetrated and sampled at three commercial wells, two in the northern margin and one in the Habibas Basin (*e.g.* Comas *et al*., 1992; Jurado and Comas, 1992; Kheidri *et al*., 2000; Cope *et al*., 2003), and a structural high of the WAB brittle tensional fracturing, which was drilled by DSDP Site 121 and ODP Site 976. Metamorphic rocks recovered from ODP Site 976 are high-grade metapelite sequence with graphite-rich schists towards the top of the cored section, migmatitic gneiss towards the bottom and interlayered marbles and occasional leucogranitic dikes and they are deformed by brittle tensional fracturing. These rocks have been correlated with units from the Apujárride Complex (Sánchez-Gómez *et al*., 1999).

Moreover, the basement of the Alboran Sea Basin comprises volcanic and plutonic rocks, which form extinct volcanic edifices predominantly located to the east of the 4ºW meridian (Figure 1-2). Some of these highs are buried and other ones outcrop in the seafloor. Most of these volcanic highs have been dredged providing samples of lavas with different ages and geochemical characteristics (*e.g.*, Gierman *et al*., 1968; Duggen *et al*., 2003, 2004 and 2008). Lavas form the Alboran Ridge and the Alboran Island are andesites and basaltic andesites. These rocks belong to the low-K tholeiitic series and calc-alkaline to K-rich igneous rocks and date ages of volcanism form ~9.4 to 9.3 Ma (Tortonian). Samples from the Yusuf Ridge, Al-Mansour Seamount, Maimónides High, Djibouti and Câbliers banks and ODP Site 977 are tholeiitic igneous rocks. Their compositions varie from basalt to andesite and their ages range from Langhian to Messinian (~15 to 6 Ma). The Ibn Batouta Bank comprises plutonic rocks, being mainly gabbros with similar age and geochemical composition.

In addition, maps of magnetic anomaly field in the Alboran Sea Basin show large "positive-negative" magnetic dipoles, which reveal the location and total dimensions of the main volcanic and plutonic bodies intruding the continental crust (*e.g.* Galdeano *et al*., 1974; Willet, 1997; Galindo-Zaldívar *et al*., 1998) (Figure 1-4). An elongated magnetic anomaly of high amplitude (300 to 550 nT) trends NE-SW parallel to the Alboran Ridge and Alboran Channel and it changes progressively direction to E-W at the northeastern end of the ridge, to finally become WNW-ESE along the Yusuf Escarpment. Other positive magnetic anomalies of smaller amplitude (50-200 nT) few kilometres of extension correlate well with some of the dredged volcanic highs, for example, the Al-Mansour Seamount, the Maimónides High and some small volcanic banks on top of the Djibouti High and the Cabo Tres Forcas Ridge (Figure 1-4). In addition, major depocentres of the basin are characterised by a relatively uniform magnetic field of ~50 nT.

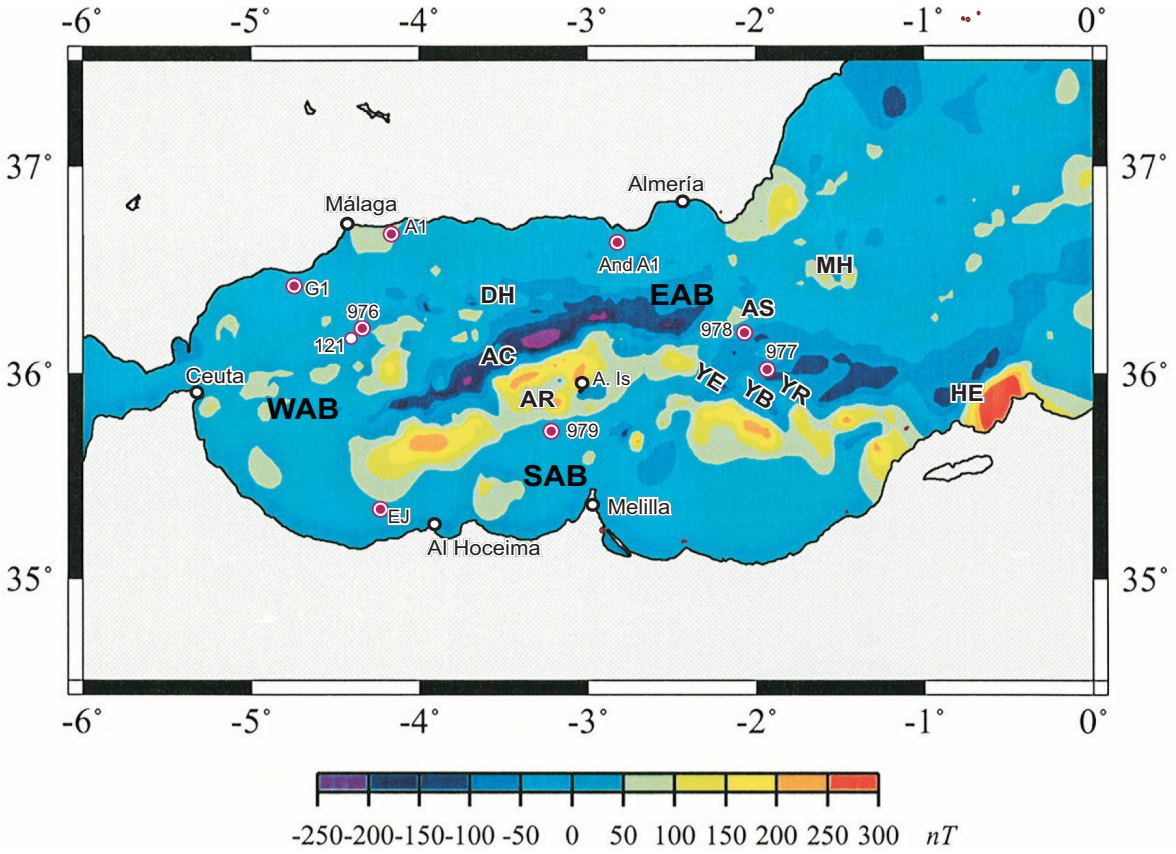

Figure 1-4. Magnetic anomaly map of the Alboran Sea Basin (taken from Willet, 1997). Data reduced to magnetic anomalies using the International Geomagnetic Reference Field of 1987 (IGRF '87). Positive magnetic anomalies generally correlate with basement outcrops. Location of commercial wells, DSDP and ODP sites is also shown for reference (Figure 1-2). Abbreviations: A. Is, Alboran Island; AR, Alboran Ridge; AC, Alboran Channel; DH, Djibouti High; EAB, East Alboran Basin; HE, Habibas Escarpment; MH, Maimonides High; SAB, South Alboran Basin; YB, Yusuf Basin; YE, Yusuf Escarpment; YR, Yusuf Ridge; WAB, West Alboran Basin.

Deep crustal seismic data and gravity modelling indicate that crustal structure of the Gibraltar Arc System is characterized by a thick arcuate bulge parallel to the orogenic arc with an abrupt thinning from the Betics and Rif (maximum crustal thicknesses of 37 km and 32 km respectively) toward the Alboran Sea Basin (minimum crustal thickness ~12-20 km) (Figure 1-5) (Working Group for Deep Seismic Sounding in the Alboran Sea 1974, 1978; Medialdea *et al*., 1986; Torné *et al*., 1992; Banda *et al*., 1993; Watts *et al*., 1993; Torné *et al*., 2000; García-Castellanos *et al*., 2002; Jiménez-Munt and Negredo, 2003; Ziegler and Dèzes, 2006; Fernández-Ibáñez *et al*., 2007; Soto *et al*., 2008). Crustal thinning occurs uniformly from the margins toward the Alboran Sea with the steepest gradient along the northern margin coinciding with the shoreline (*e.g.*, Torné and Banda, 1992; Gallart *et al*., 1995; Galindo-Zaldívar *et al*., 1997; Torné *et al*., 2000). The East Alboran Basin has thinned continental crust (< 15 km) and probably becoming oceanic in nature toward the Algerian Basin (*e.g.*, Comas *et al*., 1995; Mauffret *et al*., 2004; Booth-Rea *et al*., 2007).

Heat flow data suggest also an important thinning of the lithosphere. In Betics and Rif lithosphere thickness is ~130 km with 60–65 mW/m^2 forming an arcuate mantle bulge that thins severely towards the Alboran Sea Basin (60–50 km with > 90 mW/m^2) (Polyak *et al*., 1996; Torné *et al*., 2000) where

it exists an anomalous lithosphere with low velocity of seismic waves (7.6 to 7.9 km/s) (Working Group for Deep Seismic Sounding in the Alboran Sea 1974,1978; Seber *et al*., 1996a, 1996b; Calvert *et al*., 2000; Gurría and Mezcua, 2000; Serrano *et al*., 2005).

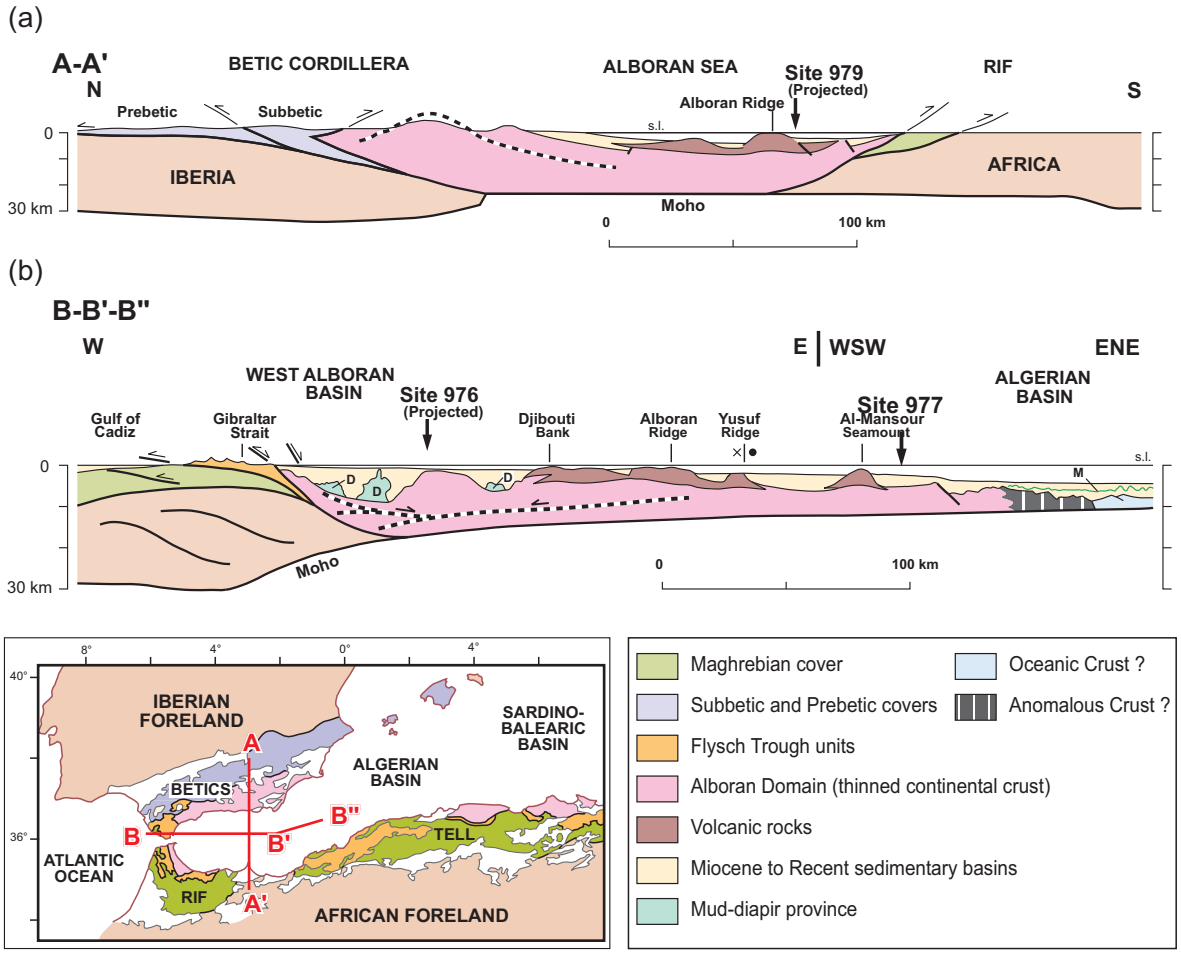

Figure 1-5. Schematic crustal sections taken from Comas *et al*., (1999). **(a)** Section illustrating the north-south crustal structure of the Alboran Basin, based on a synthesis of structural data from Spain and Morocco and Conrad seismic lines and on a density model obtained by comparing observed and calculated Bouguer anomaly data (Watts *et al*., 1993). **(b)** Crustal section from the Gibraltar Arc to the Algerian Basin illustrating the east-west crustal structure of the westernmost Mediterranean, based on a synthesis of structural data from the Gibraltar region and MCS profiles in the Alboran Sea, 3D modelling, gravity consideration, surface heat-flow, and elevation data (Torné *et al*., 2000). The intracrustal reflectors (hatched white lines) in the Alboran Domain represent extensional detachment faults or the top of the reflective lower crust.

1.1.3 Tectonic evolution of the Alboran Sea Basin

The tectonic evolution of the Alboran Sea Basin is explained as resulting from extension and basin subsidence since the Early Miocene, followed by shortening and transpression from the Late Miocene to Present (*e.g.* Comas *et al*., 1992, 1995, 1999; Docherty and Banda, 1992, 1995; Maldonado *et al*., 1992; Wooside and Maldonado, 1992; Watts *et al*. 1993; Chalouan *et al*., 1997; Alvarez-Marrón, 1999; Mauffret *et al*., 2007). According to thermal modelling of the metamorphic P-T-t

evolution of the Alboran Sea basement, crustal thinning began during the Oligocene, approximately at 27 Ma, producing rapid exhumation of metamorphic crustal rocks and concomitant heating of the lithosphere (Platt *et al*., 1996; 1998; Soto and Platt, 1999). However, the oldest deposits in the basin, forming the base of Unit VI, are marine sediments of latest Aquitanian (?) to Burdigalian age (~ 20 to 22 Ma) from the base of Unit VI (Jurado and Comas, 1992; Sautkin *et al*., 2003). These observations indicate collectively that although extension began during the Oligocene, the first marine transgression and associated syn-tectonic sedimentation occurred approximately 6 to 7 Ma after, during the Early Miocene (Figure 1-6).

Two main episodes of extension occurred in Betics and Rif during the Miocene. Extensional structures active at these times were related with the low-angle extensional detachments driven the ductile and brittle-to-ductile exhumation of the metamorphic complexes of the Alboran Domain. During the Burdigalian to Langhian an active extensional system deformed the Alpujárride Complex and produced N-S extension (García-Dueñas *et al*., 1992; Crespo-Blanc *et al*., 1994) (Figure 1-6). A second episode of extension occurred during the Late Langhian to Late Serravallian-Early Tortonian, producing NE-SW stretching along the contact between the Alpujárride and Nevado-Filábride complexes (García-Dueñas *et al*., 1988; García-Dueñas and Martínez-Martínez, 1988; Galindo-Zaldívar *et al*., 1989; García-Dueñas *et al*., 1992, 1995; Chalouan *et al*., 1997; Johnson *et al*., 1997; Martínez-Martínez *et al*., 1997, 2002). 1-D and 2-D backstripping analysis performed in the Alboran Sea Basin and onshore Neogene basins reveal two successive phases of tectonic subsidence during the Early and Middle Miocene that can be related with these two main rifting episodes (Watts *et al*., 1993; Docherty and Banda, 1995; Rodríguez-Fernández *et al*., 1999; Hanne *et al*., 2003).

In addition, the extensional processes were accompanied by magmatism and several volcanic episodes since ~15 to 6 Ma. The volcanic rocks form a broad NE–SW trending band, transecting the orogenic arc, that evolved from calc-alkaline and K-rich rocks (LREE-enriched) to tholeiitic series (LREE-depleted) (Hernandez and Bellon, 1985; Torres-Roldán *et al*., 1986; Di Battistini *et al*., 1987; Hernandez *et al*., 1987; Turner *et al*., 1999; Maury *et al*., 2000; Zeck and Williams, 2002, Duggen *et al*., 2004, 2008; Gill *et al*., 2004).

Shortening and transpression followed the end of rifting and occurred from Late Tortonian to Present. At this stage, pate convergence between Africa and Eurasia produced N-S shortening of the whole region and E-W basin elongation. The original Miocene extensional basin was divided into several sub-basins bounded by submarine highs. Deformation was dominated by strike-slip and reverse faulting and folding, forming large anticlines and fault zones (Comas *et al*., 1992; 1999; Maldonado *et al*., 1992; Woodside and Maldonado, 1992; Watts *et al*., 1993; Chalouan *et al*., 1997; Alvarez-Marrón, 1999; Mauffret *et al*., 2007). The distribution of Plio-Quaternary sediments and their facies reveal a generalized uplift in the onshore Neogene Basins and also in the Alboran Sea for this period, indicating that coeval shortening and uplift determined progressive emergence of the marine-basin margins and they are to a large degree responsible for the present-day seafloor morphology and coastline position (*e.g.* Comas *et al*. 1992; Jurado and Comas, 1992; Rodríguez-Fernández and Sanz de Galdeano, 1992, 2006; Sanz de Galdeano and Vera, 1992; Chalouan *et al*., 1997; Braga *et al*., 2003; Martín *et al*., 2003). Subsidence analyses corroborate this Plio-Quaternary uplift (Watts *et al*., 1993; Docherty and Banda, 1995; Rodríguez-Fernández *et al*., 1999; Hanne *et*

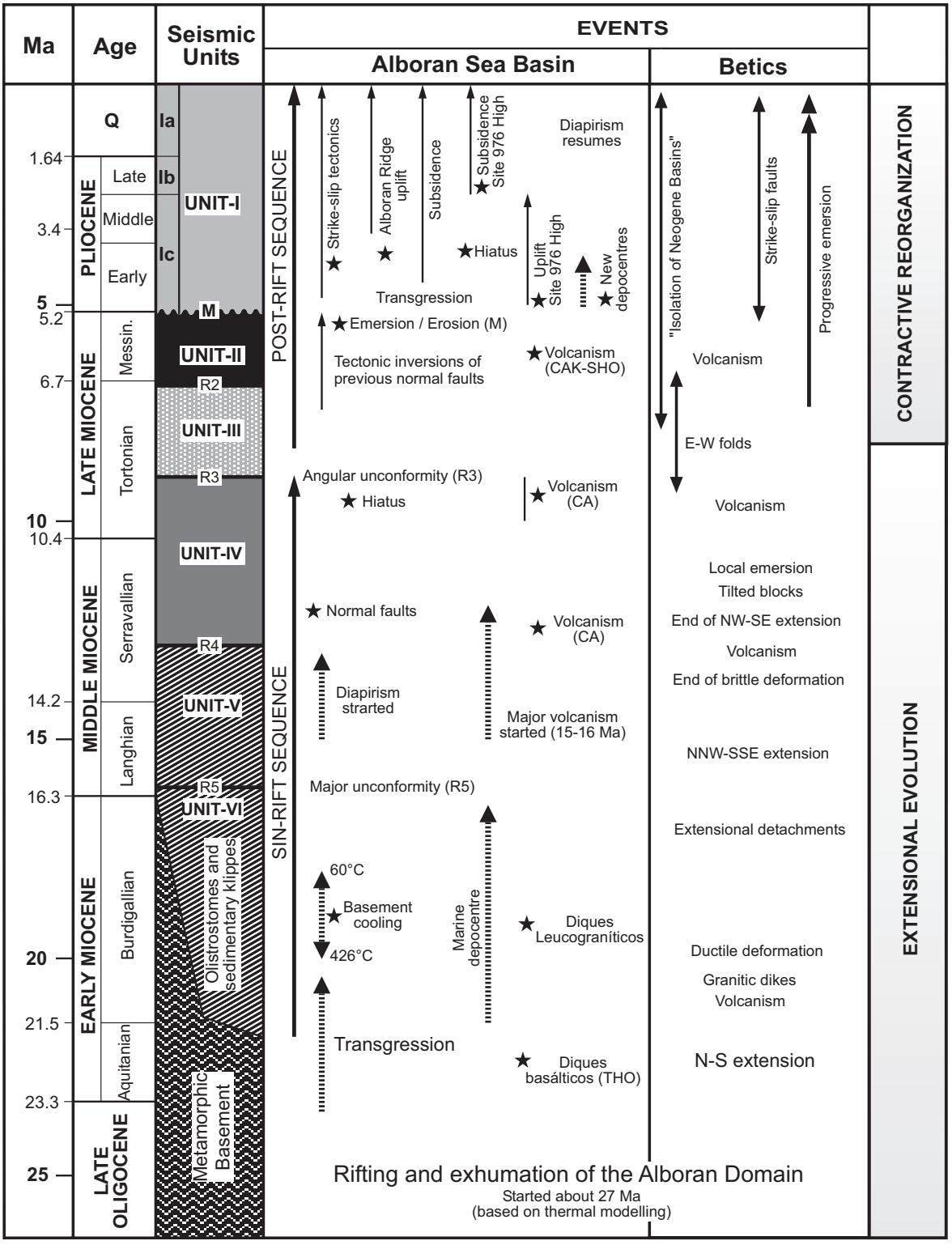

Figure 1-6. Timing of main events in the tectonic evolution of the Alboran Sea Basin compared with those in Betics and Rif (modified from Comas *et al*., 1999).

al., 2003). Shortening and transpression occurred simultaneously with calc-alkaline through K-rich (LREE-enriched) volcanism and intraplate-type alkali basaltic volcanism. The ages of these rocks range from 6.0 to 0.8 Ma and the most recent of them occur locally in the easternmost Betics, at the

western end of the Tell chain and to the south and southwest in the Atlas (*e.g.* Di Battistini *et al*., 1987; Hernandez *et al*., 1987; El Bakkali *et al*., 1998; Maury *et al*. 2000; Duggen *et al*., 2004, 2008).

The most recent tectonic evolution of the Alboran Sea Basin is controlled by two strike-slip fault systems that connect with the structures identified on land in Betics and Rif (Maldonado *et al*., 1992; Woodside and Maldonado., 1992; Fernández-Ibáñez *et al*., 2007) (Figures 1-2 and 1-6). One of these systems is formed by NE-SW to NNE-SSW left-lateral transpressive faults, including the Jebha and Nekor faults in the Rif, the fault zones along the Alboran Ridge, and the Carboneras, Palomares and Alhama de Murcia faults in the eastern Betics (*e.g.* Bousquet, 1979; Leblanc and Olivier, 1984; Montenat *et al*., 1987, 1992; Weijermars, 1987; Aït Brahim and Chotin, 1989; Morel, 1989; Bourgois *et al*., 1992; Rodríguez-Fernández and Martín-Penela, 1993; Sanz de Galdeano *et al*., 1995; Chalouan *et al*., 1997, 2008; Martínez-Díaz, 2002; Booth-Rea *et al*., 2003). The other system is a WNW-ESE right-lateral transtensive fault system that includes the Maro-Nerja Fault and other fault zones shaping the Yusuf basin and ridge (*e.g.* Mauffret *et al*., 1992, 2007; Alvarez-Marrón, 1999; Soto and Manzano, 2002). Some onshore and offshore fault segments of both systems have been reported as active faults during the Quaternary with associated instrumental seismicity and therefore they represent a potential seismic hazard (*e.g.* De Larouzière *et al*., 1988; Keller *et al*., 1995; Martínez-Díaz, 1998, 2002; Masana *et al*., 2004; Gràcia *et al*., 2006; Reicherter and Hübscher, 2007; Fernández-Ibáñez *et al*., 2007).

1.1.4 Seismicity and actual plate motions

The boundary between the African and Eurasian plates has variable character from the Western Mediterranean to the Atlantic Ocean. Along the Tell region deformation and seismicity are concentrated forming a clear plate boundary. Towards the west, this area connects with a segment of diffuse plate boundary across the Gibraltar Arc System and in the Atlantic Ocean the Gloria Fault corresponds with other segment of discrete plate boundary.

Previous studies have determined that the Gibraltar Arc System comprises a broad zone of deformation with frequent intermediate-magnitude earthquakes that show a scattered distribution (*e.g.* Grimison and Chen, 1986; Udías and Buforn, 1991; Buforn *et al*., 1991, 1995, 2004; López Casado *et al*., 2001; Stich *et al*., 2003) (Figure 1-7). Thus, the precise location and nature of the contact between the two plates across the Alboran Sea Basin is unclear and several hypotheses have been proposed (*e.g.* Klitgord and Schouten, 1986; Morel and Meghraoui, 1996; Negredo *et al*., 2002; Bird, 2003; Gutscher, 2004; Fadil *et al*., 2006; Stich *et al*., 2006; Serpelloni *et al*., 2007; Vernant *et al*., 2010; Koulali *et al*., 2011). Focal depth distribution displays abundant shallow depth, crustal earthquakes, but also intermediate depth, mantle seismic events (30–150 km) and few deep earthquakes (~600 km). Seismic tomography shows the occurrence of one or more large bodies of cold mantle and it has been argued that these data may indicate the existence of a detached portion of lithospheric mantle (*e.g.* Blanco and Spakman, 1993; Seber *et al*., 1996; Mezcua and Rueda, 1997; Calvert *et al*., 2000; Spakman and Wortel, 2004). Nevertheless, it is not clear whether the intermediate depth earthquakes are connected or not with the shallow crustal seismicity. In any case, focal depth distribution of earthquakes shows that most seismicity is in the upper crust (90% of the crustal seismicity is less than 15 km depth) and shows several seismic swarms with abundant shallow earthquakes. The biggest

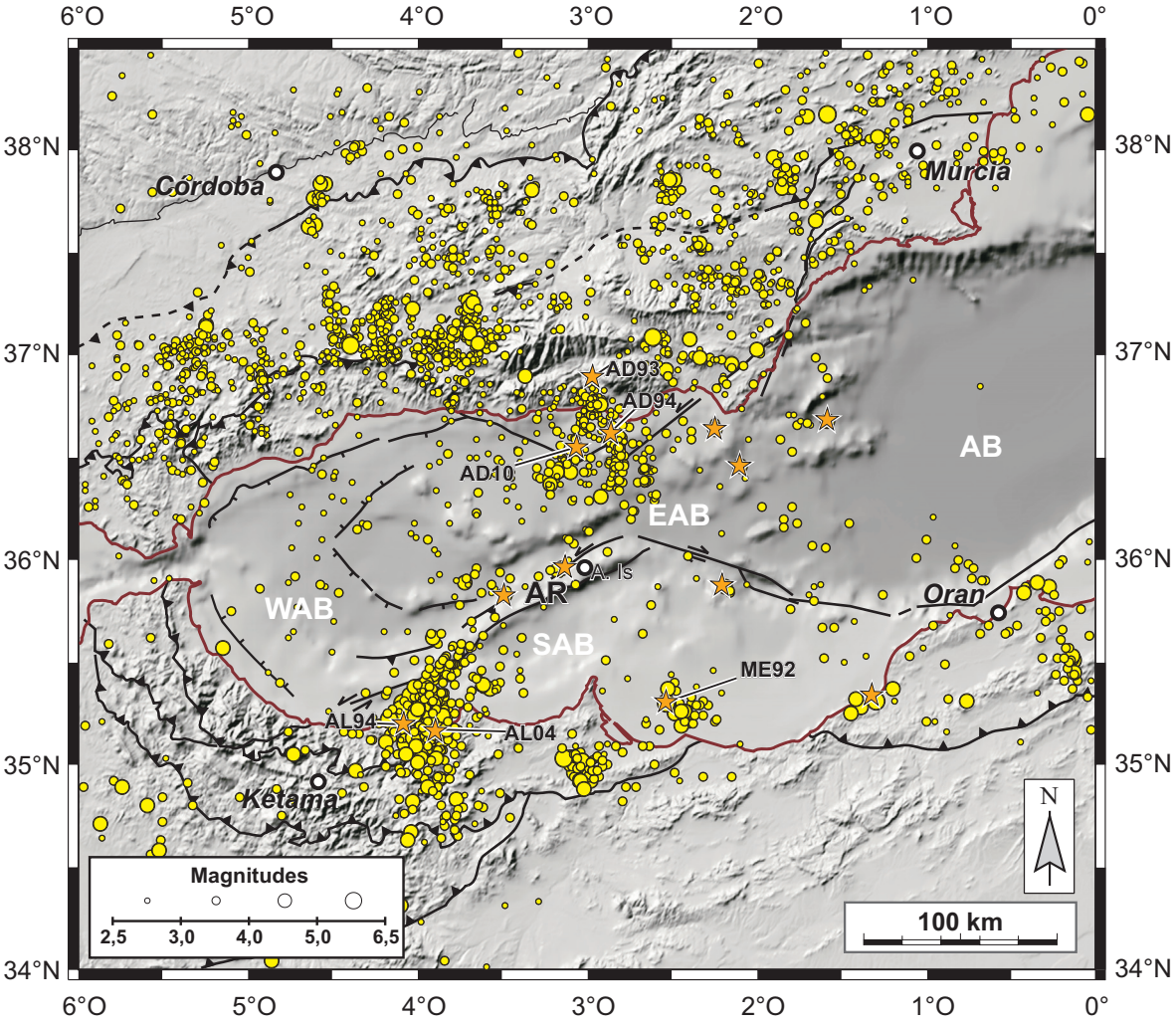

Figure 1-7. Distribution of crustal seismic events (M_w > 2.5) in the Gibraltar Arc for the 1980–2006 period (USGS catalogue) combined with topographic map and simplified major tectonic features (taken from Fernández-Ibáñez *et al*., 2007). Starts represent major earthquakes associated with the Adra and Al Hoceima seismic swarms and other offshore large earthquakes (M_w > 4.5) (Bezzeghoud and Buforn, 1999; Stich *et al*. 2001, 2003b, 2006; Biggs *et al*. 2006): AD10 Adra 1910/6/16, AD93 Adra 1993/12/23, AD94 Adra 1994/1/4, AL94 Al Hoceima 1994/5/26, AL04 Al Hoceima 2004/2/24, ME92 Melilla 1992/12/3. Abbreviations: A. Is, Alboran Island; AB, Algerian Basin; AR, Alboran Ridge; EAB, East Alboran Basin; SAB, South Alboran Basin; WAB, West Alboran Basin.

recorded earthquakes in the Alboran Sea are located next to the Moroccan coast and corresponds with the Al Hoceima seismic series in 1994 and 2004, which comprise earthquakes with maximum magnitude (M_w) of 6.3 (Stich *et al*., 2005, 2003; Biggs *et al*., 2006) (Figure 1-7). Other remarkable clusters of earthquakes are located: (1) to the east of Melilla including the 1992 Melilla earthquake (M_w = 4.8) (*e.g.* Bezzeghoud and Buforn, 1999); (2) along the Alboran Ridge, which comprises some scattered events with moderate magnitude (M_w between 4 and 5) (*e.g.* Fernández-Ibáñez *et al*., 2007; Fernández-Ibáñez and Soto, 2008); (3) in the northeastern margin forming the Adra and Motril seismic swarms (Buforn *et al*., 1995; Stich *et al*., 2001, 2003; Biggs *et al*., 2006).

The relative convergence trends along the African-Eurasian plate boundary have changed since the Cretaceous. Kinematic reconstructions suggest that this region experimented about 200 km

of N-S convergence since the Middle Oligocene to Late Miocene, followed by 50 km of oblique convergence with NW-SE since the late Tortonian (8-9 Ma) to present-day (*e.g.* Dewey *et al*., 1989; Mazzoli and Helman, 1994; Rosenbaum *et al*., 2002).

Different global space-geodetic models document the present-day moderate convergent motion of Africa towards the NW with respect to fixed Eurasia with an average velocity of convergence of ~5 mm/y (*e.g.* NUVEL-1A, DeMets *et al*., 1994; APLIM2000, Drenes and Agermann, 2001; DEOS2k, Fernades *et al*., 2003; IGSO2P09, Nocquet and Calais, 2004). This plate convergence vector shows an important oblique component with respect to the general E-W trend of the plate boundary

Additionally, GPS data from permanent and temporal stations in Iberia and North Africa indicate also predominant NW-SE convergence with an average velocity similar to those obtained from global geodesic models. However, local GPS observations in the Rif and in the vicinity of the Gibraltar Strait in the western Betics suggest a lateral escape of the frontal part of the Gibraltar Arc towards the southwest (*e.g.* Reilly *et al*., 1992; Fadil *et al*., 2006; Stich *et al*., 2006; Vernat *et al*., 2010; Koulali *et al*., 2011) (Figure 1-8).

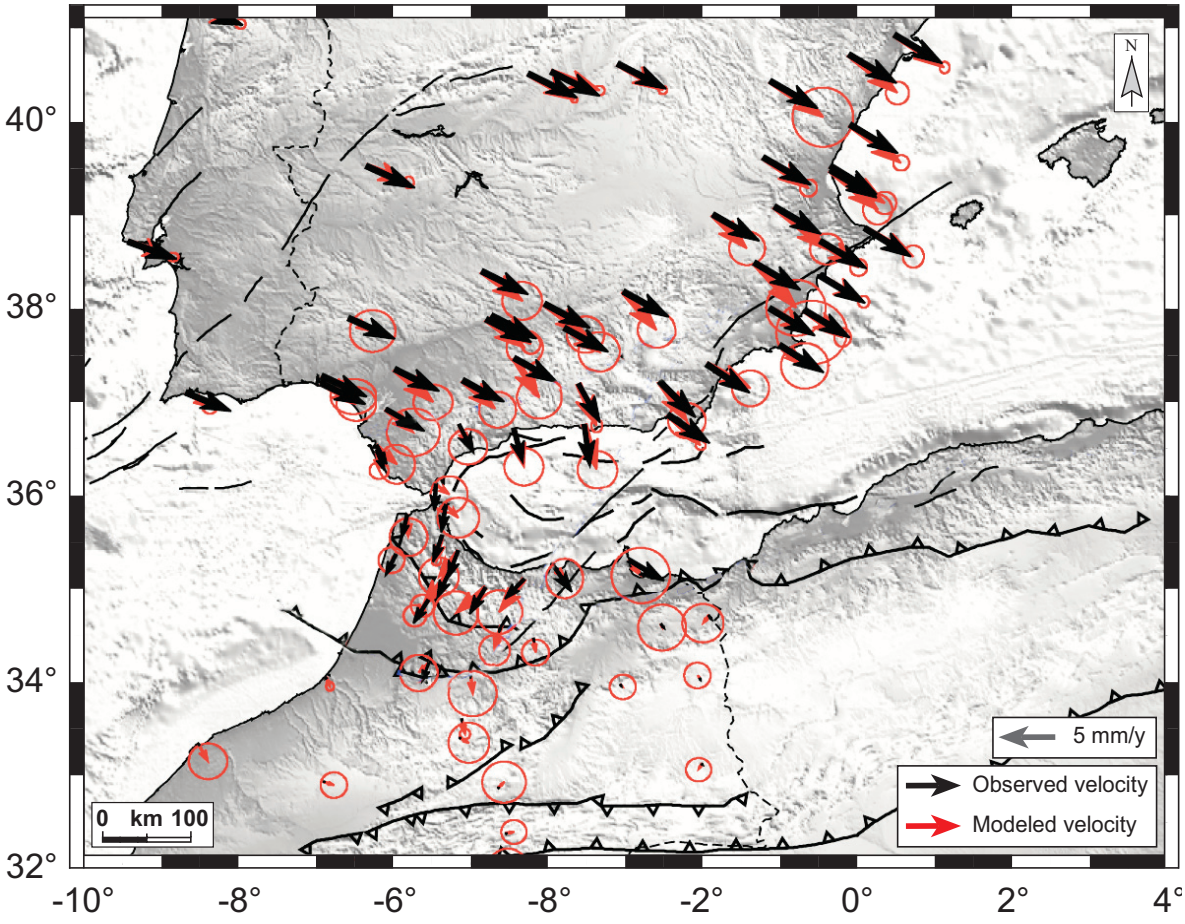

Figure 1-8. Observed and modelled GPS velocities in the westernmost Mediterranean along the Eurasian plate with respect to Africa (taken from Koulali *et al*., 2011). Red circles represent 95 % confidence ellipses. Topography and major tectonic features are also included (Figure 1-2).

1.1.5 Geodynamic models

The origin of the Alboran Sea Basin is still a matter of debate. Although it is clear that basin subsidence was linked to the formation and evolution of the surrounding Betics and Rif cordilleras, the exact tectonic mechanism responsible of the genesis of the whole Gibraltar Arc System and its relationship with the Neogene evolution of the western Mediterranean are still under discussion. Different hypothesis have been proposed to explain jointly the main geological and geophysical observations in this region: (1) the strongly arcuate shape of the orogen and its location as the westernmost peri-Mediterranean Alpine belt; (2) the existence of compressive structures in the peripheral orogenic belt, which developed coevally with extension in the inner part of the arc during the Early to Middle Miocene (*e.g.* Platt and Vissers 1989; García-Dueñas *et al.*, 1992; Watts *et al.*, 1993; Lonergan and White, 1997; Comas *et al.*, 1999); (3) the westward migration and coeval extension and exhumation of the metamorphic complexes forming the Alboran Domain (Balanyá and García-Dueñas, 1987; García-Dueñas *et al.*, 1992; Zeck *et al*., 1992; Martínez-Martínez *et al*, 1997; Augier *et al*., 2005); (4) the presence of a thin continental crust in the inner part of the hinterland corresponding with the Alboran Sea Basin (*e.g.* Hatzfeld *et al*., 1987; Torné and Banda, 1992; Platt *et al*., 1996, 1998; Soto and Platt, 1999) (5) the central part of the orogen coincide with a region of high heat flow and relatively thin lithosphere, which is underlaid by a shallow asthenosphere (*e.g.* Polyak *et al*., 1996; Rimi, 1999; Torné *et al*., 2000; Ayala *et al*., 2003; Fullea *et al*., 2007; Soto *et al*., 2008); (6) the volcanic episodes since the Middle Miocene (*e.g.* Duggen *et al.*, 2004; Gill *et al.*, 2004; Maury *et al*., 2000); (7) active tectonics with a widespread seismicity distribution and complex pattern of earthquake focal mechanisms (*e.g.* Udías and Bufforn, 1991; Bufforn, 1995; López Casado *et al*., 2001; Stich *et al*., 2003, 2006; Fernández-Ibáñez *et al*., 2007; Fernández Ibáñez and Soto, 2008); and (8) the presence of a high velocity seismic anomaly, located beneath the Gibraltar Arc, in the asthenospheric mantle with arcuate geometry and strong dip towards the east reaching ~650 m in depth (*e.g.* Blanco and Spakman, 1993; Seber *et al*., 1996; Bijwaard and Spakman, 2000; Clavert *et al*., 2000). The current geodynamic models are:

Post-orogenic collapse related with the *convective removal* of lithospheric mantle (Platt and Vissers, 1989) (Figure 1-9a). This model proposes that long-lived plate convergence generated a collisional ridge in the western Mediterranean. Lithospheric thickening resulted in the formation of a substantial cool root of lithospheric mantle by Oligocene time. This unstable lithospheric root was convectively removed and assimilated by the asthenosphere in the Late Oligocene to Early Miocene. This process would decrease the potential energy enhancing the uplift and extension of the overlying crust with a radial pattern and exhumation of metamorphic rocks (Houseman *et al*., 1981; Platt and Vissers, 1989; Houseman and Molnar, 2001). The gravitational instability is suggested to diminish during the Late Miocene and the convergence between the Eurasian and African plates promoted shortening within the peripheral orogenic belt.

Delamination of lithospheric mantle beneath the orogen (*e.g.* García-Dueñas *et al*., 1992; Seber *et al*., 1996; Calvert *et al*., 2000) (Figure 1-9b). This model has some similarities with the model of convective removal but the main differences between them refer to the driving mechanism for the lithospheric root remotion. In the case of delamination model, the lithospheric root would be progressively peeled back from east to west. The existence of a high-velocity seismic anomaly into

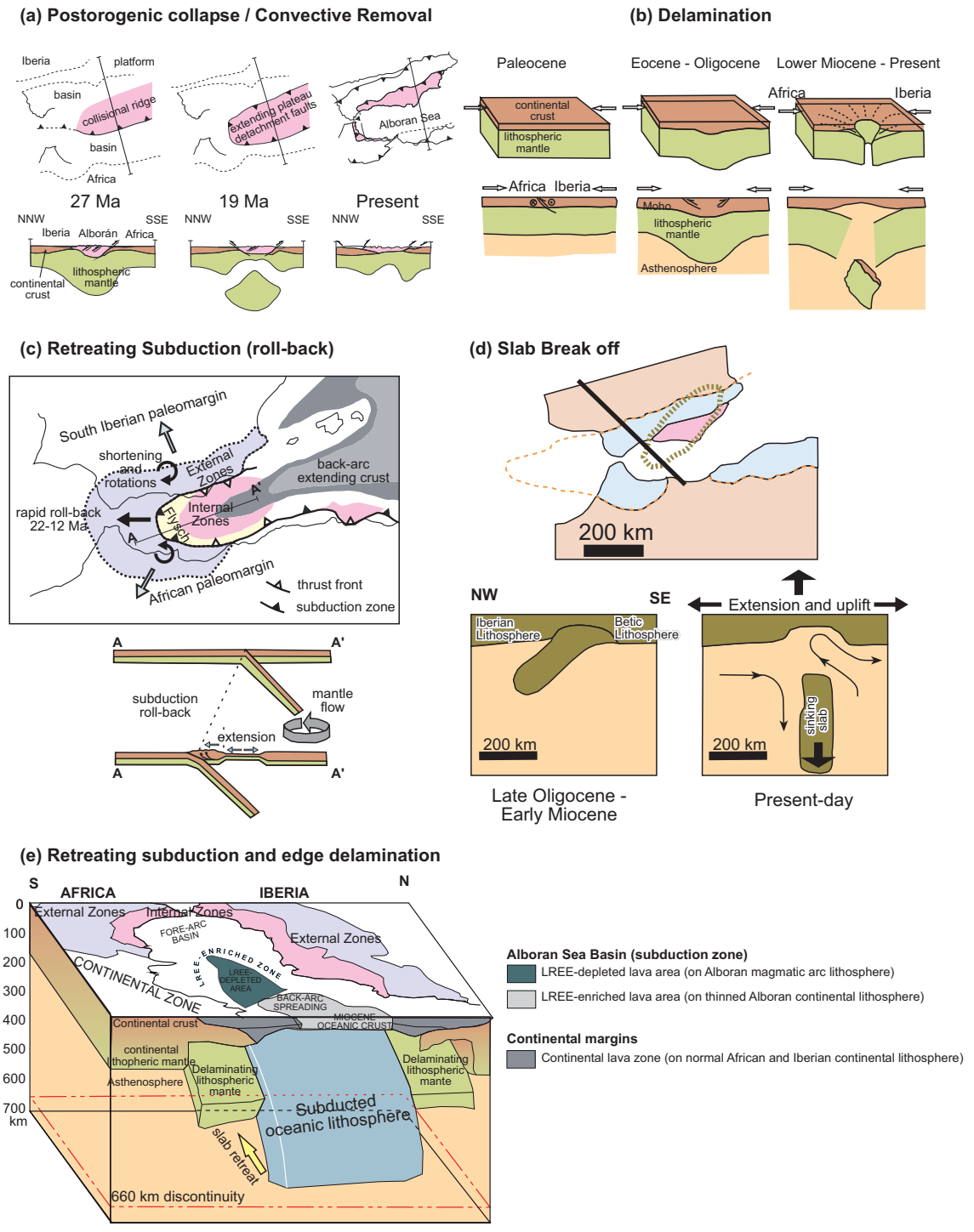

Figure 1-9. Sketches summarizing the geodynamic models proposed to explain the origin and tectonic evolution of the Gibraltar Arc System. **(a)** Convective removal of a lithospheric mantle root during the Early Miocene (taken form Platt and Vissers, 1989). **(b)** Delamination of the thickened lithosphere (taken form Seber *et al*., 1996). **(c)** Retreat from east to west of an east dipping subducting slab during the Early Miocene (taken form Lonergan and White, 1997). **(d)** Break off of a NW dipping slab during the Oligocene to Miocene transition (taken from Zeck, 1997). **(e)** Subduction of an oceanic lithosphere beneath the Alboran Sea and edge delamination beneath the continental margins (taken form Duggen *et al*., 2008).

the mantle beneath the Betics and Rif has been interpreted as a fragment of the cold upper-mantle root, which remain still connected with the crust suggesting that the delamination processes might be still active at present-day (*e.g.* Seber *et al*., 1996).

Subduction of oceanic lithosphere and associated slab "*roll-back"* and /or "*break off*" (*e.g.* Wortel and Spakman, 1992, 2000; Zeck, *et al*., 1992; Blanco and Spakman, 1993; Royden, 1993; Lonergan and White, 1997) (Figure 1-9c and 1-9d). The subducting slab would correspond with and old (probably Jurassic to Cretaceous) oceanic lithosphere, which might existed between the continental Alboran Domain and the passive paleomargins of Iberian and North-Africa and it was initially covered by the deep-water deposits of the Flysch Trough Units. This oceanic domain may have corresponded with the westernmost part of the Tethys Ocean. A number of subduction models have been proposed and they defer in the suggested geometry and sense of dip of the subducting oceanic slab (*e.g.* Torres Roldán *et al*., 1986; Spakman e al., 1993; Morales *et al*., 1999; Jolivet and Faccena, 2000; Gutscher *et al*., 2002, 2006; Ruiz-Constán *et al*., 2010). In addition, some models propose that an increase in the subduction velocity respect to the convergence rate between the Eurasian and African plates would result in a centripetal migration of the subduction zone known as "*roll-back*", which incremented the dip of the subducting slab. This process promoted extension and thinning of the overlying continental crust (Figure 1-9c). Furthermore, some subduction models suggest breaking off of the subducting slab instead of /or in addition to migration of the subduction zone. This hypothesis is called "*slab break off*" (Figure 1-9d). The detached piece of the underlying slab would progressively sink into the asthenosphere and it would be replaced by hot sub-lithospheric mantle material heating the overlying continental lithosphere and promoting its uplifting and extension (Blanco and Spakman, 1993; Zeck, 1997, 1999; Hoernle *et al*., 1999).

Some authors suggest a combination of *subduction* of oceanic lithosphere beneath the Alboran Sea and edge *delamination* beneath the continental margins (*e.g.* Duggen *et al*., 2004; 2008; Booth-Rea *et al*., 2007) (Figure 1-9e). These models propose that during the Miocene, the partially subducted Tethys oceanic lithosphere experienced *"roll-back"*, producing delamination of the subcontinental lithosphere at the southern Iberian and northwestern African continental margins. This model tries to explain the spatial, temporal and geochemical evolution of magmatism (*e.g.* El Bakkali *et al*., 1998; Maury *et al*., 2000; Gill *et al*., 2004). The upwelling of the sub-lithospheric mantle beneath the continental margins would have replaced the delaminated subcontinental lithospheric mantle inducing intensive magmatism and extension in the overlying Alboran Domain.

1.2 The scientific target

The geological and geophysical characteristics of the Alboran Sea Basin, as have been summarized above, document a complex history of basin subsidence and uplift and make this region a useful area for analysing the evolution of marine extensional basins in collisional geodynamic settings. Numerous studies have dealt on the early extensional history of this basin during the Miocene to understand how extensional collapse occurs in a collisional orogen that results from a long-lived history of plate convergence since the Cretaceous (*e.g.* Platt and Vissers, 1989; Comas *et al.*, 1992, 1999; García-Dueñas *et al.*, 1992). However, the post-extension history of this basin has received much less attention. This Ph. D thesis mainly focus on the recent history of the Alboran Sea Basin since the late Messinian, *i.e.* during the last ~5 Ma, when the original extensional basin was deformed by large-scale folds, strike-slip and reverse faults with simultaneous uplift of the basin margins (*e.g.* Bourgois *et al.*, 1992; Comas *et al*., 1992, 1999; Woodside and Maldonado, 1992). The timing of the main tectonics events during the Plio-Quaternary and the characterization of the deformations and their spatial and temporal distribution are still far from being well-established. This study aims to understand the complex interplay between the inherited pattern of Miocene structures, abundant sediment supplies from the surrounding mountains and tectonic activity, which controls the ongoing uplift and subsidence.

This thesis explores the central sector of the basin (Figure 1-10). This area depicts abrupt seafloor morphology and shows important faults and folds with recent tectonic activity (*e.g.* Campos *et al*., 1992; Maldonado *et al*. 1992; Ballesteros *et al*., 2008). The Alboran Ridge stands out in this sector as the most prominent morphological and structural feature of the Alboran Sea Basin (Figure 1-10). It corresponds with an elongated submarine high with more than 130 km in length and oriented perpendicularly to the recent NW-SE convergence trends between the Eurasian and African plates (*e.g.* Jolivet and Faccenna, 2000; Rosenbaum *et al*., 2002). Other outstanding features in the study area occur in the vicinities of the deep pull-apart Yusuf Basin. This basin is bounded by the elongated

Yusuf Ridge to the north and by the Yusuf Escarpment to the south. All these features are referred collectively in this study as the Yusuf Lineament. Previous studies have addressed the broad internal structure of the Alboran Ridge and Yusuf Lineament by means of some single and multichannel profiles, but the reconstruction of their anatomy and a detailed study of the role played by these prominent features during the Pliocene to Quaternary evolution of the Alboran Sea Basin have not been already undertaken. Moreover, their relationships with other neighbouring structures in the Gibraltar Arc System, and how they do or do not connect with the major active faults described in the onshore regions of the Betics and Rif also remain unclear (*e.g.* Hernandez *et al*., 1987; de Larouzière *et al*., 1988; Fernández-Ibáñez *et al*., 2007).

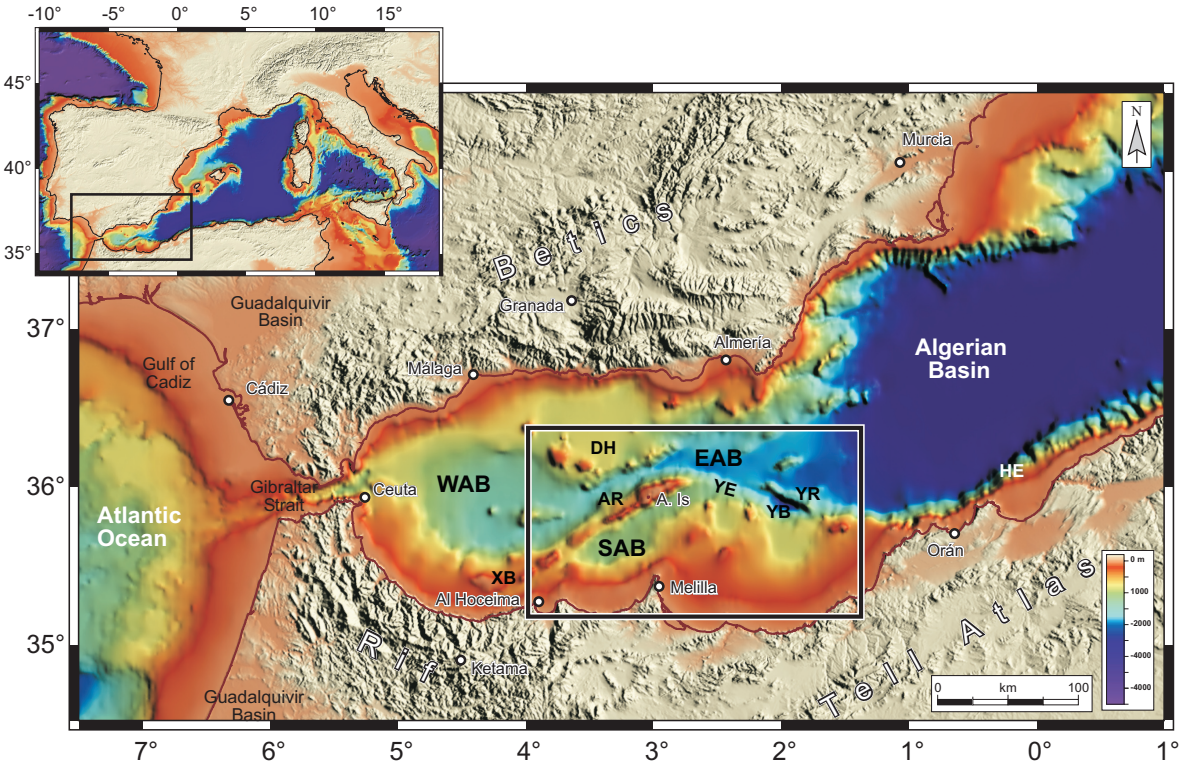

Figure 1-10. Topography of the Gibraltar Arc System and location of the study area in the Alboran Sea Basin. Study area comprises the Alboran Ridge and Yusuf regions and other surrounding realms. Inset is a topographic map of the Western Mediterranean showing the location of the Gibraltar Arc System. Digital topography is based on the SRTM (USGS652-NASA) global database combined with GEBCO 97 (IOC-IHO) for the offshore region. Abbreviations: A. Is, Alboran Island; AR, Alboran Ridge; DH, Djibouti High; EAB, East Alboran Basin; HE, Habibas Escarpment; SAB, South Alboran Basin; XB, Xauen Bank; YB, Yusuf Basin; YE, Yusuf Escarpment; YR, Yusuf Ridge and WAB, West Alboran Basin.

1.3 Objectives

This PhD Thesis aims to contribute to unravel the recent to active tectonic processes shaping the Alboran Sea Basin. It is intended to characterize the geometry and kinematics of the most recent structures discussing their correlation with the shallow, upper crust seismicity and their contribution to the abrupt seafloor physiography. In particular, this study is centred in the basin evolution during the last ~5 Ma.

Several geophysical data from the study area, including original unpublished multichannel seismic reflection profiles, high-resolution seismic profiles and bathymetry records acquired principally for this research work, have been compiled to build up a comprehensive dataset. They have been interpreted to obtain an integrated view of the shallow structure and seafloor morphology of the central and southeast Alboran Sea Basin focusing in the Alboran Ridge, the Yusuf Lineament and surrounding basins. It is expected that the whole results would help to discuss how deformation is partitioned within the Gibraltar Arc System.

The specific scientific objectives of this research work are:

- to analyze the shallow crustal structure determining the major fold and faults systems, which deform sedimentary sequences, characterizing their geometry, kinematics, and ages.
- to investigate the role of tectonic processes controlling the seafloor morphology by analyzing bathymetric features that result from active or very recent tectonics.
- to revise the Plio-Quaternary seismic stratigraphy of the central and southeast Alboran Sea Basin identifying the main seismic units and bounding unconformities, and estimating their precise age and geometry.
- to analyze the relationships between sedimentary and tectonic processes during the Pliocene

and Quaternary tectonic evolution, determining the coeval distribution and variation of sediment accumulation rates, uplift or subsidence in the Alboran Sea Basin.

- to analyze the role played by tectonic heritage from Miocene structures and basin framework in the Plio-Quaternary tectonic evolution to evaluate the likely occurrence of tectonic-inversion processes.
- to link the the present-day tectonic activity defined by the shallow seismicity and the most recent structures and the submarine instability processes, which may represent a potential seismic or tsunamigenic hazard.
- to characterize the geometry and kinematics of the Pliocene-to-Recent fault structures to finally discuss how deformation is partitioned along a diffuse plate boundary across the Alboran Sea Basin that shows scattered crustal seismicity and an oblique and moderate convergence between the African and Eurasian plates.

1.4 Thesis outline

This thesis is organized in eight chapters. In addition to the present chapter concerning to some introductory aspects and a geological overview of the whole region, the following chapters deal on the data, methodology, interpretation and discussion of results and conclusions on main findings of this study. Chapters 3 and 4 constitute papers that have been published or have accepted for publication in SCI journals. Chapters 5 and 6 are other manuscripts, which are going to be submitted in brief. The abbreviated content of every chapter of the thesis is as follows:

- *Chapter 2* ***"Dataset and Methodology"***, presents the comprehensive dataset used in this study, which came from different scientific and commercial cruises. It describes the different geophysical techniques used for data acquisition and the procedure used to digitalize the analogue records of seismic profiles. It is also presented the bio-stratigraphic and log information from several wells that have been employed to constrain the interpretation. Additionally, this chapter contains explanations about the gridding procedure used to generate contour maps and the calculus of interval velocities, depth conversions and sediment accumulation rates.

- *Chapter 3,* ***"Seafloor morphology and recent tectonics"***, presents bathymetric data and sub-bottom parametric seismic profiles and includes a description of the main faults and folds with associated Quaternary activity. Sedimentary and erosive features, as gullies, abrasion platforms and slides, have been also identified and mapped. These results are compared with shallow seismicity data and focal mechanism, in order to assess the position and kinematics of those active fault segments representing a potential seismic hazard. The discussion deals here on the role played by active tectonics, triggering instability processes and erosion. This chapter has been published in Geo-Marine Letters, 2011 (31: 19-36): *"Recent structures in the Alboran Ridge and Yusuf fault zones based on swath bathymetry and sub-bottom profiling: evidence of active tectonics"*.

- *Chapter 4,* ***"Plio-Quaternary stratigraphy and tectonic evolution",*** focus on the seismic interpretations of the shallow sedimentary sequences and structures of Plio-Quaternary age to constrain the post-Messinian basin evolution. Subsurface maps, sedimentation rate estimates and reconstructions of basin highs and active faults have been carried out throughout the Plio-Quaternary. With these interpretations it is discussed the pattern of uplift and subsidence in the basin and how they can be linked to tectonic processes. It is reconstructed the existence of several episodes of shortening since the late Messinian and it is discussed whether they can be linked to changes in the convergence between the Eurasian and African plates. This chapter has been accepted for publication in *Basin Research* with the following title: *"Strike-slip tectonics and basin inversion in the Western Mediterranean: the Post-Messinian evolution of the Alboran Sea".*

- *Chapter 5,* ***"Submarine instability processes",*** describes several types of mass transport deposits (MTD) within the Plio-Quaternary sedimentary infill using swath bathymetry data, high-resolution acoustic profiles and single and multichannel seismic reflection profiles. Age estimations are given for most of the MTD by linking seismic interpretation and bio-stratigraphic information. It is proved the occurrence of recurrent instability processes in some areas next to the main Plio-Quaternary faults and it is discussed the role of earthquakes as main triggering factor. This chapter corresponds with a manuscript under elaboration, which is entitled *"Recurrent slope instability and slides in the Alboran Sea: assessment for changing basin topography from Pliocene to Recent"* and it will be submitted to an international SCI journal.

- *Chapter 6,* ***"Tectonic inversion and geodynamic implications",*** documents pre-Messinian deformations by means of multichannel seismic profiles and compares these observations with the Plio-Quaternary structures. This contribution attempts to decipher how Miocene growth faults were inverted mainly during post-Messinian times. This chapter corresponds with a manuscript that will be submitted to an international SCI journal with the preliminary title: *"Tectonic inversion in the Alboran Sea Basin: from Miocene extension to Recent shortening".*

- *Chapter 7* summarizes the conclusions of this thesis.

- *Appendixes* contain other papers published in different non-SCI journals together with different contributions to international meetings.

2. Data and Methodology

This Ph. D thesis is based in a compilation of geophysical data along the central and southeastern parts of the Alboran Sea Basin, covering an area of 28000 km^2. This area locates between 1.35–3.95° W and 35.17–36.42º N and represents more than 50% of the total area of the Alboran Sea.

The dataset comprises swath-bathymetry mosaics, sub-bottom parametric profiles and single and multichannel seismic reflection profiles. Biostratigraphic information and log data (*Vp*, density and gamma ray) from scientific and commercial wells has been also used. Additionally, complementary seismicity data were taken from the "*United States Geological Survey*" (USGS) seismic catalog (www.usgs.gov) and focal mechanisms were compiled mainly from the *"Instituto Andaluz de Geofísica"* (www.ugr.es/~iag) and the *"Instituto Geográfico Nacional"* (www.ign.es).

2.1 Swath bathymetry

A detailed bathymetry map for the study area has been derived merging swath-bathymetric data. A bathymetric mosaic covering the Alboran Ridge and Yusuf regions was obtained during the ALBA cruise in 1992, onboard the BIO Hespérides, using an EM-12S-120 Simrad multibeam echosounder. This system is based in the emission of a series of acoustic pulses directed towards the seafloor and arranged in a fan of narrow acoustic beams (Figure 2-1). The echosounder is mounted in the hull and measures the two-way travel time (twtt) of the sound pulses between the ship and the seafloor that is immediately reflected at the water/seafloor interface. The two-way travel time of the reflected sound pulse is continuously recorded and automatically converted to depth. This conversion is performed using a mathematical function that considers changes of velocity of acoustic waves in water, which is mainly controlled by water temperature and salinity. The system works with a central frequency of 13 kHz and a power of 12 kW and emits simultaneously 81 acoustic beams forming a maximum coverage of 120º that allow to obtain an overall swath coverage of 3.5 times seafloor

depth, ranging from 50 m to 11,000 m depth. The main advantage of this system is that it provides a 100% of coverage of the seafloor, and therefore the resulting seabed maps are more detailed than those obtained using single-beam mapping. Multibeam echosounders are connected to positioning equipment, heading and motion sensing instruments, as well as sound velocity sensors in order to position the soundings correctly. XBT stations (eXpendable BatyThermograph) are systematically deployed to calibrate sound velocity profiles (SVP) during the bathymetric surveys.

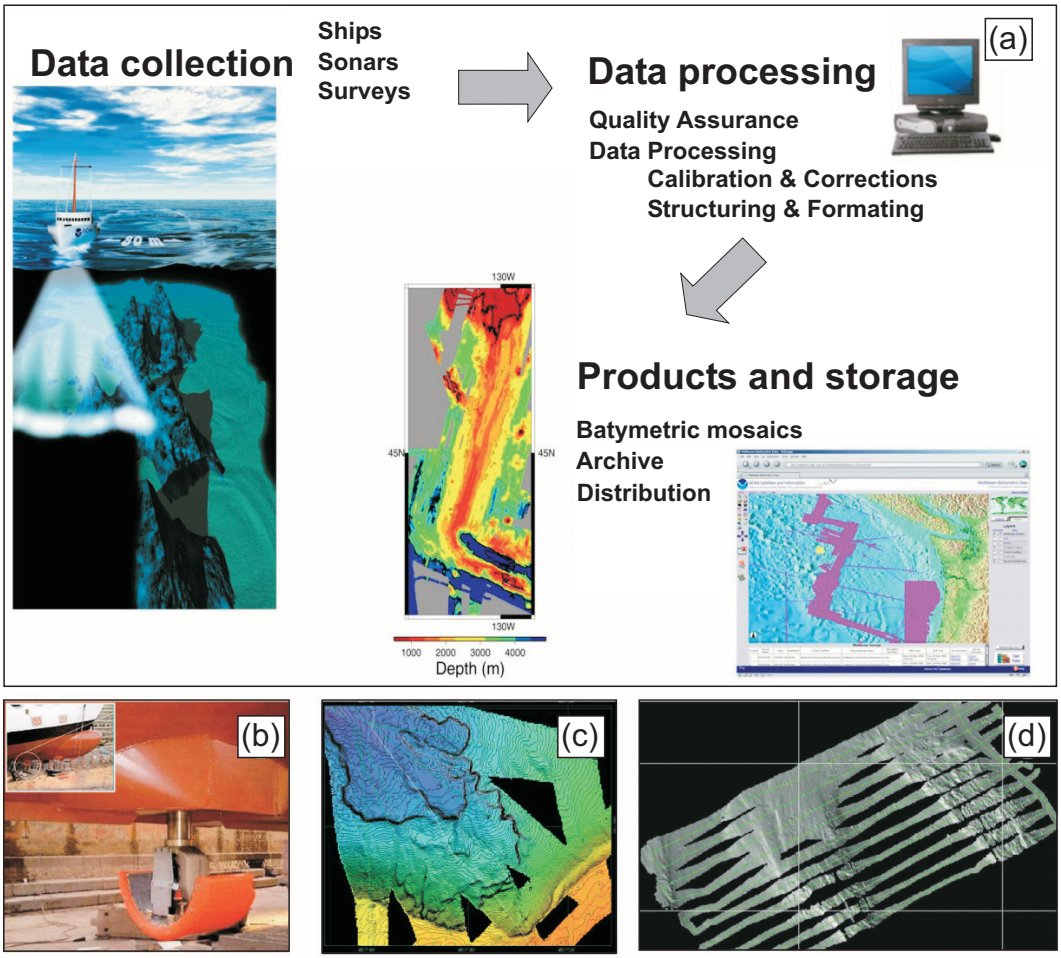

Figure 2-1. (a) Scheme of the multibeam operations covering from the data recovery during marine geological cruises to the elaboration of the final products. **(b)** Multibeam sounders mounted under the hull of the vessel. **(c)** Example of bathymetric mosaic. **(d)** Example of shaded depth relief map. (Taken from García, 2008.)

In addition to multibeam data from the ALBA cruise, several complementary dataset were used to complete the bathymetric mosaic and fill de gaps: (1) digital bathymetric atlases published by MediMap Group (2005, 2008); (2) Simrad swath-bathymetry tracks from the TECALB, HITS (Gràcia *et al*., 2006) and MARSIBAL I-06 cruises, which were conducted onboard the BIO Hespérides in 2000, 2001 and 2006 respectively; (3) bathymetric data acquired by the *"Instituto Español de Oceanografía"* (IEO) for the Spanish Fisher Office (Muñoz *et al*., 2008; Ballesteros *et al*., 2008); and (4) the GEBCO-2003 (IOC-IHO) global chart. Additionally, some data from digital topography from adjacent onshore regions along the North African margin were extracted from the

SRTM (USGS-NASA) global database (www.nasa.gov and http://dds.cr.usgs.gov/srtm). The data were stored and processed with Neptune® and Caraibes® softwares and afterwards, Surfer® and Fledermaus® softwares were used to produce digital elevation models (DEM). Different bathymetric mosaics and topography grids were interpolated separately considering different regular spacing for each case, in order to maintain the variable resolution of data (Figure 2-2). Finally, a coloured shaded-relief surface, which integrates the whole bathymetric and topographic dataset, was obtained using Surfer® and ESRI ArcGIS® softwares. In addition, a slope map showing terrain slopes in grades has been computed and several topographic profiles were built from the compiled DEM.

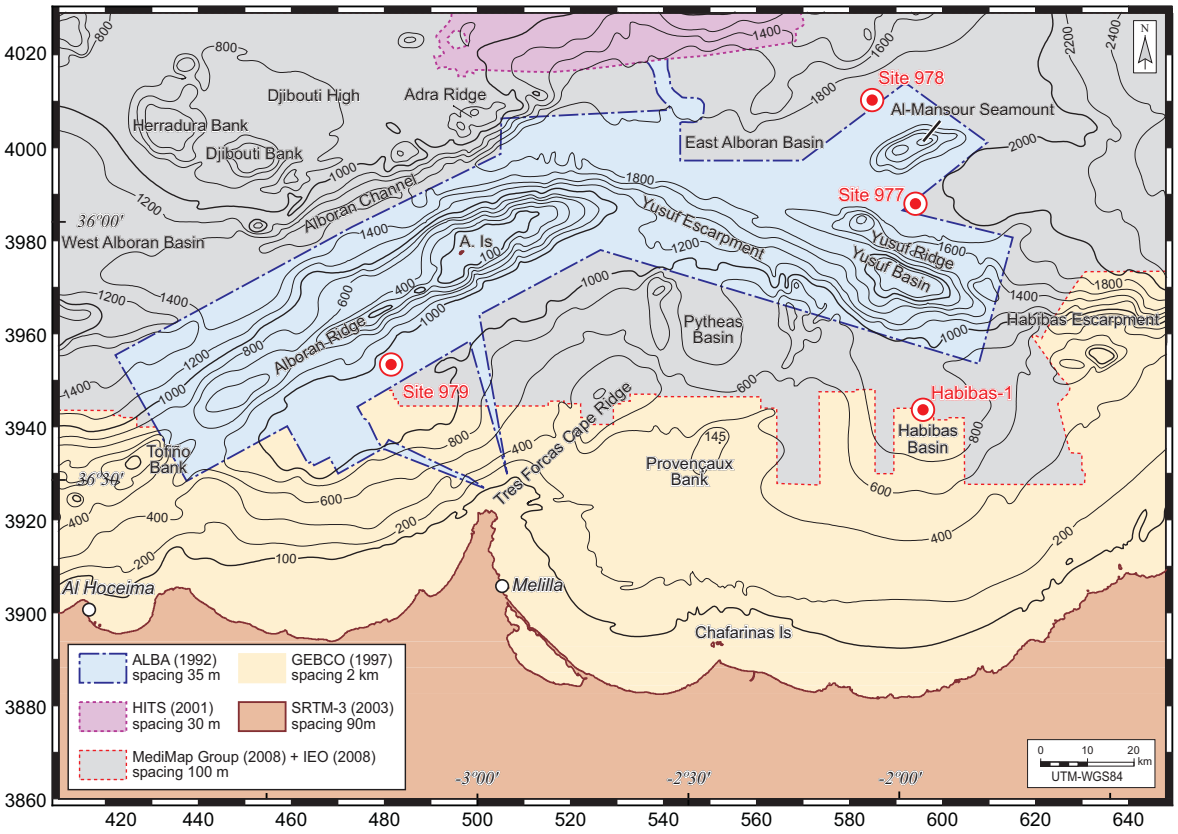

Figure 2-2. Location of the swath-bathymetry mosaics and topographic data used in this study. Data resolution is also indicated. Bathymetry contours (GEBCO-97, IOC-IHO) are in metres, contour interval 200 m. ODP Leg 161 sites and Habibas-1 well are also included. UTM projection, units in kilometres (WGS 84 ellipsoid). A. Is Alboran Island.

2.2 Sub-bottom parametric profiles

High resolution parametric profiles (TOPAS) were acquired simultaneously with bathymetric data during the ALBA, TECALB and MARSIBAL I-06 cruises. The total length of TOPAS profiles analyzed for this study is 3738 km (Figure 2-3). The TOPAS (TOpographic PA-rametric Sonar) is a low frequency (0.5-6 kHz) sub-bottom profiling system that supplies a detailed section of the shallower materials. The TOPAS system is an echosound based on the reflexion of sound waves, similarly to the swath-bathymetry system. In contrast, due to its lower frequency, the sound pulse of the TOPAS profiler penetrates some metres below the seafloor into the substratum and experiences

wave refractions along the boundaries between layers with different density before being finally reflected. The available equipment onboard the BIO Hespérides corresponds with the Simrad TOPAS PS-18 model and it was also mounted in the hull. Its main technical features are shown in table 2-1.

The penetration and resolution of TOPAS profiles depends essentially on seafloor depth, slope and sediment features. The best results are acquired from soft substratums in flat areas located at

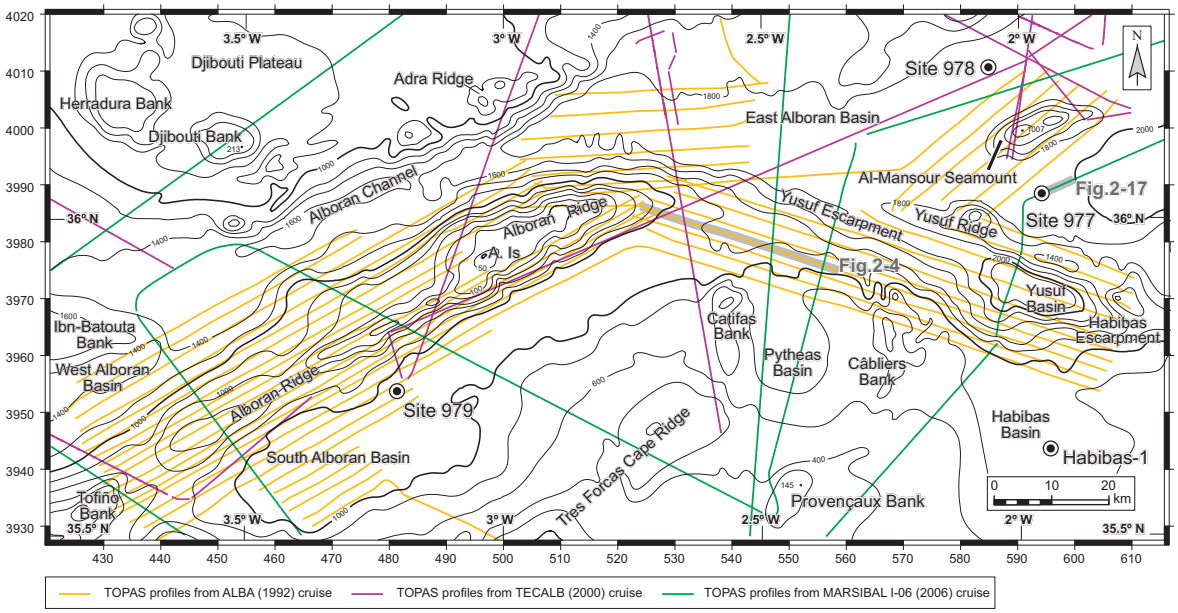

Figure 2-3. Location of TOPAS profiles from the ALBA, TECALB and MARSIBAL I-06 cruises used in this study. Bathymetry contours (GEBCO-97, IOC-IHO) are in metres, contour interval 200 m. Thick grey lines are TOPAS profiles presented in this chapter. Circles with numbers are ODP Leg 161 sites and the commercial Habibas-1 well. UTM projection, units in kilometres (WGS 84 ellipsoid). A. Is Alboran Island.

Technical specifications of the TOPAS PS-18 model	
Electrical output power	~ 32 kW
Primary source level	>204 dB//µPa@1m
Primary operating frequency	16-22 kHz
Primary beam width	~3.5º
Secondary frequency	0.5 – 6.0 kHz
Secondary beam width	~ 5º
Optional scanning sector	80º
Operational water depth	30 – 10,000 m
Penetration capability	>100 m
Resolution	< 0.3 m

Table 2-1. Technical specifications of the TOPAS PS-18 equipment onboard the BIO Hespérides.

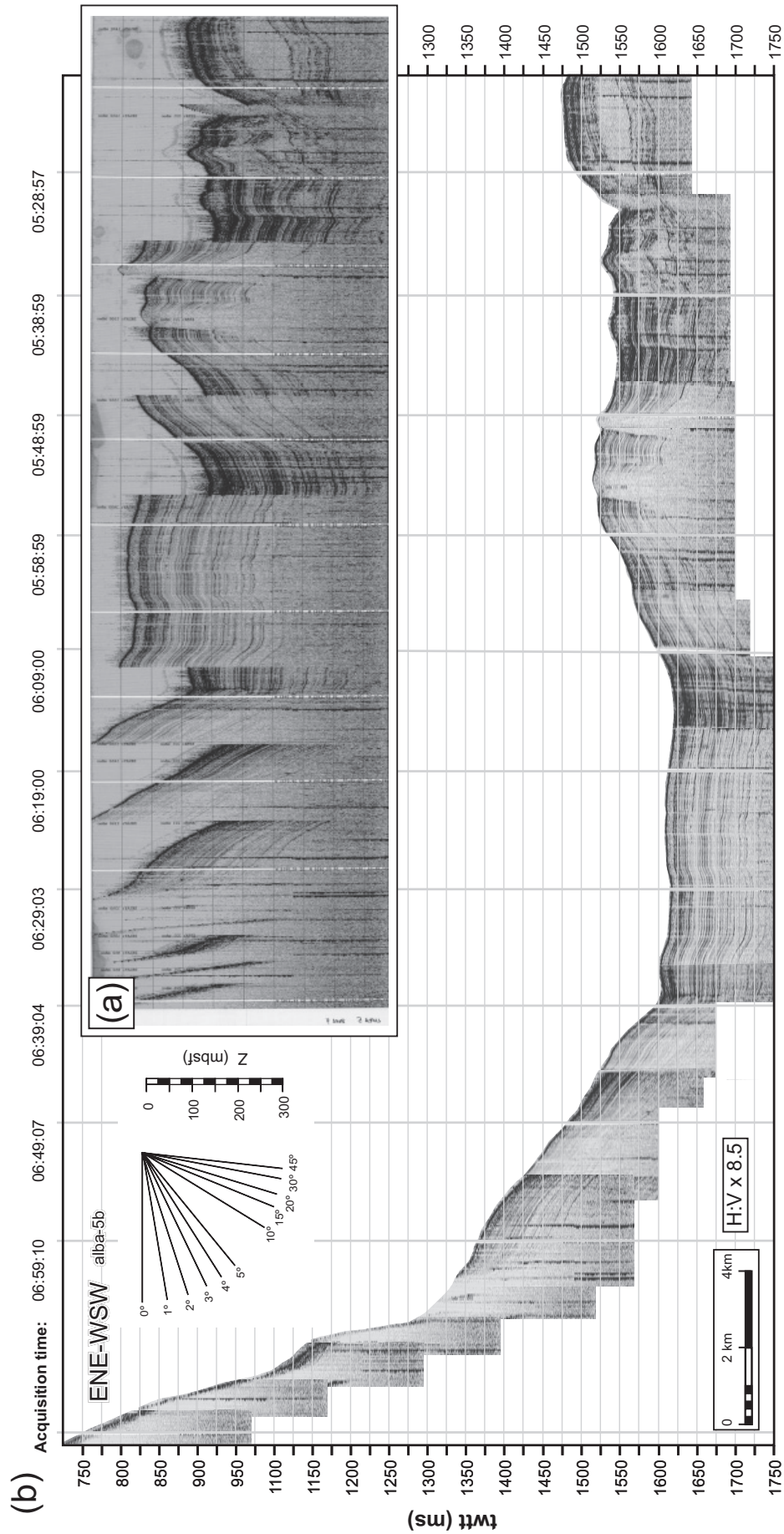

Figure 2-4. Example of water delay corrections of an analogue record of TOPAS profile from the Yusuf escarpment. **(a)** Original record comprising water delays. **(b)** Corrected TOPAS profile together with estimated depth scale and calculated dip abacus. Location is shown in figure 2-3.

intermediate depths. For example, the maximum penetration (up to 170 m) and best resolution (< 30 cm) is obtained for sediments in areas with very low slope and approximately 1000 m of water depth. A recording window of 300 or 400 ms was adopted during the surveys. Due to the variable water depths encountered in the study area, from less than 50 m to more than 2300 m, water delays were introduced to the data at the recording stage which delayed the start of the recording by a whole number of seconds. These delays are implemented to minimise the amount of redundant data collected from the water column and thus allow us to focus the record on the sub-bottom substratum reducing the final size of the recorded files. TOPAS data were processed using TOPAS® software, which allows to filter the original signal eliminating wave interferences and improving penetration and resolution of the profiles. The most recent TOPAS data from the MARSIBAL I-06 cruise were acquired in digital *"raw"* format and therefore it was possible to re-process data after the cruise and convert them to the to the standard *"segy"* format, which allows to correct water delays automatically. Nevertheless, most of TOPAS data come from antique cruises (years 1992 and 2000; Figure 2-3) and these profiles were only available in analogue records. In such cases, TOPAS profiles were scanned and all the delays were corrected manually before interpretation. Figure 2-4 is an example that shows a selected TOPAS analogue record before and after water delay corrections.

2.3 Seismic reflection profiles

2D seismic reflection data forming an irregular network of 110 profiles with a total length of 6598 km were compiled and interpreted for this study (Figure 2-5). The majority of these data, approximately 5100 km, correspond to profiles acquired in academic cruises conducted between 1970 and 2006. These cruises were: GEOMEDE in 1970, CONRAD in 1988, GC-90 in 1990, DARWIN CD 64 in 1991 and 1992, ESCIALB in 1992, ODP Leg 161 in 1995, TECALB in 2000, TTR-12 in 2002, TTR-14 in 2004 and MARSIBAL-I 06 in 2006. In addition, 1700 km of seismic data were acquired during oil and gas exploration programs since the early 1970's and constitute the RAY (1972), SH (1974), Shell-750 (1975), AS (1977), BRPM (1979) and MAP (1979) series.

Acquisition and processing techniques were similar for all the compiled data, but different equipment configurations, parameters and software were used in each cruise. Due to the high variability of sources of seismic data, this section summarizes the standard methods used to acquire and process such profiles and some technical specifications are only shown for the most recent data.

The seismic survey system comprises three main components: source of energy, reception system and acquisition-visualization of data (Figure 2-6). The depth of penetration and vertical resolution of a seismic experiment depends on the overall energy of the airgun array and the dominant frequency of the source wave. In this sense, two main categories of 2D seismic data can be distinguished: (1) single channel seismic profiles with high resolution and low penetration; and (2) multichannel seismic profiles with high penetration and low resolution.

Seismic acquisition

The seismic reflection technique is based on the physical principle of reflection of waves along a surface (interface) that bounds two materials with different properties (Figure 2-7). A special type

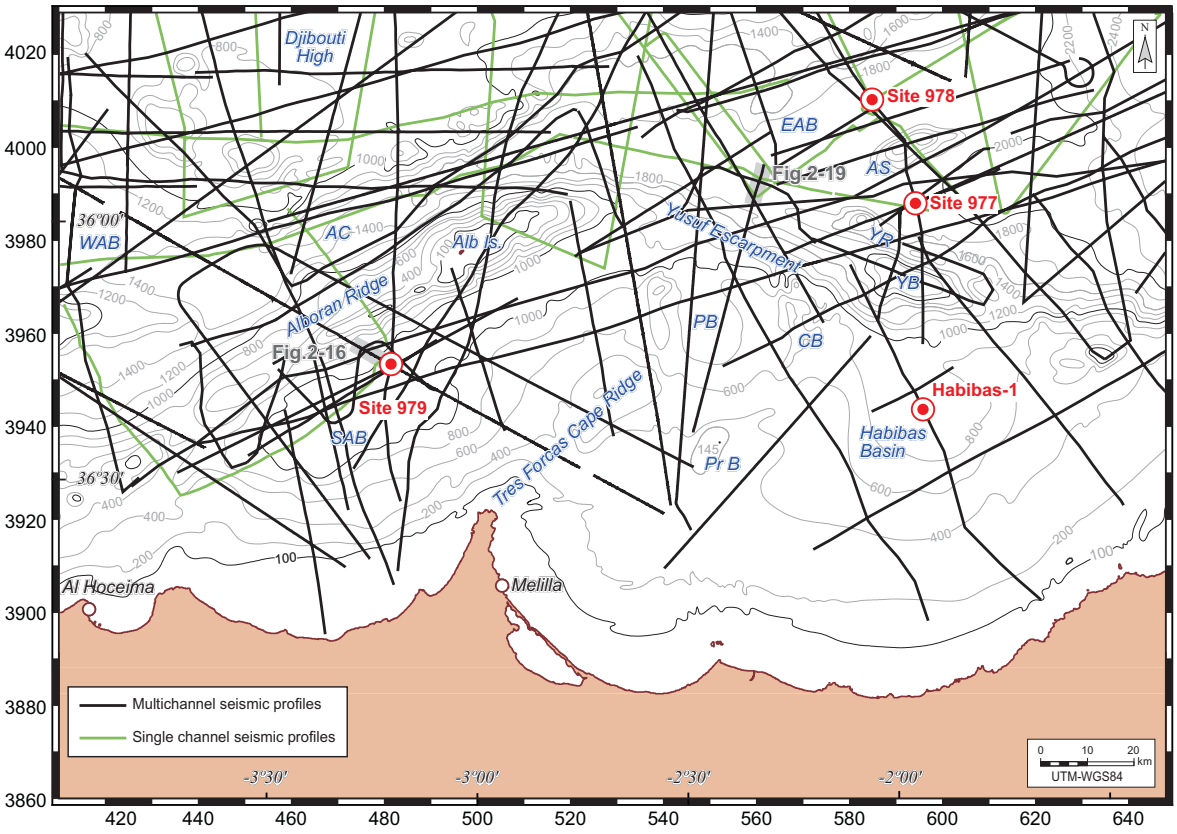

Figure 2-5. Location map of seismic profiles used in the study including data from commercial surveys (RAY, 1972; SH, 1974; Shell-750, 1975; AS, 1977; BRPM, 1979 and MAP, 1979) and scientific cruises (GEOMEDE, 1970; CONRAD, 1988; GC-90, 1990; DARWIN CD 64, 1991-1992; ESCIALB, 1992; ODP Leg 161, 1995; TECALB, 2000; TTR-12, 2002; TTR-14, 2004 and MARSIBAL-I 06, 2006). Thick grey line indicates multichannel seismic profile presented in this chapter. Location of ODP sites 977, 978, 979 and Habibas-1 well are shown as red circles. Bathymetry contours (GEBCO-97, IOC-IHO) are in metres, contour interval 200 m. Abbreviations: Alb Is, Alboran Island; AC, Alboran Channel; AS, Al-Mansour Seamount; CB, Câbliers Bank; EAB, East Alboran Basin; PB, Pytheas Basin; Pr B, Provençaux Bank; SAB, South Alboran Basin; YB, Yusuf Basin; YR, Yusuf Ridge and WAB, West Alboran Basin.

of internal waves, which propagates by compression and dilatation of material are used in these experiments and they correspond to *"compressional waves"*, also known as *"primary waves"* or *"P waves"*. During a seismic reflection experiment, the emission of P waves is controlled as they are artificially generated by an airgun source (Figure 2-6c).

Seismic energy travels along trajectories perpendicular to wave fronts, known as raypaths. A wave front is a surface along which portions of a propagating wave are in phase. Variations in the velocity of propagation of waves cause wave fronts to derivate from perfect spheres bending or "refracting" the raypaths and also may cause wave reflections (Figure 2-8).

Reflections occur when there are changes in the velocities of propagations of P waves and/or density. When seismic energy travelling in one layer encounters a layer with different acoustic impedance (product of density and velocity; ρ x V), some of the energy is reflected back into the first layer (Figure 2-7). Snell´s Law illustrates that the angle of reflection (θ_2) is exactly the same as the angle of incidence (θ_1), because both rays travel at the same velocity (V_1):

Figure 2-6. Examples of main components of the equipment used for acquisition of multichannel seismic data. **(a)** Scheme illustrating a marine seismic surrey with towed equipment. **(b)** BIO Hespérides. **(c)** Detail of airguns (source of energy). **(d)** String of airguns. **(e)** Compressor. **(f)** Buoyant analogue streamer. **(g)** Data visualization and record.

$$\frac{\sin\theta_1}{V_1} = \frac{\sin\theta_2}{V_1} \qquad [1]$$

where θ_1 is the angle of incidence; θ_2 is the angle of refraction; and V_1 is the seismic velocity of the upper layer.

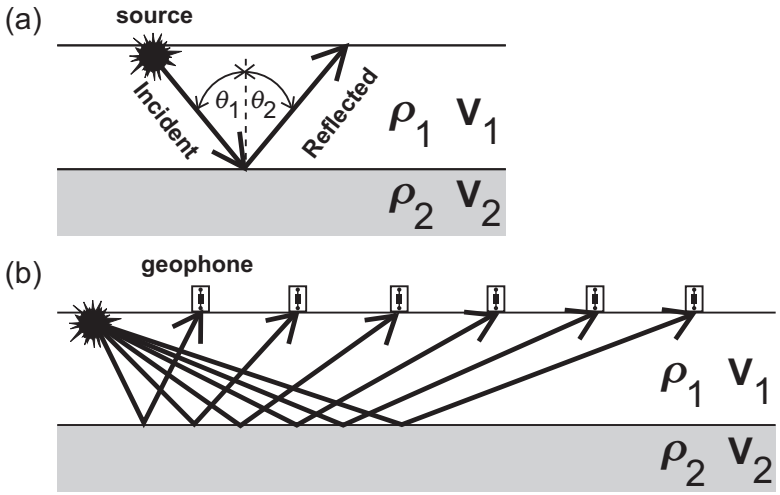

Figure 2-7. (a) A compressional wave is reflected back at an angle equal to the incident angle (θ_2) equal to the incident angle (θ_1). The densities and compressional wave velocities of the two layers are represented by ρ_1, V_1 and ρ_2, V_2. Reflection occurs when the acoustic impedance of the lower layer (ρ_2 x V_2) differs from that of the upper layer (ρ_1 x V_1). **(b)** V-shaped raypaths for a compressional wave from a source to six receivers, reflected from a horizontal interface.

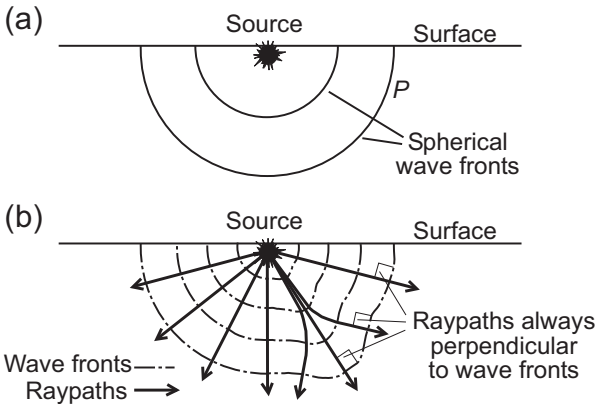

Figure 2-8. (a) Initial wave fronts for compressional waves (P). **(b)** Wave fronts for propagating P-wave. Changes in velocity cause segments of wave fronts to speed up or slow down, distorting the wave fronts from perfect spheres. Raypaths thus bend (refract) as velocity changes.

Seismic reflection data are normally recorded with several receivers offset from the source. In marine surveys, the receivers are mounted along a neutrally buoyant streamer that is towed by the ship behind the airgun source (Figure 2-6a). The optimum depth of receiver deployment is 10 – 20 m below sea level (*e.g.* Sheriff and Geldart, 1995). The receivers consist of series of hydrophones which are piezo-electric transducters that generate a voltage when pressure is applied by vibrating water particles from propagating P waves. The signals are sent by these sensors to the ship by optical fibre or cables and they are them digitized by specific software and recorded onto magnetic tapes.

A *seismic trace* is the recording of the motion of particles of rock and water particles by a receiver, plotted as a function of time. A seismic wave takes a certain amount of time to travel from the source to a receiver, depending on the distance to the receiver, the path taken by the wave, and the wave's velocity. Arrival of each wave stars as initial movement of the particles, followed by reverberations that die out with time (Figure 2-9).

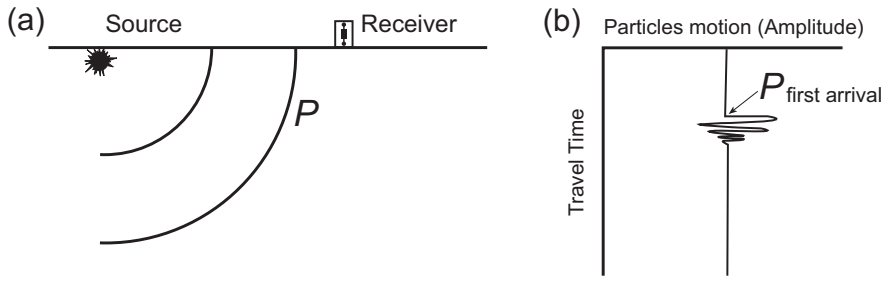

Figure 2-9. (a) Seismic waves radiating from a source to one receiver. **(b)** Seismic trace recording ground motion by the receiver, as a function of the travel time from the source to the receiver. Travel time is commonly plotted positive downward.

In order to present the seismic data in an interpretable format, acquisition and processing procedures are designed to attenuate unwanted signals and noise and to condensate the records of many shots consisting on a large number of seismic traces. A seismic reflection survey is commonly conducted in the *common midpoint* mode (*CMP*), whereby seismic traces from different shots have a common point to the surface, midway between source and receiver pairs (Figure 2-10). The CMP method provides redundant information that enhances signal-to-noise ratio and facilitates de determination of seismic velocities used in processing and interpretation.

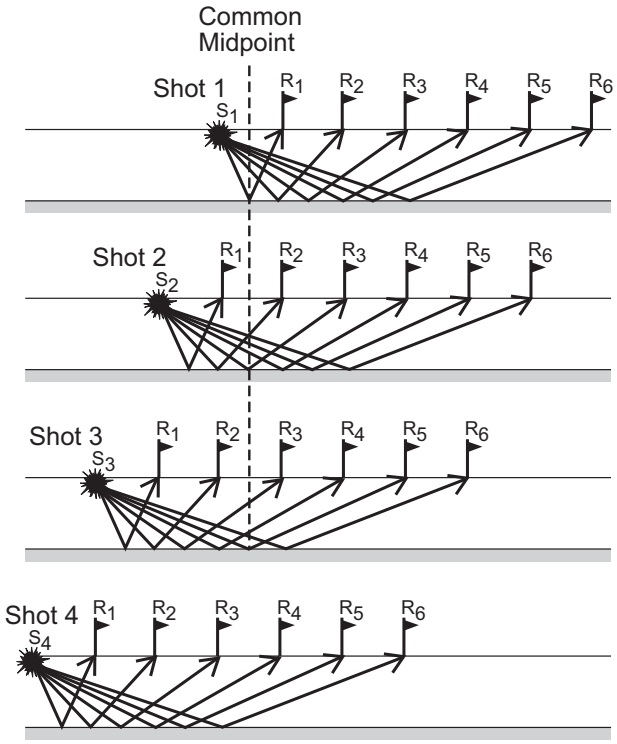

Figure 2-10. Explicative diagram of the Common midpoint method (CMP) considering a simple seismic reflection survey with four shots (S_1 to S_4) and a group of six receivers (R_1 to R_6), which are displaced in steps of one interval toward the left.

In the example of figure 2-19 one source shots and the reflected P waves are recorded by a group of six receivers. During the first shot, the source and receivers are toward the right. As the survey progresses, the source and receiver positions are displaced in steps of one interval toward the left. The location of the midpoint between the source (S_1) and the first receiver (R_1) during the first shot coincides with the midpoints for S_2/R_3 for shot 2 and also with S_3/R_5 for shot 3. Likewise, there are common midpoints for other combinations: (S_1/R_2, S_2/R_4, S_3/R_6); (S_2/R_1, S_3/R_3, S_4/R_5); and (S_2/R_2, S_3/R_4, S_4/R_6).

The record of all the seismic traces resulting from the same shot and recorded by different receivers is known as *shot gather*. For the shots illustrated in figure 2-10 each shot gather is composed by six seismic traces (Figure 2-11a). A display of traces corresponding to reflections around a common midpoint, plotted side-by-side according to horizontal distance (X) form each source is known as a *CMP gather* (Figure 2-11b). A reflection from a horizontal interface, overlain by constant velocity, appears as a hyperbola on both the shot and CMP gathers. Before all the seismic traces (three, in this example) on the CMP gather are added together ("stacked"), the event must be corrected from differences in travel time according to the hyperbola. The differences in travel time are called *normal moveout (NMO)*. The travel time for a reflection from a horizontal interface is:

$$T_f = \sqrt{t_0^2 + \frac{X^2}{V_1^2}} \qquad [2]$$

where T_f is the travel time from source, to interface, to receiver; X is the horizontal distance from source to receiver, V_1 is the seismic velocity of the layer above interface and t_0 is the time (T)-axis intercept. t_0 varies depending on the thickness; and seismic velocity of the layer above the interface (h and V_1):

$$t_0 = \frac{2h}{V_1} \qquad [3]$$

The normal moveout (T_{NMO}; Figure 2-11b) is the difference between the travel time along the hyperbola (T_f) and the intercept time (t_0):

$$T_{NMO} = T_f - t_0 \qquad [4]$$

A single trace on a seismic section is a composite of the traces from a CMP gather, corrected for T_{NMO}, then added together as a stacked trace (Figure 2-11c). The *fold of stack* is the number of traces from the CMP gather comprising a stacked trace. A resulting profile, comprising numerous stacked CMP traces, is a *stacked seismic section*. The data are plotted with the time axis downward, mimicking depth within the Earth as profiles resembling geologic sections.

Table 2-2 shows some examples of technical specifications of seismic reflection equipments available onboard the R/V Robert D. Conrad, RSS Charles Darwin and BIO Hespérides, which were used for the acquisition of most of the academic profiles during the Conrad C2911, Darwin CD 64, Tecalb and Marsibal I-06 cruises in 1988, 1991-1992, 2000 and 2006 respectively.

Seismic processing

Seismic reflection data are subjected to various processing steps to enhance reflected signals,

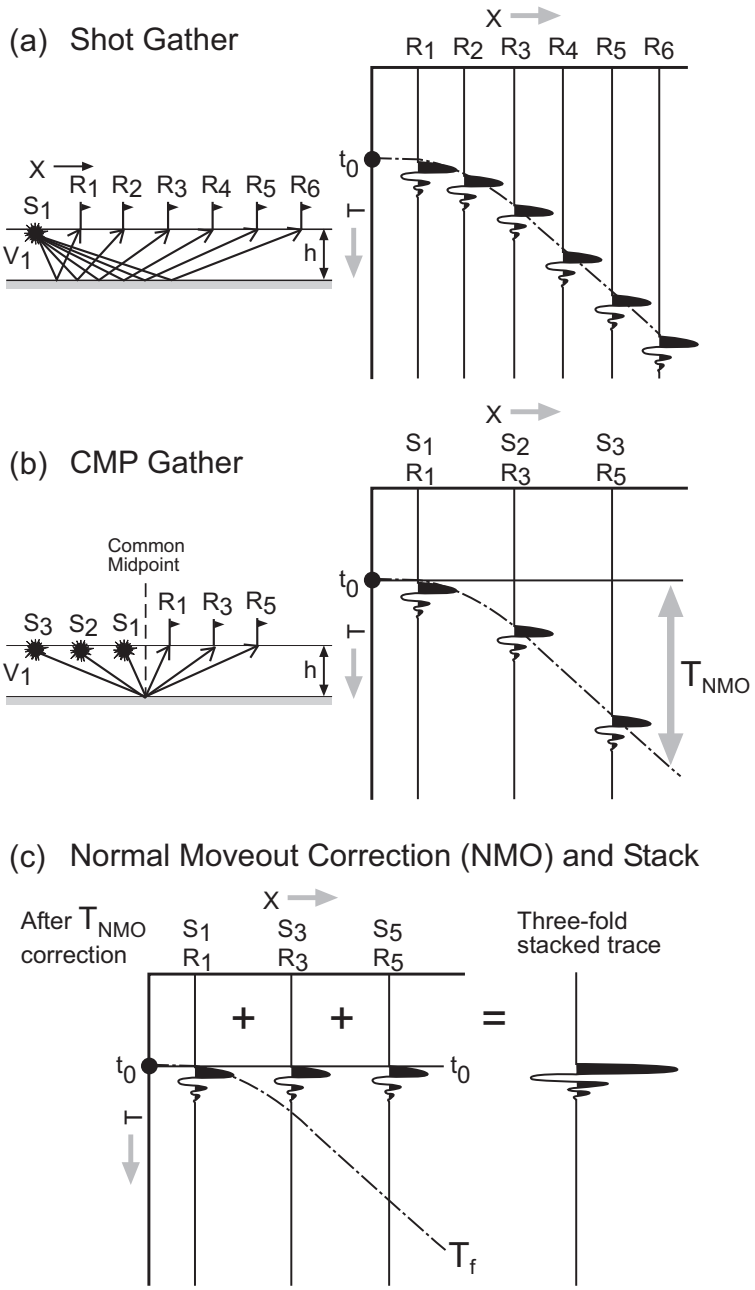

Figure 2-11. Ray path diagrams and travel-time graphs for shot and CMP gathers. **(a)** Left: raypaths for one shot with six receiver positions. Right: example of a shot gather, which results from plotting travel-times of the resulting seismic traces (T) according to horizontal distance from the source (X). **(b)** Left: example of raypaths centred on a common midpoint. Right: Common midpoint (CMP) gather. **(c)** Left: CMP gather after normal moveout (T_{NMO}) corrections. Right: Stacked trace resulting after T_{NMO} corrections. By means of the T_{NMO} corrections, peaks and troughs of different seismic traces align so that they constructively interfere when all the traces are added together.

to attenuate noise, and to present the data in a more interpretable format. In most cases, signals to be enhanced are primary reflections whilst other multiple reflections must be removed or attenuated (Figure 2-12). A *primary reflection* results from energy that undergoes only one reflection before returning to the surface (Figure 2-12a). In other cases energy reflected more than once and it forms a *multiple reflection* or *multiple* (Figure 2-12b). Multiples must be attenuated during processing so that

primary reflections are highlighted.

The general processing sequence comprises several steps that are summarized below. An

	R/V R. Conrad	RSS C. Darwin	BIO Hespérides
Average ship Speedy (knots)	~ 6	~ 6	~ 6
Airguns			
Total airgun capacity (l)	95.5	16.8	49
Number of compressors	1	1	4
Towing depth of airguns (m)	10 – 20	33	10
Shot interval (s)	30	16 (50 m)	20 – 30 (50 m)
Sample interval (ms)	2 – 4	2	2 – 4
Streamer			
Total streamer length (m)	2400	200	2800
Total number of channels	96	4	96
Number of active sections	96	4	24
Spacing interval between active sections (m)	25	50	100
Towing distance between ship and streamer (m)	315	160	167.5
Maximum penetration (s)	6 – 7	4 – 5	6 – 7

Table 2-2. Technical specifications of seismic reflection systems used during the Conrad cruise C2911 (1988, R/V Robert D. Conrad), Darwin cruise CD 64 (1991-1992, RSS Charles Darwin), Tecalb cruise (2000, BIO Hespérides) and Marsibal I-06 cruise (2006, BIO Hespérides).

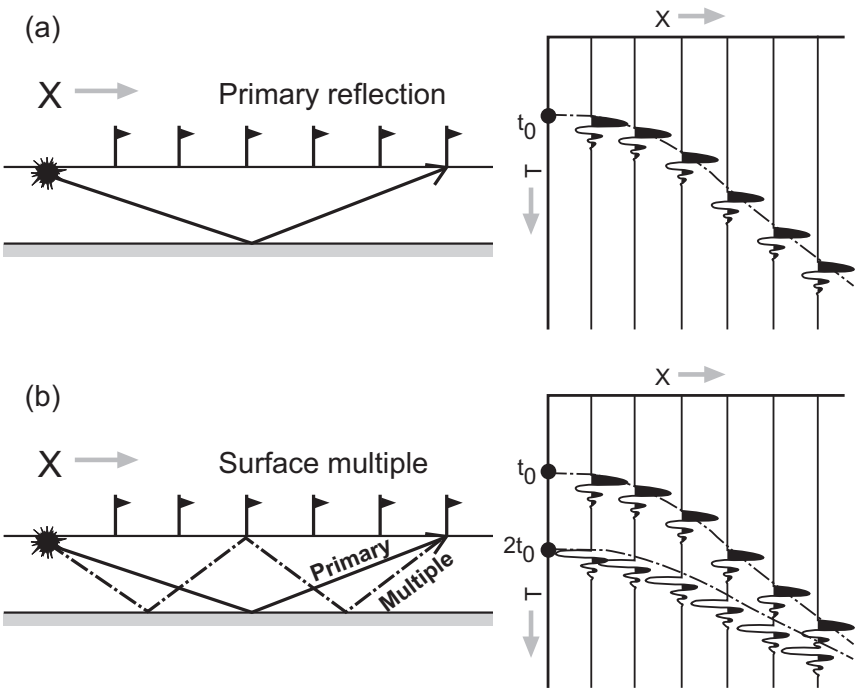

Figure 2-12. (a) Raypath and shot point gather for a primary reflection. **(b)** Comparison of primary reflection and surface multiple on raypath diagram and shot point gather.

extensive and detailed treatment of processing can be found in the bibliography (*e.g.* Yilmaz, 1987; Sheriff and Geldart, 1995).

1. *Frequency filtering* keeps only a selected band of frequencies, deleting those frequencies that are outside of the range of the input seismic signal. This step improves signal-to-noise ratio and may be done repeatedly at other stages of the processing sequence.

2. *Automatic Gain Control (AGC)*. Reflections from depth have amplitudes several orders of magnitude less than shallow reflections. This step balances amplitudes along the length of a seismic trace, generally amplifying the trace as time increases.

3. *Gather*. In this step traces from different shot gathers are rearranged as common midpoint (CMP) gathers.

4. *Velocity Analysis*. As explained above, before all the traces with a common midpoint are added together, all the seismic events in different traces must be corrected from differences in travel time according with equations [2] to [4]. The velocity analysis determines velocities that best fit primary reflections when the traces are stacked.

5. *Normal Moveout Correction* (T_{NMO}) consists on the correction of the seismic events according to the hyperbola (Figure 2-10; equations [2] to [4]).

6. *Mute.* At a distance from the source, the tops of records commonly have noise that correspond with other seismic waves generated by the airgun source (*direct P* and *S waves*) or events distorted by T_{NMO} corrections. The traces of this noise are set to zero amplitude, or muted.

7. *Deconvolution* attempts to remove the reverberations or multiples. Another post-stack deconvolution can be applied.

8. *Stack.* CMP traces are added together and displayed side-by-side to make an unmigrated time section. The display mimics the situation that would result if each seismic trace were recorded at a common source/receiver position.

9. *Migration.* The relative positions of events are distorted on time section because of vertical and lateral changes of velocity. A migrated time section attempts to move events to their true horizontal positions relative to common source/receiver positions on the surface.

Digitalization and georeferencing

Most of the seismic profiles compiled for this study were available in analogue records and only the most recent seismic surveys were in digital format. Wherefore 4200 km of profiles corresponding with the older data were digitized and transformed to the standard segy format using Lynx® software.

For each seismic profile, all the traces were reconstructed from the pixels of scanned raster images using the most appropriate vectorising method or algorithm (*e.g.* Figure 2-13). The input data were bi-level (black and white) raster of stacked and migrated seismic sections portrayed as wiggle-traces. Different vectorising algorithms and digitizing parameters have been used to suite the variable quality

of seismic images and different records comprising raster files and paper and film sections that were scanned. The resolution of the input raster maintained a minimum of 8 pixels per trace spacing. In most cases, the *VAI* (Variable Area Integration) algorithm provided the best output digitalized files. The *VAWG* (Variable Area with Wiggle) algorithm could only be used on good quality images. Very poor quality data plotted with greyscale were vectorised using the *VDR* (Variable Density Reconstruction) algorithm. Different parameters, as for example the start and end time of the seismic profiles, total number of traces, number of shoot points per trace and line thickness, are required to define the searching thresholds for the vectorizing algorithm along each seismic trace.

Calibration of raster images was performed in order to restore possible deformations caused by

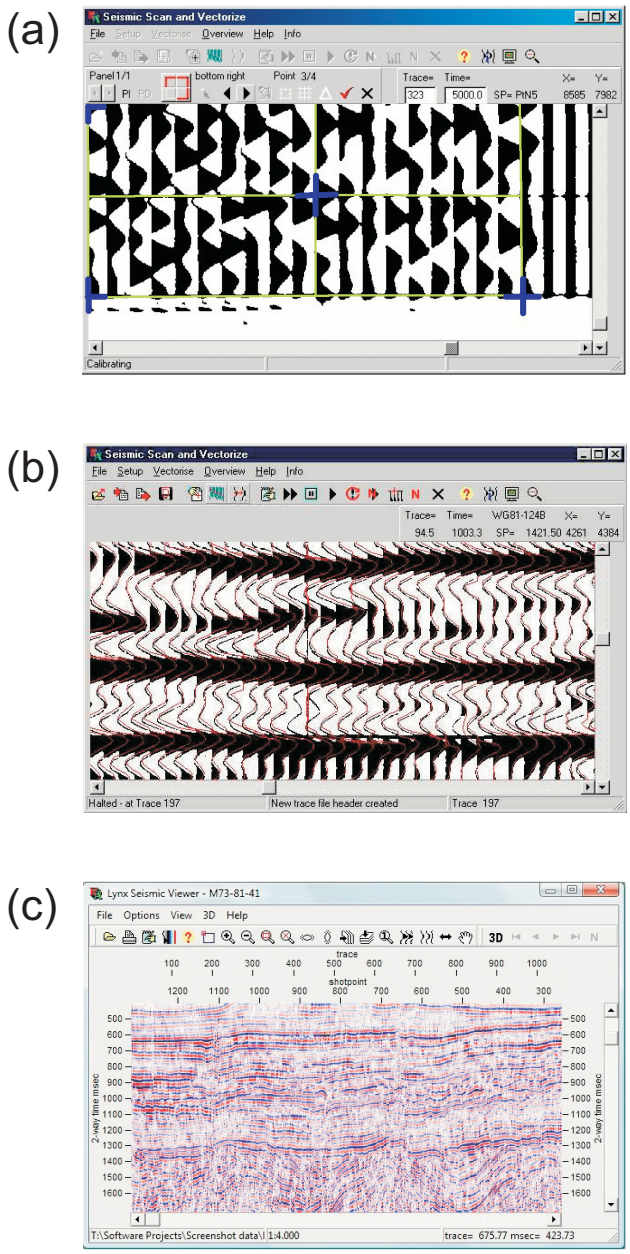

Figure 2-13. Main steps of digitalization of a scanned seismic profile using the Lynx® software. **(a)** Example of calibration. **(b)** Vectorizing of seismic traces. **(c)** Exportation of digitized seismic traces into segy files and portrayal with a colour mapped wiggle scale.

stretch of the original paper records, creases, optical distortions due to copying or small slippage through the scanner rollers. Calibration sets up the relationship between points on the raster image, as measured in pixels and the corresponding points in the rectangular trace and time coordinate system. A minimum of 200 points of calibration were entered for each seismic profile and they were used to create a network of calibrating triangles. Figure 2-13a shows a detail of an example of calibration of a scanned seismic profile. Blue crosses are the entered points of calibration and green lines indicate the resulting coordinate system, which is considered for further digitalization. Notice the good fitting between the calibrating system and the original trace and time coordinate system in the seismic profile. Digital traces were obtained after calibration and digitalization (Figure 2-13b) and they were exported into segy files and portrayed with a colour mapped wiggle scale (Figure 2-13c).

Afterwards, all the seismic profiles were integrated on a georeferenced dataset using SMT Kingdom Suite® software. Digital records of navigation were available for the most recent cruises (since year 2000). In such cases, locations of seismic profiles were directly determined from these files. Nevertheless positioning of most of the seismic surveys was only available in analogue records. Similarly to seismic profiles, positioning maps were scanned, vectorized and converted to digital format. The position of shot points were calculated using the ESRI ArcGIS® software and they were linked to the corresponding seismic traces of the digitalized segy files.

2.4 Wells

Well records provided valuable geophysical, lithological and chronostratigraphic data. They complemented the information supplied by TOPAS and seismic profiles allowing to tie seismic interpretation with precise age determinations and to correlate seismic facies with litho-facies. A total number of ten wells have been analyzed for this thesis (Figure 2-14). Andalucía-G1, Andalucía-A1, Alboran-A1, El-Jebha and Habibas-1 are commercial wells drilled during oil and gas exploration programs since the early 1970's (*e.g.* Jurado and Comas, 1992; Chalouan *et al*., 1997; Cope *et al.*, 2003; Mauffret *et al.,* 2007). DSDP Site 121 is a scientific well drilled by the *Deep Sea Drilling Project* (DSDP) during Leg 13 (Ryan *et al.*, 1973). The most recent wells are ODP Sites 976 to 979 and they were drilled during the scientific Leg 161 of the *Ocean Drilling Program* (ODP) (Comas *et al.*, 1996, 1999).

Biostratigraphic information

Precise age determinations obtained for sediments acquired during DSDP Leg 13 and ODP Leg 16 range from middle or late Miocene to Quaternary. A chronostratigraphic framework was established according to the calcareous nannofossils zonation proposed by Martini (1971) and later modified by Young (1991), which was adapted and applied for the western Mediterranean by Siesser and de Kaenel (1999) (Table 2-3). Furthermore, some of the most recent ages were recalculated by correlation of sapropels interlayered in pelagic and hemipelagic Pleistocene sediments and calibration of these datums with the orbital time scale (de Kaenel *et al*., 1999). The abundance of recorded biostratigraphic events for the last ~5.33 Ma has allowed us to determine precisely the timing of Plio-Quaternary tectonic and sedimentary events recognized in this thesis. Nevertheless, the ages

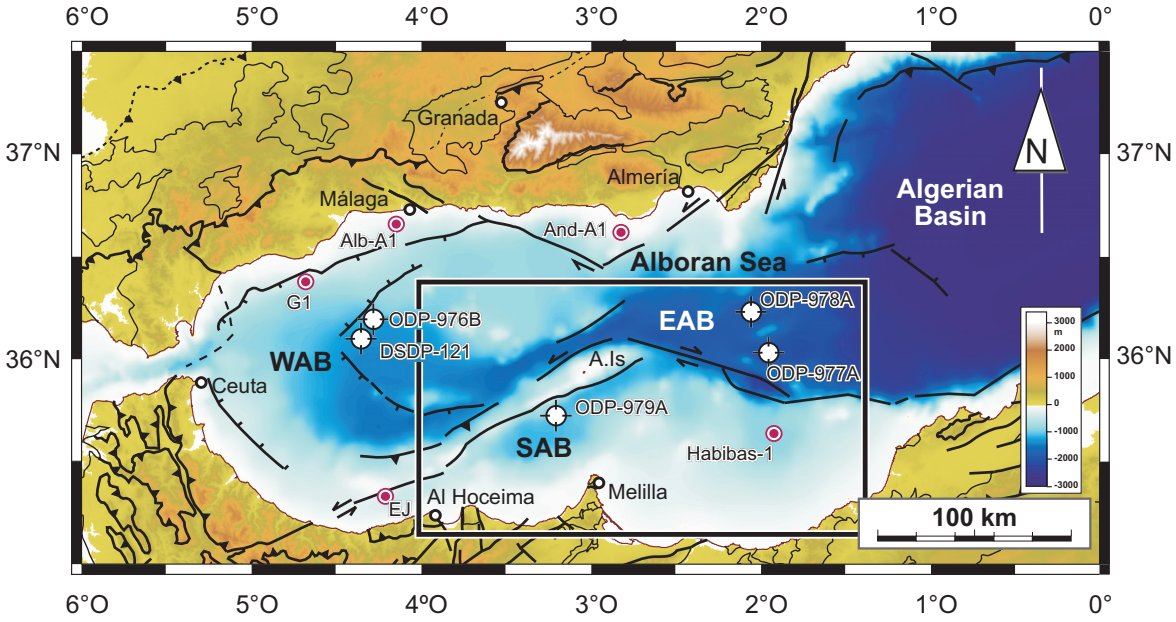

Figure 2-14. Location map of wells used in this study. Red circles are commercial wells and white circles with crosses represent scientific wells drilled by DSDP and ODP. Topography of the Gibraltar Arc and major tectonic features of the Alboran Sea (simplified from Comas *et al*. 1999) are also included. Digital topography extracted from the SRTM (USGS-NASA) global database, combined with GEBCO 97 (IOC-IHO) for the offshore region). Rectangle is the study area for this thesis. Abbreviations: A. Is, Alboran Island; Alb-A1, Alboran-A1; And-A1, Andalucía-A1; EAB, East Alboran Basin; EJ, El-Jebha; G1, Andalucía-G1; SAB, South Alboran Basin and WAB, West Alboran Basin.

of Miocene sediments in the Alboran Sea Basin are attributed from few biostratigraphic events mainly founded in commercial wells on the Spanish and Moroccan margins and they were difficult to correlate with the network of seismic profiles available for this study due to the presence of a large number of intra-basin highs (Figure 2-14). Within the study area, the whole Miocene sequence only has been penetrated at the Habibas-1 well, where the oldest sediments on top of metamorphic basement are Serravallian. ODP Site 978 only penetrated the top of the Miocene sequences ranging from mid to late Messinian ages. ODP Sites 977 and 979 did not drill any sediments below the M unconformity. Other additional age determinations for the top of the Miocene sequence come from DSDP Site 121 and ODP Site 976B, which penetrated Tortonian and Serravallian sediments on top of a structural high next to the study area (Figure 2-14). In summary, it should be noted that Miocene age attributions in this study were tentatively assigned and therefore it was difficult to establish a precise timing of Miocene events in contrast with the Plio-Quaternary evolution, which was more precisely determined.

Vp velocities and correlation between seismic and well data

Different ODP sites supplied log data and in-situ measurements of *Vp*, density and gamma ray that provided information about the physical properties of the sedimentary infill, in addition to biostratigraphic information used for age determinations. Correlation between well data and seismic profiles facilitates seismic interpretation. Thus, before interpreting, it was essential to essential to establish equivalence between the two-way travel time scale (twtt, in seconds) of seismic profiles

	Event	Age (Ma)
FO	*Emiliania huxleyi > Gephyrocapsa spp.*	0.085 [0.071]
FO	*Emiliania huxleyi*	0.26 [0.27]
LO	*Pseudoemiliania lacunosa*	0.46 [0.41]
LO	*Crenalithus asanoi (> 6,5 μm)*	0.93 [0.78]
FO	*Gephyrocapsa omega (> 4,0 μm)*	1.02 [0.96]
FO	*Crenalithus asanoi (> 6,5 μm)*	1.12
LO	*Gephyrocapsa spp. (> 6,5 μm)*	1.24
LO	*Helicosphaera sellii*	1.27
FO	*Gephyrocapsa spp.(> 5,5 μm)*	1.44 [1.61]
LO	*Calcidiscus macintyrei (> 1,1 μm)*	1.58 [1.62]
FO	*Gephyrocapsa oceanica (> 4,0 μm)*	1.75 [1.72]
LO	*Discoaster brouweri*	1.96
FO	*Globorotalia inflata*	2.13
LO	*Globorotalia bononiensis*	2.45
LO	*Discoaster pentaradiatus*	2.52
LO	*Discoaster surculus*	2.63
LO	*Discoaster tamalis*	2.78
LO	*Sphaeroidinellopsis spp.*	3.22
LO	*Globorotalia puncticulata*	3.57
LO	*Sphenolithus abies/neoabies*	3.66
LO	*Reticulofenestra psudoumbilicus (> 7 μm)*	3.82
LCO	*Globorotalia margaritae*	3.94
LCO	*Reticulofenestra pseudoumbilicus (> 7 μm)*	3.94
FCO	*Discoaster asymetricus*	4.13
FO	*Globrotalia puncticulata*	4.52
LO	*H. intermedia*	4.67
LcO	*H. intermedia*	5.07
FCO	*Globorotalia margaritae*	5.10
LO	*Reticulofenestra rotaria*	6.12
FO	*Reticulofenestra rotaria*	6.62
FRO	*Globorotalia conomiozea gr.*	7.11
LO	*Helicosphaera walbersdorfensis*	10.72
FO	*Calcidiscus macintyrei (> 11 μm)*	12.20

Table 2-3. Ages of main planktonic foraminifer and calcareous nannofossils events. FO: first occurrence, LO: last occurrence; FCO: first common occurrence; LCO: last common occurrence; FRO: first regular occurrence; LcO: last consistent occurrence. The first age estimations came from Shipboard Scientific Party (1996) and revised ages from de Kaenel *et al*. (1999) are in brackets.

and the depth scale (Z, in metres) of well records. The relationship between twtt and depth can be estimated considering the variation of *Vp* on depth as twtt and *Vp* are related as follows:

$$Vp = \frac{Z}{(twtt\ /\ 2)}\ ; \qquad twtt = \frac{2Z}{Vp} \qquad [5]$$

where *Vp* is the velocity of propagation of P waves expressed in m/s, Z is depth in metres below seafloor (m bsf) and *twtt* is the two-way travel time in seconds (s).

Therefore, it is important to know how *Vp* varies on depth. This relationship was established using both log and in-situ *Vp* measurements. For each of the wells with *Vp*-depth data, it is has been established the best-fitting function.

For ODP Site 977A, $Vp = 6 \cdot 10^{-9} \cdot Z^3 - 4 \cdot 10^{-6} \cdot Z^2 + 0.001 \cdot Z + 1.4958$ [6]

For ODP Site 978A, $Vp = 3 \cdot 10^{-8} \cdot Z^3 - 3 \cdot 10^{-5} \cdot Z^2 + 0.0104 \cdot Z + 0.4117$ [7]

For ODP Site 979A,

$$Vp = 7.07 \cdot 10^{-9} \cdot Z^4 + 1.558 \cdot 10^{-6} \cdot Z^3 - 1.3082 \cdot 10^{-3} \cdot Z^2 + 0.297 \cdot Z + 1519.7 \qquad [8]$$

For ODP Site 976B, there are two equations:

when Z is between 0 and 331 m bsf, $Vp = 1.5323 \cdot e^{0.0005 \cdot Z}$ [9]

and when Z is between 531 and 611 m bsf,

$$Vp = -2 \cdot 10^{-7} \cdot Z^6 + 6 \cdot 10^{-4} \cdot Z^5 - 0.856 \cdot Z^4 + 684.58 \cdot Z^3 - 307945 \cdot Z^2 + 7 \cdot 10^7 \cdot Z + 7 \cdot 10^9 \qquad [10]$$

Figure 2-15 shows plots of *Vp*-depth data for each well together with their best-fitting function and the corresponding coefficient of determination (R^2). It should be noted that there are not *Vp* data form some drilled segments, *i.e.* at Site 976B between 331 and 531 m, at the bottom of Site 977A between 532 and 599 m, at the top of Site 978A from 0 to 214 m and at the bottom of Site 979A from 434 to 581 m.

Using relationships [6] to [10] and substituting respectively in equation [5], the resultant equations for twtt-conversion in the different wells are:

for ODP Site 977A, $twtt = \frac{2Z}{6 \cdot 10^{-9} \cdot Z^3 - 4 \cdot 10^{-6} \cdot Z^2 + 0.001 \cdot Z + 1.4958}$ [11]

for ODP Site 978A, $twtt = \frac{2Z}{3 \cdot 10^{-8} \cdot Z^3 - 3 \cdot 10^{-5} \cdot Z^2 + 0.0104 \cdot Z + 0.4117}$ [12]

for ODP Site 979A,

$$twtt = \frac{2Z}{7.07 \cdot 10^{-9} \cdot Z^4 + 1.558 \cdot 10^{-6} \cdot Z^3 - 1.3082 \cdot 10^{-3} \cdot Z^2 + 0.297 \cdot Z + 1519.7} \qquad [13]$$

and for ODP Site 976B, there are two equations:

when Z is between 0 and 331 m bsf, $$twtt = \frac{2Z}{1.5323 \cdot e^{0.0005 \cdot Z}}$$ [14]

and when Z is between 531 and 611 m bsf,

$$twtt = \frac{2Z}{-2 \cdot 10^{-7} \cdot Z^6 + 6 \cdot 10^{-4} \cdot Z^5 - 0.856 \cdot Z^4 + 684.58 \cdot Z^3 - 307945 \cdot Z^2 + 7 \cdot 10^7 \cdot Z + 7 \cdot 10^9}$$ [15]

These equations allowed conversions of the vertical scale of well records from depth in metres to twtt and thus, it was possible to portray *Vp*, density, gamma ray and biostratigraphic data over seismic profiles. Different correlation panels were obtained, one for each well, and they were used for seismic interpretation. Figure 2-16 is an example of these correlation panels and shows correspondence between seismic line TALB-17 and well data from ODP Site 979A. All data are represented here with a twtt vertical scale in seconds (left bar). Additionally, the right bar indicates the equivalent vertical depth scale only for the well position. The change of the vertical scale of precise biostratigraphic data from depth to twtt has allowed us to establish precisely the age of the main unconformities recognized in seismic profiles. Log and in-situ data were available for the whole Plio-Quaternary sequence, which was completely penetrated at Sites 976, 977 and 978, and therefore it was possible to determine a precise chronostratigraphic framework for the last ~5.33 Ma. Three Quaternary and four Pliocene units and seven related unconformities have been identified and dated in this study. The central panels of figure 2-16 show Units Q1 to P2 and bounding key reflectors (named from top to bottom). In addition, the whole Plio-Quaternary seismic stratigraphy is widely described and illustrated with several seismic profiles in chapter 4.

Moreover, the higher resolution of TOPAS profiles allowed other more detailed correlations for the shallower sedimentary levels. Following the methodology explained above, well records for Sites 976 to 979 were portrayed with twtt vertical scales (in seconds) and directly correlated with TOPAS profiles across the wells. Thus, it was possible to estimate the approximate ages of some interpreted key reflectors in TOPAS profiles and correlate some of them with major regional unconformities recognized in seismic profiles. Figure 2-17 shows an example of these high resolution correlations between well data from ODP Site 977A and a selected segment of TOPAS profile in the East Alboran Basin. Panel c shows *Vp* logs and best fitting equation used for twtt conversions of well records. In addition, late Quaternary biostratigraphic markers recognized in this site (see table 2-2) are plotted in the central panel together with the calcareous nannofossils zonation proposed by Martini (1971).

These analyses allowed us to deduce that maximum penetration of TOPAS profiles of about 170 ms generally reaches sediments with less than ~1.15 Ma (*i.e.* middle to late Pleistocene). Therefore, TOPAS records correspond mainly with Units Q1 and the top of Unit Q2. From these correlations we conclude that deformations identified in TOPAS profiles are late Quaternary and therefore these profiles can be used to map potentially active structures (see chapter 3).

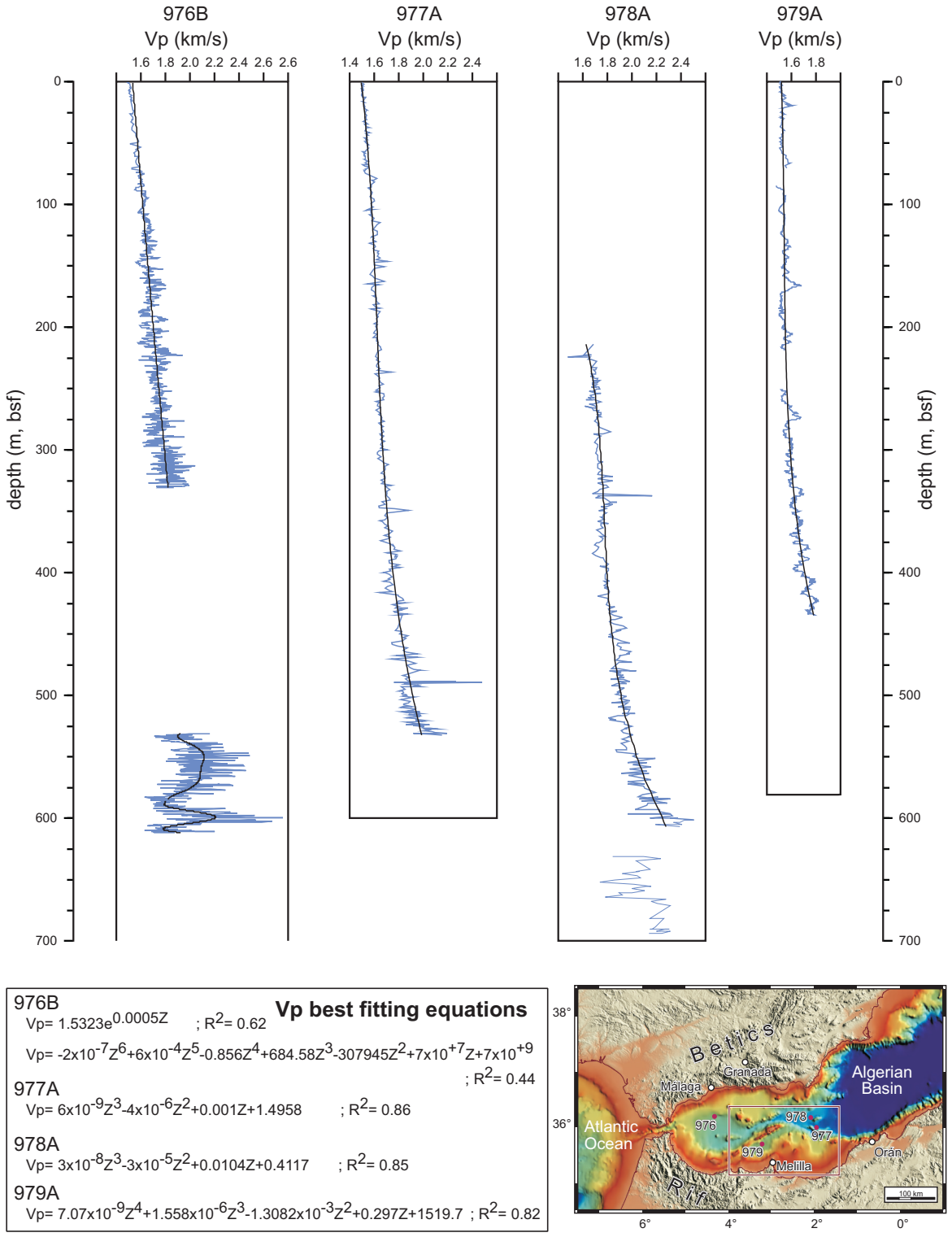

Figure 2-15. Vp log and in-situ data available for ODP Sites 976 to 979 together with their best-fitting function between *Vp* (in m/s) and depth (Z, in metres below seafloor (*m, bsf*)). The corresponding coefficient of determination (R^2) for each fitting is also shown. Inset map show well locations. Notice that there were not available Vp data from some of the drilled segments, *i.e.* at Site 976B between 331 and 531 m, at the bottom of Site 977A between 532 and 599 m, at the top of Site 978A from 0 to 214 m and at the bottom of Site 979A from 434 to 581 m.

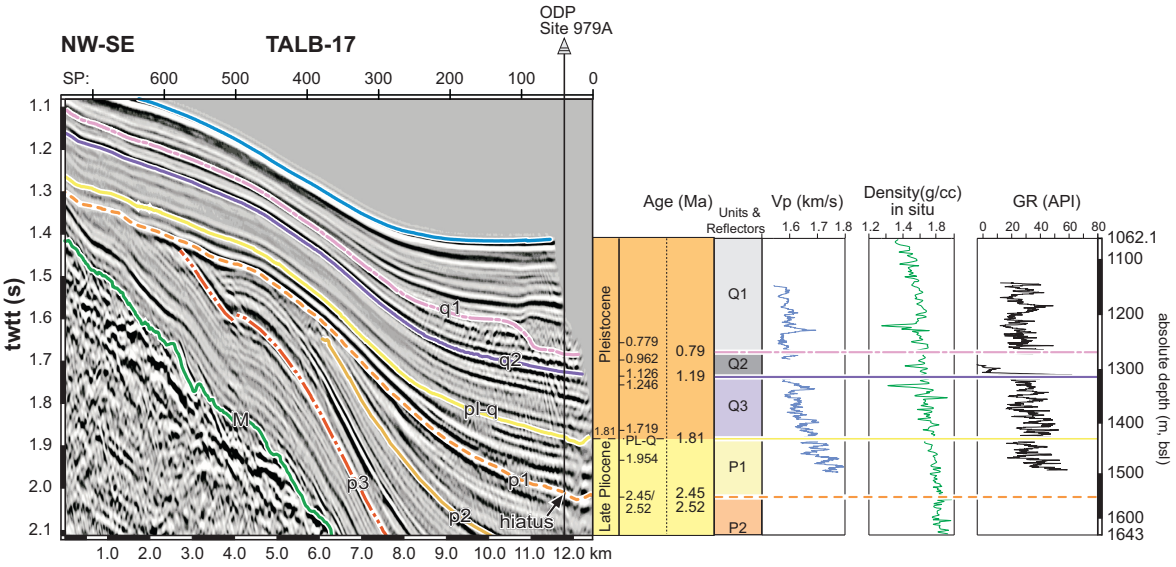

Figure 2-16. Correlation panel of seismic profile TALB-17 with log data and biostratigraphic information from ODP Site 979A in the southern slope of the Alboran Ridge. Locations in figures 2-5 and 2-18). Seismic units and key interpreted reflectors are also included showing their estimated age. twtt conversions of the vertical scale of log and biostratigraphic records have been performed using equation [13]. Abbreviations: GR, gamma ray; m bsl, metres below sea level.

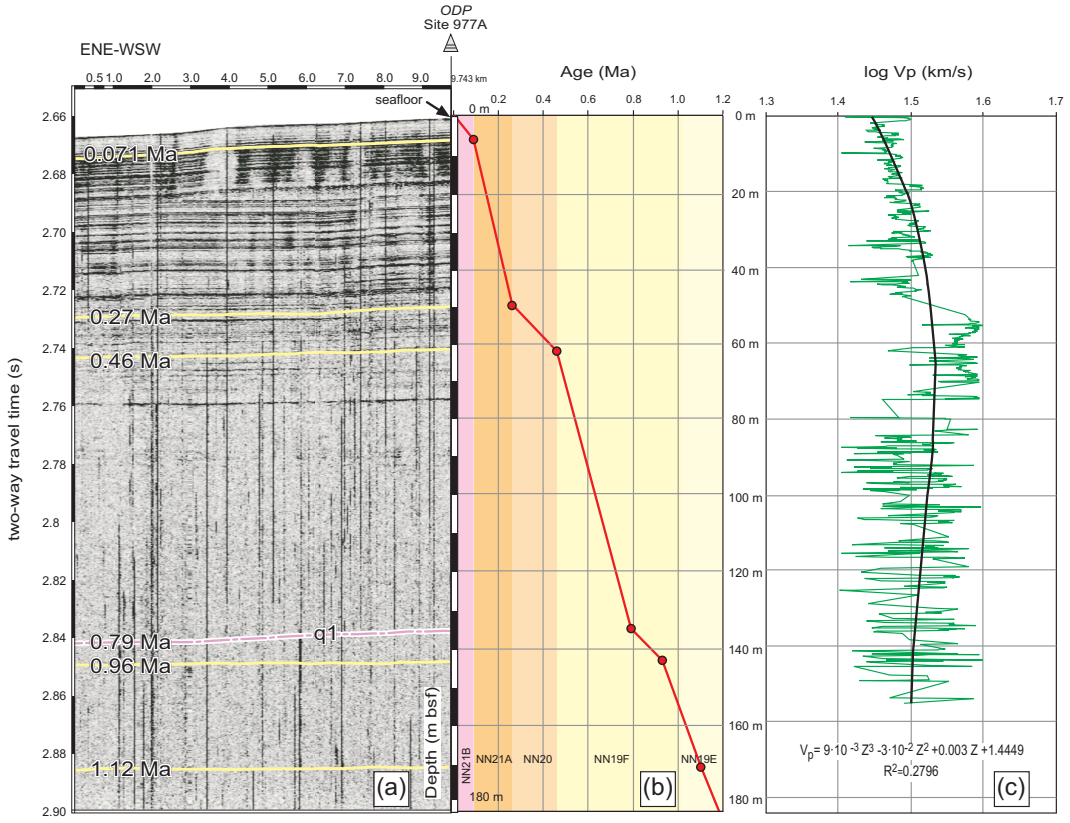

Figure 2-17. Correlation panel showing correspondence between TOPAS and well data. **(a)** Segment of TOPAS profile in the East Alboran Basin and interpreted key reflectors (location in figure 2-3). **(b)** late Quaternary biostratigraphic markers recognized in ODP Site 977A (Table 2-3) versus twtt after using the best-fitting equation shown in panel (c). Colour bars represent the calcareous nannofossils zonation proposed by Martini (1971). **(c)** Vp log from ODP Site 977A used to convert the vertical scale of biostratigrafic data from depth (in metres) to twtt (in seconds).

2.5 Seismic interpretation and gridding

Seismic interpretation was performed using the SMT Kingdom Suite® software. Those seismic profiles which cross the studied wells were interpreted firstly. Seismic discontinuities recognized along these profiles were tied with well information following the procedure explained in previous sections. Seismic interpretation was then extended from these selected profiles towards the rest of the network of seismic lines across their intersections. All the intersections were examined before interpreting and the possible vertical offsets of twtt were minimized by means of an interactive *mistie analysis* using the SMT Kingdom Suite® software. Originally, these vertical offsets of twtt or "misties" were relatively common along the seismic database due to the fact that seismic records used in this study come from different surveys. Thus, it should be noted that these data were acquired using different equipments and processed considering different velocity analysis. The most recent profiles from Marsibal I-06 cruise were assigned as reference for the mistie analysis and the rest of seismic lines were readjusted respect to them in order to minimize errors. Figure 2-18 shows the amount of residuary twtt offsets at different intersections. Locally, few offsets between 25 and 100 ms, mapped as red circles, remain at some intersections and they were not used for correlations in any case. It should be noticed that most of these biggest errors locate at bathymetric highs or escarpments, where small positioning error can produce a big offset. Positioning errors of some shoot points may be due to vectorising of position analogue maps or inaccuracy of the GPS during the oldest cruises. Seismic interpretation was carried out using preferably those intersections without vertical offsets, mapped as green circles, or alternatively those with minimum offsets (less than 20 ms twtt; yellow circles).

After seismic interpretation, the mapped events were gridded to obtain time-contour maps using the SMT Kingdom Suite® software. For each key reflector, two-way travel time values were exported together with their geographical coordinates along whole net of seismic profiles. Interpolation of these values from different 2D lines allowed generate surfaces that represent approximately the three-dimensional geometry of unconformities (in twtt) within the sedimentary infill.

Gridding algorithms are different sets of mathematical formulations that can be used to interpolate the irregularly spaced input twtt values to a rectangular mesh (grid) of output coordinate locations. Different gridding algorithms were tested in this study to produce the best grids from the available data distribution. The example in figure 2-19 illustrates that good fitting between the original interpretation of a seismic event and the resulting grid depends on the selected gridding algorithm and output spacing. Figures 2-19a to 2-19c are examples that show sections of three grids obtained for the M reflector using the Kringing, Natural Neighbor and Flex Gridding algorithms and a same spacing of 2 km. The original seismic line and interpretation are also displayed with each grid section to compare their fitting. The Flex Gridding algorithm provided the best results and therefore it was chosen to generate all time-contour maps. This algorithm uses differential equations producing an interpolated surface which pass through or at least very close of the input data in the XYZ space. The value of each grid node is calculated considering the values for a dozen of its neighbours. Thus, all nodes are coupled together, but the coupling to distant nodes is weak and indirect. Numerous iterations are needed to smooth the influence of a data across the interpolated areas. The resulting grids are smooth surfaces along interpolated areas, but they maintain very fine scale variability for the data along seismic line positions (Figure 2-19c). The spacing supplying the best results was 2

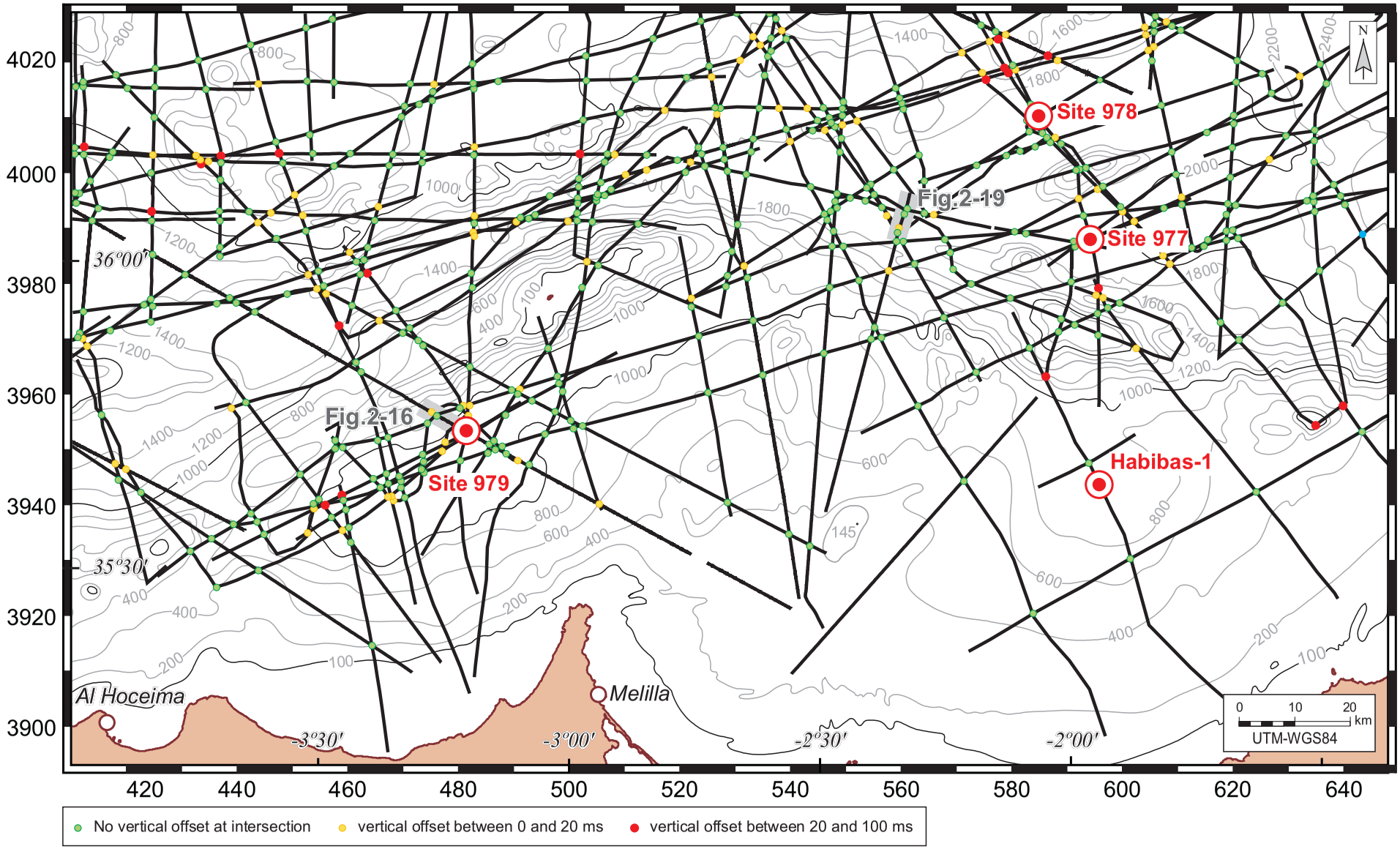

Figure 2-18. Map showing the amount of residuary twtt offsets at the different intersections between seismic profiles. Thick grey line indicates multichannel seismic profiles presented this chapter. Location of ODP sites 977, 978, 979 and Habibas-1 well are shown as red circles. Bathymetry contours (GEBCO-97, IOC-IHO) are in metres, contour interval 200 m.

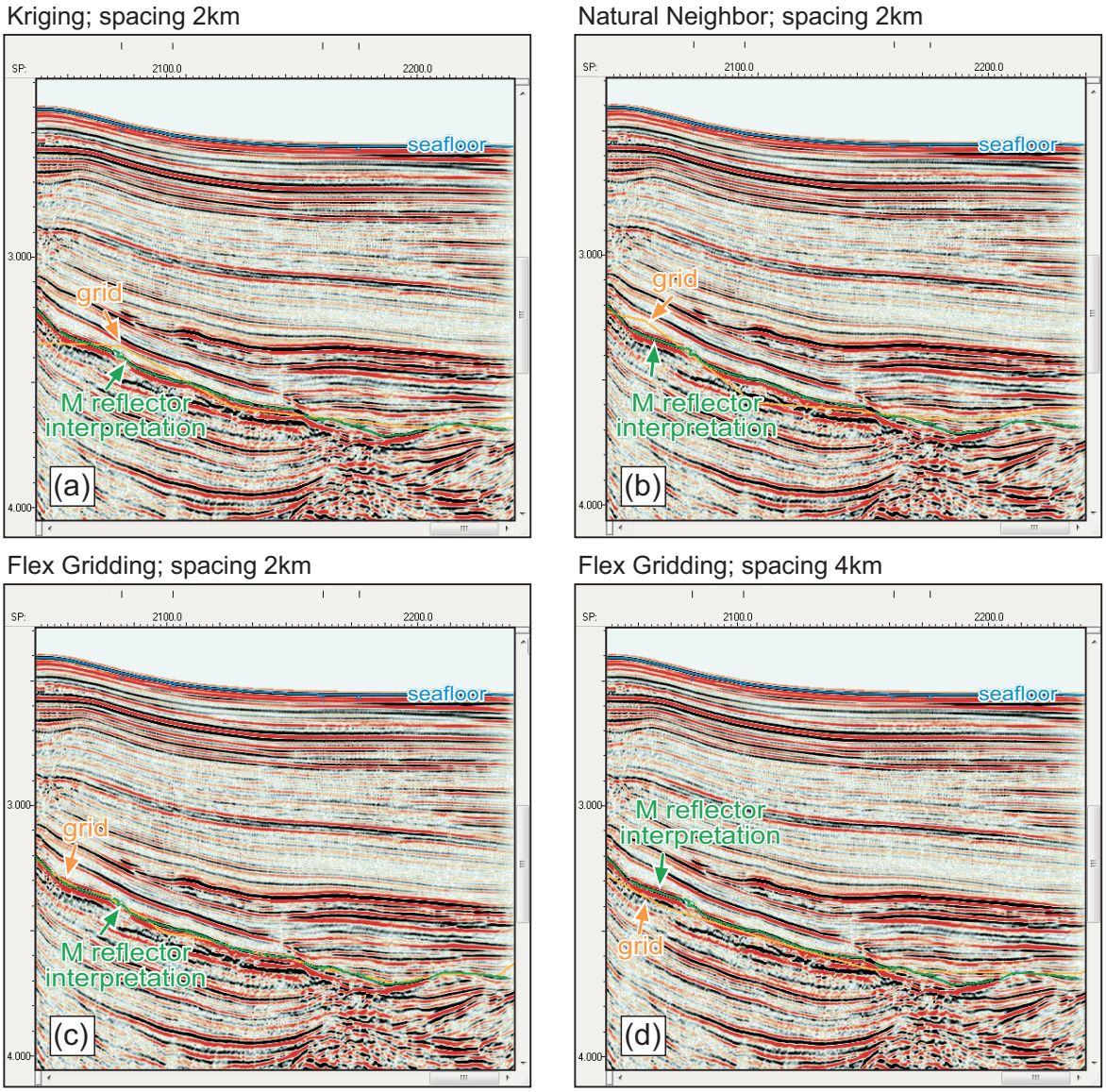

Figure 2-19. Detail of multichannel seismic section showing variable fitting between seismic interpretation of a key reflector (M) and the surfaces obtained from 3D interpolation using different gridding algorithms and spacings. Note that Flex Gridding algorithm and spacing of 2 km (panel c) supply the best-fitting results. Profile location is shown in figures 2-5 and 2-18.

km. When the Flex Gridding works with larger spacings produces grids that do not fit well with the original interpretations (Figure 2-19d, spacing 4 km). It should be noted that although the selected spacing is rather fine compared with the available distribution of seismic lines, the Flex Gridding generates very smooth surfaces for interpolated areas. The resulting grids were portrayed as coloured shaded-relief surfaces and contour maps using the Surfer® software.

An additional test was carried out to examine the accuracy of grids generated for this study: a seafloor grid obtained from seismic data was converted to depth using a standard average *Vp* of 1490 m/s for water and the result was compared with bathymetric data from GEBCO-97 database (Figure 2-20). Both surfaces were generated using the same spacing (2 km). The seismic grid reproduces rather precisely the seafloor morphology. The main realms in the study area show similar shapes,

dimensions and depths to those recognized on the bathymetric map (*cf.* figure 2-20a and figure 2-20b). The resulting depth contours on the seismic grid are to a large degree also equivalent to bathymetric contours and they only differ on details of small scale. This test indicates that gridding of seismic data using the Flex Gridding algorithms and a constant spacing of 2 km are accuracy to

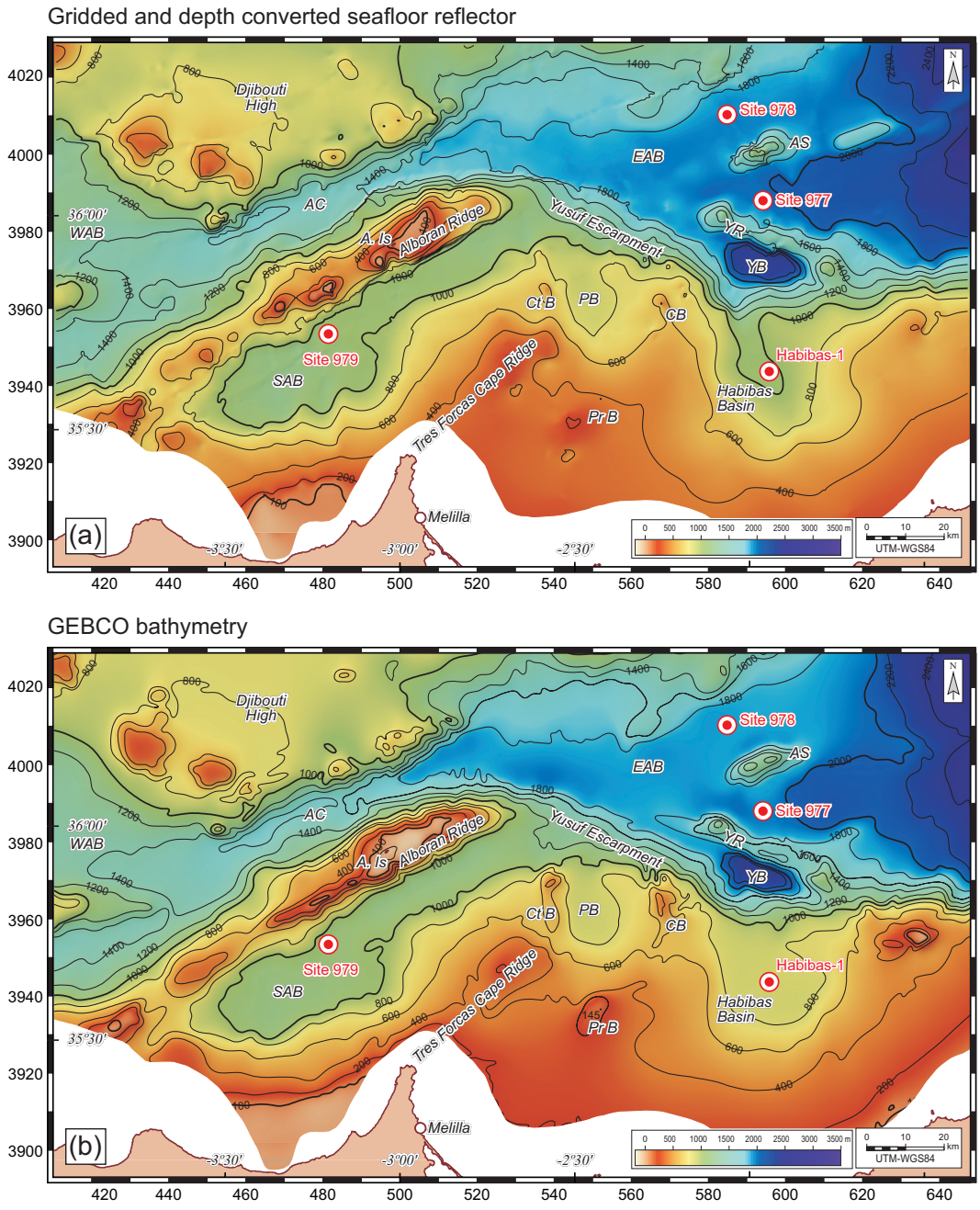

Figure 2-20. Comparison between **(a)** gridded seafloor reflector using the Flex Gridding algorithm. And **(b)** GEBCO-97 bathymetry data (IOC-IHO). The twtt gridded seafloor reflector was conveted to depth using an average *Vp* of 1490 m/s for water. In both cases grid spacing is 2 km and contour interval is 200 m. White areas correspond to domains without seismic coverage. ODP Leg 161 sites and Habibas-1 well are also included. UTM projection, units in kilometres (WGS 84 ellipsoid). Abbreviations: A. Is, Alboran Island; AC, Alboran Channel; AS, Al-Mansour Seamount; CB, Câbliers Bank; Ct B, Catifas Bank; EAB, East Alboran Basin; PB, Pytheas Basin; Pr B, Provençaux Bank; SAB, South Alboran Basin; YB, Yusuf Basin; YR, Yusuf Ridge and WAB, West Alboran Basin.

reproduce geological surfaces in the basin. However, the results should be taken as regional values, which provide general tendencies rather than precise estimations.

2.6 Interval velocities and depth conversions

Interval *Vp* were calculated in order to perform depth conversions of the twtt-contour maps. Correlations panels between seismic and well data allowed to determine the position of the reflectors at each well locations (*e.g.* Figure 2-16). The twtt data of the key reflector observed in the seismic profiles can be converted to depth using equation [5] and best-fitting functions of *Vp*-twtt data (equations [6] to [10]). It is then possible to obtain the depths (in metres) of the seismic boundaries between units at each well (Figure 2-21). Locally, some of these boundaries coincide with the hiatuses identified at ODP Sites 976, 977 and 979, as mapped events form unconformities, passing laterally

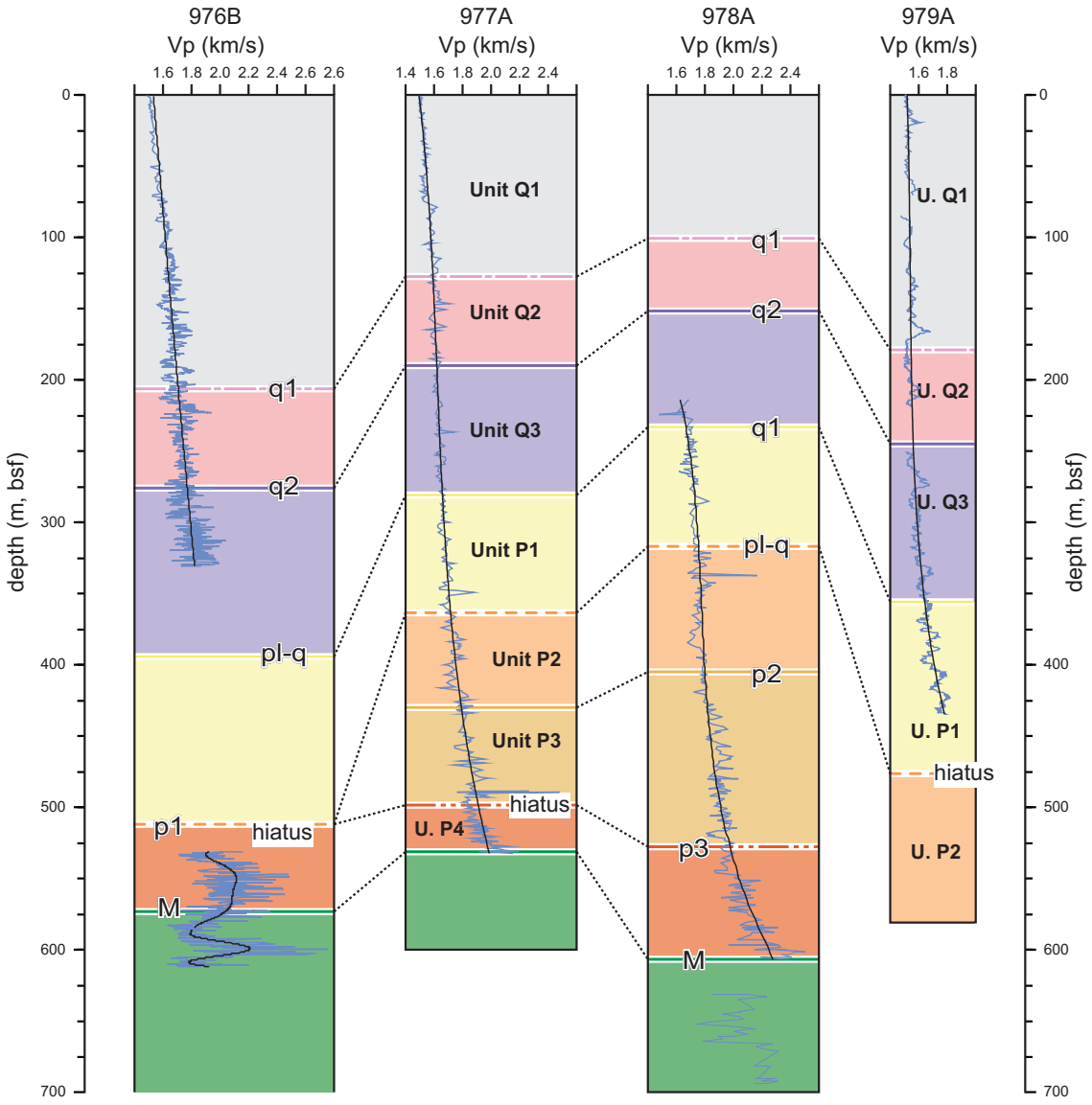

Figure 2-21. Estimated depths of key reflectors and Plio-Quaternary seismic units at ODP Sites 976 to 979 correlated with *Vp* log data and best-fitting functions (equations [6] to [10]). Position of drilled hiatuses is also indicated. *m, bsf* are metres below seafloor.

into conformable events.

An interval velocity was obtained for each seismic unit at each well using the best-fitting functions of *Vp*-depth data (equations [6] to [10]) and considering the depth of the half of the thickness of each unit. For each seismic unit, it was calculated the average of all the obtained interval *Vp* values. Figure 2-22 shows the resulting average interval sonic velocities (*Vp)* together with the rank of variability of the averaged values. Thickness maps were calculated for each seismic unit from the time-contour maps and they were converted to depth using the average sonic velocities. Therefore, it was assumed a constant *Vp* interval for each unit throughout the entire study area.

In addition, sediment accumulation maps were calculated for each seismic unit from depth converted isopach maps, knowing the age of seismic horizons and assuming a linear interpolation of ages. Because it was not conducted any decompation analysis, these sediment accumulation rates should be considered minimum values, especially for the deeper seismic units.

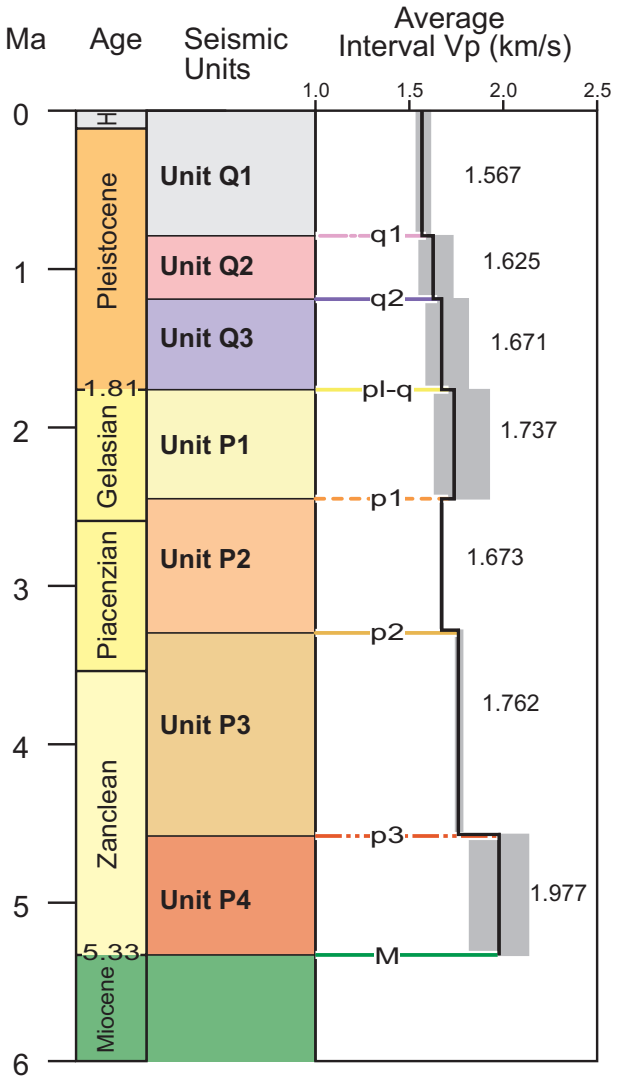

Figure 2-22. Plio-Quaternary chronostratigraphic framework established in this study including time stages, seismic units, interpreted seismic discontinuities and calculated average interval sonic velocities (*Vp*). Light grey bars indicate the range of averaged data, which come from individual estimations at ODP Sites 976 to 979.

3. Seafloor morphology and Recent tectonics

Recent structures in the Alboran Ridge and Yusuf fault zones based on swath bathymetry and sub-bottom profiling: evidence of active tectonics

Published in ***Geo-Marine Letters*** *(2011), 31, 16-39.*

Pedro Martínez-García[1], Juan I. Soto[2] and Menchu Comas[1]

[1] Instituto Andaluz de Ciencias de la Tierra (CSIC and University of Granada), Facultad de Ciencias,

[2] Instituto Andaluz de Ciencias de la Tierra (CSIC and University of Granada) and Departamento de Geodinámica, Facultad de Ciencias, Granada, Spain.

Abstract

The seafloor of the Alboran Sea in the western Mediterranean is disrupted by deformations resulting from convergence between the African and Eurasian plates. Based on a compilation of existing and new multibeam bathymetry data and high-resolution seismic profiles, our main objective was to characterize the most recent structures in the central sector, which depicts an abrupt morphology and was chosen to investigate how active tectonic processes are shaping the seafloor. The Alboran Ridge is the most prominent feature in the Alboran Sea (>130 km in length), and a key element in the Gibraltar Arc System. Recent uplift and deformation in this ridge have been caused by sub-vertical, strike-slip and reverse faults with associated folding in the most recent sediments, their trend shifting progressively from SW–NE to WNW–ESE towards the Yusuf Lineament. Present-day transtensive deformation induces faulting and subsidence in the Yusuf pull-apart basin. The Alboran Ridge and Yusuf fault zones are connected, and both constitute a wide zone of deformation reaching tens of kilometres in width and showing a complex geometry, including different active fault segments and in-relay folds. These findings demonstrate that Recent deformation is more heterogeneously distributed than commonly considered. A narrow SSW–NNE zone with folding and reverse faulting cuts across the western end of the Alboran Ridge and concentrates most of the upper crustal seismicity in the region. This zone of deformation defines a seismogenic, left-lateral fault zone connected to the south with the Al Hoceima seismic swarm, and representing a potential seismic hazard. Newly detected buried and active submarine slides along the Alboran Ridge and the Yusuf Lineament are clear signs of *submarine slope instability* in this seismically active region.

Keywords: Alboran Sea, seafloor morphology, swath bathymetry, sub-bottom profiling, strike-slip fault, active tectonics.

3.1 Introduction

In the western Mediterranean, the Alboran Sea Basin straddles the boundary between the African and Eurasian plates and evolved within a convergent plate-tectonic setting. Present-day convergence is NW–SE, clearly oblique to the trends of both the nearby Betic and Rif mountain chains and the main Alboran Sea Basin elongation (*e.g.* Fadil *et al.*, 2006). The regional seismicity is broadly distributed, being concentrated largely in the uppermost crust. Crustal seismic events can be linked with major fault structures, most with a long history of deformation during the Neogene and Quaternary (*e.g.* Udías and Buforn, 1991; Calvert *et al.*, 2000; Stich *et al.*, 2003a; Fernández-Ibáñez and Soto, 2008).

The Alboran Sea Basin is a Neogene marine back-arc basin (~54,000 km^2) within the Gibraltar Arc System, which was generated by late-orogenic crustal extension during the Early Miocene (*e.g.* Platt and Vissers, 1989; Comas *et al.*,1992, 1999; García-Dueñas *et al.*, 1992; Maldonado *et al.*, 1992; Watts *et al.*, 1993). In the Gibraltar Arc System, the Miocene extension was accompanied by extensive magmatism and several volcanic episodes (*e.g.* Duggen *et al.*, 2004). This extensional episode was followed by a contractive reorganization from the Late Miocene to the Holocene (Comas *et al.*, 1992, 1999; Watts *et al.*, 1993; Chalouan *et al.*, 1997). The tectonic processes occurring in the basin during the Plio-Quaternary are to a large degree responsible for the present seafloor physiography (*e.g.* Woodside and Maldonado, 1992; Bourgois *et al.*, 1992; Campos *et al.*, 1992; Gràcia *et al.*, 2006; Ballesteros *et al.*, 2008).

The continental Alboran Sea Basin is shallower than the oceanic Algerian Basin to the east. The westward connection with the deeper Atlantic Ocean occurs through a narrow, channelled threshold in the Gibraltar Strait. The floor of the Alboran Sea is morphologically complex, with isolated highs or seamounts of volcanic origin and locally emerged ridges hundreds of kilometres long (*e.g.* the Alboran Ridge, Figure 3-1). These submarine reliefs bound three main basins known as the West, East and South Alboran basins. The Alboran Ridge trends NE–SW and constitutes a major linear relief in the Alboran Sea, extending eastwards to the NW–SE Yusuf Lineament, which ultimately merges with the steep southern margin of the Algerian Basin, known as the Habibas Escarpment (Figure 3-1). It is well known that these major elongated reliefs are morphological expressions of two strike-slip fault systems, the Alboran Ridge and Yusuf fault zones. These show evidence of present-day seismic activity and may link with the structures identified on land in the Betics and Rif mountains (*e.g.* Woodside and Maldonado, 1992; Bourgois *et al.*, 1992; Campos *et al.*, 1992; Comas *et al.*, 1992; Maldonado *et al.*, 1992; Chalouan *et al.*, 1997; Ammar *et al.*, 2007; Fernández-Ibáñez *et al.*, 2007; Mauffret *et al.*, 2007; Ballesteros *et al.*, 2008). Although the seafloor morphology and physiographic domains of various sectors of the Alboran Sea have been well documented in previous work using swath bathymetry and seismic profiling (*e.g.* Alonso and Maldonado, 1992; Ercilla *et al.*, 1992; Vázquez, 2001; Alonso and Ercilla, 2003; Martín-Serrano, 2005; Gràcia *et al.*, 2006; Ballesteros *et al.*, 2008; Muñoz *et al.*, 2008), the relationship between the Alboran Ridge and the Yusuf fault zones remains unclear and the characterization of active structures in the central Alboran Sea is still far from being well-established.

In an attempt to contribute to the Alboran tectonic scenario from the Quaternary to the Present, we performed a geomorphological and structural study in the central sector of the Alboran Sea (Figure 3-1). Our main aims were (1) to investigate the shallow structure of the Alboran Ridge and

Yusuf fault zones in more detail, (2) to determine the temporal and spatial relationships between the different fault zones during the Quaternary, and (3) to identify the active fault segments, exploring their relation with the shallow seismicity to infer fault kinematics. For this purpose, we compiled a swath-bathymetry mosaic incorporating new as well as published data, notably those of MediMap Group (2008). The multibeam bathymetry published recently by Ballesteros *et al.* (2008) and Muñoz *et al.* (2008) covers the north-western part of our study area and represents an outstanding reference to constrain our work. In addition, seafloor topography was linked to sub-bottom shallow structures evaluated by means of high-resolution seismic profiles.

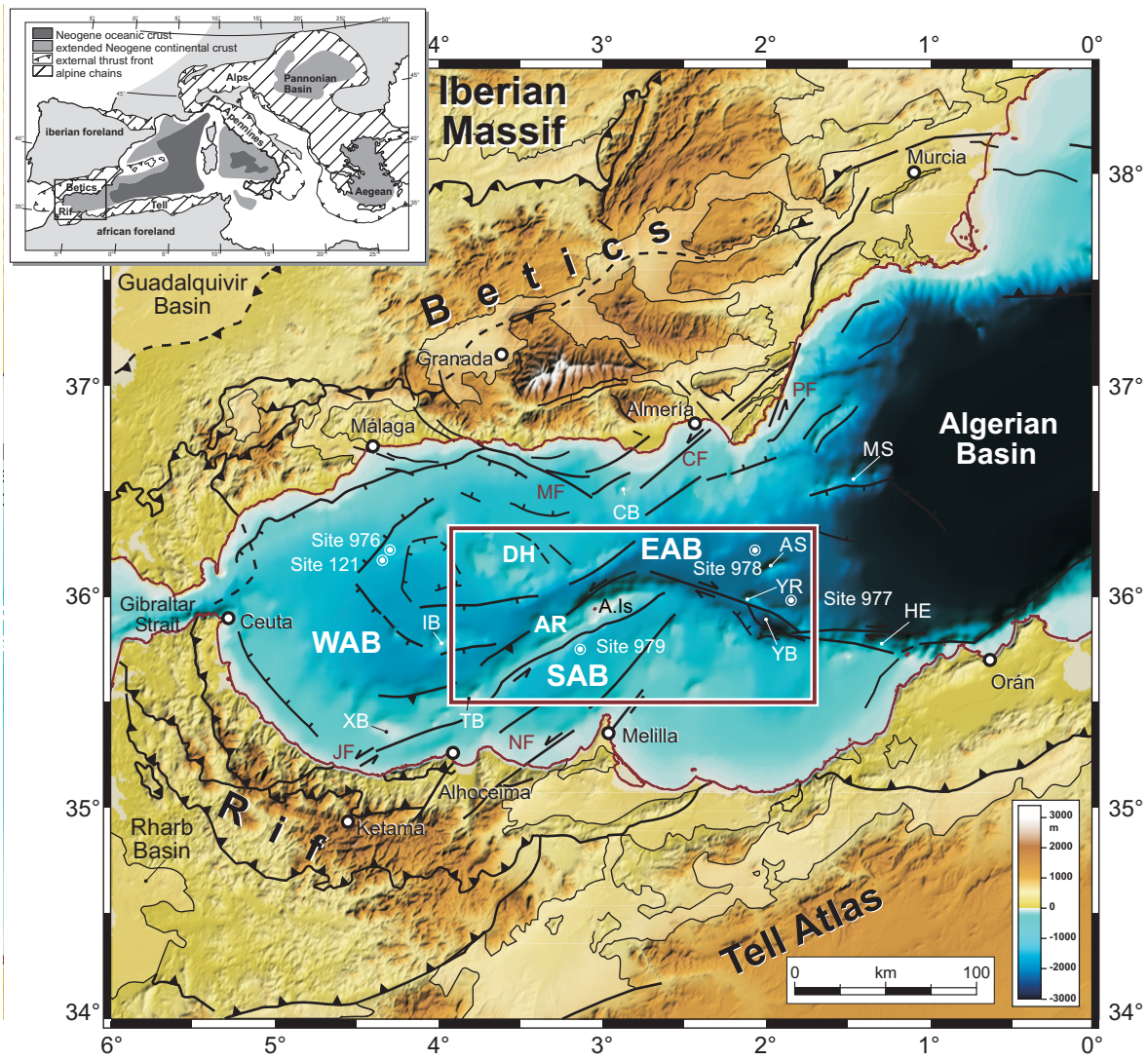

Figure 3-1. Topography of the Gibraltar Arc and major tectonic features of the Alboran Sea study region (simplified from Comas et al. 1999), also showing the locations of ODP Leg 161 sites and DSDP Site 121 (digital topography extracted from the SRTM (USGS-NASA) global database, combined with GEBCO 97 (IOC-IHO) for the offshore region). Rectangle delimits the study area, comprising the Alboran Ridge and surrounding sectors. Inset map is a tectonic sketch of the Mediterranean Sea, showing the Neogene extensional basins and the fronts of the surrounding Alpine thrust belts (from Comas et al., 1999). Abbreviations: A. Is, Alboran Island; AR, Alboran Ridge; AS, Al-Mansour Seamount; CB, Chella Bank; CF, Carboneras Fault; DP, Djibouti High; EAB, East Alboran Basin; HE, Habibas Escarpment; IB, Ibn-Batouta Bank; JF, Jebha Fault; MF, Maro-Nerja Fault; MS, Maimonides Seamount; NF, Nekor Fault; PF, Palomares Fault; SAB, South Alboran Basin; TB, Tofiño Bank; XB, Xauen Bank; YB, Yusuf Basin; YR, Yusuf Ridge; WAB, West Alboran Basin.

3.2 Materials and methods

We generated a bathymetry map of the central sector of the Alboran Sea at about 3.8–1.7ºW and 35.5–36.3ºN (Figure 3-2), covering an area of about 14400 km^2. Swath-bathymetric datasets were acquired with a Simrad EM-12S-120 multibeam echosounder during the ALBA cruise of 1992, complemented with more recent Simrad tracks from the TECALB (2000) and MARSIBAL I-06 (2006) cruises aboard the BIO Hespérides. Other data were extracted from bathymetric atlases published by the MediMap Group (2008).

Sub-bottom parametric seismic TOPAS (TOpographic PArametric Sonar) profiles (in total, ~3738 km length) were acquired simultaneously with the bathymetry. The ALBA mosaic includes longitudinal TOPAS profiles along major tracks with variable spacings of 1–3 km. In this work we show representative segments of this comprehensive dataset. The Simrad TOPAS is a low-frequency (0.5–6 kHz) sub-bottom seismic profiling system for which maximum penetration and resolution depend essentially on water depth and sediment characteristics. Information on the age of Recent sediments was extracted from ODP reports for ODP Leg 161 sites 976, 977 and 978 drilled in the central Alboran Sea (Comas *et al.*, 1996). Vp data and biostratigraphic information for these wells served to convert two-way time into depth and to estimate the age of some key seismic events in the TOPAS profiles.

Seismicity data at shallow depths (≤11 km) were taken from the USGS 1979–2006 seismic catalogue. In addition, a set of 13 focal mechanisms was available from the Instituto Andaluz de Geofísica (www.ugr.es/~iag). These are considered reliable since they were calculated through moment tension inversion (*e.g.* Stich *et al.*, 2003a).

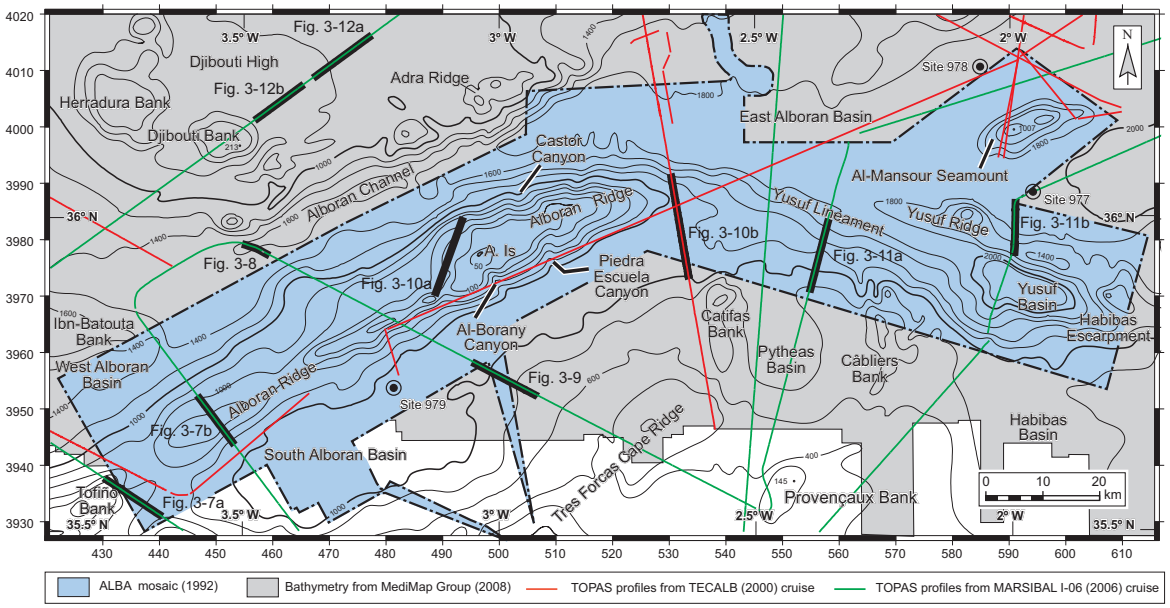

Figure 3-2. Bathymetry contours of the study area in the central Alboran Sea (GEBCO 97, IOC-IHO), showing the location of the swath-bathymetry mosaics of the ALBA cruise, completed with Medi-Map Group (2008). The locations of TOPAS profiles from the TECALB and MARSIBAL I-06 cruises are also indicated. Circles with numbers represent ODP Leg 161 sites. Thick black lines indicate TOPAS profiles presented in figures 3-7, 3-8, 3-9, 3-10, 3-11, 2-12 and 3-13. Bathymetry contours are in metres, contour interval 200 m, UTM projection, units in kilometres (WGS 84 ellipsoid). A. Is Alboran Island.

3.3 Results

Seafloor topography

Combining bathymetry, slope inspection and topographic sections, five physiographic domains can be distinguished in the central Alboran Sea (Figures 3-3, 3-4 and 3-5): (1) the Alboran Ridge; (2) the Yusuf Lineament, including the associated basin and ridge; (3) a basin plain corresponding to the East Alboran Basin; (4) the Djibouti High, a submarine promontory including several seamounts (Adra Ridge, Djibouti and Herradura banks); and (5) the Alboran Channel. Below, we identify new findings on the otherwise well-known Alboran Ridge and Yusuf Lineament and describe the sedimentary and tectonic structures identified there and nearby.

Alboran Ridge

The Alboran Ridge constitutes a SW-NE-trending seamount over 130 km long and rising 1850 m above the seafloor. It has a flat top in its north-eastern sector and emerges locally in the Alboran Island (Figures 3-3 and 3-5d). To the southwest, it has a narrow, elongated crest (>50 km long and up to 70 m high, Figure 3-5c), including a depression at about 3.4ºW. To the south, the Alboran Ridge bounds the South Alboran Basin (SAB) (Figures 3-5b to 3-5g), an elongated depression (20–10 km wide and ~90 km long) trending N70°E with a basin plain delimited by the 1000 m isobath. Further to the east, the ridge trend shifts from SW–NE to E–W.

The highest slope gradients (>20º) of the Alboran Ridge are located in its eastern sector (~3ºW; Figure 3-4). The southern slope has an irregular surface varying along strike. To the west, the slope shows a smooth, undulating topography with a relatively low gradient (<13º) (Figures 3-5b and 3-5c). By contrast, the eastern slope corresponds to a narrow, SE-facing escarpment with a steeper gradient (>13º) and a staircase profile, ~900 m above the seafloor of the South Alboran Basin (e.g., Figure 3-5e). The northern slope (between 2.5º and 3.1ºW) is wide, steep (commonly >12–13º) and concave (southwards), rising about 1800 m above the valley of the Alboran Channel (Figures 3-5c to 3-5f). Locally, other secondary and smaller concave (south-eastwards) domains with high slopes are located between 3.05º and 3.2ºW.

Towards the southwest, the Alboran Ridge connects with the Tofiño and Xauen banks (Figure 3-1). These seamounts bound the West Alboran Basin (WAB), this being the main basin in the Alboran Sea. Along this margin, the WAB has low slope gradients (<5º) and the 1400 m contour line bounds the basin plain. The Ibn-Batouta Bank rises 650 m above the WAB basin plain (Figure 3-3).

Yusuf Lineament

Our results reveal that the Alboran Ridge turns eastwards into a curved, north-dipping slope gradually shifting from SW–NE to NW–SE (between 3º and 2.5ºW). In this sector, the Alboran Ridge connects with the Yusuf Ridge and Yusuf Basin (Mauffret *et al.*, 1992) through a relatively narrow slope (~10 km wide and <7–8º; Figures 3-4 and 3-5g). Collectively, we refer to this elongated domain as the Yusuf Lineament, constituting the western prolongation of the Habibas Escarpment which bounds the Algerian Basin (Figure 3-1). We discovered numerous gullies and short, discrete submarine canyons which erode this escarpment (Figures 3-3 and 3-6). The Yusuf Lineament presents

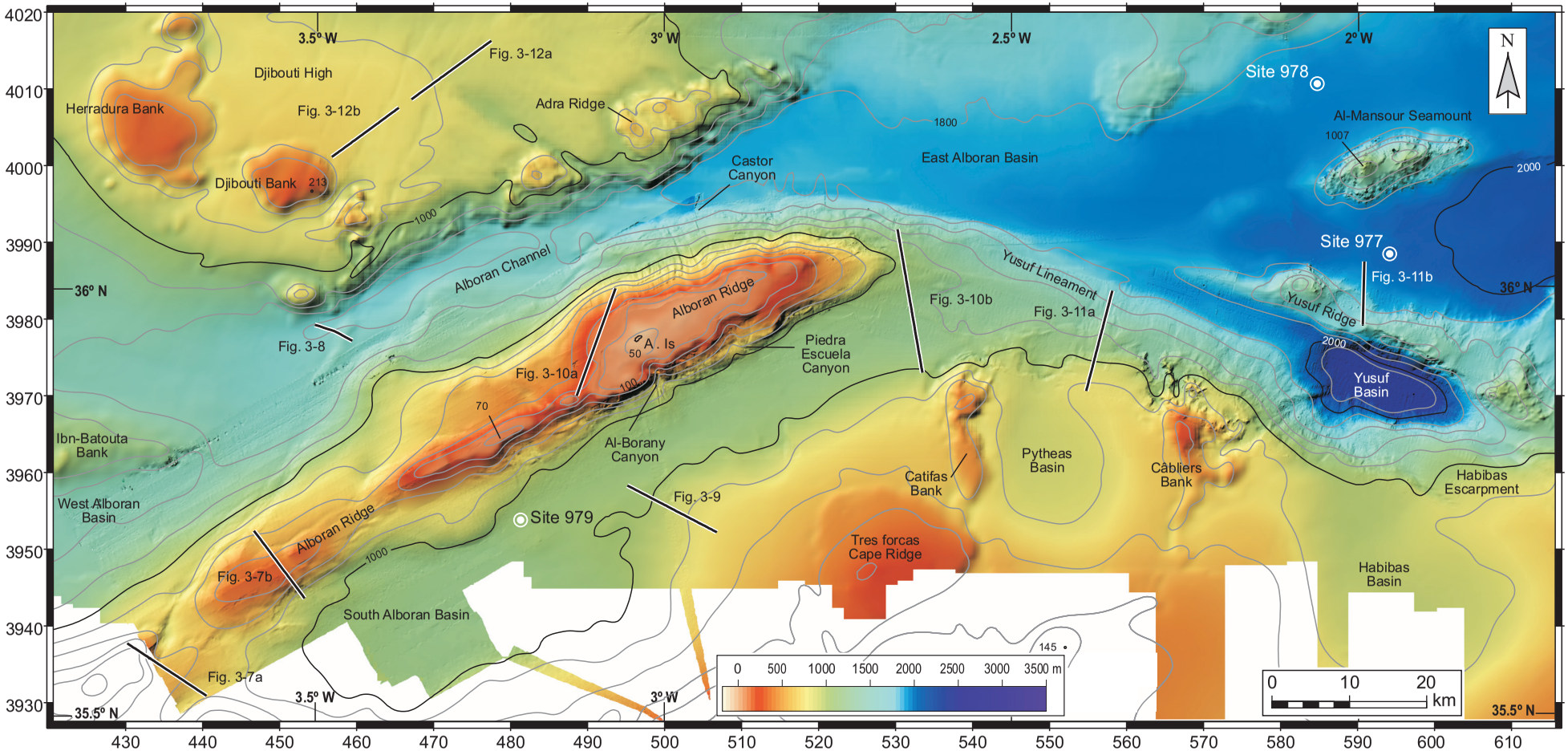

Figure 3-3. Coloured shaded-relief bathymetric mosaic of the central Alboran Sea. Thick black lines indicate TOPAS profiles presented in figures 3-7, 3-8, 3-9, 3-10, 3-11, 2-12 and 3-13. White circles represent ODP Leg 161 sites. Bathymetry contours (GEBCO 97, IOC-IHO) are in metres, contour interval 200 m, UTM projection, units in kilometres (WGS 84 ellipsoid).

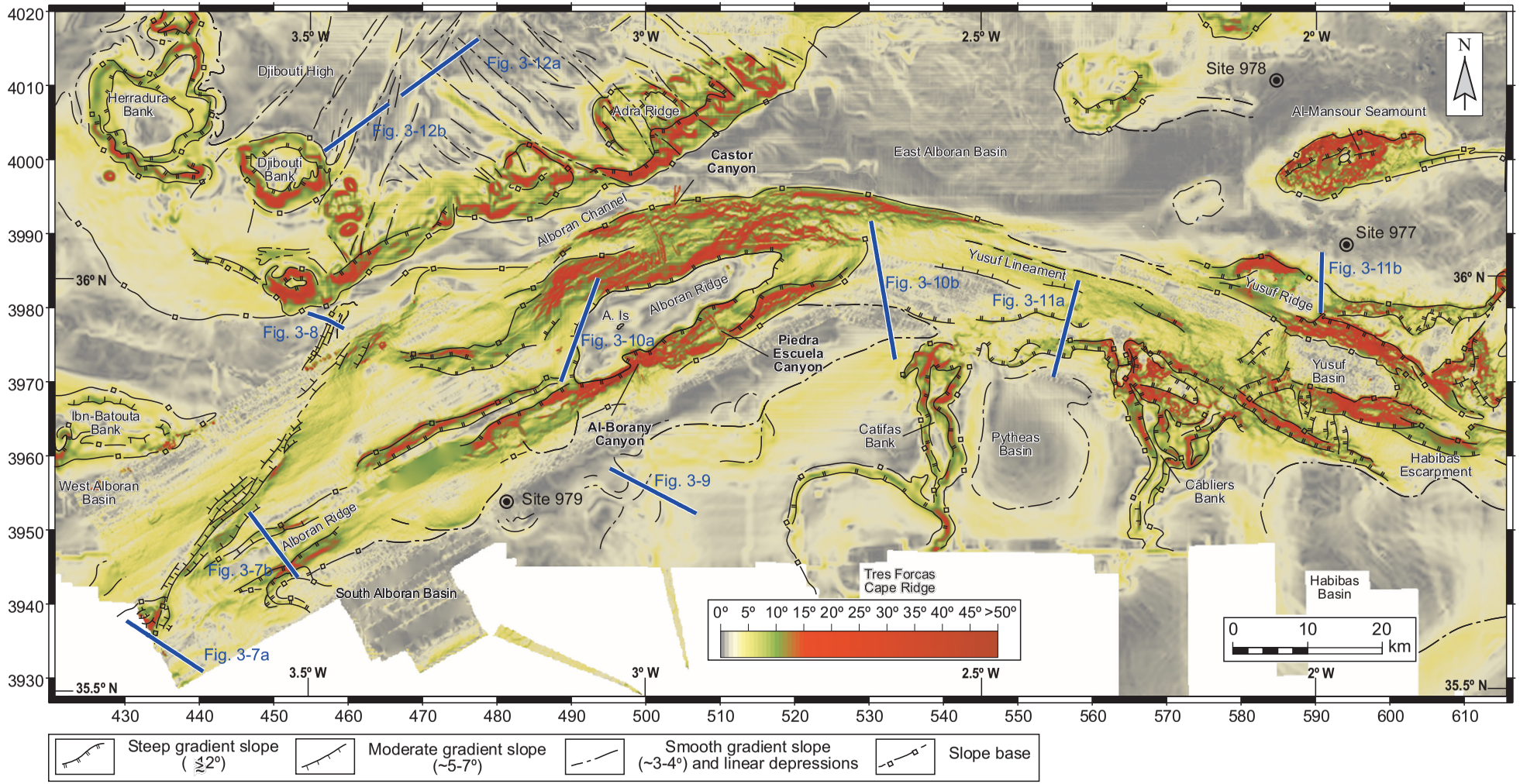

Figure 3-4. Slope map of the central Alboran Sea (colour scale degree of slope, in degrees). Thick blue lines indicate TOPAS profiles presented in figures 3-7, 3-8, 3-9, 3-10, 3-11, 2-12 and 3-13. Circles represent ODP Leg 161 sites. UTM projection, units in kilometres (WGS 84 ellipsoid).

the highest slope gradients in the central Alboran Sea, with values locally exceeding 70º bordering the Yusuf Basin. The Yusuf Ridge (~40 km long) is an abrupt seamount which bounds the deep, isolated Yusuf Basin (~2300 m depth), the latter having a flat floor and asymmetric margins (Figures 3-3, 3-5j and 3-5k). The northern and southern slopes form straight, narrow and steep (>20°) margins, whereas the western and eastern limits are curved and show a staircase profile with a moderate average slope (<10°).

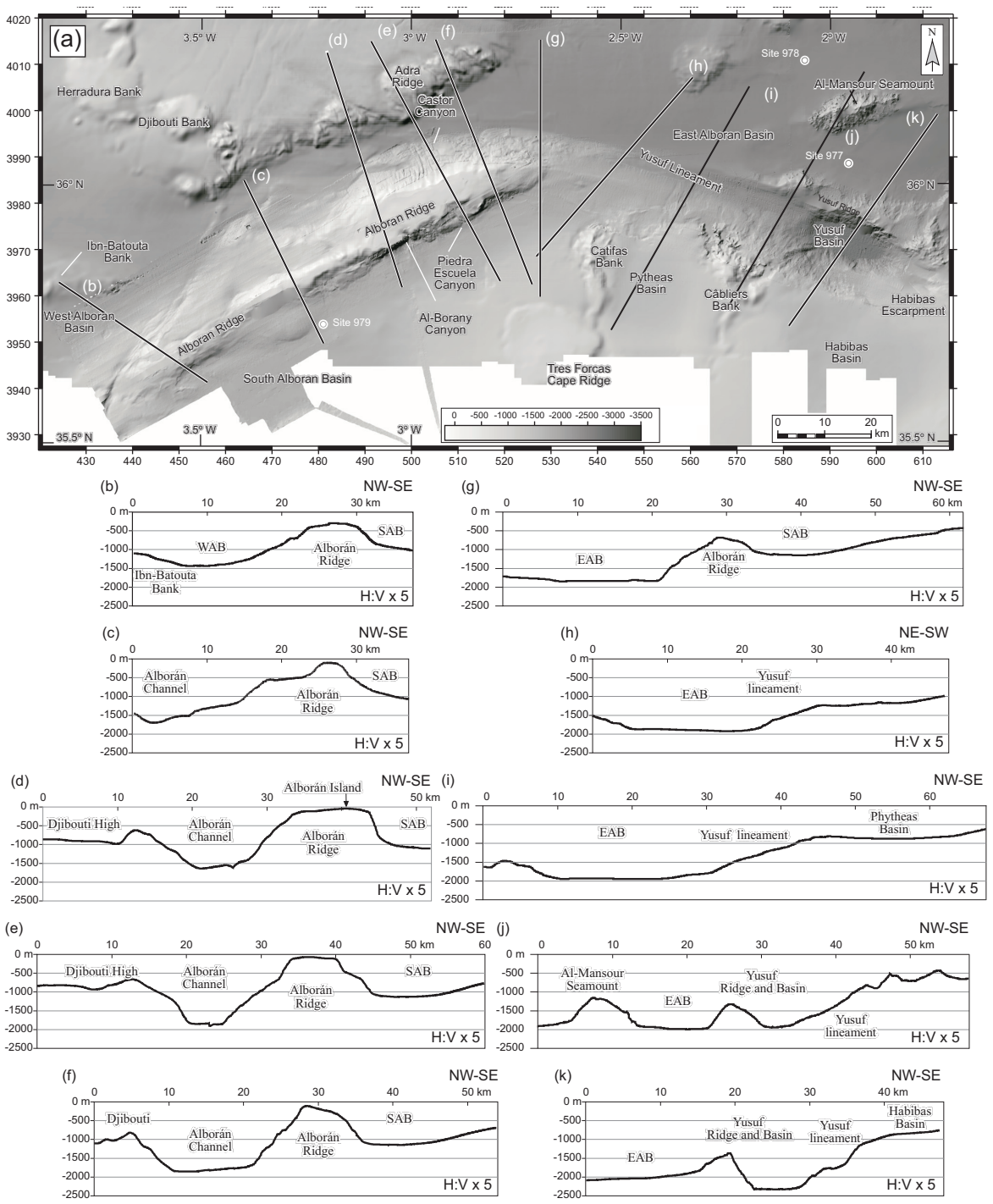

Figure 3-5. **(a)** Bathymetric map of the Alboran Ridge and surrounding areas including position of seafloor profiles shown in **(b)** to **(k)**. Abbreviations: EAB, East Alboran Basin; SAB, South Alboran Basin; WAB, West Alboran Basin.

In this region, the southern margin of the Alboran Sea (between 1.5ºW and 3ºW) constitutes a large, smooth slope gently dipping northwards and connecting with the Yusuf Lineament. This margin shows several seamounts, such as the Câbliers, Catifas and Provençaux banks and the Tres Forcas Cape Ridge, comprising small depressions such as the Pytheas and Habibas sub-basins.

East Alboran Basin

The East Alboran Basin (EAB) is delimited by the 1900 m isobath (Figure 3-3). Towards the east the EAB broadens and deepens, connecting with the Algerian Basin at about 1ºW through a gentle slope (~5º; Figure 3-1). The southern slope of the EAB is steep and is bounded by the Yusuf Lineament and the northern slope of the Alboran Ridge. The isolated Al-Mansour seamount rises ~500 m above the surrounding basin plain, with steep slopes (~25º; Figures 3-4 and 3-5j).

Alboran Channel

The Alboran Channel is a narrow trough more than 70 km long. It displays a flat and narrow floor, with variable width (from 4 to 8 km) connecting the West Alboran Basin with the deeper East Alboran Basin (Figures 3-3). This channel is delimited by the southern escarpment of the Djibouti High and the Alboran Ridge (Figures 3-5d to 3-5f), showing a sub-parallel SW-NE trend.

Djibouti High

A wide promontory lying northwest of the Alboran Ridge includes several seamounts: the Adra Ridge (Estrada *et al.*, 1997), the Herradura Bank (Muñoz *et al.*, 2008), the Djibouti Bank (Watts *et al.*, 1993) and other, unnamed seamounts (Figure 3-3). We have collectively named this region the Djibouti High, which overall rises about 800 m above the surrounding basins (Figures 3-5d and 3-5e). In plan view, the various seamounts are circular in shape, tens of kilometres in diameter, several hundred metres high, and are surrounded by deep moats. We identified numerous crosscutting linear depressions tens of kilometres long, showing two contrasting orientations (NNE–SSW and NW–SE; Figures 3-4 and 3-6).

The Djibouti High is bounded to the south by a slope trending SW–NE which shows locally steep gradients (~10–25°). This plateau slope includes several volcanic seamounts, such as the Adra Ridge and three other small, unnamed highs.

Sedimentary, erosive and tectonic features

The main base of slopes and slope breaks bound several subordinate basins comprising basin plain areas with <2º slopes. The basin plains located north of the Alboran Ridge and the Yusuf Lineament are over 1400 m deep (*e.g.* the WAB, EAB, Alboran Channel and Yusuf Basin). South of these lineaments, the South Alboran Basin, and the Pytheas and Habibas basins have basin floors shallower than 1200 m (Figures 3-3, 3-5f, 3-5i and 3-5k).

Most of the seamounts show conspicuous abrasion platforms (Figure 3-6), occurring particularly

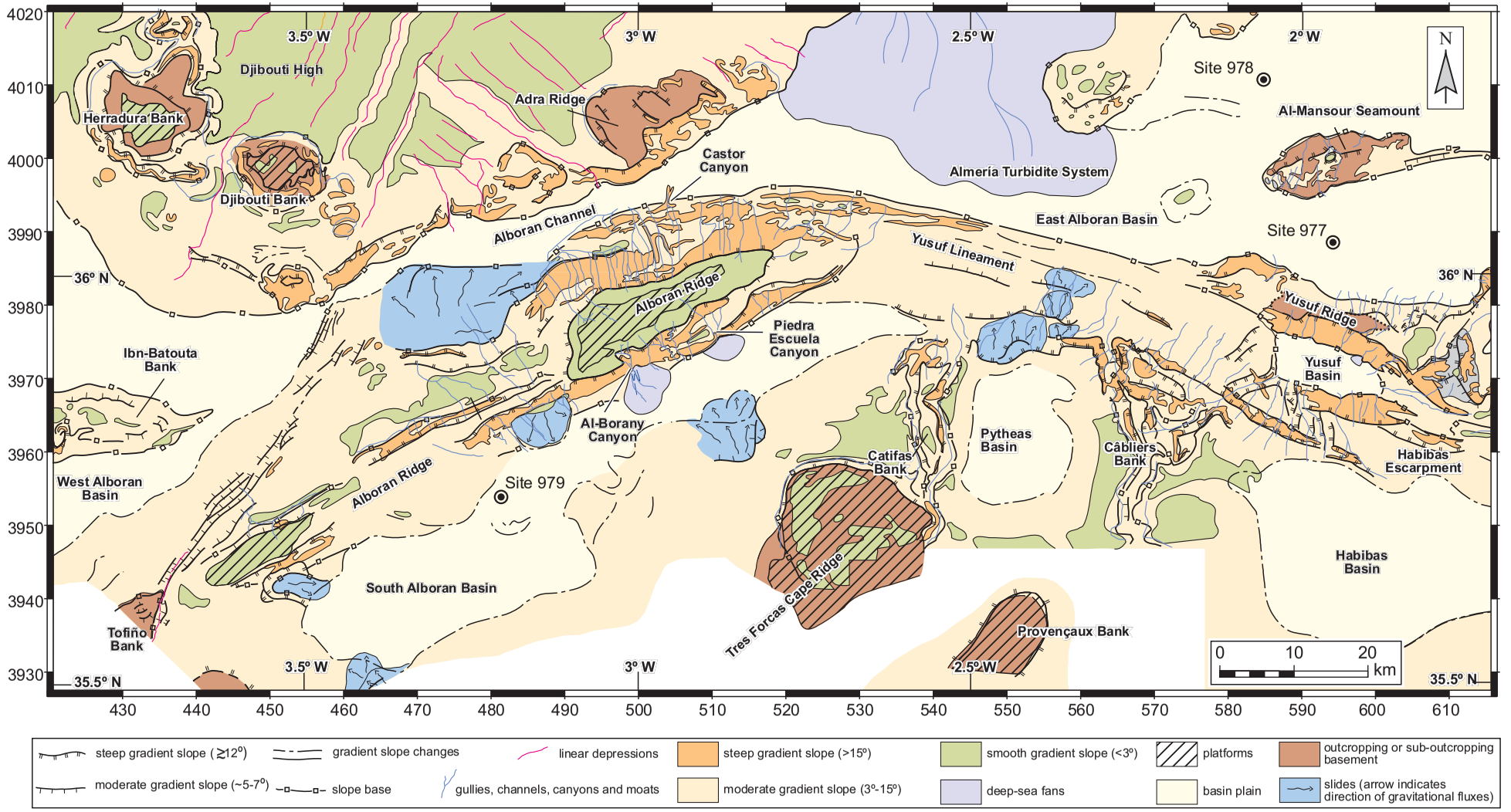

Figure 3-6. Geomorphological map of the central Alboran Sea. UTM projection, units in kilometres (WGS 84 ellipsoid).

where their summits are approx. 200 m deep. Major abrasion platforms, covering tens of km^2, are found at the top of the Alboran Ridge, the Djibouti High seamounts (*e.g.* Herradura Bank), the Cabo Tres Forcas Ridge and the Provençaux Bank.

Other common erosive features are gullies, canyons and channels which appear mainly across the slopes of the Alboran Ridge and Yusuf Lineament (Figure 3-6). We identified a parallel network of regularly spaced gullies (≤10–12 km in length) covering an area of about 500 km^2 and cutting across the northern slope of the Alboran Ridge from platforms (~150–200 m deep) to basin plain areas (EAB and Alboran Channel; 1600–1800 m deep; Figure 3-6). This system consists largely of small-scale (≤10–12 km), regularly spaced longitudinal incisions running mainly N–S across the slope. Deflected paths are visible in some down-slope gullies, as, for example, in the northern slope of the Alboran Ridge gullies where the general N–S orientation locally changes to ENE–WSW (~3ºW, 36ºN), merging into a single valley (Figures 3-3 and 3-6). Gullies and small canyons are also observed along the southern slope of the Alboran Ridge. They extend down to the South Alboran Basin (1000 m deep) covering an area of approx. 150 km^2. Some of these canyons (*e.g.* the Al-Borani and Piedra Escuela canyons (Figure 3-6)) form discrete submarine fans at the base of slope. Another network of gullies cuts across the Yusuf Lineament and Ridge. This comprises numerous incisions (≤11 km in length) which mainly run SW–NE, ending in the Yusuf Basin and the East Alboran Basin and covering an area of about 700 km^2. Sinuous, distal channels are found along the northern margin of the EAB (Almería Margin), corresponding to the distal portion of the Almería turbidite system flowing into the EAB (Alonso and Ercilla, 2003; García *et al.*, 2006; Gràcia *et al.*, 2006).

Small to moderate-scale slides and slump structures are also common throughout the study area. These occur associated with high-gradient slopes, as, for example, in the Alboran Ridge and Yusuf Lineament, where slide scars are seen with slopes of up to 10–25º (Figure 3-6).

The main escarpments along the Alboran Ridge are the morphological expression of faults with SW–NE trend (*e.g.* Campos *et al.*, 1992). Elongated seafloor undulations sub-parallel to these escarpments correspond to associated folds. The northern slope of the Alboran Ridge (between 3.2º and 2.5ºW) corresponds to fault escarpments showing a general curved outline changing from a SW to a SE trend (Figure 3-4). Towards the west, the Alboran Ridge is affected by an oblique, deformed zone visible on the seafloor (Figure 3-4). Bathymetric data reveal an elongated, NE-SW-trending narrow zone (average trend N30°E and 2–5 km wide) characterized by escarpments and seafloor undulations, extending northwards across the Alboran Channel. This zone is at least 50 km long and merges with some of the SSW–NNE linear depressions observed on the Djibouti High.

Most of the lineaments identified on the Djibouti High correspond to linear depressions and display the two main trends (NNE–SSW and NW–SE; Figure 3-6). Based on seismic profiles (see following section), we interpret these depressions to be surface expressions of faults. The southern slope of this plateau is formed by an escarpment which has an average alignment of N65ºE but which has repeatedly been displaced by faults oriented N120°–126ºE. Some of these faults connect with some of the linear depressions seen in the plateau (Figure 3-6).

The Yusuf Lineament and Ridge shows NW-SE-oriented escarpments which are the morphological expression of a fault zone (*e.g.* Mauffret *et al.*, 1992). Fault escarpments delimit the narrow and sub-parallel Yusuf Basin.

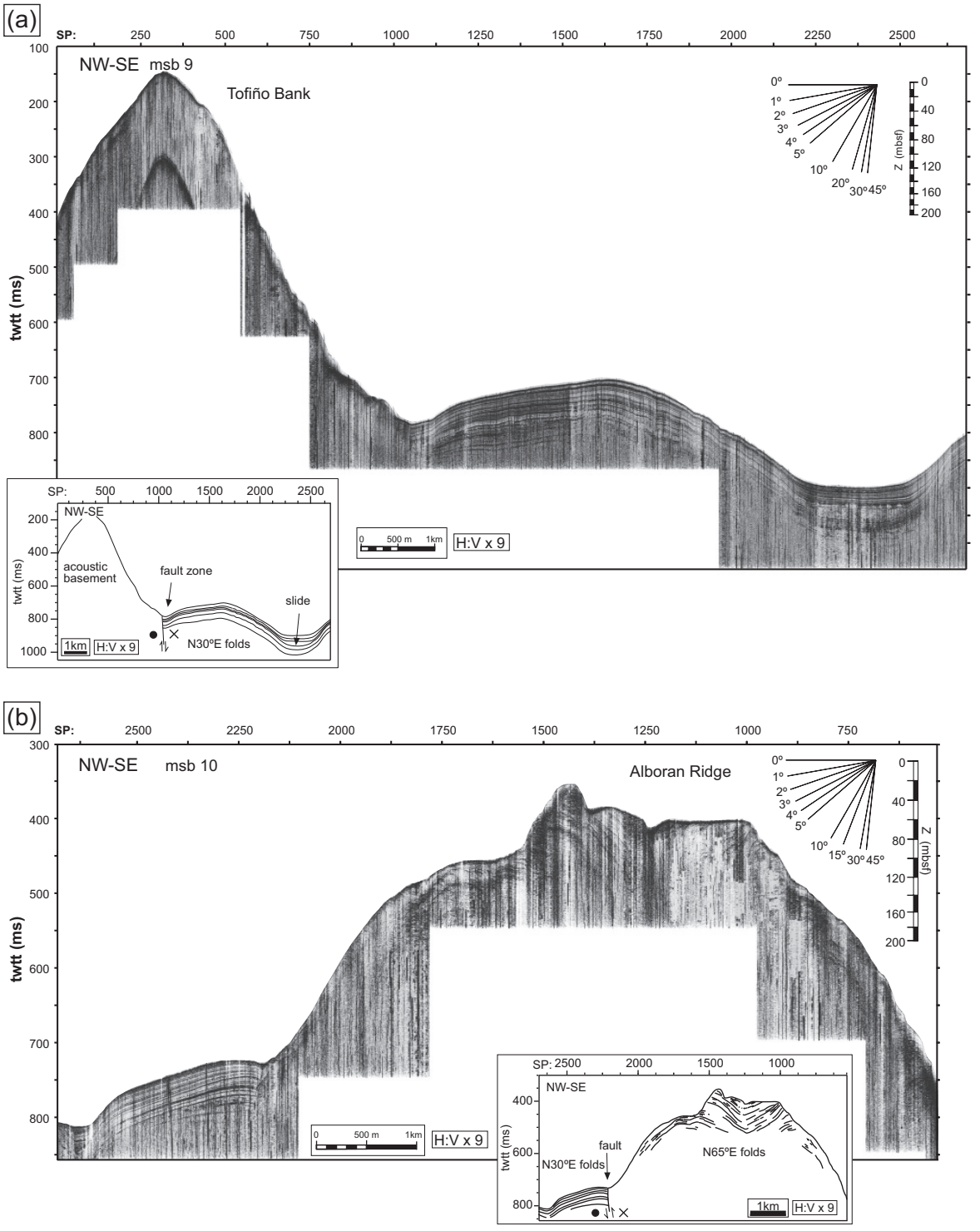

Figure 3-7. Examples of interpreted TOPAS profiles in the western sector of the Alboran Ridge, together with estimated depth scale and calculated dip abacus. Dots and crosses in the fault zones illustrate the strike-slip component of an oblique-slip fault with block motion towards and from the observer respectively: **(a)** faults and folds crosscutting the western extremity of the ridge; **(b)** faults and folds more to the east. Locations are shown in figure 3-2.

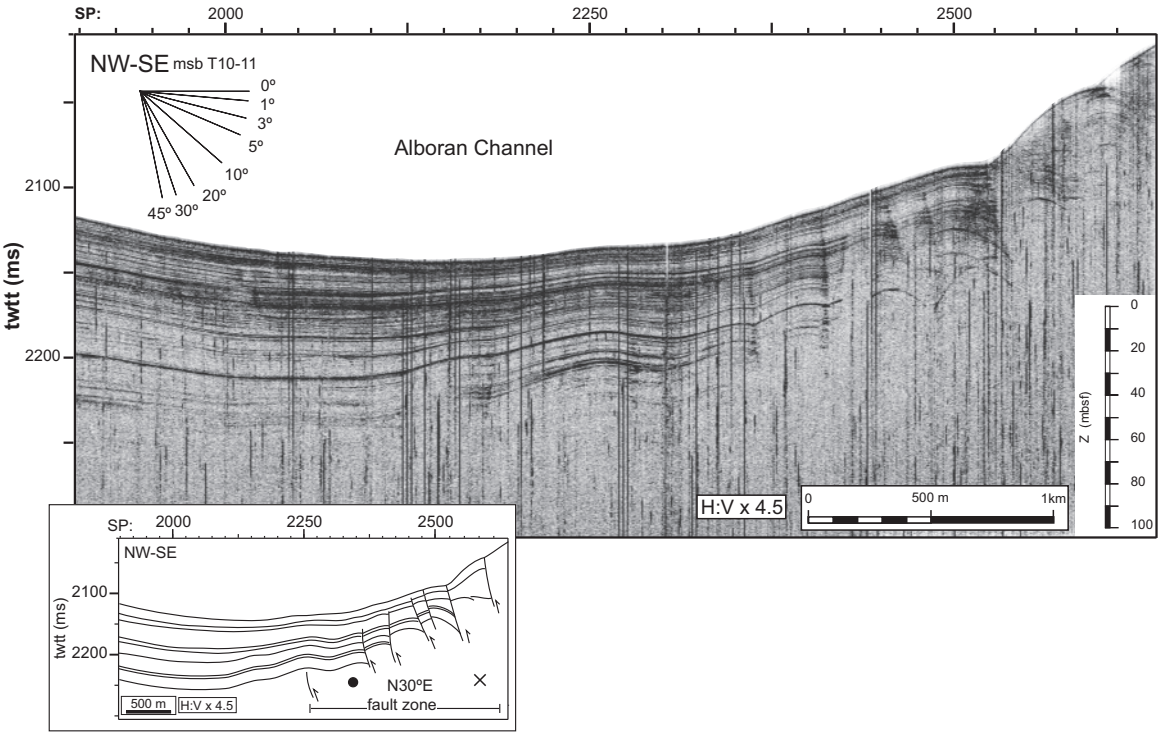

Figure 3-8. Example of interpreted TOPAS profile in the Alboran Channel, together with estimated depth scale and calculated dip abacus. Dots and crosses in the fault zones illustrate the strike-slip component of an oblique-slip fault with block motion towards and from the observer respectively. Location is shown in figure 3-2.

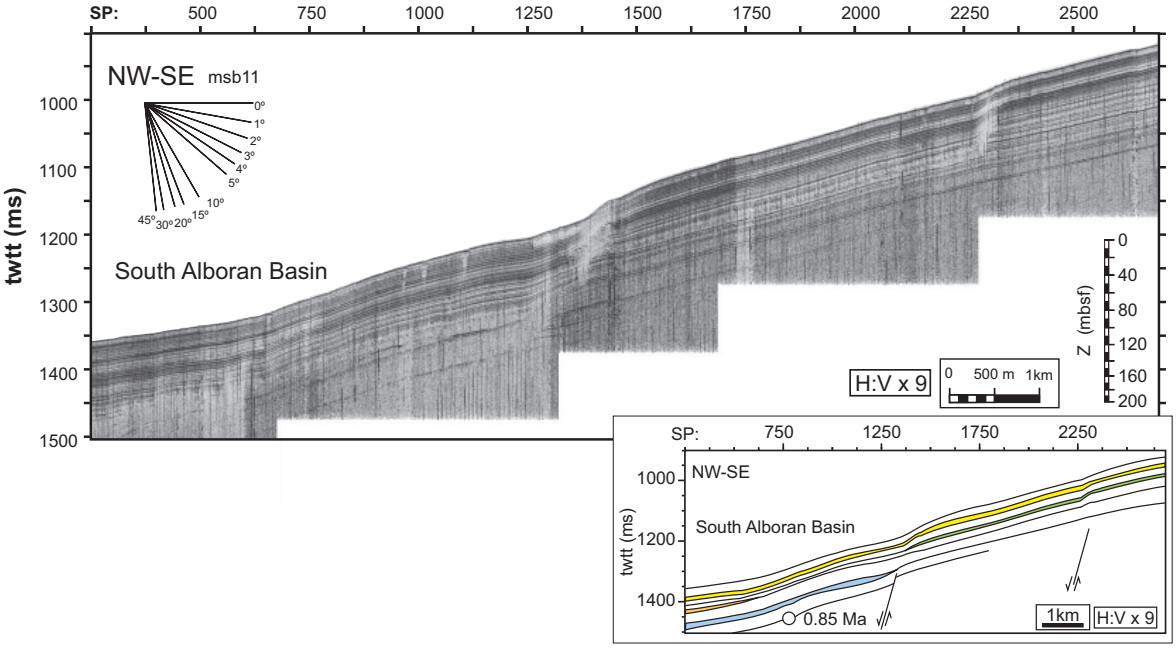

Figure 3-9. Example of interpreted TOPAS profile showing onlaps and pinch-out geometries above fault tips in the South Alboran Basin, together with estimated depth scale and calculated dip abacus. Location is shown in figure 3-2. Note the estimated age of a key seismic event obtained by correlation with ODP wells.

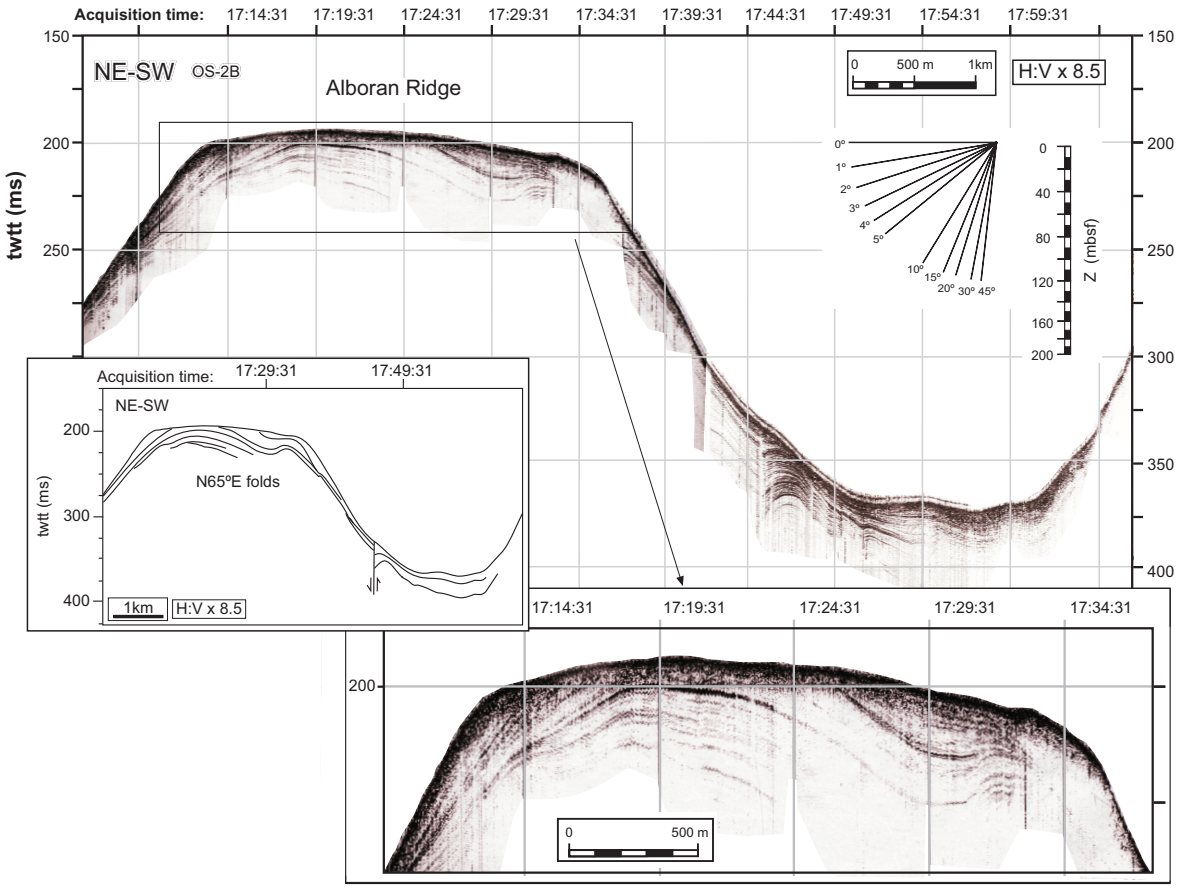

Figure 3-10. Interpreted TOPAS profile in the central sector of the Alboran Ridge showing fold structure cut by the platform of the Alboran Island, together with estimated depth scale and calculated dip abacus. Location is shown in figure 3-2.

Shallow structure

Selected TOPAS profiles shown in figures 3-7 to 3-13 illustrate the structural style of Recent faults and folds in the study area, their orientations being plotted in figure 3-14. In addition, we present a simplified structural map showing the distribution of the most recent fault-and-fold systems and their spatial relationship with seismicity (Figure 3-15).

TOPAS profiles across the central Alboran Ridge show open anticlines and synclines with low-dipping flanks (<10–12º). These structures are asymmetric, their layer dip increasing with depth, and they are cut by the seafloor surface (Figures 3-7b and 3-10). Sub-vertical faults show reverse displacement and appear associated with these folds. Fault traces and fold axes in the central and western Alboran Ridge are sub-parallel and have a N64°–65ºE average trend (Figure 3-7a, b). In the vicinity of the central Alboran Ridge, folds show a clear culmination with double-plunging hinges dipping south-westwards (at 3.2–3.4ºW) and eastwards (at 2.5–2.7ºW). The folds at the summit are cut by the abrasion platform surrounding Alboran Island (Figure 3-10). Towards the east, and at greater water depth, folds with an average trend of N92°–93ºE deform the seafloor, suggesting that such structures are active or very recent (Figure 3-11). This seismic profile across the eastern Alboran Ridge shows open anticlines displaying shoulder geometries and changing dip in their flanks. Moreover, this profile shows a recent depocentre associated with an open syncline corresponding to

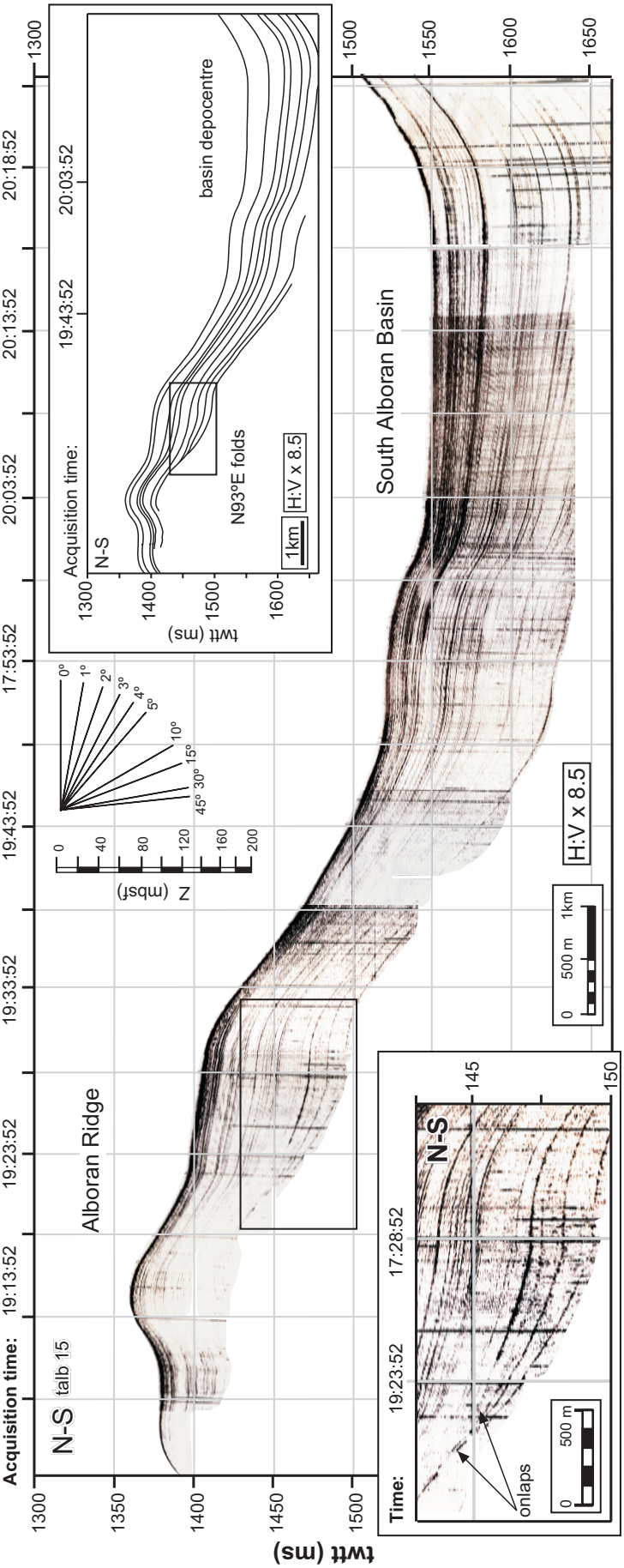

Figure 3-11. Example of interpreted TOPAS profile at the eastern extremity of the ridge showing open folds and progressive onlap geometries. Location is shown in figure 3-2.

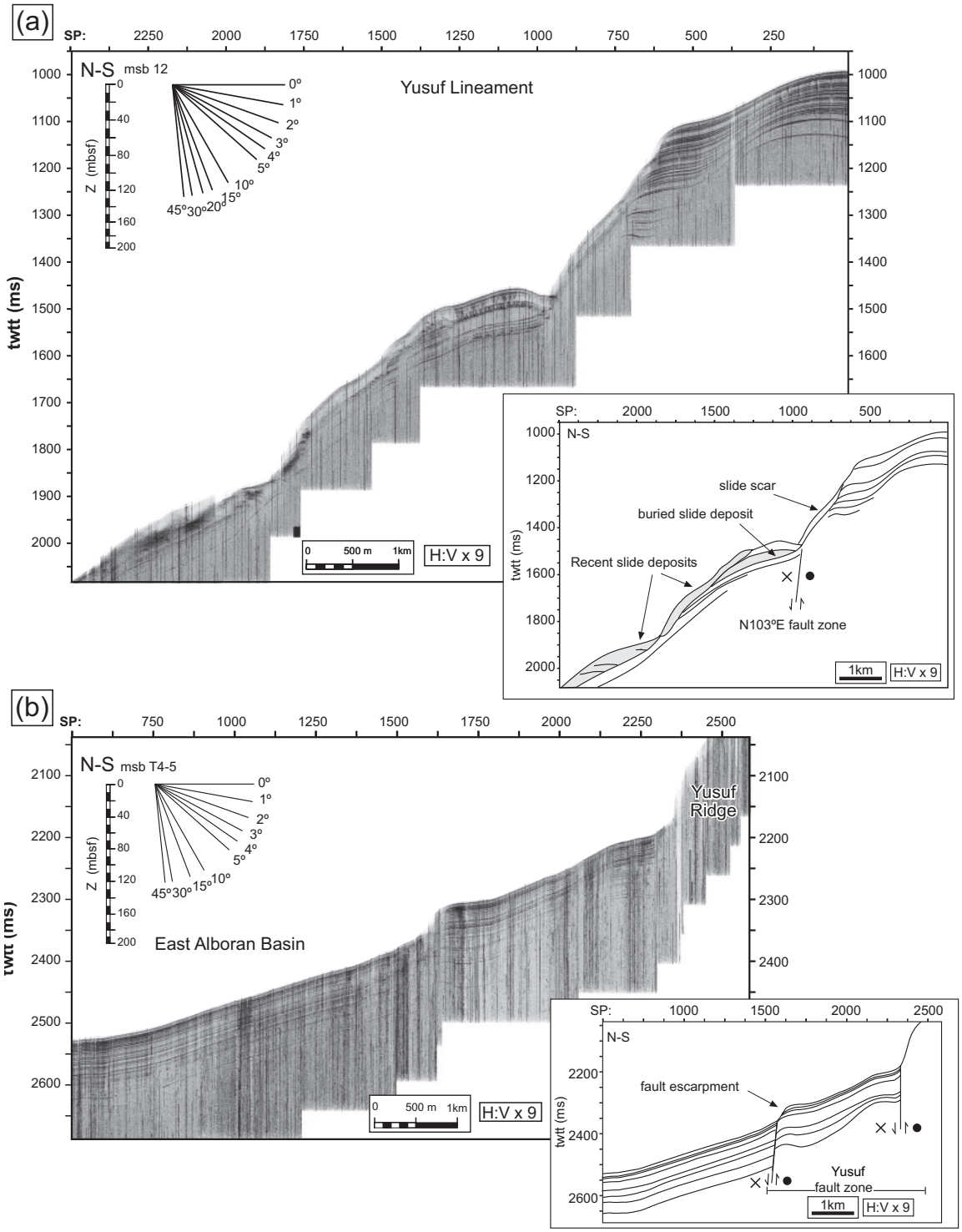

Figure 3-12. Examples of interpreted TOPAS profiles in the Yusuf Lineament, together with estimated depth scale and calculated dip abacus. Dots and crosses in the fault zones illustrate the strike-slip component of an oblique-slip fault with block motion towards and from the observer respectively: **(a)** slides related with faults; **(b)** fault escarpments in the northern slope of the Yusuf Ridge. Locations are shown in figure 3-2.

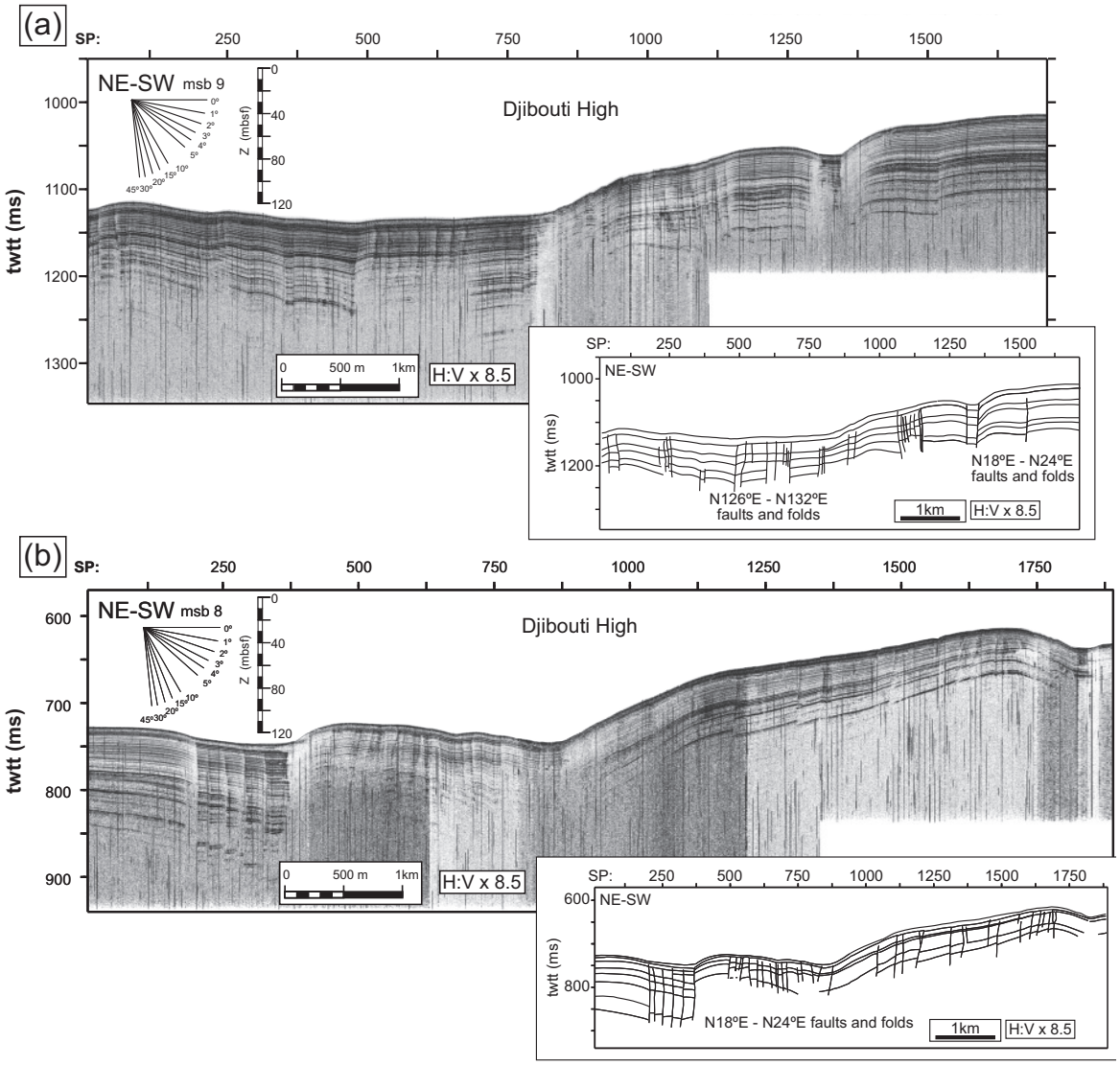

Figure 3-13. Examples of interpreted TOPAS profiles on the Djibouti High to the north of the Alboran Ridge, together with estimated depth scale and calculated dip abacus: **(a)** active faults and folds immediately east of the Djibouti Bank; **(b)** active structures close to the Djibouti Bank culmination. Locations are shown in figure 3-2.

the South Alboran Basin. Maximum thickness of the most recent sedimentary layers is found in this basin, becoming thinner towards the elevated antiform of the Alboran Ridge with conspicuous pinch-out geometries (*cf.* detail on Figure 3-11). Pinch-out geometries and onlap terminations can be observed also in the southern margin of the SAB (Figure 3-9).

In the western sector of the Alboran Ridge, the various fold-and-fault systems described above are cut obliquely by a deforming band (2–5 km) with a N24º–30ºE trend (Figure 3-14a, b). Seismic profiles across this zone reveal the presence of folds associated (at depth) with reverse faults (Figure 3-7a and 3-8), which display in-relay geometries in plan view (Figure 3-15). This fault-and-fold system separates the Alboran Ridge from the Tofiño Bank. The seismic profile shown in figure 3-7a demonstrates that the band of discrete seafloor undulation corresponds to folds which show asymmetric flanks and deform the most recent sediments. Towards the NE, the seismic section

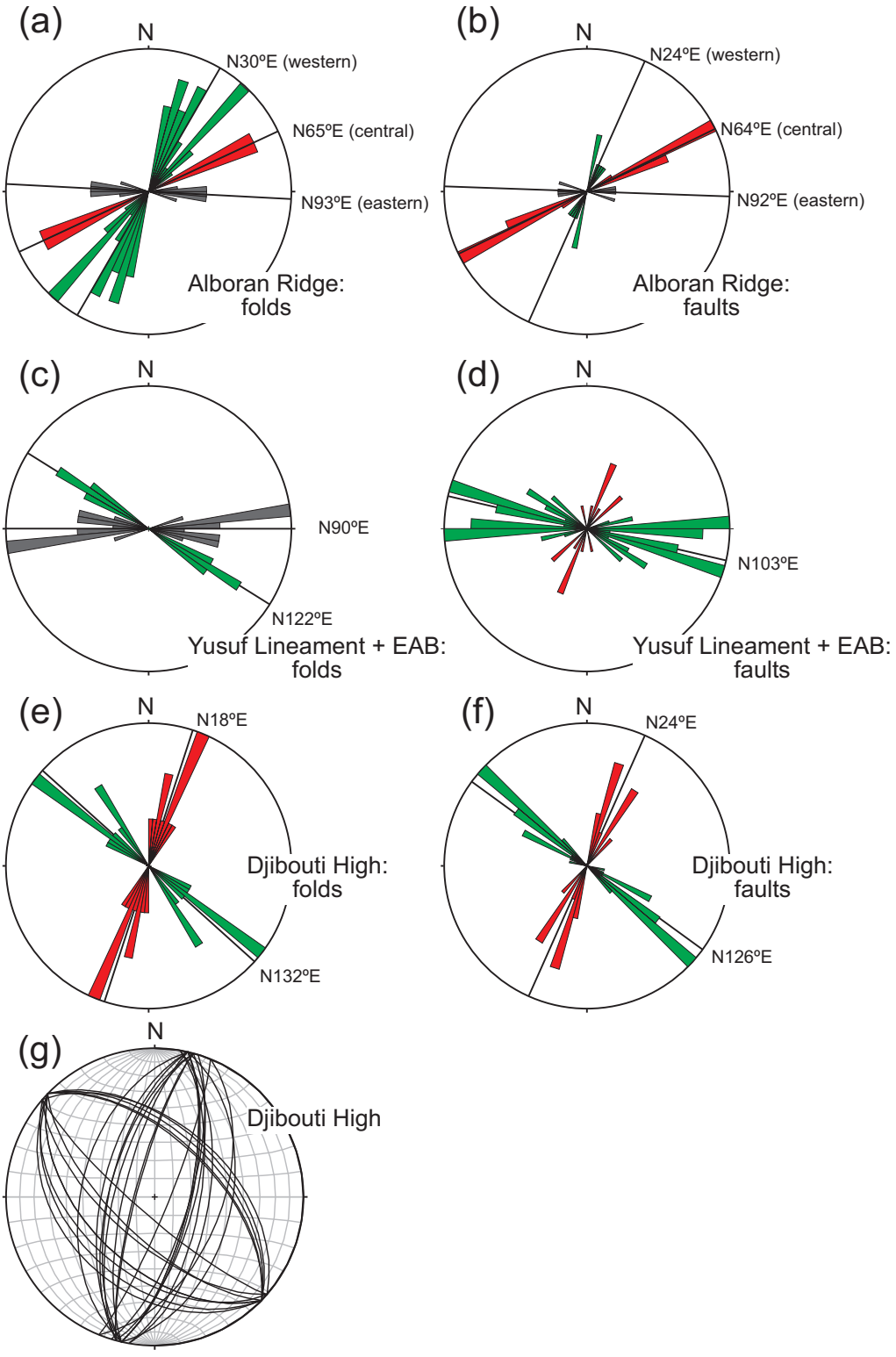

Figure 3-14. Rose diagrams showing the orientation of faults and folds on the seafloor and their average trends for individual groups at 5º resolution: **(a)** folds in the Alboran Ridge (n=41, circle=12% of measurements); **(b)** faults in the Alboran Ridge (n=19, circle=26% of measurements); **(c)** folds in the Yusuf Lineament and East Alboran Basin (EAB; n=20, circle=20% of measurements); **(d)** faults in the Yusuf Lineament and EAB (n=40, circle=15% of measurements); **(e)** folds in the Djibouti High (n=19, circle=16% of measurements); **(f)** faults in the Djibouti High (n=40, circle=20% of measurements); **(g)** synthetic stereogram representing main fault planes reconstructed for the Djibouti High (equi-areal projection, lower hemisphere).

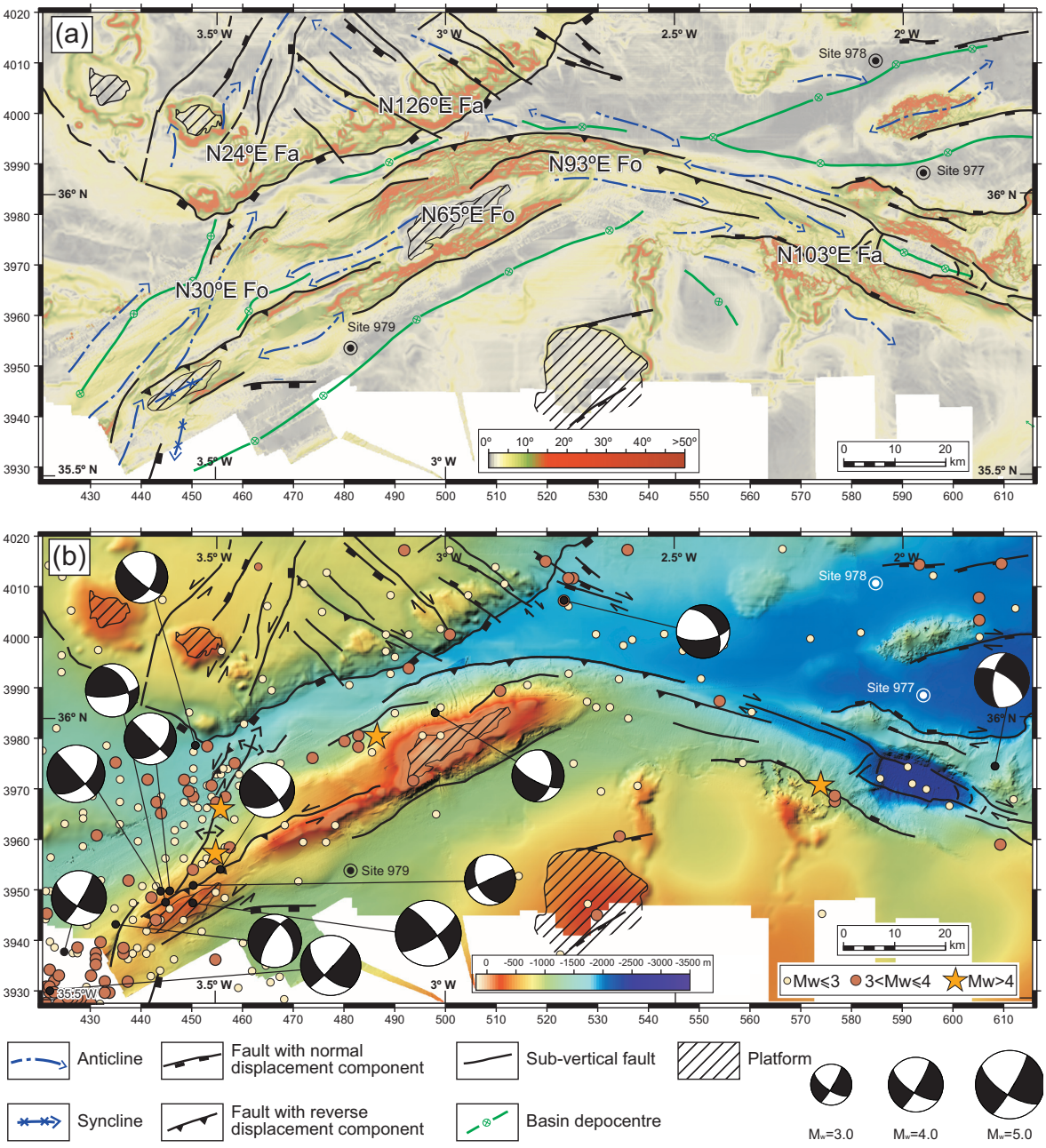

Figure 3-15. (a) Simplified structural map of the most recent structures in the central Alboran Sea, showing the general orientations of fault-and-fold systems, combined with the bathymetry. Circles represent ODP Leg 161 sites. UTM projection, units in kilometres (WGS 84 ellipsoid). Abbreviations: Fa, Faults; Fo, Folds. **(b)** Simplified uppermost crustal structure of the central Alboran Sea, and distribution of shallow seismicity (≤11 km) for the period 1979–2006 (extracted from the USGS catalogue) combined with the bathymetry. Focal mechanisms (moment tensor inversion) are shown for 13 events (lower hemisphere, equal-area projection, dilatational quadrant in white; extracted from Stich *et al.*, 2003a).

of figure 3-8 reveals a buried zone of deformation with a minimum width of 2.5 km. Asymmetric folds here are clearly associated with high-angle (>45º) reverse faults. The different fault planes affect progressively younger sediments to the SE, thus revealing a back-stepping fault-and-fold sequence. Along this fault-and-fold zone (N30ºE) fold culminations vary in height, showing structural saddles and plunging terminations, and most of the anticlines display a general immersion towards the north.

The Yusuf Lineament corresponds to a sub-vertical fault zone including different fault segments in relay (N103ºE trend; Figure 3-14d) accommodated by en-echelon folds (average trend N122ºE; Figure 3-14c). These faults extend south-eastwards where they bound the Yusuf Ridge and Basin (Figure 3-14). The seismic profiles show faults affecting present-day sediments and the seafloor. Relative displacements in these fault segments show a normal slip component (Figure 3-12). Slides and slump structures are common also along the Yusuf Lineament. Figure 3-12a is a profile across this lineament and shows slide scars and outcropping and sub-outcropping slide sediments with chaotic to semi-transparent facies, which can be related to fault escarpments and Recent faulting pulses.

High-resolution seismic profiles across the Djibouti High demonstrate that most of the linear depressions correspond to high-angle fault planes (Figure 3-13). In plan view these faults display two main trends (average orientations N18ºE and N132°E) and represent two fault systems with associated sub-parallel folds (Figure 3-14e, f). Some of the fault planes change dip direction along the vertical section, showing both reverse and normal displacements (Figure 3-13). Using the fault trace measured on the seafloor and the fault apparent dip estimated in the TOPAS profiles, we reconstructed the real fault dip in figure 3-14g. The Djibouti High thus has two systems with average N18ºE and N132°E orientations and dipping 50–60º, which may correspond to conjugate fault systems with sub-parallel associated folds.

3.4 Discussion and conclusions

Our results confirm that Recent deformation in the central Alboran Sea is widespread, heterogeneously distributed and characterized by different structural styles. Recent tectonic activity is the main controlling factor in the present-day geomorphology of the central Alboran Sea, although sedimentary and erosive processes should also be taken into account.

Influence of sedimentary processes on seafloor morphology

The networks of gullies and discrete canyons identified along the slopes of the Alboran Ridge and the Yusuf Lineament are the main erosive features in the region. Comparable networks have been described, for example, on the Almería margin by Alonso and Ercilla (2003), García *et al.* (2006) and Gràcia *et al.* (2006). Networks of gullies and discrete canyons are conditioned by tectonic processes. Fault zones along the Alboran Ridge, Djibouti High and Yusuf region produce linear escarpments on the seafloor with abrupt slopes eroded by gullies. Most of these erosive features follow the main slope of the escarpments, although deflected paths are visible in some gullies (for example, on the northern slope of the Alboran Ridge; Figure 3-6). Deflected paths of gullies occur along fault traces. Such gully deflections are linked to fault zones associated with friable lithologies.

Successions of slide scars exist along the Yusuf Lineament and along the slopes of the Alboran Ridge. We interpret that most of the slides and mass-wasting structures (Figure 3-6) probably derive from unstable seafloor escarpments. The slides are commonly located along fault escarpments and many are Recent deposits, as they are not draped by hemipelagic sediments (*e.g.* Figure 3-12a).

In addition, many of the shallow platforms developed on top of shallower reliefs (*e.g.* Alboran Ridge, Herradura Bank and Djibouti Bank) are probably related to the effects of waves, shallow oceanic currents and erosion during Quaternary sea-level lowstands (*e.g.* Heburn and La Violette, 1990; Lobo *et al.*, 2008). The existence of a shallow platform at the top of the Alboran Ridge was previously reported by Bárcenas *et al.* (2004) and Maestro-González *et al.* (2008). High-resolution seismic profiles reveal a thin, reflective layer (<10 m) crosscutting previous structures (*e.g.* Figure 3-10), which may correspond to a carbonate crust associated with an abrasion platform. This is certainly the case for most of the shallow platforms found along the Alboran Ridge, which resemble the carbonate incrustations described for the Cabo de Gata promontory and the Chella Bank by Gràcia *et al.* (2006), Ballesteros *et al.* (2008) and Lo Iacono *et al.* (2008). Some of these seamounts are surrounded by moats, probably resulting from sea-bottom currents similar to those described by Ballesteros *et al.* (2008) in the vicinity of the Chella Bank.

Active tectonic stuctures

According to chronostratigraphic determinations at sites 977 to 979 (Siesser and de Kaenel, 1999; de Kaenel *et al.*, 1999), the estimated maximum penetration of the TOPAS profiles (~170–180 m) corresponds to sediments of about 0.8–1.1 Ma, i.e. mid to late Pleistocene. The structures identified deforming the seafloor can therefore be considered as active structures, and the faults and folds controlling the submarine physiography may represent structures with a potential seismic hazard. Hypocentre distribution, magnitude, and focal mechanisms enable us to assess the position and nature of those active fault segments.

Most of the shallow seismicity in our study area is concentrated in the western part of the Alboran Ridge, related to the fault-and-fold zone (trending N30ºE) depicted in figure 3-15 and connecting with a seismic swarm located at about 35.3ºN and 4ºW. This seismic swarm corresponds to the Al Hoceima seismic series to the south (Biggs *et al.*, 2006). Focal mechanisms in this sector correspond to left-lateral, strike-slip to reverse faulting. We identify that focal mechanisms along the Alboran Ridge coincide with the outlined trace of a reverse fault in figure 3-15. This fault has been identified in high-resolution seismic profiles (*e.g.* Figure 3-7b) and has a N65ºE trend, occurring along the SW culmination of the Alboran Ridge.

Seismicity in the central and eastern Alboran Ridge is widespread, but a few moderate magnitude earthquakes are concentrated near mapped faults between 2.25ºW and 2.35ºW. The single focal mechanism available here indicates normal faulting with a strike-slip component, but nodal fault planes (N10ºE and N100ºE) are clearly oblique to the fault traces observed in the uppermost sedimentary sequence (N65ºE).

In the Yusuf Lineament seismicity is scarce, occurring partially along the main faults identified here (Figure 3-15b). Moreover, some low-magnitude earthquakes (M_w<3) in the Yusuf Basin clearly show that some of the bounding faults are active at present (Figure 3-15b). The single focal mechanism available for the Yusuf Ridge reveals right-lateral, transtensive deformation, for faults trending NW–SE. This kinematics is coherent with normal displacements observed along active faults observed in this zone from high-resolution seismic profiles (Figure 3-12). These observations

support previous interpretations (*e.g.* Mauffret *et al.*, 1992; Alvarez-Marrón, 1999; Comas *et al.*, 1999; Fernández-Ibáñez *et al.*, 2007) of the Yusuf Lineament as a fault structure with right-lateral, transtensive deformation.

Shallow seismicity in the Djibouti High is scattered with low to moderate magnitude events (Figure 3-15b). Only a single focal mechanism is available here, at about 3.5ºW, and coincides with the southern slope of the plateau. It occurs in a position where the general N65ºE trend of the escarpment turns to NW–SE orientation. This focal mechanism is coherent with right-lateral, strike-slip faulting along a sub-vertical fault trending N130ºE. This orientation is sub-parallel to other faults seen as linear depressions in the plateau (Figure 3-15).

The southern slope of the Djibouti High corresponds to a fault zone trending SW–NE which is coincident with a seamount lineation of confirmed Miocene volcanic rocks and some metamorphic basement outcrops (*e.g.* Ballesteros *et al.*, 2008). The SW–NE escarpment of this plateau is clearly displaced by NW–SE high-angle faults, similar to the interpretation of Ballesteros *et al.* (2008). The westernmost fault of this system could be seismically active, and the available focal mechanism here (depth <11 km) reflects a right-lateral fault. The Djibouti High itself is affected by two conjugate fault systems with NNE–SSW and NW–SE orientations. Since no focal mechanism exists in this case, the fault kinematics of these two fault systems remains speculative. Nevertheless, the displacements observed indicate a right-lateral, strike-slip component for the NW–SE fault system. We suggest that they correspond to conjugate strike-slip fault systems (Figure 3-16), with a fault kinematics in agreement with the neighbouring Adra seismic swarm (Stich *et al.*, 2003b). This interpretation is consistent with the present-day plate convergence and the associated regional stress field, oriented NW–SE (*e.g.* Fernández-Ibáñez *et al.*, 2007).

The signature of the Carboneras Fault (*e.g.* Gràcia *et al.*, 2006; Reicherter and Hübscher, 2007) on the seafloor extends south-westwards to the Djibouti High in the area of the Adra seismic swarm (Stich *et al.*, 2001). Whether there is any relationship between the two fault systems on the Djibouti High and the Carboneras Fault is not clear from our data and deserves further studies.

Previous studies have established that the most recent tectonic evolution of the Alboran Basin is controlled by two conjugate strike-slip fault systems which connect with the structures identified on land in the Betics and Rif (Figure 3-16; Woodside and Maldonado, 1992; Maldonado *et al.*, 1992; Fernández-Ibáñez *et al.*, 2007). One of these systems is formed by NE–SW to NNE–SSW left-lateral transpressive faults, including the Jebha and Nekor faults in the Rif, the fault zones along the Alboran Ridge, and the Carboneras Fault and the N-S-striking Palomares Fault in the eastern Betics. The conjugate system is a WNW–ESE right-lateral transtensive fault system which includes fault zones shaping the Yusuf Basin and Ridge. Some fault segments of these conjugate structures have been reported as active faults during the Quaternary (*e.g.* de Larouzière *et al.*, 1988; Masana *et al.*, 2004; Gràcia *et al.*, 2006; Reicherter and Hübscher, 2007; Fernández-Ibáñez *et al.*, 2007).

The linear shape of the Alboran Ridge is controlled by active faults and folds which deform the seafloor (Figure 3-15). Using multichannel and single-channel seismic profiles, different authors have traditionally described the existence of a fault zone with a probable left-lateral strike motion along the Alboran Ridge (*e.g.* Woodside and Maldonado, 1992; Bourgois *et al.*, 1992; Campos *et al.*, 1992;

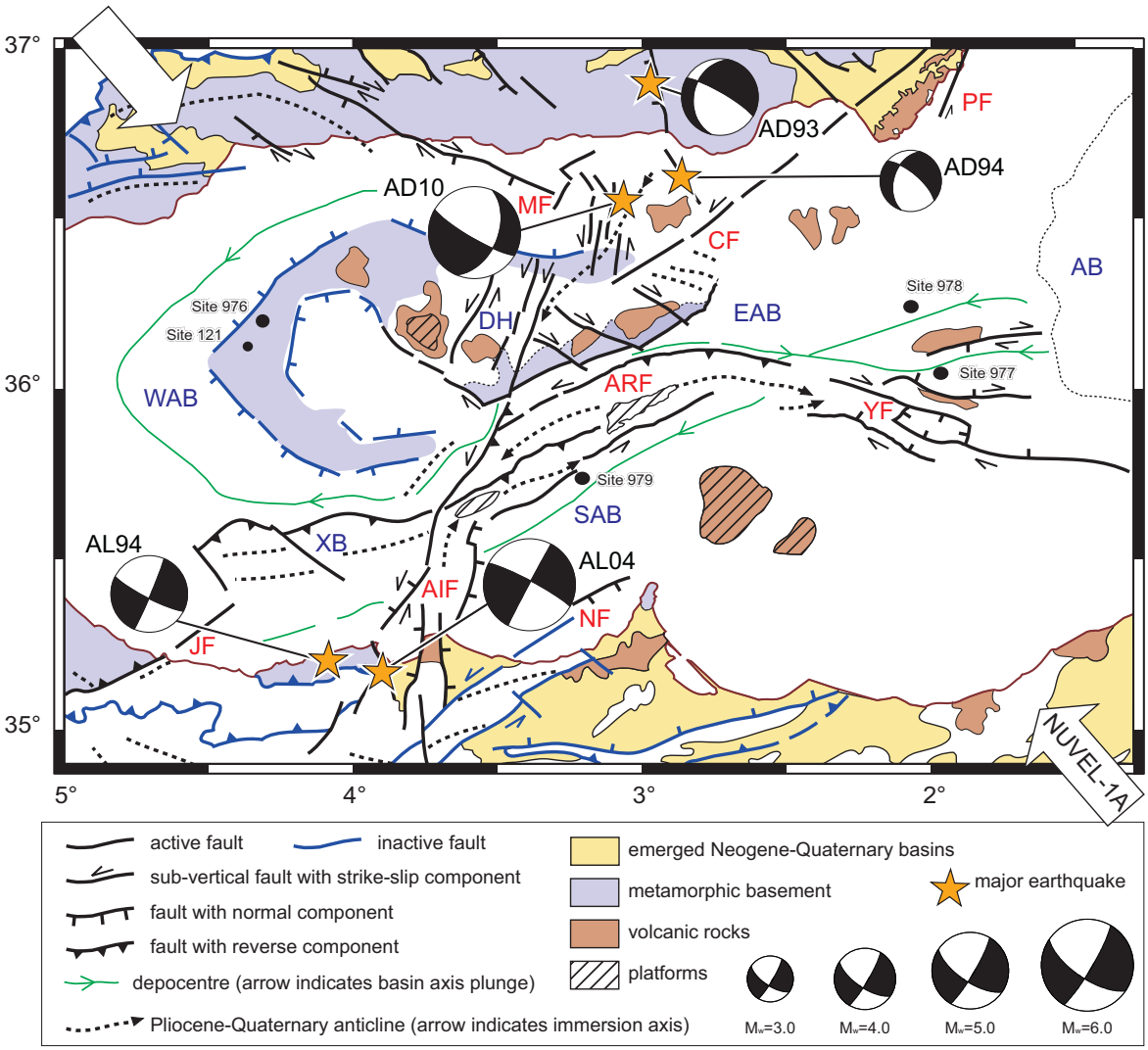

Figure 3-16. Structural map of the Alboran Sea Basin and surrounding areas showing Recent structures and main sedimentary depocentres (simplified), based on own interpretation and complementary data sources: Maldonado *et al.* (1992), Mauffret *et al.* (1992), Medina (1995), Galindo-Zaldívar *et al.* (1997), López Garrido and Sanz de Galdeano (2000); Alfaro *et al.* (2001); Sanz de Galdeano *et al.* (2001), Aït Brahim *et al.* (2002), Soto and Manzano (2002), Booth-Rea *et al.* (2003), Reicherter *et al.* (2003), Schoorl and Veldkamp (2003); Guerra-Merchán *et al.* (2004), Benmakhlouf *et al.* (2005), Gràcia *et al.* (2006), Ammar *et al.* (2007), Ballesteros *et al.* (2008), Chalouan *et al.* (2008) and Galindo-Zaldívar *et al.* (2009). Black dots represent ODP Leg 161 sites. Large arrows indicate trend of plate convergence according to NUVEL-1A model (DeMets *et al.*, 1994). Major earthquakes and focal mechanisms associated with the Adra and Al Hoceima seismic swarms (Stich *et al.*, 2001, 2003b; Biggs *et al.*, 2006) are plotted: AD10 Adra 1910/6/16, AD93 Adra 1993/12/23, AD94 Adra 1994/1/4, AL94 Al Hoceima 1994/5/26, AL04 Al Hoceima 2004/2/24. Abbreviations: AB, Algerian Basin; AIF, Al Idrisi fault zone; ARF, Alboran Ridge fault zone; CF, Carboneras Fault; DP, Djibouti High; EAB, East Alboran Basin; JF, Jebha Fault; MF, Maro-Nerja Fault; NF, Nekor Fault; PF, Palomares Fault; SAB, South Alboran Basin; WAB, West Alboran Basin; XB, Xauen Bank; YF, Yusuf fault zone. Offshore metamorphic and volcanic rocks are outcropping or sub-outcropping.

Comas *et al.*, 1992, 1999; Maldonado *et al.*, 1992; Mauffret *et al.*, 1992; Watts *et al.*, 1993; Chalouan *et al.*, 1997; Estrada *et al.*, 1997; Willet, 1997). Our results reveal that both flanks of the Alboran Ridge correspond to steep slopes with linear and curved outlines. We have recognized that shallow structures along the western Alboran Ridge are open, ENE folds and parallel, high-angle faults. Fault kinematics deduced from focal mechanisms in this sector of the Alboran Ridge corresponds to left-lateral, strike-slip to reverse faults (Figures 3-15 and 3-16). These results support previous interpretations of the Alboran Ridge as a left-lateral, strike-slip fault zone. Our analysis reveals that this bathymetric high corresponds to a long (~130 km) curved fault zone varying in width from 8 to 22 km. The orientation of this structure changes progressively from SW–NE (west of Alboran Island) to WNW–ESE (at 2.5ºW), and ultimately connects with the Yusuf fault zone towards the east. The northern escarpment of the ridge (between 2.5º and 3.1ºW) is an arcuate front corresponding to a south-dipping reverse fault. In addition, fold axes plunge towards the SW and ENE on both sides of the shallow platform surrounding Alboran Island (Figure 3-16). These observations collectively suggest that the Alboran Ridge has experienced Recent uplift and was mainly controlled by left-lateral strike-slip faults with a reverse component. On the other hand, the Quaternary depocentre of the South Alboran Basin shows sedimentary layers that become thinner towards the Alboran Ridge and comprise pinch-out geometries on their flanks (Figure 3-11), demonstrating a Recent and synsedimentary uplift of the Alboran Ridge.

In the western sector, the Alboran Ridge is cut by an oblique, narrow (2–5 km wide) fault-and-fold zone (trending N30ºE) which continues northwards to the Djibouti Bank (Figure 3-16). This deformed zone consists of surficial folds and some active reverse faults (Figure 3-8). This fault zone is certainly a younger structure than the folds and faults along the Alboran Ridge (trending N65ºE).

Based on these findings, we interpret that there have been two contrasting Recent folding and faulting episodes. The older structure is observed along the core of the Alboran Ridge, gradually changing in orientation from SW–NE to W–E and finally NW–SE in the Yusuf Lineament. The structural culmination of this fold structure is being eroded on the abrasion platform developed around Alboran Island. The younger, narrow fault zone trending N30ºE crosscuts the western sector of the Alboran Ridge and extends northwards, connecting with the parallel fault group on the Djibouti High (Figure 3-16). Surficial folds along this fault zone are interpreted as the shallow termination of a deeper, blind fault. Seismicity suggests that faulting in the uppermost crust occurred through left-lateral faults with a reverse component. This fault zone connects southwards with the Al Idrissi fault zone depicted by Ammar *et al.* (2007). This fault zone represents the offshore continuation of the N-S-trending normal faults (Medina, 1995; Aït Brahim *et al.*, 2002; Galindo-Zaldívar *et al.*, 2009) observed close to the Al Hoceima seismic swarm (major earthquake in 1994, M_w=5.9 and 2004, M_w=6.5; Biggs *et al.*, 2006). Focal mechanisms in this area confirm that active NNE–SSW faults have a left-lateral, strike-slip component (Figure 3-16).

The Jebha Fault in the Rif has a SW–NE trend, parallel to the Alboran Ridge fault zone (Figure 3-16). According to Chalouan *et al.* (2008), this fault is NW dipping and shows a reverse component. The most recent activity of the Jebha Fault in the onshore region has been analyzed by Benmakhlouf *et al.* (2005), who found evidence of both a left- and a right-lateral motion of this structure along a high-angle fault dipping to the NW. Thus, we propose that the identified N30ºE

narrow fault zone represents a transform fault transferring reverse faulting between the Alboran Ridge fault zone and the Recent structures forming the Xauen Bank and Jebha Fault.

Using the scarce geodetic data available, the actual pattern of deformation in the region can be inferred as moderate (4.5 mm/yr), NW–SE convergence between the Eurasian and African plates. Recent local GPS observations in the western Betics and Rif suggest a lateral motion of the western Gibraltar Arc towards the W and SW (Fadil *et al.*, 2006). Both the Alboran Ridge fault zone and the Al Idrisi fault zone represent active strike-slip, left-lateral fault zones which partition the present-day plate convergence and conduct lateral escape of the Gibraltar Arc towards the southwest (*e.g.* Maldonado *et al.*, 1992; Fernández-Ibáñez *et al.*, 2007).

Our results reveal that previously described fault zones in the central Alboran Sea (Alboran Ridge and Yusuf fault zones) are connected and comprise a wide zone of deformation with scattered associated seismicity. These fault zones have a complex geometry characterized by different active fault segments and in-relay folds. Moreover, our results reveal the existence of previously unknown oblique structures in the central sector of the Alboran Sea, notably on the Djibouti High and crosscutting the western sector of the Alboran Ridge. This seismically active fault zone trending N30ºE is the youngest structure in the region and represents a seismic hazard zone connected to the south with the Al Hoceima seismic swarm.

4. Plio-Quaternary stratigraphy and tectonic evolution

Strike-slip tectonics and basin inversion in the Western Mediterranean: the Post-Messinian evolution of the Alboran Sea

*Accepted in **Basin Research** (Submitted on 10 December 2011).*

Pedro Martínez-García[1], Menchu Comas[1], Juan I. Soto[2], Lidia Lonergan[3] and Anthony B. Watts[4]

[1] Instituto Andaluz de Ciencias de la Tierra (CSIC and University of Granada), Facultad de Ciencias,

[2] Instituto Andaluz de Ciencias de la Tierra (CSIC and University of Granada) and Departamento de Geodinámica, Facultad de Ciencias, Granada, Spain.

[3] Department of Earth Science and Engineering (Imperial College London), South Kensington Campus, London, United Kingdom.

[4] Department of Earth Sciences, University of Oxford, Oxford. United Kingdom.

Abstract

A comprehensive sediment thickness dataset consisting of single and multichannel seismic profiles integrated with bio-stratigraphic and log information from nearby DSDP and ODP wells have been used to constrain the Late Miocene to Quaternary basin evolution of the central part of the Alboran Sea Basin. We find that deformation is heterogeneously distributed in space and time and that three major shortening phases have affected the basin as a result of continuing convergence between the Eurasian and African plates. During the Messinian salinity crisis, intense erosion and local subsidence resulted in small, isolated, basins with shallow marine and lacustrine sedimentation. The first shortening event occurred during the Early Pliocene (~5.33 to 4.57 Ma) along the Alboran Ridge. This was followed by a major transgression widening the basin and increasing sediment accumulation rates. The second and main phase of shortening on the Alboran Ridge took place during the Late Pliocene (~3.28 to 2.59 Ma) as a result of thrusting and folding which was accompanied by a rotation of the Eurasian/African plate convergence vector from NW-SE to WNW-ESE. This phase also caused uplift of the southern basins and right-lateral transtension along the WNW-ENE Yusuf fault zone. Deformation along the Yusuf and Alboran ridges continued during the early Pleistocene (~1.81 to 1.19 Ma) and the NNE-SSW trending Al-Idrisi strike-slip fault appears to be active at the present day. The Alboran Sea Basin is a region of complex interplay between sediment supply from the surrounding Betic and Rif mountains, and tectonics in a zone of transpression between the converging African and European plates. The inherited basin geometry from pre-Messinian time has resulted in a partitioning of the subsequent deformation and the resulting subsidence and uplift in the Pliocene to recent basin.

Keywords: strike-slip tectonics, inversion, transpression, Messinian salinity crisis, basin analysis, Alboran Ridge, Yusuf Basin, Alboran Sea

4.1 Introduction

The Alboran Sea is one of a number of basins in the Mediterranean Sea that formed during the Neogene within a region of convergence between the African and Eurasian plates. These basins, which include the Alboran Sea, the Pannonian Basin and Tyrrenhian Sea, are located at the centre of the curved Alpine orogenic arcs (Horvath and Berckhemer, 1982). Basin subsidence initiated about 25-30 Ma by orogenic collapse, accompanied by thinning and heating of the lithosphere (*e.g.* Platt and Vissers, 1989; Jolivet and Faccenna, 2000; Faccenna *et al.*, 2004). During Late Miocene to Recent times, these basins were subject to varying degrees of shortening (*e.g.* Comas *et al.*, 1999; Cloetingh *et al.*, 2008; Strzerzynski, *et al.*, 2010).

Whilst the early extensional history of the Alboran Sea has been extensively studied because of its significance for models of orogenic collapse (Comas *et al.*, 1992, 1999; García-Dueñas *et al.*, 1992; Watts *et al.*, 1993; Chalouan *et al.*, 1997; Mauffret *et al.*, 2007), the post-extensional history has received much less attention. Since the Early Pliocene, for example, the Alboran Sea Basin underwent tectonic inversion with the development of strike-slip and reverse faults, folds and uplift of the basin margins (e.g. Bourgois *et al.*, 1992; Campos *et al.*, 1992; Maldonado *et al.*, 1992; Woodside and Maldonado, 1992; Ballesteros *et al.*, 2008; Fernández-Ibáñez and Soto, 2008; Martínez-García *et al*., 2011).

In this paper, we use an extensive database of seismic reflection profiles correlated with DSDP and ODP biostratigraphic data (Leg 13 and Leg 161; Ryan *et al.*, 1973; Comas *et al.*, 1996; de Kaenel *et al.*, 1999; Siesser and de Kaenel, 1999) to: (1) document the geometry of the Plio-Quaternary sedimentary infill by mapping the main seismic units and related unconformities; (2) calculate the changes in sediment accumulation rates during the Plio-Quaternary to describe the location and magnitude of uplift and subsidence in the different basin domains; and (3) determine the geometry, position and kinematics of the post-Messinian deformation structures.

4.2 Regional setting and background

The Gibraltar Arc System is a strongly arcuate Alpine orogen in the western Mediterranean. It comprises the Betic and Rif mountains and a deep sedimentary basin, the Alboran Sea Basin that developed within the orogenic belt (Figure 4-1). This system was formed during the Early Miocene by westward migration of the mountain belt and coeval extension in a context of NW-SE convergence between the African and Eurasian plates (*e.g.* Platt and Vissers 1989; García-Dueñas *et al.*, 1992; Watts *et al.*, 1993; Lonergan and White, 1997; Comas *et al.*, 1999; Jolivet and Faccenna, 2000). Miocene extension was accompanied by several volcanic episodes (*e.g.* Duggen *et al.*, 2004; Gill *et al.*, 2004). Extinct volcanic edifices and intrusions form most of the bathymetric highs in the Alboran Sea. In the Alboran Ridge in particular, the volcanism dates from 9.4 to 9.3 Ma, indicating that part of this high was an active volcanic edifice during the Late Miocene (Fernández-Soler *et al.*, 2000; Duggen *et al.*, 2004).

The Alboran Sea Basin is generally considered to have formed by crustal thinning and heating and cooling of the lithosphere following an Early-to-Late Miocene rifting event (Comas *et al.*, 1992,

1999; Docherty and Banda, 1992, 1995; Watts *et al.*, 1993; Chalouan *et al.*, 1997; Platt *et al.*, 1998; Jolivet *et al.*, 2006). Later shortening caused partial basin inversion through folding and reverse and strike-slip faulting in both NE-SW and NNE-SSW orientations. These structures have been active throughout the Plio-Quaternary, producing shortening of the whole region and are responsible for the coeval uplift of the basin margins and the present-day seafloor morphology (Bourgois *et al.*, 1992;

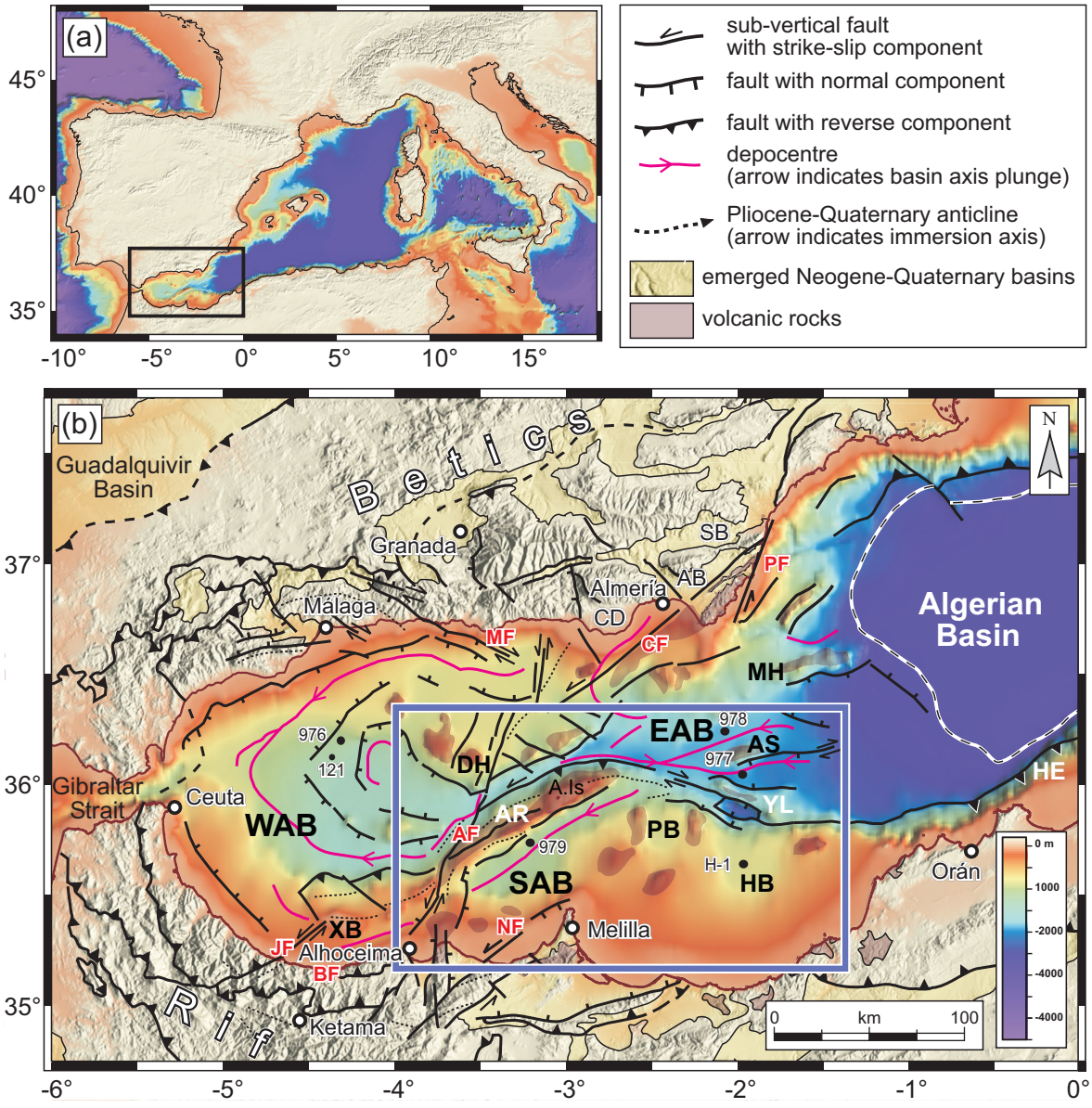

Figure 4-1. (a) Topographic map of the western Mediterranean region with study area. **(b)** Topography and tectonic map of the Gibraltar Arc System (modified from Comas et al., 1999 and Martínez-García et al., 2011). Digital topography is based on the SRTM (USGS-NASA) global database combined with GEBCO 97 (IOC-IHO) for the offshore region. Blue box is study area in the central part of the Alboran Sea. Black dots are ODP sites (976 to 979), DSDP Site 121 and Habibas-1 well (H-1). Abbreviations: A. Is, Alboran Island; AB, Almería-Níjar Basin; AF, Al-Idrisi Fault; AR, Alboran Ridge; AS, Al-Mansour Seamount; BF, North Bokkoya Fault; CD, Campo de Dalías; CF, Carboneras Fault; DH, Djibouti High; EAB, East Alboran Basin; HB, Habibas Basin; HE, Habibas Escarpment; JF, Jebha Fault; MF, Maro-Nerja Fault; MH, Maimonides High; NF, Nekor Fault; PB, Pytheas Basin; PF, Palomares Fault; SAB, South Alboran Basin; SB, Sorbas Basin; XB, Xauen Bank; YL, Yusuf Lineament and WAB, West Alboran Basin.

Maldonado *et al.*, 1992; Woodside and Maldonado, 1992; Álvarez-Marrón, 1999; Mauffret *et al.*, 2007; Fernández-Ibáñez *et al.*, 2007; Fernández-Ibáñez and Soto, 2008).

The Miocene sedimentary sequence of the Alboran Sea Basin is similar to that found in the onshore basins of the Betic and Rif mountains, suggesting that the basin was wider during the Miocene than it is at present (*e.g.* Comas *et al.* 1992; Jurado and Comas, 1992; Rodríguez-Fernández and Sanz de Galdeano, 1992, 2006; Chalouan *et al.*, 1997). The isolation of the onshore basins from the Alboran Sea Basin has been documented to occur after the Early Pliocene (Sanz de Galdeano and Vera, 1992; Braga *et al.*, 2003). In contrast to the terrestrial deposits found in the onshore basins, the whole Plio-Quaternary sequence of the basin is composed of marine sediments with hemipelagic marls, muddy turbidites and rare sandy-silty turbidites (Alonso *et al.*, 1999). These deposits overlie a Messinian sequence consisting of fine-grained marine siliciclastic sediments and shallow carbonates, interbedded with sandy turbidite deposits and occasional volcanoclastic layers. It should be noted that the Messinian deposits of the Alboran Sea Basin lack a thick evaporitic sequence: they are depleted of salt and only occasional thin gypsum and anhydrite intervals appear towards the top of the section (*e.g.* Jurado and Comas, 1992; Kheidri *et al.*, 2000). A strong erosional unconformity marks the boundary between the Plio-Quaternary and Messinian sequence. This event is a prominent seismic marker known as the M-reflector and is recognized throughout the Mediterranean (Hsü *et al.*, 1973; Ryan *et al.*, 1973). It is interpreted as having formed because of deep desiccation and erosion during the Messinian salinity crisis, at about 5.6-5.5 Ma. (*e.g.* Clauzon *et al.*, 1996; Krijgsman *et al.*, 1999a; Blanc, 2002; Sprovieri *et al.*, 2008; Bache *et al.*, 2009; García-Castellanos *et al.*, 2009; Estrada *et al.*, 2011).

The seismic stratigraphy of the Plio-Quaternary sequence of the Alboran Sea Basin is well established and several seismic units are recognised based on seismic interpretation and well information from DSDP Site 121 and ODP Leg 161. Most previous researchers have divided this sequence into two Pliocene and two Quaternary units which are distinguished by their seismic characteristics (Alonso and Maldonado, 1992; Campillo *et al.*, 1992; Ercilla *et al.*, 1992; Maldonado *et al.*, 1992; Hernández-Molina *et al.*, 1994; 2002; Estrada *et al.*, 1997; Pérez-Belzuz *et al.*, 1997; Tandon *et al.* 1998; Alonso *et al.*, 1999; Comas *et al.*, 1999; Alonso and Ercilla, 2000, 2003; Talukder *et al.*, 2003).

The Plio-Quaternary tectonic subsidence and uplift history of the basin has been determined using 1-dimensional and 2-dimensional backstripping techniques and comparison made with onshore regions (Watts *et al.*, 1993; Docherty and Banda, 1995; Estrada *et al.*, 1997; Rodríguez-Fernández *et al.*, 1999; Hanne *et al.,* 2003; Martínez-García and Soto, 2006). These studies document a significant reduction in the magnitude of the tectonic subsidence during the Late Pliocene and Quaternary in the Alboran Sea Basin, together with a simultaneous tectonic uplift in the vicinity of the Alboran Ridge.

The Alboran Ridge is a prominent bathymetric high that bounds three main sub-basins: the West, East and South Alboran basins (WAB, EAB and SAB respectively) (Figure 4-1). The high is a 130 km long, 1.8 km high, volcanic ridge, with a WSW-ENE orientation, perpendicular to the Neogene plate-convergence vector of the Eurasian and African plates (*e.g.* Rosenbaum *et al.*, 2002). The Alboran Ridge is poorly imaged on seismic reflection profiles and so its internal structure is not known. Most previous studies have reported the occurrence of a fault zone, with probable left-lateral

movement along the northern flank of the ridge (*e.g.* Bourgois *et al.*, 1992; Campos *et al.*, 1992; Comas *et al.*, 1992, 1999; Maldonado *et al.*, 1992; Mauffret *et al.*, 1992; Woodside and Maldonado, 1992; Watts *et al.*, 1993; Chalouan *et al.*, 1997; Estrada *et al.*, 1997; Willet, 1997; Ammar *et al.*, 2007). The relationships with other fault structures in the region and whether or not this structure connects with the major active faults described in the onshore regions of the Betics and Rif is also unclear (see discussion in Fernández-Ibáñez *et al.*, 2007; Ballesteros *et al.*, 2008; Martínez-García *et al.*, 2011).

4.3 Data and methodology

This study used seismic reflection profiles covering an area of 28,000 km^2 located between 1.35–3.95° W and 35.17–36.42º N (Figure 4-2). The dataset comprises 6598 km of single-channel and multi-channel seismic reflection profiles, most of which were collected on academic cruises, while some 1700 km are commercial data from oil companies. All the older analogue seismic profiles were scanned and converted to segy format using Lynx® software. Seismic profiles used in the figures in this paper come from the following cruises: Robert D. Conrad cruise C2911 (1988), RRS Charles Darwin cruise CD64 (1991-1992), R/V BIO Hesperides Tecalb and Marsibal I-06 cruises (2000 and 2006).

The seismic lines and available well information for study area were interpreted using the SMT Kingdom Suite® software. Seismic events were tied to chrono-stratigraphic and log data (V_p, density and gamma ray) from DSDP Site 121 and ODP Sites 976 to 979 (Ryan *et al.*, 1973; Comas *et al.*, 1996, 1999; de Kaenel *et al.*, 1999; Siesser and de Kaenel, 1999). In addition, we used the commercial Habibas-1 well located to the southeast of the study area in a zone with low density of seismic coverage (Kheidri *et al.*, 2000; Cope *et al.*, 2003; Mauffret *et al.,* 2007) (Figure 4-2).

We used the lithologic and bio-stratigraphic information from these wells to build up a chrono-stratigraphic framework for the Pliocene-to-Recent sedimentary history of the basin. This is summarized in figure 4-3, which shows the different seismic units and the bounding seismic reflectors that were mapped regionally. The mapped surfaces and unconformities are presented as time-contour maps (in two-way travel time, twtt). Faults and folds that were active at the relevant time are included on the maps. From the time-contour maps we calculated thickness maps for each seismic unit, which were depth converted using average sonic velocities (V_p; Table 4-1). Knowing the age of the seismic horizons (Figure 4-3), sediment accumulation rate maps were calculated for each seismic unit, assuming a linear interpolation of ages. Because we did not conduct any decompaction analysis the sediment accumulation rates are minimum values, especially for the deeper seismic units.

4.4 Plio-Quaternary seismic stratigraphy

The seismic stratigraphy through the Plio-Quaternary interval is illustrated in figure 4-3. Many of the mapped events form unconformities on the basin margins or in intra-basin highs, passing laterally into conformable events in the main depocentres. The principal reflectors and seismic units are described below from oldest to youngest.

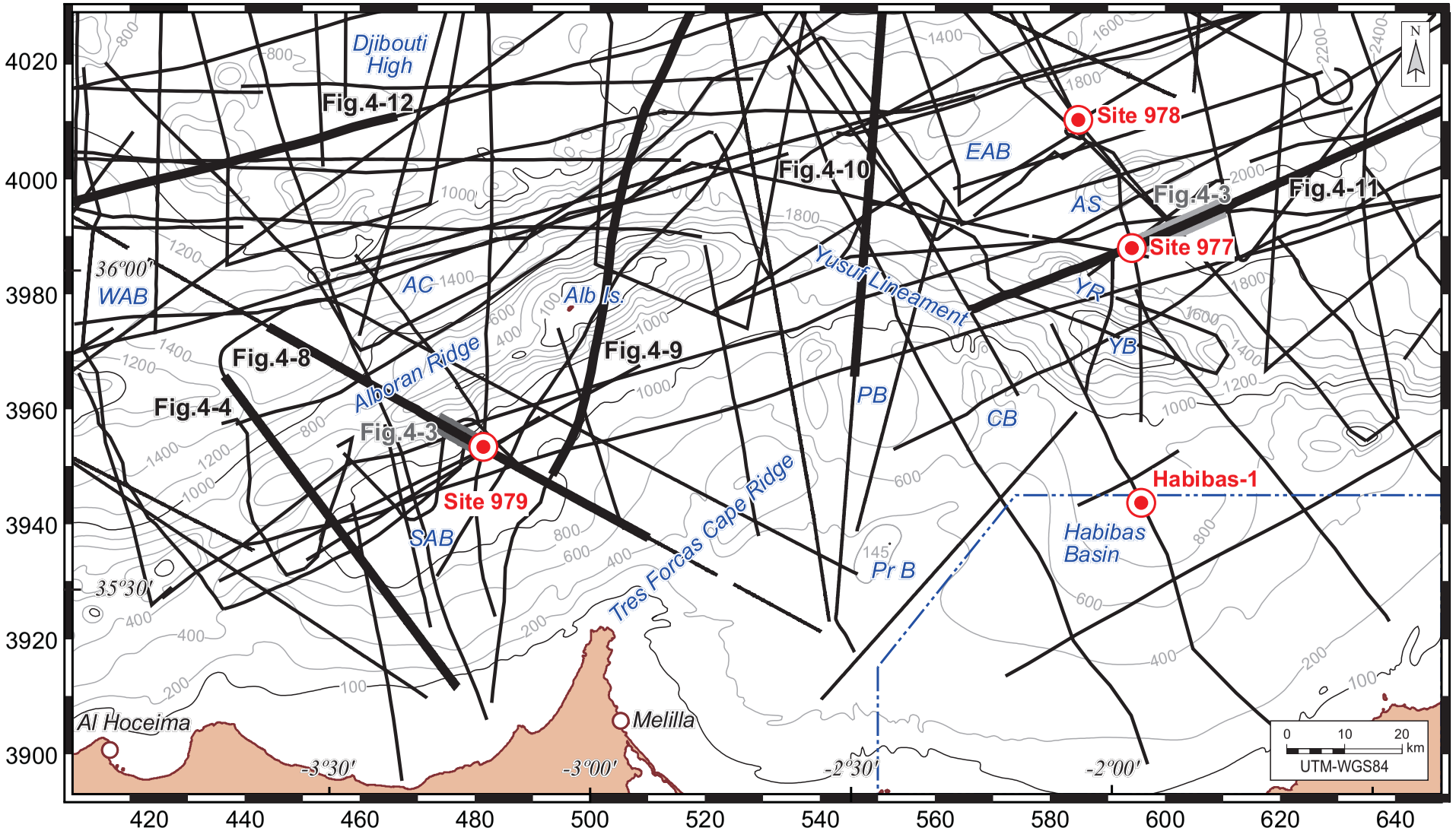

Figure 4-2. Location map of seismic profiles used in the study (rectangle in figure 4-1) including data from commercial surveys (RAY, 1972; SH, 1974; Shell-750, 1975; AS, 1977; BRPM, 1979 and MAP, 1979) and scientific cruises (GEOMEDE, 1970; CONRAD, 1988; GC-90, 1990; DARWIN CD 64, 1991-1992; ESCIALB, 1992; ODP Leg 161, 1995; TECALB, 2000; TTR-12, 2002; TTR-14, 2004 and MARSIBAL-I 06, 2006). Thick black lines indicate multichannel seismic profiles presented in other figures. Location of ODP sites 977, 978, 979 and Habibas-1 well are shown as red circles. Bathymetry contours (GEBCO-97, IOC-IHO) are in metres, contour interval 200 m. Abbreviations: Alb Is, Alboran Island; AC, Alboran Channel; AS, Al-Mansour Seamount; CB, Câbliers Bank; EAB, East Alboran Basin; PB, Pytheas Basin; Pr B, Provençaux Bank; SAB, South Alboran Basin; YB, Yusuf Basin; YR, Yusuf Ridge and WAB, West Alboran Basin.

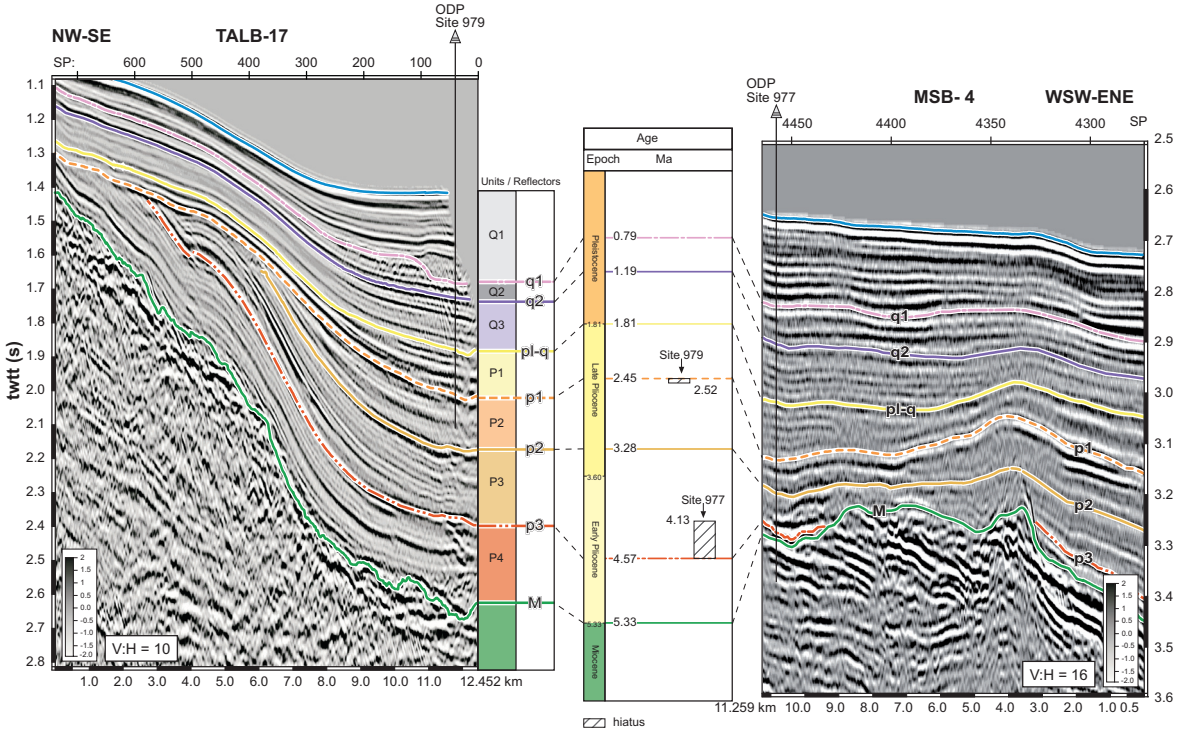

Figure 4-3. Correlation of multichannel seismic data (see location in figure 4-2) with biostratigraphic data from ODP sites 979 and 977. Depths are in two-way travel time (twtt; two-way travel time) below sea-level.

Seismic Unit	Interval Vp (m/s) ODP 976 B	Interval Vp (m/s) ODP 977A	Interval Vp (m/s) ODP 978A	Interval Vp (m/s) ODP 979A	Average interval Vp (m/s)	σ (m/s)
Unit Q1	1613.4	1551.22	-	1537.39	1567.34	± 33.06
Unit Q2	1728.66	1593.69	-	1553.03	1625.13	± 75.07
Unit Q3	1811.84	1610.35	-	1590.75	1670.98	± 99.92
Unit P1	1921.96	1633.74	1649.45	1741.09	1736.56	± 114.62
Unit P2	-	1677.29	1667.83	-	1672.56	± 4.73
Unit P3	-	1744.72	1780.06	-	1762.39	± 17.67
Unit P4	-	1820.74	2133.79	-	1977.27	± 156.53

Table 4-1. Interval sonic velocities (m/s) for the different seismic units calculated by best-fitting functions of V_p log data and in-situ measurements from ODP sites 976, 977, 978 and 979. Average values of the interval velocities and the estimated standard deviation (σ) are also indicated.

M reflector

The M reflector, which defines the Miocene-Pliocene boundary, appears as a prominent, high amplitude, laterally continuous reflection. It is clearly recognized also at ODP Sites 976 and 978 and in the Habibas-1 Well (Figure 4-1). This event is dated at 5.33 Ma (Clauzon *et al.*, 1996; Gradstein *et al.*, 2004). However it should be noted that it may involve an hiatus of significant duration due to its strong erosive nature.

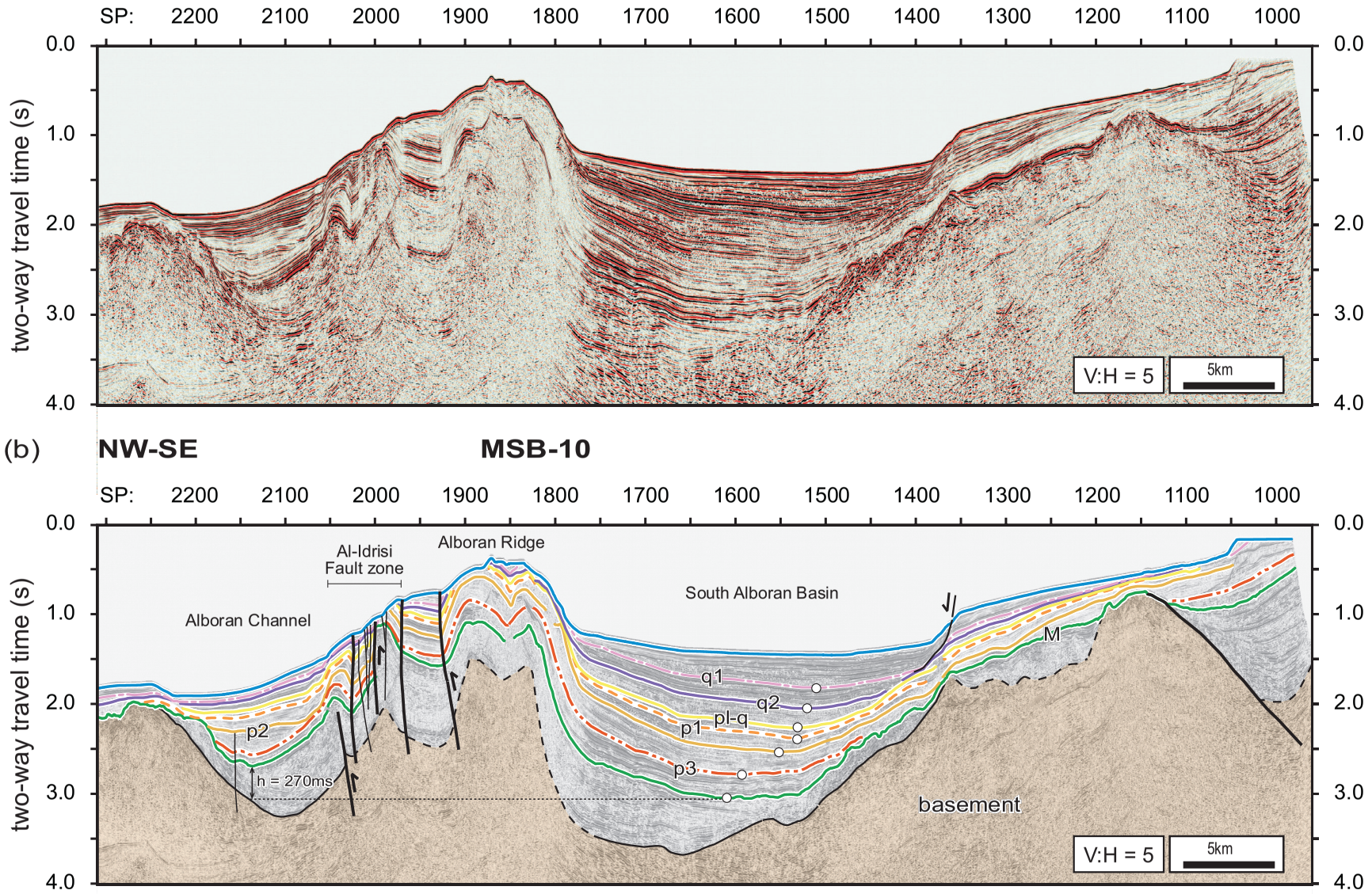

Figure 4-4. (a) Uninterpreted and **(b)** interpreted multichannel seismic section across the western Alboran Ridge and South Alboran Basin. Seismic reflectors, age of unconformities and seismic units as defined in figure 4-3. Note migration of syncline hinge (white circles) and associated depocentre towards the SE in the SAB. Vertical offset between the Plio-Quaternary depocentres of the Alboran Channel and the SAB is also indicated (h = 270 ms twtt). Uncertainty on the position of the top of basement is indicated by dashed lines. Location of seismic line is shown in figures 4-4-2, 4-5 and 4-6.

The M reflector forms the lower boundary of the Plio-Quaternary succession and is an angular erosional unconformity on the basin margins and basement highs that changes laterally to a concordant surface in some basinal areas (*e.g.* Figure 4-4). In areas where the M-reflector is concordant it overlies a thin seismic unit formed by alternating and parallel, strong reflections of probably Messinian age (*e.g.* shot point 1600 in figure 4-4).

The time-contour map in figure 4-5 illustrates the geometry of the M reflector, and identifies the faults thought to be active during the latest Messinian. The surface has a complex, undulating geometry reaching a maximum depth of ~3950 ms (twtt) toward the north-east of the studied area, close to the Algerian Basin. Several, NE-SW elongated depressions, tens of kilometres long can be recognised on the M-reflector map. These are the Alboran Channel, the South Alboran Basin (SAB) and the Habibas and Pytheas basins. These lows are separated by sub-parallel highs, such as the Alboran Ridge, the Cabo Tres Forcas Ridge, and the Provençaux- Câbliers banks. In the East Alboran Basin (EAB), ODP Sites 978 and 979 are located within two major troughs trending NE-SW to ENE-WSW and separating the Al-Mansour Seamount. These troughs deepen toward the south-west, reaching a maximum depth of about 3800 ms (twtt) close to the northern slope of the Alboran Ridge.

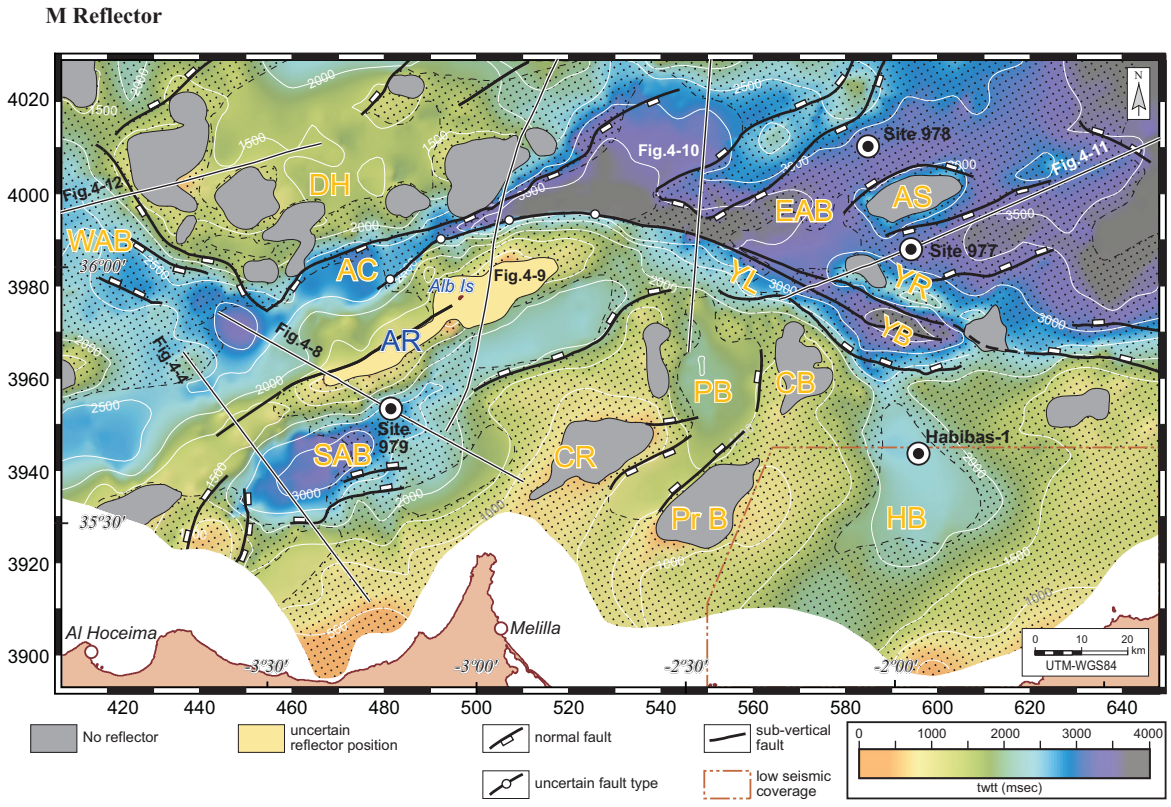

Figure 4-5. Contour map of the M reflector. Stippled areas indicate where the event has an unconformable relationship with underlying strata. Structures active at this time are also shown. Contour interval is 500 ms twtt (two-way travel time). Grey areas are outcropping basement or Miocene sedimentary sequences. Yellow shows areas where the position of the M reflector remains unclear. Multichannel seismic profiles for figures 4-4, 4-8, 4-9, 4-10, 4-11 and 4-12 are also shown. Abbreviations: Alb Is, Alboran Island; AC, Alboran Channel; AR, Alboran Ridge; AS, Al-Mansour Seamount; CB, Câbliers Bank; CR, Cabo Tres Forcas Ridge; DH, Djibouti High; EAB, East Alboran Basin; HB, Habibas Basin; PB, Pytheas Basin; Pr B, Provençaux Bank; SAB, South Alboran Basin; YB, Yusuf Basin; YL, Yusuf Lineament; YR, Yusuf Ridge; and WAB, West Alboran Basin.

The WNW-ESE trending Yusuf Basin is also an obvious deep trough in Messinian times where the M-reflector reaches a depth of ~3500 ms (twtt). We note that the M reflector is locally concordant with the underlying strata, as in the EAB, SAB, Pytheas and Habibas basins, in most of the Djibouti High and in the south-western sector of the Alboran Ridge.

Pliocene Sequences

Unit P4 (Early Pliocene) has semi-transparent seismic facies with continuous parallel reflectors and locally high amplitudes (*e.g.* Figure 4-3). The top of the unit is defined by the p3 reflector with an estimated age of ~4.57 Ma. Correlation with the ODP Site 977 shows that is event corresponds locally with an important Early Pliocene hiatus (~4.13 to 5.07 Ma; Figure 4-3). The p3 reflector has a limited presence in the area, being absent over wide areas of the Djibouti High, the NE Alboran Ridge and the Algerian margin (Figure 4-6a). Unit P4 has maximum thickness of about 400 ms twtt in the south-western Alboran Ridge, the EAB and the SAB. On the African margin, downlapping reflector geometries are observed within this unit that we interpret as prograding deltas building out from North Africa.

The Early-Late Pliocene Unit P3, has fairly transparent seismic facies with continuous and parallel, low-amplitude reflectors (*e.g.* Figure 4-3). In general, this unit onlaps basement highs and the underlying sedimentary sequences. The p2 reflector forms the upper boundary of this unit and its estimated age is ~3.28 Ma. This seismic event locally truncates the underlying reflectors (Figures 4-4 and 4-6b). Unit P3 is up to 500 ms (twtt) thick in SAB and EAB, and is very thin or absent over most of the main submarine highs.

The early Late Pliocene P2 unit has semi-transparent seismic facies, including well-stratified medium-amplitude reflectors and few high amplitude events (*e.g.* Figure 4-3). The unit also contains some lens-shaped bodies with both chaotic and stratified infill, which we interpret as channels. The p1 reflector forms the upper boundary of this unit and it is a high-amplitude, strongly erosional event on the flanks of the bathymetric highs. As with the other major unconformities it becomes more conformable towards the basin centres (Figures 4-3, 4-4 and 4-6c). Correlation to ODP Site 979 shows that this reflector corresponds with a hiatus from 2.52 to 2.45 Ma (Figure 4-3). The amount of early Pliocene sediments eroded increases towards some of the highs, suggesting that the unconformity has probably a longer duration on the basin margins and intra-basin highs.

Unit P1, of Late Pliocene age, is a thin unit with parallel seismic fabric formed by continuous high-amplitude reflectors that locally have moderate-amplitudes. This unit is approximately tabular with a broadly constant thickness of about 150 ms (twtt) (Figure 4-4). Its upper boundary is the pl-q reflector, which corresponds with the 1.81Ma Pliocene-Quaternary boundary (Figures 4-3 and 4-4).

Quaternary Sequences

The early Pleistocene Q3 unit has a lower semi-transparent seismic facies with stronger parallel high-amplitude reflectors developed towards its top. The unit frequently contains lenses with chaotic reflectivity, which we interpret to be submarine slide deposits. As a whole, Unit Q3 exhibits a concave

geometry reaching maximum thickness of about 300 ms (twtt) in the basin centres (Figure 4-4).

The q2 reflector forms the boundary between Q3 unit and the overlying middle Pleistocene (1.19-0.79 Ma), Q2 unit (Figures 4-3 and 4-4). Unit Q3 thins onto some highs as can be observed between shot points 200-300 in figure 4-3 which suggests growth of structures such as the Alboran Ridge and Yusuf Lineament at this time. Unit Q2 has strong parallel high-amplitude reflectors and, locally, has chaotic seismic facies that we interpret as buried submarine slides. Unit Q2 has an approximate maximum thickness of 200 ms twtt and thins markedly toward the Alboran Ridge (*e.g.* Figure 4-4). The q1 reflector, forming the top of Unit Q2, has an estimated age of ~0.79 Ma.

The seismic facies of the late Pleistocene to Holocene aged Unit Q1 (0.79 Ma to Present) consist of high-to-moderate amplitude reflectors with abundant intercalations of lenses with chaotic seismic facies, interpreted to be submarine slides. The unit varies considerably in thickness, ranging from minimum values on the Djibouti High and the Alboran Ridge to a maximum thickness of about 400 ms (twtt) within the Alboran Channel, the Habibas Basin and the SAB (Figure 4-4).

Sediment accumulation rates

Sediment accumulation rates calculated for the seismic units mapped in the studied area are shown in figure 4-7. The structures interpreted to have been active in the relevant time intervals periods, are also shown.

The most obvious feature of these maps is how variable the sediment accumulation rates were in both time and space. For example the SAB had high accumulation rates (>0.4 mm/yr) in the Early Pliocene and again in the Quaternary, but for much of the Pliocene only accumulated average amounts of sediments (~0.2 mm/yr). In comparison the Habibas Basin, further to the east, had high sediment accumulation rates in Unit P2 times and again in the Quaternary. The basins to the north of the Alboran Ridge and Yusuf Lineament had consistently high sediment accumulation rates (up to 0.5 mm/yr) except for a brief period in the Late Pliocene (Unit P1 times), but even in these basins the locus of maximum sedimentation varies laterally, responding to changes in fault activity.

In the Early Pliocene (Unit P4) small, restricted basins existed in the area with highly variable but locally high sediment accumulation rates of up to 0.55 mm/yr (Figure 4-7a). For example the south-western part of the SAB had high rates averaging about 0.4 mm/yr. Similar rates are observed close to the North African margin (> 0.25 mm/yr) in the southernmost part of the SAB, where prograding deltas have been interpreted (between 3º10'-3º30' W). Another important depocentre occurs in the western part of the EAB, trending parallel to the WNW-ESE Yusuf Lineament (average of 0.3 mm/yr). Conversely, other areas were emergent at this time or had very low sediment accumulation rates (~0.1-0.15 mm/yr).

In general the sediment accumulation rates in the Early to Late Pliocene (P3 unit; ~4.57-3.28 Ma), are lower than in the underlying P4 unit (average of ~0.1 mm/yr; Figure 4-7b) although the basins increased in area during this time. Only two areas with high sediment accumulation rates are identified in this period: one, a small region in the SAB, to the south-west of ODP Site 979 (0.15-0.3 mm/yr) and the other in the EAB (0.15-0.35 mm/yr), where maximum rates occur on the south-east

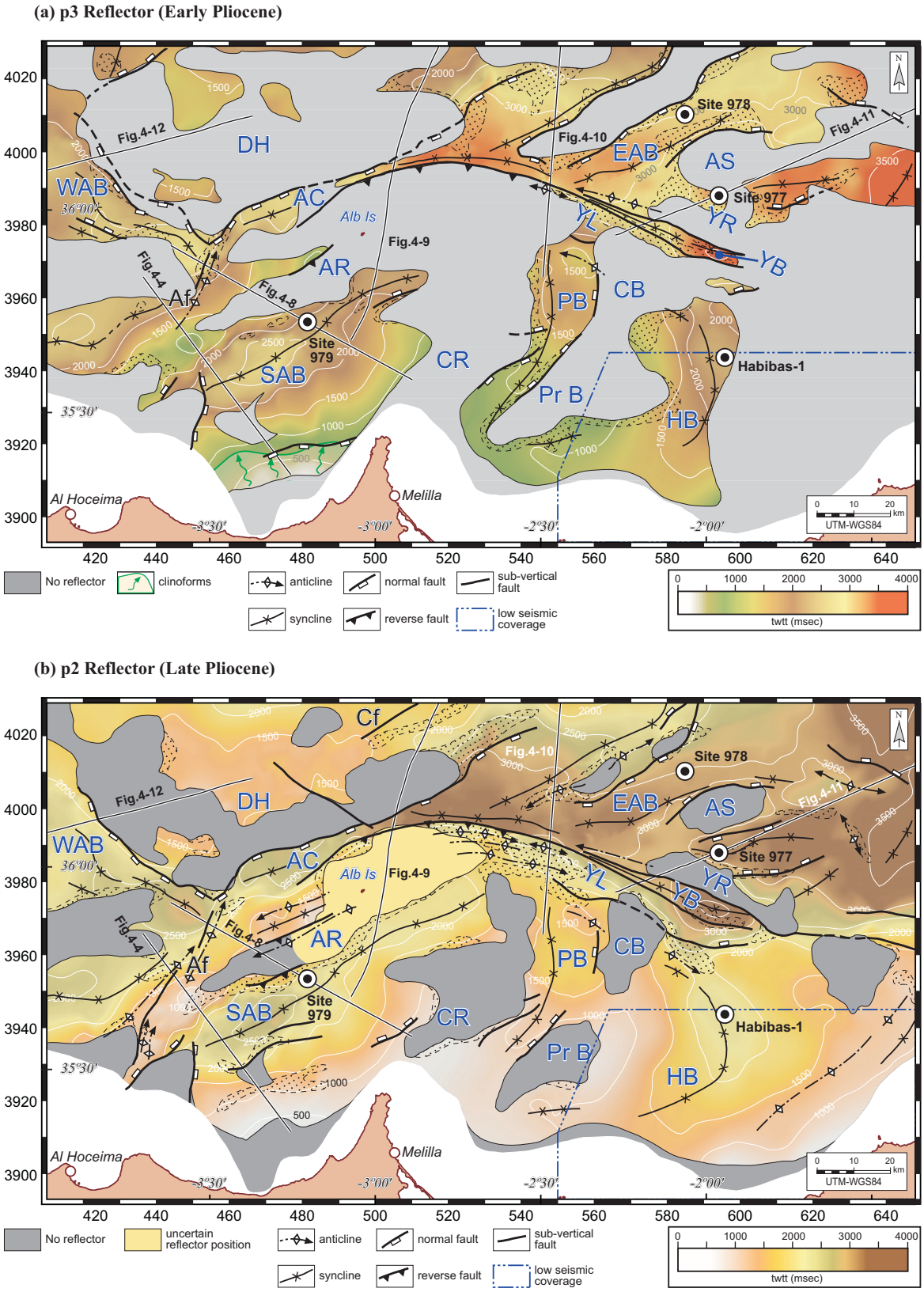

Figure 4-6. Contour maps and structural interpretation of **(a)** p3 reflector **(b)** p2 reflector **(c)** p1 reflector and **(d)** q2 reflector (see age in figure 4-3). Structures active at this time are also shown. Contour interval is 500 ms twtt (two-way travel time). Stippled areas indicate where the event has an unconformable relationship with underlying strata. Yellow shows areas of thin Plio-Quaternary sequence. Multichannel seismic profiles for figures 4-4, 4-8, 4-9, 4-10, 4-11 and 4-12 are also shown. Abbreviations: Alb Is, Alboran Island; AC, ▶

(c) p1 Reflector (Late Pliocene)

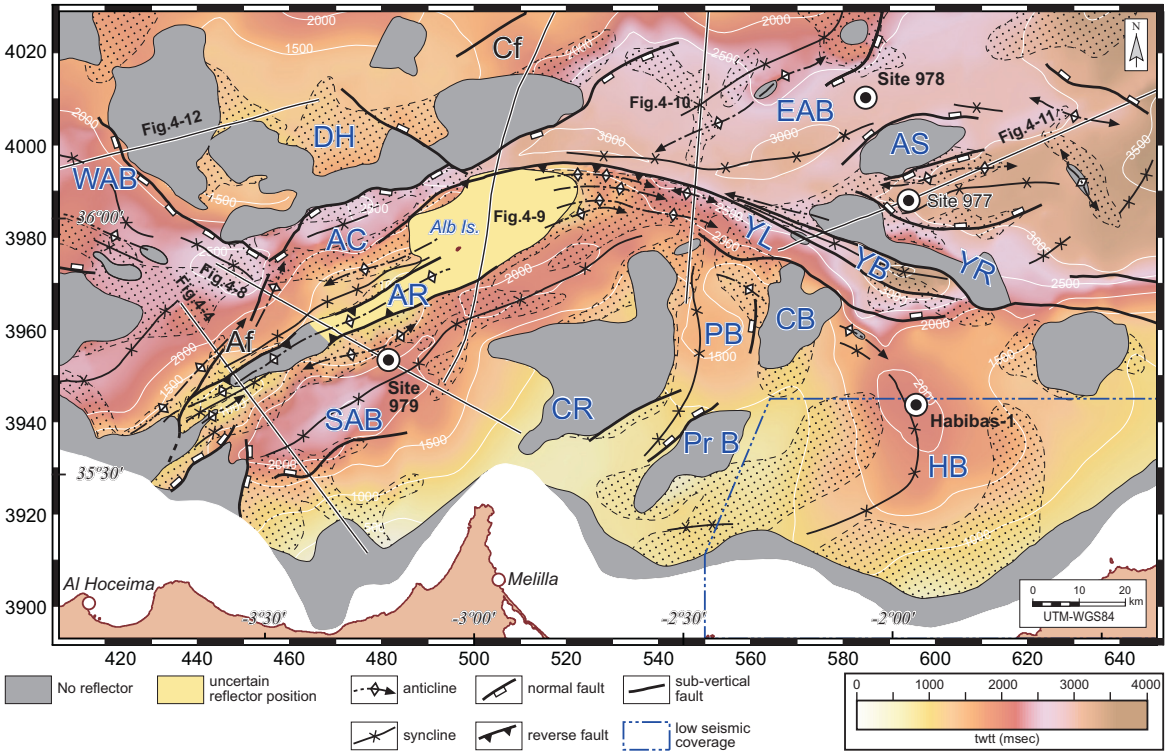

(d) q2 Reflector (Quaternary)

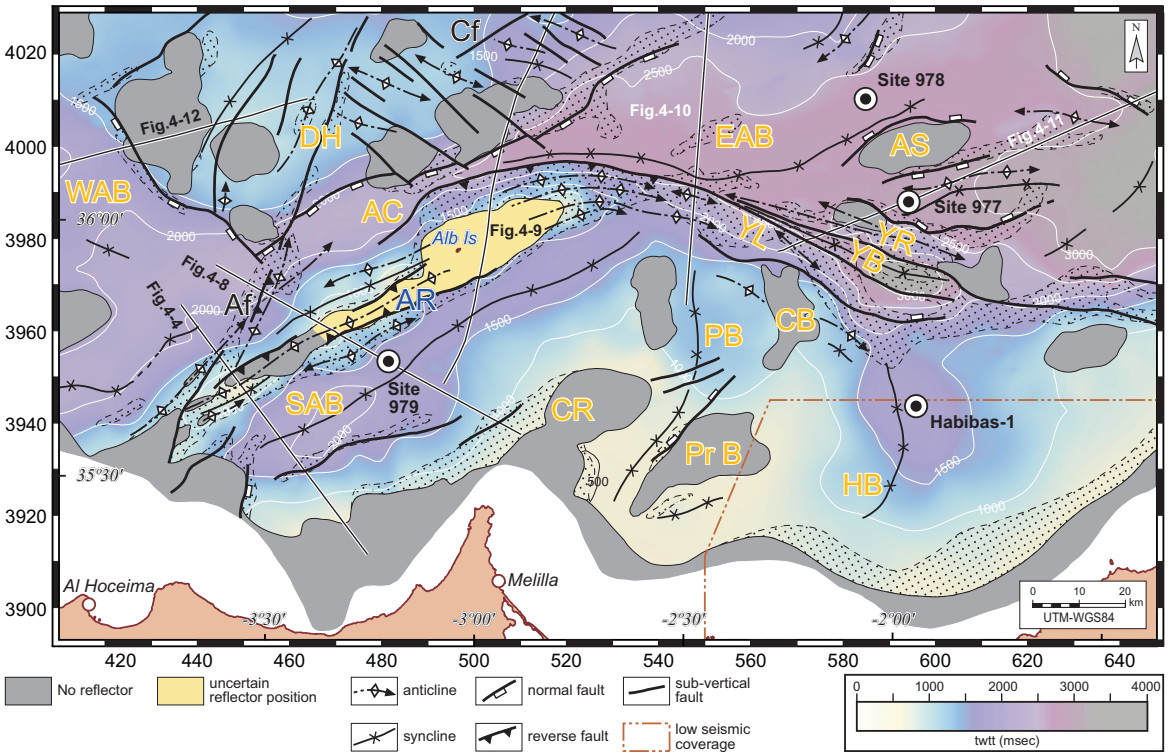

Alboran Channel; Af, Al-Idrisi fault zone; AR, Alboran Ridge; AS, Al-Mansour Seamount; CB, Câbliers Bank; Cf, Carboneras fault zone; CR, Cabo Tres Forcas Ridge; DH, Djibouti High; EAB, East Alboran Basin; HB, Habibas Basin; PB, Pytheas Basin; Pr B, Provençaux Bank; SAB, South Alboran Basin; YB, Yusuf Basin; YL, Yusuf Lineament; YR, Yusuf Ridge; and WAB, West Alboran Basin.

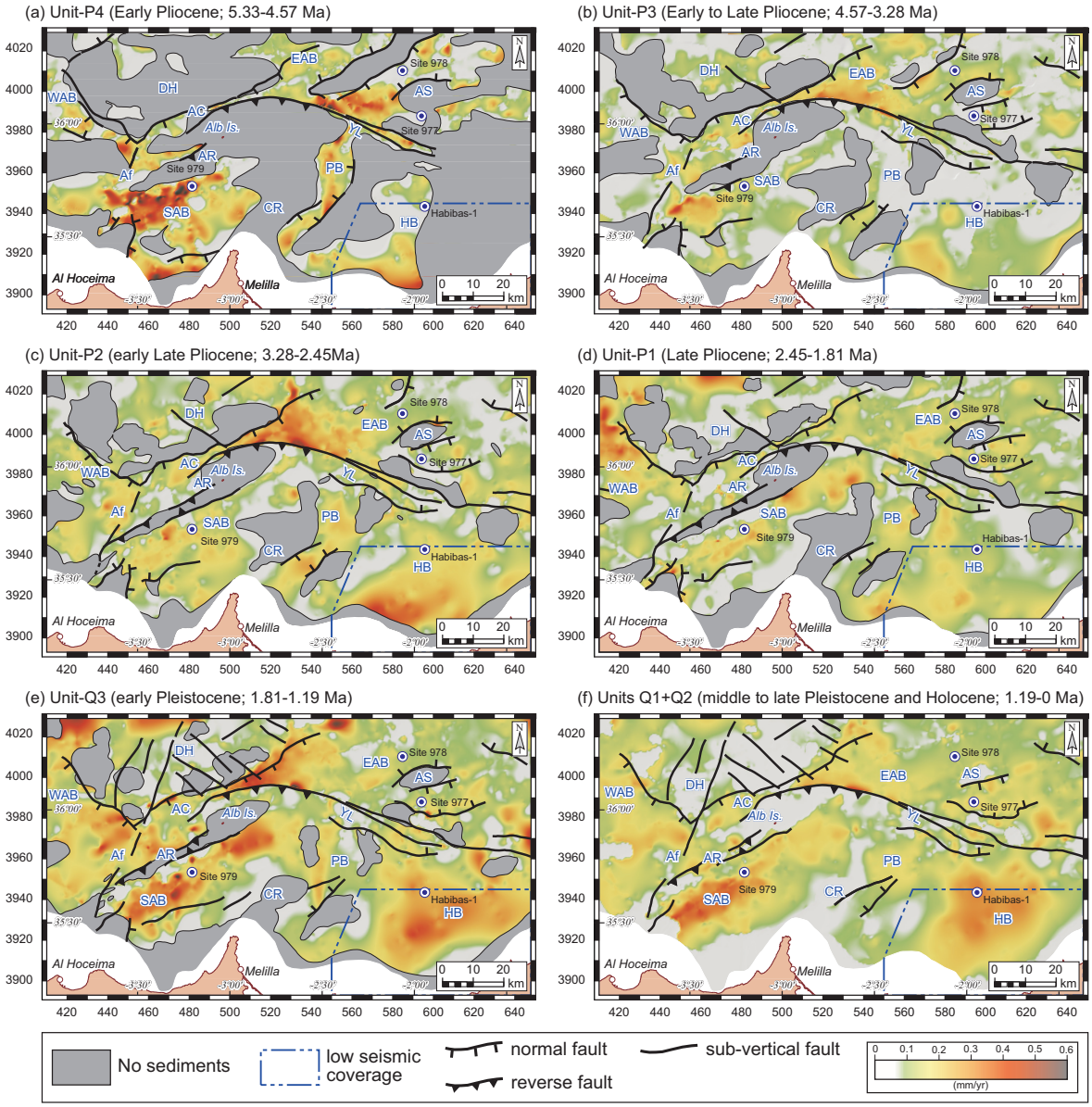

Figure 4-7. Maps of sediment accumulation rates (mm/yr) for the Plio-Quaternary units (see ages in figure 4-3). The sediment accumulation rates have not been decompacted and hence are minimum values. Abbreviations: Alb Is., Alboran Island; AC, Alboran Channel; Af, Al-Idrisi fault zone; AR, Alboran Ridge; AS, Al-Mansour Seamount; CR, Cabo Tres Forcas Ridge; DH, Djibouti High; EAB, East Alboran Basin; HB, Habibas Basin; PB, Pytheas Basin; SAB, South Alboran Basin; YL, Yusuf Lineament; and WAB, West Alboran Basin.

side of the basin close to the Alboran Ridge and the Yusuf Lineament.

In Late Pliocene times (P2 unit; ~3.28-2.45 Ma) the eastern and southern sides of the EAB continued to have high sediment accumulation rates (up to 0.45 mm/yr), with higher values than in P3 times. In the north part of the EAB, close to the Spanish margin (at ~2º 20' W), we can see high sediment input associated with the turbidite systems feeding down the Almeria Canyon into the basin. Towards the east, rates diminish progressively to less than 0.1 mm/yr. In the Habibas Basin, similarly to other sub-basins south of the Alboran Ridge, some of the high sediment accumulation

rates inferred in this period (0.25-0.4 mm/yr) most likely reflect the contribution of sedimentary systems coming from the North African margin.

The pattern of sedimentation changes in the Late Pliocene P1 unit (~2.45-1.81 Ma). Rates reduce significantly around highs such as the Djibouti High and to the NW of the Cabo Tres Forcas Ridge, and for the first time the EAB shows as significant reduction of sediment accumulation at this time (rates 0.1-0.15 mm/yr). In contrast deposition increases in the eastern WAB and on the northern margin of the Djibouti High close to the Spanish shelf with local maxima up to 0.4 mm/yr (Figure 4-7d).

A marked increase in sediment accumulation rates up to 0.45 mm/yr is observed in most basinal areas at the beginning of the Quaternary (~1.81-1.19 Ma; Figure 4-7e). In the NE-SW trending SAB and Habibas Basin high rates continue to this day, in contrast to the Spanish side of the basin where rates have decreased since 1.19 Ma (Figure 4-7f). The EAB depocentre in front of the Alboran Ridge and Yusuf Lineament, switches on again in the early Pleistocene (Q3 times) reaching rates of ~0.45 mm/yr, but reduces to moderate rates of ~0.2-0.3 mm/yr in the last 1.19 Ma (Units Q2 and Q1) (Figures 4-7e and 4-7f), which largely reflect the continuing input of sediment of the Almeria turbidite system.

Aside from the continued high sediment accumulation rates in the South Alboran and Habibas Basins during the last 1.19 Ma (Figure 4-7f) the most notable feature of Q2 and Q1 times is the very low rates of <0.1 mm/yr over large areas of the Alboran Ridge, Yusuf Lineament, Djibouti High, Cabo Tres Forcas Ridge and most of the African margin.

4.5 Post-Messinian structure

The main structures that influence Plio-Quaternary sedimentation are illustrated on several regional seismic lines in figures 4-4 and 4-8 to 4-12. The faults and folds are also mapped on the time-contour maps of the P3 to Q3 reflectors (Figure 4-6). It should be noted that these maps only show those structures active at time of the mapped event, illustrating the progressive change in structural complexity, and therefore tectonic activity, through time in the area.

Alboran Ridge and Yusuf fault zones

The Alboran Ridge is deformed by two main fault-and-fold systems with different orientations: the Al-Idrisi fault zone trending NNE-SSW and the Alboran Ridge fault zone trending NE-SW (Martínez-García *et al.*, 2011). The Al-Idrisi fault zone is a narrow deformation zone, 2-7 km wide, with sub-vertical faults and associated folds that cuts the western sector of the Alboran Ridge (*e.g.* Ammar *et al.*, 2007) (Figures 4-4 and 4-8). This zone comprises faults and folds in relay with a mean orientation N30ºE and it extends northward across the Djibouti High (Figures 4-6c and 4-6d). Most of these faults cut the whole Plio-Quaternary sequence indicating very recent tectonic activity and show a reverse slip component (Figures 4-4 and 4-8). Thickness of most of the seismic units is similar on both sides of the fault zone but there is some thickening of sediments adjacent to the fault in units P4, Q2 and Q3 (*e.g.* Figure 4-8 at shot points 2750 to 3250). We therefore infer two main

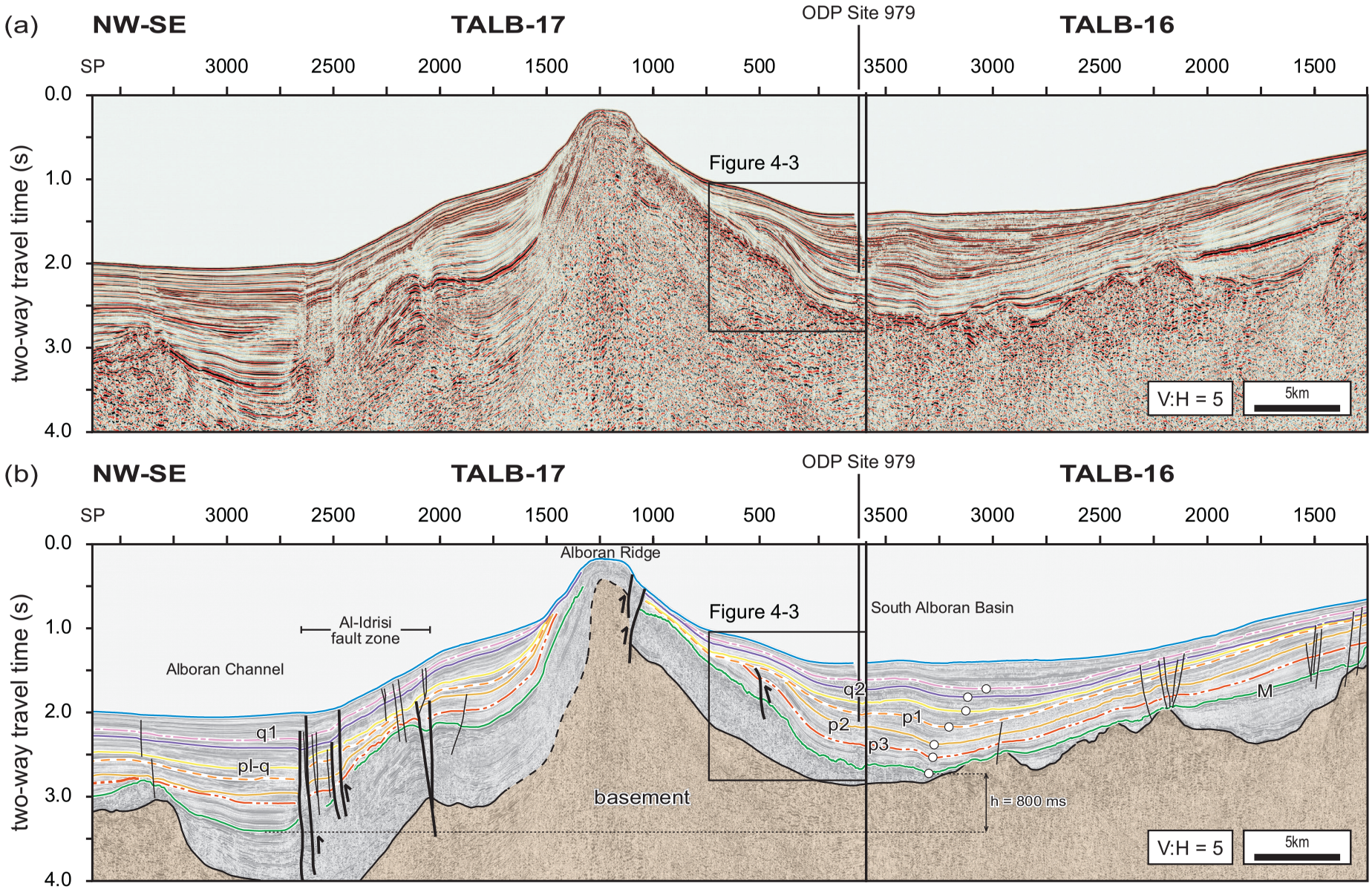

Figure 4-8. (a) Uninterpreted and **(b)** interpreted multichannel seismic section across the central Alboran Ridge, Al-Idrisi fault zone, Alboran Channel and South Alboran Basin (SAB). Seismic reflectors, age of unconformities and seismic units as defined in figure 4-3. Location of the ODP Site 979, used to tie the seismic interpretation, is shown. Note migration of syncline hinge (white circles) and associated depocentre towards the SE in the SAB. Vertical offset between the Plio-Quaternary depocentres of the Alboran Channel and the SAB is also indicated (h = 800 ms twtt; two-way travel time). Uncertainty regarding position of top of basement is indicated by dashed lines. Location of seismic line is shown in figures 4-2, 4-5 and 4-6.

phases of faulting, one in the Early Pliocene and the other during the Quaternary.

Along the crest of the Alboran Ridge, the Plio-Quaternary sedimentary sequences are folded in open, N65ºE trending, asymmetric folds (Figure 4-6). Seismic units are usually thicker over the fold hinge, thinning progressively toward the fold flanks. The folds have nucleated over a basement high and are associated with a reverse fault dipping towards the southeast (*e.g.* Figure 4-4 between shot points 1900 and 1950). In plan view, the fault trace and associated fold axes are rectilinear and define a zone of deformation extending for 60 km (Figure 4-6).

The structure in the central sector the Alboran Ridge is illustrated by the seismic section shown in figure 4-8. The fold-and-fault system, with a mean N65ºE orientation, forms a zone of deformation some 20 km wide. The structure consists of a major faulted anticline accompanied by open asymmetric folds in its flanks. The Plio-Quaternary units are uplifted and eroded toward the anticline culmination where the underlying basement sub-crops. The units of Early Pliocene age (P4 and P3) have similar thickness along the western Alboran Ridge and the SAB indicating that main folding episodes occurred in this area after their deposition (Figures 4-4 and 4-8). However units P1 to Q1 thin towards the fold-system of the Alboran Ridge. It should be noted that there are several unconformities along the flanks of the ridge, as demonstrated by the q2, p1 and p2 events which have erosive angular truncations in the western and central ridge (*e.g.* Figure 4-4 between shot points 1750 and 2100 and figure 4-8 between shot points 2500 and 2750 in line TALB-17).

Towards the east of the Alboran Ridge, the structure is approximately 22 km wide, with asymmetric flanks bounded by high-angle faults (Figure 4-9). The M reflector truncates the pre-Messinian sequences and the Plio-Quaternary sequence, which has a thickness of about 1000 ms (twtt) in the adjacent basins, thins to thickness of ~ 300-400 ms (twtt) toward the Alboran Ridge anticline. The angle between flanks tends to diminish upward progressively. All these observations suggest a recent progressive and syn-sedimentary uplift of the Alboran Ridge.

Between 2.5º and 3.1º W, fold axial traces along the Alboran Ridge fault zone curve and their orientation changes progressively from SW-NE to WNW-ESE, linking eastward with the structures in the Yusuf fault zone (Figure 4-6). In this area the northern flank of the Alboran Ridge is an arcuate south-dipping reverse fault, which has led to the thrusting of the Alboran Ridge over the southern margin of the East Alboran Basin (Figure 4-10).

The Yusuf fault zone trends N105ºE and has a complex geometry changing from west to east (Figure 4-6). In its western part, the structure consists of a narrow, ~4 km wide fault connecting with the reverse fault on the northern side of the Alboran Ridge. Towards the east the fault zone has a progressively higher dip and becomes wider, reaching a maximum width of 22 km and with several overlapping fault strands which separate two main oblique folds: an anticline on the Yusuf Ridge and a syncline along the Yusuf Basin. The entire sedimentary sequence of the Yusuf Basin is cut by high-angle faults with a normal slip component (Figure 4-11). The Plio-Quaternary sequence thins to ~400 ms (twtt) above the Yusuf Ridge, where the volcanic basement outcrops locally. Sedimentary thickness increases to the west into the Yusuf Basin with an open Plio-Quaternary syncline reaching a thickness of 800-1000 ms (twtt) in its centre. Some units show thickening towards the NE, which is consistent with growth faulting during the early Pleistocene (*e.g.* Unit Q3 in figure 4-11). Some of the

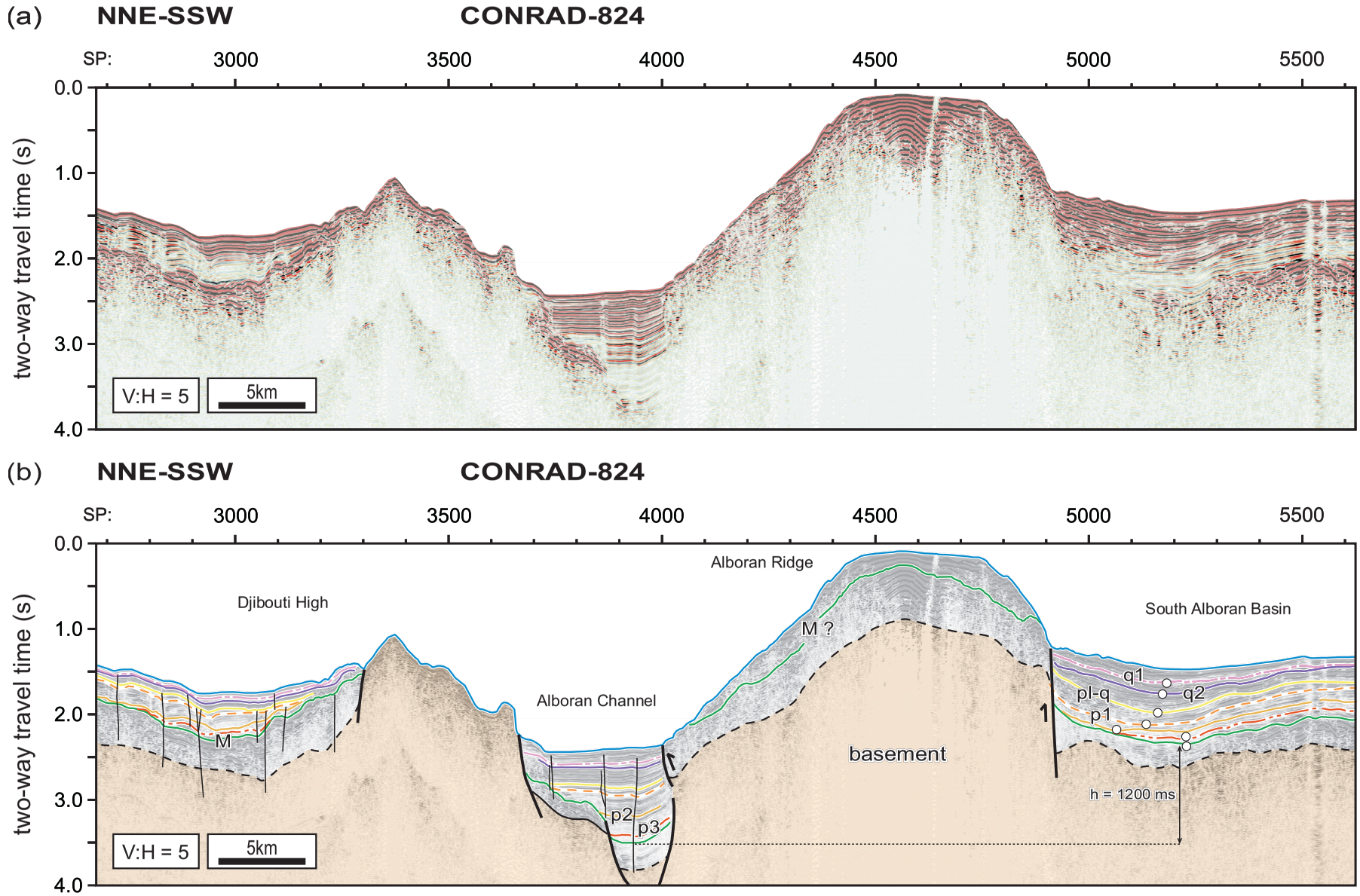

Figure 4-9. (a) Uninterpreted and **(b)** interpreted multichannel seismic section across the Djibouti High, eastern Alboran Ridge to the South Alboran Basin (SAB). Seismic reflectors, age of unconformities and seismic units as defined in figure 4-3. Note also migration of syncline hinge of the SAB (white circles) and associated depocentre for the Plio-Quaternary series. Vertical offset between the Plio-Quaternary depocentres of the Alboran Channel and the SAB is also indicated (h = 1200 ms twtt; two-way travel time). Uncertainty regarding position of top of basement is indicated by dashed lines. Location of seismic line is shown in figures 4-2, 4-5 and 4-6.

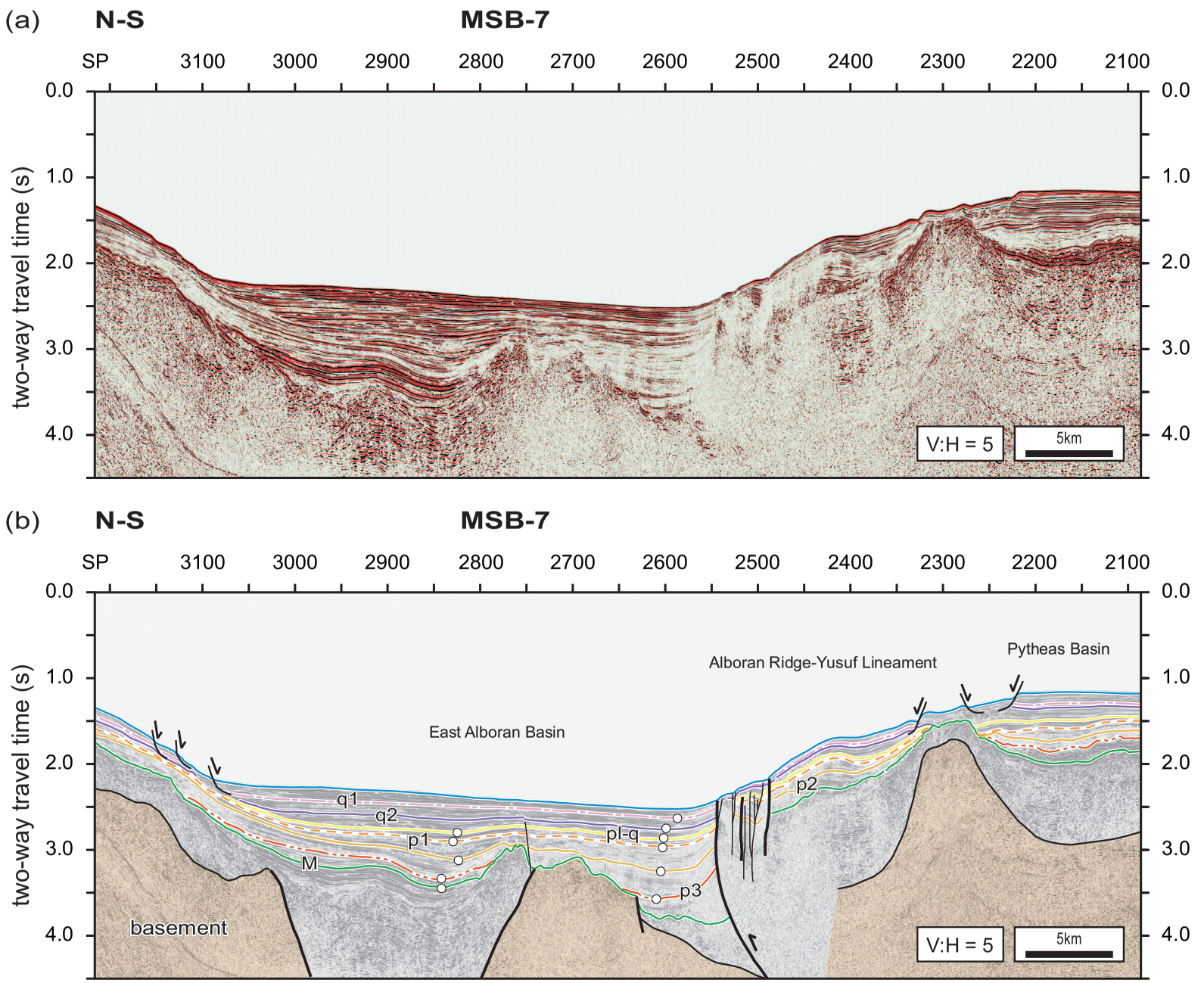

Figure 4-10. (a) Uninterpreted and **(b)** interpreted multichannel seismic section across the East Alboran Basin (EAB) and Yusuf Lineament. Seismic reflectors, age of unconformities and seismic units as defined in figure 4-3. Notice differences in thicknesses of the different Plio-Quaternary seismic units between the EAB and the Pytheas Basin. White circles indicate position of syncline hinges. Location of seismic line is shown in figures 4-2, 4-5 and 4-6.

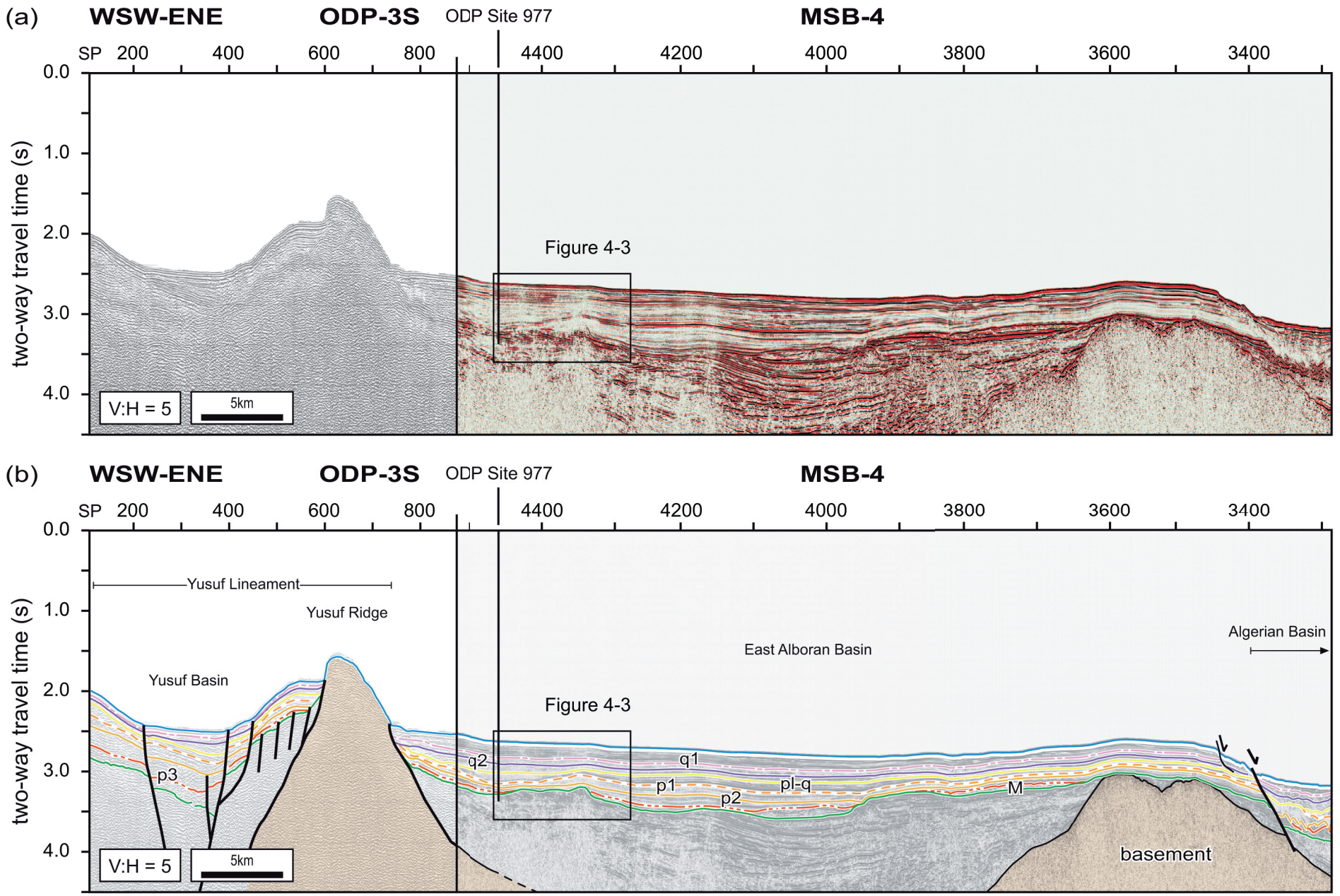

Figure 4-11. (a) Uninterpreted and **(b)** interpreted composite, multichannel seismic section across the East Alboran Basin (EAB) and Yusuf Lineament. Seismic reflectors, age of unconformities and seismic units as defined in figure 4-3. Location of the ODP Site 977, used to tie the seismic interpretation, is shown. Location of seismic line is shown in figures 4-2, 4-5 and 4-6.

regional unconformities truncate underlying reflectors along the flanks of the Yusuf Ridge, as is seen on the Alboran Ridge. The q2 reflector is the largest angular unconformity (*e.g.* around shot point 800 in figure 4-11) documenting an important phase of deformation during the Quaternary.

South and East Alboran basins and Alboran Channel

The South Alboran Basin and the Alboran Channel are two open synclines trending NE-SW, parallel to the Alboran Ridge and containing Plio-Quaternary depocentres (Figure 4-6). Along the syncline of the Alboran Channel, the angle between fold limbs decreases progressively upward (*e.g.* Figure 4-4 between shot points 2050 and 2200). Moreover the youngest sequences in the same area (units P1 to Q1), which are not affected by this syncline and appear tilted towards the NW. These observations suggest that folding had ended by the end of the Late Pliocene. However, the syncline of the SAB deforms all the seismic units and displays a hinge that migrated south-eastwards (Figures 4-4, 4-8 and 4-9), thus demonstrating a progressive tilting of the basin depocentre throughout the Plio-Quaternary.

In addition, a significant vertical offset occurs between the Plio-Quaternary depocentre in the SAB with respect to the Alboran Channel. In the western part of the Alboran Ridge the M-reflector unconformity has a minimum vertical offset of 270 ms (twtt) (Figure 4-4), which increases progressively towards the north-east, where the vertical offset is 800 and 1200 ms (Figures 4-8 and 4-9).

In the East Alboran Basin deformation is produced by folds and faults oriented NE-SW to WSW-ENE that also deform the syncline in the foot wall of the Alboran Ridge reverse fault (Figure 4-6). This syncline has a curved axial trace and the fold hinge migrates southward through the Plio-Quaternary depocentre (Figure 4-10 at shot point 2600). Other structures in this basin include a basement high bounded by SW-NE normal faults and two synclines plunging to the SW (Figure 4-6). The normal faults bounding the high affect only the Early Pliocene units and with no offsets above the p2 reflector. The Late Pliocene series, units P2 and P1, describe an open anticline above the underlying faults.

The Djibouti High

The structure of the Djibouti High and the adjacent areas of the West Alboran Basin is illustrated in figure 4-12. A NW-SE trending high-angle fault forms the boundary between the high and the adjacent basin. To the south it changes strike to a SW-NE trend (Figure 4-6). Plio-Quaternary units onlap the Herradura volcanic bank and are gently folded towards the east. The whole sedimentary sequence to the NE of the Djibouti High is faulted by sub-vertical faults with both reverse and normal displacements (Figures 4-9 and 4-12). These faults trend both NNE-SSW and NW-SE, and they deform the present day seabed as described by Martínez-García *et al.* (2011).

4.6 Timing of deformation

We interpret that central Alboran Sea Basin was deformed by three major tectonic events in the last 5 million years. Deformation was accompanied by sedimentation and controlled the thinning

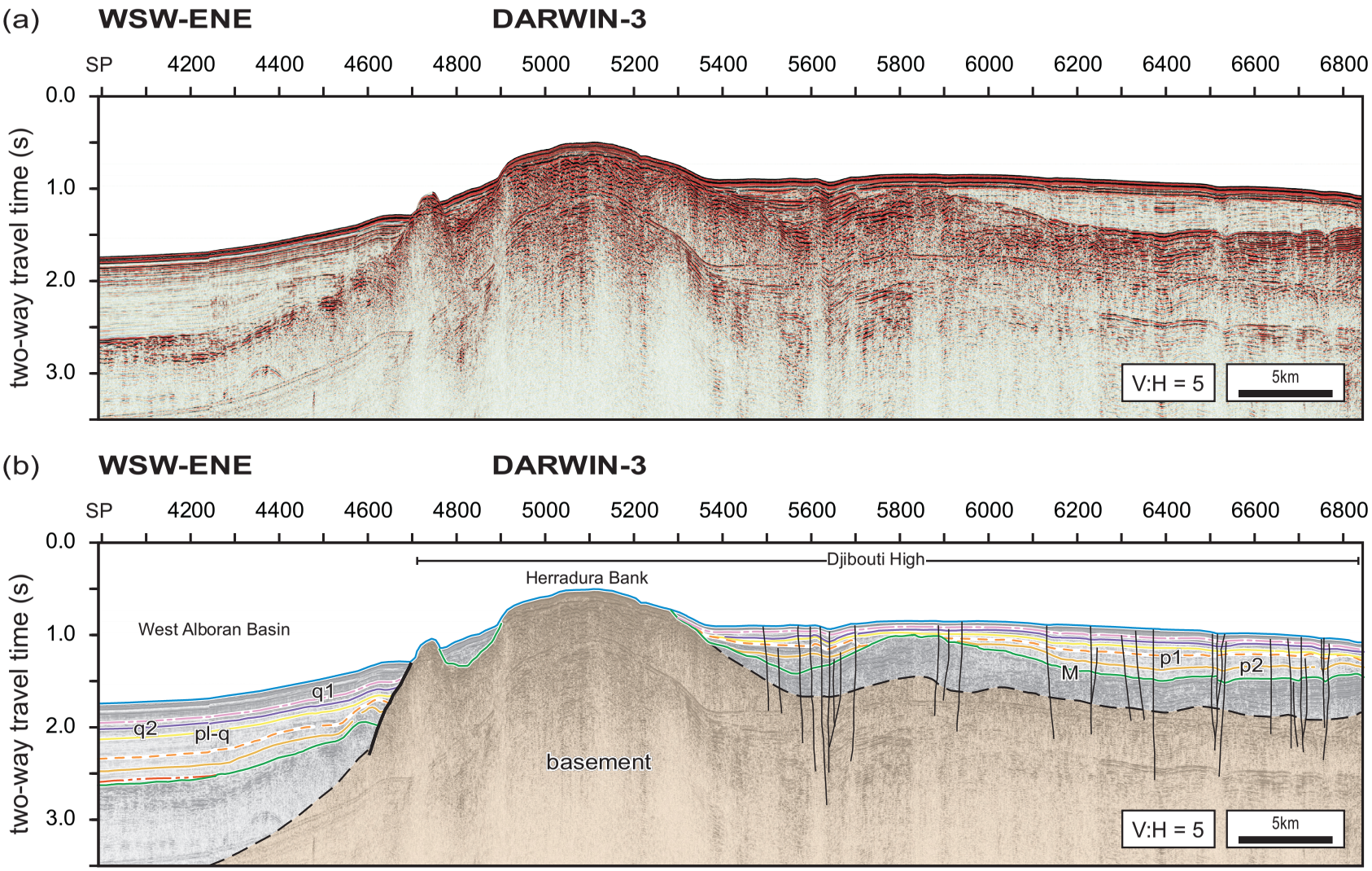

Figure 4-12. (a) Uninterpreted and **(b)** interpreted multichannel seismic section across the WAB and the Djibouti High. Seismic reflectors, age of unconformities and seismic units as defined in figure 4-3. Uncertainty regarding position of top of basement is indicated by dashed lines. Location of seismic line is shown in figures 4-2, 4-5 and 4-6.

of sedimentary units, erosion and the formation of major regional unconformities such as the late Pliocene p2 event. We have dated the deformation using detailed biostratigraphy from de Kaenel *et al.* (1999) and Siesser and de Kaenel (1999) in ODP-Leg 161 sites. The chronology of the main deformation events with average sediment accumulation rates for the main basin area are correlated in figure 4-13.

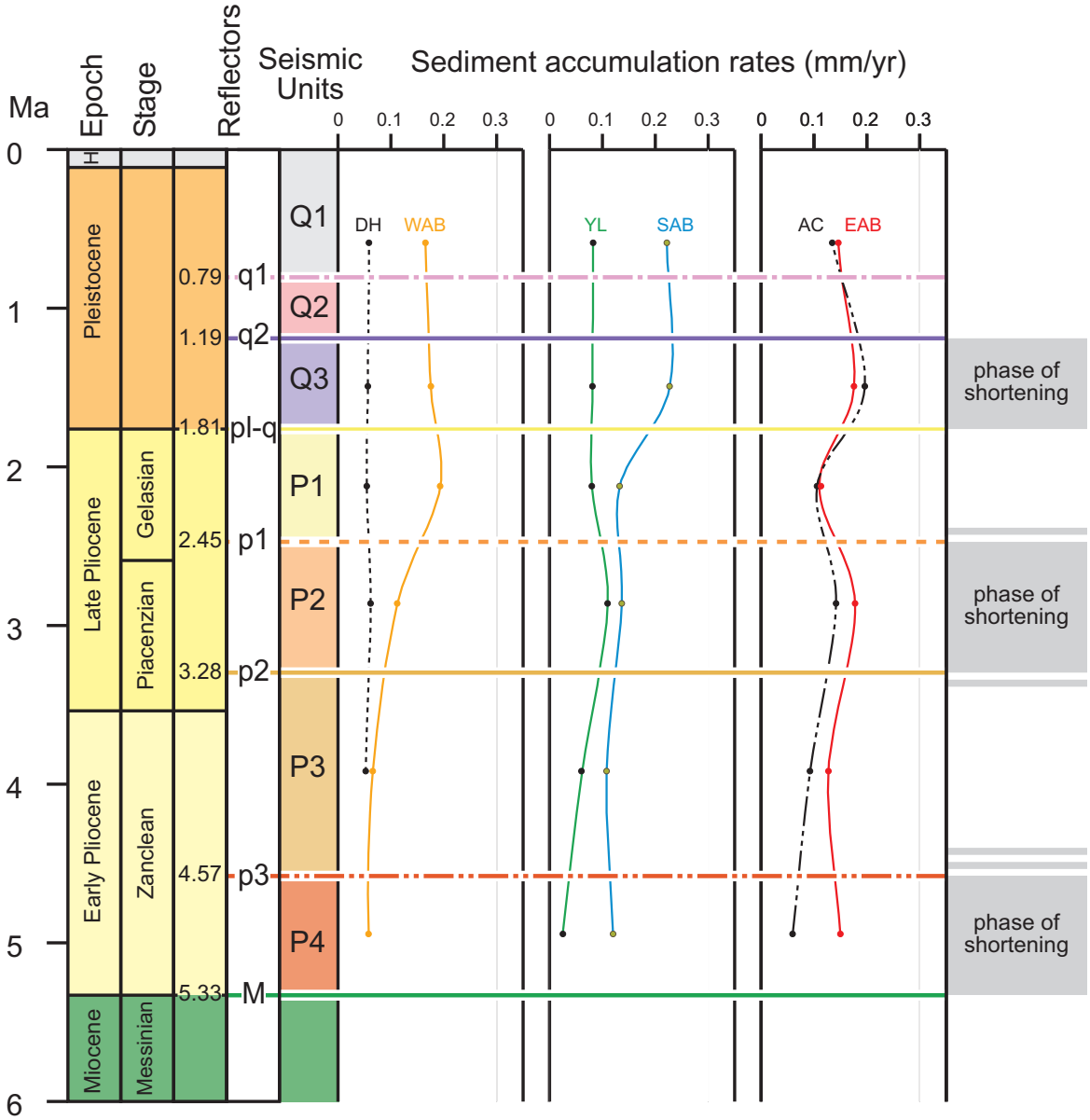

Figure 4-13. Correlation between seismic stratigraphy and changes in average sediment accumulation rates (mm/yr) during the Plio-Quaternary for the main sedimentary depocentres in the studied area: the Alboran Channel (AC), the Djibouti High (DH), the East Alboran Basin (EAB), the South Alboran Basin (SAB), the Yusuf Lineament (YL) and the West Alboran Basin (WAB). Average sediment accumulation rates have been calculated in areas with a continuous Plio-Quaternary sequence and good seismic coverage. Notice that curve for the Djibouti High (DH) begins at Unit P3 because Unit P4 has little distribution here. Dates for the Plio-Quaternary are from Gradstein et al. (2004).

Early Pliocene

The first episode of shortening occurred during deposition of Unit P4 in the earliest Pliocene (~5.33 to 4.57 Ma; Zanclean). The main active structure at this time was a reverse fault on the northern side of the Alboran Ridge, which generated a significant elevation difference between the two fault blocks (*e.g.* Figure 4-10). Unit P4 is thickest in the foot wall block (the EAB) and it is thin or absent on the Alboran Ridge-Yusuf Lineament hanging wall block. Two further observations supporting this interpretation of early Pliocene movement on the Alboran Ridge fault; firstly, the Miocene sub-basins located to the south of this contact (*e.g.* the SAB and the Pytheas basins) are uplifted and had reduced sediment accumulation rates during the Early Pliocene (Figure 4-13); secondly, the p3 reflector, forms an unconformity on the margins of the Alboran Ridge and has a locally important Zanclean hiatus (~4.13 to 5.07 Ma).

The Yusuf and Al-Idrisi fault zones were also active at the same time. Unit P4 thickens in the Yusuf Basin, whereas it is thin or absent above the Yusuf Ridge (Figure 4-11), and hence suggests that the Yusuf fault zone was active during the Zanclean. In the Alboran Channel, Unit P4 thickens towards the central segment of the Al-Idrisi fault (Figure 4-8). In detail, this fault zone propagated southwards because deformation in the southernmost segments is younger than the p3 reflector, *i.e.*, it occurred after 4.57 Ma (Figure 4-4).

Late Pliocene

During the transition from the Early to Late Pliocene, during Unit P3 times (~4.57 to 3.28 Ma), there were very low deposition rates in the basins with many areas being eroded or having no deposition (Figure 4-13). The continuity of Unit P3 from the WAB to the EAB provides evidence of a connection between both basins through the Alboran Channel. Major structures such as the Alboran Ridge and the Yusuf Lineament formed significant intra-basin highs at this time, as suggested by the onlap geometries throughout Unit P3 and its low sediment accumulation rates (Figure 4-7b). The south-western sector of the Alboran Ridge remained relatively undeformed during the Early Pliocene because Unit P3 has similar thickness to those in the adjacent SAB (*e.g.* Figures 4-4 and 4-8).

A second phase of deformation took place during the deposition of Unit P2 at the beginning of the Late Pliocene (~3.28 to 2.45 Ma; Piacenzian to earliest Gelasian). Folds of this age are identified in the hanging wall of the north-directed thrust, on the east of Alboran Island, and also in the south-western sector of the Alboran Ridge (Figure 4-6b). We suggest this event was also contractional because firstly there is considerable thinning of Unit P2 on to the Alboran Ridge, in contrast with uniform thicknesses of underlying units (Figures 4-4 and 4-8); secondly the Alboran ridge had very low sediment accumulation rates (~0.05 mm/yr) in this period; and thirdly the presence of a widespread angular unconformity (the p1 event) in many parts of the basin associated with significant erosion (Figure 4-6c). Similar observations can be made in the EAB, where Unit P2 and occasionally the lower part of Unit P1 thin towards the NE-SW-trending anticlines (Figure 4-11) and above the basement high shown in figure 4-10 (between shot points 2600 and 2850). The uplift during this phase of contraction could have provided sediments that contributed to the higher deposition rates in the surrounding Habibas, Alboran Channel, EAB and WAB basins.

The Late Pliocene (Gelasian) corresponds with a period of relative tectonic quiescence, with the deposition of the thin and relatively uniform Unit P1 (2.45-1.81 Ma). Regional sediment accumulation rates diminish to average values of about 0.1 mm/yr (Figures 4-7d and 4-13).

Pleistocene

The youngest episode of deformation occurred during the earliest Pleistocene, during deposition of Unit Q3 (~1.81 to 1.19 Ma) (Figure 4-13). Unit Q3 thins progressively towards the Alboran Ridge high and the q2 event truncates underlying strata of Q3 age (*e.g.* Figure 4-8) suggesting syn-sedimentary deformation of the Alboran Ridge (Figures 4-7e and 4-13).

The Yusuf Lineament was also active at this time. Unit Q3 thickens in the hanging wall of the northern, normal fault (Figure 4-11), which suggest a phase of extensional to transtensional deformation as also documented by Mauffret *et al.* (1992, 2007), Alvarez-Marrón (1999) and Fernández-Ibáñez *et al.* (2007). The Yusuf Lineament seems then to have undergone a later more recent phase of strike slip faulting as suggested by a constant thickness of Unit Q2 (1.19-0.79 Ma, middle Pleistocene) and progressive thinning of Unit Q1 (< 0.79 Ma, late Pleistocene) across the structure (Figure 4-10 and 4-11).

Reverse slip also occurred on the Al-Idrisi fault zone during the early Quaternary (Figures 4-4 and 4-8). Units Q2 and Q1 are also deformed by the fault zone, but the similar thicknesses across the fault suggests a predominantly strike-slip regime. During this time this fault propagated north-wards forming two conjugate fault sets on the Djibouti High: one trending NNE-SSW, parallel to the Al-Idrisi fault, and the other trending NW-SE (Figures 4-6d and 4-12).

Uplift of the Alboran Ridge continued throughout the Quaternary, as inferred by the significant thinning shown by the youngest units (Q2 and Q1) towards this high (Figures 4-4, 4-8 and 4-9). The Alboran Channel accumulated less sediments during the most recent Quaternary (~0.15 mm/yr), suggesting that it was narrowing due to increased shortening (Figures 4-7f and 4-13). Recent tectonic activity has affected the seabed and is thought to have triggered a number of mass-transport complexes sourced from the Alboran Ridge (Martínez-García *et al.*, 2009).

4.7 Discussion

In the discussion we shall firstly, consider how two main fault systems have controlled the recent evolution of the central Alboran Basin. Secondly we will comment on the geometry of the basin in Messinian times and implications that this has for events associated with the Messinian salinity crisis. Finally we shall summarize the basin evolution through the Pliocene and Quaternary, focussing on the timing of deformation and how the deformation has controlled basin subsidence.

Plio-Quaternary tectonic evolution

Previous studies have suggested that the Alboran Ridge and Yusuf fault zones are two strike-slip systems that connect with structures identified in the Betics and Rif (*e.g.* Maldonado *et al.*,

1992; Woodside and Maldonado, 1992; Fernández-Ibáñez *et al.*, 2007). The Alboran Ridge has been considered part of a left-lateral transpressive system linked to other NE-SE and NNE-SSW trending segments, such as the Jebha Fault in the Rif (*e.g.* Benmaklouf *et al.*, 2005; Chalouan *et al.* 2008) and the Carboneras and Palomares faults in the eastern Betics (*e.g.* Rodríguez-Fernández and Martín-Penela, 1993; Gràcia *et al.*, 2006; Reicherter and Hübscher, 2007). This structure is probably a conjugate system formed of the NW-SE striking right-lateral transtensional Maro-Nerja and the Yusuf Faults (*e.g.* Mauffret *et al.*, 1992; Alvarez-Marrón, 1999; Soto and Manzano, 2002). How the different faults connect remains unclear (see discussion in Fernández-Ibáñez *et al.*, 2007). Some authors suggest that the left-lateral strike-slip faults forms a crustal-scale shear zone that crosscut the entire region from the eastern Betics to the Rif (the Trans-Alboran shear zone; Hernandez *et al.*, 1987; de Larouzière *et al.*, 1988). In contrast, other studies argue that the different fault segments with a NE-SW orientation are not connected and therefore, they do not form a single shear zone crosscutting the region (*e.g.* Bourgois *et al.*, 1992; Mauffret *et al.*, 1992; Ammar *et al.*, 2007).

The connection between the Yusuf fault zone and other NW-SE trending fault segments is also subject to debate. It is not clear if the Yusuf fault terminates on the northern side of the Alboran Ridge (Willet, 1997) or if it continues through the Alboran Channel and deforms the Djibouti High as suggested by Ammar *et al.* (2007) and Ballesteros *et al.* (2008).

Our results show that the Alboran Ridge and Carboneras fault zones are not connected, and therefore do not form a single fault structure crosscutting the Alboran Sea Basin from the Betics to the Rif (Figure 4-6). In fact, the fault and fold systems along the Alboran Ridge change progressively from SW-NE to E-W, to connect finally with the Yusuf fault zone (trending NW-SE). The link between the Alboran Ridge and Yusuf fault zones is accommodated by a curved reverse fault. We have shown that the Alboran Ridge and Yusuf fault zones form a wide and continuous zone of deformation, moving at different times throughout the Plio-Quaternary (Figures 4-6 and 4-10), triggering a progressive southward migration and tilting of the SAB, Pytheas and Habibas basin depocentres (Figure 4-7). We also show that the Yusuf fault zone does not connect with the NW-SE faults deforming the Djibouti High during the Plio-Quaternary in contrast with previous interpretations (*e.g.* Ammar *et al.*, 2007; Ballesteros *et al.*, 2008). The shape and evolution of the depocentre located in the western part of the EAB and the Alboran Channel support this interpretation, because it mimics always the curved trend defined by the Alboran Ridge and Yusuf fault zones (Figure 4-7).

We summarize the evolution of the basin throughout the Pliocene and Quaternary in figure 4-14, with identification of the main faults and folds active in each time interval. These maps also include the convergence vector of the African and Eurasian plates for the relevant time period (Mazzoli and Helman, 1994; Rosenbaum *et al.*, 2002). For comparison, we include the present seafloor bathymetry with the most recently active structures (Martínez-García *et al.*, 2011) and present day plate convergence vectors (DeMets *et al.*, 1994; Fernandes *et al.*, 2003; Nocquet and Calais, 2004).

Implications for the Messinian Salinity Crisis and reflooding of the Mediterranean

The change in sea level in the Mediterranean during the Messinian salinity crisis is estimated to be between 1300 and 1500 m (*e.g.* Bache *et al.*, 2009; Urgeles *et al.*, 2011). Our reconstruction

of the M-reflector shows that in small areas in the centre of the Habibas and Pytheas basins, the SAB, the Alboran Channel and the EAB and even on the Djibouti High the event is a concordant surface with underlying sequences indicating that residual small basins existed during the salinity crisis (Figure 4-14a). Data from Jurado and Comas (1992), Iaccarino and Bossio (1999), Kheidri *et al.* (2000) and Cope *et al.* (2003) show that the sedimentary infill of these small basins consists of

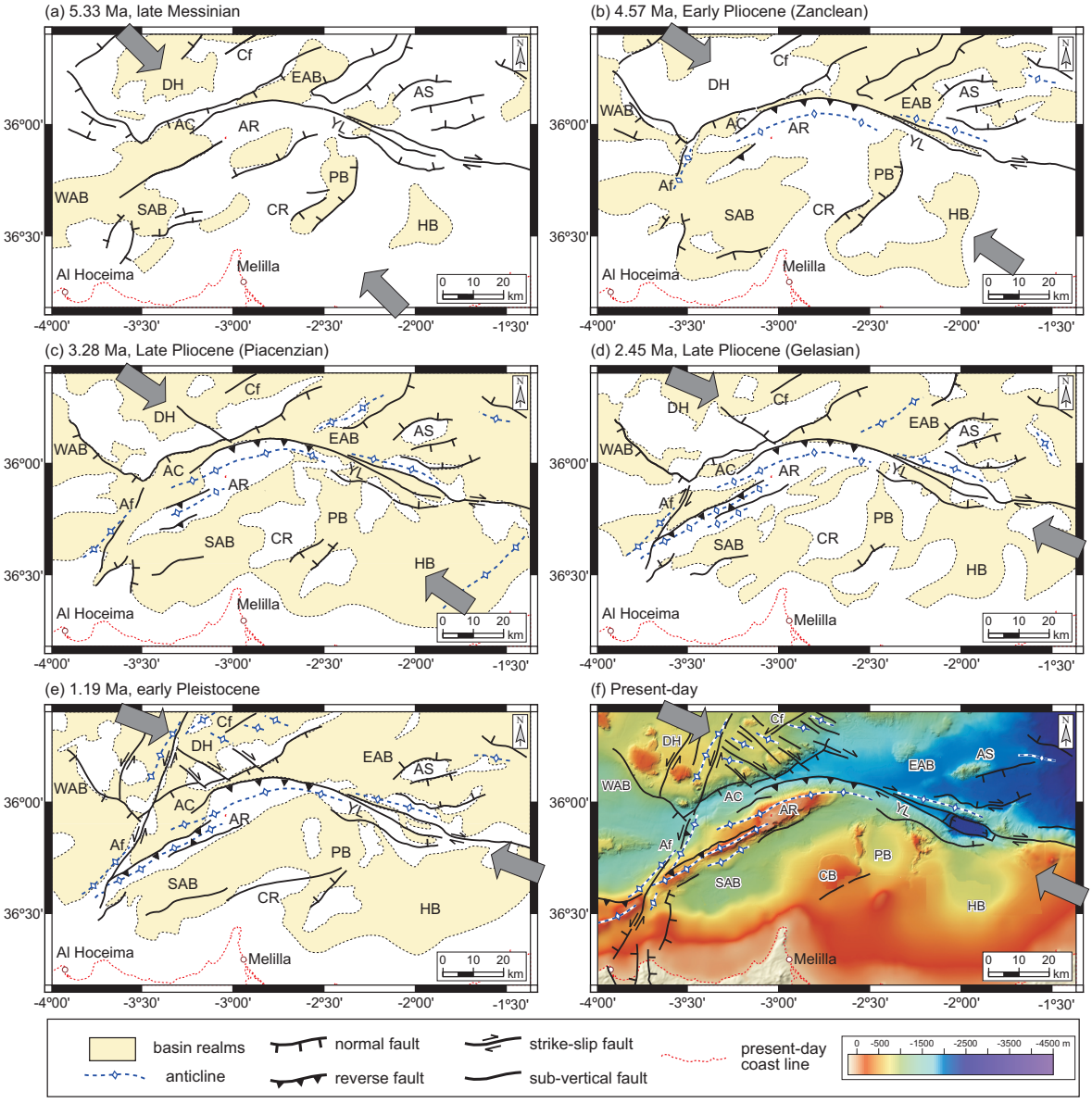

Figure 4-14. Summary maps showing the basin extents and active structures since late Messinian. Stages (panels a to e) correspond to the main events distinguished in the area. Present-day structure and bathymetry shown in (f) is taken from Martínez-García et al. (2011). Large arrows indicate plate convergence vectors between the African and Eurasian plates for each time interval, inferred from plate kinematics reconstructions of Mazzoli and Helman (1994) and Rosenbaum et al. (2002). Present-day plate convergence vector is the average value of the geodetic models of DeMets et al. (1994), Fernandes et al. (2003) and Nocquet and Calais (2004). Abbreviations: AC, Alboran Channel; Af, Al-Idrisi fault zone; AR, Alboran Ridge; AS, Al-Mansour Seamount; Cf, Carboneras fault zone; CR, Cabo Tres Forcas Ridge; DH, Djibouti High; EAB, East Alboran Basin; HB, Habi-bas Basin; PB, Pytheas Basin; SAB, South Alboran Basin; YL, Yusuf Lineament; and WAB, West Alboran Basin.

shallow carbonates, sandy turbidites and gypsum deposits, indicative of shallow marine or lacustrine conditions comparable to those inferred for the isolated marginal basins of the Betics (*e.g.* Martín and Braga, 1994).

Our data also shows that there was a connection between the SAB and the Alboran Channel at the western end of Alboran Ridge (Figure 4-14a). This part of the Alboran Ridge was therefore a basin during the Messinian and was subsequently inverted and uplifted, likewise the Djibouti High. This interpretation agrees with that proposed for the Xauen Bank offshore Morocco by Bourgois *et al.* (1992) where they show an uplifted and folded Miocene depocentre formed during tectonic inversion of the southern WAB (Figure 4-1).

The opening of the Gibraltar Strait at the end of the Messinian caused Atlantic waters to re-enter the Mediterranean (*e.g.* Iaccarino and Bossio, 1999; Krijgsman *et al.*, 1999; Blanc, 2002; Loget *et al.*, 2005). The oldest Pliocene sediments in the region (Unit P4) onlap the M surface and contain abundant channels formed during a major transgression. Previous studies have suggested that hemipelagic sedimentation and low-energy turbidity currents were dominant at that time, infilling the remnant Messinian topography (Estrada *et al.*, 1997; Alonso *et al.*, 1999).

Plio-Quaternary Basin Evolution

The distribution of Unit P4 (Early Pliocene) is restricted in the basin and there are large areas over which there was no sedimentation (Figure 4-7a). These observations agree with data from the nearby WAB, where the Early Pliocene around the ODP Site 976 high is almost totally eroded (Campillo *et al.*, 1992; Comas *et al.*, 1992, 1999; Comas and Soto, 1999). The first deformation event occurred in Unit P4 times uplifting the Alboran Ridge, the Yusuf Lineament and the basin margins (Figure 4-13). The reverse faulting along the Alboran Ridge fault zone and the right-lateral displacement along a sub-vertical Yusuf fault zone are an expression of the NW-SE convergence of the African and Eurasian plates at this time (Figure 4-14b). This phase of shortening appears to have had regional expression and was not just localised to structures within the Alboran Sea Basin as we note that the onshore coastal areas of the Betics, became almost completely emergent during the Early Pliocene despite the post-Messinian marine transgression inferred for that time (*e.g.* Aguirre, 1998; Braga *et al.*, 2003; Martín *et al.*, 2003).

During the Early to Late Pliocene, we observe a considerable widening of the basin areas (Figure 4-14c). However, low sediment accumulation rates on the Alboran Ridge and Yusuf Lineament (average ~0.06 mm/yr) together with the local unconformity developed on the highs (reflector p2; ~ 3.28 Ma) suggest that uplift continued on these structures (Figure 4-7b). Other authors have also recognized an important onshore unconformity of comparable age (~3.6-3.2 Ma; Montenat *et al.*, 1990; Aguirre, 1998). The p2 reflector (~3.28 Ma) correlates well with this intra-Pliocene age.

During the early Late Pliocene, coinciding with the second phase of shortening (~3.28-2.45 Ma), reverse faulting and associated folding propagated to the southwest along the Alboran Ridge (Figure 4-14 d). Plate reconstructions for this period suggest a smooth change in the convergence trend between the African and Eurasian plates from NW-SE to WNW-ESE (*e.g.* Mazzoli and Helman,

1994). This period coincides with a major uplift of the Alboran Ridge, which has minimum sediment accumulation rates for Unit P2 (Figure 4-13). However, the Yusuf Lineament simultaneously underwent an increase in subsidence and sediment accumulation rates (~0.1 mm/yr). This was probably due to active transtensional displacement along the Yusuf fault zone (*e.g.* Campos *et al.*, 1992; Maldonado *et al.*, 1992; Mauffret *et al.*, 1992, 2007; Alvarez-Marrón *et al*., 1999), which is sub parallel to the plate convergence vector at that time.

For the first time sediment supply through the Almeria Canyon into the basin is observed (see sediment accumulation rate maps; Figure 4-7c) and it corresponds with a first important contribution of the Almeria turbidite system (*e.g.* Estrada el al., 1997; Alonso and Ercilla, 2003). We consider that shortening during the Late Pliocene event, coeval with a possible fall in sea-level (Hernández-Molina *et al.*, 2002), led to erosion around the basin margins and on intrabasin highs such as the highest portions of the Alboran Ridge and Yusuf Lineament, which could have been partially emergent during this time.

In contrast the Djibouti High, was not affected by significant deformation during the Late Pliocene and it remained as a residual normal fault bounded Miocene high. Condensed sequences and associated low sediment accumulation rates suggest that this block remained elevated during most of the Plio-Quaternary (Figures 4-7 and 4-13). Another residual high similarly bounded by high-angle Miocene faults is the buried basement high identified in the EAB (Figures 4-14b and 4-14c). The folded Plio-Quaternary sequence capping these highs indicates that during the Late Pliocene some older extensional-related structures were reactivated and shortened (*e.g.* Comas and Soto, 1999).

The late Pliocene shortening is also identified in the Rif region by the inversion of earlier normal faults such as the North Bokkoya fault (Figure 4-1), which is parallel in strike to the Alboran Ridge (Chalouan *et al.*, 1997). Integrating these data with our results in the Alboran Sea Basin, allows us to infer that although most of the contraction was accommodated on the Alboran Ridge and the Yusuf Lineament, deformation was heterogeneously distributed during the Late Pliocene tectonic event.

The Alboran Ridge and Yusuf Lineament experienced a further phase of shortening during the early Pleistocene (~1.81-1.19 Ma; *e.g.* Figures 4-8 and 4-11). This event is recorded in uplifted terraces along the coast of southern Spain (*e.g.* Rodríguez-Fernández and Martín-Penela, 1993; Zazo *et al.*, 2003). The NE-SW folds and associated reverse faults that developed throughout the Quaternary on the Alboran Ridge were probably driven by the NW-SE orientation of plate-convergence (Figure 4-14e). The two fault and fold systems identified in the Djibouti High started at this time period. They are interpreted as conjugate systems with a significant component of lateral motion (Figure 4-14f; Martínez-García *et al.*, 2011). Their fault kinematics is also consistent with the present-day NW-SE regional stress field oriented (Fernández-Ibáñez *et al.*, 2007).

Further subsidence of NE-SW-trending depocentres, parallel to the Alboran Ridge, continued after early Pleistocene shortening (Figures 4-7e and 4-13). The expansion of the main basin realms during the Quaternary was accompanied by an increase in sediment accumulation rates (Figure 4-14e). The episodes of high sea-level during this period (up to 120-150 m) might have also encouraged seabed gravity-instability processes (Hernández-Molina *et al.*, 1994, 2000; Estrada *et al.*, 1997; Lobo *et al.*, 1999). Tectonic uplift of the Alboran Ridge has probably continued up to the

present day. Deformation processes, combined with the effects of sea-level falls during the most recent Quaternary, are thus responsible for the present day shape of the emergent Alboran Island.

4.8 Conclusions

1) Through a new interpretation of a dense grid of seismic reflection profiles, correlated to nearby DSDP and ODP sites, we have identified and assigned ages to four Pliocene and three Quarternary units in the Alboran Sea. Our reconstructions of basin structures and sediment accumulation rates document how the palaeogeography has evolved since the Messinian in a region characterised by complex interactions between inherited structures, sediment supply from the surrounding Betic and Rif mountains, deformation and subsidence.

2) We have described the internal structure and the subsidence/uplift history of the SW-NE trending Alboran Ridge and the WNW-ESE trending Yusuf Lineament through the Pliocene and Quaternary. We have identified three contractional deformation phases that have affected these important fault zones causing shortening, uplift and transpression or transtension depending on their angle with respect to the prevailing plate convergence trend. Main deformation pulses occurred during the Early Pliocene (~5.33 to 4.57 Ma), the Late Pliocene (~3.28 to 2.45 Ma) and within the early Pleistocene (~1.81 to 1.19 Ma).

3) The main uplift of the Alboran Ridge occurred during the Late Pliocene, at the same time as the plate convergence between the African and Eurasian plates changed from NW-SE to WNW-ESE. North-directed reverse faults thrusted the ridge over the Alboran Channel and EAB. The accompanying folding caused erosion of the high during this time and a reduction in the sedimentation rates in basins located in its the hanging wall (*e.g.* the South Alboran Basin and the Pytheas Basin).

4) During the most recent phase of shortening new fault systems have developed across the western part of the Alboran Ridge. Most of the deformation has been partitioned during the Quaternary along the left-lateral, NNE-SSW trending, Al-Idrisi fault and in conjugate fault systems on the Djibouti High.

5) In summary, we have documented how the Plio-Quaternary Alboran Sea Basin has evolved on a complicated template inherited from previous tectonic events. Our work shows that shortening and partial inversion, very complex kinematics and patterns of relative subsidence/uplift evolved in a short time frame of only 5 Million years. In large part this complexity is a function of the distribution of local basins and intra-basinal highs inherited from pre-Messinian times, within a zone of transpressional deformation.

5. Submarine instability processes

Recurrent slope instability and slides in the Alboran Sea Basin: assessment for changing basin topography from Pliocene to Recent

Manuscript under elaboration (to be submitted).

Pedro Martínez-García[1], Menchu Comas[1], Juan I. Soto[2] and Lidia Lonergan[3]

[1] Instituto Andaluz de Ciencias de la Tierra (CSIC and University of Granada), Facultad de Ciencias,

[2] Instituto Andaluz de Ciencias de la Tierra (CSIC and University of Granada) and Departamento de Geodinámica, Facultad de Ciencias, Granada, Spain.

[3] Department of Earth Science and Engineering (Imperial College London), South Kensington Campus, London, United Kingdom.

Abstract

From swath bathymetry data, high-resolution acoustic profiles (TOPAS) and multichannel seismic reflection profiles, several mass transport deposits (MTD) have been imaged in the eastern Alboran Sea (western Mediterranean). Submarine instability processes occur along several submarine slopes including the Yusuf Escarpment and the Alboran Ridge. The identified gravitational deposits in the Plio-Quaternary record show variable internal structures including deposits with transparent and chaotic facies and tilted blocks with low degree of internal deformation. They extend in areas of up to 19 km^2 and appear in water depths ranging between 640 and 2580 m. The occurrence of slides deposits along fault escarpments affecting the seafloor reveals that submarine instability processes in the region are mainly controlled by tectonics. Moreover, some mass transport deposits are composed internally by several lobes of sediments. This fact suggests that instability processes are recurrent throughout the Plio-Quaternary and they may be related with recurrent events of faulting and uplift. Submarine instability processes are tied to the well known Plio-Quaternary tectonic evolution of the central and southeastern Alboran Sea. Numerous submarine instability processes are recent to active as most of the slides deposits are outcropping or buried by thin layer of hemipelagic sediments. It is therefore demonstrated that instability processes represent a geological risk in the Alboran Sea that should be surveyed and analyzed in the future in order to determine its tsunamigenic potential in the Mediterranean region.

Keywords: slides, instability processes, swath-bathymetry; Alboran Sea, active tectonics, Plio-Quaternary.

5.1 Introduction

Submarine gravitational instability processes are responsible to a large degree for the morphology and evolution of the seafloor and they display considerable magnitude in continental slopes in oceanic environments. The progressive increasing development of geophysics techniques and direct methods that allow to observe the marine seafloor and to obtain information from the shallower sediments, has propitiated successive discoveries of numerous submarine slides in different geological and geomorphological settings (*e.g.*, Tricardini and Argnani, 1990; Gardner *et al.*, 1999; McAdoo *et al.*, 2000; Imbo *et al.*, 2003; Canals *et al.*, 2004; Lastras *et al.*, 2004, 2006; Casas *et al.*, 2003, Hjelstuen *et al.*, 2007). Moreover the study of submarine instability processes has economical and social interest as they represent a major geological hazard for nearby coastal areas and offshore infrastructures (*e.g.* Synloakis *et al.*, 1997)

In the Western Mediterranean, the Alboran Sea Basin is well known about aspects related with its sedimentary infilling, structure, tectonic evolution and peculiar geophysical features (Comas *et al.*, 1992, 1999; Docherty and Banda 1992, 1995; García-Dueñas *et al.*, 1992; Jurado and Comas, 1992; Maldonado *et al.*, 1992; Woodside and Maldonado 1992; Watts *et al.*, 1993; Polyak *et al.*, 1996; Lonergan and White, 1997; Torné *et al.*, 2000, Talukder *et al.*, 2003, Gràcia et al 2006; Ballesteros *et al.*, 2008, among others). However the characterization of mass-transport deposits and the study of their origin has received much less specific attention (*e.g.*, Alonso *et al.*, 1999; Lo Iacono *et al.*, 2008) and it deserves to be studied in detail similarly to other studies in the western Mediterranean (*e.g.*, Alonso *et al.*, 1990; Tricardini and Argnani, 1990; Hernández-Molina *et al.*, 1994; Lastras *et al.*, 2002; 2004; 2006; Casas *et al.*, 2003; Canals *et al.*, 2000; 2004; Giresse *et al.*, 2009).

In this work we show and analyze some cases of sedimentary instability processes and related deposits (*Mass Transport Deposits* - MTD) that have been recognized in the eastern sector of the Alboran Sea (Figure 5-1) This work is based on the analysis of bathymetric, seismic reflection and high resolution acoustic data. The study comprises the description and mapping of these structures and discusses the mechanisms and main controlling factors that have produced submarine slides and slumps during the Pliocene to Quaternary evolution of this region. We believe that these new data would be useful to evaluate the geologic hazards in the western Mediterranean.

5.2 Geological setting

The Alboran Sea Basin deepens and opens eastward to the abyssal plane of the Algerian Basin (Figure 5-1). The westward connection with the deeper Atlantic Ocean occurs through a narrow, channelled threshold in the Gibraltar Strait. The seafloor of the Alboran Sea is morphologically complex, with numerous isolated highs from different origins (structural ridges, volcanic highs and mud volcanoes) (Figure 5-1). The Alboran Ridge is the major bathymetric high in the Alboran Sea Basin, and bounds three main sub-basins: the West, East and South Alboran basins (WAB, EAB and SAB respectively) (Figure 5-1). This bathymetric high is a 130 km long volcanic ridge with SW-NE orientation. Eastwards the Alboran Ridge turns into a north-dipping slope and its orientation change progressively from SW-NE to E-W, to connect finally with the Yusuf Escarpment. This escarpment constitutes the western prolongation of the Habibas Escarpment, which forms the steep southern

margin of the Algerian Basin. The Yusuf Escarpment presents the highest slope gradients in the Alboran Sea, with values locally exceeding 70° bordering the Yusuf Basin (Figure 5-1).

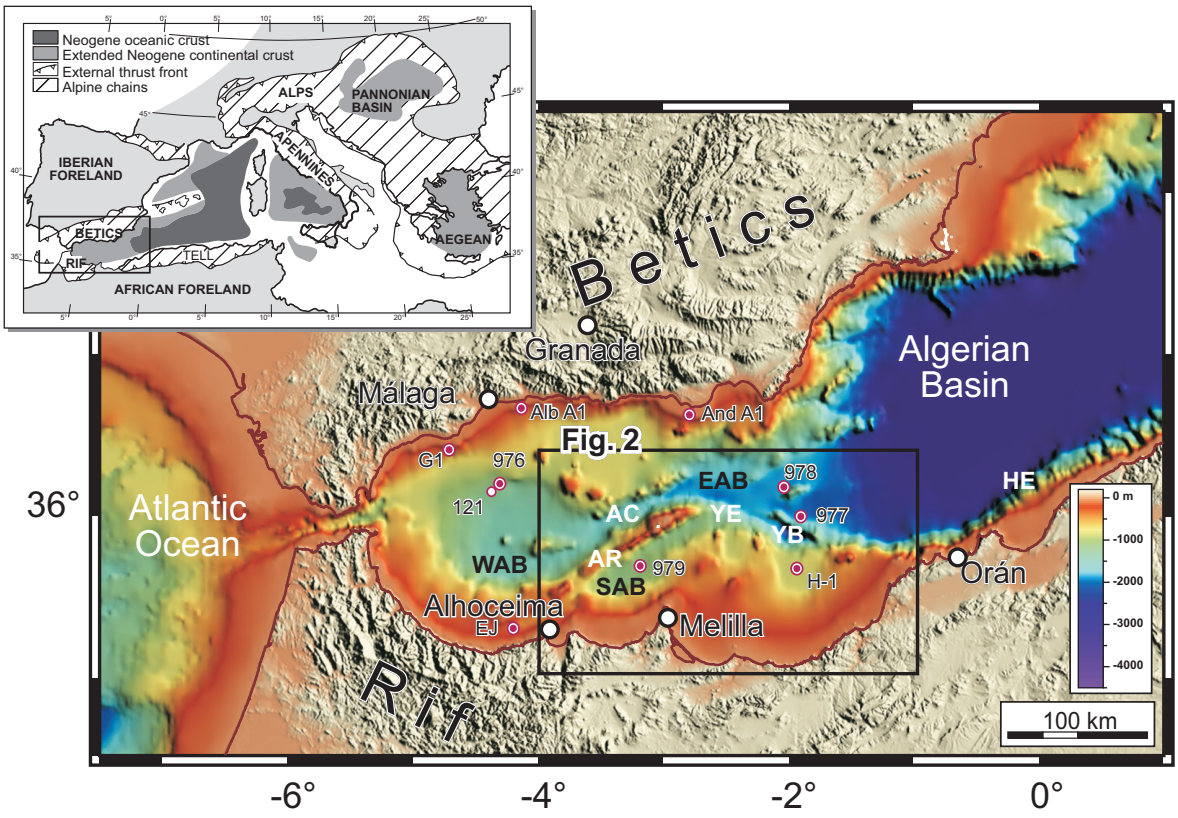

Figure 5-1. Topography of the Gibraltar Arc System. Digital topography is built on the SRTM (USGS-NASA) global database combined with GEBCO 97 (IOC-IHO) for the offshore region. Rectangle delimits the studied area in the Alboran Sea and its transition towards the Algerian Basin. Circles show location of ODP Leg 161 sites (976 to 979), DSDP site 121 and commercial boreholes offshore (G1, Andalucía-G1; A1, Alboran-A1; And-A1, Andalucía-A1; EJ, El-Jebha; H-1, Habibas-1). Inset map is a tectonic sketch of the Mediterranean Sea, showing Neogene extensional basins and external front of surrounding Alpine thrust belts (from Comas *et al.* 1999). Abbreviations: AR, Alboran Ridge; AC, Alboran Channel; EAB, East Alboran Basin; HE, Habibas Escarpment; SAB, South Alboran Basin; YB, Yusuf Basin; YE, Yusuf Escarpment; WAB, West Alboran Basin.

The Alboran Sea Basin is one of a number of basins in the Mediterranean Sea that formed during the Neogene within a region of convergence between the African and Eurasian plates (Horvath and Berckhemer, 1982). The Alboran Sea Basin locates at the centre of the Gibraltar Arc System, which is a strongly arcuate Alpine orogen comprising also the Betic and Rif mountains. This system was formed during the Early Miocene by westward migration of the mountain belt and coeval extension in a context of NW-SE plate convergence (*e.g.* Platt and Vissers 1989; García-Dueñas *et al.*, 1992; Watts *et al.*, 1993; Lonergan and White, 1997; Comas *et al.*, 1999; Jolivet and Faccenna, 2000). Eastwards, the Algerian Basin corresponds with an abyssal plain (maximum depth 2800 m) and it is probably floored by oceanic crust formed during the middle to late Miocene as result of crustal back-arc extension (Rehault *et al.*, 1985; Dewey *et al.*, 1989; Mauffret *et al.*, 2004; Booth-Rea *et al.* 2007).

Later shortening caused basin inversion, folding and reverse and strike-slip faulting in the Alboran Sea Basin. These structures have been active throughout the Plio-Quaternary, producing shortening of the whole region and uplift of the basin margins (Bourgois *et al.*, 1992; Woodside and Maldonado, 1992; Morel and Meghraoui *et al.*, 1996; Meghraoui *et al.*, 2004; Déverchère *et al.*, 2005; Mauffret *et al.*, 2007; Fernández-Ibáñez *et al.*, 2007; Yelles *et al.*, 2009; Strzerynski *et al.*, 2010).

Continental crustal basement underlies a sedimentary cover up to 8 km thick in the Alboran Sea Basin (*e.g.*, Platt *et al.*, 1998; Comas *et al.*, 1992; 1999). The seismic stratigraphy of the Miocene to Recent sequences is well established and several seismic units are recognised based on seismic interpretation and well information from commercial wells and DSDP Site 121 and ODP Leg 161. (*e.g.*, Comas *et al.*, 1992, 1999; Ercilla *et al.* 1992; Jurado y Comas, 1992; Maldonado *et al.*, 1992; Chalouan *et al.*, 1997; Estrada *et al.* 1997; Vázquez 2001; Talukder *et al.*, 2003).

The Pliocene-Quaternary record of the Alboran Sea Basin was well characterized by the *Ocean Drilling Program* during Leg 161. Quaternary and Holocene sedimentary deposits that were recovered in the ODP Sites 976 to 979, show abundant turbiditic intervals and redeposited shale-rich facies (Comas *et al.*, 1996; Alonso et. al, 1999). Particularly in Site 979, which drilled the southern side of the Alboran Ridge, the Quaternary-Holocene sequence, constituted by hemipelagic deposits with scarce detritic intercalations, has several hiatus and slumping intervals attributed to episodes of sedimentary instability caused by the coeval uplifting of the Alboran Ridge (Comas *et al.*, 1996; 1999).

5.3 Dataset and Methodology

This work is based on the study and interpretation of swath bathymetry mosaics, high resolution acoustic sections and multichannel seismic profiles. The swath bathymetric datasets belong to different marine cruises conducted in the region on board the BIO Hesperides, corresponding to the ALBA cruise (1992), TECALB (2000), and MARSIBAL I-06 (in 2006) cruises. Other complementary data used to complete the mosaic locally are the bathymetric atlases of MediMap Group (2005, 2008).

Slides identified in the bathymetric mosaic have been analyzed in vertical sections from high-resolution TOPAS and multichannel seismic reflection profiles, in order to study its internal structure. The Simrad TOPAS (TOpographic PArametric Sonar) is a low frequency (0.5-6 kHz) sub-bottom profiling system which provides detailed images of the shallower deposits (maximum penetration is around 170-180 m). Moreover, deep structure has been analyzed by means of multichannel seismic reflection profiles (Figure 5-2a). It includes available data from commercial seismic surveys during the early seventies and also academical data acquired during the TECALB (2000) and MARSIBAL I-06 (2006) cruises conducted onboard the R/V BIO Hespérides. Seismic interpretation was performed using the SMT Kingdom Suite® software. Key seismic horizons of regional distribution as identified by Martínez-García *et al.*, (*submitted for publication*) were correlated to define precisely the timing of MTD events. This seismic stratigraphy proposed on the basis of the correlation with DSDP Site 121 and ODP sites 976 to 979 (Ryan *et al.*, 1973;Comas *et al.*, 1996, 1999). In addition, we used the commercial Habibas-1 well located to the southeast of the study area (Kheidri *et al.*, 2000; Cope *et*

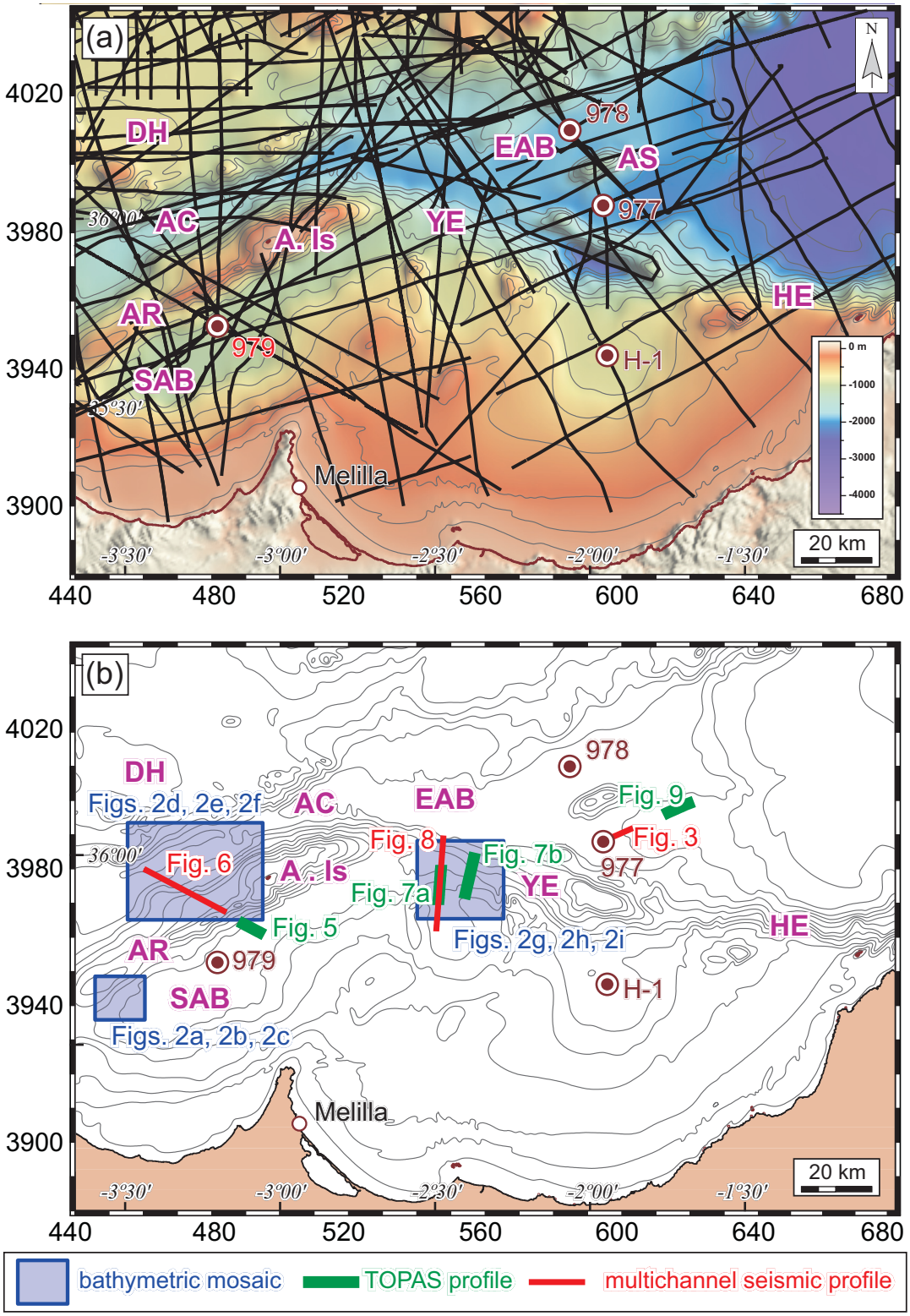

Figure 5-2. (a) Location map of seismic profiles and wells used in the study (rectangle in Figure 5-1). Detail of the studied area in the eastern Alboran Sea, showing location of ODP Leg 161 sites and studied seismic profiles. **(b)** Bathymetry contours of the studied area (from GEBCO 97), showing location of the bathymetric mosaics, TOPAS profiles and multichannel seismic profiles presented in other figures. Bathymetry contours in metres; contour interval is 200 m. UTM projection, units in kilometres (WGS 84 ellipsoid). Abbreviations: A. Is, Alboran Island; AR, Alboran Ridge; AC, Alboran Channel; DH, Djibouti High; EAB, East Alboran Basin; HE, Habibas Escarpment; SAB, South Alboran Basin; YE, Yusuf Escarpment; WAB, West Alboran Basin.

al., 2003; Mauffret *et al.,* 2007) (Figure 5-2). Selected reflectors correspond with local or regional unconformities whose age is well know form biostratigraphic studies (de Kaenel *et al.* 1999; Siesser and de Kaenel, 1999). Seismic events were tied to well log data (Vp, density and gamma ray). Figure 5-3 shows an example of correlation between seismic and biostratigraphic data in the ODP Site 977.

High resolution bathymetric data were acquired using an EM-12S-120 Simrad multibeam echosounder. This system has a swath coverage of 3.5 times seafloor depth and covers water depths ranging from 50 to 11 000 m. These data were processed with the CARIBES software to obtain a 3D high-quality mosaic. Examples of the resultant seafloor image are shown in figure 5-4. The seafloor analysis was completed by calculating terrain slopes (Figures 5-4b, 5-4e, 5-4h, and 5-4k).

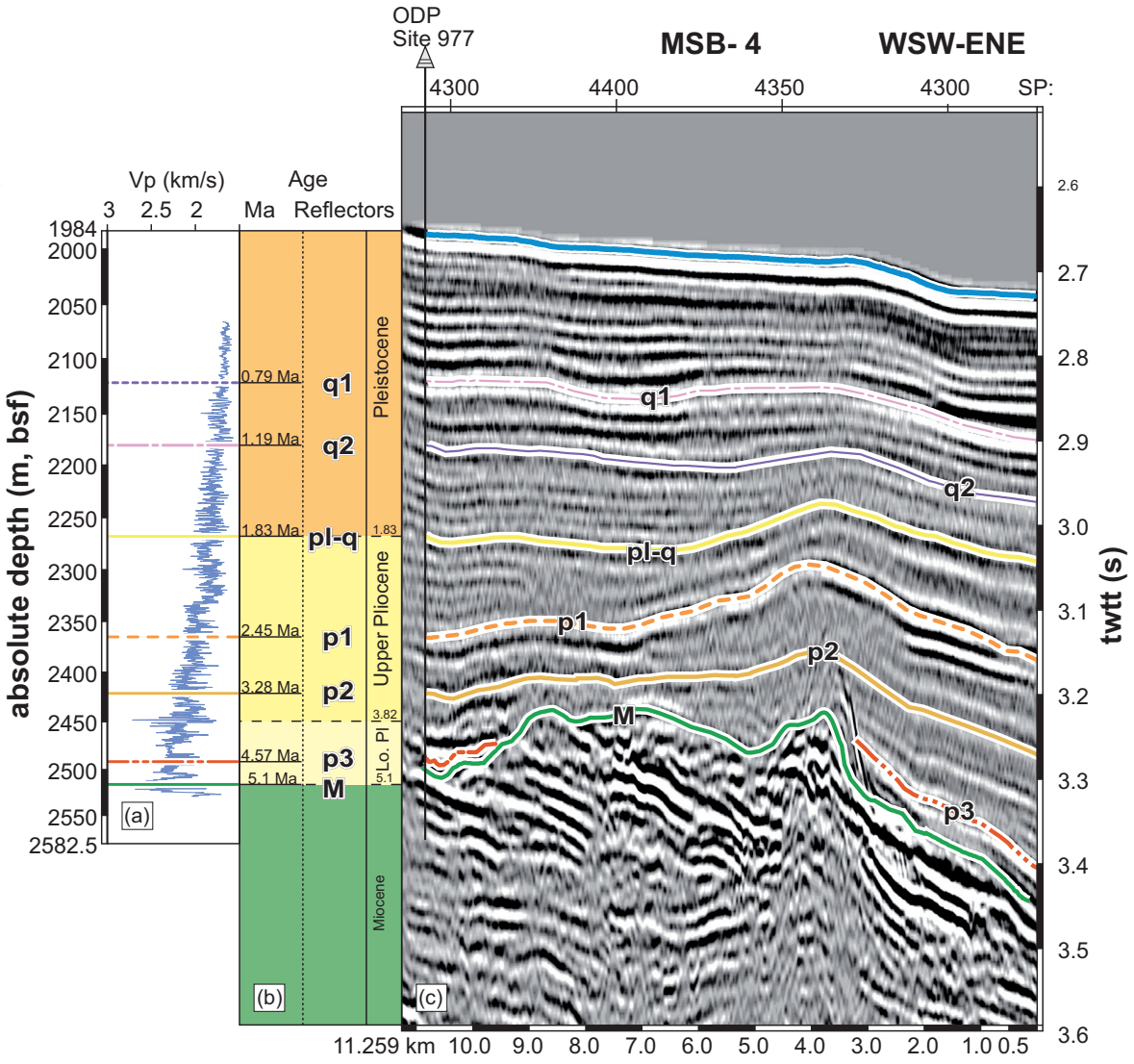

Figure 5-3. Comparative panel showing correlation between: **(a)** Vp data from the Site 977; **(b)** chronostratigraphic determinations (de Kaenel *et al.*, 1999; Siesser and de Kaenel, 1999); and **(c)** multichannel seismic profile across the EAB (line MSB-4). Location in figure 5-2b.

5.4 Plio-Quaternary seismic stratigraphy

We have identified and assigned ages to four Pliocene and three Quaternary seismic units, which are bounded by key reflectors (Figure 5-3). The M reflector forms the lower boundary of the Plio-Quaternary succession and appears as a prominent, high amplitude, laterally continuous reflection. This event is dated at 5.33 Ma (Clauzon *et al.*, 1996). However it should be noted that it may involve an hiatus of significant duration due to its strong erosive nature. Unit P4 is Early Pliocene. Its bottom is the M-reflector and its top corresponds with the p3 reflector with an estimated age of ~4.57 Ma. Unit P3 is Early-Late Pliocene. The p2 reflector forms the upper boundary of this unit and its estimated age is ~3.28 Ma. The early Late Pliocene P2 is bounded on top by the p1 reflector. Correlation to ODP Site 979 shows that this reflector corresponds with a hiatus from 2.52 to 2.45 Ma. As with the other major unconformities it becomes conformable towards the basin centres. Unit P1, of Late Pliocene age, is delimited on top by the pl-q reflector, which corresponds with the 1.81Ma Pliocene-Quaternary boundary. Unit Q3 is early Pleistocene. The q2 reflector (1.19 Ma) forms the boundary between this unit and the overlying middle Pleistocene Q2 Unit. The q1 reflector, forming the top of Unit Q2, has an estimated age of ~0.79 Ma. The shallowest seismic unit is Q1 and its age ranges from late Pleistocene to Holocene (~0.79 to 0 Ma).

5.5 Evidences of slides and Mass Transport Deposits

On the bathymetric mosaic covering different sectors of the Alboran Sea, we have recognized numerous slides and slumps structures in water depths ranging between 640 and 2580 m. Slide scars are escarpments with slopes over and 10-25º and concave geometries towards the base of the slopes. Mass Transport Deposits (MTD) are recognized as lobes delimitated by changes of slope terrain gradient at their bases. MTD mainly locate in the slopes of the Alboran Ridge, along the Yusuf Escarpment, in the EAB and along the step between the EAB and the Algerian Basin (Figure 5-1).

Southern Slope of the Alboran Ridge

A slide scar has been identified between 35º 36'N - 35º 39'N and 3º34'W - 3º28'W covering a minimum area of 19 km^2. The bathymetric image and slope map in figures 5-4a and 5-4b is show a clear scar with a concave shape towards the SW. The curved outline of the main scar has a total length of about 10 km and in detail, it is composed by several small secondary concave scars conforming a general lobulated shape in the headwall area. This scar extends from -640 to -815 m, and it is located on the base of a linear escarpment with SW-NE orientation and a variable slope between 10º and 25º (Figure 5-1). Some other buried MTD have been identifed in TOPAS profiles towards the east of this same escarpment. For example, figure 5-5 shows sub-outcropping slides buried by thin layers of hemipelagic sediments around 35º 47'N and -3º7'W. Slides display lens geometries and transparent acoustic facies. This fact indicates that MTD are chaotic deposits. Slide bodies dip toward the southeast and show basal failure planes dipping ~3º (Figure 5-5). The mean thickness of these slide deposits is over 15 m but the different bodies are usually thicker downslope, towards their toe fronts.

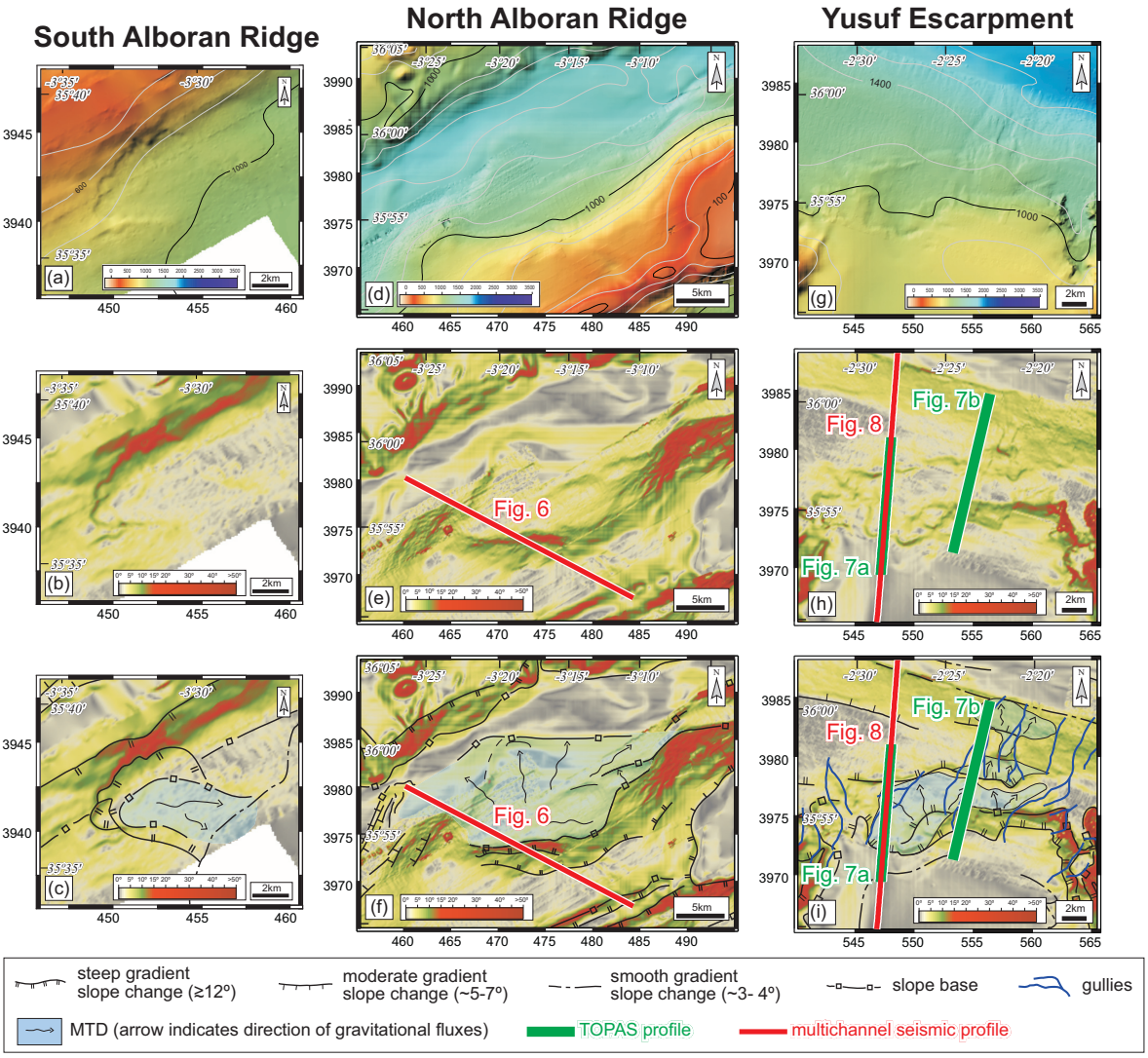

Figure 5-4. Bathymetric mosaics, slope maps and interpretation of different slides in the central and eastern Alboran Sea. Locations in figure 2b. **(a)**, **(b)** and **(c)** southern slope of the Alboran Ridge; **(d)**, **(e)** and **(f)** northern slope of the Alboran Ridge; **(g)**, **(h)** and **(i)** Yusuf Escarpment. Bathymetry contours in metres from GEBCO 97 (IOC-IHO); contour interval is 200 m. UTM projection, units in kilometres (WGS 84 ellipsoid).

Northern Slope of the Alboran Ridge

We have identified a wide sector affected by instability sedimentary in the northern slope of the Alboran Ridge . Resulting slides are located between 35º 26'N - 36º 0'N and 3º27'W -3º7'W, in water depths ranging between -880 and -1650 m. This area covers approximately 230 km^2 and has a peculiar staircase profile: different steps are narrow and concave domains with high slope (12-25º) and hundred metres in height that bound areas with smooth or undulating topography with a relatively low gradient (<7°) (Figures 5-4d to 5-4f). The main scar locates between 600 and 1000 m depth and is concave towards the NW. Its curved outline measures about 33 km.

The stratigraphic architecture of this slope is illustrated by the multichannel seismic profile shown in figure 5-6. This section displays numerous high-angle faults that deform Plio-Quaternary sediments. Even some of these faults condition the morphology of the seafloor, indicating that they are active at present (Martínez-García *et al.*, 2011). Three recent slides have been interpreted within the

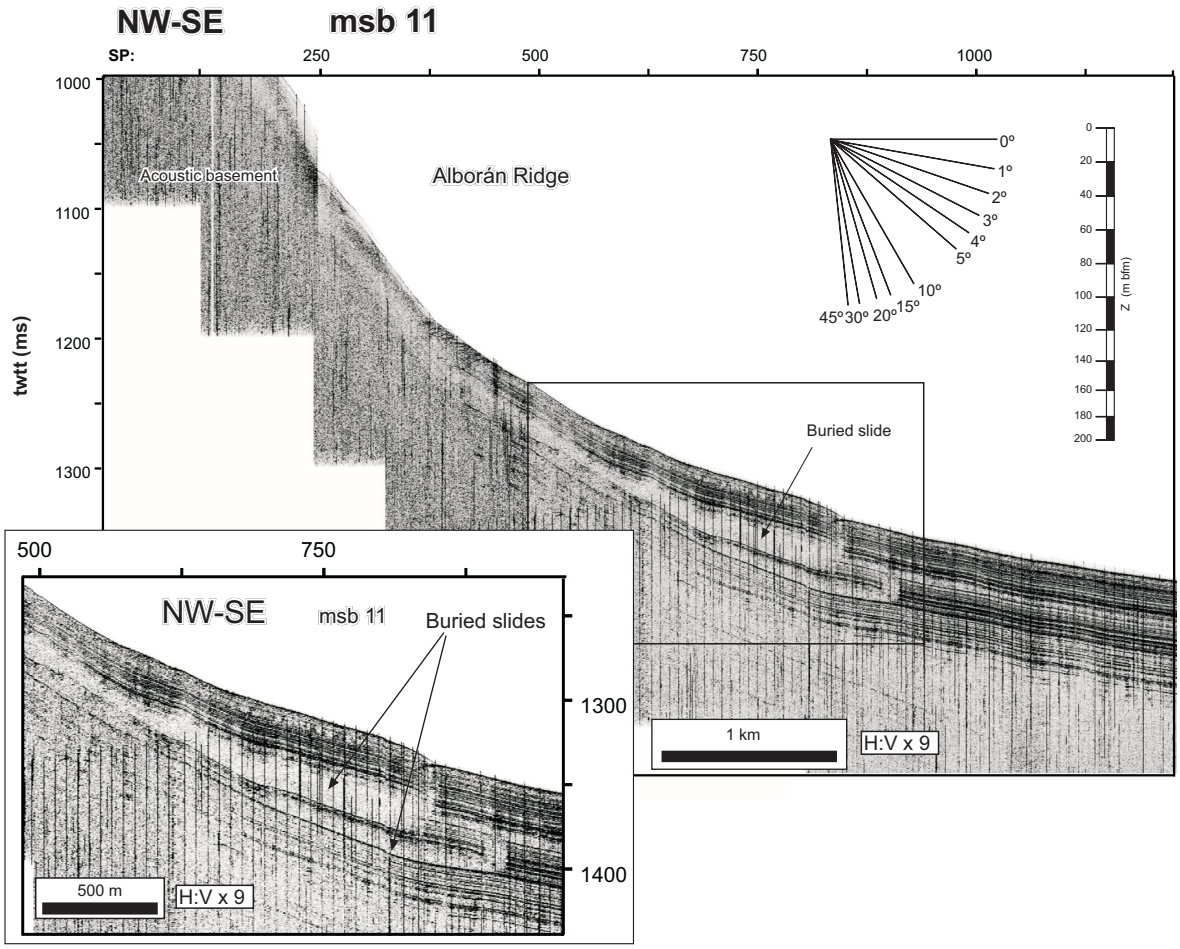

Figure 5-5. TOPAS profile showing buried slides in the southern slope of the Alboran Ridge. Estimated depth scale and calculated dip abacus are shown for comparison. Location in figures 5-2b, 5-4e and 5-4f.

Plio-Quaternary sequence (above the M-reflector), based on their chaotic and semi-transparent facies. Gravitational detachments (failure planes or slip planes) at their bases are clearly visible. Different slide bodies have similar mean thickness of about 150 ms (twtt) (~112 m) and their extension varies from ~4 to 10 km. The different slides are overlapping and they all together form a system of MTD extending ~20 km. Two types of seismic facies have been identified. The shallower slide deposit, labelled as Slide 3, and the frontal part of Slide 2, show chaotic semi-transparent facies alternating with some levels of stratified facies. Conversely, the deeper MTD corresponding with Slide 3 and the upper part of Slide 2, display discontinuous and irregular high-amplitude facies (Fig. 6).

Yusuf Escarpment

Several scars and MTD have been identified in this escarpment, being located in an area comprised between 35º26'N-36º0'N and 3º27'W-3º7'W, in water depths ranging between -900 and -1620 m. Numerous minor slide scars with variable curvature form the headwall area of these slides. In some cases scars are eroded by gullies that flow downslope across the Yusuf Escarpment (Figures 5-4g and 5-4i). Figure 5-7a is a TOPAS profile across one of the MTD recognized in the bathymetric mosaic, which locates on the upper part of the escarpment (Figures 5-4g to 5-4i). The TOPAS profile

shows that sediments on the slide headwall adjacent to the main scar display stratified facies and are deformed by open folds with low-dipping flanks (<10-12º) and low angle normal faults (30º) dipping towards the NE. We interpreted these structures as slumps. A multichannel seismic reflection profile, coincident with this TOPAS profile, reveals that these faults are shallow structures that are rooted on a basal detachment (Figure 5-8). This failure plane corresponds with a layer within the Quaternary sequence and it is parallel to the sediment stratification. Below this surface, Pliocene sediments are not affected by these shallow faults (shot points 2225-2275 and 2325-2350). Moreover, the central part of these MTD lay on top of a basement high (shot points 2275-2325).

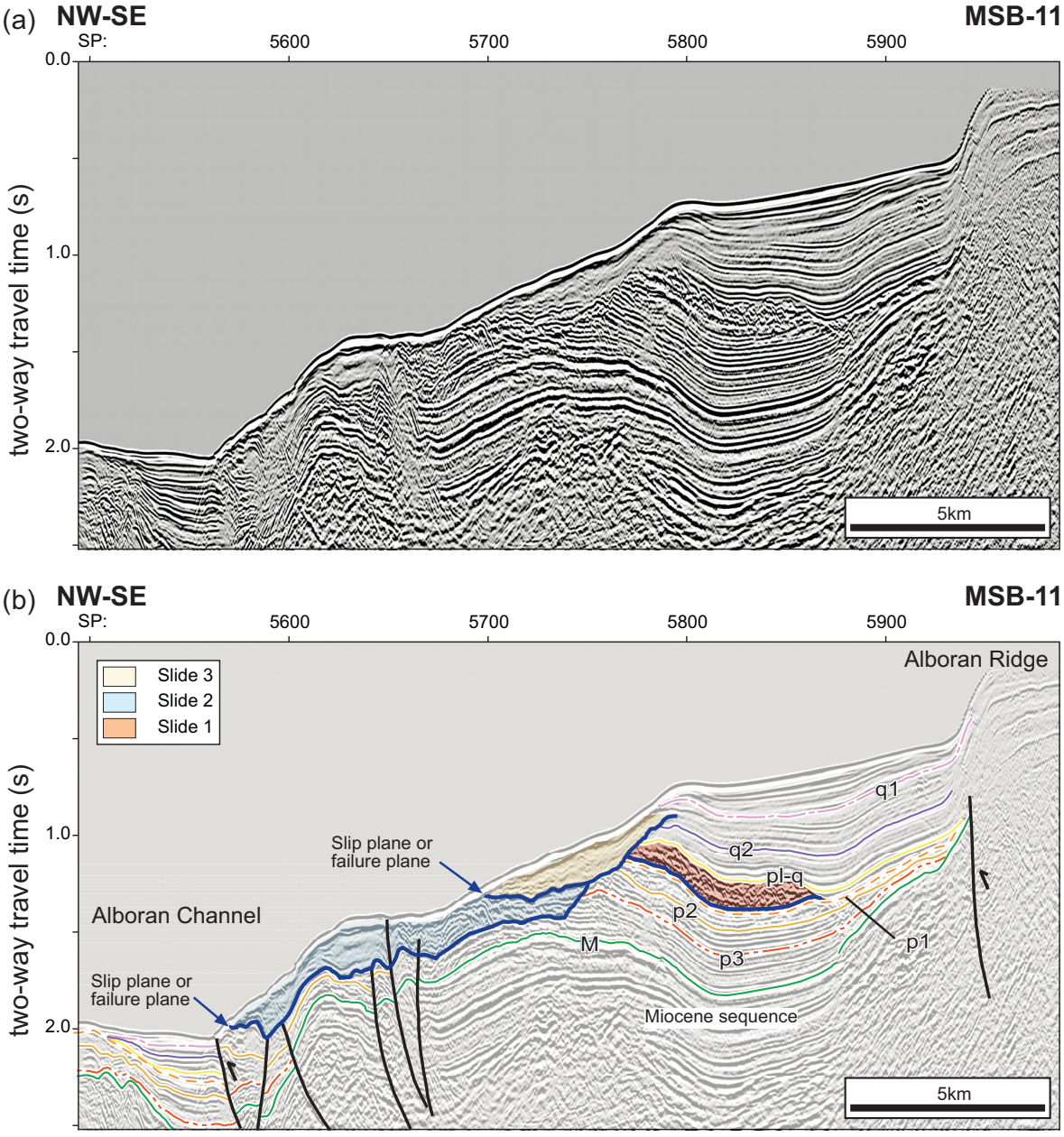

Figure 5-6. Multichannel seismic reflection profile across the northern slope of the Alboran Ridge showing the internal structure of several slides. Location in figures 5-2b, 5-2e and 5-2f.

Figure 7b corresponds with another TOPAS profile across the entire Yusuf Escarpment and to the east of the slumps in the upper part of the escarpment (Figures 5-4g to 5-4i). In this case the shallower deposits consist in several superposed lobes with semi-transparent facies that has been interpreted as MTD with chaotic facies. Slides show biconvex geometries and the lower one displays a slump fold on its head (shot points 1870-2000). Total volume of slides recognized in Yusuf has been estimated over 1.4 km^3, considering a minimum area of 70 km^2 (calculated form the bathymetric mosaic, figure 5-4i) and mean thickness of these deposits over 20 m (according to TOPAS profile shown in figure 5-7b).

East Alboran Basin (EAB)

MTD have been identified in the EAB, towards the southeast of the Al-Mansour Seamount (Figure 5-2). TOPAS profile showed in figure 5-9 evidences the presence of a sub-outcropping slide deposit in a relatively low slope area (<3º) in water depths over 2100 m. The minimum length of the slide body is 9.5 km and its thickness increases downslope from 7 ms to 45 ms in the slide toe (~ 5 m to 33 m) (around shot point 500). MTD shows chaotic transparent acoustic facies and are covered by thin layers of hemipelagic sediments with well-stratified facies. An undulating basal slip plane, corresponding with a high amplitude reflector, is clearly observable in this section (between shot points 500 and 1380).

5.6 Discusion

Age of slides

MTD studied in this work are recent structures. From seismic interpretation and correlation with available biostratigraphic ages from ODP wells (Figure 5-3), we determine that the age of the recognized deposits ranges from Upper Pliocene to Quaternary similarly to other slides previously identified in the northern margin of the Alboran Sea (*e.g.* Lo Iacono *et al.*, 2008; Ercilla *et al.*, 2009).

Relative ages of some of slides can be determined from their position in the sedimentary sequence and by the cross-correlation with key horizons. In the northern slope of the Alboran Ridge (Figure 5-6) Slide 1 lies above the p1 reflector (2.45 Ma) and it is limited above by the Pliocene-Quaternary boundary (pl-q; 1.83 Ma) suggesting that this MTD is Late Pliocene in age. Slide 2 erodes the reflector p3 (4.57 Ma). As this slide is eroded by the younger Slide 3, stratigraphic relationships between Slide 2 and other key horizons (post-4.57 Ma) can not be determined. Nevertheless Slide 2 is outcropping suggesting a recent age, certainly of Quaternary age and older than Slide 3. Slide 3 is the most recent one, as it overlies and erodes Slides 1 and 2. It erodes horizons p1, pl-q and q2 suggesting that this event is younger than 1.19Ma.

In the Yusuf Escarpment slip surfaces are located above the pl-q boundary and cut the q1 (1.19 Ma) and q2 (0.78 Ma) horizons (Figure 5-8). These observations show that these failure structures are younger than 0.78 Ma. Moreover normal faults bounding the glided blocks, affect the seafloor, evidencing a very recent age for these processes and deposits (Figures 5-4g to 5-4i).

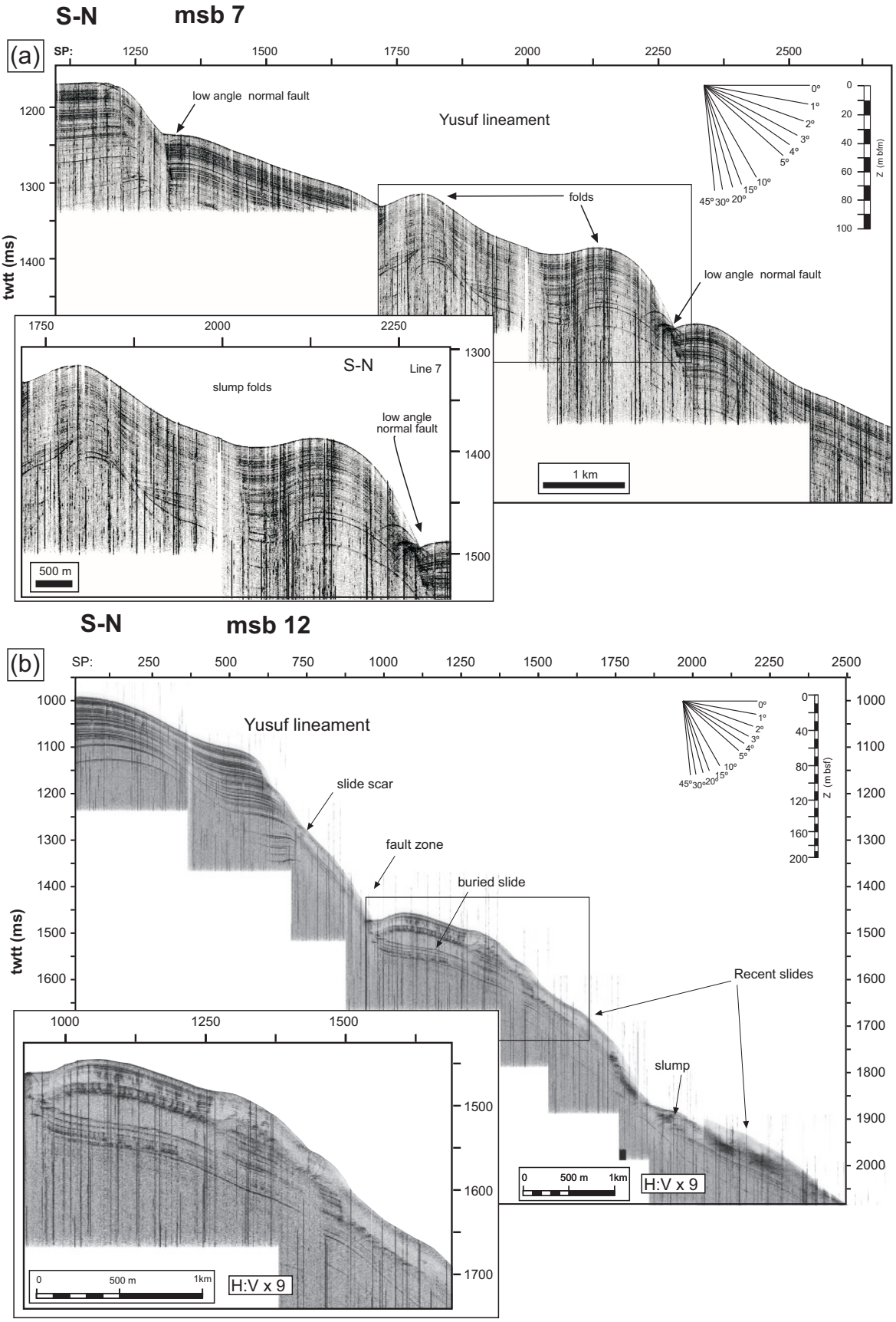

Figure 5-7. TOPAS profiles across the Yusuf Escarpment. Estimated depth scale and calculated dip abacus are shown for comparison. Location in figures 5-2b, 5-4h and 5-4i. **(a)** Slump folds and faults in the upper part of the escarpment. **(b)** Outcropping and buried slides and associated scars.

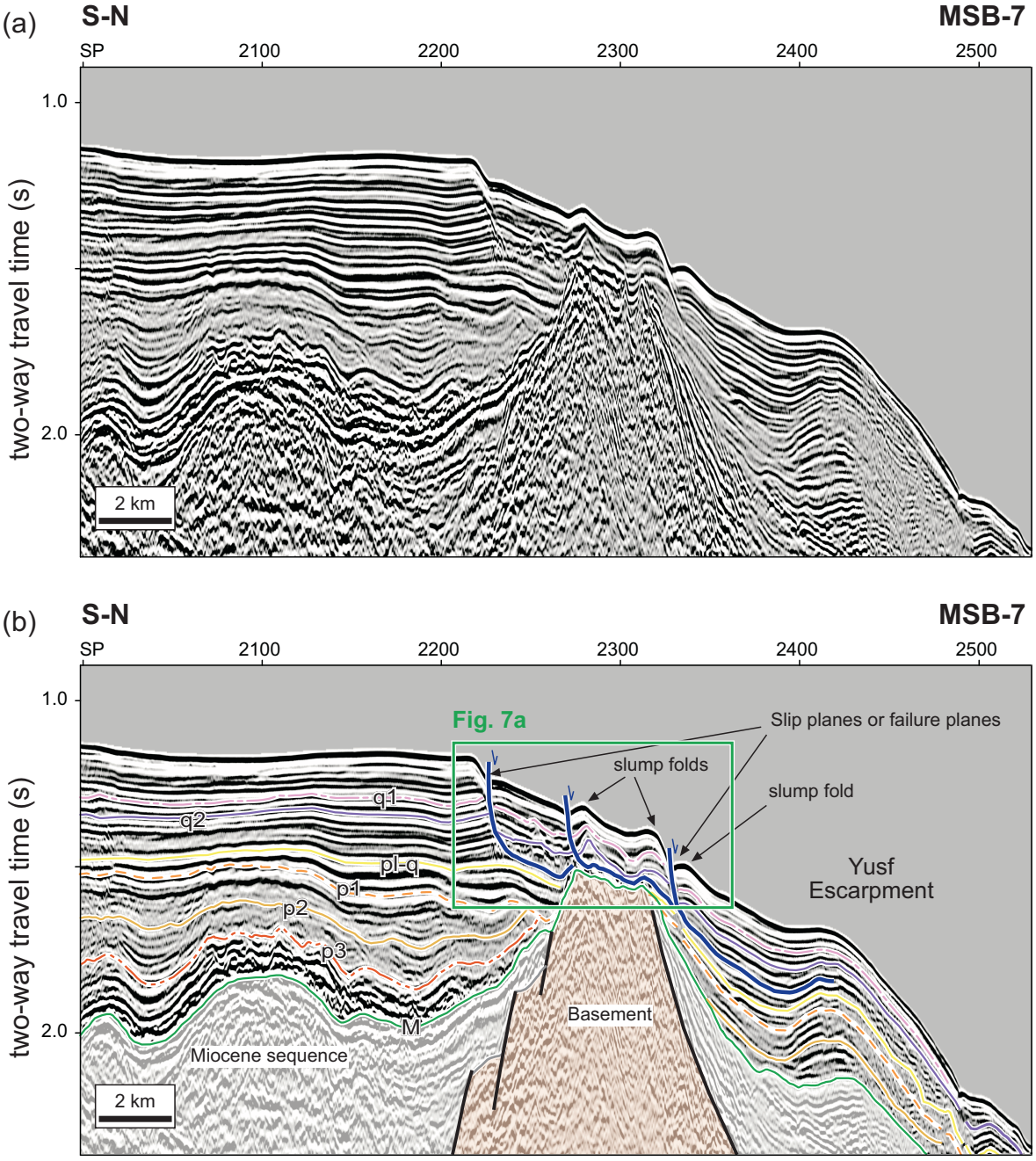

Figure 5-8. Multichannel seismic reflection profile across the Yusuf escarpment showing slump folds and faults rooted on a basal detachment within the Quaternary sequence. Location in figure 5-2b.

The existence of Quaternary MTD in the EAB has been reported previously by Estrada *et al.* (1997). Additionally, lower Pliocene slump structures have been drilled in the EAB, in Site 977 (Comas *et al.*, 1996). MTD in the EAB studied in this work are seen in TOPAS profiles as very shallow deposits covered by a thin package of hemipelagic sediments (~15 m thick) (Figure 5-9). The age of this slide can be deduced form the draping layer, which is about 0.1-0.12 Ma (de Kaenel *et al.*, 1999; Siesser and de Kaenel, 1999), *i.e.* Late Pleistocene.

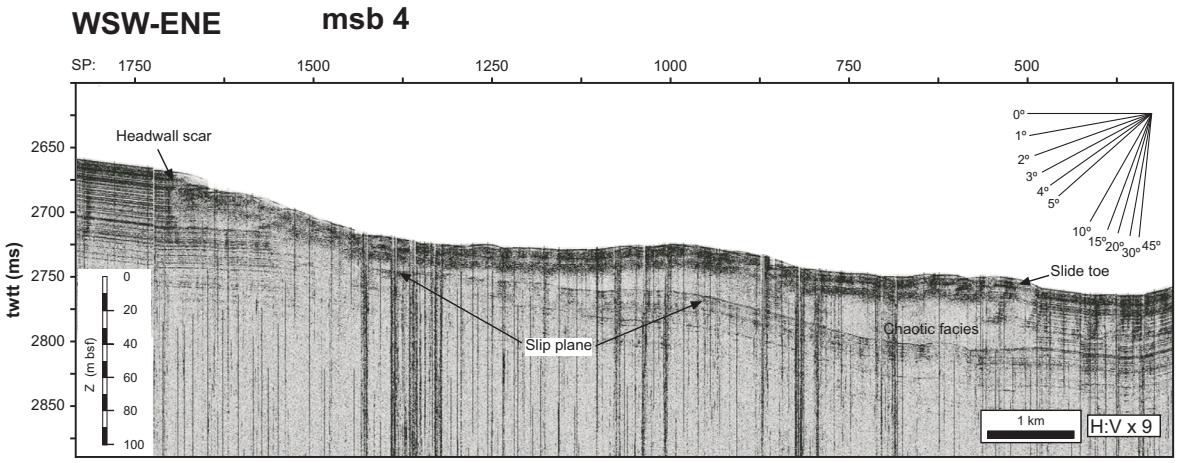

Figure 5-9. TOPAS profiles from the East Alboran Basin (EAB) showing a sub-outcropping slide. Estimated depth scale and calculated dip abacus are shown for comparison. Location in figure 5-2b.

Submarine instability processes and active tectonics

Submarine slides are effective mechanisms for transference of sediments from platforms, continental slopes, or submarine highs to basin floors. They are known to be caused by different proceses: seismic activity (earthquakes), aseismic tectonic deformations affecting the seafloor (*e.g.*, basinfloor tilting), volcanism, eustatic changes (glaciations), desestabilization of gas hydrates (methane emissions), presence of over-pressurized intervals, and gravity-loading (high sedimentation rates) (*e.g.*, Masson *et al.*, 2007). In this work we do not precise the contribution or occurence of each of these triggering factors. We focus on comparing the different types of MTD founded in the study area trying to unravel the main origin for each case.

Analyzed data form the continental slopes of the Alboran Ridge, the Yusuf Escarpment and the East Alboran Basins, evidence the existente of submarine slides with moderate extension and suggest that MTD are constituted by both slumps and debris flow deposits (Figure 5-10). Transport directions of these fluxes seem to occur parallel to the maximum slope of the escarpments, perpendicularly to both the outline curvature of the scars and the lobulated fronts of their deposits in plan view (Fig. 4). The Occasional occurrence of gullies in these escarpments is also indicative of active sediment transference downslope.

Slides in the eastern Alboran Sea have a variable size and morphology (Figure 5-10). They display similar features and dimension to other slides previously depicted in the western Mediterranean. Slides on the Yusuf Escarpment and the southern slope of the Alboran Ridge cover areas of tens of square kilometres, comparable to small slides identified in the northern margin of the Alboran Sea (García *et al.*, 2006; Lo Iacono *et al.*, 2008), the platform around the Alboran Island (Bárcenas *et al.*, 2004) and in the Evissa Channel (Lastras *et al.*, 2004; 2006). MTD on the northern slope of the Alboran Ridge covers an area of 230 km^2 comparable to other moderate-scale slides studied in the Ebro Continental slope (*e.g.* Martínez del Olmo, 1984; Baraza *et al.*, 1990; Casas *et al.*, 2003).

The MTD analyzed in this study display variable internal structure suggesting differences in transport and depositional processes. Some slides show chaotic internal structure indicating that sediments have been displaced, distorted and mixed as the slide moved downslope. This is certainly

the case for most of shallower slides on the northern slope of the Alboran Ridge, on the EAB and the lower part of the Yusuf Escarpment (Figures 5-5, 5-6 and 5-7b). The lack of bedding in these slides suggests that the low consolidated sediments forming the MTD displaced moderate to large distances downslope. Conversely slides on the upper slope of the Yusuf Escarpment (Figures 5-7a and 5-8) are formed by cohesive, stratified sediment bodies or blocks associated to scar-slump structures. These packages exhibit low degree of internal deformation suggesting a moderate downslope transportation, comparable to the process described for slides in offshore Sicily (Tricardini and Argnani, 1990 and Hjestuen et al 2007), in slump complexes in the Israel margin (Martinez *et al.*, 2005) and in the Bjørnøya Slide on the North Sea (Hjelstuen *et al.*, 2007).

In addition, chaotic facies of most slides along the Alboran Ridge and Yusuf Escarpment, indicate that there, MTD were re-deposited and experienced several phases of transport and deformation. Conversely, MTD with limited deformation of their internal structure, which maintain the original stratified facies and therefore, they probably correspond with a single failure event (Casas *et al.*, 2003). This is certainly the case of the slump folds located in the upper part of the Yusuf Escarpment.

Multichannel seismic refection profiles across the Alboran Ridge and Yusuf Escarpment shows that MTD recognized in these reliefs are generated by sedimentary instability processes caused by contemporary active tectonics. For example, some MTD on the Alboran Ridge appear folded and deformed by faults (*e.g.*, Slide 2 in figure 5-6) revealing compressive deformations after the deposit of these sediments (post-Late Pliocene).

Previous studies have suggested that both, the Alboran Ridge and the Yusuf Escarpment correspond with two strike-slip fault systems that connect with structures identified in the Betics and Rif (*e.g.* Maldonado *et al.*, 1992; Woodside and Maldonado, 1992; Fernández-Ibáñez *et al.*, 2007). The Alboran Ridge has been considered part of a left-lateral transpressive system linked to other NE-SE and NNE-SSW trending segments, such as the Jebha Fault in the Rif (*e.g.* Benmakhlouf *et al.*, 2005; Chalouan *et al.* 2008) and the Carboneras and Palomares faults in the eastern Betics (*e.g.* Rodríguez-Fernández and Martín-Penela, 1993; Gràcia *et al.*, 2006; Reicherter and Hübscher, 2007). This structure is probably a conjugate system formed of the NW-SE striking right-lateral transtensional Maro-Nerja and the Yusuf Faults (*e.g.* Mauffret *et al.*, 1992; Alvarez-Marrón, 1999; Soto and Manzano, 2002). In addition, reverse to left-lateral slip occur also on the Al-Idrisi fault zone, which cuts obliquely the western sector of the Alboran Ridge. This fault zone has reported Quaternary to Recent activity and concentrates most of the shallow seismicity in the area (Ammar *et al.*, 2007; Martínez-García *et al.*, 2011) (Figure 5-10).

Superposition and coalescence of slide masses suggest a significant recurrence of sedimentary instability processes in the Alboran Ridge and Yusuf Escarpment. Occasionally, the irregular and semi-transparent facies of MTD are draped by thins layers of hemipelagic sediments. This fact indicates that MTD are chaotic deposits whose accumulation is recurrent in time and shows alternating episodes of chaotic deposits and other with hemipelagic sedimentation. Similarly, the presence of several scars on the same headwall areas and the superposition of several MTD are other indications of multiple instability phases. Location of slides on fault escarpments with reported present-day seismic activity (*e.g.*, Fernández-Ibáñez *et al.*, 2007 and references therein), suggest that MTD were probably triggered by earthquakes. In fact, some of the major recent earthquakes in the region (M_w>4)

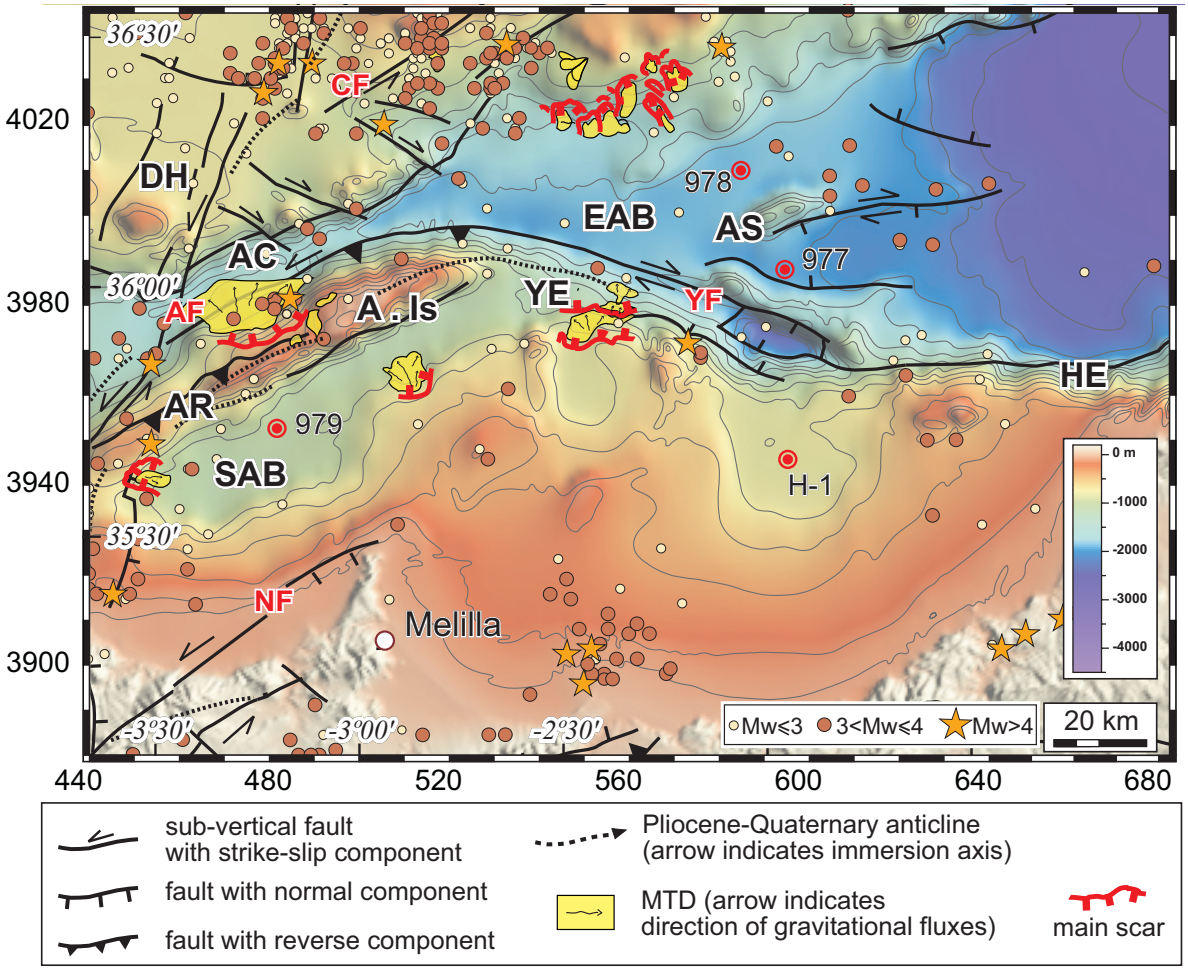

Figure 5-10. Map of the eastern Alboran Sea and its transition towards the Algerian Basin showing location of the different mass transport deposits (MTD) identified in this work and others previously depicted by Bárcenas *et al.*, 2006 and Lo Iacono *et al.*, 2008. It shows also position of main tectonic structures (taken from Martínez-García *et al.*, 2011) on top of the bathymetry and the distribution of shallow seismicity (for the period 1979-2009) (USGS catalogue). Circles show location of ODP Leg 161 sites (976 to 979), DSDP site 121 and the commercial Habibas-1 well. Abbreviations: A. Is, Alboran Island; AC, Alboran Channel; AF, Al-Idrisi fault; AR, Alboran Ridge; AS, Al-Mansour Seamount; CF, Carboneras fault; DH, Djibouti High; EAB, East Alboran Basin; HE, Habibas Escarpment; NF, Nekor fault; SAB, South Alboran Basin; YE, Yusuf Escarpment; YF, Yusuf fault; WAB, West Alboran Basin.

have occurred on the vicinity of mapped slides (Figure 5-10). The slides identified along the Alboran Ridge slopes and the Yusuf Escarpment are interpreted to occur related to tectonic pulses of active seismogenic faults. Slides with similar size and characteristics, triggered by earthquakes have been also reported in the strike-slip North Anatolian fault zone in the Marmara Sea and the northeastern Aegean Sea (Gazioğlu *et al.*, 2005; Gökaşan *et al.*, 2003; Ustaömer *et al.*, 2008).

The occurrence of massive slides in the Alboran region could also had been influenced by others factors as eustatic changes or sedimentary loading. The determination of the influence of these triggering mechanisms would require well cores and could be interesting for future studies in the region.

We demonstrate the occurrence of very recent, and eventually present-day, instability

processes in the Alboran Sea resulting in moderate to large scale slides and MTD, which represents a potential geological hazard with an important socio-economic impact. For this reason, the existence of other possible slides and the accurate quantification of their volumes and location deserve to be surveyed in the future, making possible a detailed characterization of the tsunamigenic potential in this region.

5.7 Conclusions

We have reported the existence of different MTD in the central and eastern sectors of the Alboran Sea. These structures have small to moderate dimensions (~20 to 1300 km^2) and are constituted by slump and debris flow deposits. Most of them are outcropping deposits or are draped by thin layers of hemipelagic sediments. The age of recognized deposits ranges from Late Pliocene to Quaternary (post- 2.45 to ~0Ma) and they have a associated marks visible in the present-day seafloor morphology.

Recurrent slide deposits and lobulated headwall formed by several minor scars locate on both sides of the Alboran Ridge and the Yusuf Escarpment and they have produced headwall degradation by retrogressive slide processes.

Distances of displacement of MTD are variable: some slides show chaotic internal structure indicating a moderate to large downslope displacement of unconsolidated sediments; in other cases MTD exhibit a low-degree of internal deformation suggesting a minor downslope transportation of cohesive material.

MTD on the slopes of the Alboran Ridge and the Yusuf Escarpment are interpreted to be triggered by earthquakes. The superposition of recurrent chaotic slides is attributed to recent strike-slip faulting pulses along the Alboran Ridge and Yusuf fault zones. Others factors as eustatic changes or sedimentary loading could have also contributed to create these instability-related deposits.

6. Tectonic inversion and geodynamic implications

Tectonic inversion in the Alboran Sea Basin: from Miocene extension to Recent shortening

Manuscript under elaboration (to be submitted).

Pedro Martínez-García[1], Juan I. Soto[2], Menchu Comas[1], Lidia Lonergan[3] and Anthony B. Watts[4]

[1] Instituto Andaluz de Ciencias de la Tierra (CSIC and University of Granada), Facultad de Ciencias,

[2] Instituto Andaluz de Ciencias de la Tierra (CSIC and University of Granada) and Departamento de Geodinámica, Facultad de Ciencias, Granada, Spain.

[3] Department of Earth Science and Engineering (Imperial College London), South Kensington Campus, London, United Kingdom.

[4] Department of Earth Sciences, University of Oxford, Oxford. United Kingdom.

Abstract

An extensive database of seismic reflection profiles correlated with bio-stratigraphic and log information from nearby DSDP, ODP and commercial wells have been used to document the evolution of the central and southeastern Alboran Sea from a Miocene extensional basin to complex, comparimentalised sub-basin dominated by strike-slip and reverse faulting during the Plio-Quaternary. NE-SW High-angle normal faults, tilted basement blocks and growth wedges indicate that Miocene rifting here was predominating NW-SE trending and promoted a reduced amount of extension. Miocene depocentres in the study area are thinner (maximum thickness ~2.5-3 km) and younger than the major basin depocentres in the western and northern sectors (up to 8.5 km thick), suggesting that rifting progressed from west to east. Plio-Quaternary NW-SE shortening coexisted with thermal subsidence and reactivated some extensional structures as reverse faults and folds. Tectonic inversion was partial and only occurs along some of the Miocene NE-SW faults. The Alboran Ridge, in the centre of the basin, accommodated most of shortening since the Late Pliocene. Tectonic inversion along its western sector was simultaneous with formation other new south-dipping reverse faults along its northeastern slope. Relict Miocene magmatic intrusions along this relief formed rheological anisotropies with favourable orientation respect to the Recent NW-SE convergence between the African and Eurasian plates. Tectonic inversion in the Alboran Sea resembles to those along the Algerian margin. The entire region comprises different NE-SW trending segments (~125-180 km in length), which are displaced by a number of NW-SE to WNW-ESE right-lateral, strike-slip transfer faults zones between the compressive segments. These structures are long-lived zones of weakness formed during the Miocene basin opening in the westernmost Mediterranean and they control the actual distribution and partition of deformation.

Keywords: tectonic inversion, strike-slip tectonics, shortening, conjugate faults, basin analysis, Alboran Ridge, Yusuf Escarpment, Western Mediterranean

6.1 Introduction

Positive tectonic inversion refers to the contractional reactivation of inherited normal faults due to a change in tectonic regime from crustal extension to compression and it is frequently proposed as an important controlling factor in the structures of collisional belts. In many cases fault reactivation is highly selective and only affects to few structures or some individual fault segments from an extensive set of pre-existing normal faults. In these regions, slip is frequently partitioned between the different long-lived zones of weakness with favourable orientation respect to the renewed trend of shortening resulting in either strike-slip or dip slip displacements (*e.g.* Bally, 1984; Hayward and Graham, 1989; Tikoff and Teyssier, 1994; Coward, 1996; Jones *et al.*, 2004). Other factors controlling this selective mechanism are; (1) the existence of rheological anisotropies in the crustal basement such as lithological contacts, (2) the presence of low friction material along particular faults and (3) the heterogeneous distribution of fluid overpressures (*e.g.* Sibson, 1995; De Paola *et al.*, 2005). During the last decades such inversion structures have been widely studied due to their role as traps for hydrocarbons (*e.g.* Bally, 1983; Faster and Gawthorpe, 1990; Butler *et al.*, 1990). They have been recognised worldwide in both onshore and offshore regions such as the Alps (*e.g.* Bally, 1984; Butler, 1989), the Pyrenees (*e.g.* Saura and Teixel, 2006), the Zagros (*e.g.* Jackson, 1980), the NE Atlantic Margin (Jackson and Larsen, 2008; Ritchie *et al.*, 2008) and North Sea (*e.g.* Badley *et al.*, 1989; de Lugt *et al.*, 2003), the Canadian Rockies (*e.g.* Bally *et al.*, 1966; McClay *et al.*, 1989), the California borderland (*e.g.* Crouch and Suppe, 1993; Gutiérrez-Alonso and Gross, 1997), the Andes (*e.g.* Grier *et al.*, 1991; Godoy *et al.*, 1999; Carrera *et al.*, 2006) and back-arc basins in Costa Rica (*e.g.* Brandes *et al.*, 2007) and Japan (*e.g.* Tamaki and Honza, 1985).

In the Mediterranean, several extensional basins were formed during the Miocene by collapse of the Alpine-aged orogenens (at about 25-30 Ma). Some of these basins were later partially inverted and deformed under a transpressional regimen during the Plio-Quaternary within a convergent tectonic setting between the African and Eurasian plates (*e.g.* Horvath and Berckhemer, 1982; Platt and Vissers, 1989; Jolivet and Faccenna, 2000; Rosenbaum *et al.*, 2002; Faccenna *et al.*, 2004). The Alboran Sea Basin is the westernmost of these inverted basins and it has experienced a complex Plio-Quaternary tectonic evolution forming reverse, strike-slip faults and folds and general uplift of basin margins (Bourgois *et al.*, 1992; Comas *et al.*, 1992; 1999; Campos *et al.*, 1992; Woodside and

Figure 6-1. (a) Geological map of the Alboran Sea Basin and surrounding areas showing early Miocene to Holocene structures and main sedimentary depocentres (compiled from Comas *et al.*, 1999 and Martínez-García *et al.*, 2011). Directions of Miocene extension are indicated by blue arrows. Rectangle marks the position of the study area in central and southeastern sectors of the basin. Red circles show location of ODP leg 161 sites (976 to 979), DSDP site 121 and commercial boreholes offshore (G1: Andalucía G1, A1: Alboran A1, And-A1: Andalucía A1, and EJ: El-Jebha, H-1: Habibas-1). Inset map shows main tectonic elements in the western Mediterranean (from Comas *et al.*, 1999). **(b)** Topographic and structural map of the Alboran Sea region combined with distribution of crustal seismic events (M > 2.5) for the period 1980-2006 (USGS catalogue) (taken from Fernández-Ibáñez *et al.*, 2007). Digital topography is built on the SRTM (USGS-NASA) global database combined with GEBCO 97 (IOC-IHO) for the offshore region. Three hypotheses for the geometry of the plate boundary are also shown in pink (Klitgord and Schouten, 1986), yellow (Bird, 2003) and blue (Gutscher, 2004). Abbreviations: A. Is, Alboran Island; AIF; Al-Idrisi fault; AR, Alboran Ridge; CF, Carboneras Fault; DH, Djibouti High; EAB, East Alboran Basin; GSB, Gharb-Saïss Basin: HB, Habibas Basin; HE, Habibas Escarpment; JF, Jebha Fault; MF, Maro-Nerja Fault; MH, Maimonides High; NF, Nekor Fault; PB, Pytheas Basin; PF, Palomares Fault; SAB, South Alboran Basin; XB, Xauen Bank; YR, Yusuf Ridge and WAB, West Alboran Basin.

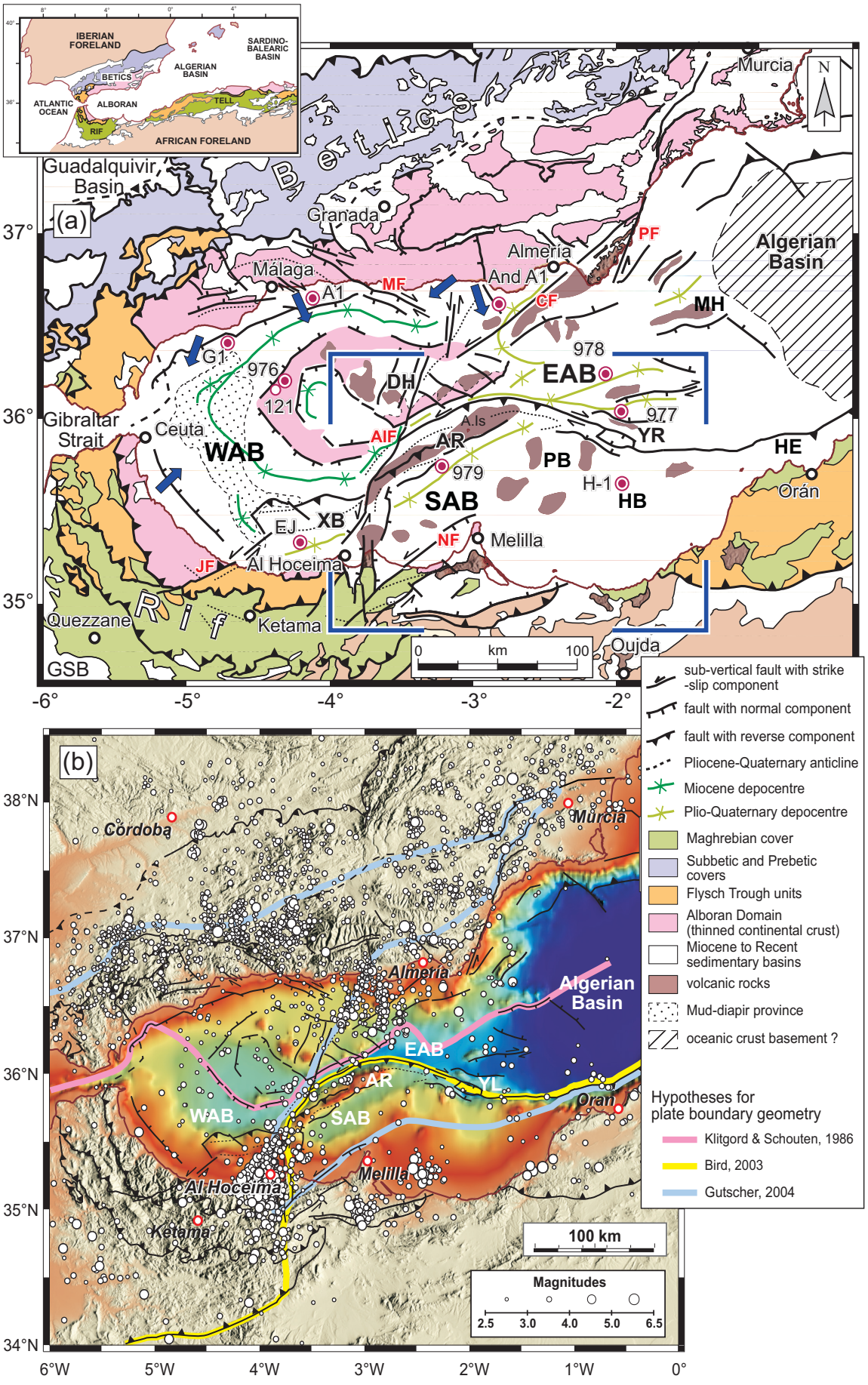
IBERIAN FORELAND
SARDINO-BALEARIC BASIN
ALGERIAN BASIN
BETICS
ATLANTIC OCEAN
ALBORAN
TELL
RIF
AFRICAN FORELAND
(a)
Guadalquivir Basin
Betics
Granada
Murcia
N
Málaga
A1
MF
Almería
And A1
PF
CF
Algerian Basin
MH
G1
976
121
DH
978
EAB
977
YR
HE
Gibraltar Strait
Ceuta
WAB
AIF
AR
A.Is
PB
979
H-1
HB
Orán
SAB
EJ
XB
NF
Melilla
JF
Al Hoceima
Rif
Quezzane
Ketama
Oujda
GSB
0
km
100
37°
36°
35°
-6°
-5°
-4°
-3°
-2°
(b)
Córdoba
Murcia
Almería
Algerian Basin
EAB
AR
YL
Oran
WAB
SAB
Melilla
Al Hoceima
Ketama
100 km
Magnitudes
2.5
3.0
4.0
5.0
6.5
38°N
37°N
36°N
35°N
34°N
6°W
5°W
4°W
3°W
2°W
1°W
0°
sub-vertical fault with strike -slip component
fault with normal component
fault with reverse component
Pliocene-Quaternary anticline
Miocene depocentre
Plio-Quaternary depocentre
Maghrebian cover
Subbetic and Prebetic covers
Flysch Trough units
Alboran Domain (thinned continental crust)
Miocene to Recent sedimentary basins
volcanic rocks
Mud-diapir province
oceanic crust basement ?
Hypotheses for plate boundary geometry
Klitgord & Schouten, 1986
Bird, 2003
Gutscher, 2004

Maldonado, 1992; Watts *et al.*, 1993; Docherty and Banda, 1995; Chalouan *et al.*, 1997; Willet, 1997; Alvarez-Marrón *et al.*, 1999; Rodríguez-Fernández *et al.*, 1999; Gràcia *et al.*, 2006; Mauffret *et al.*, 2007; Ballesteros *et al.*, 2008; Martínez-García *et al.*, 2011) (Figure 6-1a). All these characteristics make this region a useful area for analysing the evolution of marine extensional basins in collisional settings.

At present-day, deformation and seismicity are distributed over a wide band along the Alboran Sea Basin and the surrounding Betic and Rif chains and the whole region constitutes a diffuse plate boundary accommodating continent-continent collision (Figure 6-1b). Earthquakes are low to moderate magnitude and mostly occur at shallow depths ($M_w < 6.5$ and depths < 50 km) (*e.g.* Buforn *et al.*, 1995; Stich *et al.*, 2003a; Fernández-Ibáñez and Soto, 2008). Several hypotheses for the precise geometry of the Africa-Eurasia plate boundary have been proposed attending to the location of several zones of preferential accommodation of deformation and seismicity, GPS measurements, and numerical modelling. However, the existence of a discrete plate boundary is equivocal and remains controversial (*e.g.* Klitgord and Schouten, 1986; Morel and Meghraoui, 1996; Negredo *et al.*, 2002; Bird, 2003; Gutscher, 2004; Fadil *et al.*, 2006; Vernant *et al.*, 2010; Koulali *et al.*, 2011).

The extensional history of the Alboran Sea Basin has been extensively studied in its western and northern sectors and also throughout the surrounding Betics and Rif, where the continental crustal basement flooring the basin outcrops widely. However, few is known about the rifting geometry in the central and southeastern parts of the Alboran Sea Basin that concentrate a number of structures with Plio-Quaternary activity (*e.g.* Platt and Vissers, 1989; Bourgois *et al.*, 1992; Comas *et al.*, 1992; 1999; García-Dueñas *et al.*, 1992; Maldonado *et al.*, 1992; Watts *et al.*, 1993; Platt *et al.*, 1998, 2003). Additionally, the role of pre-existing Miocene faults during the shortening phase and whether or not these structures were reused and helped to localize compressive deformations is still unclear.

The aims of this work are to perform seismic interpretation of an extensive database of seismic reflection profiles to: (1) determine precisely the deeper structure of the basin to better constrain the Miocene rifting geometry; (3) reconstruct the geometry and thickness of the sedimentary filling comparing the distribution and features of syn-rift depocentres with those post-rift generated by shortening; (2) understand the partial tectonic inversion processes and the role played by inherited extensional structures during the later shortening; (4) study the partitioning of deformation and transference of slip into a diffuse plate boundary determining the type, geometry position and kinematics of active structures with associated seismic hazard in the western Mediterranean.

6.2 Geological setting

The Alboran Sea Basin, in the western Mediterranean, is a major extensional basin surrounded by an Alpine orogenic belt, which comprises the Betic and Rif mountain chains and a frontal sedimentary wedge in the Gulf of Cadiz. The whole system is known as the Gibraltar Arc System and it was formed during the Neogene by simultaneous westward thrusting in the mountain front and extensional collapse in the inner part of the arc within a general setting of plate convergence between the African and Eurasian plates (*e.g.* Dewey, 1988; Platt and Vissers, 1989; Comas *et al.*, 1992, 1999; García-Dueñas *et al.*, 1992; Watts *et al.*, 1993; Lonergan and White, 1997; Jolivet and

Faccenna, 2000; Rosenbaum *et al.*, 2002; Platt *et al.*, 2003). Several pre-Neogene crustal domains were involved in the formation of this collisional orogen (Figure 6-1a): (1) the Subbetic, Prebetic and Maghrebian covers representing passive continental margins consisting of Mesozoic and Tertiary sedimentary rocks, which were deposited in basinal and shelf enviroments on the South Iberian and North African margins of the Tethyan Ocean; (2) the Flysch Trough Units, mainly located in the Rif, the westernmost Betics and the Tell regions, comprising Early Cretaceous to Early Miocene allochtonous deep marine clastic deposits that originally covered oceanic troughs or very thin continental crust; and (3) the Alboran Domain: Paleozoic and Mesozoic metamorphic rocks arranged into a thrust stack of three nappe complexes, which constitute the internal Betics and Rif and the thinned continental basement beneath the Alboran Sea itself.

During the Early to middle Miocene, the covers of the Iberian and African paleomargins and the Flysch Units were deformed by thin skinned thrusting and folding as consequence of westward movement and emplacement over them of the Alboran Domain (*e.g.* Andrieux *et al.*, 1971; Balanyá and García-Dueñas, 1987; Frizon de Lamotte *et al.*, 1991; García-Dueñas *et al.*, 1992; Morley, 1992; Lonergan *et al.*, 1994). This event produced shortening of the peripheral belt accompanied by the development of the external flexural foreland basins of Guadalquivir and Gharb-Saïss (Figure 6-1). At the same time crustal extension occurred in the Alboran Domain by means of low-angle normal faults and locally inversion of previous thrusts resulting in the formation of the Alboran Sea Basin (*e.g.* Platt, 1986; Galindo-Zaldívar *et al.*, 1989; Platt and Vissers, 1989; García-Dueñas *et al.*, 1992; Comas *et al.*, 1992; Jabaloy *et al.*, 1993; Watts *et al.*, 1993; Lonergan and Platt, 1995; Azañón and Crespo-Blanc, 2000; Martínez-Martínez and Azañón, 1997; Martínez-Martínez *et al.*, 2002). Extension was accompanied by crustal melting, magmatism and several volcanic episodes (*e.g.* Platt *et al.*, 1998; Hoernle *et al.*, 1999; Soto and Platt, 1999; Turner *et al.*, 1999; Duggen *et al.*, 2004, 2008; Gill *et al.*, 2004) resulting in a pattern of volcanic ridges, particularly in the central and eastern Alboran Sea, which is shown by aeromagnetic maps (Galdeano *et al.*, 1974). Causes of extension are still under debate and several tectonic models have been proposed to explain the origin of the Alboran Sea Basin: (1) radial extensional postorogenic collapse caused by rapid convective removal of the lithospheric root (*e.g.* Dewey, 1988; Platt and Vissers, 1989; Platt *et al.*, 2003; Molnar and Houseman, 2004); (2) delamination of lithosphere (*e.g.* García-Dueñas *et al.*, 1992; Docherty and Banda, 1995; Seber *et al.*, 1996; Calvert *et al.*, 2000); and (3) subduction zone rollback beneath the curst of the Alboran Domain considering different geometries and directions for the subducting slab (*e.g.* Torres-Roldán *et al.*, 1986; Sanz de Galdeano, 1990; Zeck *et al.*, 1992; Royden, 1993; Lonergan and White, 1997; Hoernle *et al.*, 1999; Morales *et al.*, 1999; Jolivet and Faccenna, 2000; Gutscher *et al.*, 2002; Faccenna *et al.*, 2004); (4) Combined models considering both subduction rollback and edge delamination beneath the continental margins (*e.g.* Duggen *et al.*, 2004; 2008; Booth-Rea *et al.*, 2007).

The extensional episode and associated subsidence in the Alboran Sea Basin occurred throughout the Miocene ceasing at approximately 9-8 Ma (Tortonian, Late Miocene). Relative motion between the Eurasian and African plates was N-S at this time coexisting with the westwards motion of the Alboran Domain. A further phase of shortening occurred during the Plio-Quaternary, when the dynamic processes below the curst ended or become residuary and the renewed NW–SE plate convergence controlled recent deformation causing partial inversion of older normal faults and

strike-slip tectonics (Dewey *et al.*, 1989; Bourgois *et al.*, 1992; Comas *et al.*, 1992, 1999; Watts *et al.*, 1993; Docherty and Banda, 1995; Chalouan *et al.*, 1997; Rosenbaum *et al.*, 2002; Mauffret *et al.*, 2007).

Continuous syn-tectonic sedimentation resulted in significant thickness variations of the sedimentary cover and basin compartmentalization into three main sub-basins: the West Alboran Basin (WAB), East Alboran Basin (EAB) and South Alboran Basin (SAB) (Figure 6-1). The major depocentre is located in the WAB where the sedimentary pile is up to 8.5 km thick and displays a curved geometry that mimics the orogenic front of the Gibraltar Arc System (Comas *et al.*, 1992; Soto *et al.*, 1996; Chalouan *et al.*, 1997). Towards the East, the thickness of the sedimentary filling decreases to 2-3 km in the EAB and in the SAB maximum sediment accumulation reaches 3 km (Comas *et al.*, 1995; Booth-Rea *et al.*, 2007; Mauffret *et al.*, 2007). Correlation of seismic reflection data with lithologic and chrono-stratigraphic information supplied by wells show that the sedimentary cover comprises different regional unconformities limiting major seismic units. The seismostratigraphy established by Comas *et al.* (1992) and Jurado and Comas (1992) for the western and northern sectors of the basin differentiates six lithoseismic units (I-VI; labelled from top to bottom), which are comparable to those identified by Chalouan *et al*., (1997) for the SW margin of the basin.

Unit I is Pliocene to Quaternary and mainly consists of pelagic marls, muddy turbidites, and rare silty-sand turbidites (Alonso *et al.*, 1999). The base of this unit corresponds with the M reflector recognized throughout the Mediterranean that locally is a strong erosional unconformity resulting from basin desiccation and subaerial erosion at the end of the Miocene during the Messinian salinity crisis (Hsü *et al.*, 1973; Ryan *et al.*, 1973). The Messinian aged Unit II is composed of marine and lacustrine sandy turbidites interbedded with fine-laminated sediments and shallow carbonate facies, with occasional gypsum and thin anhydrite intervals (Jurado and Comas, 1992; Iaccarino and Bossio, 1999). The R2 reflector at the base of this unit is a Late Tortonian regional unconformity. Tortonian sediments from Unit III mainly consist of sandstone intervals with claystone and silty clay beds with turbiditic facies. The R3 reflector is an angular unconformity at the base of Unit III and appears to mark the end of Miocene rifting in the WAB (Comas *et al.*, 1999). Unit IV (Serravallian to Early Tortonian) is formed by graded sand-silt-clay turbidites and turbiditic muds and is bounded at its base by the R4 reflector. Unit V is subdivided into two subunits: subunit Va (late Langhian to Serravallian) with similar lithostratigraphy to the overlying Unit IV; and subunit Vb (Langhian) that is constituted by undercompacted shales with interbedded sandy and sandy-pebbly intervals. The R5 reflector at the base of Unit V is a major unconformity. Both R4 and R5 unconformities are probably result of pulses of fault activity during the rifting processes (Comas *et al.*, 1999). Unit VI comprises the lowermost deposits in the basin with late Aquitanian to Burdigalian age (Jurado and Comas, 1992; Sautkin *et al.*, 2003) and consists of marine olistoliths and rock breccia embedded into an undercompacted matrix of shale.

6.3 Data and methodology

The database comprises a dense grid of 110 industrial and academic seismic reflection profiles totalling 6598 km and covering an area of 28,000 km^2 in the central and southeastern parts of the

Alboran Sea Basin (Figs. 1 and 2). Some 4200 km of profiles corresponds with the older analogue records, which were digitized and transformed to the standard segy format using Lynx® software. Representative seismic profiles illustrating this work come from the following cruises: Marsibal I-06 and Tecalb (BIO Hespérides, 2006 and 2000), Conrad cruise C2911 (R/V Robert D. Conrad, 1988), MAP-79 (Eniepsa, 1979), BRPM (Compagnie Generale de Geophysique, 1975), SH (Sonatrach, 1974). The seismic data were interpreted using the SMT´s Kingdom Suite® software. Seismic events were correlated with several scientific and commercial well records from DSDP Site 121, ODP Sites 976, 977, 978 and 979 and Habibas-1 well (Figure 6-2) (Comas *et al.*, 1996, 1999; de Kaenel *et al.*, 1999; Siesser and de Kaenel, 1999; Kheidri *et al.*, 2000; Cope *et al.*, 2003). Detailed chrono-stratigraphic and log information available for the last ~5 Ma and good resolution of seismic data in the shallower parts of the seismic profiles have allowed us to recognize several seismic units and bounding discontinuities for the Plio-Quaternary sequence. However, seismic resolution decreases in the deeper parts of the profiles and the older sedimentary sequences under the M reflector were not drilled in most of the studied wells. Thus intra-Miocene discontinuities were only locally mapped and their age attributions should be considered tentative.

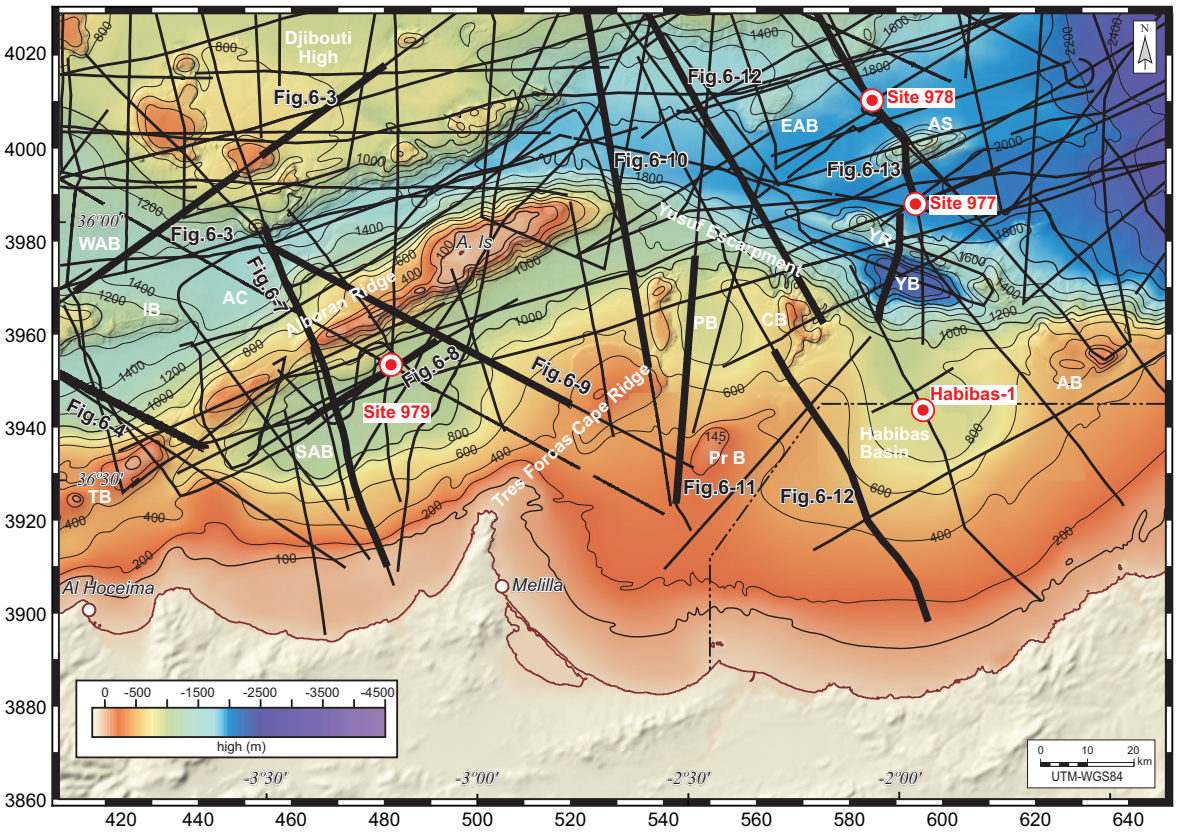

Figure 6-2. Location map showing bathymetry and position of the complete dataset of seismic profiles interpreted in the study. Thick black lines indicate multichannel seismic profiles presented in other figures. Location of ODP Leg 161 sites 977, 978, 979 and the commercial borehole Habibas-1 are also included. Bathymetry contours (GEBCO-97, IOC-IHO) are in metres, contour interval 200 m. UTM projection, units in kilometres. Abbreviations: A. Is, Alboran Island; AB, Alidade Bank; AC, Alboran Channel; AS, Al-Mansour Seamount; CB, Câbliers Bank; EAB, East Alboran Basin; IB, Ibn-Batouta Bank; PB, Pytheas Basin; Pr B, Provençaux Bank; SAB, South Alboran Basin; TB, Tofiño Bank; YB, Yusuf Basin; YR, Yusuf Ridge and WAB, West Alboran Basin.

Time-contour maps were obtained for the different mapped unconformities by griding and then isopach maps were calculated separately for the Plio-Quaternary and Miocene sequences. Then time-thickness maps were converted to depth using average sonic velocities (Vp) according to Martínez-García *et al.* (submitted for publication) and Talukder (2003) for the Plio-Quaternary and Miocene sequences respectively. Isopachs are presented as contour maps together with active structures at the relevant time.

In addition to seismic data, we have compiled several published swath-bathymetry mosaics and focal mechanisms in order to compare the present-day active structures and basin configuration with the previous Plio-Quaternary and Miocene stages. Bathymetric data from Martínez-García *et al.* (2011) have been merged with other complementary data from MediMap Group (2008) and GEBCO-03 (IOC-IHO) (Figure 6-2). A set of 47 focal mechanisms of earthquakes has been compiled and analyzed for this study.

6.4 Key reflectors and main seismic units

Acoustic basement

The top of acoustic basement corresponds with several discontinuous reflections of high amplitude and normal polarity (*e.g.* Figure 6-3). This reflector is a major unconformity that bounds a package with high to moderate reflectivity and well stratified seismic facies representing the sedimentary cover from an underlying seismic unit with chaotic and semitransparent facies with low coherence from the crustal basement. In those areas with a thin sedimentary cover (*i.e.* ~thinner than 1 s twtt) the top of basement is clearly visible as a strong reflector with great lateral continuity. However, this reflector is more difficult to recognize when it lies at great depths under thicker sedimentary cover due to the lower resolution of seismic profiles in deep. In such cases, it should be note that the top of basement has been inferred considering the position of the deepest stratified facies that may represent the oldest sediments lying directly on top of basement. These uncertainties about the precise position of top of basement are indicated by dashed lines in the interpreted seismic sections. Locally the top of basement coincide with erosion surfaces that constitute paleo-reliefs. In other cases this reflector corresponds with fault surfaces bounding structural basement highs and tilted blocks (*e.g.* Figure 6-3). Additionally, some seismic sections show the top of basement forming conic morphologies that outcrop locally at the seafloor and they are attributed to volcanic edifices (*e.g.* Figure 6-3 between shot points 3200 and 3400).

In the southeastern part of the study area the basement was drilled by Habibas-1 well at 4496.5 m depth and it is constituted by metamorphic rocks (schist) from the Alboran Domain (Kheidri *et al.*, 2000; Cope *et al.*, 2003) similarly to those forming the basement high drilled by DSDP Site 121 and ODP Site 976 in the western part of the basin and also the basement along northern margin drilled by the commercial wells Alboran A-1 and Andalucía A-1 (Figure 6-1) (*e.g.* Ryan *et al.*, 1973; Jurado and Comas, 1992; Comas *et al.*, 1996; Soto and Platt, 1999).

Miocene Sequence

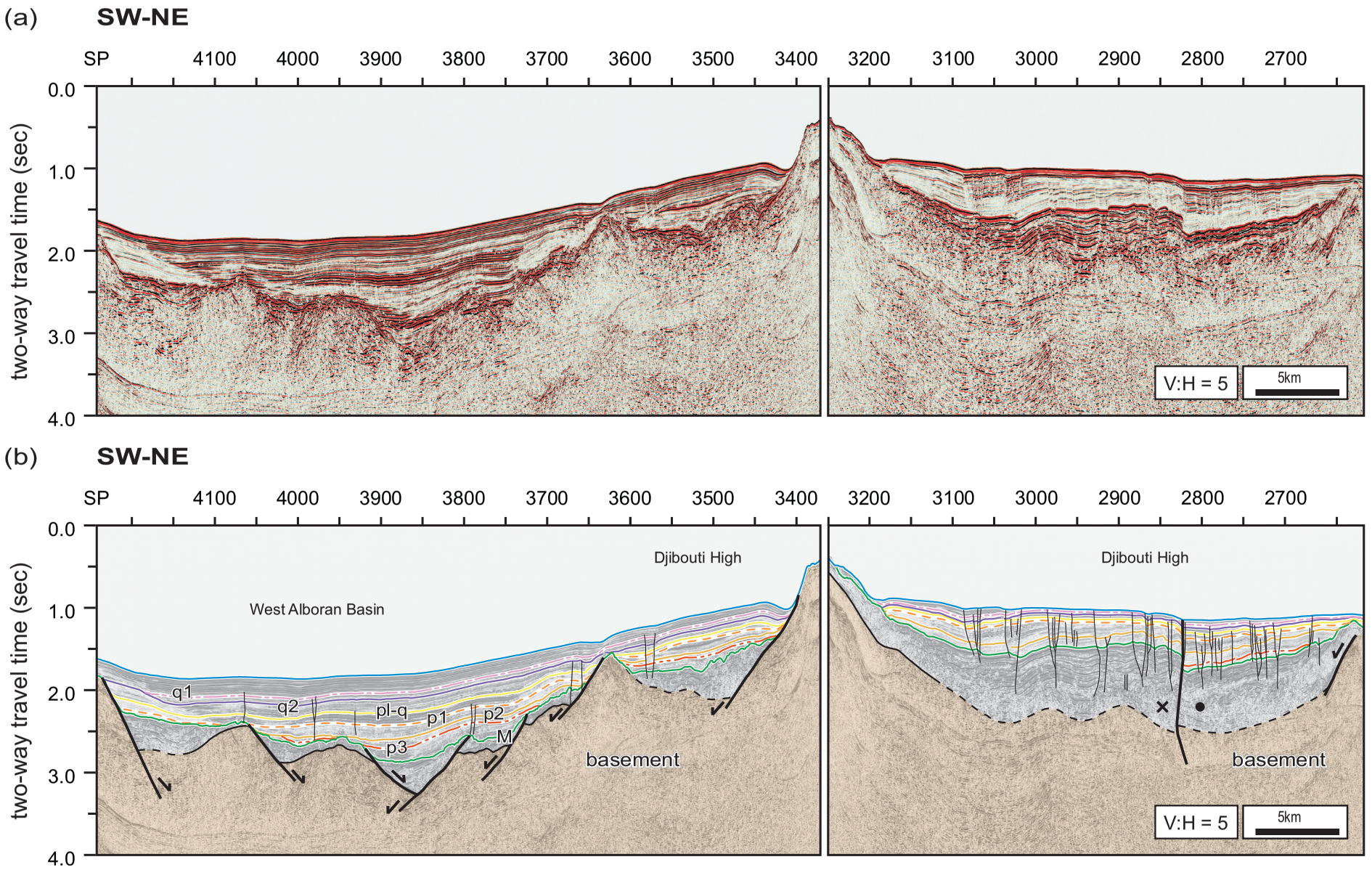

Figure 6-3. (a) Uninterpreted and **(b)** interpreted multichannel seismic section across the West Alboran Basin (WAB) and the Djibouti High. M to q1 reflectors, age of unconformities and Plio-Quaternary seismic units as defined by Martínez-García et al. (submitted for publication). Note that Miocene extensional structures are sealed by Plio-Quaternary deposits in the WAB. Tentative position of top of basement is indicated by dashed lines. Location of seismic line is shown in figures 2, 5 and 6.

Different major angular or erosional unconformities can be recognized within the sedimentary infill and they generally coincide with prominent reflectors and changes of seismic facies. In this section we focus on the different discontinuities identified within the Miocene infill, *i.e.*, below the conspicuous M reflector. Well data are scare for the Miocene sequence in the study area as it was only completely drilled at Habbibas-1 well. Additionally ODP Site 978 penetrated the uppermost Messinian deposits. Thus Miocene age attributions are tentatively assigned and correlated with previous studies in other sectors of the Alboran Sea Basin. The principal Miocene reflectors and seismic units are described below from oldest to youngest.

The R4 reflector is an angular unconformity locally recognized within the lower part of the Miocene sequence. Its seismic character changes laterally from strong and high amplitude reflections to more semitransparent zones (*e.g.* Figure 6-4). This reflector corresponds with an erosional truncation over large areas and changes laterally to a concordant surface in some basinal realms. At Habibas-1 well the R4 reflector is a concordant surface within a sedimentary sequence of Serravallian age. The seismic unit bounded on top by the R4 reflector represents the oldest deposits, which lay directly over the acoustic basement. This unit has high amplitude semitransparent facies and fills fault-related depressions. At Habibas-1 well these deposits are Serravallian carbonate clays interbedded with sandy levels. Moreover the R4 unconformity is the base of other seismic unit with strong reflectors of low lateral continuity alternating with semitransparent and locally transparent to chaotic facies corresponding with alternating clays, silts and sandy lenses.

The Tortonian R3 reflector has very continuous strong character and high amplitude and it frequently truncates the underlying sequences (*e.g.* Figure 6-4). This reflector forms the lower boundary of a late Tortonian unit with fairly transparent facies formed by parallel continuous reflectors and including also well-stratified medium to high amplitude reflections. These facies represent fine grained clays and marls interbedded with sandstone levels.

The high amplitude R2 reflector occasionally has reverse polarity and corresponds approximately with the Tortonian-Messinian boundary. It is the base of a thin seismic unit with strong parallel high-amplitude reflectors and locally chaotic facies (*e.g.* Figure 6-4). Correlation with the Habibas-1 well indicates that these reflections correspond with Messinian sediments, mainly consisting of gypsum-clays, anhydrite, marls and levels of volcanic ashes towards its top.

Seismic reflectors R4, R3 and R2 correlates with the main Miocene seismo-stratigraphic discontinuities identified by Comas *et al.*, (1992) and Jurado and Comas, (1992) and comparable to those used by Chalouan *et al.*, (1997).

M reflector

The M reflector marks the Miocene-Pliocene boundary at about 5. 33 Ma and is a surface with strong erosional character of variable magnitude that truncates Late Miocene deposits and basement highs (*e.g.* Figure 6-3). Figure 6-5 is a depth-converted contour map of the M reflector showing its complex present-day geometry characterized by several NE-SW and WNW-ESE troughs bounded by a number of highs with tens of kilometres in length. In most of the study area the M reflector locates at top of the thin Messinian unit with high amplitude, which represent detrital and evaporitic deposits

probably related to the Messinian salinity crisis (*e.g.* Figures 3 and 4). In other cases the M reflector locally erodes the top of basement as in the Ibn-Batouta, Provençaux, Câbliers and Alidade banks, the Cabo Tres Forcas Ridge, the edges of the Djibouti High, the eastern part of the Yusuf Ridge and Basin and in the unnamed buried high in the EAB.

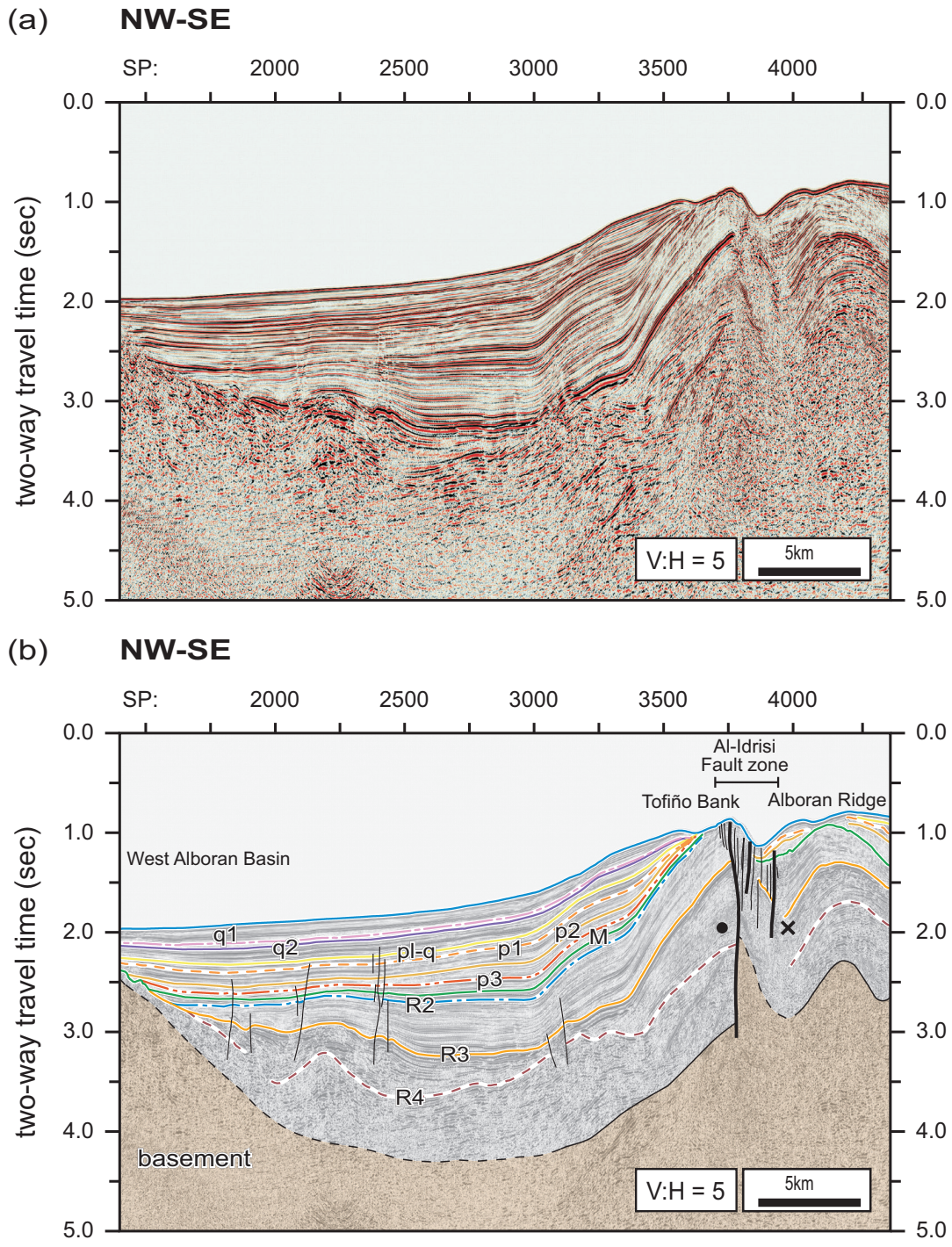

Figure 6-4. (a) Uninterpreted and **(b)** interpreted multichannel seismic section across the West Alboran Basin, Al-Idrisi fault zone and Tofiño Bank. R4 to q1 reflectors, age of unconformities and seismic units as defined by Jurado and Comas (1992) for the Miocene sequences (below the M-reflector), and by Martínez-García et al. (submitted for publication) for the Plio-Quaternary sequences. Tentative position of top of basement is indicated by dashed lines. Location of seismic line is shown in figures 2, 5 and 6.

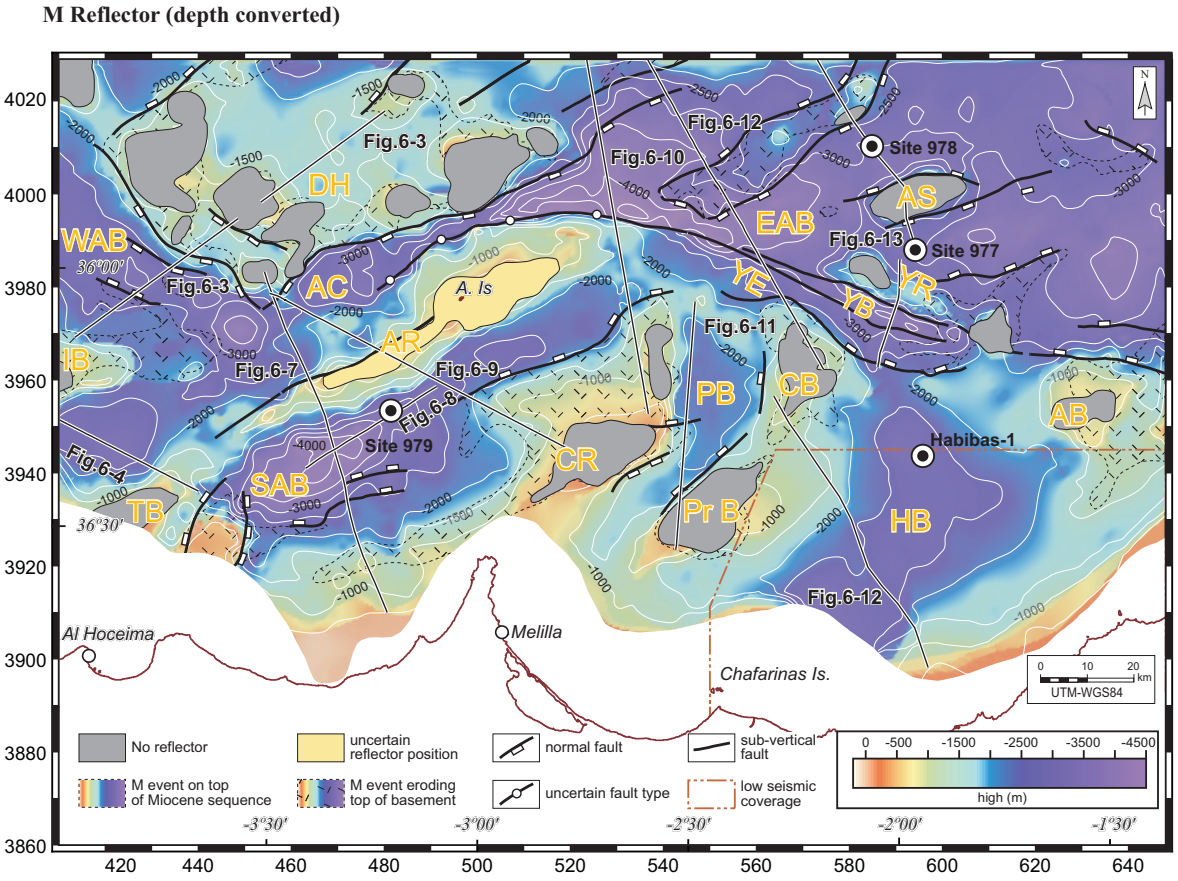

Figure 6-5. Depth-converted contour map of the M reflector in the study area showing variability of underlying materials from Miocene sediments to basement. Streaky areas indicate where the M event is an unconformity eroding the top of basement. Ornamented areas are present-day outcropping basement or Miocene sedimentary sequences. Yellow shows areas where the position of the M reflector remains uncertain. Main structures active at this time are also represented. Contour interval is 500 m. UTM projection, units in kilometres. Position of multichannel seismic profiles from Figs 3, 4, 7, 8, 9, 10, 11, 12 and 13 is indicated. Location of ODP Leg 161 sites 977, 978, 979 and the commercial borehole Habibas-1 are also included. Abbreviations: A. Is, Alboran Island; AB, Alidade Bank; AC, Alboran Channel; AR, Alboran Ridge; AS, Al-Mansour Seamount; CB, Câbliers Bank; CR, Cabo Tres Forcas Ridge; DH, Djibouti High; EAB, East Alboran Basin; HB, Habibas Basin; IB, Ibn-Batouta Bank; PB, Pytheas Basin; Pr B, Provençaux Bank; SAB, South Alboran Basin; TB, Tofiño Bank; YB, Yusuf Basin; YE, Yusuf Escarpment; YR, Yusuf Ridge; and WAB, West Alboran Basin.

The depth of the M reflector ranges from minimum values about 35 m in the Moroccan margin next to the coastline between Al Hoceima and Melilla to maximum depths up to 4000 m in some basin centres. Significant vertical offsets of the M reflector surface coincide with the location of active faults in Messinian times or further during the Plio-Quaternary (Figure 6-5). For example, a maximum vertical offset of approximately 2000 m can be calculated for the northern slope of the Alboran Ridge, considering the position of the M reflector at the base of the slope at 2500 m depth and at the bottom of the adjacent EAB at more than 4500 m. Other local maximum depth values of the M reflector occur at the southwestern parts of the SAB and Alboran Channel, were this surface reaches up to 4000 m and 3500 m depth respectively, indicating that these basins were deep troughs in Messinian times. Similarly the M reflector is up to 3500 m depth along the WNW-ESE elongated Yusuf Basin.

Plio-Quaternary sequence

The Plio-Quaternary sequence on top of the M reflector comprises several seismic units bounded by the following regional unconformities: p3 (~4.57 Ma; Early Pliocene), p2 (~3.28 Ma; Late Pliocene), p1 (remarkable Late Pliocene hiatus from 2.52 to 2.45 Ma in site 979), pl-q (~1.81 Ma; Pliocene-Quaternary boundary), q2 (~1.19 Ma; Pleistocene), q1 (~0.79 Ma; Pleistocene). The lowermost Pliocene units are dominated by semi-transparent seismic facies with continuous parallel reflectors and locally lens-shaped and channel features that correspond with dominantly clay lithologies with some interbedded carbonate and sandy levels. In contrast, the uppermost Late Pliocene and Quaternary units have high-to-moderate amplitude reflectors with abundant intercalations of chaotic seismic facies, interpreted to be slides. These series are mainly composed by clay, silt and sandstone. A more detailed description of each seismic unit and the bounding seismic reflectors has been presented in Martínez-García *et al.* (submitted for publication).

Isopach maps

Figure 6-6a shows the estimated thickness of Miocene sediments. Isopachs should be considered as approximate values in this case due to: (1) local uncertainties about the precise position of the top of basement as it is indicated in the interpreted seismic sections from Figures 3, 4 and 7 to 13; (2) volcanic intrusions from ~18 to 6 Ma that form the acoustic basement in some places may overlie older sediments (*e.g.* Hoernle *et al.*, 1999; Duggen *et al.*, 2008); (3) the existence of major unconformities within the Miocene sedimentary cover, specially the M reflector at its top that has erosive nature in most of the study area, indicate that part of the original deposits were removed. Thus sediment thickness presented here should be taken as regional values providing general tendencies and locally representing minimum values.

The Miocene infill shows a number of depocentres associated with normal faults (Figure 6-6a). The EAB comprises four of these depocentres with NE-SW orientation; two of them are separated by the Al-Mansour Seamount and reach maximum thicknesses up to 2.5 km and other two are up to 1.5 km thick and locate in the westernmost part of the EAB next to the Djibouti High and in the easternmost part, close to the Algerian Basin. The SAB contains other Miocene depocentre with average NE-SW orientation and ~120 km length. Maximum thickness up to 2 km occurs in its southern part, which connects throughout the western end of the Alboran Ridge with other remarkable depocentres in the SW Alboran Chanel and the southern branch of the WAB. Other small depocentre with similar NE-SW orientation occurs to the NW of the peninsula of Melilla and contains more than 1.5 km of Miocene sediments. The Habibas Basin comprises an extensive Miocene depocentre with elliptical shape in plan view (~70 km long and 45 km wide). The axis of this elongated depocentre has NNE-SSW orientation and comprises maximum Miocene thickness up to 2.4 km, which was drilled at Habibas-1 well. Additionally, NW-SE to WNW-ESE elongated Miocene depocentres, tens of kilometres long, can be recognized along the Yusuf Basin and Escarpment and in the WAB.

A number of NE-SW trending Plio-Quaternary depocentres coincide in location with those Miocene ones along the Alboran Channel, SAB, Pytheas and Habibas basins (Figure 6-6b).

Isopach map of Miocene sediments (depth converted)

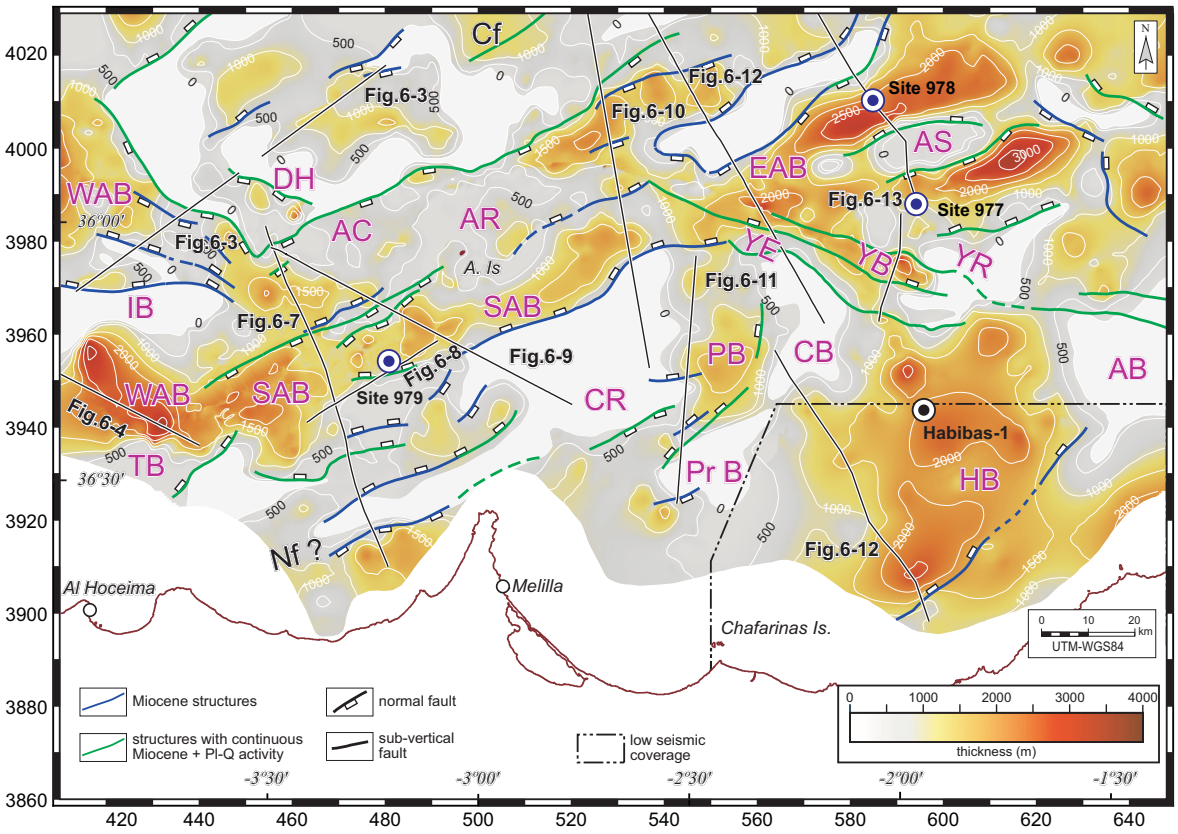

Isopach map of Plio-Quaternary sediments (depth converted)

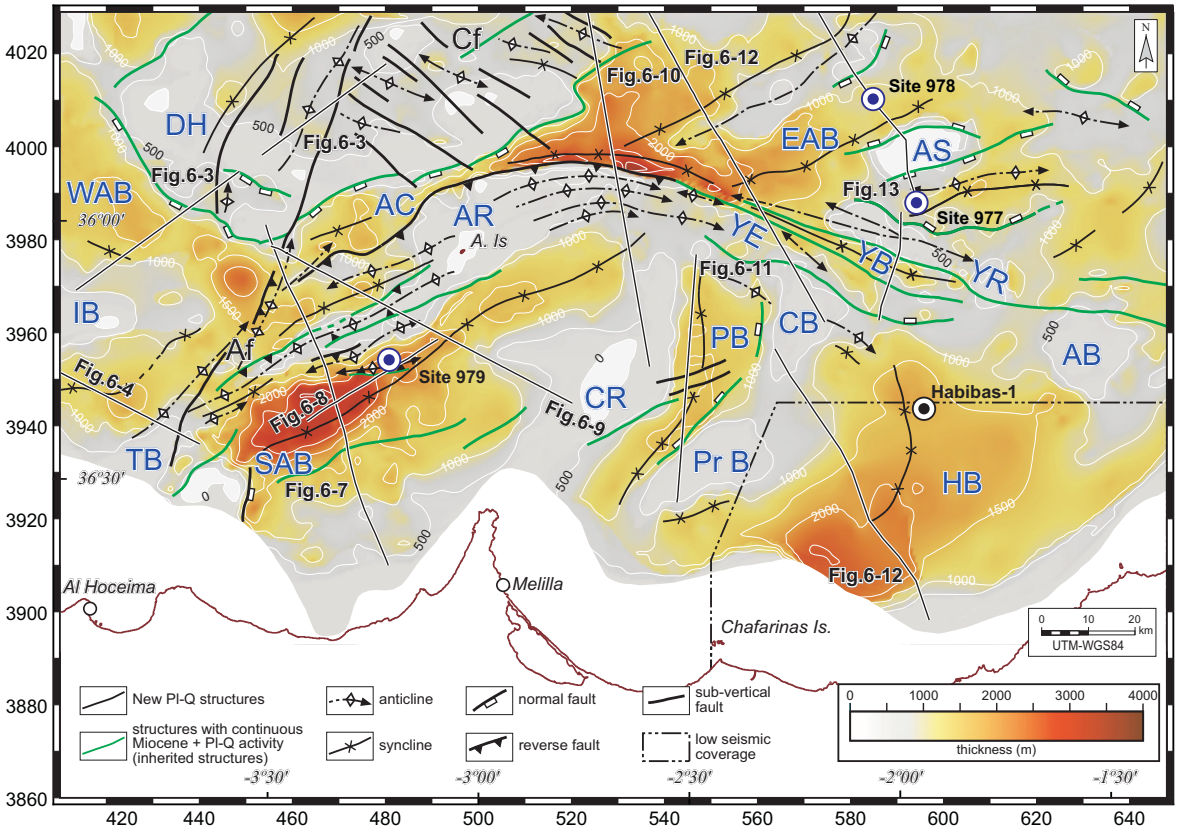

The depocentre of the Alboran Channel has a singular shape as it merges with another NW-SE perpendicular axis along the WAB. Otherwise, the Plio-Quaternary depocentre of the EAB shows a complex geometry: several NE-SW to ENE-WSW elongated axes containing up to 1 km of post-Messinian sediments, which were drilled at ODP Sites 977 and 978, are located at the same position than previous Miocene depocentres being separated by basement highs (*cf.* Figures 6a and 6b), but the two westernmost of these Plio-Quaternary axes thicken and deepen towards the SW where they merge with another new depocentre axis in front of the Alboran Ridge and Yusuf Escarpment. This last Plio-Quaternary axis is curved in plan view changing from SW-NE to WNW trend and connecting with the narrow depocentre along the Yusuf Basin. The southern part of this asymmetric depocentre in the EAB contains maximum Plio-Quaternary thickness in the study area reaching up to 3 km. Other local maxima up to 2.5 km are in the SW of the SAB and Habibas Basin.

Comparing both maps, the most significative feature is the change in the location and magnitude of main sedimentary depocentres between the Miocene and Plio-Quaternary suggesting important changes on the distribution of main basinal areas. Even some long-lived sub-basins show lateral variations of the locus of maximum thickness responding to changes in tectonic activity. For example, both the SAB and Habibas Basin show rather uniform distribution of sediment thickness along their axes during the Miocene, but the Plio-Quaternary the depocentres become asymmetric containing maximum thicknesses at their SW sectors suggesting a recent tilting of these basin axes. Additionally, the EAB experienced a change in the locus of maximum sediment accumulation from its eastern part during the Miocene along major NE-SW troughs to its western part, mainly in front of the Alboran Ridge and Yusuf Escarpment, during the Plio-Quaternary. In addition, some Miocene depocentres do not reflect high sediment accumulation any more during the Plio-Quaternary. This is the case of depocentres along the Yusuf Escarpment, the SW Alboran Ridge and to the NW of Melilla. Most basement highs are depleted of Miocene sediments o covered by thin sequences (< 500 m) forming areas that remained elevated at this time and trend parallel to the main depocentres. The Plio-Quaternary sequence also thins towards these highs and the isopach map of Figure 6-6b shows that the elongated shape of some of these highs was enhanced during the Plio-Quaternary.

6.5 Fault structure

The principal faults and folds in the study area are shown in multichannel seismic sections of Figures 3, 4 and 7 to 13. These structures are also mapped on the depth-contour map of the M reflector (Figure 6-5) and on the isopach maps of sediments accumulated during the Miocene and Plio-Quaternary respectively (Figure 6-6). Fault and folds represented in each map are those thought to be

Figure 6-6. Isopach maps showing thickness in metres of: **(a)** the Miocene sequences and **(b)** the Plio-Quaternary sequences. Main structures active at these time intervals are also represented. Contour interval is 500 m. UTM projection, units in kilometres. Position of multichannel seismic profiles from Figs 3, 4, 7, 8, 9, 10, 11, 12 and 13 is indicated. Blue circles are ODP sites 977, 978, 979 and the commercial borehole Habibas-1. Abbreviations: A. Is, Alboran Island; AB, Alidade Bank; AC, Alboran Channel; Af, Al-Idrisi fault zone; AR, Alboran Ridge; AS, Al-Mansour Seamount; CB, Câbliers Bank; Cf, Carboneras fault zone; CR, Cabo Tres Forcas Ridge; DH, Djibouti High; EAB, East Alboran Basin; HB, Habibas Basin; IB, Ibn-Batouta Bank; PB, Pytheas Basin; Pr B, Provençaux Bank; SAB, South Alboran Basin; TB, Tofiño Bank; YB, Yusuf Basin; YE, Yusuf Escarpment; YR, Yusuf Ridge; and WAB, West Alboran Basin.

active at the time of the mapped event. These maps show the change from a dominating extensional pattern to a complex framework dominated by contractional structures comprising inherited fault zones and other newly generated during the Plio-Quaternary.

Miocene structures

Different extensional fault systems were active during the Miocene producing remarkable associated depocentres (Figure 6-6a). Figure 6-3 shows a number of normal faults deforming the acoustic basement and the lowermost part of the sedimentary infill in the West Alboran Basin and the westernmost part of the Djibouti High. These structures trend NW-SE to E-W and arrange into two groups of synthetic faults. The two fault sets dip towards each other forming an overall conjugate convergent geometry. There are some tilted fault blocks of basement and growth wedges below the M reflector. Syn-sedimentary thickenings towards the foot wall scarps indicate that these Miocene deposits are syn-rift.

Other Miocene normal faults deforming the Djibouti High are NE-SW trending. These structures have small depocentres associated and show a divergent pattern (Figure 6-6a). The most remarkable of these faults occurs along the southeastern edge of the Djibouti High bounding the Alboran Channel (Figures 6a and 7). Other sub-parallel, NE-SW to ENE-WSW trending, high angle normal faults with associated Miocene depocentres occur along the Alboran Ridge, South and East Alboran basins and the North African margin. These structures display a general, in-relay geometry with lateral ramps between the different fault segments (Figure 6-6a). For example, Figures 7 and 9 shows faulted blocks of basement and old deposits below the M reflector. Most of these structures are overlain by a thick sequence of sediments of Pliocene to Recent age. The southernmost part of Figure 6-7 shows a half-graben structure with a south-facing border fault and Miocene deposits thickening towards the NW in the hanging wall, which is consistent with growth faulting during the Miocene. Towards the NW of this structure, other sub parallel Miocene normal faults cut the southern margin of the SAB where the top of basement has a staircase profile. The structures in the SAB predominantly dip in an opposite sense respect to the fault in the Moroccan margin, thus forming two divergent conjugate systems (Figures 6a, and 7).

Miocene fault surfaces are not clearly imaged along the Alboran Ridge due to intense Plio-Quaternary deformation and abundant magmatic intrusions, which produce chaotic reflections. However, we observed several asymmetric wedges of Miocene sediments that indicate the location of possible old extensional syn-sedimentary structures. For example, Figure 6-7 shows that the core of the western Alboran Ridge comprises an asymmetric depocentre of folded Miocene sediments (between shot points 2100 and 2500). At present-day, these deposits form the hanging wall of a Plio-Quaternary reverse fault, but they have a wedge geometry thickening towards the NW. These observations suggest that the southeast-dipping fault had extensional regime during the Miocene forming a half-graben filled by sediments that were later uplifted and folded. Similarly, Figure 6-9 shows other growth wedge geometry in the southern slope of the Alboran Ridge (between shot points 6025 and 6300). In this case the R3 and M reflectors delimitate a Late Miocene sedimentary sequence thickening towards the NW that indicates the existence of a southeast-dipping extensional fault active at this time.

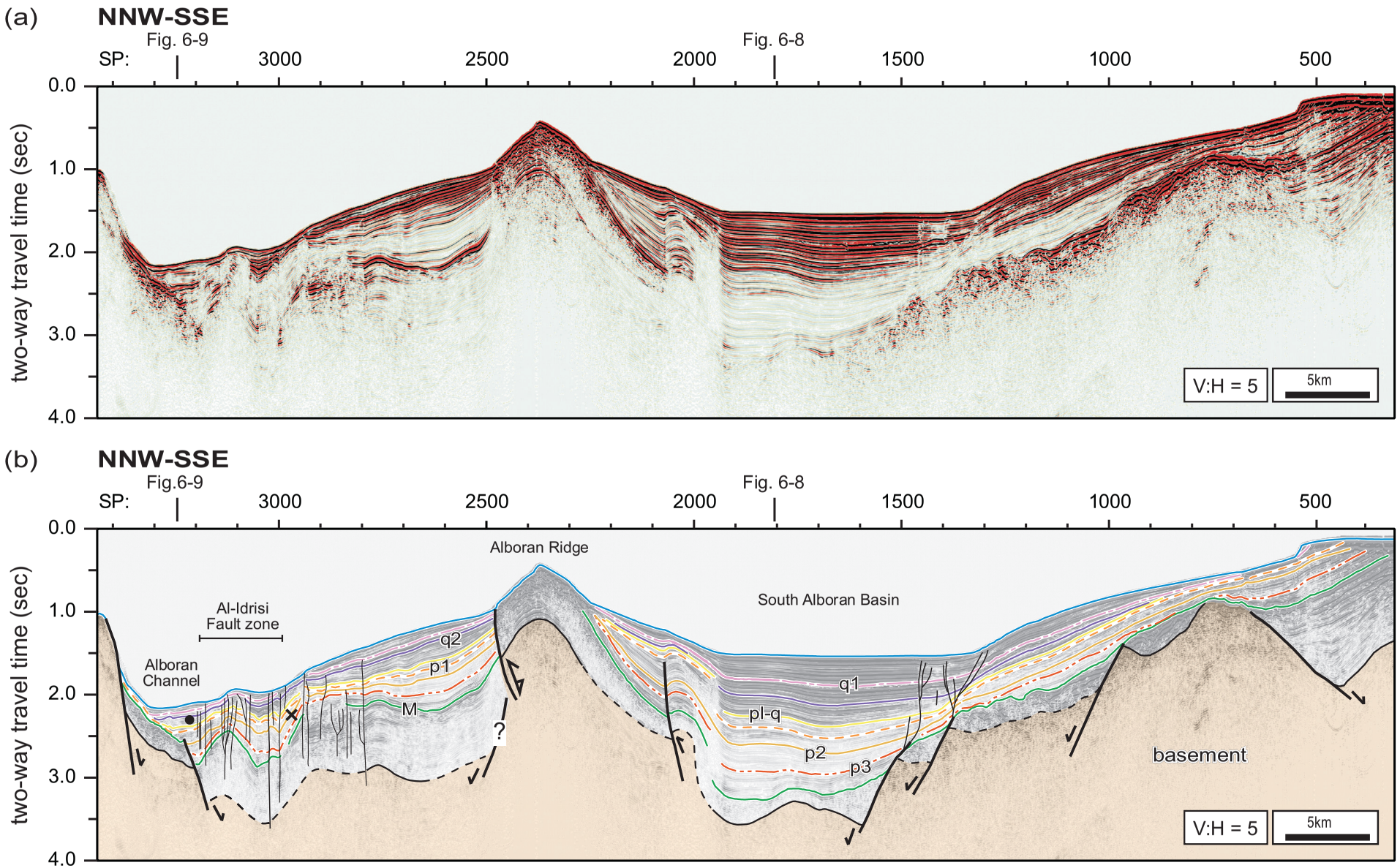

Figure 6-7. (a) Uninterpreted and **(b)** interpreted multichannel seismic section from the Alboran Channel to the North African margin and across the western Alboran Ridge and the South Alboran Basin. M to q1 reflectors, age of unconformities and Plio-Quaternary seismic units as defined by Martínez-García et al. (submitted for publication). Tentative position of top of basement is indicated by dashed lines. Double arrow indicates Miocene normal fault inverted as reverse during the Plio-Quaternary. Location of seismic line is shown in figures 2, 5 and 6.

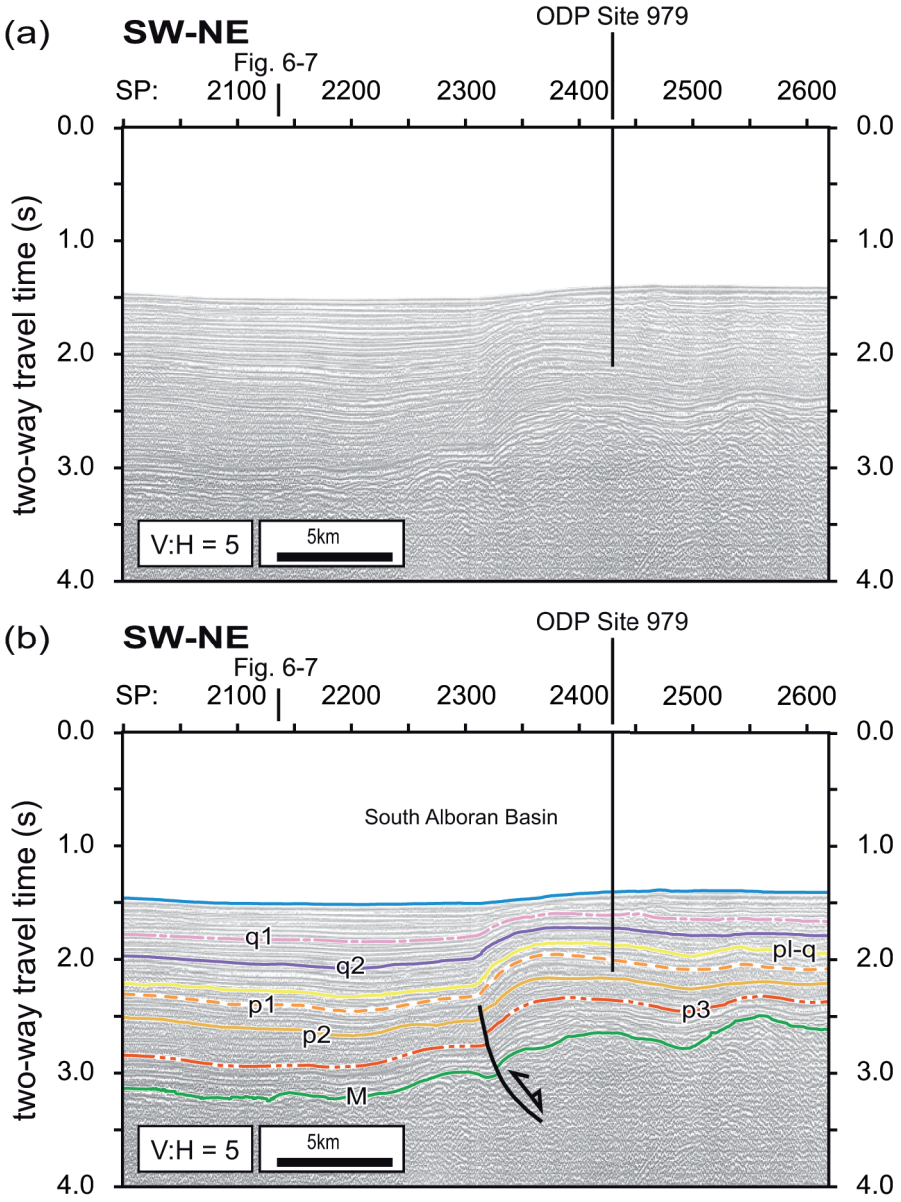

Figure 6-8. (a) Uninterpreted and **(b)** interpreted multichannel seismic section showing an inverted structure in the South Alboran Basin. M to q1 reflectors, age of unconformities and Plio-Quaternary seismic units as defined by Martínez-García et al. (submitted for publication). Double arrow indicates Miocene normal fault inverted as reverse during the Plio-Quaternary. Location of seismic line is shown in figures 2, 5 and 6.

The seismic section shown in Figure 6-10 illustrates the structure in the East Alboran Basin and the western sectors of the Alboran Ridge and South Alboran Basin. In the EAB, we have interpreted a system of Miocene synthetic normal faults with NE-SW orientation. The sedimentary sequence of Middle Miocene age show tilted strata associated with the faults and these sediments are truncated by the R4 reflector on top. The R3 reflector seals most of these extensional structures in the EAB (Figure 6-10). This seismic section shows also that the Miocene infill in the eastern part of the SAB is associated with a northwest-dipping fault, which has a significant normal slip component. This fault continued being active during the Pliocene as in this case the unconformity that seals the normal fault is the pl-q reflector. To the south of this structure, the Pytheas Basin comprises also normal faults with NE-SW to NNE-SSW trend (Figures 6a and 11). N to NW dipping faults bound tilted blocks

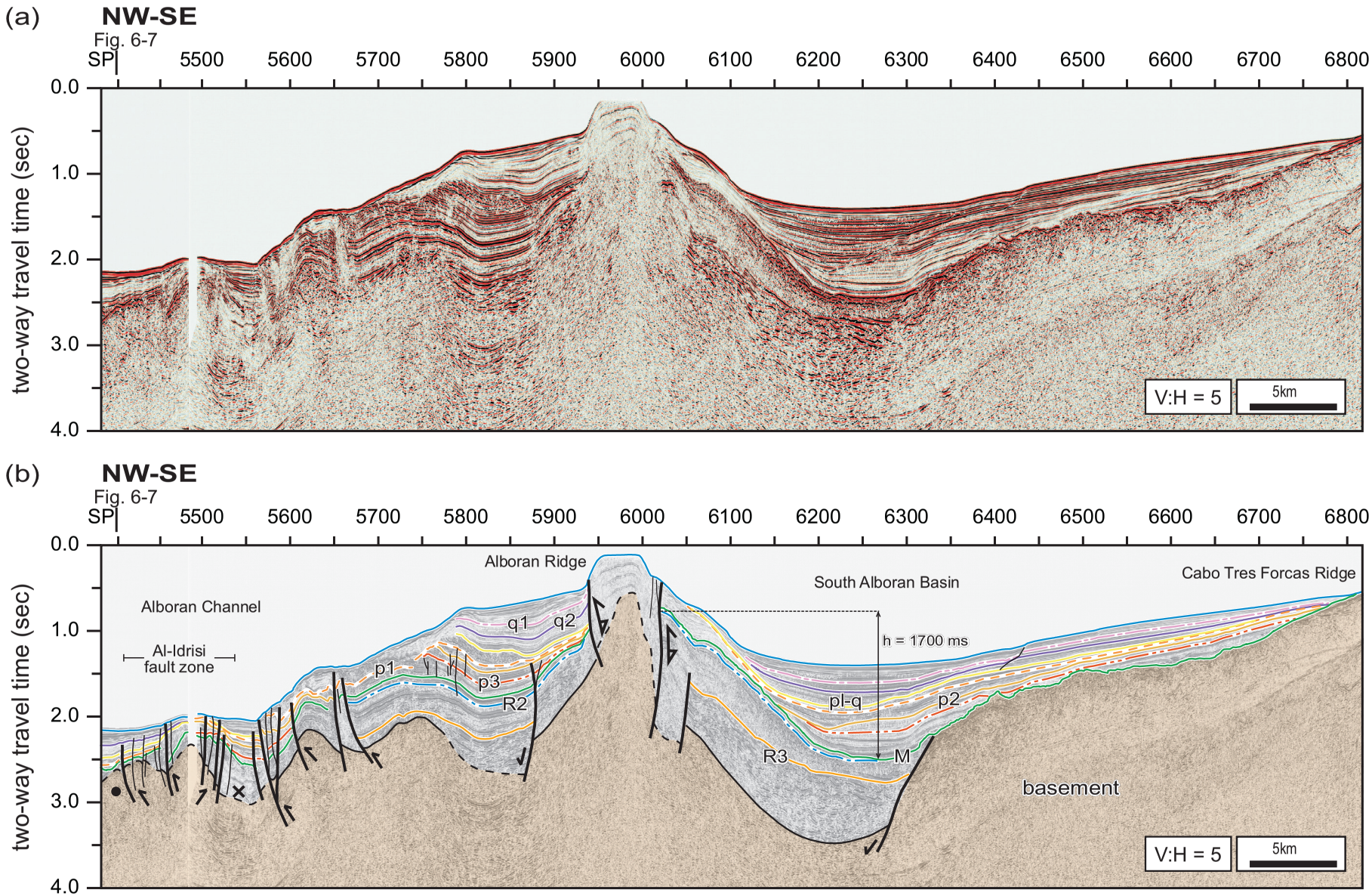

Figure 6-9. (a) Uninterpreted and **(b)** interpreted multichannel seismic section across the Alboran Channel, central Alboran Ridge and South Alboran Basin to the Cabo Tres Forcas Ridge. R3 to q1 reflectors, age of unconformities and seismic units as defined by Jurado and Comas (1992) for the Miocene sequences (below the M-reflector), and by Martínez-García et al. (submitted for publication) for the Plio-Quaternary sequences. Tentative position of top of basement is indicated by dashed lines. Double arrows indicate Miocene normal fault inverted as reverse during the Plio-Quaternary. Notice the two growth wedges in Miocene sediments in the southern slope of the Alboran Ridge and the SAB that thicken in opposite senses (shot points 6050-6125): Unit IV (*i.e.*, below R3 reflector) thickens towards the SE, whilst Unit III (*i.e.*, between R3 and R2 reflectors) thickens towards the NW. Notice also that wedge of Unit III is inverted and uplifted towards the Alboran Ridge. Location of seismic line is shown in figures 2, 5 and 6.

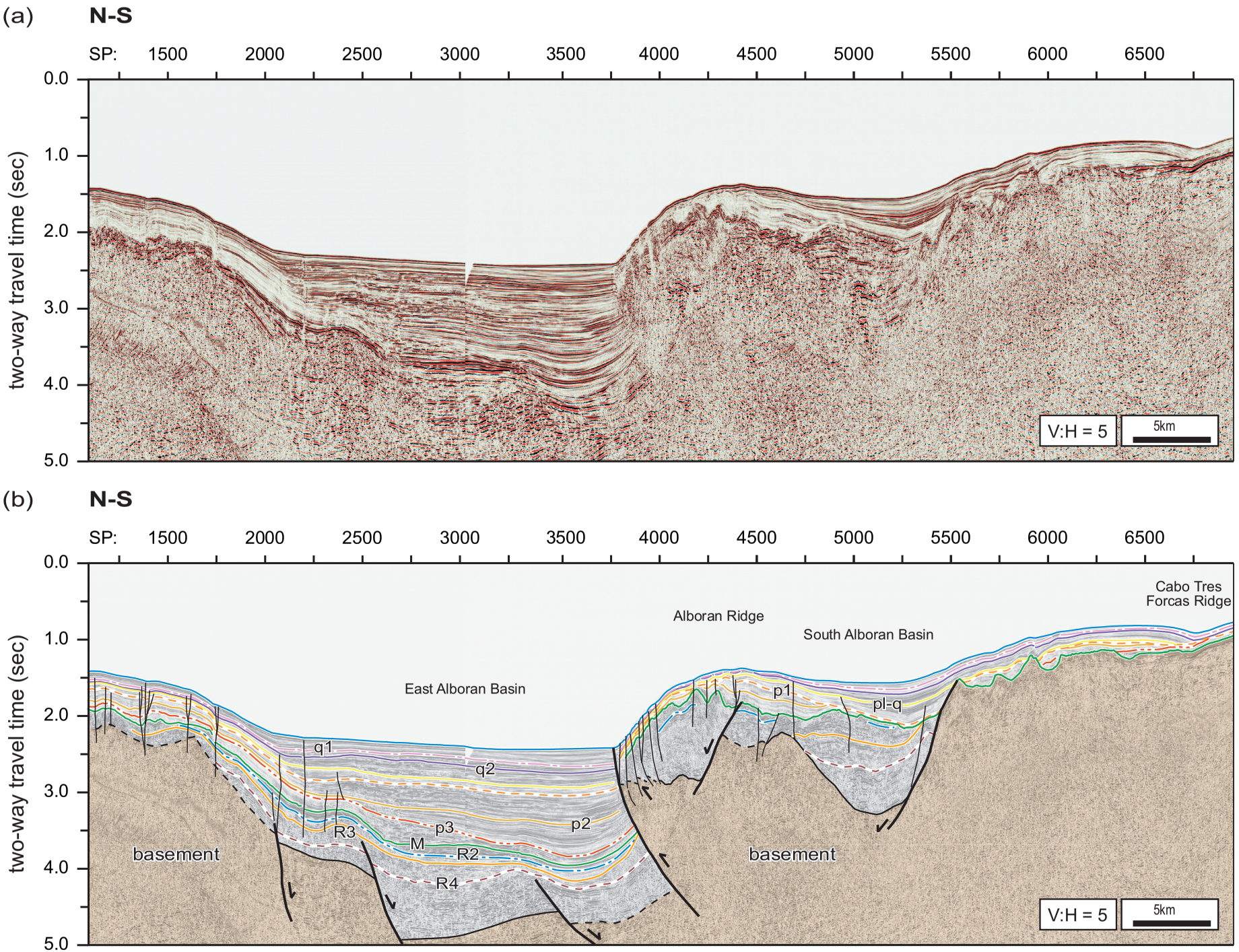
(a)
N-S
SP:
1500
2000
2500
3000
3500
4000
4500
5000
5500
6000
6500
0.0
1.0
2.0
3.0
4.0
5.0
two-way travel time (sec)
V:H = 5
5km
(b)
N-S
SP:
1500
2000
2500
3000
3500
4000
4500
5000
5500
6000
6500
0.0
1.0
2.0
3.0
4.0
5.0
two-way travel time (sec)
Cabo Tres
Forcas Ridge
Alboran Ridge
South Alboran Basin
East Alboran Basin
p1
pl-q
q1
q2
p2
p3
R3
M
R2
R4
basement
basement
V:H = 5
5km

Figure 6-10. (a) Uninterpreted and **(b)** interpreted multichannel seismic section across the East Alboran Basin, eastern Alboran Ridge, South Alboran Basin to the Cabo Tres Forcas Ridge. R4 to q1 reflectors, age of unconformities and seismic units as defined by Jurado and Comas (1992) for the Miocene sequences (below the M-reflector), and by Martínez-García et al. (submitted for publication) for the Plio-Quaternary sequences. Note Miocene high angle extensional structures and Plio-Quaternary inversion and uplift of southern basins caused by north-directed thrusting along the northern side of the Alboran Ridge. Tentative position of top of basement is indicated by dashed lines. Location of seismic line is shown in figures 2, 5 and 6.

of basement and growth wedges of Miocene deposits that thicken towards the fault scarps. In the southern margin of this basin, the Provençaux Bank is a basement high bounded by two divergent high-angle normal faults forming a host structure. Most of the normal faults in this profile are sealed by the M reflector, but the fault around shot point 1550 affects to the entire Plio-Quaternary sequence.

Figure 6-12 is a composite seismic section with NNW-SSE trend that crosses the whole study area from the East Alboran Basin to the Habibas Basin and shows different Miocene extensional structures. The Miocene sequences thicken towards the Yusuf Escarpment, where we interpret a system of high-angle faults with normal slip components that have WNW-ENE orientation (Figure 6-6a). In the EAB, this profile crosses the same system of synthetic southeastern-dipping normal faults with NE-SW orientation previously shown in figure 6-10 (*cf.* shot points 400 to 750 in figure 6-12 and 2000 to 3500 in figure 6-10) and other basement high located in the central part that is bounded by two conjugate divergent faults forming an elongated NE-SW horst. Most of these extensional structures become inactive at the end of the Miocene, as they do not cut the M reflector. Only some segments of the faults delimitating the basement horst in the EAB affect to the lowermost Pliocene sediments and are sealed by the p1 reflector (*e.g.* shot points 900 to 1000 in figure 6-12).

Figure 6-12 shows also that the Habibas Basin, to the south of the Yusuf Escarpment, comprise a Miocene half-graben structure with a northwest-facing border fault along its southeastern margin. This structure has a NE-SW trend, similarly to those Miocene structures previously depicted for other realms (Figure 6-6a). The half-graben is filled in by a syn-tectonic Miocene sequence, penetrated at Habibas-1 well, which expands towards the footwall scarp and reaches a maximum thickness up to 1700 ms (twtt) (around shot point 2450).

Figure 6-13 illustrates the structure in the eastern sector of the EAB. Here the basin is sub-divided into three troughs separated by basement highs, which are bounded by divergent high-angle faults: (1) the Yusuf Ridge; (2) the Al-Mansour Seamount; and (3) the unnamed buried horst of basement previously imaged in figure 6-12 that outcrops here and has asymmetric flanks (*cf.* shot points 900 to 1000 in figure 6-12 and shot points 2600 to 2900 in figure 6-13). Pre-Messinian sequences, thicker than 1000 ms (twtt), fill the lower part of these troughs with graben and half-graben structures. In the Yusuf Basin, high-angle conjugate convergent faults with WNW-ESE orientation bound a thick Miocene sedimentary depocentre (up to 1300 ms (twtt)) (Figures 6a and 13). Some of these faults show significant normal slip component and the entire Miocene sequence shows thickening towards the NE, which is consistent with growth faulting at this time.

Plio-Quaternary structures

Most faults in the West Alboran Basin are sealed by the M unconformity indicating that tectonic

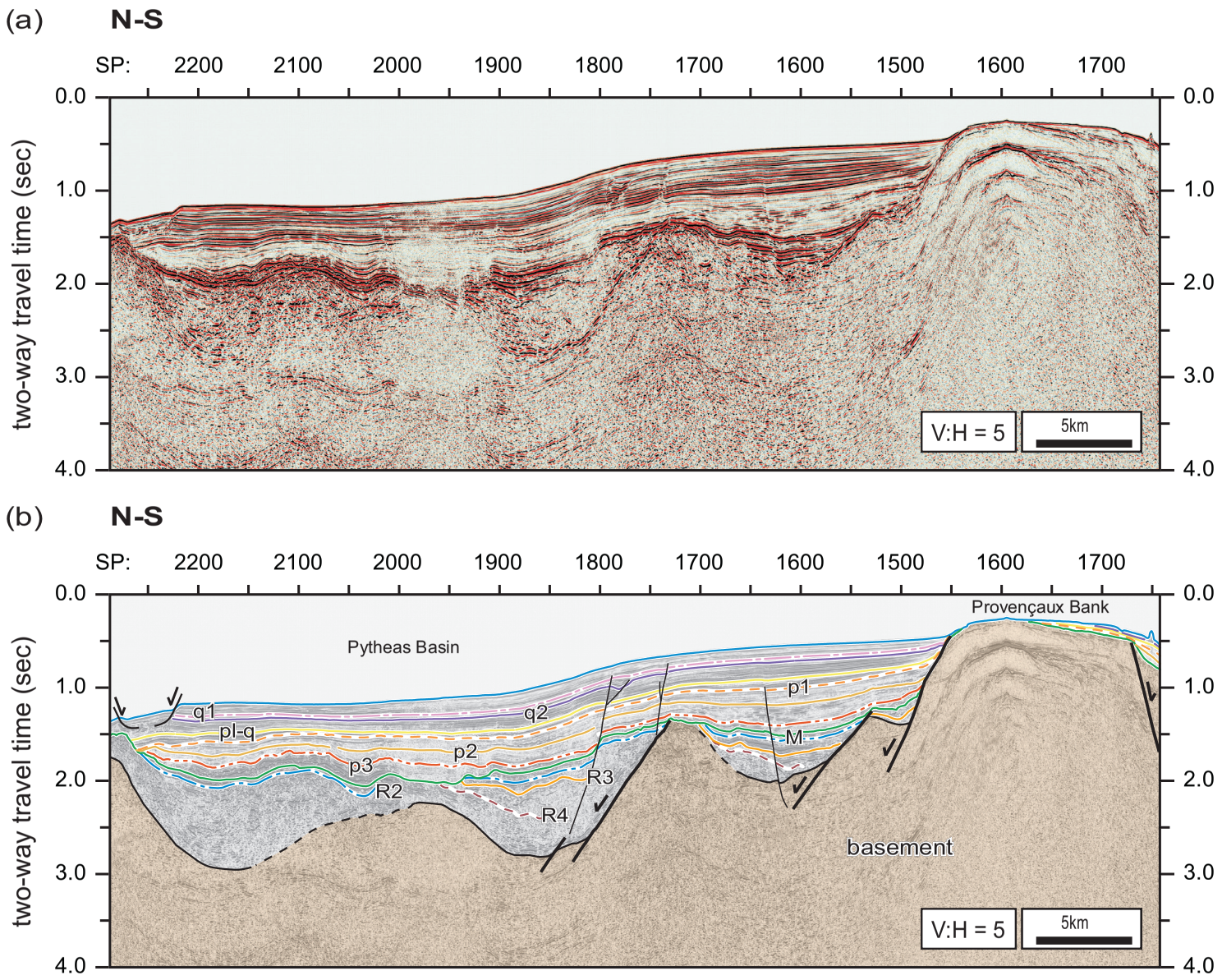

Figure 6-11. (a) Uninterpreted and **(b)** interpreted multichannel seismic section across the Pytheas Basin and Provençaux Bank. R4 to q1 reflectors, age of unconformities and seismic units as defined by Jurado and Comas (1992) for the Miocene sequences (below the M-reflector), and by Martínez-García et al. (submitted for publication) for the Plio-Quaternary sequences. Tentative position of top of basement is indicated by dashed lines. Note that most of pre-M extensional structures are sealed by Plio-Quaternary deposits. Location of seismic line is shown in figures 2, 5 and 6.

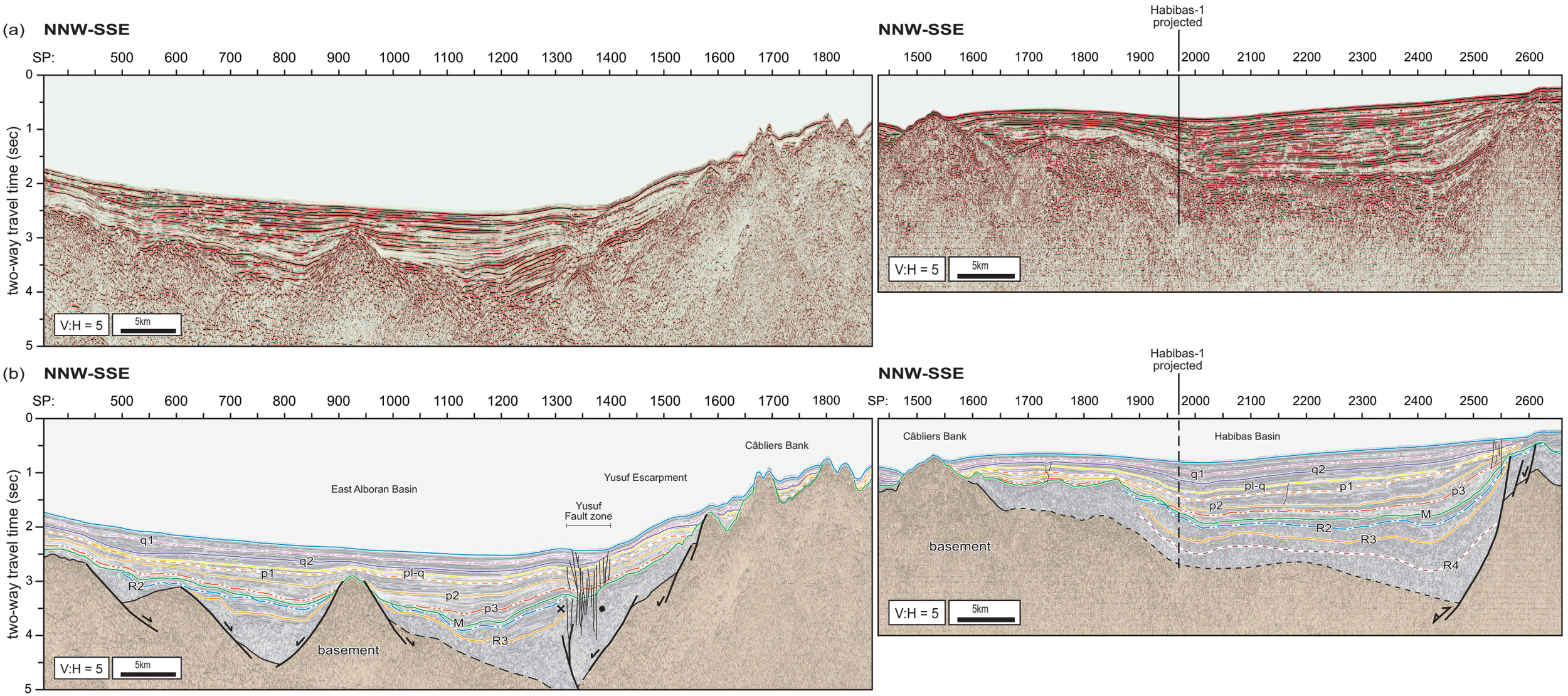

Figure 6-12. (a) Uninterpreted and **(b)** interpreted multichannel composite seismic section across the East Alboran Basin (EAB), Yusuf Escarpment and Habibas Basin. Habibas-1 well is projected from approximately 20 km northeast. R4 to q1 reflectors, age of unconformities and seismic units as defined by Jurado and Comas (1992) for the Miocene sequences (below the M-reflector), and by Martínez-García et al. (submitted for publication) for the Plio-Quaternary sequences. Note pre-M extensional structures, tilted blocks sealed by Plio-Quaternary sediments in the EAB and growth wedge geometry for the lowermost deposits of the Habibas Basin. Double arrow indicates inverted fault. Tentative position of top of basement is indicated by dashed lines. Location of seismic line is shown in figures 2, 5 and 6.

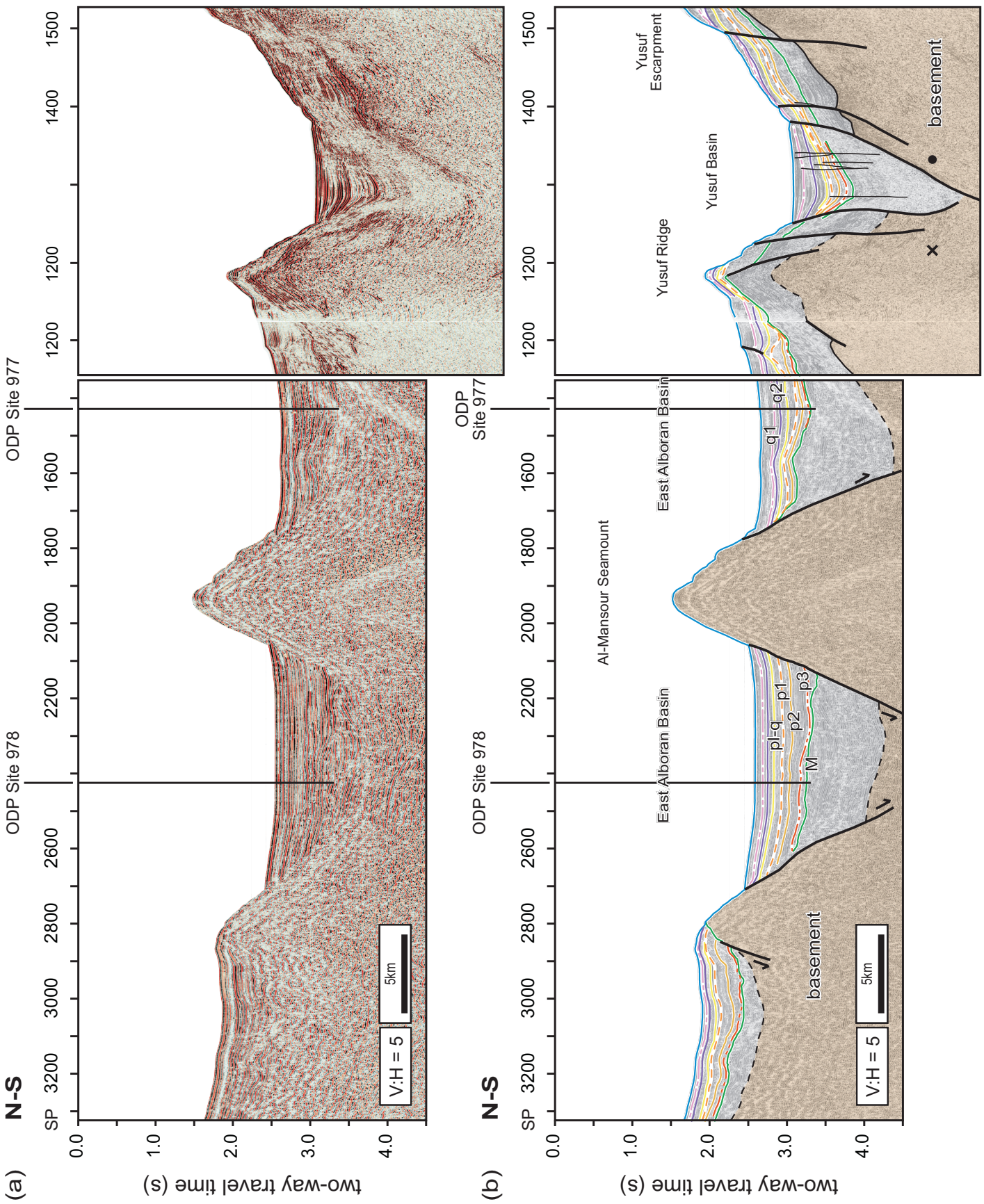
(a)
N-S
SP
3200
3000
2800
2600
2200
2000
1800
1600
1400
1200
1200
1500
ODP Site 978
ODP Site 977
two-way travel time (s)
0.0
1.0
2.0
3.0
4.0
V:H = 5
5km
(b)
N-S
Al-Mansour Seamount
East Alboran Basin
East Alboran Basin
Yusuf Ridge
Yusuf Basin
Yusuf Escarpment
basement
basement
q1
q2
pl-q
p1
p2
p3
M
ODP Site 978
ODP Site 977
two-way travel time (s)
V:H = 5
5km

Figure 6-13. (a) Uninterpreted and **(b)** interpreted multichannel composite seismic section across the East Alboran Basin and Yusuf Basin and Ridge. Note two small sub-basins separated by a basement high in the EAB and perched sedimentary sequences on the margins of the Yusuf Basin. Tentative position position of top of basement is indicated by dashed lines. Location of seismic line is shown in figures 2, 5 and 6.

activity was scarce in this realm during the most recent times (Figure 6-3). The Plio-Quaternary cover locally shapes some small drape folds on top of crests of faulted basement blocks (*e.g.* around shot points 3950 and 3800 in figure 6-3). Only the two most external faults of the normal conjugate fault system affect to the lowermost Plio-Quaternary sediments and these structures are finally sealed by the q2 reflector (shot points 4250 and 3625 in figure 6-3).In these cases, none of the most recent seismic units show wedges geometries thickening towards the fault scarps, in contrast to the previous Miocene deposits. This observation indicates that the vertical normal-slip components of these faults were reduced at Plio-Quaternary times.

Similarly to the WAB, most of the normal faults deforming the Djibouti High are sealed by the M reflector (*e.g.* shot point 2650 in figure 6-3). However, the structures forming its southern edge cut the Plio-Quaternary sequence (Figure 6-6b). In the western part of this scarp, the inherited Miocene NW-SE trending structures turning to NE-SW orientation maintain a significant normal slip component, but there are not thickening of Plio-Quaternary sediments adjacent to these faults (*e.g.* shot points 3400 in figure 6-3 and 3400 in figure 6-7). Towards the east, their vertical slip component decrease and fault surfaces at the base of the escarp are sub-vertical with limited displacement of Plio-Quaternary reflectors (*e.g.* around shot point 2100 in figure 6-10). Moreover, the inner part of the Djibouti High is deformed by many sub-vertical faults, which produce both reverse and normal displacements of the entire sedimentary cover and deform the seafloor suggesting a recent origin (*e.g.* Figure 6-3 between shot points 3100 and 2650). These faults have got associated oblique open folds and arrange into two conjugate systems with average NNE-SSW and NW-SE orientations forming an angle of approximately 65º between them (Figure 6-b). The NW-SE fault system cuts and displaces previous NE-SW trending faults at the southern escarpment of the Djibouti High.

Two fault-and-fold systems with different orientations deform the Plio-Quaternary sediments along the Alboran Ridge: the Alboran Ridge fault zone trending NE-SW, which controls the elongated shape of the ridge and the Al-Idrisi fault zone that is NNE-SSW trending and cuts obliquely the westernmost sector of this bathymetric high (Martínez-García *et al.*, 2011). (Figure 6-b). The Al-Idrisi fault zone consists of several sub-vertical faults with a reverse-slip component and associated folds (Figures 4, 7 and 9). In plan view, the different fault segments display in-relay geometries with anticlines plunging towards the north. Figure 6-4 shows a section of the Al-Idrisi fault zone in its southern part, where this structure separates the Alboran Ridge from the Tofiño Bank and crosscuts an old Miocene depocentre. Here, the Miocene sequence has similar thickness of ~ 1500-1700 ms (twtt) at both faults blocks, but significant changes of thickness occur for the Plio-Quaternary seismic units. The Plio-Quaternary cover thins to thicknesses of ~ 200-400 ms (twtt) towards the Alboran Ridge, which comprises the hanging wall block, and expands away from the fault along the northern side of the Tofiño Bank, which constitutes the foot wall block, reaching maximum thickness of about 1200 ms (twtt). These observations collectively indicate that the Al-Idrisi fault zone is a post-Messinian structure that produced a recent progressive and syn-sedimentary uplift of the western part

of the Alboran Ridge.

The Plio-Quaternary Alboran Ridge fault zone runs parallel to previous Miocene structures with NE-SW orientation and comprises several fault segments dipping in both northwest and southeast senses with a remarkable reverse slip component. Faults are associated with sub parallel folds in-relay with plunging terminations (Figures 6b, 7, 9 and 10). Some of these faults are inverted inherited extensional surfaces (*e.g.* fault at shot point 2500 in figure 6-7). In these cases, the previous Miocene depocentres showing growth wedge geometries appear folded and uplifted on the hanging wall of reverse faults that cut the entire Plio-Quaternary sequence. Other example is the inverted wedge of pre-Messinian sediments in the southern slope of the Alboran Ridge shown in figure 6-9. This wedge is folded and covered by a thick Plio-Quaternary sequence of about 1200 ms (twtt) in the SAB that progressively thins to ~ 200-400 ms (twtt) in the slope of the Alboran Ridge, where the wedge is uplifted about 1700 ms (twtt) respect the wedge apex in the centre of the SAB. All these observations suggest a post-Messinian tectonic inversion of the Miocene extensional structures and dominance of syn-sedimentary uplift and folding of the Alboran Ridge during the Plio-Quaternary.

The seismic profile of Figure 6-8 crosscuts obliquely other inverted structure at the base of the southern flank of the Alboran Ridge. In this case a Plio-Quaternary asymmetric fold is associated with a reverse fault in depth, *i.e.* under the p1 reflector. It should be noted that all the Plio-Quaternary seismic units over the p3 reflector are thinned on the hanging wall, corresponding with an anticline, and they thicken in the foot wall. These geometries are coherent with reverse faulting and associated folding. However, the lowermost Pliocene unit, bounded by the p3 and M reflectors, is thicker in the hanging wall than in the foot wall. Along the hanging wall, between shot points 2300 and 2550, this unit progressively thickens towards the fault plane showing a growth wedge geometry that is consistent with normal faulting at Early Pliocene times.

Other compressive structures along the Alboran Ridge fault zone are not associated with wedges of Miocene sediments, but they also deform the entire Plio-Quaternary sequence (*e.g.* fault and fold between shot points 2100 and 2000 in figure 6-7). They are interpreted as structures newly generated during the Plio-Quaternary and are sub parallel to other inherited structures (Figure 6-b).

Between 2.5º and 3.1º, the Alboran Ridge fault zone become curve; fold and faults orientations progressively change from NE-SW to WNW-ESE, linking eastward with the structures in the Yusuf fault zone (Figure 6-b). In this area the northern flank of the Alboran Ridge is a south-dipping reverse fault with arcuate trace in plan view and listric geometry in section (Figure 6-10). This structure produces significant vertical displacements of all the recognized key reflectors and comprises remarkable thickness differences between both fault blocks. All the Plio-Quaternary seismic units are thickest in the foot wall block of this reverse contact and they are thin or absent on the Alboran Ridge hanging wall block. It remains unclear whether or not this reverse fault was active before the late Messinian, as it was not possible to correlate none of the intra-Miocene unconformities at both sides of this structure. Additionally, it should be noted that there are several Plio-Quaternary unconformities along the flanks of the ridge. For example, the p1 reflector is a remarkable unconformity between shot points 4750 and 5500 in figure 6-10 and locally erodes most of the previous Pliocene deposits. These observations document important episodes of shortening and uplifting of the Alboran Ridge

at post- Messinian times.

The seismic section of Figure 6-12 shows the western part of the Yusuf fault zone. Here the structure is a narrow deformation zone, ~ 4 km wide, with many sub-vertical fault surfaces that cut the whole Plio-Quaternary sequence. Some of these faults show a small vertical slip component and they form a narrow depression along the fault zone. Here, the set of faults deforming the Plio-Quaternary deposits do not connect directly with those Miocene extensional structures along the Yusuf Escarpment. Nevertheless, they maintain the same WNW-ENE orientation and location at the base of the escarpment (*cf.* Figure 6-a and 6b). Towards the east, the Yusuf fault zone becomes wider and comprises several overlapping fault segments. Figure 6-13 shows that in this sector the main Plio-Quaternary faults are high-angle and have a normal slip component. They display a convergent geometry forming a depressed and elongate area between them: the Yusuf Basin, which contains a folded Plio-Quaternary depocentre. This depocentre shows some thickening of sediments towards the NE similarly to previous Miocene sequences here. The angle between asymmetric flanks of this syncline tends to diminish upward progressively. These observations suggest recent growth faulting along the Yusuf fault zone and progressive and syn-sedimentary folding of the Yusuf Basin. In addition, it should be noted that in the eastern sector of the Yusuf fault zone, Plio-Quaternary faulting occurs along the same fault planes associated with Miocene deformations suggesting that inherited structures were reused here, in contrast to the western sector where new fault planes where generated during the Plio-Quaternary (*cf.* Figure 6-12 and 13).

Most of the sub-basins located to the south of the Alboran Ridge and Yusuf fault zones show few evidences of recent deformations. The Plio-Quaternary cover drapes previous Miocene structures and show thickening of sediments towards the basin centre (*e.g.* Figures 7 and 9 to 11). These geometries are interpreted to be result from filling of residual accommodation space form previous rifting events and latter shortening forming open synclines along the basin axis. Locally, in the southern margin of the SAB, there are some networks of fractures with very small vertical slip components that cut all the Plio-Quaternary seismic units. These structures locate on top of crests of faulted Miocene blocks (*e.g.* between shot points 1500 and 1700 in figure 6-7).

The southern margin of the Pytheas basin also comprises a residual high-angle normal fault affecting to the Plio-Quaternary deposits (shot point 1550 in figure 6-11). In this case none of the Plio-Quaternary seismic units comprise growth wedges associated with the fault and instead they show expansion of sedimentary sequences away from this structure and thinning strata towards the basement high. These observations suggest that this basement high experienced a continuous progressive syn-sedimentary uplift during the Plio-Quaternary, but the normal slip component of the fault at its northern margin was limited.

Active structures

Some of the depicted structures with a long-lived history of deformation during the Plio-Quaternary affect the seabed and control its present day morphology. Figure 6-14 is an example of combined swath bathymetry and multichannel seismic data illustrating the relationship between the internal structure and present-day anatomy of the Alboran Ridge and other surrounding realms.

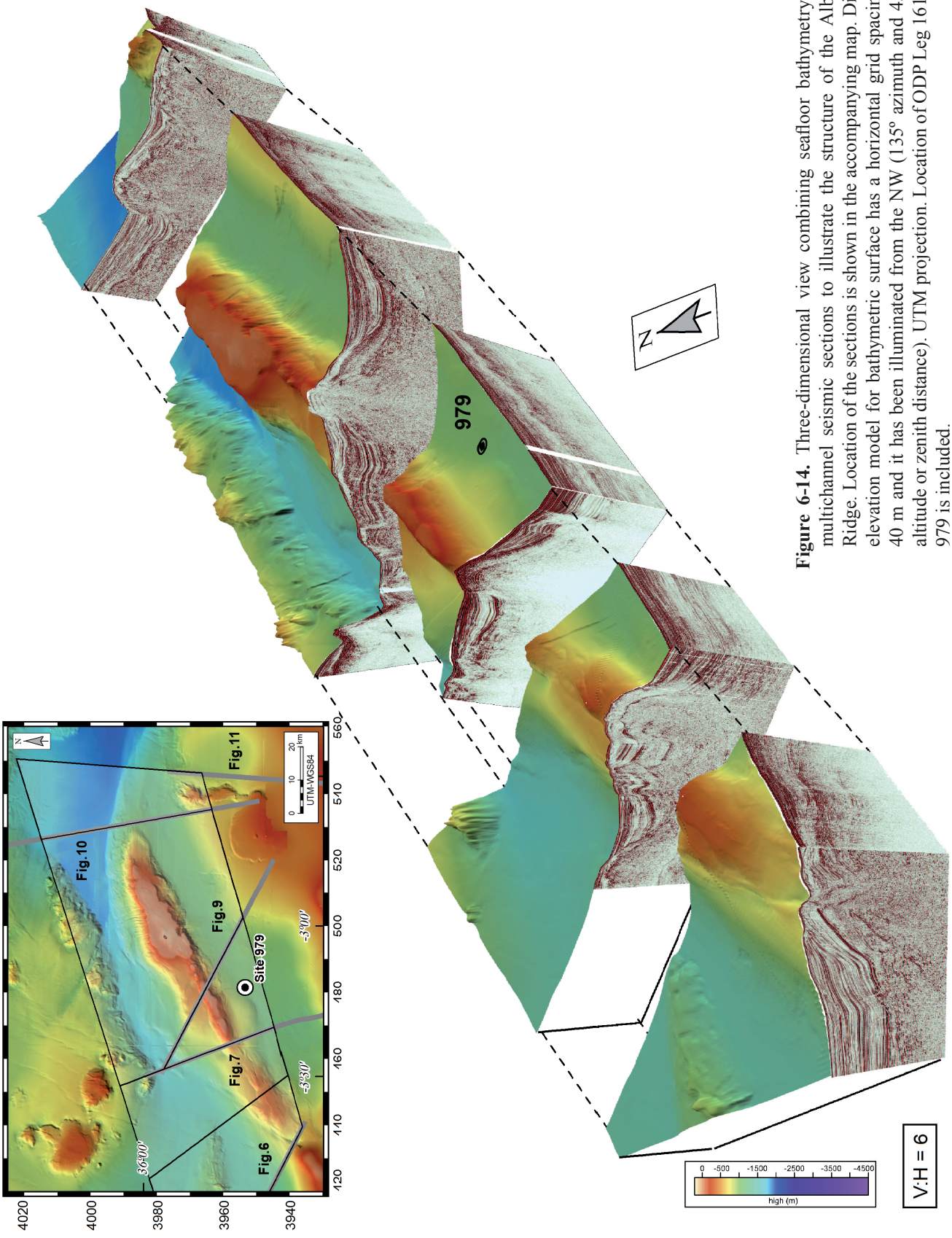

Figure 6-14. Three-dimensional view combining seafloor bathymetry and multichannel seismic sections to illustrate the structure of the Alboran Ridge. Location of the sections is shown in the accompanying map. Digital elevation model for bathymetric surface has a horizontal grid spacing of 40 m and it has been illuminated from the NW (135° azimuth and 45° of altitude or zenith distance). UTM projection. Location of ODP Leg 161 Site 979 is included.

This 3D block shows that the elongated relief of the Alboran Ridge is mainly conditioned by folds and reverse faults with NE-SW trend that in some cases have got associated Miocene depocentres and correspond with inverted structures. The summit of the ridge is cut by a wide abrasion platform around the Alboran Island. This area comprising the highest elevations corresponds with the maximum vertical offset of the south-dipping reverse fault along the northern slope. The SAB located to the south of this compressive structure is uplifted respect to other basin realms to the north (EAB and Alboran Channel) and it results in a more reduced accumulation of Recent sediments and shallower seafloor. This Figure 6-also shows that the Al-Idrisi fault zone is an active structure producing very Recent deformations in the western part of the Alboran Ridge and Alboran Channel. Moreover, the fault zone forming southern edge of the Djibouti High is seen as abrupt escarpment coincident with a seamount lineation of extinct volcanic edifices.

The map in figure 6-15 shows all the active structures in the study area deforming the present-day seafloor together with a compilation of focal mechanisms that enable us to assess the location and kinematics of active structures. Most of the focal mechanisms are concentrated along the Al-Idrisi fault zone and correspond with dominating left-lateral, strike-slip faulting with a reverse component along fault planes with NNE-SSW orientation. Other focal mechanisms indicate active faulting with a main reverse component for faults trending NE-SW to E-W along the core of the ridge (*e.g.* focal mechanism 9, 12, 46 and 44). An isolated focal mechanism in the southeastern margin of the Habibas Basin indicates active reverse faulting along NE-SW trending faults, similarly to the Alboran Ridge. The single focal mechanism available for the Yusuf fault zone indicates active right-lateral transtensive faulting for NW-SE trending structures.

Focal mechanisms in the Djibouti High and the western part of the East Alboran Basin reveals dominating strike-slip faulting along sub-vertical planes for the conjugated fault systems with NNE-SSW and NW-SE orientations. Focal mechanisms 14, 15 and 16 indicate a main left-lateral strike-slip component for NNE-SSW nodal planes, parallel to the Al-Idrisi fault zone. The conjugated NW-SE fault system is right-lateral strike-slip according to focal mechanisms 3, 4, 13, 20 and 40.

6.6 DISCUSSION

Miocene rifting in the Alboran Sea Basin

Previous studies have determined that rifting of the Alboran Domain started during the late Oligocene, at about 27 Ma, according to exhumation histories of metamorphic rocks forming the basement of the basin (*e.g.* Platt *et al.*, 1998; Comas *et al.*, 1999). This process started while the region was elevated above sea level and denuded the thickened continental curst in the inner part of the Alpine collisional orogen. The marine transgression that created the Alboran Sea began at about 23 Ma in the western and northern parts of the basin as evidenced by the occurrence of Aquitanian-Burdigalian marine sediments in the West Alboran Basin (*e.g.* Jurado and Comas, 1992; Chalouan *et al.*, 1997; Sautkin *et al.*, 2003). In this sector, low-angle normal faults produced continuous extension and basin subsidence until the early Tortonian. The directions of extension change from dominating S to SE along the northern part of the WAB to N to NE along its southwestern part (Comas *et al.*, 1992; Chalouan *et al.*, 1997). The same pattern of extension is observed for low-angle normal

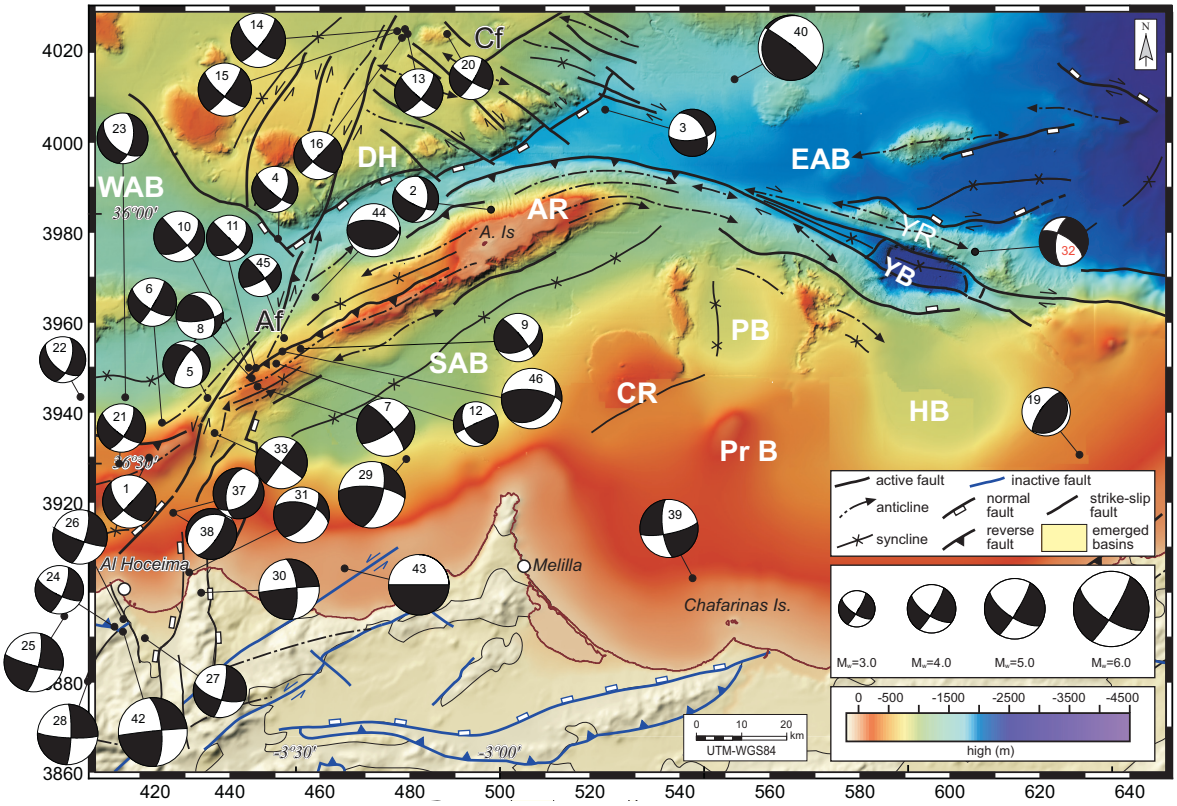

Figure 6-15. Simplified map of the most recent structures in the study area and adjacent onshore basins in Northern Morocco combined with colour shaded-relief and focal mechanism for 47 earthquakes for the period 1959- 2009 (extracted from Hatzfeld, 1978; Vidal, 1986; Medina and Cherkaoui, 1992; Coca and Buforn, 1994; Coca and Buforn, 1994; Buforn *et al.*, 1995; Medina, 1995; Bezzeghoud and Buforn, 1999; Stich *et al.*, 2001, 2003a, 2009; Biggs *et al.*, 2006 and www.ign.es). Focal mechanism projections are equal-area and lower hemisphere; dilatational quadrants in white. Note concentration of earthquakes (M_w >3.5) along the Al-Idrisi fault zone and around Al Hoceima, indicating present-day left-lateral faulting. UTM projection, units in kilometres.

faults recognized onshore. They indicate N to NW and NE extensional trends of Late Burdigalian to Langhian-Serravallian age in the Betics and NE trends in the internal Rif during the Late Burdigalian to Langhian (García-Dueñas *et al.*, 1992; Chalouan *et al.*, 1995). In addition, N-S extension of Late Miocene age has controlled the formation of some onshore basin in northern Morocco (Azdimousa *et al.*, 2007).

Our results show that the Miocene phase of rifting affected also to the central and southeastern sectors of the Alboran Sea Basin forming high-angle normal faults bounding tilted basement blocks and asymmetric basins filled by syn-rift sequences with growth wedge geometries (Figures 3, 7, 9, 10, 11, 12 and 13). In this area the predominating direction of extension was NW-SE and resulted in several elongated NE-SW to ENE-WSW Miocene depocentres. Contrasting NE-SW to N-S trends of extension have been also determined for the easternmost extremity of the WAB, the Yusuf Escarpment and the eastern most part of the EAB close to the Algerian Basin (Figure 6-a). In addition to these contrasting directions of extension, the Miocene structure is characterized by a complex structural pattern formed by a widespread distribution of in relay short fault segments (generally less than 60 km in length) with both synthetic and antithetic configurations. These observations collectively

indicate that the extensional system was immature in this part of the basin and that rifting finished before the formation of any master fault.

NW-SE extension in the study area was oblique to the ~ 200 km of N-S convergence between the Eurasian and African plates during the Miocene and synchronous with the westwards migration by 100-200 km of the entire Alboran Domain (*e.g.* Andrieux *et al.*, 1971; Dewey *et al.*, 1989; Platt and Vissers, 1989; García-Dueñas *et al.*, 1992; Vissers *et al.*, 1995; Rosenbaum *et al.*, 2002). Thus, it is possible that these NE-SW trending high-angle normal faults would have had a significant strike-slip left-lateral component at this time (Figure 6-16). This interpretation agrees with onshore studies in northern Morocco that show a remarkable Miocene strike-slip movement of the NE-SW trending Jebha and Nekor faults due to the oblique collision of the Alboran Domain respect to Africa at this time (*e.g.* Asebriy *et al.*, 1993; Chalouan and Michard, 2004; Azdimousa *et al.*, 2007; Chalouan *et al.* 2008). Moreover, it is probable that the Alboran Channel began to form at this time as a pull-apart basin in a transtensive zone between two NE-SW trending faults with an important left-lateral strike-slip component (Willet, 1997).

A multidirectional extensional system with an overall radial pattern that mimics the curved shape of the orogenic front can be reconstructed comparing the directions of extension deduced for the study area with those previously identified in the western part of the Alboran Sea Basin (*cf.* Figure 6-1 and 16). Additionally, it should be noted that whilst the Miocene sequences in the study area have maximum thickness of 2.5-3 km and oldest deposits are Serravallian, the WAB and the northern margin have at least 6 km of Miocene sediments and comprise the oldest deposits in the basin of Aquitanian-Burdigalian age (*e.g.* Comas *et al.*, 1992; Jurado and Comas, 1992; Chalouan *et al.*, 1997; Willet., 1997). These observations collectively suggest that rifting and associated subsidence initiated before in the western part of the Alboran Sea Basin. The thinner Miocene sequence in the central and eastern parts of the basin may also indicate that there the active extensional realms remained next to the sea level and limited accommodation space was generated at that time.

Moreover, seismic profiles indicate that the end of rifting was also diachronous across the basin. According to Comas *et al.* (1999) the R3 reflector (mid Tortonian age) appears to mark the end of rifting in the WAB and the northern margin. A similar age can be deduced for the inverted half-graben of the Habibas Basin as the top of the syn-rif sequences is also a Tortonian unconformity (R3 reflector; Figure 6-12). Similarly, most of the extensional structures in the westernmost part of the EAB are sealed by the R3 reflector (Figure 6-10). However, towards the east of the EAB some normal faults continued being active during the rest of the Miocene and locally during the Early Pliocene as the unconformities sealing these structures are the M and p1 reflectors of late Messinian and Early Pliocene ages respectively (Figure 6-12). In the southwestern part of the SAB normal faults and tilted blocks of basement are sealed by the M reflector (Figures 7 and 9), but in the northeastern part of this sub-basin a northwest-dipping normal fault continued active during the Pliocene and was finally sealed by the pl-q reflector (Figure 6-10). These observations indicate that the end of rifting in the SAB progress from west to east, similarly to the EAB. For the inverted fault in the southern flank of the Alboran Ridge, the end of extension occurred during the Early Pliocene as the p3 reflector marks the boundary between the syn-rif sequence with growth wedge geometry and the post-rift sequence denoting inversion (Figure 6-8). In the Pytheas Basin the M reflector marks

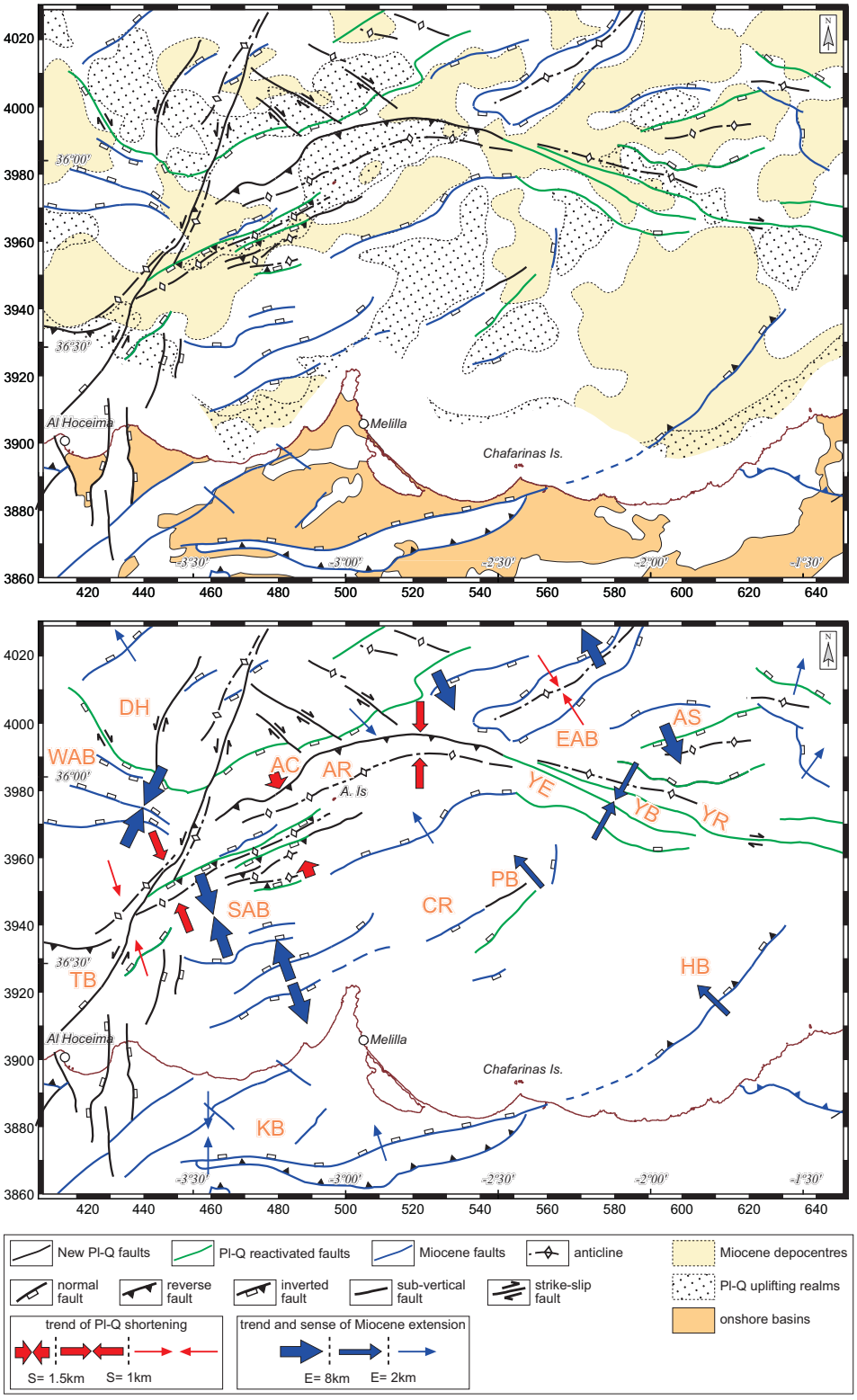

Figure 6-16. Map summarizing the partial inversion in the Alboran Sea Basin. It is compared the distribution of Miocene depocentres with the Plio-Quaternary uplifting realms. Magnitude and trend of the Miocene extension (E) and Late Pliocene to Recent shortening (S) have been estimated for the top of basement and p2 reflector (~3.28 Ma) respectively. Abbreviations: A. Is, Alboran Island; Af, Al-Idrisi fault zone; AC, Alboran Channel; AR, Alboran Ridge; AS, Al-Mansour Seamount; Cf, Carboneras fault zone; CR, Cabo Tres Forcas Ridge; DH, Djibouti High; EAB, East Alboran Basin; HB, Habibas Basin; KB, Kert Basin; PB, Pytheas Basin; Pr B, Provençaux Bank; SAB, South Alboran Basin; TB, Tofiño Bank; YB, Yusuf Basin; YE, Yusuf Escarpment; YR, Yusuf Ridge; and WAB, West Alboran Basin.

the end of extension and only the southernmost fault bounding the Provençaux Bank cut the Plio-Quaternary sediments (Figure 6-11). However, none of the post-Messinian units show any growth wedge geometries indicating that the normal slip component of this fault was limited for the most recent times and probably it was reused as a strike-slip structure.

The observations summarized above collectively suggest a younger extension in the most internal and eastern parts of the Alboran Sea Basin. In spite of the observed radial pattern of extension, timing evidences do not appear to support an extensional collapse model for the origin of the basin, which would produce a synchronous extension throughout the entire region (*e.g.* Dewey, 1988; Platt and Vissers, 1989; Docherty and Banda, 1995; Tandon *et al.*, 1998).

Miocene extension is also evident along the southern margin of the Algerian Basin, eastwards of our study area. There, normal fault systems have a similar NE-SW to ENE-WSW trend, but in this case they had an overall synthetic pattern predominantly dipping towards the basin centre, which is floored by oceanic crust (Galdeano, 1973; Catalano *et al.*, 2000; Cope *et al.*, 2003; Mauffret et al, 2004). These facts indicate a more mature rifting process in this sector compared to the Alboran Sea. Miocene sub-basin along the Algerian margin are formed on top of tilted blocks of basement and are filled by Miocene syn-rift sequences that are mostly sealed by onlapping Messinian deposits (*e.g.*, Rehault *et al.*, 1984; Yelles *et al.*, 2009; Mauffret, 2007). In addition the extensional segments are cut by sub-vertical strike-slip faults with ~N120º trend like the Salah-El-Din and Thenia faults (Figure 6-16). These faults have been interpreted to be transform faults during the opening of the Algerian Basin transferring slip between the different NE-SW extensional systems (*e.g.*, Schettino and Turco, 2006; Mauffret, 2007; Strzerzynski *et al.*, 2010). Similarly, we propose that the high-angle overlapping fault segments with WNW-ESE trend along the Yusuf Escarpment and Ridge constituted a Miocene transfer fault zone transferring extension from the central and southeastern Alboran Sea to the westernmost part of the Algerian margin.

Plio-Quaternary partial basin inversion

Seismic profiles show that although most of the studied extensional structures become inactive throughout the end of the Miocene to earliest Pliocene, some few normal Miocene faults were reactivated after the end of rifting. The renewed NW-SE convergence from the latest Tortonian to

Figure 6-17. Tectonic map of the Western Mediterranean showing the main tectonic features merging our data with other sources (references in the text). Main features of the Algerian are simplified from Morel and Meghraoui *et al.*, 1996; Déverchère *et al.*, 2005; Domzig *et al.*, 2006; Yelles-Chaouche *et al.*, 2006; Mauffret, 2007; Yelles *et al.*, 2009; Strzerzynski *et al.*, 2010. Red dots show location of ODP leg 161 sites (976 to 979), DSDP site 121 and commercial boreholes offshore (G1, Andalucía-G1; A1, Alboran-A1; And-A1, Andalucía-A1; EJ, El-Jebha; H-1, Habibas-1; Ar, Arzew-1 ; Al, Algiers-1). Inset map shows topography and recent structures combined with distribution of crustal seismic events (M_w > 3) for the period 1973-2012 (taken from the USGS catalogue). Digital topography is built on the SRTM (USGS-NASA) global database combined with GEBCO 97 (IOC-IHO) for the offshore region. Abbreviations: AIF, Al-Idrisi fault zone; ARF, Alboran Ridge fault zone; CB, Cheliff Basin; CF, Carboneras fault; DH; Djibouti High; EAB, East Alboran Basin; HB, Habibas Basin; HE, Habibas Escarpment; JF, Jebha fault; KB, Kert Basin; MB, Mitidja Basin; M-HB, Mleta and Habra basins; MF, Maro-Nerja fault; NF, Nekor fault; PF, Palomares fault; SAB, South Alboran Basin; SF, Salah El Din fault; TF, Thenia fault; XB, Xauen Bank; YF, Yusuf fault zone and WAB, West Alboran Basin. ▶

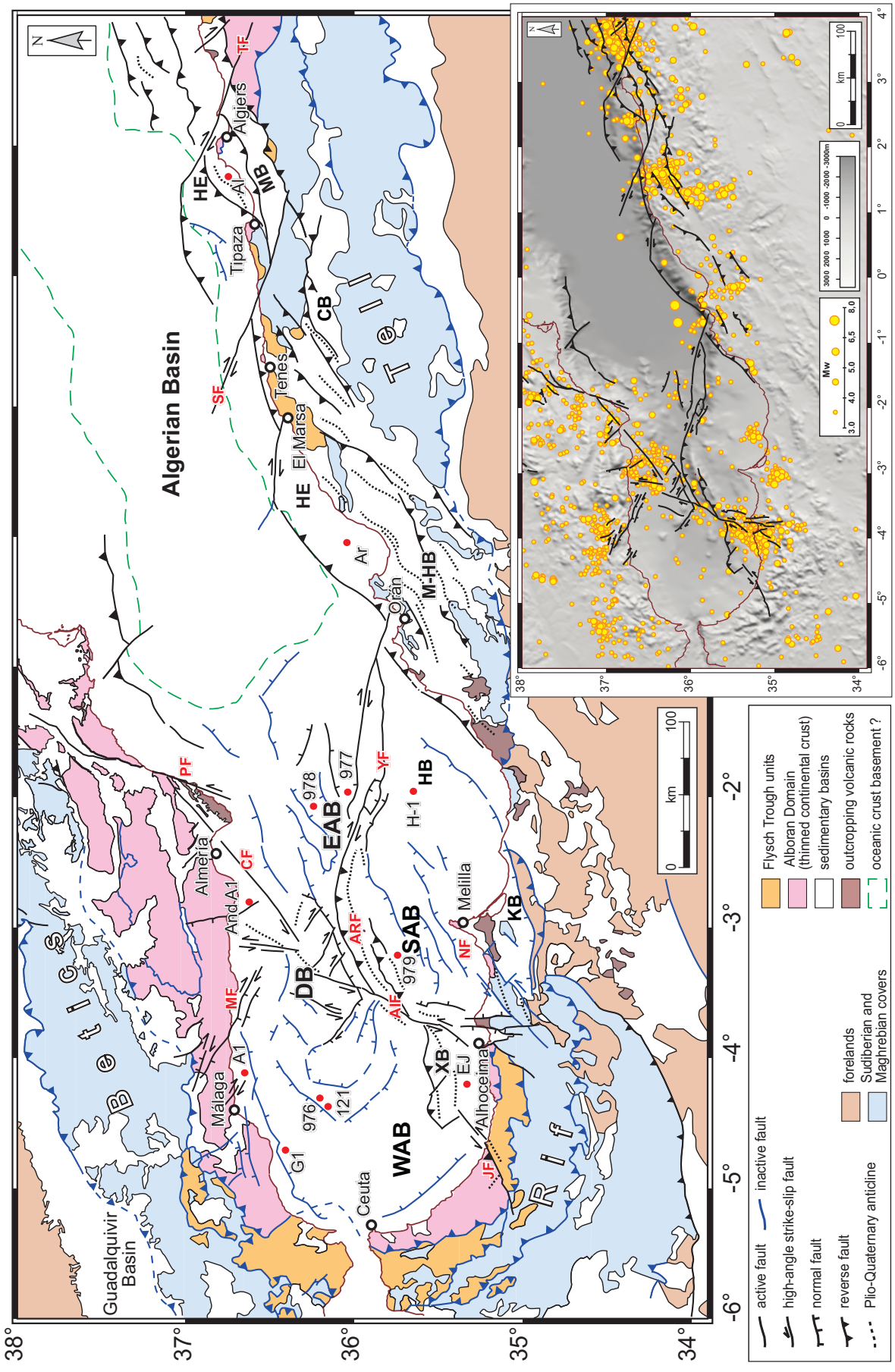
Algerian Basin
Guadalquivir Basin
Betics
Rif
Tell
Algiers
Tipaza
Tenes
El Marsa
Oran
Almeria
Málaga
Melilla
Alhoceima
Ceuta
HE
MB
CB
M-HB
HB
EAB
SAB
DB
WAB
KB
XB
TF
SF
PF
CF
ARF
YF
NF
AIF
JF
ME
A1
And.A1
G1
976
121
978
977
979
H-1
EJ
Mw
3.0 4.0 5.0 6.5 8.0
3000 2000 1000 0 -1000 -2000 -3000m
0 km 100
active fault
inactive fault
high-angle strike-slip fault
normal fault
reverse fault
Plio-Quaternary anticline
forelands
Sudiberian and Maghrebian covers
Flysch Trough units
Alboran Domain (thinned continental crust)
sedimentary basins
outcropping volcanic rocks
oceanic crust basement ?

present-day, which produced about 50 km of shortening throughout the entire Gibraltar Arc System (Dewey *et al.*, 1989; Srivastava *et al.*, 1990; Mazzoli and Helman, 1994; Morel and Meghraoui, 1996), controlled the new kinematics of the reactivated faults.

Our results indicate also that after rifting ceased in the late Miocene to Early Pliocene, the Alboran Sea Basin experienced rather uniform thermal subsidence. Most of the intrabasin highs were formed during the Miocene as they are not covered by sediments of this age, but they experienced general subsidence during the most recent times, which favoured the accumulation of thin Plio-Quaternary sequences on their summits reaching 500 m of thickness over most of them (*cf.* Figures 6a and 6b). However, previous backstripping analysis show that subsidence values differ considerably from some sectors of the Alboran Sea Basin to others indicating local and coeval uplift probably caused tectonic processes (Watts *et al.*, 1993; Docherty and Banda, 1995; Rodríguez-Fernández *et al.*, 1999; Hanne *et al.*, 2003). Plio-Quaternary shortening was synchronous with the residual thermal subsidence and in some realms, as the Alboran Ridge, it resulted in a general reduction in the amount of subsidence during the Late Pliocene and Quaternary (Docherty and Banda, 1995; Estrada *et al.*, 1997; Rodríguez-Fernández *et al.*, 1999; Martínez-García and Soto, 2006).

Our results show different examples of Miocene normal faults reactivated by shortening that put syn-rift marker horizons into contraction. Along inverted structures, these markers may regain its original regional elevation and them they appear like unfaulted horizons. If shortening continues, the syn-rif markers can even be expelled out and the antique downthrown block of the previous normal fault become them the upthrown block of the new inverted fault producing reverse displacement. But in some cases shortening detains during this process and then the upper part of the syn-rift sequence may be in net contraction whilst the lower part remains in net extension. The point of change between net extension to net contraction is known as the null point (*e.g.* Hayward and Graham, 1989; Williams *et al.*, 1989).

In the study area positive inversion structures occur mainly along the Alboran Ridge and the Habibas Basin, where several wedges of Miocene sediments appear folded and uplifted on the hanging wall of reverse Plio-Quaternary faults. Different grades of inversion can be deduced from observations along these structures. Figures 9 and 12 (shot points 6025 to 6300 and 1600 to 2550, respectively) show that in some cases tectonic inversion was partial and shortening do not compensated the bigger amount of Miocene extension. In this case the uplifted hanging wall comprising deformed syn-rif sequences, still remains sunken respect to the foot wall and none of the syn-rift markers have reached their null points. Thus, the location of Plio-Quaternary depocentres roughly coincides with those from previous Miocene ones on the hanging walls. There, sedimentary units synchronous with these partial inversions structures are only thinned next to the fault plane (*e.g.* units up to p1 reflector in figure 6-9 between shot points 6000 to 6150), but they thicken along the rest of the hanging wall where there is residual subsidence and sediment compaction. We interpret that some of subsidence is probably still accommodation space from Miocene rift events.

In the Habibas Basin the contents of the Middle Miocene half-graben structure (below R3 reflector) began to be extruded and become elevated in the still downthrown hanging wall block. It happened at Tortonian to Messinian times as seismic units on top of R3 reflector do not show any

more growth wedges towards the footwall scarp (Figure 6-12). The M reflector seals this inverted structure indicating that it become inactive before the Plio-Quaternary. Shortening detained before to compensate the previous extension and basin inversion concentrated next to the main fault plane for the Tortonian to Messinian sequences. Since the late Messinian the residual accommodation space from Miocene extension, which was not compensated by shortening, was filled by thicker Plio-Quaternary sediments in the basin centre where there has been more subsidence and compaction.

In the southwestern Alboran Ridge tectonic inversion of previous normal faults was complete and the syn-rift horizons are above their null point. For example, in figure 6-8 the lowermost Pliocene unit thickens on the hanging wall indicating active extension at this time, but after shortening compensated the original amount extension at post-p3 times the hanging wall block did not coincide any more with the maximum depocentre. Sedimentary units deposited since them (between p3 reflector and seafloor) thicken on the foot wall coherently with the formation of a reverse blind fault and the associated anticline in the hanging wall.

A complete tectonic inversion is also evident along the westernmost part of the core of the Alboran Ridge. There, the syn-rif sequence, originally deposited along a Miocene half-graben, has been completely expelled and folded (Figure 6-7). In this case, part of the originally subsiding area occupied by a Miocene depocentre has become an uplifting high with none or very thin Plio-Quaternary sequences on its top (*cf.* Figures 6a and 6b). The Xauen Bank offshore Morocco, which constitutes the southwestern prolongation of the Alboran Ridge, comprises also an uplifted and folded Miocene depocentre with thin Pliocene sequences on top (penetrated at El-Jebha well, Figure 6-1) (*e.g.* Chalouan *et al.*, 1997). Following the interpretations by Bourgois *et al.* (1992) we consider that both the Xauen Bank and the southwestern Alboran Ridge resulted from tectonic inversion of the southern part of the WAB that originally connected with the SAB during the Miocene (Figure 6-a). The precise timing of inversion in these realms can be inferred from the Plio-Quaternary seismic architecture. The youngest Early Pliocene unit (between M and p3 reflectors) is approximately tabular indicating that uplifting occurred in this area after its deposition (Figure 6-7). Moreover, successive Late Pliocene to Quaternary unconformities and expansion of sedimentary sequence away from the Alboran Ridge indicate that tectonic inversion and folding in the westernmost Alboran Ridge occurred since Late Pliocene. In addition, the p1 reflector is a prominent Late Pliocene unconformity indicating an important uplift episode (Martínez-García *et al.*, submitted for publication). This event corresponds with a major change of seismic facies in the basin from predominantly transparent layers for the Early Pliocene sediments to mostly high-amplitude for the Late Pliocene and Quaternary units. This change may reflect a change to more coarse grained lithologies as a consequence of the relief generation.

Additionally to the classical structures of positive tectonic inversion, we have found that some of the antique Miocene normal faults in the Alboran Sea are not inverted, but reused as high-angle strike-slip faults. The southern margin of the SAB locally shows an example of this kind of reactivations (shot points 1500 to 1700 in figure 6-7). There, some Plio-Quaternary high angle faults with few vertical displacement are rooted together on depth and locate on top of Miocene tilted blocks suggesting a change from extensional regimen to predominantly strike-slip kinematics. Other examples of these residual structures can be seen in the Pytheas Basin (Figure 6-11). The

most significant is the Plio-Quaternary fault separating this basin from the Provençaux Bank. This structure has tilted blocks associated on depth, below the M reflector, but its vertical slip component is scarce for the Plio-Quaternary sediments suggesting a predominant strike-slip movement at these times.

Previous studies have determined that the WNW-ESE striking Yusuf fault zone has had right-lateral strike-slip kinematics during the Plio-Quaternary and two overlapping fault segments formed the pull-apart Yusuf Basin (*e.g.* Mauffret *et al.*, 1992; Woodside and Maldonado, 1992; Willet, 1997; Alvarez-Marrón, 1999; Fernández-Ibáñez *et al.*, 2007). Our results show that the easternmost part of this fault zone reuses previous Miocene high-angle fault planes with a remarkable normal slip component suggesting a case of reactivation similar to those proposed for the structures in the southern South Alboran and Pytheas basin (Figure 6-13). However, the eastern part of the Plio-Quaternary Yusuf fault zone, which connects with the reverse fault on the northern side of the Alboran Ridge, runs parallel to the previous Miocene extensional faults, but do not reuses the antique fault planes. Instead, new sub-vertical fault planes were generated across the old Miocene depocentre in this sector (*cf.* Figure 6-a and 6b and Figure 6-12).

Seismic profiles along the eastern part of the Alboran Ridge do not show remarkable evidences of reactivation of Miocene faults conversely to its western sector (Figure 6-b). The main structure here is a curved south-dipping thrust whose hanging wall is folded in a wide anticline (Figures 6b and 10). It was not possible to observe any syn-rift growth wedges associated with this fault, which might indicate a previous Miocene extensional regime. Abundant chaotic facies forming the core of this fold correlate with magmatic intrusions, which have been dragged from previous studies. They indicate that this part of the Alboran Ridge was an active volcanic edifice during the Late Miocene about 9.4 Ma and it extinguished during the Plio-Quaternary (*e.g.* Fernández Soler *et al.*, 2000; Duggen *et al.*, 2004, 2008). We discard a simple inversion of previous normal faults in this sector of the Alboran Ridge. Instead we propose that the recent contractional deformations focussed along the northern slope of the Miocene volcanic edifice resulting into the birth of a new curved fault of opposite vergence to those remaining on the hanging wall (Figure 6-10). This interpretation agrees with that proposed for the Pliocene to Recent tectonic inversion of the Algerian margin by Yelles *et al.* (2009) and Strzerzynski *et al.* (2010).

Seismic profiles indicate that tectonic inversion and fault reactivation of the Alboran Sea Basin was partial and only affected to few fault segments from the extensive set of pre-existing faults (Figure 6-6). The reactivated structures mainly concentrate along the Alboran Ridge and Yusuf fault zones, which include also some new fault segments and folds and accommodated most of the Plio-Quaternary shortening. Trusting, folding and strike-slip faulting promoted uplift of reliefs along Alboran Ridge and the Yusuf Escarpment and also triggered a southward tilting of the basin axis basins located in the hanging wall block (SAB, Pytheas and Habibas basins) (*cf.* Figure 6-6a and 6-6b). Thus, the southernmost Miocene depocentres become perched basins during the Plio-Quaternary (*e.g.* Figure 6-10). A similar evolution has been proposed for some sub-parallel NE-SW elongated basins in northern Algeria due to tectonic inversion of this margin (Figure 6-17) (Morel and Meghraoui *et al.*, 1996; Déverchère *et al.*, 2005; Mauffret, 2007; Strzerzynski *et al.*, 2010).

Our results show that basin inversion of the Alboran Sea Basin was highly selective. The

existence of previous Miocene normal faults with NE-SW trend was an important controlling factor. These segments are perpendicularly oriented respect to the renewed NW-SE convergence (*e.g.* Dewey, 1988; Mazzoli and Helman, 1994; Rosenbaum *et al.*, 2002) and so they have a favourable orientation to be inverted as reverse faults. However, it was not the unique cause of inversion as only few of these NE-SW fault segments were reactivated. Moreover, in the Yusuf fault zone the reactivated structures have WNW-ESE trend and they are oblique to sub-parallel to the Plio-Quaternary convergence vector. Thus, we consider that the presence of Miocene volcanic intrusions forming rheological anisotropies in the continental crust was an additional controlling factor for such inversion and reactivation of structures.

Active deformations and along the present-day Africa-Eurasia plate boundary in the western Mediterranean

The data set and interpretations we present can be integrated with previous geophysical, seismological and geodetic results to precise the distribution and transference of deformation in the western Mediterranean. Quaternary structures and seismicity in this area spread over a wide band of deformation with roughly E-W trend, which comprises the Gibraltar Arc and the Tell Mountains and the north Algerian margin (Figure 6-17). Geodetic models indicate that the present-day convergence vectors are NE-SW trending with a moderate rate of about 4.5 mm/y resulting in a zone of transpresional crustal deformation (DeMets *et al.*, 1994; Fernandes *et al.*, 2003; Nocquet and Calais, 2004). Additionally, recent local GPS observations in the Rif and the western Betics suggest a lateral escape of the western part of the Gibraltar Arc towards the southwest with a rate of ~2-3 mm/y (Fadil *et al.*, 2006; Pérouse *et al.*, 2010; Vernant *et al.*, 2010; Kolulali *et al.*, 2011).

Most previous studies have reported a probable present-day left-lateral movement along the Alboran Ridge fault zone (*e.g.* Bourgois *et al.*, 1992; Campos *et al.*, 1992; Comas *et al.*, 1992, 1999; Maldonado *et al.*, 1992; Mauffret *et al.*, 1992; Woodside and Maldonado, 1992; Watts *et al.*, 1993; Chalouan *et al.*, 1997; Estrada *et al.*, 1997; Willet, 1997; Ammar *et al.*, 2007). However, detailed structural mapping together with a new compilation of available focal mechanism show that most of the left-lateral strike-slip faulting occurs along the NNE-SSW Al-Idrisi fault zone, which cuts obliquely the Alboran Ridge (Figure 6-15). In contrast, some focal mechanisms with NE-SW nodal fault planes along the ridge indicate a predominant reverse component for the Alboran Ridge fault zone. The perpendicular orientation of this relief respect to the NW-SE present-day convergence vectors and the dominance of reverse faults and folds along it reinforce this interpretation (Figures 7 to 10 and 14).

On the other hand, the role of the Al-Idrisi fault zone in the present-day distribution of deformation deserves also to be discussed. It should be noted that both tip lines of this fault correspond with two remarkable seismic swarms; one next to Al Hoceima and other one offshore to the southwest of Almería (Figure 6-17) (Stich *et al.*, 2001, 2003b; Biggs *et al.*, 2006; Martínez-García *et al.*, 2011). This fact suggests active propagation of this fault, both northwards and southwards. In addition, the Al-Idrisi fault zone may transfer slip motion from the Alboran Ridge to the Rif. This interpretation agrees with the existence of active reverse faults along the southern edge of the Rif (Zizi, 2002; Moratti *et al.*, 2003; Chalouan *et al.*, 2006).Moreover, we consider that the Al-Idrisi fault zone is to a large

degree responsible for the lateral escape of the frontal part of the Gibraltar Arc depicted by previous studies (*e.g.* Negredo *et al.*, 2002; Chalouan *et al.*, 2006; Fadil *et al.*, 2006; Fernández-Ibáñez *et al.*, 2007). The left-lateral strike-slip motion of this structure may contribute to the clockwise rotation of the GPS velocity field in the western Betics and Rif recently reported by Koulali *et al.* (2011).

Figure 6-17 shows that the active tectonic framework in the eastern part of the Alboran Sea Basin resembles to that in the Algerian margin (Morel and Meghraoui *et al.*, 1996; Déverchère *et al.*, 2005; Domzig *et al.*, 2006; Yelles-Chaouche *et al.*, 2006; Mauffret, 2007; Yelles *et al.*, 2009; Strzerzynski *et al.*, 2010). Along the entire Algerian margin shortening is accommodated by a set of NE-SW trending reverse faults and associated folds, similarly to the structures along the Alboran Ridge and Xauen Bank. In addition, other system of NW-SE to WNW-ESE right-lateral strike-slip faults, comprising the Yusuf fault zone, transfers slip between the different reverse segments about 125-180 km in length. This tectonic framework resulted from inversion of the previous Miocene rifting structure, which comprised a number of NE-SW extensional segments dissected by NW-SE to WNW-ESE transform faults according to seismic and magnetic data (*e.g.* Durand-Delga, 1980; Rehault *et al.*, 1984; Sanz de Galdeano, 1990). Thus, we consider that the present-day partitioning of the deformation in the eastern Alboran Sea and Algerian margin and the slip transference between different active segments are both strongly conditioned by the existence of previous zones of weakness generated during the phase of basin opening.

Different works have proposed an incipient subduction of the oceanic crust flooring the Algerian Basin below the continental northern Algerian margin (*e.g.* Auzende *et al.*, 1972; Déverchère *et al.*, 2005). Southward dipping reverse faulting and folding predominantly located at the foot of the continental slope, dominance of reverse focal mechanisms and uplift of the continental costal areas support this interpretation (*e.g.* Meghraoui *et al.*, 2004; Strzerzynski *et al.*, 2010). Our results show that his incipient subduction in northern Algeria connects westwards with compressive deformations along the Alboran Ridge by means of the transfer strike-slip Yusuf fault zone. Thus, at present-day there is an offshore transition between young ocean-continent collision to continent-continent collision (*e.g.* Meghraoui *et al.*, 1996; Negredo *et al.*, 2002). The wider distribution of deformations in the Alboran Sea Basin reaching some sectors of the Betics and Rif (Figure 6-17) can be explained considering the different decoupling/coupling in collisional settings (*e.g.*, Handy *et al.*, 2005; Willingshofer and Sokoutis, 2009). A strong decoupling can be expected in the ocean-continent collision along the Algerian margin as most shortening is taken up by trusting along the decoupled boundary at the foot of the continental slope. However, in the Alboran Sea collision occurs within a thinned continental crust. In this case the buoyancy of continental lithosphere obstructs the subduction of one block below other and deformation is widely distributed affecting to both blocks in collision (Willingshofer and Sokoutis, 2009).

6.7 conclusions

1) High-angle normal faults, tilted blocks of basement and asymmetric basins filled by syn-rift Miocene sequences with growth wedge geometries document Miocene extension with a predominant NE-SW trend in the central and southeastern parts of the Alboran Sea Basin. The widespread distribution of in relay short fault segments and the existence of other contrasting

secondary NE-SW to N-S trends of extension indicate an immature rifting process in these sectors.

2) The entire Alboran Sea Basin shows an overall multidirectional extensional system with radial pattern. Miocene depocentres in the central and southeastern parts of the basin are thinner (maximum thickness 2.5-3 km) and probably younger than those in the western and northern parts. It suggests that rifting progressed from west to east. The end of extension was also diachronous. It finished at mid Tortonian times in the WAB, the westernmost EAB and the sub-basins located along the southern margins. However, normal faults along the SAB and the easternmost EAB continued active until the late Messinian and locally until the Early Pliocene.

3) Plio-Quaternary NW-SE shortening coexisted with thermal subsidence and reactivated some old Miocene faults. We document different grades of positive tectonic inversion forming NE-SW reverse faults and folds. In most cases tectonic inversion was partial and shortening was not able to compensate the bigger amount of previous extension. Additionally, some Plio-Quaternary strike-slip faults, as the Yusuf fault zone, also reactivated partially some segments of previous Miocene normal faults.

4) The most significant positive tectonic inversion occurred along the western Alboran Ridge since the Late Pliocene. In the western part of the ridge, the existence of Miocene magmatic intrusions determined the formation of new Plio-Quaternary north-directed reverse faults and folds. Shortening caused uplift of the Alboran Ridge itself and of the previous Miocene basins located in the hanging wall, which were tilted towards the south and become Plio-Quaternary perched basins.

5) The eastern part of the Alboran Sea Basin and the Algerian margin comprise a wide band of Plio-Quaternary deformation formed by different NE-SW reverse segments separated by NW-SE to WNW-ESE right lateral strike-slip transfer faults. This template is controlled by an inherited Miocene rifting geometry which determined previous basin openings. Present-day shortening is partitioned between the different long-lived zones of weakness which are perpendicularly oriented to the NW-SE trend of convergence between the African and Eurasian plates. The Miocene transform faults, which are sub-parallel to oblique respect to the convergence trend, has been also reactivated as strike-slip faults transferring slip between the different reverse segments.

6) Present day continent-continent collision occurs along the Alboran Sea connecting with the ocean-continent collision along the Algerian margin. The stronger coupling between continental crusts expected for the Alboran Sea determine a more distributed deformation which affects to both blocks in collision and extends northwards and southwards across the Betics and Rif.

7. Conclusions

This chapter summarizes the main results of this thesis and it discusses briefly how they contribute to the knowledge of the stratigraphic and tectonic evolution of the Alboran Sea Basin. The studied active processes, which affect the seafloor, should be considered in any further detailed study of geological risk in the region. It is also presented the influence of previous geological processes, which are inactive at present-day, conditioning the actual location and geometry of active sedimentary and tectonic structures.

It has been conducted a detailed geomorphological and structural study based on high-resolution geophysical techniques, like swath bathymetry and TOPAS profiles, in the central sector of the Alboran Sea, around the Alboran Ridge and Yusuf regions (**Chapter 3**) (Figures 3-6 and 3-15). Recent faults and folds deform the seafloor and the most recent Quaternary sediments, control the canyon and channel network and form seafloor escarpments causing seafloor instabilities that explain most of the discovered submarine slides. Mapped faults and folds are demonstrated to be active structures considering the hypocenter distribution, magnitude and focal mechanisms of shallow crustal seismicity (< 11 km) (Figure 3-15). The location and kinematics of active structures in the study area was compared with other surrounding faults, resulting a map of active structures for the entire Alboran Sea Basin (Figure 3-16).

These results confirm that the Alboran Ridge and Yusuf fault zones, previously identified as Plio-Quaternary structures, are active at present-day. Moreover, this study reveals that these two fault zones are connected forming a wide and continuous band of deformation with scattered, associated seismicity. The orientation of these fault zones varies from west to east, changing progressively from SW-NE to WNW-ESE trend. In the Alboran Ridge, reverse faults and folds with SW-NE trend are the predominant structures. They are oriented perpendicular to the NW-SE plate convergence vector inferred by geodetic models and accommodate most of shortening. Structural mapping and focal mechanisms indicate a predominant reverse component for the Alboran Ridge fault zone. The fault

and fold systems along the Alboran Ridge change progressively from SW-NE to E-W, to connect finally with the Yusuf fault zone, which has WNW-ESE orientation. There, structures are oblique or sub-parallel to the actual plate convergence vector resulting in important strike-slip faulting with a right-lateral component. Transtensional displacements occur between overlapping fault segments.

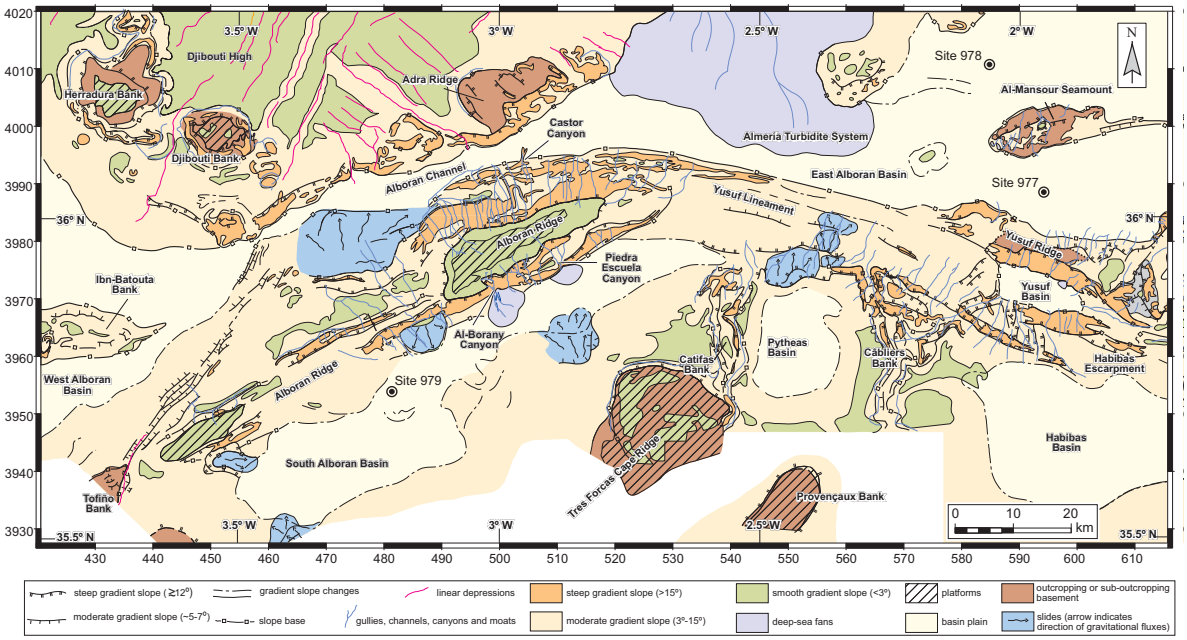

Figure 3-6. Geomorphological map of the central Alboran Sea. Details in chapter 3.

Additionally, data demonstrate the existence of a previously unknown narrow, NNE-SSW zone with folding and reverse faulting, which cuts obliquely the western Alboran Ridge .This structure, named Al-Idrisi fault zone, concentrates most of the upper crustal seismicity in the Alboran Sea region (Figure 3-15). Fault kinematics deduced from focal mechanisms corresponds to left-lateral, strike-slip to reverse faulting. The Al-Idrisi fault zone connects southwards with a seismic swarm located around Al Hoceima, in the Moroccan shoreline, which comprises large earthquakes (M_w>6). Moreover, other seismic swarm occurs next to the northern termination of the Al-Idrisi fault zone corresponding with the Adra seismic series (Figure 3-16). The occurrence of these two seismic swarms at both ends of the fault may indicate active fault propagation along both, the northern and southern tip lines.

The Al-Idrisi fault zone is certainly younger than folds and faults along the Alboran Ridge and Yusuf Escarpment, and it may represent an important contribution to seismic hazard in the Alboran Sea area. The documented strike-slip movement of this fault conducts to the lateral escape of the frontal part of the Gibraltar Arc towards the southwest. The Al-Idrisi fault corresponds with the eastern boundary of this block, which comprises the southwestern Betics, the western Alboran Sea and the Rif. The internal clockwise rotation of this block, recognized by recent GPS measurements, may be promoted by the left-lateral kinematics of the Al-Idrisi fault.

The northern part of the Al-Idrisi fault zone deforms the Djibouti High, where other active

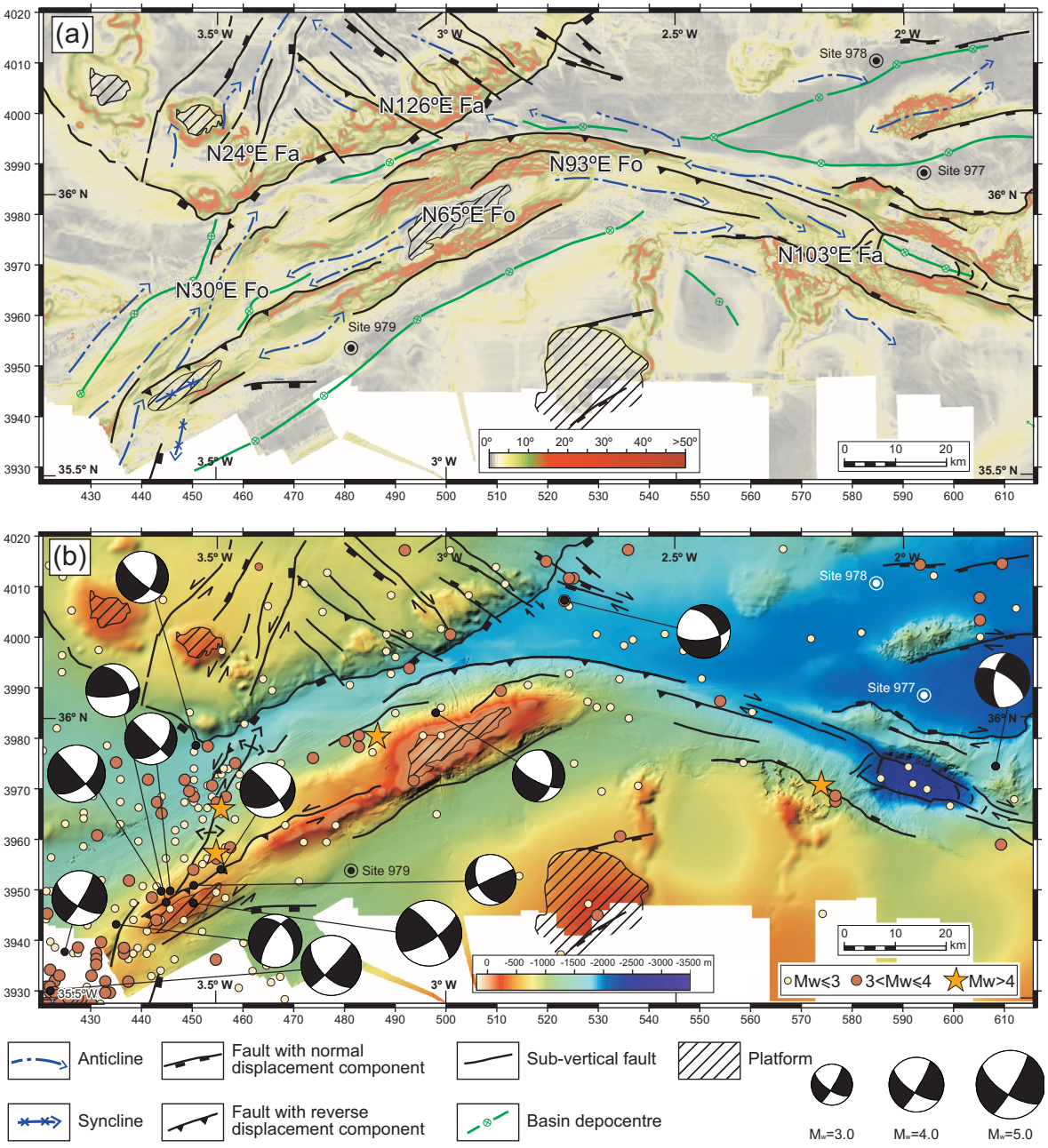

Figure 3-15. (a) Simplified structural map of the most recent structures in the central Alboran Sea **(b)** Simplified uppermost crustal structure of the central Alboran Sea. Details in chapter 3.

structures have been also founded. Some of these faults are NNE-SSW trending and has a left-lateral, strike-slip movement, similarly to the Al-Idrisi fault. There are other faults trending NW-SE with a dominant right-lateral, strike-slip component. They correspond to two conjugate strike-slip fault systems that locate at the southwestern termination of the Carboneras fault (Figures 3-15 and 3-16).

A dense grid of single and multichannel seismic profiles, correlated to nearby DSDP and ODP sites and commercial wells, have been used to constrain the evolution of the Alboran Sea Basin. Detailed bio-stratigraphic and log information for the Late Miocene to Quaternary sediments has allowed a precise study for the last ~5.33 Ma (**Chapter 4**) (Figures 4-8 and 4-13). Reconstructions

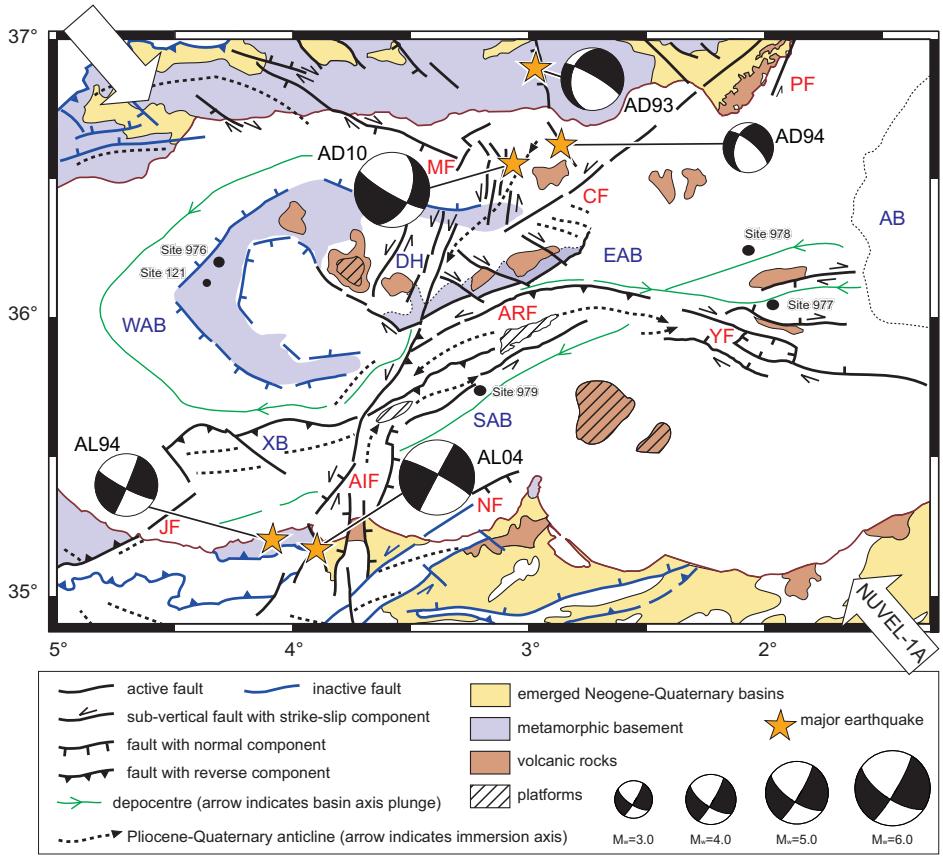

Figure 3-16. Structural map of the Alboran Sea Basin and surrounding areas showing Recent structures and main sedimentary depocentres (simplified). Major earthquakes: AD10 Adra 1910/6/16, AD93 Adra 1993/12/23, AD94 Adra 1994/1/4, AL94 Al Hoceima 1994/5/26, AL04 Al Hoceima 2004/2 /24. Abbreviations: AB, Algerian Basin; AIF, Al Idrisi fault zone; ARF, Alboran Ridge fault zone; CF, Carboneras Fault; DP, Djibouti High; EAB, East Alboran Basin; JF, Jebha Fault; MF, Maro-Nerja Fault; NF, Nekor Fault; PF, Palomares Fault; SAB, South Alboran Basin; WAB, West Alboran Basin; XB, Xauen Bank; YF, Yusuf fault zone. Other details in chapter 3.

of basin structures and sediment accumulation rates document how the paleogeography has evolved since the Messinian and indicate that this region experienced complex interactions between plate convergence, inherited structures, sediment supply from the surrounding Betic and Rif mountains, deformation and subsidence (Figure 4-14).

Fault and fold systems along the Alboran Ridge were already connected with the structures along the Yusuf region during the Plio-Quaternary and they moved at different times, causing shortening, uplift and transpression or transtension depending on the angle between these structures and the prevailing convergence trend at each time. Main deformation pulses occurred during the Early Pliocene (~5.33 to 622 4.57 Ma), the Late Pliocene (~3.28 to 2.45 Ma) and within the early Pleistocene (~1.81 to 1.19 Ma) (**Chapter 4**). Detailed structural mapping show that the Alboran Ridge and Carboneras fault zones were not connected during the Plio-Quaternary and therefore do not form a single fault structure crosscutting the Alboran Sea Basin from the Betics to the Rif (Figure 4-14).

The link between the Alboran Ridge and Yusuf fault zones is accommodated by an arcuate south-

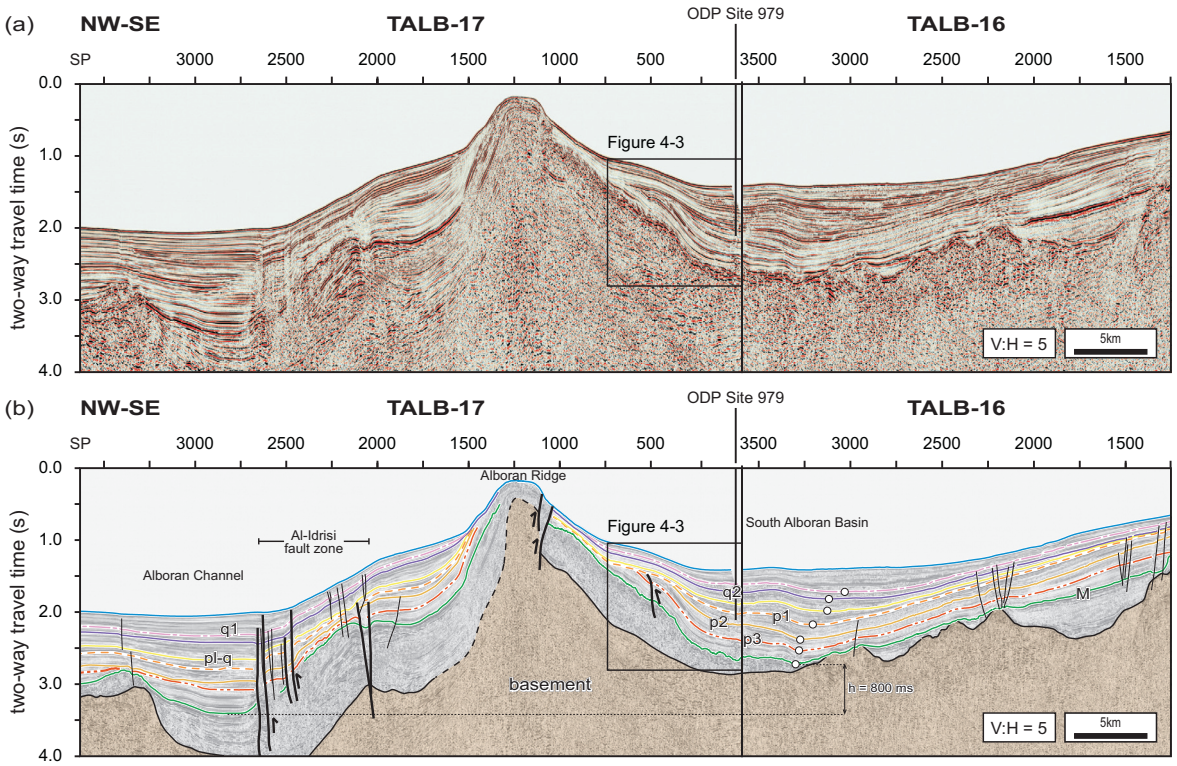

Figure 4-8. (a) Uninterpreted and **(b)** interpreted multichannel seismic section across the central Alboran Ridge, Al-Idrisi fault zone, Alboran Channel and South Alboran Basin (SAB). Details in chapter 4.

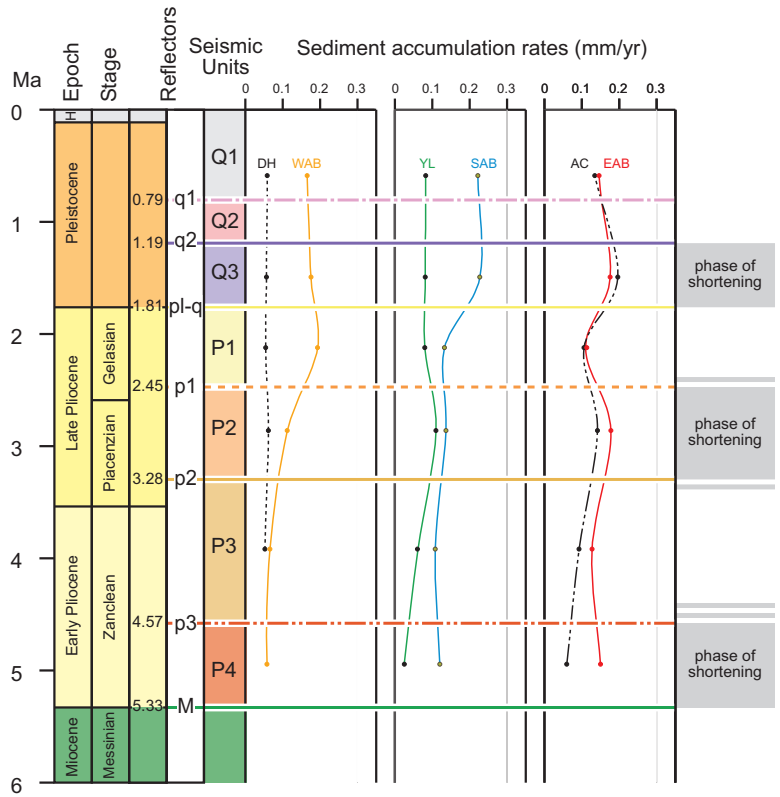

Figure 4-13. Correlation between seismic stratigraphy and changes in average sediment accumulation rates (mm/yr) during the Plio-Quaternary for the main sedimentary depocentres in the studied area: the Alboran Channel (AC), the Djibouti High (DH), the East Alboran Basin (EAB), the South Alboran Basin (SAB), the Yusuf Lineament (YL) and the West Alboran Basin (WAB). Details in chapter 4.

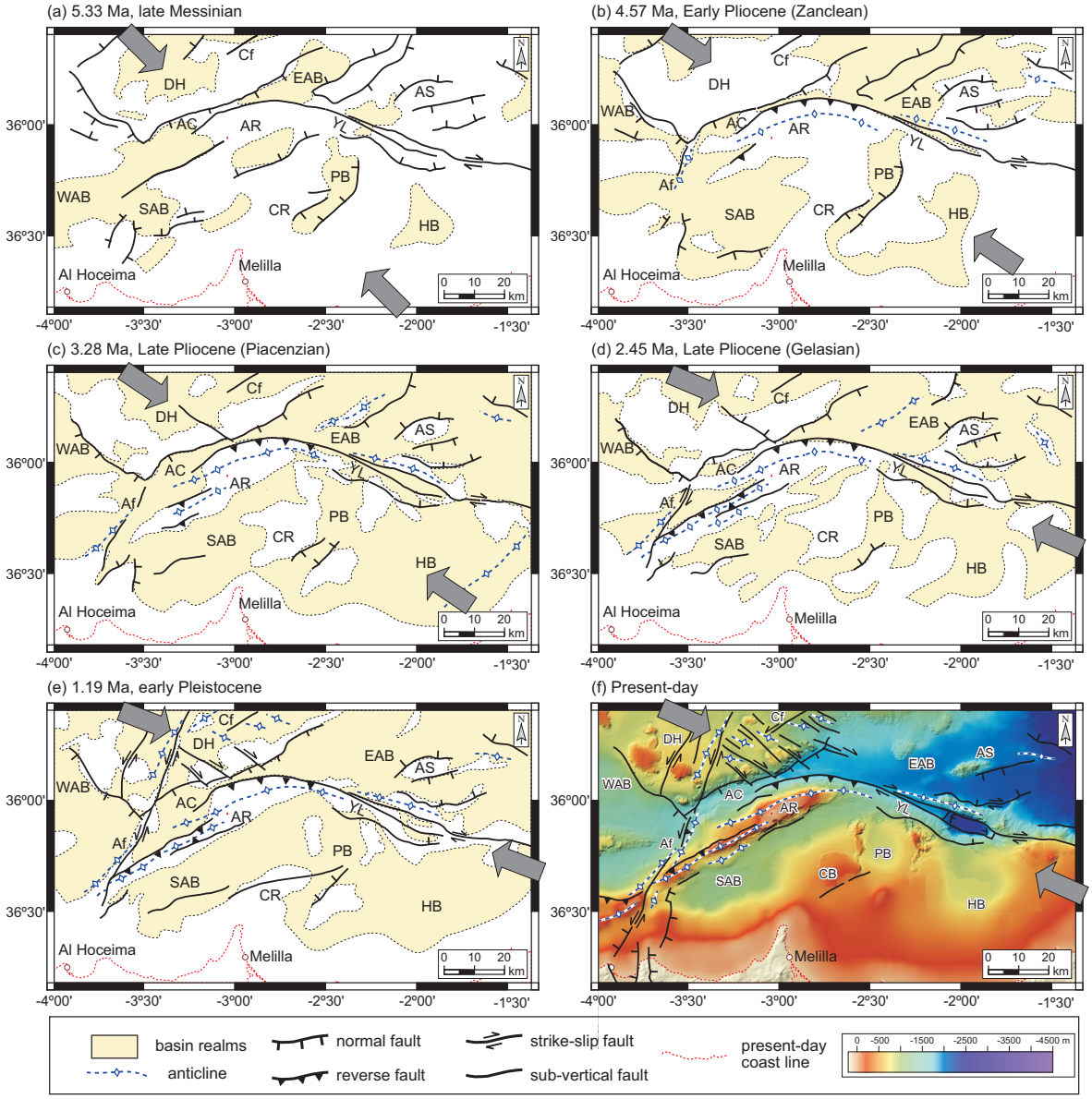

Figure 4-14. Summary maps showing the basin extents and active structures since late Messinian. Abbreviations: AC, Alboran Channel; Af, Al-Idrisi fault zone; AR, Alboran Ridge; AS, Al-Mansour Seamount; Cf, Carboneras fault zone; CR, Cabo Tres Forcas Ridge; DH, Djibouti High; EAB, East Alboran Basin; HB, Habi-bas Basin; PB, Pytheas Basin; SAB, South Alboran Basin; YL, Yusuf Lineament; and WAB, West Alboran Basin. Details in chapter 4.

dipping reverse fault, which has led to the thrusting of the Alboran Ridge over the southern margin of the East Alboran Basin. Localized deformations along the Alboran Ridge and Yusuf Escapement triggered progressive southwards migration and tilting of depocentres in the southern basins located on the hanging wall of the reverse fault. Thus, the SAB, Pytheas and Habibas basins become Plio-Quaternary, perched basins and experienced a significant reduction in the sediment accumulation rates (Figure 4-13 and 4-14).

The main uplift of the Alboran Ridge occurred during the Late Pliocene, at the same time as the plate convergence between the African and Eurasian plates changed from NW-SE to WNW-ESE (Figure 4-14d). Along the western part of the Alboran Ridge previous extensional structures with

NE-SW trend were reactivated and inverted, similarly to the Xauen Bank. The uplift of these reliefs resulted in the disconnection between the WAB and the SAB, which had been connected during the Miocene. Moreover, in the eastern Alboran Ridge the existence of Miocene magmatic intrusions determined the formation of new north-directed reverse faults and folds, which were active since at least the Early Pliocene. The main phase of shortening and uplift during the Late Pliocene (Figure 4-13) coincided with the first important contribution of the Almeria turbidite system into the Alboran Sea Basin. Seafloor uplift favoured erosion and accumulation of more coarse grained lithologies during the Late Pliocene and Quaternary and also encouraged abundant gravity-instability processes (**Chapter 5**).

Mass Transport Deposits (MTD) has been mainly found along the slopes of the Alboran Ridge and the Yusuf Escarpment and their ages range from Late Pliocene to present. The superposition of slides, draped by thins layers of stratified sediments, and their location in fault escarpments suggest that they were probably triggered by earthquakes during tectonic pulses of active faults. These processes occurred at least since the Late Pliocene and alternated with periods of relative tectonic quiescence dominated by hemipelagic sedimentation.

The Djibouti High was not affected by significant deformation during the Pliocene and it remained as a residual high from Miocene rift events. However, during the early Pleistocene, coinciding with the most recent phase of shortening, the NNE-SSW trending strike-slip Al-Idrisi fault zone propagated northwards deforming the Djibouti High (Figure 4-14e). Simultaneously the two conjugated high-angle strike-slip fault systems (NNE-SSW and NW-SE) were formed there.

A complicated tectonic template was inherited from previous Miocene rifting events and it conditioned strongly the further Plio-Quaternary evolution (**Chapter 6**). High-angle faults, tilted blocks of basement and asymmetric basins filled by syn-rift, Miocene deposits document a predominant NW-SE extension in the study area during the Middle to Late Miocene. It is possible that these SW-NE trending structures had a significant left-lateral, strike-slip component, as they were oblique to the prevailing N-S convergence at this time. In this sector of the Alboran Sea Basin, the rifting produced a limited amount of extension as is evidenced by the following observations: (1) existence of several contrasting secondary extensional faults with NW-SE to E-W orientation, in addition to the main SW-NE extensional structures (Figure 6-17); (2) scattered distribution of in-relay, short fault segments with both synthetic and antithetic configurations; and (3) Miocene depocentres are smaller than those in the western and northern parts of the basin and achieve a maximum thickness of 2.5-3 km.

The entire Alboran Sea Basin shows an overall multidirectional extensional system with radial pattern that mimics the curved shape of the entire orogen. Both, the onset and end of rifting were diachronous. Rifting began in the early Miocene in the west and north of the basin. However, syn-rift sequences in the eastern and southern basins (*e.g.* EAB, SAB) are dominated by Late Miocene to Early Pliocene sediments indicating that accommodation space from rifting was generated here later. It is also possible that part of the extension occurred while the central and southeastern sectors of the basin were next to the sea level or even elevated above it. Rifting finished in the WAB during the Tortonian, similarly to the Habibas Basin and the westernmost part of the EAB. However, normal faults along the SAB and the easternmost EAB continued active until the late Messinian and locally,

until the Early Pliocene. Therefore, extension was younger in the most internal and eastern parts of the Alboran Sea Basin.

At the end of the Miocene, during the Messinian salinity crisis, the region experienced deep desiccation as consequence of the closure of marine passages between the Atlantic Ocean and the Mediterranean Sea. However, a number of residual shallow marine or lacustrine basins existed in the Alboran Sea region at this time and they were comparable to other marginal basins in the onshore Betics (**Chapter 4**). During the late Messinian, there were still connection between the SAB and the Alboran Channel at the western end of the Alboran Ridge (Figure 4-14a).

After rifting ceased during the Late Miocene to Early Pliocene, the Alboran Sea Basin experienced uniform thermal subsidence, which resulted in the accumulation of a rather tabular thin layer of Plio-Quaternary sediments (< 500 m of thickness) on top of most of the inherited Miocene intrabasin highs. However, this residual thermal subsidence coexisted with shortening and some of these residual highs were reactivated and uplifted during the Plio-Quaternary. In such cases the Plio-Quaternary sequences on top of highs are folded and show onlapping of growth strata onto the crest of folds and thickening of sedimentary sequences away from these structures (Figures 4-8 and 4-14).

Reactivation and shortening of some of the old extensional-related Miocene structures document a partial tectonic inversion process in the Alboran Sea Basin (**Chapter 6**). Seismic profiles and structural maps illustrate that several NE-SW reverse faults and associated folds have experienced variable magnitude and timing of inversion (**Chapter 6**; Figure 6-16). These structures occur mainly along the Alboran Ridge and Habibas Basin. In most cases, tectonic inversion was partial and shortening was not able to compensate the larger amount of previous Miocene extension. Maximum extension up to 8 km has been recorded in the SAB, EAB and the easternmost WAB and it was mainly caused by Miocene rifting events. In contrast, the calculated Recent shortening is considerably smaller reaching maximum values about 2 km since the Late Pliocene and being mainly accommodated in the Alboran Ridge region. This fact explains that the location of Plio-Quaternary depocentres roughly coincides with those realms which experienced remarkable Miocene extension, where there is still residual accommodation space favouring recent subsidence and compaction.

In addition to the structures of positive tectonic inversion, the Alboran Sea Basin comprises some other examples of partial reactivation of Miocene normal faults as strike-slip structures during the Plio-Quaternary. The WNW-ESE, Yusuf fault zone is the clearest example of this type of structures. Reactivation has occurred mainly along the eastern sector of the Yusuf fault zone, where the Plio-Quaternary right-lateral strike-slip fault planes with small vertical-slip component are rooted on high-angle conjugate-convergent normal faults, which bound a thick Miocene depocentre. However, strike-slip faults along the western part of this fault zone, *i.e.*, along the Yusuf Escarpment, are not linked with previous extensional structures indicating that strike-slip reactivation of Miocene faults was also partial.

Plio-Quaternary tectonic inversion and fault reactivation in the Alboran Sea Basin only affected some of the structures or individual fault segments that form the Miocene extensional-system (Figure 6-17). At least two main factors controlled this selective reactivation: (1) the orientation of previous structures respect to the renewed NW-SE convergence vector between the Eurasian and

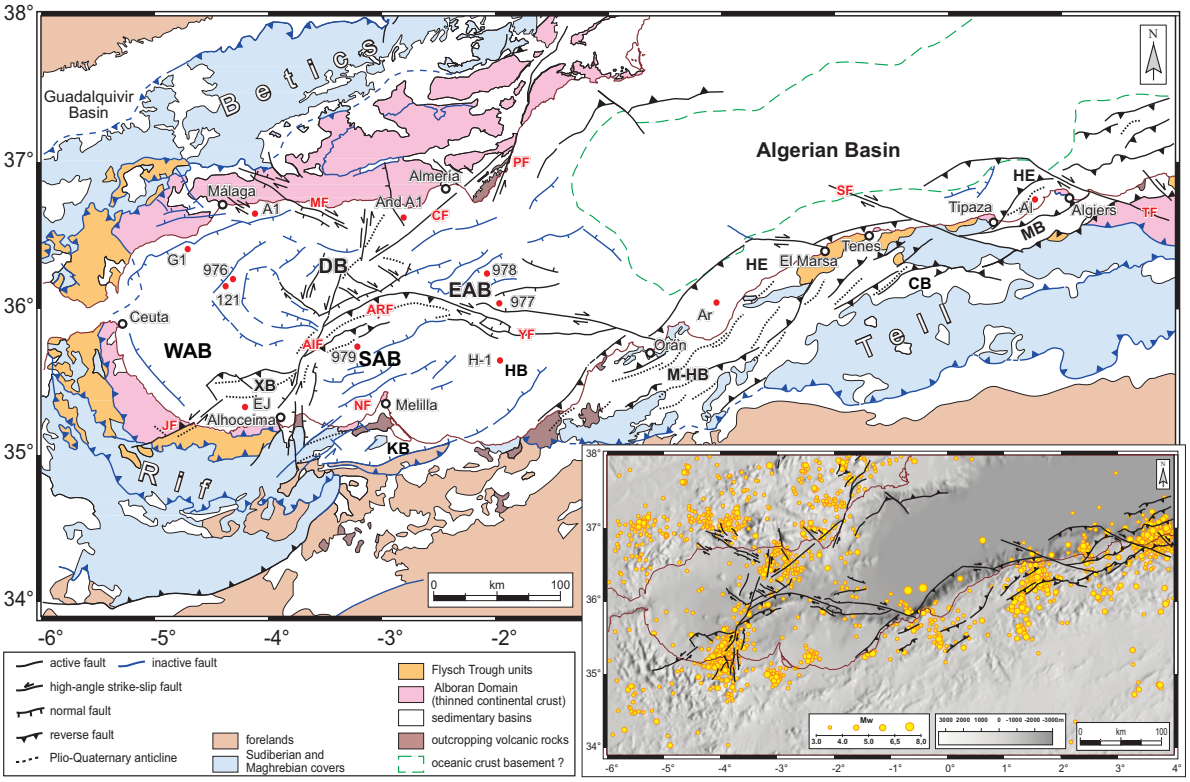

Figure 6-17. Tectonic map of the Western Mediterranean showing the main tectonic features merging our data with other sources. Abbreviations: A1, Alboran-A1 well; AIF, Al-Idrisi fault zone; Al, Algiers-1 well; And-A1, Andalucía-A1 well; Ar, Arzew-1 well; ARF, Alboran Ridge fault zone; CB, Cheliff Basin; CF, Carboneras fault; DH; Djibouti High; EAB, East Alboran Basin; EJ, El-Jebha well; G1, Andalucía-G1 well; H-1, Habibas-1well; HB, Habibas Basin; HE, Habibas Escarpment; JF, Jebha fault; KB, Kert Basin; MB, Mitidja Basin; M-HB, Mleta and Habra basins; MF, Maro-Nerja fault; NF, Nekor fault; PF, Palomares fault; SAB, South Alboran Basin; SF, Salah El Din fault; TF, Thenia fault; XB, Xauen Bank; YF, Yusuf fault zone and WAB, West Alboran Basin. Other details in chapter 6.

African plates; (2) the existence of previous volcanic intrusions, which are aligned with some of the reactivated fault segments and constitute rheological anisotropies within the crustal basement.

The distribution and orientation of Plio-Quaternary to active structures in the central and southeastern part of the Alboran Sea Basin resembles to those existing towards the east, along the Algerian margin (Figure 6-17). The entire region comprises different NE-SW trending segments about 125-180 km in length, which are roughly perpendicular to the present-day vector of convergence between the Eurasian and African plates, and accommodate most of shortening by means of reverse faulting and folding. These segments are displaced by a number of NW-SE to WNW-ESE right-lateral, strike-slip fault zones that act as transfer faults connecting the different reverse NE-SW segments. The whole system resulted from inversion and reactivation of previous extensional-related structures which were formed during the Miocene phase of basin opening in the westernmost Mediterranean.

At present-day, continent-young ocean plate convergence occurs along the foot of the continental slope of the Algerian margin. Compressional and strike-slip structures along this region connect towards the west with the wide band of deformation, which comprises the Alboran Ridge and Yusuf fault zones in the Alboran Sea Basin. A stronger coupling within the Alboran Sea Basin can

be expected, as crustal basement is continental at both sides of the collisional band. In this case the buoyancy of continental lithosphere obstructs the onset of a new subduction or obduction and deformation is widely distributed affecting to both blocks under collision and extending northwards and southwards across Betics and Rif.

7. Conclusiones

Este capítulo resume los principales resultados de esta tesis y discute brevemente su contribución al conocimiento de la evolución estratigráfica y tectónica de la Cuenca del Mar de Alborán. Los procesos activos estudiados aquí, que afectan al fondo marino, deben ser considerados en futuros estudios detallados del riesgo geológico en la región. También se considera la influencia de procesos geológicos previos, que son inactivos en la actualidad, pero condicionaron la posición y geometría de las estructuras tectónicas y sedimentarias actuales.

Se ha realizado un detallado estudio geomorfológico y estructural basado en técnicas geofísicas de alta resolución, como batimetría multihaz y perfiles TOPAS, en el sector central del Mar de Alborán, alrededor de la Cresta de Alborán y la región de Yusuf (**Capítulo 3**) (Figuras 3-6 y 3-15). Las fallas y pliegues identificados deforman el fondo marino y los sedimentos cuaternarios más recientes, controlan la red de cañones y canales y forman escarpes batimétricos donde se producen inestabilidades de fondo marino que explican la mayoría de los deslizamientos submarinos descubiertos. Considerando la distribución, magnitud y mecanismos focales de la sismicidad más somera en la corteza (< 11 km), se demuestra que los pliegues y fallas cartografiados son estructuras activas (Figura 3-15). La localización y cinemática de la estas estructuras en el área de estudio se ha comparado con otras fallas adyacentes, obteniéndose un mapa de estructuras activas para toda la Cuenca del Mar de Alborán (Figura 3-16).

Los resultados de esta tesis confirman que las zonas de falla de la Cresta de Alborán y Yusuf, previamente identificadas como estructuras Plio-Cuaternarias, son activas en la actualidad. Además, este estudio revela que estas dos zonas de falla están conectadas formando una ancha y continua banda de deformación con sismicidad asociada y distribuida. La orientación de estas zonas de falla varía de Oeste a Este cambiando progresivamente desde orientación SO-NE a ONO-ESE. En la Cresta de Alboran predominan las fallas inversas y pliegues de dirección SO-NE. Estas estructuras están orientadas perpendicularmente a vector NO-SE de convergencia de placas inferido por modelos

geodésicos y acomodan la mayoría del acortamiento. El mapeo estructural y los mecanismos focales indican que la zona de falla de la Cresta de Alborán tiene una componente predominante inversa. Los sistemas de pliegues y fallas cambian progresivamente de orientación SO-NE a E-O y finalmente conectan con la zona de falla de Yusuf, que tiene orientación ONO-ESE. Allí las estructuras son oblicuas o sub-paralelas al vector actual de convergencia de placas, de modo que el la cinemática predominante es de salto en dirección con una importante componente dextra. Los desplazamientos transtensivos ocurren entre distintos segmentos de falla solapantes.

Además, los datos demuestran la existencia de una estrecha zona de falla previamente desconocida que tiene orientación NNE-SSO y corta oblicuamente el sector occidental de la Cresta de Alborán. Esta estructura, llamada zona de falla de Al-Idrisi, concentra la mayoría de la sismicidad de la corteza superior en la región del Mar de Alborán (Figura 3-15). La cinemática de esta falla, deducida a partir de mecanismos focales, corresponde con fallas de salto en dirección sinistras a inversas. La falla de Al-Idrisi conecta hacia el sur con un enjambre sísmico que se localiza alrededor de Alhucemas, en la costa marroquí y que comprende terremotos grandes (M_w>6). Además otro enjambre sísmico ocurre cerca de la terminación septentrional de la zona de falla de Al-Idrisi y corresponde con las series sísmicas de Adra (Figura 3-16). La existencia de estos dos enjambres sísmicos en ambos extremos de la falla puede indicar que esta estructura se propaga activamente a lo largo de ambas terminaciones, hacia el Sur y hacia el Norte.

La falla de Al-Idrisi es claramente más joven que los pliegues y fallas a lo largo de la Cresta de Alborán y el Escarpe de Yusuf y puede representar un importante riesgo sísmico en el área del Mar de Alborán. El movimiento de salto en dirección documentado en esta falla conduce el escape lateral de la parte frontal del Arco de Gibraltar hacia el Suroeste. La falla de Al-Idrisi corresponde con el límite oriental de este bloque que comprende el Suroeste de las Béticas, la parte oriental del Mar de Alborán y el Rif. La rotación horaria interna reconocida en este bloque mediante medidas recientes de GPS, puede estar impulsada por la cinemática sinstra de la falla de Al-Idrisi.

La parte Norte de la zona de falla de Al-Idrisi deforma el Alto de Djibouti, donde también han sido encontradas otras estructuras activas. Algunas de esas fallas tienen orientación NNE-SSO y movimiento en salto en dirección izquierdo, similarmente a la falla de Al-Idrisi. Existen otras fallas con orientación NO-SE con una componente predominante de salto en dirección dexta. Todas estas estructuras activas en el Alto de Djibouti forman dos sistemas conjugados de fallas de salto en dirección que se localizan en la terminación SO de la falla de Carboneras (Figuras 3-15 y 3-16).

Para determinar la evolución de la Cuenca del Mar de Alboran se ha empleado una densa malla de perfiles de sísmica monocanal y multicanal correlacionados con sondeos cercanos del DSDP, ODP y otros comerciales. La detallada información bio-estratigráfica y los datos de diagrafías para sedimentos de edad Mioceno final a Cuaternario ha permitido un estudio preciso para los últimos ~5.33 Ma (**Capítulo 4**) (Figuras 4-8 y 3-13). Las reconstrucciones de estructuras y cuencas y las tasas de acumulación de sedimentos documentan cómo ha evolucionado la paleogeografía desde el Messiniense e indican que en esta región ocurrieron complejas interacciones entre la convergencia de placas, las estructuras heredadas, el aporte sedimentario desde las los relieves circundantes (Béticas y Rif), la deformación y la subsidencia (Figura 4-14).

Los sistemas de pliegues y fallas a lo largo de la Cresta de Alboran ya estaban conectados con las estructuras en la región de Yusuf durante el Plio-Cuaternario y se movieron en diferentes intervalos de tiempo causando acortamiento, levantamiento, transpresión o transtensión dependiendo del ángulo que formaban estas estructuras con la dirección de convergencia predominante en cada momento. Los principales pulsos de deformación ocurrieron durante el Plioceno Inferior (~5.33 a 622 4.57 Ma), el Plioceno Superior (~3.28 a 2.45 Ma) y dentro del Pleistoceno más temprano (~1.81 a 1.19 Ma) (**Capítulo 4**).

La conexión entre las zonas de falla de la Cresta de Alborán y Yusuf se acomoda por una falla inversa con traza arqueada que buza hacia el sur y ha permitido el cabalgamiento de la Cresta de Alborán sobre el margen sur de la Cuenca Este de Alborán. Las deformaciones localizadas a lo largo de la Cresta de Alboran y el Escarpe de Yusuf provocaron el basculamiento y migración progresiva hacia el sur de los depocentros de las cuencas meridionales, situadas en el boque de techo de la falla inversa. Así las cuencas de Pytheas, Habibas y Sur de Alboran pasaron a ser cuencas colgadas durante el Plio-Cuaternario y experimentaron una importante reducción en las tasas de acumulación de sedimentos (Figuras 4-13 y 4-14).

La mayor parte del levantamiento de la Cresta de Alborán ocurrió durante el Plioceno Superior, al mismo tiempo que la convergencia entre las placas Euroasiática y Africana cambió de NO-SE a ONO-ESE (Figura 4-14d). En la parte occidental de la Cresta de Alborán algunas estructuras extensionales previas con orientación SO-NE fueron reactivadas e invertidas, similarmente al Banco de Xauen. El levantamiento de estos relieves produjo la desconexión entre las cuencas Oeste y Sur de Alborán que habían permanecido conectadas durante el Mioceno. Además, en el Este de la Cresta de Alborán, la existencia de intrusiones magmáticas determinó la formación de nuevas fallas inversas vergentes al norte y pliegues. Estas estructuras fueron activas, al menos, desde el Plioceno Inferior. La principal fase de acortamiento y levantamiento durante el Plioceno Superior (Figura 4-13) condicionó la primera contribución importante del sistema turbidítico de Almería dentro de la Cuenca del Mar de Alborán. La generación de relieve favoreció la erosión y acumulación de sedimentos de tamaño de grano grueso durante el Plioceno Superior y el Cuaternario y también desencadenó abundantes procesos de inestabilidad gravitatoria (**Capítulo 5**).

Se han identificado depósitos transportados en masa (Mass Transport Deposits, MTD) de edad Plioceno Superior a actual en las laderas de la Cresta de Alborán y en el Escarpe de Yusuf. La superposición de deslizamientos, cubiertos por finas capas de sedimentos estratificados, y su localización a lo largo de escarpes de falla con sismicidad asociada sugiere que estos depósitos fueron probablemente provocados por terremotos durante pulsos de movimiento de fallas activas. Estos procesos recurrentes ocurrieron al menos desde el Plioceno Superior y alternaron con periodos de baja actividad tectónica, en los que predominaba la sedimentación hemipelágica.

El Alto de Djibouti no estuvo afectado por deformaciones significativas durante el Plioceno y permaneció como un alto residual de los eventos de rifting Miocenos. Sin embargo, durante el inicio del Pleistoceno, coincidiendo con la fase de acortamiento más reciente, la falla de salto en dirección de Al-Idrisi, con orientación NNE-SSO, se propagó hacia el Norte deformando el Alto de Djibouti (Figura 4-14e). Simultáneamente, los dos sistemas conjugados de fallas de salto en dirección de alto ángulo (NNE-SSO y NO-SE) se formaron en ese alto.

Los eventos previos de rifting Mioceno dieron lugar a un complicado patrón tectónico que fue heredado durante el Plio-Cuaternario y condicionó significativamente la evolución más reciente de la cuenca (**Capítulo 6**). Las fallas de alto ángulo, los bloques basculados de basamento y las cuencas asimétricas rellenas por sedimentos Miocenos syn-rift, documentan una extensión de dirección predominantemente NO-SE en el área de estudio, durante el Mioceno Medio a Superior. Es posible que esas fallas normales de orientación SO-NE tuvieran originalmente una importante componente de salto en dirección izquierdo, ya que eran oblicuas a la convergencia N-S predominante en aquel tiempo. Distintas observaciones indican que el rifting produjo una cantidad de extensión limitada en este sector de la Cuenca del Mar de Alborán: (1) existencia de otras fallas normales secundarias con orientaciones NO-SE a E-O que contrastan con las principales estructural extensionales de dirección SO-NE (Figura 6-17); (2) los segmentos de falla son cortos y aparecen ampliamente distribuidos y dispuestos en relevo con configuraciones sintéticas y también antitéticas; y (3) los depocentros Miocenos alcanzan aquí un espesor máximo de 2,5 a 3 km, siendo más pequeños y menos potentes que aquellos existentes en las partes occidental y septentrional de la cuenca.

Considerando la Cuenca del Mar de Alborán en su conjunto, se observa un sistema general de extensión multidireccional con un patrón radial que reproduce la forma curvada del orógeno completo. El comienzo y el final de la extensión fueron ambos diacrónicos a lo largo de la cuenca. El rifting comenzó en el Mioceno Inferior en el Oeste y en el Norte. Sin embargo, las secuencias syn-rift en las sub-cuencas meridionales y orientales (*e.g.* Cuencas Este y Sur de Alborán) están compuestas predominantemente por sedimentos de edad Mioceno Superior a Plioceno Inferior. Este hecho indica que en estas zonas los eventos de rifting generaron espacio de acomodación más tarde que en los sectores occidental y septentrional. También es posible que parte de la extensión ocurriese mientras los sectores central y suroriental de la cuenca se encontraban próximos al nivel del mar o incluso, emergidos sobre él. El rifting terminó en la Cuenca Oeste de Alborán durante el Tortoniense, similarmente a la Cuenca de Habibas y la parte más occidental de la Cuenca Este de Alborán. Sin embargo, las fallas normales a lo largo de la Cuenca Sur de Alborán y la parte más oriental de la Cuenca Este de Alborán, continuaron siendo activas hasta el final de Messiniense y localmente hasta el Plioceno Inferior. Por tanto, la extensión fue más joven en las partes más internas y orientales de la Cuenca del Mar de Alborán.

Al final del Mioceno, durante la crisis de salinidad Messiniense, la región experimentó una intensa desecación como consecuencia del cierre de los corredores marinos que conectaban el Océano Atlántico y el Mar Mediterráneo. Sin embargo, en la región del Mar de Alborán existieron durante esa época algunas cuencas residuales marinas someras o lacustres, comparables a las cuencas marginales emergidas en Béticas (**Capítulo 4**). Durante el final del Messiniense todavía existía conexión entre la Cuenca Sur de Alborán y el Canal de Alborán a través la parte occidental de la Cresta de Alborán (Figura 4-14a).

Después del final del rifting, durante el Mioceno Superior al Plioceno Inferior, la Cuenca del Mar de Alborán experimentó una subsidencia térmica uniforme que dio lugar a la acumulación de una delgada capa tabular de sedimentos Plio-Cuaternarios (< 500 m de espesor) que recubre la mayoría de los altos entre cuencas heredados del Mioceno. Sin embargo, esta subsidencia térmica residual coexistió con el acortamiento y algunos de esos altos residuales fueren reactivados y levantados

durante el Plio-Cuaternario. En esos casos, las secuencias Plio-Cuaternarias que cubren los altos están plegadas y muestran geometrías en onlap hacia las crestas de los pliegues y engrosamiento de las secuencias sedimentarias hacia el exterior de esas estructuras (Figuras 4-8 y 4-14).

La reactivación y el acortamiento de algunas de las antiguas fallas relacionadas con la extensión Miocena documentan un proceso de inversión tectónica parcial en la Cuenca del Mar de Alborán (**Capítulo 6**). Los perfiles sísmicos y los mapas estructurales muestran que varias fallas inversas de dirección SO-NE y pliegues asociados han experimentado una inversión de magnitud y edad variables (**Capítulo 6;** Figura 6-16). Estas estructuras se localizan fundamentalmente en la Cresta de Alborán y en la Cuenca de Habibas. En la mayoría de los casos, la inversión tectónica fue parcial y el acortamiento no fue capaz de compensar la mayor cantidad de extensión miocena previa. Se han registrado valores máximos de extensión para el área de estudio, de más de 8 km, en la Cuenca Sur y Este de Alboran y en la parte más oriental de la Cuenca Oeste de Alborán. Esta extensión fue causada principalmente por los eventos de rifting en el Mioceno. Sin embargo, el acortamiento reciente calculado es considerablemente más pequeño, alcanzando valores máximos de unos 2 km desde el Plioceno Superior y fue principalmente acomodado en la región de la Cresta de Alborán. Esto explica que la localización de los mayores depocentros Plio-Cuaternarios coincide aproximadamente con aquellos dominios que experimentaron una significativa extensión miocena, donde existe todavía espacio de acomodación residual que favorece la subsidencia reciente y la compactación.

Además de las estructuras de inversión tectónica positiva, la Cuenca del Mar de Alboran comprende otros ejemplos de reactivación parcial de fallas normales miocenas como estructuras de salto en dirección durante el Plio-Cuaternario. La zona de falla de Yusuf, con orientación ONO-ESE, es el ejemplo más claro de este tipo de estructuras. La reactivación ha ocurrido principalmente a lo largo del sector oriental de la zona de falla de Yusuf, donde los planos de fallas Cuaternarias de salto en dirección dextras, que tienen pequeñas componentes verticales de salto, están enraizados en fallas conjugadas-convergentes de alto ángulo que limitan un potente depocentro mioceno. Sin embargo, las fallas de salto en dirección en la parte occidental de esta zona de falla, *i.e.*, a lo largo del Escarpe de Yusuf, no están conectadas con estructuras extensionales previas, indicando que la reactivación en salto en dirección de fallas miocenas también fue parcial.

La inversión tectónica y la reactivación de fallas durante el Plio-Cuaternario sólo afectaron a algunas estructuras o segmentos de fallas individuales que formaban parte del sistema extensional mioceno (Figura 6-17). Al menos dos factores controlaron esta reactivación selectiva: (1) la orientación de las estructuras previas respecto a la nueva orientación del vector de convergencia entre las placas Euroasiática y Africana (NO-SE); (2) la existencia de intrusiones volcánicas previas, que están alineadas con algunos de los segmentos de fallas reactivados y constituyen anisotropías reológicas dentro del basamento cortical.

La distribución y orientación de estructuras Plio-Cuaternarias a activas en los sectores central y suroriental de la Cuenca del Mar de Alborán se asemejan a aquellas existentes hacia el Este, a lo largo del margen argelino (Figura 6-17). Toda esta región comprende diferentes segmentos con orientación NE-SO y longitudes de unos 125 a 180 km que son aproximadamente perpendiculares al vector de convergencia actual entre las placas Euroasiática y Africana y acomodan la mayoría del

acortamiento mediante fallamiento inverso y plegamiento. Estos segmentos están desplazados por varias zonas de falla de salto en dirección y orientación NO-SE a ONO-ESE que actúan como fallas transfer conectando los distintos segmentos sometidos a acortamiento. El sistema completo resultó de la inversión y reactivación de estructuras relacionadas con extensión que se formaron durante la fase miocena de apertura de cuencas en el Mediterráneo más occidental.

En la actualidad, al pie del margen argelino tiene lugar la colisión entre un segmento de placa de naturaza continental y otro de naturaleza oceánica joven (inicio de subducción). Las estructuras compresivas y de salto en dirección de esta región conectan hacia el Oeste, en el Mar de Alboran, con una banda de deformación ancha que comprende las zonas de falla de la Cresta de Alborán y Yusuf. Dentro del Mar de Alboran, es esperable un mayor acoplamiento entre los dos bloques a ambos lados de esa banda de colisión, ya que el basamento tiene naturaleza continental. En este caso la flotabilidad de la litosfera continental impide el nacimiento de una nueva zona de subducción u obducción y la deformación es ampliamente distribuida afectando a los dos bloques en colisión y extendiéndose hacia el Norte y el Sur a lo largo de las Béticas y el Rif.

8. References

ADAMS, C.G., BENSON, R.H., KIDD, R.B., RYAN, W.B.F. and WRIGHT, R.C. (1977). The Messinian salinity crisis and evidence of late Miocene eustatic changes in the world ocean. Nature, 269, 383-386.

AGUIRRE, J. (1998). El Plioceno del SE de la Península Ibérica (Provincia de Almería). Síntesis estratigráfica, sedimentaria, bioestratigráfica y paleogeográfica. Revista de la Sociedad Geológica de España, 11(3-4), 297-315.

AÏT BRAHIM, L. and CHOTIN, P. (1989). Genése et deformation des bassins néogènes du Rif Central (Maroc) au cours du rapprochement Europa-Africa. . Geodin. Acta (Paris), 3, 295–304.

AÏT BRAHIM, L., CHOTIN, P., HINAJ, S., ABDELOUAFI, A., EL ADRAOUI, A., NAKCHA, C., DHONT, D., CHARROUD, M., SOSSEY ALAOUI, F., AMRHAR, M., BOUAZA, A., TABYAOUI, H. and CHAOUNI, A. (2002). Paleostress evolution in the Moroccan African margin from Triassic to Present. Tectonophysics, 357, 187-205.

AKOGLU, A.M., CAKIR, Z., MEGHRAOUI, M., BELABBES, S., EL ALAMI, S.O., ERGINTAV, S. and AKYUZ, H.S. (2006). The 1994-2004 Al Hoceima (Morocco) earthquake sequence: Conjugate fault ruptures deduced from InSAR. Earth and Planetary Science Letters, 252, 467-480.

ALFARO, P., GALINDO ZALDÍVAR, J., JABALOY, A., LÓPEZ GARRIDO, A.C. and SANZ DE GALDEANO, C. (2001). Evidence for the activity and paleoseismicity of the Padul fault (Betic Cordillera, southern Spain). Acta Geológica Hispánica, 36, 283-295.

ALLEN, P.A. and ALLEN, J.R. (2005). Basin Analysis. Blackwell, Padstow.

ALONSO, B. and MALDONADO, A. (1990). Late Quaternary sedimentation patterns of the Ebro turbidite systems (northwestern Mediterranean): Two styles of deep-sea deposition. In: The Ebro Margin (Ed. by C. H. Nelson and A. Maldonado), 95, 353-377. Marine Geology.

ALONSO, B. and MALDONADO, A. (1992). Plio-Quaternary margin growth pattern in a complex tectonic setting: Northeastern Alboran Sea. Geo-Marine Letters, 12, 137-143.

ALONSO, B., ERCILLA, G., MARTÍNEZ-RUÍZ, F., BARAZA, J. and GALIMONT, A. (1999). Pliocene-Pleistoce sedimentary facies at site 976: depositional history in the northwestern Alboran Sea. In: Proceedings ODP, Scientific Results (Ed. by R. Zahn, M. C. Comas and A. Klaus), 161, 57-68. Ocean Drilling Program, College Station, TX.

ALONSO, B. and ERCILLA, G. (2000). Sistemas turbidíticos y canales medio-oceánicos. In: Valles submarinos y sistemas turbidíticos modernos (Ed. by B. Alonso and G. Ercilla), 19-66. CSIC, Barcelona.

ALONSO, B. and ERCILLA, G. (2003). Small turbidite systems in a complex tectonic setting (SW Mediterranean Sea): morphology and growth patterns. Marine and Petroleum Geology, 19,

1225-1240.

ALVAREZ-MARRÓN, J. (1999). Pliocene to Holocene structure of the eastern Alboran Sea (Western Mediterranean). In: Proceedings ODP, Scientific Results (Ed. by R. Zahn, M. C. Comas and A. Klaus), 161, 345-355. Ocean Drilling Program, College Station, TX.

AMMAR, A., MAUFFRET, A., GORINI, C. and JABO, H. (2007). The tectonic structure of the Alboran margin of Morocco. Sociedad Geológica de España, 20, 247-271.

ANDRIEUX, J., FONTBOTE, J.M. and MATTAUER, M. (1971). Sur un modele explicatif de l'arc de Gibraltar. Earth and Planetary Science Letters, 12, 191-198.

ASEBRIY, L., BOURGOIS, J., CHERKAOUI, T.E. and AZDIMOUSA, A. (1993). Evolution tectonique récente de la zone de faille du Nékor: importance paléogéographique et structurale dans le Rif externe, Maroc. Journal of African Earth Sciences (and the Middle East), 17, 65-74.

AUGIER, R., JOLIVET, L. and ROBIN, C. (2005). Late Orogenic doming in the eastern Betic Cordilleras: Final exhumation of the Nevado-Filabride complex and its relation to basin genesis. Tectonics, 24, TC4003.

AUZENDE, J.M., BONNIN, J., OLIVET, J.L. and PAUTOT, G. (1971). Upper Miocene salt layer in the western Mediterranean basin. Nature, Phys Sci, 230, 82-84.

AUZENDE, J.M., OLIVET, J.L. and BONNIN, J. (1972). Une structure compressive au nord del'Algérie? Deep Sea Research and Oceanographic Abstracts, 19, 149-155.

AYALA, C., TORNE, M. and POUS, J. (2003). The lithosphere-asthenosphere boundary in the western Mediterranean from 3D joint gravity and geoid modeling: tectonic implications. Earth and Planetary Science Letters, 209, 275-290.

AZAÑÓN, J.M., GARCÍA-DUEÑAS, V. and GOFFÉ, B. (1998). Exhumation of high-pressure metapelites and coeval crustal extension in the Alpujarride complex (Betic Cordillera). Tectonophysics, 285, 231-252.

AZAÑÓN, J.M. and CRESPO-BLANC, A. (2000). Exhumation during continental collision inferred from the tectonometamorphic evolution of the Alpujarride Complex in the central Betics (Alboran Domain, SE Spain). Tectonics, 19, 549-565.

AZDIMOUSA, A., JABALOY, A., ASEBRIY, L., BOOTH-REA, G., GONZÁLEZ-LODEIRO, F. and BOURGOIS, J. (2007). Lithostratigraphy and structure of the Temsamane Unit (Eastern External Rif, Morocco). Revista de la Sociedad Geológica de España, 20 (3-4), 187-200.

BACHE, F., OLIVET, J.L., GORINI, C., RABINEAU, M., BAZTAN, J., ASLANIAN, D. and SUC, J.-P. (2009). Messinian erosional and salinity crises: View from the Provence Basin (Gulf of Lions, Western Mediterranean). Earth and Planetary Science Letters, 286, 139-157.

BACHE, F., POPESCU, S.-M., RABINEAU, M., GORINI, C., SUC, J.-P., CLAUZON, G., OLIVET, J.-L., RUBINO, J.-L., MELINTE-DOBRINESCU, M.C., ESTRADA, F., LONDEIX, L., ARMIJO, R., MEYER, B., JOLIVET, L., JOUANNIC, G., LEROUX, E., ASLANIAN, D., REIS, A.T.D., MOCOCHAIN, L., DUMURDŽANOV, N., ZAGORCHEV, I., LESIĆ, V., TOMIĆ, D., NAMıK ÇAĞATAY, M., BRUN, J.-P., SOKOUTIS, D., CSATO, I., UCARKUS, G. and ÇAKıR, Z. (2012). A two-step process for the reflooding of the Mediterranean after the Messinian Salinity Crisis. Basin Research, 24, 125-153.

BAKKER, H.E., DE JONG, K., HELMERS, H. and BIERMANN, C. (1989). The geodynamic evolution of the internal zone of the Betic Cordilleras (south-east Spain): A model based on the structural analysis and geothermobarometry. Journal of Metamorphic Geology, 7, 359-381.

BALANYÁ, J.C. and GARCÍA-DUEÑAS, V. (1987). Les directions structurales dans le Domaine d'Alboran de parts et d'outre du Detroit de Gibralter. Comptes Rendus Acad. Sci. Paris, 304, 929-933.

BALANYÁ, J.C. and GARCÍA-DUEÑAS, V. (1988). El Cabalgamiento cortical de Gibraltar y la tectónica de Béticas y Rif. II Congreso Geológico de España. Simposium sobre Cinturones Orogénicos.

BALLESTEROS, M., RIVERA, J., MUÑOZ, A., MUÑOZ-MARTÍN, A., ACOSTA, J., CARBÓ, A. and UCHUPI, E. (2008). Alboran basin, Southern Spain. Part II: Neogene tectonic implications for the orogenic float model. Marine and Petroleum Geology, 25, 75-101.

BANDA, E., GALLART, J., GARCÍA-DUEÑAS, V., DAÑOBEITIA, J.J. and MAKRIS, J. (1993). Lateral variation of the crust in the Iberian peninsula: new evidence from the Betic Cordillera. Tectonophysics, 221, 53-66.

BARAZA, J., LEE, J., KAYEN, R. and HAMPTON, M.A. (1990). Geotechnical characteristics and slope stability on the Ebro margin, western Mediterranean. In: The Ebro Margin (Ed. by C. H.

Nelson and A. Maldonado), 95, 379-393. Marine Geology.

BÁRCENAS, P., VÁZQUEZ, J.T., DÍAZ DEL RÍO, V. and FERNÁNDEZ-SALAS, L.M. (2004). Geomorfología del Banco de la Isla de Alborán. Geo-Temas, 6, 209-212.

BENMAKHLOUF, M., GALINDO-ZALDÍVAR, J., CHALOUAN, A., SANZ DE GALDEANO, C., AHMAMOU, M. and LÓPEZ-GARRIDO, A.C. (2005). Cinemática y paleoesfuerzos en la zona de falla transcurrente de Jebha-Chrafate (Rif septentrional, Marruecos). Geogaceta, 38, 71-74.

BENSON, R.H., RAKIC-EL BIED, K. and BONADUCE, G. (1991). An Important Current Reversal (Influx) in the Rifian Corridor (Morocco) at the Tortonian-Messinian Boundary: The End of Tethys Ocean. Paleoceanography, 6, 165-192.

BERÁSTEGUI, X., BANKS, C., PUIG, C., TABERNER, C., WALTHAM, D. and FERNÀNDEZ, M. (1998). Lateral diapiric emplacement of Triassic evaporites at the southern margin of the Guadalquivir Basin, Spain. In: Cenozoic Foreland Basins of Western Europe (Ed. by A. Mascle, C. Puigdefàbregas, H. P. Luterbacher and M. Fernàndez), 134, 49-68. Geological Society of London Special Publications, London.

BEZZEGHOUD, M. and BUFORN, E. (1999). Source Parameters of the 1992 Melilla (Spain, Mw = 4.8), 1994 Alhoceima (Morocco, Mw = 5.8), and 1994 Mascara (Algeria, Mw - 5.7) Earthquakes and Seismotectonic Implications. Bulletin of the Seismological Society of America, 89, 359-372.

BIGGS, J., BERGMAN, E., EMMERSON, B., FUNNING, G.J., JACKSON, J.A., PARSONS, B. and WRIGH, T.J. (2006). Fault identification for buried strike-slip earthquakes using InSAR: The 1994 and 2004 Al Hoceima, Morocco earthquakes. Geophysical Journal International, 166, 1347-1362.

BIJWAARD, H. and SPAKMAN, W. (2000). Non-linear global p-wave tomography by iterated linearizad inversion. Geophysical Journal International, 141, 71-82.

BILLI, A., PRESTI, D., FACCENNA, C., NERI, G. and ORECCHIO, B. (2007). Seismotectonics of the Nubia plate compressive margin in the south Tyrrhenian region, Italy: Clues for subduction inception. Journal of Geophysical Research, 112, B08302, doi:08310.01029/02006JB004837.

BIRD, P. (2003). An updated digital model of plate boundaries. Geochemistry, geophysics, geosystems, 4, 1027, doi:1010.1029/2001GC000252.

BLANC, P.-L. (2002). The opening of the Plio-Quaternary Gibraltar Strait: assessing the size of a cataclysm. Geodinamica Acta, 15, 303-317.

BLANCO, M.J. and SPAKMAN, W. (1993). The P-wave velocity structure of the mantle below the Iberian Peninsula: evidence for subducted lithosphere below southern Spain. Tectonophysics, 221, 13-34.

BOOTH-REA, G., AZAÑÓN, J.M., GARCÍA-DUEÑAS, V. and AUGIER, R. (2003). Uppermost Tortonian to Quaternary depocentre migration related with segmentation of the strike-slip Palomares Fault Zone, Vera Basin (SE Spain). Comptes Rendus Geoscience, 335, 751-761.

BOOTH-REA, G., RANERO, C.R., MARTÍNEZ-MARTÍNEZ, J.M. and GREVEMEYER, I. (2007). Crustal types and Terciary tectonic evolution of the Alboran sea, western Mediterranean. Geochemistry Geophysics Geosystems, 8, Q10005, doi: 10010.11029/12007GC001639.

BOURGOIS, J., MAUFFRET, A., AMMAR, A. and DEMNATI, A. (1992). Multichannel Seismic Data Imaging of Inversion Tectonics of the Alboran Ridge (Western Mediterranean Sea). Geo-Marine Letters, 12, 117-122.

BOUSQUET, J.C. (1979). Quaternary strike-slip faults in southeastern Spain. Tectonophysics, 52, 277-286.

BRAGA, J.C., MARTÍN, J.M. and QUESADA, C. (2003). Patterns and average rates of late Neogene–Recent uplift of the Betic Cordillera, SE Spain. Geomorphology, 50, 3-26.

BRANDES, C., ASTORGA, A., BLISNIUK, P., LITTKE, R. and WINSEMANN, J. (2009). Anatomy of Anticlines, Piggy-Back Basins and Growth Strata: A Case Study from the Limón Fold-and-Thrust Belt, Costa Rica. In: Sedimentary Processes, Environments and Basins (Ed. by, 91-110. Blackwell Publishing Ltd.

BRYDEN, H.L. and STOMMEL, H.M. (1982). Origin of the Mediterranean outflow. Journal of Marine Research, 40, 55-71.

BUFORN, E., UDIAS, A. and MADARIAGA, R. (1991). Intermediate and deep earthquakes in Spain. Pageoph., 136, 375-393.

BUFORN, E., SANZ DE GALDEANO, C. and UDÍAS, A. (1995). Sismotectonics of the Ibero-Maghrebian region. Tectonophysics, 248, 247-261.

BUFORN, E., BEZZEGHOUD, M., UDÍAS, A. and PRO, C. (2004). Seismic sources on the Iberia-African plate boundary and their tectonic

implications. Pure and Applied Geophysics, 161, 623-646.

BURBANK, D.W. and ANDERSON, R.S., eds. (2001). Tectonic Geomorphology. Blackwell Science, Maldem, Massachusetts.

BUROLLET, P.F., SAID, A. AND TROUVE, P., and 1978. (1987). Slim holes drilled on the Algerian shelf. In: Initial Reports of Deep Sea Drilling Project. In: Initial Reports of Deep Sea Drilling Project (Ed. by D. A. Ross and Y. P. Neprocnov), 42, 1181–1184. Government Press, Washington, DC.

CALVERT, A., SANDVOL, E., SEBER, D., BARAZANGI, M., ROECKER, T., MOURABIT, F., VIDAL, F., ALGUACIL, G. and JABOUR, N. (2000). Geodynamic evolution of the lithosphere and upper-mantle beneath the Alboran Region of the western Mediterranean - constraints for travel.time tomography. Journal of Geophysical Research, 105, 10871-10898.

CAMPILLO, A.C., MALDONADO, A. and MAUFFRET, A. (1992). Stratigraphic and Tectonic Evolution of the Western Alboran Sea: Late Miocene to Recent. Geo-Marine Letters, 12, 165-172.

CAMPOS, J., MALDONADO, A. and CAMPILLO, A.C. (1992). Post-Messinian evolutional patterns of the central Alboran Sea. Geo-Marine Letters, 12, 173-178.

CANALS, M., CASAMOR, J.L., URGELES, R., LASTRAS, G., MASSON, D., BERNE, S., ALONSO, B. and DE BATIST, M. (2000). The Ebro continental margin, Western Mediterranean Sea: interplay between canyon-channel systems and mass wasting processes. In: Deep-Water Reservoirs of the World (CD) (Ed. by P. Weimer and H. Nelson), 152–174. Gulf Coast Section SEPM Foundation, Houston.

CANALS, M., LASTRAS, G., URGELES, R., CASAMOR, J.L., MIENERT, J., CATTANEO, A., DE BATIST, M., HAFLIDASON, H., IMBO, Y., LABERG, J.S., LOCAT, J., LONG, D., LONGVA, O., MASSON, D.G., SULTAN, N., TRINCARDI, F. and BRYN, P. (2004). Slope failure dynamics and impacts from seafloor and shallow sub-seafloor geophysical data: case studies from the COSTA project. Marine Geology, 213, 9-72.

CARRERA, N., MUÑOZ, J.A., SÀBAT, F., MON, R. and ROCA, E. (2006). The role of inversion tectonics in the structure of the Cordillera Oriental (NW Argentinean Andes). Journal of Structural Geology, 28, 1921-1932.

CASAS, D., ERCILLA, G., BARAZA, J., ALONSO, B. and MALDONADO, A. (2003). Recent mass-movement processes on the Ebro continental slope (NW Mediterranean). Marine and Petroleum Geology, 20, 445-447.

CASAS, D., ERCILLA, G., BARAZA, J., ALONSO, B. and MALDONADO, A. (2003). Recent mass-movement processes on the Ebro continental slope (NW Mediterranean). Marine and Petroleum Geology, 20, 445-447.

CASTAGNA, J.P., BATZLE, M.L. and EASTWOOD, R.L. (1985). Relationship between compressional and shear-wvave velocity in clastic silicate rocks. Geophysics, 50, 571-581.

CATALANO, R., FRANCHINO, A., MERLINI, S. and SULLI, A. (2000). A crustal section from the Eastern Algerian basin to the Ionian ocean (Central Mediterranean). Memorie della Societd Geologica d' Italia, 55, 71–85.

CHALOUAN, A. and MICHARD, A. (1990). The Ghomarides nappes, Rif costal range, Morocco: A variscan chip in the Alpine belt. Tectonics, 9, 1565-1583.

CHALOUAN, A., OUAZANI-TOUHAMI, A., MOUHIR, L., SAJI, R. and BENMAKHLOUF, M. (1995). Les failles normales à faible pendage du Rif interne (Maroc) et leur effet sur l'amincissement crustal du domaine d'Alboran. Geogaceta, 17, 107-109.

CHALOUAN, A., SAJI, R., MICHARD, A. and BALLY, A.W. (1997). Neogene tectonic evolution of the southwestern Alboran Basin as inferred from seismic data off Morocco. American Association of Petroleum Geologists Bulletin, 81, 1161-1184.

CHALOUAN, A. and MICHARD, A. (2004). The Alpine Rif Belt (Morocco): A Case of Mountain Building in a Subduction-Subduction-Transform Fault Triple Junction. Pure and Applied Geophysics, 161, 489-519.

CHALOUAN, A., MICHARD, A., EL KADIRI, K., NEGRO, F., FRIZON DE LAMOTTE, D., SOTO, J.I. and SADDIQI, O. (2008). The Rift Belt. In: The Rif belt continental evolution: the geology of Morocco. Structure, stratigraphy, and tectonics of the Africa-Atlantic-Mediterranean triple junction. Lecture in Earth Sciences (Ed. by A. Michard, O. Saddiqi, A. Chalouan and D. Frizon de Lamotte), 116, 203-302. Springer, Berlin.

CLAUZON, G., SUC, J.-P., GAUTIER, F., BERGER, A. and LOUTRE, M.-F. (1996). Alternate interpretation of the Messinian salinity crisis: Controversy resolved? Geology, 24, 363-366.

CLOETINGH, S., VAN DER BEEK, P.A., VAN

REES, D., ROEP, T.B., BIERMANN, C. and STEPHENSON, A. (1992). Flexural Interaction and the Dynamics of Neogene Extensional Basin Formation in the Alboran-Betic Region. Geo-Marine Letters, 12, 66-75.

CLOETINGH, S., BEEKMAN, F., VAN WEES, J.D., ZIEGLER, P.A. and SOKOUTIS, D. (2008). Post-rift compressional reactivation potential of passive margins and extensional basins. In: The nature and origin of compression in passive margins (Ed. by e. a. H. Johnson), 306, 27-70. Geol. Soc. Lond. Spec. Publ., London.

COCA, P. and BUFORN, E. (1994). Mecanismos focales en el Sur de España: Periodo 1965-1985. Estudios Geol., 50, 33-45.

COMAS, M.C., GARCÍA-DUEÑAS, V. and JURADO, M.J. (1992). Neogene tectonic evolution of The Alboran Sea from MCS data. Geo-Marine Letters, 12, 157-164.

COMAS, M., DAÑOBEITIA, J.J., ALVAREZ-MARRÓN, J. and SOTO, J.I. (1995). Crustal reflections and structure in the Alboran Basin: preliminary results of the ESCI-Alborán Survey. Revista de la Sociedad Geológica de España, 8, 76-88.

COMAS, M.C., ZAHN, R., KLAUS, A. and AL., E., eds. (1996). Proceedings ODP, Initial Reports. Ocean Drilling Program, College Station, TX.

COMAS, M.C., PLATT, J.P., SOTO, J.I. and WATTS, A.B. (1999). The origin and tectonic history of the Alboran Basin: Insights from Leg 161 results. In: Proceedings ODP, Scientific Results (Ed. by R. Zahn, M. C. Comas and A. Klaus), 161, 555-580. Ocean Drilling Program, College Station, TX.

COMAS, M.C. and SOTO, J.I. (1999). Breccias on top of basement at Site 976 (West Alboran Sea basin): tectonic significance. In: Proceedings ODP, Scientific Results (Ed. by R. Zahn, M. C. Comas and A. Klaus), 161, 331-344. Ocean Drilling Program, College Station, TX.

COMAS, M.C. and SOTO, J.I. (1999). Brittle deformattion in the metamorphyc basement at site 976: Implications for middle Miocene extensional tectonics in the western Alboran basin. In: Proceedings of the Ocean Drilling Program, Scientific Results (Ed. by R. Zahn, M. C. Comas and A. Klaus), 161, 331-344. Ocean Drilling Program, College Station, TX.

COMAS, M., IVANOV, M.K. and SHIPBOARD SCIENTIFIC PARTY OF TTR-12, LEG 3 (2003). Alboran Basin (Leg 3). In: Interdisciplinary Geoscience Research on the north East Atlantic Margin, Mediterranean Sea and Mid-Atlantic Ridge (Ed. by N. H. Kenyon, M. K. Ivanov, A. M. Akhmetzhanov and G. G. Akhmanov), IOC Technical Series, No. 67. UNESCO, 2003 (English).

COPE, M.J. (2003). Algerian licensing round may offer opportunity for exploration plays in deep offshore frontier. First Break, 21, 37–42.

CRESPO BLANC, A., OROZCO, M. and GARCÍA-DUEÑAS, V. (1994). Extension versus compression during the Miocene tectonic evolution of the Betic chain. Late folding of normal fault systems. Tectonics, 13, 78-88.

CRESPO-BLANC, A. and CAMPOS, J. (2001). Structure and kinematics of the South Iberian paleomargin and its relationship with the Flysch Trough units: extensional tectonics within the Gibraltar Arc fold-and-thrust belt (western Betics). Journal of Structural Geology.

CRESPO-BLANC, A. and FRIZON DE LAMOTTE, D. (2006). Structural evolution of the external zones derived from the flysch trough and the South Iberian and Maghrebian paleomargins around the Gibraltar arc: a comparative study. Bulletin de la Société Géologique de France, 177, 267-282.

DE JONG, K. (1991). Tectono-Metamorphic studies an radiometric dating in the Betic Cordilleras (SE Spain): with implications for the dynamics of extension and compression in the western Mediterranean area. Doctoral Thesis, Vrije University, Amsterdam, Netherlands.

DE KAENEL, E.P., SIESSER, W.G. and MURAT, A. (1999). Pleistocene calcareous nannofossil biostratigraphy and the western mediterranean sapropels, sites 974 to 977 and 979. In: Proceedings of the Ocean Drilling Program, Scientific Results (Ed. by R. Zahn, M. C. Comas and A. Klaus), 161, 159-183, College Station, TX.

DE LA LINDE, J., COMAS, M. and SOTO, J.I. (1996). Morfología del basamento en el noroeste del Mar de Alborán. Geogaceta, 20, 355-358.

DE LAROUZIÈRE, F.D., BOLZE, J., BORDET, P., HERNANDEZ, J., MONTENAT, C. and OTT D'ESTEVOU, P. (1988). The Betic segment of the lithospheric trans-Alboran shear zone during the Late Miocene. Tectonophysics, 152, 41-52.

DE LUGT, I.R., VAN WEES, J.D. and WONG, T.E. (2003). The tectonic evolution of the southern Dutch North Sea during the Palaeogene: basin inversion in distinct pulses. Tectonophysics, 373, 141-159.

DE PAOLA, N., HOLDSWORTH, R.E., MCCAFFREY, K.J.W. and BARCHI, M.R.

(2005). Partitioned transtension: an alternative to basin inversion models. Journal of Structural Geology, 27, 607-625.

DEMETS, C., GORDON, R.G., ARGUS, D.F. and STEIN, S. (1994). Effect of recent revisions to the geomagnetic reversal time scale on estimate of current plate motions. Geophys. Res. Lett., 21, 2191-2194.

DÉVERCHÈRE, J., YELLES, K., DOMZIG, A., MERCIER-DE-LÉPINAY, B., BOUILLIN, J.-P., GAULLIER, V., BRACÈNE, R., CALAIS, E., SAVOYE, B., KHERROUBI, A., ROY, P.L., PAUC, H. and DAN, G. (2005). Active thrust faulting offshore Boumerdes, Algeria, and its relations to the 2003 Mw 6.9 earthquake. Geophysical Research Letters, 32, L04311, doi:04310.01029/02004GL021646.

DEWEY, J.F. (1988). Extensional collapse of orogens. Tectonics, 7, 1123-1139.

DEWEY, J.F., HELMAN, M.L., TURCO, E., HUTTON, D.H.W.A. and KNOTT, S.D. (1989). Kinematics of the Western Mediterranean. In: Conference on Alpine tectonics (Ed. by M. P. Coward, D. Dietrich and R. G. Park), Geological Society Special Publication, 265-283. Geological Society of London Special Publications, London.

DOCHERTY, C. and BANDA, E. (1992). A Note on the Subsidence History of the Northern Margin of the Alboran Basin. Geo-Marine Letters, 12, 82-87.

DOCHERTY, C. and BANDA, E. (1995). Evidence for the eastward migration of the Alboran Sea based on regional subsidence analysis: A case for basin formation by delamination of the subcrustal lithosphere. Tectonics, 14, 804-818.

DOMIZG, A., YELLES, K., LE ROY, C., J., D., BOUILLIN, J.P., BRACÈNE, R., MERCIER DE LÉPINAY, B., LE ROY, P., CALAIS, E., KHERROUBI, A., GAULLIER, V., SAVOYE, B. and PAUC, H. (2006). Searching for the Arica-Eurasia Miocene boundary offshore western Algeria (MARADJA'03). Comptes Rendus Geoscience, 338, 80-91.

DUGGEN, S., HOERNLE, K., VAN DEN BOGAARD, P., RUPKE, L. and PHIPPS MORGAN, J. (2003). Deep roots of the Messinian salinity crisis. Nature, 422, 602-606.

DUGGEN, S., HOERNLE, K., VAN DEN BOGAARD, P. and HARRIS, C. (2004). Magmatic evolution of the Alboran region: The role of subduction in forming the western Mediterranean and causing the Messinian Salinity Crisis. Earth and Planetary Science Letters, 218, 91-108.

DUGGEN, S., HOERNLE, K., KLÜGEL, A., GELDMACHER, J., THIRLWALL, M., HAUFF, F., LOWRY, D. and OATES, N. (2008). Geochemical zonation of the Miocene Alborán Basin volcanism (westernmost Mediterranean):geodynamic implications. Contributions to Mineralogy and Petrology, doi:10.1007/s00410-00008-00302-00414.

DURAND-DELGA, M., ESCALIER-DES-ORRES, P. and FERNEX, F. (1962). Sur la présence de Jurassique et d'Oligocène a l'ouest de Carthagene (Espagne méridionale). Comptes Rendus Acad. Sci. Paris, 255, 1753-1755.

DURAND-DELGA, M. (1980). La Méditerranée occidentale: Etapes de sa genèse et problèmes structuraux liés à celle-ci. Mem. Soc. Géol. Fr., 10, 203-224.

DURAND-DELGA, M. and FONBOTÉ, J.M. (1980). Le cadre structural de la Méditerranée occidentale. 26º Congrès Géol. Intern. Paris, Colloque nº 5 (Les chaines alpines issues de la Téthys), Mem. B.R.G.M.

DURAND-DELGA, M., ROSSI, P., OLIVIER, P. and PUGLISI, D. (2000). Situation structurale et nature ophiolitique de roches basiques jurassiques associées aux flyschs maghrébins du Rif (Maroc) et de Sicile (Italie). Comptes Rendus Acad. Sci. Paris, 331, 29-38.

EL BAKKALI, S., GOURGAUD, A., BOURDIER, J.-L., BELLON, H. and GUNDOGDU, N. (1998). Post-collision neogene volcanism of the Eastern Rif (Morocco): magmatic evolution through time. Lithos, 45, 523-543.

ERCILLA, G. (1992). Sedimentación en márgenes continentales y cuencas del Mediterráneo occidental durante el Quaternario (Península Ibérica). Published Ph.D thesis, Universitat Politécnica de Cataluña, Barcelona.

ERCILLA, G., ALONSO, B. and BARAZA, J. (1992). Sedimentary Evolution of the Northwestern Alboran Sea during the Quaternary. Geo-Marine Letters, 12, 144-149.

ERCILLA, G., ALONSO, B. and BARAZA, J. (1994). Post-Calabrian sequence stratigraphy of the northwestern Alboran Sea (southwestern Mediterranean). Marine Geology, 120, 249-265.

ERCILLA, G. and ALONSO, B. (1996). Quaternary siliciclastic sequence stratigraphy of western Mediterranean passive and tectonically active margins: the role of global versus local controlling factors In: Geological Society Special Publication, Geology of Siliciclastic shelf sea (Ed. by M. De Batist and M. Jacobs), 117, 125-137. The

Geological Society, London.

ERCILLA, G., FERRÁN, E., YENES, M., CASAS, D., ALONSO, B., FARRAN, M. and TEAM, S. (2009). The Baraza Slide: defining its dinamic (northern Alboran Sea). International Conference on Seafloor Mapping for Geohazard Assessment (Fioro d'lschia, Italy, May 11-13, 2009).

ESTRADA, F., ERCILLA, G. and ALONSO, B. (1997). Pliocene-Quaternary tectonic-sedimentary evolution of the NE Alboran Sea (SW Mediterranean Sea). Tectonophysics, 282, 423-442.

ESTRADA, F., ERCILLA, G., GORINI, C., ALONSO, B., VÁZQUEZ, J., GARCÍA-CASTELLANOS, D., JUAN, C., MALDONADO, A., AMMAR, A. and ELABBASSI, M. (2011). Impact of pulsed Atlantic water inflow into the Alboran Basin at the time of the Zanclean flooding. Geo-Marine Letters, 1-16.

FACCENNA, C., PIROMALLO, C., CRESPO-BLANC, A., JOLIVET, L. and ROSSETTI, F. (2004). Lateral slab deformation and the origin of the western Mediterranean arcs. Tectonics, 23, doi:10.1029/2002TC001488.

FADIL, A., VERNANT, P., MCCLUSKY, S., REILINGER, R., GOMEZ, F., BEN SARI, D., MOURABIT, T., FEIGL, K. and BARAZANGI, M. (2006). Active tectonics of the western Mediterranean: Geodetic evidence for rollback of a delaminated subcontinental lithospheric slab beneath the Rif Mountains, Morocco. Geology, 34, 529-532.

FAUQUETTE, S., SUC, J.-P., BERTINI, A., POPESCU, S.-M., WARNY, S., BACHIRI TAOUFIQ, N., PEREZ VILLA, M.-J., CHIKHI, H., FEDDI, N., SUBALLY, D., CLAUZON, G. and FERRIER, J. (2006). How much did climate force the Messinian salinity crisis? Quantified climatic conditions from pollen records in the Mediterranean region. Palaeogeography, Palaeoclimatology, Palaeoecology, 238, 281-301.

FERNANDES, R., AMBROSIUS, B.A.C., NOOMEN, R., BASTOS, L., WORTEL, M.J.R., SPAKMAN, W. and GOVERS, R. (2003). The relative motion between Africa and Eurasia as derived from ITRF2000 and GPS data. Geophys. Res. Lett., 30, 16, 1828, doi:1810.1029/2003GL017089.

FERNÁNDEZ SOLER, J., MARTÍNEZ-RUÍZ, F., AKHMANOV, G., AKHMETZHANOV, A., STADNITSKAYA, A., KOZLOVA, E., SAUTKIN, A., MAZURENKO, L., OVSYANNIKOV, D., SADEKOV, A., BELENKAYA, I., SUSLOVA, E. and GONCHAROV, D. (1999). Bottom sampling. In: Multidisciplinary Study of Geological Processes on the North East Atlantic and Western Mediterranean Margins, Preliminary results of geological and geophysical investigations during the TTR-9 of R/V Professor Logachev, June-July, 1999 (Ed. by N. H. Kenyon, M. K. Ivanov, A. M. Azhmetzhanov and G. G. Akhmanov), IOC Technical Series, 56, 85-91. UNESCO.

FERNÁNDEZ-IBÁÑEZ, F. (2007). Sismicidad, reología y estructura térmica de la corteza del Arco de Gibraltar, Univ. Granada, Granada.

FERNÁNDEZ-IBÁÑEZ, F., SOTO, J.I., ZOBACK, M.D. and MORALES, J. (2007). Present-day stress field in the Gibraltar Arc (western Mediterranean). Journal of Geophysical Research, 112, B08404, doi:08410.01029/ 02006JB004683.

FERNÁNDEZ-IBÁÑEZ, F. and SOTO, J.I. (2008). Crustal rheology and seismicity in the Gibraltar Arc (western Mediterranean). Tectonics, 27, TC2007, doi:2010.1029/2007TC002192,002008.

FIELD, M.E. and GARDNER, J.V. (1991). Valencia gorge: Possible Messinian refill channel for the western Mediterranean Sea. Geology, 19, 1129-1132.

FLINCH, J.F. (1996). Accretion and extensional collapse of the external Western Rif (Northern Morocco). In: Peri-Tethys Memoir 2: Structure and Prospects of Alpine Basins and Forelands (Ed. by P. A. Ziegler and F. Horvath), Mém. Mus. natn. Hist nat, 170, 61-85. Editions du Museum, Paris.

FRASER, A.J. and GAWTHORPE, R.L. (1990). Tectono-stratigraphic development and hydrocarbon habitat of the Carboniferous in northern England. Geological Society, London, Special Publications, 55, 49-86.

FRIZON DE LAMOTTE, D., ANDRIEUX, J. and GUÉZOU, J.-C. (1991). Cinématique des chévauchements Néogènes dans l'arc Bético-Rifain: discussion sur les modèles géodynamiques. Bulletin de la Societé Géologique de France, 4, 611-626.

FRIZON DE LAMOTTE, D., CRESPO-BLANC, A., SAINT-BÉZAR, B., COMAS, M., FERNÀNDEZ, M., ZEYEN, H., AYARZA, P., ROBERT-CHARRUE, C., CHALOUAN, A., ZIZI, M., TEIXELL, A., ARBOLEYA, M.-L., ALVAREZ-LOBATO, F., JULIVERT, M. and MICHARD, A. (2004). TRANSMED Transect I. In: The TRANSMED Atlas - The Mediterranean region from crust to mantle. (Ed. by W. Cavazza, F. Roure, W. Spakman, G. M. Stampfli and P. Ziegler). Springer-Verlag, Berlin Heidelberg.

FULLEA, J., FERNANDEZ, M., ZEYEN, H. and

VERGES, J. (2007). A rapid method to map the crustal and lithospheric thickness using elevation, geoid anomaly and thermal analysis. Application to the Gibraltar Arc System, Atlas Mountains and adjacent zones. Tectonophysics, In Press, Corrected Proof.

GALDEANO, A., COURTILLOT, V., LE BORGNE, E., LE MOUEL, J.-L. and ROSSIGNOL, J.-C. (1974). An aeromagnetic survey of the southwest of the western Mediterranean: Description and tectonic implications. Earth and Planetary Science Letters, 23, 323-336.

GALINDO-ZALDÍVAR, J., GONZÁLEZ LODEIRO, F. and JABALOY, A. (1989). Progressive extensional shear structures in a detachment contact in the Western Sierra Nevada (Betic Cordilleras, Spain). Geodinamica Acta, 3, 73-85.

GALINDO-ZALDÍVAR, J., JABALOY, A., GONZÁLEZ LODEIRO, F. and ALDAYA, F. (1997). Crustal structure of the central sector of the Betic Cordillera (SE Spain). Tectonics, 16, 18-37.

GALINDO-ZALDÍVAR, J., GONZALEZ-LODEIRO, F., JABALOY, A., MALDONADO, A. and SCHEIDER, A.A. (1998). Models of magnetic and Bouguer gravity anomalies for the deep structure of the central Alboran Sea basin. Geo-Marine Letters, 18, 10-18.

GALINDO-ZALDÍVAR, J., CHALOUAN, A., AZZOUZ, O., SANZ DE GALDEANO, C., ANAHNAH, F., AMEZA, L., RUANO, P., PEDRERA, A., RUIZ-CONSTÁN, A., MARÍN-LECHADO, C., BENMAKHLOUF, M., LÓPEZ-GARRIDO, A.C., AHMAMOU, M., SAJI, R., ROLDÁN-GARCÍA, F.J., AKIL, M. and CHABLI, A. (2009). Are the seismological and geological observations of the Al Hoceima (Morocco, Rif) 2004 earthquake (M = 6.3) contradictory? Tectonophysics, 475, 59-67.

GALLART, J., DÍAZ, J., VIDAL, N. and DAÑOBEITIA, J.J. (1995). The base of the crust at the Betic-Alborán Sea transition: evidence for an abrupt structural variation from wide-angle ESCI data. Revista de la Sociedad Geológica de España, 8, 519-527.

GARCÍA, M., ALONSO, B., ERCILLA, G. and GRÀCIA, E. (2006). The tributary valley systems of the Almeria Canyon (Alboran Sea, SW Mediterranean): sedimentary architecture. Marine Geology, 226, 207-223.

GARCÍA, M. (2008). Post-rift sedimentary evolution of the central Bransfield Basin (Antartic Peninsula). Doctoral Thesis, University of Barcelona, Barcelona.

GARCIA-CASTELLANOS, D., FERNÀNDEZ, M. and TORNÉ, M. (2002). Modelling the evolution of the Guadalquivir foreland basin (souther Spain). Tectonics, 21, 9-1/9-17.

GARCIA-CASTELLANOS, D., ESTRADA, F., JIMÉNEZ-MUNT, I., GORINI, C., FERNÀNDEZ, M., VERGÉS, J. and DE VICENTE, R. (2009). Catastrophic flood of the Mediterranean after the Messinian salinity crisis. Nature, 462, 778-781 doi:710.1038/nature08555.

GARCÍA-DUEÑAS, V., MARTÍNEZ-MARTÍNEZ, J.M. and SOTO, J.I. (1988). Los Nevado-Filábrides, una pila de pliegue-mantos separados por zonas de cizalla. II Congreso Geológico de España. Simposios, 17-26.

GARCÍA-DUEÑAS, V., BALANYÁ, J.C. and MARTÍNEZ-MARTÍNEZ, J.M. (1992). Miocene extensional detachments in the outcropping basement of the northern Alboran basin (Betics) and their tectonic implications. Geo-Marine Letters, 12, 88-95.

GARCÍA-HERNÁNDEZ, M., LÓPEZ-GARRIDO, A.C., RIVAS, P., SANZ DE GALDEANO, C. and VERA, J.A. (1980). Mesozoic paleogeographic evolution on the external zones of the Betic cordillera. Geologie en Mijnbouw, 50, 155-168.

GARDNER, J.V., PRIOR, D.B. and FIELD , M.E. (1999). Humboldt Slide — a large shear-dominated retrogressive slope failure. Marine Geology, 154, 323-338.

GARZIGLIA, S.B., MIGEON, S.B., DUCASSOU, E., LONCKE, L. and MASCLE, J. (2008). Mass-transport deposits on the Rosetta province (NW Nile deep-sea turbidite system, Egyptian margin): Characteristics, distribution, and potential causal processes. Marine Geology, 250, 180-198.

GAUER, P., KVALSTAD, T.J., FORSBERG, C.F., BRYN, P. and BERG, K. (2005). The last phase of the Storegga Slide: simulation of retrogressive slide dynamics and comparison with slide-scar morphology. Marine and Petroleum Geology, 22, 171-178.

GELATI, R., MORATTI, G. and PAPANI, G. (2000). The Late Cenozoic sedimentary succession of the Taza-Guercif Basin, South Rifian Corridor, Morocco. Marine and Petroleum Geology, 17, 373-390.

GIERMAN, G., PFANNENSTIEL, M. and WIMMENAUER, W. (1968). Relation entre morphologie tectonique et volcanisme en mer d'Alboran (Mediterranée occidentale). Résultats

préliminaires de la campagne J. Charcot (1967). C. R. Somm. Soc. Geol. France, 4, 116-118.

GILL, R.C.O., APARICIO, A., EL AZZOUZI, M., HERNÁNDEZ, J., THIRLWALL, M.F., BOURGOIS, J. and MARRINER, G.F. (2004). Depleted arc volcanism in the Alborán Sea and shoshonitic volcanism in Morocco: geochemical and isotopic constraints on Neogene tectonic processes. Lithos, 78, 363-388.

GIRESSE, P., PAUC, H., DÉVERCHÈRE, J. and THE MARADJA SHIPBOARD SCIENTIFIC PARTY (2009). Sedimentary processes and origin of sediment gravity-flow deposits on the western Algerian margin during late Pleistocene and Holocene. Marine and Petroleum Geology, 26, 695-710.

GODOY, E., YAÑEZ, G. and VERA, E. (1999). Inversion of an Oligocene volcano-tectonic basin and uplifting of its superimposed Miocene magmatic arc in the Chilean Central Andes: first seismic and gravity evidences. Tectonophysics, 306, 217-236.

GOFFÉ, B., MICHARD, A., GARCÍA-DUEÑAS, V., GONZÁLEZ-LODEIRO, F., MONIÉ, P., CAMPOS, J., GALINDO-ZALDIVAR, J., JABALOY, A., MARTÍNEZ-MARTÍNEZ, J.M. and SIMANCAS, J.F. (1989). First evidence of high-pressure, low-tempurature metamorphism in the Alpujárride nappes, Betic Cordilleras (SE Spain). European Journal of Mineralogy, 1, 139-142.

GOVERS, R., MEIJER, P. and KRIJGSMAN, W. (2009). Regional isostatic response to Messinian Salinity Crisis events. Tectonophysics, 463, 109-129.

GRÀCIA, E., PALLÀS, R., SOTO, J.I., COMAS, M., MORENO, X., MASANA, E., SANTANACH, P., DIEZ, S., GARCÍA, M. and DAÑOBEITIA, J. (2006). Active faulting offshore SE Spain (Alboran Sea): Implications for earthquake hazard assessment in the Southern Iberian Margin. Earth and Planetary Science Letters, 241, 734-749.

GRADSTEIN, F.M., OGG, J.G., SMITH, A.G., AGTERGERG, F.P., BLEEKER, W., COOPER, R.A., DAVYDOV, V., GIBBARD, P., HINNOV, L.A., HOUSE, M.R., LOURENS, L., LUTERBACHER, H.-P., MCARTHUR, J., MELCHIN, M.J., ROBB, L.J., SHERGOLD, J., VILLENEUVE, M., WARDLAW, B.R., ALI, J., BRINKHUIS, H., HILGEN, F.J., HOOKER, J., HOWARTH, R.J., KNOLL, A.H., LASKAR, J., MONECHI, S., POWELL, J., PLUMB, K.A., RAFFI, I., RÖHL, U., SANFILIPPO, A., SCHMITZ, B., SHACKLETON, N.J., SHIELDS, G.A., STRAUSS, H., VAN DAM, J., VEIZER, J., VAN KOLFSCHOTEN, T. and WILSON, D., eds. (2004). A Geologic Time Scale 2004. Cambridge University Press, Cambridge.

GRIER, M.E., SALFITY, J.A. and ALLMENDINGER, R.W. (1991). Andean reactivation of the Cretaceous Salta rift, northwestern Argentina. Journal of South American Earth Sciences, 4, 351-372.

GRIMISON, N.L. and CHEN, W.P. (1986). The Azores-Gibraltar plate boundary: focal mechanisms, depths of earthquakes, and their tectonic implications. J. Geophys. Res., 91, 2029-2047.

GUERRA-MERCHÁN, A., SERRANO, F. and RAMALLO, D. (2004). Geomorphic and sedimentary Plio-Pleistocene evolution of the Nerja area (northern Alboran basin, Spain). Geomorphology, 60, 89-105.

GUTSCHER, M.A., MALOD, J., REHAULT, J.P., CONTRUCCI, I., KLINGELHOEFER, F., MENDES, V.L. and SPAKMAN, W. (2002). Evidence for active subduction beneath Gibraltar. Geology, 30, 1071-1074.

GUTSCHER, M.A. (2004). What caused the great Lisbon earthquake? Science, 305, 1247-1248.

GUTSCHER, M.A., BAPTISTA, M.A. and MIRANDA, J.M. (2006). The Gibraltar Arc seismogenic zone (part 2): Constraints on a shallow east dipping fault-plane source for the 1755 Lisbon earthquake provided by tsunami modeling and seismic intensity. Tectonophysics, 426, 153-166.

HAFLIDASON, H., SEJRUP, H.P., NYGÁRD, A., MIENERT, J., BRYN, P., LIEN, R., FORSBERG, C.F., BERG, K. and MASSON, D. (2004). The Soregga Slide: architecture, geometry and slide development. Marine Geology, 213, 201-234.

HANDY, M.R., BABIST, J., WAGNER, R., ROSENBERG, C. and KONRAD, M. (2005). Decoupling and its relation to strain partitioning in continental lithosphere: insight from the Periadriatic fault system (European Alps). Geological Society, London, Special Publications, 243, 249-276.

HANNE, D., WHITE, N. and LONERGAN, L. (2003). Subsidence Analyses from the Betic Cordillera, Southeast Spain. Basin Research, 15, 1-21.

HAQ, B.U., HARDEBOL, J. and VAIL, P.R. (1987). Chronology of fludtuating sea levels since the Triassic (250 Myr ago to present). Science, 235, 1156-1167.

HEBURN, G.W. and LA VIOLETTE, P.E. (1990).

Variations in the Structure of the Anticyclonic Gyres Found in the Alboran Sea. Journal of Geophysical Research, 95, 1599-1613.

HERNANDEZ, J. and BELLON, H. (1985). Chronologie K-Ar du volcanisme miocene du Rif oriental (Maroc): implications tectoniques et magmatique. Revue de Géographie Physique et de Géologie Dynamique, 26, 85-94.

HERNÁNDEZ, J., DE LAROUZIÈRE, F.D., BOLZE, J. and BORDET, P. (1987). Le magmatisme Néogène bético-rifain et le couloir de décrochement trans-Alborán. Bulletin de la Société Géologique de France, 8 III, 257-267.

HERNÁNDEZ, J., DE LAROUZIÈRE, F.D., BOLZE, J. and BORDET, P. (1987). Le magmatisme Néogène bético-rifain et le couloir de décrochement trans-Alborán. Bulletin de la Société Géologique de France, 8 III, 257-267.

HERNÁNDEZ-MOLINA, F.J., SOMOZA, L., REY, J. and POMAR, L. (1994). Late Pleistocene-Holocene sediments on the Spanish continental shelves: Model for very high resolution sequence stratigraphy. Marine Geology, 120, 129-174.

HERNÁNDEZ-MOLINA, F.J., SOMOZA, L. and LOBO, F.J. (2000). Seismic stratigraphy of the Gulf of Cádiz continental shelf: a model for Late Quaternary very high-resolution sequence stratigraphy and response to sea-level fall. In: Sedimentary Responses to Forced Regressions (Ed. by D. Hunt and R. L. G. Gawthorpe), 172, 329–361. Geological Society of London Special Publication.

HERNÁNDEZ-MOLINA, F.J., SOMOZA, L., VAZQUEZ, J.T., LOBO, F., FERNANDEZ-PUGA, M.C., LLAVE, E. and DIAZ-DEL RIO, V. (2002). Quaternary stratigraphic stacking patterns on the continental shelves of the southern Iberian Peninsula: their relationship with global climate and palaeoceanographic changes. Quaternary International, 92, 5-23.

HJELSTUEN, B.O., ELDHOLM, O. and FALEIDE, J.I. (2007). Recurrent Pleistocene mega-failures on the SW Barents Sea margin. Earth and Planetary Science Letters, 258, 605-618.

HODELL, D.A., ELMSTROM, K.M. and KENNETT, J.P. (1986). Latest Miocene benthic d18O changes, global ice volume, sea level and the 'Messinian salinity crisis'. Nature, 320, 411–414.

HODELL, D.A., J.H. CURTIS, F.J. SIERRO, AND M.E. RAYMO (2001). Correlation of Late Miocene to Early Pliocene sequences between the Mediterranean and North Atlantic. Paloceanography, 16(2), 164-178.

HOERNLE, K., VAN DEN BOGAARD, P., DUGGEN, S., MOCEK, B. and GARBE-SCHÖNBERG, D. (1999). Evidence for Miocene subduction beneath the Alboran Sea: 40AR/39AR dating and geochemistry of vocanic rocks from holes 977A and 978A1. In: Proceedings ODP, Scientific Results (Ed. by R. Zahn, M. C. Comas and A. Klaus), 161, 357-373. Ocean Drilling Program, College Station, TX.

HORVATH, F. and BERCKHEMER, H. (1982). Mediterranean backarc basins. In: Alpine Mediterranean geodynamics (Ed. by H. Berkhemer and K. Hsü), 141-173. American Geophysical Union, Washington.

HOUSEMAN, G.A., MCKENZIE, D.P. and MOLNAR, P. (1981). Convective instability of a thickened boundary layer and its relevance for the thermal evolution of continental convergent belts. J. Geophys. Res., 86, 6115-6132.

HOUSEMAN, G.A. and MOLNAR, P. (2001). Mechanisms of lithospheric rejuvenation associated with continental orogeny. In: Continental Reactivation and Reworking (Ed. by J. A. Miller, R. E. Holdsworth, I. S. Buick and M. Hand), 184, 13-38. Geol. Soc. London, Spe. Publ., London.

HSÜ, K.J., RYAN, W.B.F. and CITA, M.B. (1973). Late Miocene Desiccation of the Mediterranean. Nature, 242, 240-244.

IACCARINO, S.M. and BOSSIO, A. (1999). Paleoenvironment of Uppermost Messinian Sequences in the Western Mediterranean (Sites 974, 975, and 978). In: Proceedings of the Ocean Drilling Program, Scientific Results (Ed. by R. Zahn, M. C. Comas and A. Klaus), 161, 529-541. Ocean Drilling Program, College Station, TX.

IMBO, Y., DE BATIST, M., CANALS, M., PRIETO, M.J. and BARAZA, J. (2003). The Gebra Slide: a submarine slide on the Trinity Peninsula Margin, Antarctica. Marine Geology, 193, 235-232.

IRIBARREN, L., VERGÉS, J., FULLEA, J. and FERNÀNDEZ, M. (2003). Balance volumétrico de sedimentos neógenos y cuaternarios en el margen Sud-Ibérico: implicaciones tectónicas. Geotemas, 5, 129-132.

JABALOY, A., GALINDO-ZALDÍVAR, J. and GONZÁLEZ LODEIRO, F. (1993). The Alpujárride-Nevado-Filábride extensional shear zone, Betic Cordillera, SE Spain. Journal of Structural Geology, 15, 555-569.

JABALOY, A., GALINDO-ZALDÍVAR, J. and GONZÁLEZ LODEIRO, F. (1993). The Alpujárride-Nevado-Filábride extensional shear

zone, Betic Cordillera, SE Spain. Journal of Structural Geology, 15, 555-569.

JACKSON, J.A. (1980). Reactivation of basement faults and crustal shortening in orogenic belts. Nature, 283, 343-346.

JACKSON, C.A.L. and LARSEN, E. (2008). Temporal constraints on basin inversion provided by 3D seismic and well data: a case study from the South Viking Graben, offshore Norway. Basin Research, 20, 397-417.

JOHNSON, C. (1997). Resolving denudational histories in orogenic belts with apatite fission-track thermochronology and structural data: An example from southern Spain. Geology, 25, 623-626.

JOLIVET, L. and FACCENNA, C. (2000). Mediterranean extension and the Africa-Eurasia collision. Tectonics, 19, 1095-1106.

JOLIVET, L., AUGIER, R., ROBIN, C., SUC, J.-P. and ROUCHY, J.M. (2006). Lithospheric-scale geodynamic context of the Messinian salinity crisis. Sedimentary Geology, 188-189, 9-33.

JONES, R.R., HOLDSWORTH, R.E., CLEGG, P., MCCAFFREY, K. and TAVARNELLI, E. (2004). Inclined transpression. Journal of Structural Geology, 26, 1531-1548.

JURADO, M.J. and COMAS, M.C. (1992). Well Log interpretation and seismic character of the Cenozoic sequence in the northern Alboran Sea. Geo-Marine Letters, 12, 129-136.

JUST, J., HÜBSCHER, C., BETZLER, C., LÜDMANN, T. and REICHERTER, K. (2011). Erosion of continental margins in the Western Mediterranean due to sea-level stagnancy during the Messinian Salinity Crisis. Geo-Marine Letters, 31, 51-64.

KELLER, J.V.A., HALL, S.H., DART, C.J. and MCCLAY, K.R. (1995). The geometry and evolution of a transpresional strike-slip system - The Carboneras Fault, SE Spain. Journal of the Geological Society of London, 152, 339-351.

KELLER, E.A. and PINTER, N., eds. (2002). Active Tectonics, earthquakes, uplift and landscape. Prentice Hall, New Jersey.

KHEIDRI, L.H., BENABDELMOUNEN, M.S. and ZAZOUN, R.S. (2000). Evolution structurale de la partie orientale du bassin d'Alboran au cours du Néogène (offshore occidental, Algérie). In: African Continental Margin of the Mediterranean Sea, CIESM Workshop Series (Ed. by F. Briand), CIESM Workshop Series, 13, 40–43. CIESM, Djerba, Tunisia.

KHÉLIFI, N., SARNTHEIN, M., ANDERSEN, N., BLANZ, T., FRANK, M., GARBE-SCHÖNBERG, D., HALEY, B.A., STUMPF, R. and WEINELT, M. (2009). A major and long-term Pliocene intensification of the Mediterranean outflow, 3.5 -3.3 Ma ago. Geology, 37, 811-814.

KLITGORD, K.D. and SCHOUTEN, H. (1986). Plate kinematics of the central Atlantic. In: The Geology of North America (Ed. by P. R. Vogt and B. E. Tucholke), The western North Atlantic Region, decada of North American Geology, Series1, M, 351-377. Geol. Soc. America, Boulder, Colorado.

KOULALI, A., OUAZAR, D., TAHAYT, A., KING, R.W., VERNANT, P., REILINGER, R.E., MCCLUSKY, S., MOURABIT, T., DAVILA, J.M. and AMRAOUI, N. (2011). New GPS constraints on active deformation along the Africa-Iberia plate boundary. Earth and Planetary Science Letters, 308, 211-217.

KRIJGSMAN, W., HILGEN, F.J., RAFFI, I., SIERRO, F.J. and WILSON, D.S. (1999a). Chronology, causesand progression of the Mesinian salinity crisis. Letters to nature, 400, 652-655.

KRIJGSMAN, W., LANGEREIS, C.G., ZACHARIASSE, W.J., BOCCALETTI, M., MORATTI, G., GELATI, R., IACCARINO, S., PAPANI, G. and VILLA, G. (1999b). Late Neogene evolution of the Taza-Guercif Basin (Rifian Corridor, Morocco) and implications for the Messinian salinity crisis. Marine Geology, 153, 147-160.

KRIJGSMAN, W. (2002). The Mediterranean: Mare Nostrum of Earth sciences. Earth and Planetary Science Letters, 205, 1-12.

KVALSTAD, T.J., ANDRESEN, L., FORSBERG, C.F., BERG, K., BRYN, P. and WANGEN, M. (2005). The Storegga slide: evaluation of triggering sources and slide mechanics. Marine and Petroleum Geology, 22, 245-256.

LASTRAS, G., CANALS, M. and URGELES, R. (2003). Lessons from sea-floor and subsea-floor imagery of the BIG'95 debris flow scar and deposit. In: Submarine mass movements and their consequences (Ed. by J. Locat and J. Mienert), 425-431. Kluwer, Dordrecht.

LASTRAS, G., CANALS, M., URGELES, R., HUGHES-CLARKE, J.E. and ACOSTA, J. (2004). Shallow slides and pockmark swarms in the Eivissa Channel, western Mediterranean Sea. Sedimentology, 51, 837-850.

LASTRAS, G., CANALS, M., AMBLAS, D., IVANOV, M., DENNIELOU, B., DROZ, L., AKHMETZHANOV, A. and PARTY, T.-L.S.S.

(2006). Eivissa slides, western Mediterranean Sea: morphology and processes Geo-Marine Letters, 26, 225-233.

LASTRAS, G., CANALS, M., AMBLAS, D., IVANOV, M., DENNIELOU, B., DROZ, L., AKHMETZHANOV, A. and PARTY, T.-L.S.S. (2006). Eivissa slides, western Mediterranean Sea: morphology and processes Geo-Marine Letters, 26, 225-233.

LEBLANC, D. and OLIVIER, P. (1984). Role of strike-slip faults in the Betic-Rifian orogeny. Tectonophysics, 101, 345-355.

LO IACONO, C., GRÀCIA, E., DIEZ, S., BOZZANO, G., MORENO, X., DAÑOBEITIA, J. and ALONSO, B. (2008). Seafloor characterization and backscatter variability of the Almería Margin (Alboran Sea, SW Mediterranean) based on high-resolution acoustic data. Marine Geology, 250, 1-18.

LOBO, F.J., HERNÁNDEZ-MOLINA, F.J., SOMOZA, L. and DÍAZ DEL RÍO, V. (1999). Paleoenvironments, relative sea level changes and tectonic influence on the Quaternary seismic units of the Huelva continental shelf (Gulf of Cadiz, Southwestern Iberian Peninsula). In: Oceanography of the Iberian Continental Margin (Ed. by F. J. Hernández Molina and J. T. Vázquez), 15(1–4), 161–180. Boletin Instituto Español de Oceanografia.

LOBO, F.J., MALDONADO, A., HERNANDEZ-MOLINA, F.J., FERNANDEZ-SALAS, L.M., ERCILLA, G. and ALONSO, B. (2008). Growth patterns of a proximal terrigenous margin offshore the Guadalfeo River, northern Alboran Sea (SW Mediterranean Sea): glacio-eustatic control and disturbing tectonic factors. Marine Geophysical Researches, 29, 195-216.

LOGET, N., VAN DEN DRIESSCHE, J. and DAVY, P. (2005). How did the Messinian Salinity Crisis end? Terranova, 17, 414-419.

LONCKE, L., GAULLIER, V., MASCLE, J., VENDEVILLE, B. and CAMERA, L. (2006). The Nile deep-sea fan: An example of interacting sedimentation, salt tectonics, and inherited subsalt paleotopographic features. Marine and Petroleum Geology, 23, 297-315.

LONERGAN, L., PLATT, J.P. and GALLAGHER, L. (1994). The Internal-External zone boundary in the eastern Betic Cordillera, SE Spain: Reply. Journal of Geophysical Research, 18, 525-527.

LONERGAN, L. and PLATT, J.P. (1995). The Maláguide-Alpujárride boundary: a major extensional contact in the internal zone of the eastern Betic Cordillera, SE Spain. Journal of Structural Geology, 17, 1655-1671.

LONERGAN, L. and WHITE, N. (1997). Origin of the Betic-Rif mountain belt. Tectonics, 16, 504-522.

LÓPEZ CASADO, C., SANZ DE GALDEANO, C., MOLINA PALACIOS, S. and HENARES ROMERO, J. (2001). The structure of the Alboran Sea: interpretation from seismological and geological data. Tectonophysics, 338, 79-95.

LÓPEZ GARRIDO, A.C. and SANZ DE GALDEANO, C. (2000). Las fallas tortonienses a cuaternarias entre Granada y la costa: el límite occidental del Nevado-Filábride y de las unidades alpujárrides inferiores. Rev. Soc. Geol. Esp., 13, 519-528.

MAESTRO-GONZÁLEZ, A., BÁRCENAS, P., VÁZQUEZ, T. and DÍAZ-DEL-RÍO, V. (2008). The role of basement inheritance faults in the recent fracture system of the inner shelf around Alboran Island, Western Mediterranean. Geo-Marine Letters, 28, 53-64.

MAGARA, K. (1976). Water Expulsion from Clastic Sediments during Compaction_Directions and Volumes. The American Association of Petroleum Geologists Bulletin, 60, 543-553.

MALDONADO, A., CAMPILLO, A.C., MAUFFRET, A., ALONSO, B., WOODISDE, J. and CAMPOS, J. (1992). Alboran Sea Late Cenozoic tectonic and Stratigraphic evolution. Geo-Marine Letters, 12, 179-186.

MARSAGLIA, K.M., LATTER, K.K. and CLINE, V. (1999). Sand provenance in the Alboran and Tyrrhenian basin. In: Proc. ODP, Sci. Results (Ed. by R. Zahn, M. C. Comas and A. Klaus), 161, 37-56. Ocean Drilling Program, College Station, TX.

MARTIN, J.M., BRAGA, J.C. and BETZLER, C. (2003). Late Neogene-Recent uplift of the Cabo de Gata volcanic province, Almeria, SE Spain. Geomorphology, 50, 27-42.

MARTÍN, J. and BRAGA, J.C. (1994). Messinian events in the Sorbas Basin in southeastern Spain and their implications in the recent history of the Mediterranean. Sedimentary Geology, 90, 257-268.

MARTÍN ALGARRA, A. (1987). Evolución geológica alpina del contacto entre las Zonas Internas y las Zonas Externas de la Cordillera Bética (sector centro-occidental). Doctoral Thesis, Universidad de Granada.

MARTINEZ DEL OLMO, W. (1984). Un ejemplo actual y reciente de abanico turbidítico profundo:

Columbretes fan. I Congreso Español de Geología.

MARTÍNEZ DEL OLMO, W., GARCÍA MALLO, J., LERET VERDU, G., SERRANO OÑATE, A. and SUAREZ ALBA, J. (1984). Modelo tectosedimentario del Bajo Guadalquivir. I Congreso Español de Geología, Segovia, 199-213.

MARTÍNEZ-DÍAZ, J.J. (1998). Neotectónica y tectónica activa del Sector Centro-Occidental de la Región de Murcia y Sur de Almeria (Cordillera Bética-España). Doctoral Thesis, Universidad Complutense de Madrid, Madrid.

MARTÍNEZ-DÍAZ, J.J. (2002). Stress field variation related to fault reactivation in a reverse oblique-slip fault: the Alhama de Murcia fault, Betic Cordillera, Spain. Tectonophysics, 356, 291-305.

MARTÍNEZ-GARCÍA, P. and SOTO, J.I. (2006). Valores de subsidencia reciente (Plioceno-Cuaternario) en el Mar de Alborán mediante análisis de "backstripping". Geogaceta, 40, 63-66.

MARTÍNEZ-GARCÍA, P., COMAS, M.C., SOTO, J.I., LONERGAN, L. and PÉREZ-HERNÁNDEZ, S. (2009). Deslizamientos submarinos recientes en la Cresta de Alborán (mar de Alborán). Geogaceta, 47, 89-92.

MARTÍNEZ-GARCÍA, P., SOTO, J.I. and COMAS, M. (2011). Recent structures in the Alboran Ridge and Yusuf fault zones based on swath bathymetry and sub-bottom profiling: evidence of active tectonics. Geo-Marine Letters, 31, 16-39.

MARTÍNEZ-GARCÍA, P., COMAS, M., SOTO, J.I., LONERGAN, L. and WATTS, A.B. (submitted for publication). Strike-slip tectonics and basin inversion in the Western Mediterranean: the Post-Messinian evolution of the Alboran Sea. Basin Research.

MARTÍNEZ-MARTÍNEZ, J.M. and AZAÑÓN, J.M. (1997). Mode of extensional tectonics in the southeastern Betics (SE Spain): Implications for the tectonic evolution of the peri-Alborán orogenic system. Tectonics, 16, 205-225.

MARTÍNEZ-MARTÍNEZ, J.M., SOTO, J.I. and BALANYÁ, J.C. (2002). Orthogonal folding of extensional detachements: Structure and origin of the Sierra Nevada elongated dome (Betics, SE Spain). Tectonics, 21, 1-21.

MARTINI, E. (1971). Standard Tertiary and Quaternary calcareous nannoplankton zonation. Proceeding on the Second International Conference on Planktonic Microfossils, Tecnosci.

MARTÍN-SERRANO, A. (2005). Mapa geomorfológico de España y del margen continental a escala 1:1.000.000, Instituto Geológico y Minero de España. Madrid.

MASANA, E., MARTÍNEZ-DÍAZ, J.J., HERNÁNDEZ-ENRILE, P. and SANTANACH, P. (2004). The Alhama de Murcia fault (SE Spain), a seismogenic fault in a diffuse plate boundary: seismotectonic implications for the Ibero-Magrebian region. Journal of Geophysical Research, 109, B01301, doi:01310.01029/02002JB 002359.

MAUFFRET, A., EL-ROBRINI, M. and GENNESSEAUX, M. (1987). Indice de la compression récente en mer Méditerranée: un bassin losangique sur la marge nor-algérienne. Bull. Soc. Géol. France, 8, 1195-1206.

MAUFFRET, A., MALDONADO, A. and CAMPILLO, A.C. (1992). Tectonic framework of the eastern Alboran and western Alboran basins, western Mediterranean. Geo-Marine Letters, 12, 104-110.

MAUFFRET, A., FRIZON-DE-LAMOTTE, D., LALLEMANT, S., GORINI, C. and MAILLARD, A. (2004). E–W opening of the Algerian Basin (Western Mediterranean). Terra Nova, 16, 257-264.

MAUFFRET, A. (2007). The Northwestern (Maghreb) boundary of the Nubia (Africa) Plate. Tectonophysics, 429, 21-44.

MAUFFRET, A., AMMAR, A., GORINI, C. and JABOUR, H. (2007). The Alboran Sea (Western Mediterranean) revisited with a view from the Moroccan Margin. Terra Nova, 19, 195-203.

MAURY, R.C., FOURCADE, S., COULON, C., EL AZZOUZI, M., BELLON, H., COUTELLE, A., OUABADI, A., SEMROUND, B., MEGARTSI, M., COTTEN, J., BELANTEUR, O., LOUNI-HACINI, A., PIQUÉ, A., CAPDEVILA, R., HERNÁNDEZ, J. and RÉHAULT, J.P. (2000). Post-collisional Neogene magmatism of the Mediterranean Maghreb margin: a consequence of slab breakoff. 331, 159-173.

MAZZOLI, S. and HELMAN, M. (1994). Neogene patterns of relative plate motion for Africa-Europe: some implications for recent central Mediterranean tectonics. International Journal of Earth Sciences, 83, 464-468.

MCADOO, B.G., PRATSON, L.F. and ORANGE, D.L. (2000). Submarine landslide geomorphology, US continental slope. Marine Geology, 169, 103-136.

MCCLAY, K.R. and ANDERTON, R. (1989). Inversion of the Kechika Trough, Northeastern British Columbia, Canada. Geological Society,

London, Special Publications, 44, 235-257.

MCCULLOCH, M.T. and DECKKER, P.D. (1989). Sr isotope constraints on the Mediterranean environment at the end of the Messinian salinity crisis. Nature, 342, 62-65.

MCKENZIE, D. and JACKSON, J.A. (1983). The relationship between strain rates, crustal thickening, paleomagnetism, finite strain and fault movements within a deforming zone. Earth and Planetary Science Letters, 65, 182-202.

MEDIALDEA, T., SURIÑACH, E., VEGAS, R., BANDA, E. and ANSORGE, J. (1986). Crustal structure under the western end of the Betic Cordillera (Spain). Annales Geophysicae, 4, 345-355.

MEDIMAP-GROUP (2005). Morpho-bathymetry of the Mediterranean Sea, Editions Ifremer. ISBN 2-84433-147-5 (France), CIESM /Ifremer Spetial Publication, Atlases and Maps, two maps at 1/ 2000000.

MEDIMAP-GROUP (2008). Morpho-bathymetry of the Mediterranean Sea, Editions Ifremer. Plouzané (France), CIESM /Ifremer Spetial Publication, Atlases and Maps, two maps at 1/ 2000000.

MEDINA, F. (1995). Present-day state of stress in northern Morocco from focal mechanism analysis. Journal of Structural Geology, 17, 1035-1046.

MEZCUA, J. and RUEDA, J. (1997). Seismological evidence for a delamination process in the lithosphere under the Alboran Sea. Geophys. J. Int., 129, F1-F8.

MILLER, K.G., KOMINZ, M.A., BROWNING, J.V., WRIGHT, J.D., MOUNTAIN, G.S., KATZ, M.E., SUGARMAN, P.J., CRAMER, B.S., CHISTIE-BLICK, N. and PEKAR, S.F. (2005). The Phanerozoic Record of Global Sea-Level Change. Science, 310, 1293 (2005) DOI: 1210.1126/ science.1116412.

MILLIOT, C. (1999). Circulation in the Western Mediterranean Sea. Journal of Marine Systems, 20, 423-442.

MOLNAR, P. and HOUSEMAN, G.A. (2004). The effects of buoyant crust on the gravitational instability of thickened mantle lithosphere at zones of intracontinental convergence. Geophysical Journal International, 158, 1134-1150.

MONTENAT, C., OTT D'ESTEVOU, P. and MASSE, P. (1987). Tectonic-Sedimentary characters of the Betic Neogene Basins evolving in a crustal transcurrent shear zone (SE Spain). Bull. Centres Rech. Explor. Prod. Elf-Aquitaine, 11, 1-22.

MONTENAT, C., OTT D'ESTEVOU, P. and DE LA CHAPELLE, G. (1990). Le Bassin de Nijar-Carboneras et le Couloir du Bas-Andarax. In: Les Bassins Néogènes du Domaine Bétique Orientale (Espagne) (Ed. by C. Montenat), Doc. et Trav. IGAL, 12-13, 129-164. Institut Geologique Albert de Lapparent, Paris.

MORALES, J., SERRANO, I., JABALOY, A., GALINDO-ZALDÍVAR, J., ZHAO, D., TORCAL, F., VIDAL, F. and GONZÁLEZ LODEIRO, F. (1999). Active continental subduction beneath the Betic Cordillera and the Alborán Sea. Geology, 27, 735-738.

MORATTI, G., PICCARDI, L., VANNUCCI, G., BELARDINELLI, M.E., DAHMANI, M., BENDKIK, A. and CHENAKEB, M. (2003). The 1755 "Meknes" earthquake (Morocco): field data and geodynamic implications. Journal of Geodynamics, 36, 305-322.

MOREL, J.L. (1989). Etats de contrainte et cinematique de la chaine rifaine (Maroc) du Tortonien a l'actuel. . Geodin. Acta, 3, 238–294.

MOREL, J.L. and MEGHRAOUI, M. (1996). Goringe-Alboran-Tell tectonic zone: A transpression system along the Africa-Eurasia plate boundary. Geology, 24, 755-758.

MORLEY, C.K. (1992). Notes on Neogene basin history of the western Alboran Sea and its implications for the tectonic evolution of the Rif-Betic orogenic belt. Journal of African Earth Sciences, 14, 57-66.

MULDER, C.J. and PARRY, G.R. (1977). Late Tertiary evolution of the Alboran Sea at the eastern entrance of the Straits of Gibraltar. International Symposium Structural History of the Mediterranean Basins., Split (Yugoslavia), Editions Technip, Paris.

MUÑOZ, A., BALLESTEROS, M., MONTOYA, I., RIVERA, J., ACOSTA, J. and UCHUPI, E. (2008). Alboran basin, Southern Spain. Part I: Geomorphology. Marine and Petroleum Geology, 25, 59-73.

NEGREDO, A.M., BIRD, P., SANZ DE GALDEANO, C. and BUFORN, E. (2002). Neotectonic modeling of the Ibero-Maghrebian region. Journal of Geophysical Research, 107, B11, 2292, doi:2210.1029/2001JB000743.

NOCQUET, J.M. and CALAIS, E. (2004). Geodetic measurements of crustal deformation in the Western Mediterranean and Europe. Pure and Applied Geophysics, 161, 661-681.

NORMAN, S.E. and CHASE, C.G. (1986). Uplift

of the shores of the western Mediterranean due to Messinian desiccation and flexural isostasy. Nature, 322, 450-451.

PARRILLA, G., KINDER, T.H. and PRELLER, R.H. (1986). Deep and Intermediate Mediterranean Water in the western Alboran Sea. Deep Sea Research, 33, 55-88.

PÉREZ BELZUZ, F., ALONSO, B. and ERCILLA, G. (1997). History of mud diapirism and triggering mechanisms in the Western Alboran Sea. Tectonophysics, 282, 399-423.

PÈROUSE, E., VERNANT, P., CHÉRY, J., REILINGER, R. and MCCLUSKY, S. (2010). Active surface deformation and sub-lithospheric processes in the western Mediterranean constrained by numerical models. Geology, 38, 823-826.

PLATT, J.P. (1986). Dynamics of orogenic wedges and the uplift of high-pressure metamorphic rocks. Geological Society of America Bulletin, 97, 1037-1053.

PLATT, J.P. and VISSERS, R.L.M. (1989). Extensional collapse of thickened continental lithosphere: A working hypothesis for the Alboran Sea and Gibraltar Arc. Geology, 17, 540-543.

PLATT, J.P., SOTO, J.I., COMAS, M.C. and LEG 161 SHIPBOARD, S. (1996). Decompression and high-temperature-low-pressure metamorphism in the exhumed floor of an extensional basin, Alboran Sea, western Mediterranean. Geology, 24, 447-450.

PLATT, J.P., SOTO, J.I., WHITEHOUSE, M.J., HURFORD, A.J. and KELLEY, S.P. (1998). Thermal evolution, rate of exhumation, and tectonic significance of metamorphic rocks from the floor of the Alboran extensional basin, Western Mediterranean. Tectonics, 17, 671-689.

PLATT, J.P., ALLERTON, S., KIRKER, A., MANDEVILLE, C., MAYFIELD, A., PLATZMAN, E.S. and RIMI, A. (2003). The ultimate arc: Differential displacement, oroclinal bending, and vertical axis rotation in the External Betic-Rif arc. Tectonics, 22, 1017-1046.

POLYAK, B.G., FERNÀNDEZ, M., KHUTORSKOY, M.D., SOTO, J.I., BASOV, I.A., COMAS, M.C., KHAIN, V.Y., ALONSO, B., AGAPOVA, G.V., MAZURAVA, I.S., NEGREDO, A., TOCHITSKY, V.O., DE LA LINDE, J., BOGDANOV, N.A. and BANDA, E. (1996). Heat flow in the Alboran Sea, western Mediterranean. Tectonophysics, 263, 191-218.

POUPON, A. and GAYMARD, R. (1970). The evaluation of clay content from logs. Transaction of the Society of Professional Well Log Analysts. 11th Logging Symposium.

PUGA, E., NIETO, J.M. and DÍAZ DE FEDERICO, A. (2000). Contrasting P-T paths in eclogites of the Betic ophiolitic association, Mulhacén Complex, Southeastern Spain. Canadian Mineralogist, 38, 1137-1161.

REHAULT, J.P., BOILLOT, G. and MAUFFRET, A. (1984). The Western Mediterranean Basin geological evolution. Marine Geology, 55, 447-477.

REICHERTER, K.R., JABALOY, A., GALINDO-ZALDÍVAR, J., RUANO, P., BECKER-HEIDMANN, P., MORALES, J., REISS, S. and GONZÁLEZ-LODEIRO, F. (2003). Repeated palaeoseismic activity of the Ventas de Zafarraya fault (S Spain) and its relation with the 1884 Andalusian earthquake. Intertantional Journal of Earth Sciences, 92, 912–922. DOI 910.1007/s00531-00003-00366-00533.

REICHERTER, K. and HÜBSCHER, C. (2007). Evidence for a seafloor rupture of the Carboneras Fault Zone (Southern Spain): Relation to the 1522 Almería earthquake? Journal of Seismology, 11, 15-26.

REILLY, W.I., FREDRICH, G., HEIN, G.W., LANDAU, H., ALMAZÁN, J.L. and CATURLA, J.L. (1992). Geodetic determination of crustal deformation across the Strait of Gibraltar. Geophysical Journal International, 111, 391-398.

RIMI, A. (1999). Mantle heat-flow and geotherms for the main geologic domains in Morocco. International Journal of Earth Sciences, 88, 458-466.

RIO, M.-H., POULAIN, P.-M., PASCUAL, A., MAURI, E., LARNICOL, G. and SANTOLERI, R. (2007). A Mean Dynamic Topogrphy ot the Mediterranean Sea computed for altimetric data, in-situ measurements and a general circulation model. Journal of Marine Systems, 65, 484-508.

RITCHIE, J.D., JOHNSON, H., QUINN, M.F. and GATLIFF, R.W. (2008). The effects of Cenozoic compression within the Faroe-Shetland Basin and adjacent areas. Geological Society, London, Special Publications, 306, 121-136.

RODRÍGUEZ-FERNÁNDEZ, J. and SANZ DE GALDEANO, C. (1992). Onshore Neogene Stratigraphy in the North of the Alboran Sea (Betic Internal Zones): Paleogeographic Implications. Geo-Marine Letters, 12, 123-128.

RODRÍGUEZ-FERNÁNDEZ, J. and MARTÍN-PENELA, J. (1993). Neogene Evolution of the

campo de dalias and the surrounding Offshore Areas - (Northeastern Alboran Sea). Geodinamica Acta, 6, 1-16.

RODRÍGUEZ-FERNÁNDEZ, J., COMAS, M.C., SORÍA, J., MARTÍN-PÉREZ, J.A. and SOTO, J.I. (1999). The sedimentary record of the Alboran Basin: an attempt at sedimentary sequence correlation and subsidence analysis. In: Proceedings of the Ocean Drilling Program, Scientific Results (Ed. by R. Zahn, M. C. Comas and A. Klaus), 161, 69-76. Ocean Drilling Program, College Station, TX.

RODRÍGUEZ-FERNÁNDEZ, J. and SANZ DE GALDEANO, C. (2006). Late orogenic intramontane basin development: the Granada basin, Betics (southern Spain). Basin Research, 18, 85-102.

ROSENBAUM, G., LISTER, G.S. and DUBOZ, C. (2002). Relative motions of Africa, Iberia and Europe during Alpine orogeny. Tectonophysics, 359, 117-129.

ROYDEN, L.H. (1993). Evolution of retreating subduction boundaries formed during continental collision. Tectonics, 12, 629-638.

RUIZ-CONSTÁN, A., GALINDO-ZALDÍVAR, J., PEDRERA, A., ARZATE, J.A., POUS, J., ANAHNAH, F., HEISE, W., MONTEIRO SANTOS, F.A. and C., M.-L. (2010). Deep deformation pattern from electrical anisotropy in an arched orogen (Betic Cordillera, western Mediterranean). Geology, 38, 731–734.

RYAN, W.B.F., HSÜ, K.J., CITA, M.B., DUMITRICA, P., LORT, J., MAYNC, W., NESTEROFF, W.D., PAUTOT, G., STRDUER, H. and WEZAE, F.C. (1973). Western Alboran Basin-Site 121. In: Initial Reports of the Deep Sea Drilling Project. (Ed. by W. B. F. Ryan and K. J. e. a. Hsü), 13, 43-89. Govt. Printing Office, Washington D.C.

SÁNCHEZ-GÓMEZ, M., AZAÑÓN, J.M., GARCÍA-DUEÑAS, V. and SOTO, J.I. (1999). Correlation between the metamorphic rocks recovered from Site 976 and the Alpujarride rocks of the Western Betics. In: Proceedings of the Ocean Drilling Program, Scientific Results (Ed. by Z. Klaus, M. C. Comas and A. Klaus), 161, 307-318. Ocean Drilling Program, College Station, TX.

SANZ DE GALDEANO, C. (1990). Geologic evolution of the Betic Cordilleras in the Western Mediterranean, Miocene to the Present. Tectonophysics, 172, 107-119.

SANZ DE GALDEANO, C. and VERA, J. (1992). Stratigraphic record and paleogeographical context of the Neogene basins in the Betic Cordillera Spain. Basin Research, 4, 21:36.

SANZ DE GALDEANO, C., LÓPEZ CASADO, C., DELGADO, J. and PEINADO, M.A. (1995). Shallow seismicity and active faults in the Betic Cordillera: A preliminary approach to seismic sources associated with specific faults. Tectonophysics, 248, 293-302.

SANZ DE GALDEANO, C., ANDREO, B. and LÓPEZ-GARRIDO, A.C. (2001). Comment on the paper “Late exhumation stages of the Alpujarride Complex (western Betic Cordilleras, Spain):new thermochronological and structural data on Los Reales and Ojen nappes”by Marc Sosson, Anne-Claire Morillon, Jacques Bourgois, Gilbert Féraud, Gérard Poupeau, Pierre Saint-Marc. Tectonophysics, 331, 413-417.

SAUTKIN, A., TALUKDER, A.R., COMAS, M.C., SOTO, J.I. and ALEKSEEV, A. (2003). Mud volcanoes in the Alboran Sea: evidence from micropaleontological and geophysical data. Marine Geology, 195, 237-261.

SCHETTINO, A. and TURCO, E. (2006). Plate Kinematics of the Western Mediterranean region during the Oligocene and Early Miocene. Geophysical Journal International Tectonics and geodynamics, 166, 1398-1423.

SCHOORL, J.M. and VELDKAMP, A. (2003). Late Cenozoic landscape development and its tectonic implications for the Guadalhorce valley near Álora (Southern Spain). Geomorphology, 50, 43-57.

SCLATER, J.G. and CHRISTIE, P.A.F. (1980). Continental stretching: an explanation of the post-Mid-Cretaceous subsidence of the central North Sea Basin. Journal of Geophysical Research, 85, 3711-3739.

SEBER, D., BARAZANGI, M., IBENBRAHIM, A. and DEMNATI, A. (1996). Geophysical evidence for lithospheric delamination beneath the Alboran Sea and Rif-Betics mountains. Nature, 379, 785-790.

SELLA, G.F., DIXON, T.H. and MAO, A. (2002). REVEL: A model for Recent plate velocities from space geodesy. Journal of Geophysical Research, 107, B4, 2081, doi: 2010.1029/2000JB000033.

SERPELLONI, E., VANNUCCI, G., PONDRELLI, S., ARGNANI, A., CASULA, G., ANZIDEI, M., BALDI, P. and GASPERINI, P. (2007). Kinematics of the Western Africa-Eurasia plate boundary from focal mechanisms and GPS data. Geophysiscs Journal International, 169, 1180-1200.

SHERIFF, R.E. and GELDART, L.P. (1995). Exploration Seismology (2nd edition). Cambridge

University Press, Cambridge.

SHIPBOARD SCIENTIFIC PARTY (1996). Explanatory notes (Ed. by R. Zahn, M. C. Comas, A. Klaus and e. al.), 161, 21-49. Ocean Drilling Program, College Station, TX.

SIERRO, F.J., GONZÁLEZ DELGADO, J.A., DABRIO, C.J., FLORES, C.J. and CIVIS, J. (1996). Late Neogene depositional sequences in the foreland basin of Guadalquivir (SW Spain). In: Tertiary basins of Spain, the stratigraphic record of crustal kinematics (Ed. by P. F. Friend and C. J. Dabrio), 339-345. Cambridge University Press.

SIESSER, W.G. and DE KAENEL, E.P. (1999). Neogene calcareous nannofossils: western mediterranean biostratigraphy and paleoclimatology. In: Proceedings of the Ocean Drilling Program, Scientific Results (Ed. by R. Zahn, M. C. Comas and A. Klaus), 161, 223-237. Ocean Drilling Program, College Station, TX.

SOTO, J.I., COMAS, M.C. and DE LA LINDE, J. (1996). Espesor de sedimentos en la cuenca de Alborán mediante una conversión sísmica corregida. Geogaceta (Geological Society of Spain), 20, 382-385.

SOTO, J.I. and PLATT, J.P. (1999). Petrological and Structural Evolution of High-Grade Metamorphic Rocks from the Floor of the Alboran Sea Basin, Western Mediterranean. Journal of Petrology, 40, 21-60.

SOTO, J.I. and MANZANO, F.J. (2002). Geometría y cinemática de fallas recientes en e margen septentrional del Mar de Alborán (Sector de Maro, Provincia de Málaga). Geogaceta, 31, 139-142.

SOTO, J.I., FERNÁNDEZ-IBÁÑEZ, F., FERNÁNDEZ, M. and GARCÍA-CASCO, A. (2008). Thermal structure of the crust in the Gibraltar Arc: Influence on active tectonics in the western Mediterranean. Geochemistry, Geophysics and Geosystems, 9, Q10011, doi:10010.11029/12008GC002061.

SPAKMAN, W., VAN-DER-LEE, S. and VAN-DER-HILST, R. (1993). Travel-time tomography of the European-Mediterranean mantle down to 1400 km. Physics of the Earth and Planetary Interiors, 79, 3-74.

SPAKMAN, W. and WORTEL, M.J.R. (2004). A tomographic view on western Mediterranean geodynamics. In: The TRANSMED Atlas - The Mediterranean region from crust to mantle. (Ed. by W. Cavazza, F. Roure, W. Spakman, G. M. Stampfli and P. Ziegler), 31-52. Springer, Berlin Heidelberg.

SPROVIERI, M., D'ALCALA, M.R., MANTA, D.S., BELLANCA, A., NERI, R., LIRER, F., TABERNER, C., PUEYO, J.J. and SAMMARTINO, S. (2008). Ba/Ca evolution in water masses of the Mediterranean late Neogene. Paleoceanography, 23, PA3205, doi:3210.1029/2007pa001469.

SRIVASTAVA, S.P., ROEST, W.R., KOVACS, L.C., OAKEY, G., LEVESQUE, S., VERHOEF, J. and MACNAB, R. (1990). Motion of Iberia since the Late Jurassic: Results from detailed aeromagnetic measurements in the Newfoundland Basin. Tectonophysics, 184, 229-260.

STICH, D., ALGUACIL, G. and MORALES, J. (2001). The relative location of multiplets in the vicinity of the Western Almeria (southern Spain) earthquake series of 1993-1994. Geophysical Journal International, 146, 801-812.

STICH, D., AMMON, C.J. and MORALES, J. (2003a). Moment tensor solutions for small and moderate earthquakes in the Ibero-Maghreb region. Journal of Geophysical Research, 108, 2148, doi2110.1029/2002JB002057.

STICH, D., BATLLO, J., MORALES, J., MACIA, R. and DINEVA, S. (2003b). Source parameters of the Mw=6.1, 1910 Adra earthquake (southern Spain). Geophysical Journal International, 155, 539-546.

STICH, D., MANCILLA, D., BAUMONT, D. and MORALES, J. (2005). Source analysis of the Mw 6.3 2004 Al Hoceima earthquake (Morocco) using regional apparent source time functions. Journal of Geophysical Research, 110, B06306, doi:06310.01029/02004JB003366.

STICH, D., SERPELLONI, E., MANCILLA, F.D. and MORALES, J. (2006). Kinematics of the Iberia-Maghreb plate contact from seismic moment tensors and GPS observations. Tectonophysics, 426, 295-317.

STRZERZYNSKI, P., DÉVERCHÈRE, J., CATTANEO, A., DOMZIG, A., YELLES, K., DE LÉPINAY, B.M., BABONNEAU, N. and BOUDIAF, A. (2010). Tectonic inheritance and Pliocene-Pleistocene inversion of the Algerian margin around Algiers: Insights from multibeam and seismic reflection data. Tectonics, 29, doi:10.1029/2009TC002547.

SULTAN, N., VOISSET, M., MARSSET, B., MARSSET, T., CAUQUIL, E. and COLLIAT, J.L. (2007). Potential role of compressional structures in generating submarine slope failures in the Niger Delta. Marine Geology, 237, 169-190.

SYNLOAKIS, C.E., LUI, P., GARRIER, G. and YEH,

H. (1997). Tsunamigenic sea-floor defromation. Science, 278, 598-600.

TALUKDER, A.R., COMAS, M. and SOTO, J.I. (2003). Pliocene to Recent mud diapirsm and related mud volcanoes in the Alboran Sea (Western Mediterranean). In: Mobilisation of subsurface sediments (Ed. by A. Maltman, P. V. Rensbergen, C. Morley and J. Cartwright.). Geol. Soc. London, Spe. Publ., London.

TALUKDER, M.A.R. (2003). La Provincia Diapírica de lodo en la Cuenca Oeste del Mar de Alborán: Estructuras, Génesis y Evolución. Doctoral Thesis, University of Granada, Granada.

TAMAKI, K. and HONZA, E. (1985). Incipient subduction and deduction along the eastern margin of the Japan Sea. Tectonophysics, 119, 381-406.

TANDON, K., LORENZO, J.M. and DE LA LINDE RUBIO, J. (1998). Timing of rifting in the Alboran Sea basin-correlation of borehole (ODP Leg 161 and Andalucia A-1) to seismic reflection data: implications for basin formation. Marine Geology, 144, 275-294.

TIKOFF, B. and TEYSSIER, C. (1994). Strain modeling of displacement-field partitioning in transpressional orogens. Journal of Structural Geology, 16, 1575-1588.

TORNÉ, M. and BANDA, E. (1992). Crustal thinning from the Betic cordillera to the Alboran Sea. Geo-Marine Letters, 12, 76-81.

TORNÉ, M., FERNÀNDEZ, M., COMAS, M.C. and SOTO, J.I. (2000). Lithospheric structure beneath the Alboran Basin: results from 3D gravity modeling and tectonic relevance. Journal of Geophysical Research, 105, 3209-3228.

TORRES-ROLDAN, R., POLI, G. and PECCERILLO, A. (1986). An early Miocene arc-tholeiitic magmatic dike event from the Alboran Sea — Evidence for precollisional subduction and back-arc crustal extension in the westernmost Mediterranean. Geologische Rundschau, 75, 219-234.

TRICARDINI, F. and ARGNANI, A. (1990). Gela Submarine Slide: A Major Basin-Wide Event in the Plio-Quaternary Foredepp of Sicily. Geo-Mar. lett., 10, 13-21.

TUBIA, J.M. and GIL IBARGUCHI, J.L. (1991). Eclogites of the Ojen nappe: a record of subduction in the Alpujárride complex (Betic Cordilleras, southern Spain). Journal of the Geological Society of London, 148, 801-805.

TURNER, S.P., PLATT, J.P., GEORGE, R.M.M., KELLEY, S.P., PEARSON, D.G. and NOWELL, G.M. (1999). Magmatism Associated with Orogenic Collapse of the Betic-Alboran Domain. SE Spain. Journal of Petrology, 40, 1011-1036.

UDÍAS, A. and BUFORN, E. (1991). Regional stresses along the Eurasia-Africa plate boudary deriven from focal mechanisms of large earthquakes. Pure and Applied Geophysics, 136, 433-448.

URGELES, R., CAMERLENGHI, A., GARCIA-CASTELLANOS, D., DE MOL, B., GARCÉS, M., VERGÉS, J., HASLAM, I. and HARDMAN, M. (2011). New constraints on the Messinian sealevel drawdown from 3D seismic data of the Ebro Margin, western Mediterranean. Basin Research, 23, 123-145.

VAIL, P.R., MITCHUM, R.M.L., TODD, R.G., WIDMMIER, J.M., THOMPSON, S., SANGREE, J.B. and BUBB, J.N. (1977). Seismic stratigraphy and global changes in sea level. In: Seimic stratigraphy: its applications to hydrocarbon exploration. (Ed. by C. E. Payton), 26, 49-212. Am. Ass. Petrol Geol. Mem.

VARGAS-YÁÑEZ, M., PLAZA, F., GARCÍA-LAFUENTE, J., SARHAN, T., VARGAS, J.M. and VÉLEZ-BELCHI, P. (2002). About seasonal variability of the Alboran Sea circulation. Journal of Marine Systems, 35, 229-248.

VÁZQUEZ, J. (2001). Estructura del margen septentrional del Mar de Alborán, Universidad Complutense de Madrid, Madrid.

VERA, J.A. (1983). Las Zonas Externas de las Cordilleras Béticas. In: Geología de España, Libro Jubilar J. M. Ríos (Ed. by I.G.M.E.), II, 218-251. I.G.M.E., Madrid.

VERA, J.A. (2000). El Terciario de la Cordillera Bética: estado actual de conocimientos. Revista de la Sociedad Geológica de España, 13, 345-373.

VERA, J.A. (2001). Evolution of the South Iberian continental margin. In: PeriThethys Memoir: Peri Tethyan Rif/wrench basins and passive margins (Ed. by P. A. Ziegler, W. Cavazza and A. F. H. Robertson), 109-143. Mémoires du Muséum national d'histoire naturelle, Paris.

VERNANT, P., FADIL, A., MOURABIT, T., OUAZAR, D., KOULALI, A., DAVILA, J.M., GARATE, J., MCCLUSKY, S. and REILINGER, R. (2010). Geodetic constraints on active tectonics of the Western Mediterranean: Implications for the kinematics and dynamics of the Nubia-Eurasia plate boundary zone. Journal of Geodynamics, 49, 123-129.

VIDAL, F. (1986). Sismotectónica de la región Béticas-Mar de Alborán. Doctoral Thesis,

Universidad de Granada, Granada.

VIDAL, L., BICKERT, T., WEFER, G. and RÖHL, U. (2002). Late Miocene stable isotope stratigraphy of SE Atlantic ODP Site 1085: Relation to Messinian events. Marine Geology, 180, 71-85.

VIUDEZ, A., TINTORÉ, J. and HANEY, R. (1996). Circulation in the Alboran Sea as determined by quasi-synoptic hydrographic observations: Part I. Three-dimensional structure of the two anticiclonic gyres. Journal of Physical Oceanography, 26, 684-705.

WATSON, J.A. and JOHSON, G.L. (1968). Mediterranean diapiric structures. Bull Am Assoc Petrol Geol, 52, 2247-2249.

WATTS, A.B., PLATT, J.P. and BUHL, P. (1993). Tectonic evolution of the Alboran Sea basin. Basin Research, 5, 153-177.

WATTS, A.B. (2001). Isostasy and Flexure of the Lithosphere. Cambridge University Press, Cambridge.

WEIJERMARS, R. (1987). The Palomares brittle-ductile Shear Zone of southern Spain. Journal of Structural Geology, 9, 139-158.

WILDI, W., NOLD, M. and UTTINGER, J. (1977). La Dorsale calcaire entre Tetouan et Assifane (Rif interne, Maroc). Eclogae Geologicae Helvetiae, 72, 371-415.

WILDI, W. (1983). Les chames tello-rifaines (Algérie, Maroc, Tunisie): structure. stratigraphie et évolution du Trias au Miocéne. Revue de Géographie Physique et de Géologie Dynamique, 24, 201-297.

WILLET, A. (1997). Marine geophysical investigations of the Alboran Sea. Doctoral Thesis, Oxford University, Oxford.

WILLINGSHOFER, E. and SOKOUTIS, D. (2009). Decoupling along plate boundaries: Key variable controlling the mode of deformation and the geometry of collisional mountain belts. Geology, 37, 39-42.

WOODSIDE, J.M. and MALDONADO, A. (1992). Styles of compressional neotectonics in the Eastern Alboran Sea. Geo-Marine Letters, 12, 111-116.

WOODSIDE, J., IVANOV, M.K., KOELEWIJN, R., ZELDENRUST, I. and SHASHKIN, P. (2000). Alboran Basin (diapiric province): Sidescan sonar data. In: Multidisciplinary study of geological processes on the northeast Atlantic and western Mediterranean margins: Preliminary results of geological and geophysical investigations during the TTR-9 cruise of R/V Professor Logachev (Ed. by N. H. Kenyon, M. K. Ivanov, A. M. Akhmetzhanov and G. G. Akhmanov), Intergovernmental Oceanographic Commission, Technical Series, 56, 82-84. UNESCO.

WORKING GROUP FOR THE DEEP SOUNDING IN THE ALBORAN SEA 1974 (1978). Crustal seismic profiles in the Alboran Sea - Preliminary results. Pure and Applied Geophysics, 116, 167-180.

WORTEL, M.J.R. and SPAKMAN, W. (2000). Subduction and Slab Detachment in the Mediterranean-Carpathian Region. Science, 290, 1910-1917.

YELLES, A., DOMZIG, A., DÉVERCHÈRE, J., BRACÈNE, R., MERCIER DE LÉPINAY, B., STRZERZYNSKI, P., BERTRAND, G., BOUDIAF, A., WINTER, T., KHERROUBI, A., LE ROY, P. and DJELLIT, H. (2009). Plio-Quaternary reactivation of the Neogene margin off NW Algiers, Algeria: The Khayr al Din bank. Tectonophysics, 475, 98-116.

YILMAZ, Ö. (1987). Seismic data processing. Society of Exploration Geophysicists, Tulsa, OK.

YOUNG, J.R. (1991). A Quaternary nannofossil range chart. Newsletter of the International Nannoplankton Association, 13, 14-17.

ZAZO, C., GOY, J.L., DABRIO, C.J., BARDAJI, T., HILLAIRE-MARCEL, C., GHALEB, B., GONZALEZ-DELGADO, J.A. and SOLER, V. (2003). Pleistocene raised marine terraces of the Spanish Mediterranean and Atlantic coasts: records of coastal uplift, sea-level highstands and climate changes. Marine Geology, 194, 103-133.

ZECK, H.P., MONIE, P. and VILLA, I.M. (1992). Very high-rates of cooling and uplift in the Alpine belt of the Betic Cordilleras, southern Spain - Reply. Geology, 20, 1053-1054.

ZECK, H.P. (1997). Mantle peridotites outlining the Gibraltar Arc - centrifugal extensional allochthons derived from the earlier Alpine, westward subducted nappe pile. Tectonophysics, 281, 195-207.

ZECK, H.P. (1999). Alpine plate kinematics in the western Mediterrranean: a westward-directed subduction regime followed by slab roll-back and slab detachment. In: The Mediterranean Basins: Tertiary Extensions within the Alpine Orogen (Ed. by B. Durand, L. Jolivet, F. Horvath and M. Séranne), 134, 109-120. Geological Society of London Special Publications, London.

ZECK, H.P. and WILLIAMS, I.S. (2002). Inherited and Magmatic Zircon from Neogene Hoyazo

Cordierite Dacite, SE Spain - Anatectic Source Rock Provenance and Magmatic Evolution. Journal of Petrology, 43, 1089-1104.

ZIZI, M. (2002). Triassic-Jurassic estensional systems and their Neogene reactivation in Northern Morocco: the rides prerifaines and Guercif basin. Doctoral Thesis, University of Rabat, Rabat.

ZOUHRI, L. (2002). The aquifer of the Mamora Basin, Morocco: geometry and groundwater flow. Journal of African Earth Sciences, 32, 837-850.

ZOUHRI, L. (2004). Structural evolution of the southern Rif Cordillera (Morocco): tectonics and synsedimentary fault processes. Geological Journal, 39, 81-93.

9. Appendixes

Structural analysis and Recent tectonics in the central Alboran Sea

Published in ***Trabajos de Geología*** *(2010), 30, 44-48.*
(contribution to YORSGET-2008 meeting)

Pedro Martínez-García[1], Juan I. Soto[1] and Menchu Comas[1]

[1] Instituto Andaluz de Ciencias de la Tierra (CSIC and University of Granada), Facultad de Ciencias, Campus Fuentenueva s/n, 18002 Granada (Spain). Email: matez@ugr.es.

Abstract

We analyze the distribution and character of recent deformations in the Alboran Ridge and neighbouring areas in the Alboran Sea (within the Gibraltar Arc System, in the Western Mediterranean). Shallow structure has been analyzed integrating different geophysical data sets, as multibeam swath-bathymetry and sub-bottom profiling and comparing with deeper sections shown in multichannel seismic profiles. We explore relationships between upper-crustal structures and shallow seismicity, to decipher the position and nature of active fault segments. Pliocene to recent uplift of the Alboran Ridge has been produced by reverse to strike-slip faulting along NE-SW trending fault-systems that show transpressive character. Major faults bounding the Ridge change gradually their direction from NE-SW to NW-SE, and connect with the transtensional Yusuf fault system, which includes the Yusuf Ridge and Basin. Towards the West the Ridge is affected by NNE-SSW trending folds, associated with high-angle faults at depth. Those structures define a seismogenic, left-lateral fault-zone connected to the South with the Al Hoceima seismic swarm.

Keywords: Alboran Ridge, active fault, strike-slip tectonics, seismic profiles.

Introduction and setting

Structural analysis of marine survey data can be used also to investigate the geometry, nature, and tectonic evolution of structures in submerged regions. In this way, we have characterized the recent structure in the major tectonic lineament of the Alboran Sea Basin, the Alboran Ridge and its connection with the Yusuf fault zone, by integrating different geophysical data from marine surveys. The main objective of this work is to reconstruct the structure of faults and folds that deform the most recent sedimentary cover, commonly up to the seafloor. A detailed structural map have been accomplished for the studied region, comparing finally the geometry, type, and age of the faults with the distribution and character of the seismicity in the upper crust. Fault structures and earthquake information have been linked to reconstruct the present-day stress field, which is compared with the overall actual convergence between the African and Eurasian plates.

The Alboran Sea Basin is a back-arc basin developed behind the Gibraltar Arc, formed by the Betic and Rif mountain ranges (Figure 1, inset map). The basin originated from crustal thinning, rifting, and basin subsidence, which started during the early Miocene (~18 Ma) and resumed by the late Miocene (~8-9 Ma). Miocene extensional tectonics resulted in half-graben structures that accommodate deep depocenters of Miocene sediments, particularly in the West Alboran Basin and in the Málaga Basin (Figure 1). Subsequent contractive tectonics, producing folding, high-angle faulting and tectonic inversion, occurred from the Late Miocene (Late Tortonian-Messinian, ~5-8 Ma) until Recent (Comas *et al*., 1992, 1999; Watts *et al*., 1993; Chalouan *et al*., 1997; Mauffret *et al*., 2004, 2007). Contractive tectonics results in roughly N-S shortening of the whole basin, and conditioned the present day structure of the Alboran Basin (Figure 1).

In the Alboran Basin we investigate the Alboran Ridge and the Yusuf fault zones (Figure 1). The Alboran Ridge represents the major, bathymetric high of the Alboran Sea. With a general SW-NE trend, the Ridge continues to the SW in the Xauen Bank (Figure 1). To the East, the Ridge connects with the NW-SE Yusuf escarpment that in turns prologues with the Yusuf Ridge and the Yusuf Basin. These morphological lineaments in the basin seem to be related to major fault systems. The Alboran Ridge corresponds actually with a left-lateral transpressive fault zone, whereas the Yusuf Ridge and Basin have been interpreted as resulting from a right-lateral, transtensive fault system (Comas *et al.*, 1999; Álvarez-Marrón, 1999; Fernández-Ibáñez *et al*., 2007).

Dataset and methods

The present study integrates data sets acquired during different geophysical. Multi-channel seismic profiles (MCS), processed until 7 sec (twtt) depth, acquired during the TECALB (2000) and MARSIBAL-06 (2006) cruises onboard the R/V BIO HESPÉRIDES, have been analyzed to better understand deep structures around and across the Alboran Ridge. Single channel seismic and very high-resolution acoustic sub-bottom profiling (TOPAS: Topographic PArametric Sonar, 0.5-6 kHz frequency), as well as swath-bathymetry (SIMRAD) data were acquired during these surveys. Complementary datasets from the ALBA cruise (R/V BIO HESPÉRIDES, 1992) and swath-bathymetry from the IFREMER-CIESM compilation (MediMap Group, 2005) were merged in an area of the central Alboran Sea to accomplish a bathymetry mosaic of 14,400 km^2 where our structural

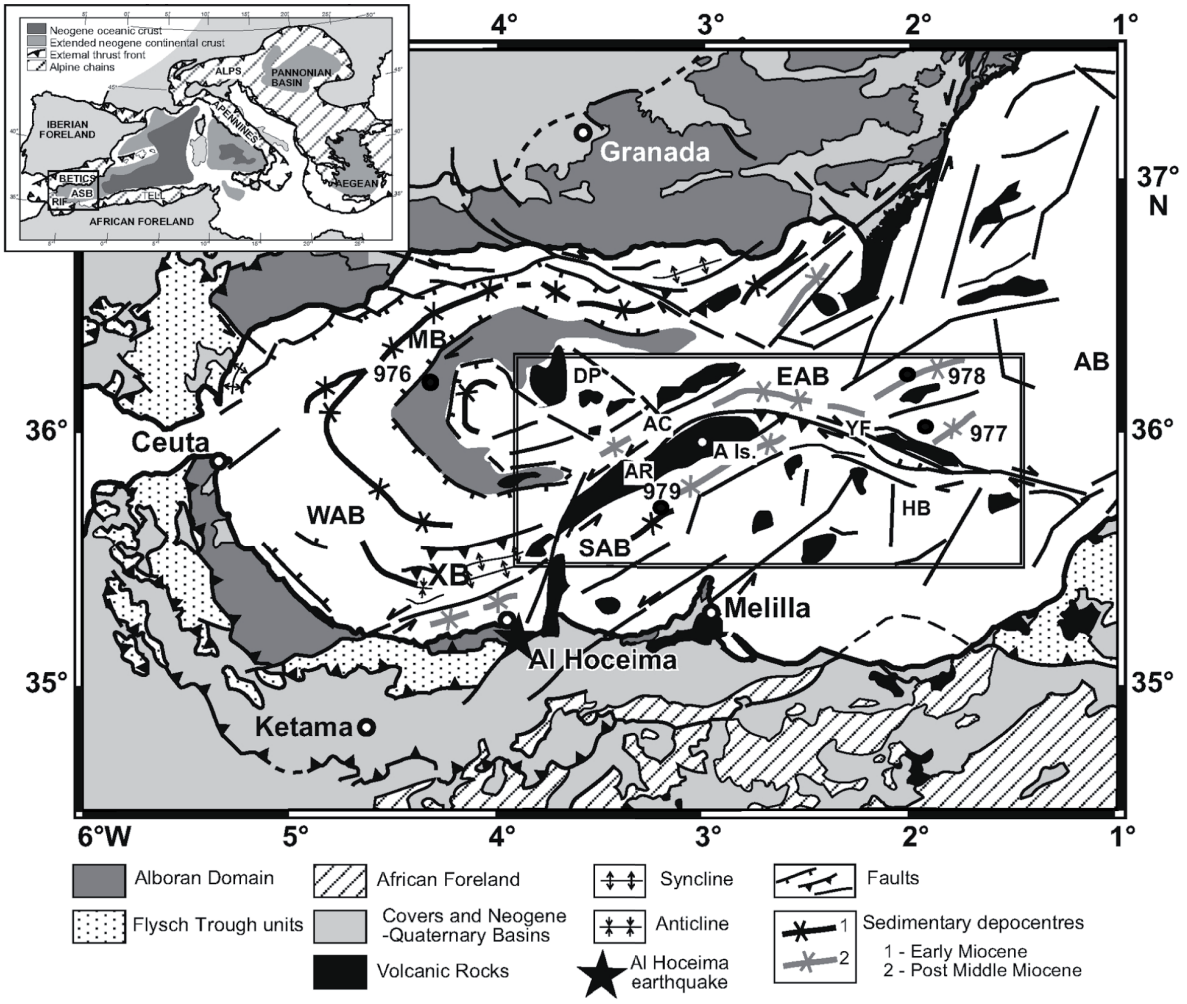

Figure 1. Structural map of the Alboran Sea Basin and surrounding areas (modified from Comas et al., 1999). The studied area is shown with a rectangle. Position of ODP Leg 161 Sites (976 to 979) is noted. Al Hoceima earthquake taken form Akoglu et al., 2006. AB: Algerian Basin; AC: Alboran Chanel; A Is: Alboran Island; AR: Alboran Ridge; ASB: Alboran Sea Basin; DB: Djibouti Bank; EAB: East Alboran Basin; HB: Habibas Basin; MB: Málaga Basin; SAB: South Alboran Basin; YS: Yusuf fault zone; WAB: West Alboran Basin; XB: Xauen Bank.

analysis has been carried out.

Seismic interpretation and depth conversion of seismic profiles have been accomplished using well data (Figure 1). This study considers logging information from several ODP sites drilled in the Alboran Sea during ODP Leg 161 (Comas *et al*., 1996).

Deep structure

The structure beneath the Alboran Sea, as shows in figure 1, results from the interpretation of a dense grid of MCS profiles including commercial and academic ones (Comas *et al*., 1999).

The Alboran Ridge, the major NE-SW trending seamount of the Alboran Basin, is imaged in MCS as a large, complex antiform bounded by strike-slip to reverse fault zones. The resulting

structure encompasses uplift, subsidiary folding, and basin inversion. Sediments in the Ridge consist of Plio-Quaternary deposits laying on top the volcanic acoustic basement. Tilted strata at the antiform limbs show significant angular unconformities indicating discontinuous uplift of the Alboran Ridge along the Plio-Quaternary.

The northern escarpment of the Alboran Ridge, adjacent to the Alboran Channel, corresponds to a major left-lateral strike-slip fault zone at depth. At the eastern end of the Ridge the master fault shows high-angle dip and a reverse displacement, whereas towards the west left-lateral strike-slip components dominate. The southern escarpment of the Ridge, flanking the South Alboran Basin, corresponds to a near vertical fault zone at depth (Figure 1).

The Yusuf fault zone to the east, is a dextral NE-SW fault system, includes two master normal faults that produce local transtension and forming the Yusuf pull-apart basin. The temporal and spatial relationship between the Alboran-Ridge and the Yusuf fault zones remains still unclear.

Post-Messinian deformation affects from the basement up to the Pliocene-to-Holocene sedimentary sequences. However, folding and strike-slip faulting seems to have started from the late Miocene.

Shallow structure

Recent tectonic processes in the Alboran Sea Basin are mainly responsible of its complex seafloor physiography. Shallow structures in the central Alboran Sea, around the Alboran Ridge have been analyzed and mapped (Figure 2). This map shows fault and folds affecting the seafloor and the uppermost hundreds of meters beneath the seafloor (< 200 m). Mean structural directions are shown by sectors in table 1. Shallow structures are open folds associated with high-angle faults, which produce seafloor escarpments. High-resolution profiles provide oblique seismic sections showing apparent dips from predominant structures and we identify fault traces and fold culminations in the bathymetry. Moreover, depth conversions have been done using velocity profiles from ODP well logging.

Recent deformation is heterogeneously distributed and show different structural styles (Figure 2). Shallow structures in the Alboran Ridge are open NE folds and parallel, high angle faults (av. 65º±01). Fold axes are tilted towards the SW and ENE at both sides of the shallow platform surrounding the Alboran Island. Toward the SW (Figure 2), these structures are cut by an oblique system (NE-SW; av. 30º±01) formed by a fold-and-fault system that continues northward to the Djibouti Bank. The northern escarpment of the Alboran Ridge represents a recent reverse fault affecting the seafloor. To the east this fault turns to have a NW-SE orientation (av., from 93º±08 to 102-122º±01). The Yusuf fault zone shows different segments with lateral tips in relay, accommodated by "en-echelon" folds, suggesting transtensive deformation.

Seismicity and active faults

The distribution and character of the shallow-crustal seimicity (Figure 2) have been used to

constrain the location and nature of active faults. Hypocenter distribution, magnitude, and focal mechanisms allow determining the position and kinematics of active fault segments. A set of 13 focal mechanisms has been compiled for this study (Figure 2). Focal mechanisms in the Alboran Ridge mostly correspond to strike-slip (left lateral) to reverse faults. In the East Alboran Basin and the Yusuf region, the scarce focal mechanisms show normal faulting with an important strike-slip component.

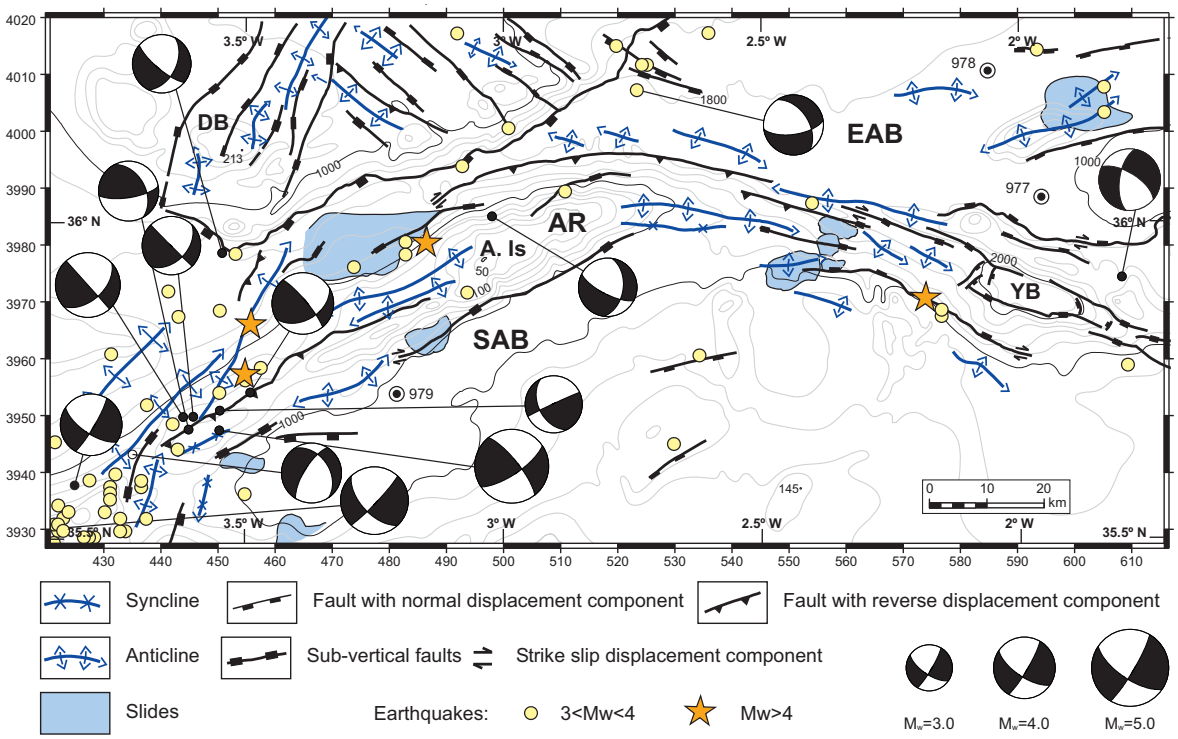

Figure 2. Shallow structure and crustal seismicity in the central Alboran Sea. Seismic events (M_w > 3) from the USGS (period 1979-2007) and focal mechanisms from moment tensor inversion (Instituto Andaluz de Geofísica database). Position of ODP Leg 161 Sites (977 to 979) is shown. Bathymetric contour lines (in m) from GEBCO-97 (IOC-IHO). A Is: Alboran Island; AR: Alboran Ridge; DB: Djibouti Bank; EAB: East Alboran Basin; SAB: South Alboran Basin; YB: Yusuf Basin.

Sector	Folds		Faults	
	Mean orientations (1)	N	Mean orientations 1)	N
Djibouti Bank Region	018 ± 6º & 132 ±9º	19	024 ± 4º & 126 ±3º	40
Western Alborán Ridge	030 ±4.5º	25	024 ± 9º	6
Central Alborán Ridge	065 ±1º	7	064 ± 1.5º	9
Eastern Alborán Ridge	093 ± 5º	8	092 ± 13º	4
Yusuf Escarpment	122 ± 3º	7	103 ± 6º	27
East Alborán Basin	090 ±5º	11	092 ±4º	16

Table 1. Faults and folds orientation in the studied region. (1) Mean vector (azimuth) is accompanied by the 95% value of the distribution. N: number of measurements.

Slumps and mass wasting structures identified, probably derive from unstable seafloor escarpments conditioned by active faulting. Shallow crustal seismicity occurs along the Alboran Ridge and Yusuf region. In the western part of the Ridge, a seismic swarm connects southward with the Al Hoceima seismic series. We propose the existence of an active NNE-SSW; left lateral fault zone crosscutting obliquely the Alboran Ridge (Figures 1 and 2).

Present-day stress field in the region has been calculated integrating the shallow-fault pattern and focal-mechanism data. The resultant S_{Hmax} (av. azimuth 011º) in the studied region shows a significant (~55º) clockwise rotation of the local stress field, with respect to the regional orientation imposed by the ongoing plate convergence between Africa and Eurasia (*e.g.*, DeMets *et al*., 1994). This sort of rotation reinforced the interpretation that active faults crosscutting the Alboran Ridge represent segments of a weak, strike-slip (left-lateral) fault zone.

Conclusions

As a whole, seafloor morphology and seismic images from the studied region corroborates that the actual structural pattern in the Alboran Basin is mainly conditioned by post-Messinian, roughly N-S contractive tectonics. Two main conjugated, NE-SW (Yusuf fault zone) and NW-SE (Alboran Ridge fault zone) strike-slip fault systems and associated folding were developed. These faults accomplished for substantial WSW-ENE elongation of the Alboran Sea Basin and contribute to the westward escape of the Gibraltar Arc front (Fernández-Ibáñez *et al*., 2007, and references therein).

Seafloor deformations connect with deeper structures. Superficial fold systems are linked with sub-vertical faults with seismogenic segments. The relationships between faults and seismicity suggest that present-day deformation is concentrated along a NNE-SSW fault-zone crosscutting the Alboran Ridge and connecting southward with the Al Hoceima seismic swarm. This discovered fault zone may therefore represent an area of potential seismic hazard in the Alboran Sea.

Pliocene to Quaternary subsidence rates in the Alboran Sea from backstripping analysis

Valores de subsidencia reciente (Plioceno-Cuaternario) en el Mar de Alborán mediante análisis de "backstripping"

Published in ***Geogaceta*** *(2006), 40, 63-66.*

Pedro Martínez-García[1] and Juan I. Soto[1]

[1] Instituto Andaluz de Ciencias de la Tierra (CSIC-Universidad de Granada) y Dpto. Geodinámica. Facultad de Ciencias, Campus Fuentenueva s/n. 18002 Granada. e-mail: matez@ugr.es, jsoto@ugr.es.

Abstract

A backstripping analysis is presented for the different scientific ODP wells in the Alboran Sea (Leg 161, Holes 976B, 977A, 978A, and 979A). The study has been performed for the complete Pliocene-to-Quaternary sedimentary sequence, based on the detailed paleontological dataset available in these wells. Logging data together with in-situ determinations of porosity and density have been fitted to obtain robust estimates of the appropriate variables to perform the backstripping study (*e.g.*, porosity, density). The total subsidence pattern shows a remarkable coincidence in all the wells (Y=310-355 m) equivalent to a subsidence rate of 0.06-0.07 mm/y for the last 5.1 Ma. In regions where a significant intra-Pliocene hiatus (2.2-5.0 Ma) occurred, like the Site 976-basement high in the West Alboran Basin or the Alboran Ridge, we infer the existence of a major tectonic pulse with high subsidence rates (2.2-5.0 mm/y) that diminishes towards the Quaternary (0.07-0.11 mm/y). According to these results, the estimated stretching factor (β) for this basin is 1.35-1.42.

Keywords: *porosity, backstripping analysis, subsidence rates, Alboran Basin.*

Introducción

El Mar de Alborán (en el Mediterráneo occidental) se sitúa en la parte interna de un cinturón orogénico arqueado que comprende las Cordilleras Béticas y el Rif conectadas a través del Arco de Gibraltar (Figura 1). Se trata de la más occidental de las cadenas mediterráneas alpinas, resultantes de la colisión entre las placas Euroasiática y Africana. La región conecta hacia el Este con la Cuenca Argelino-Balear, cuyo substrato puede ser de naturaleza oceánica (Comas *et al.*, 1999).

Aunque el origen de esta cuenca y sus relaciones con los procesos tectónicos que durante el Neógeno configuraron las cadenas circundantes son ampliamente debatidos, el relleno sedimentario y su estructuración tectónica (*e.g.*, Comas *et al.*, 1992, 1999; Watts *et al.*, 1993; Chalouan *et al.*, 1997), junto con la modelización térmica de la evolución de su substrato metamórfico (Platt *et al.*, 1998), demuestran que la Cuenca del Mar de Alborán se originó en el Mioceno inferior (*ca.* post-27 Ma) por un proceso de adelgazamiento litosférico severo. Los procesos tectónicos que ocurrieron durante el Plio-Cuaternario, son en gran medida, los responsables de la fisiografía del fondo marino actual y de la posición de la línea de costas (Comas *et al.*, 1992, 1999). En este sentido, conocer y cuantificar la subsidencia (con sus componentes tectónica y térmica) durante este periodo aportará datos de gran interés para comprender la evolución más reciente de esta región.

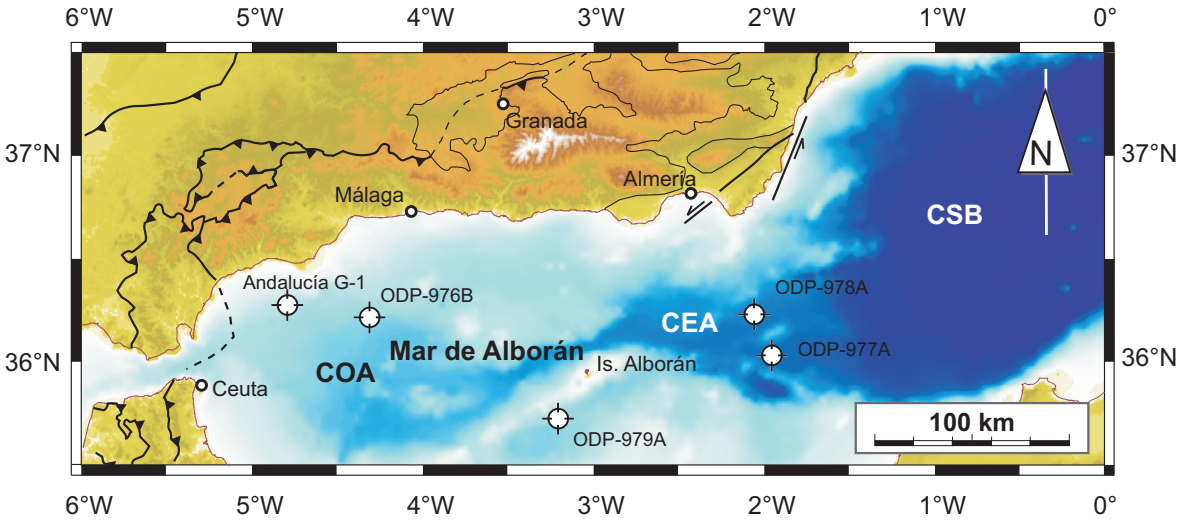

Figura 1. Mapa geológico simplificado y localización de los pozos estudiados mediante "*backstripping*" en el Mar de Alborán. COA: Cuenca Oeste de Alborán; CEA: Cuenca Este de Alborán; CSB; Cuenca Sur Balear.

Figure 1. *Simplified geological and location of the studied wells in Alboran Sea (western Mediterranean) where backstripping analysis has been carried out. COA: West Alboran Basin; CEA: East Alboran Basin, and CSB: South Balearic Basin.*

Análisis de "backstripping" en Alborán

En la región existen análisis de subsidencia previos, tanto en el Mar de Alborán como en algunas de las cuencas Neógenas emergidas (en Béticas) realizados mediante la técnica de "*backstripping*" (*e.g.*, Cloething *et al.*, 1992; Docherty y Banda, 1992, 1995; Watts *et al.*, 1993; Rodríguez-Fernández *et al.*, 1999; Hanne *et al.*, 2003). Todos estos estudios se han realizado en pozos profundos aplicando siempre valores estándar de porosidad y densidad de sedimentos, tomados normalmente de la

tabulación según litologías propuesta por Sclater y Christie (1980). En nuestro caso el análisis de subsidencia se sustenta en la obtención de estos parámetros según un estudio de las diagrafías ("*logging*") de los pozos analizados (*e.g*. Figura 2). Se han seleccionado aquellos pozos profundos del Mar de Alborán en los que para la sucesión sedimentaria de edad Plio-Cuaternaria (post-Messiniense, *i.e.* post-reflector M) existen datos precisos de parámetros físicos medidos in-situ y/o mediante diagrafías (*e.g*., Jurado y Comas, 1992), y en los que se tiene un buen control paleontológico. El estudio que aquí presentamos se sustenta en el análisis de la subsidencia reciente (durante el Plioceno y Cuaternario, *i.e.* últimos 5,1 Ma) en los pozos de ODP-Sites 976, 977, 978 y 979 (Leg 161; Comas *et al.*, 1996, 1999) (Figura 1).

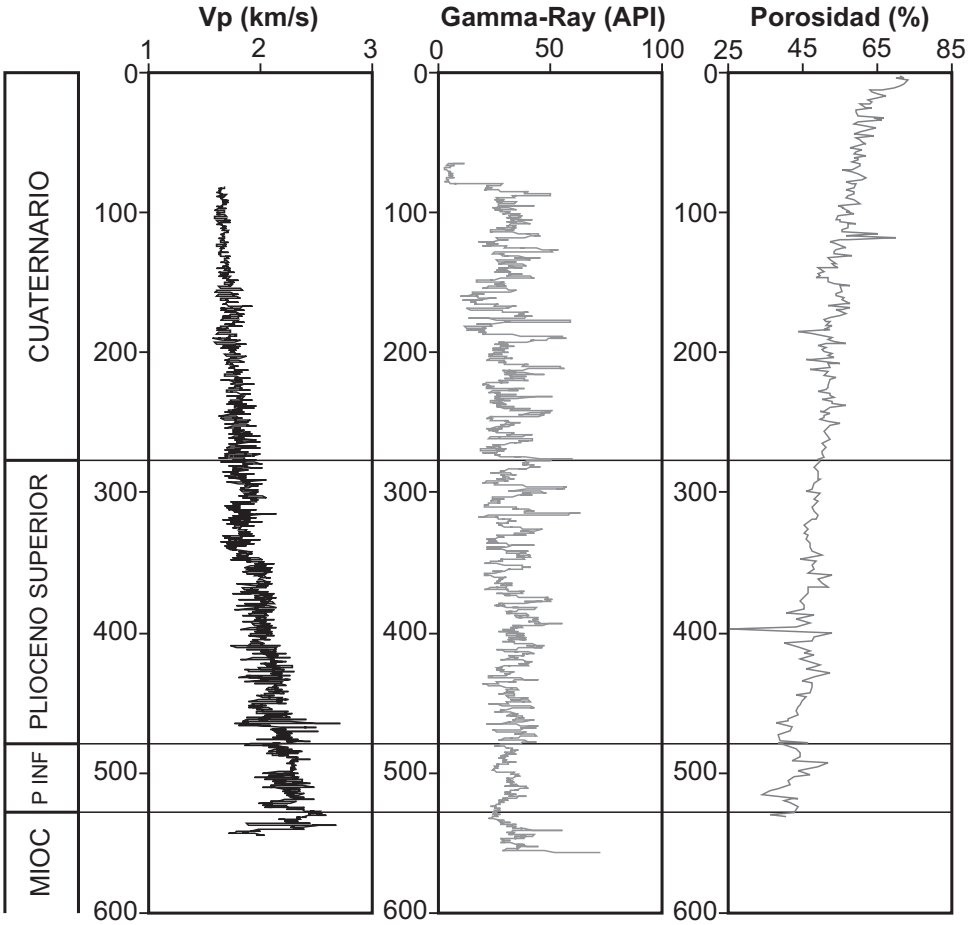

Figura 2. Datos de diagrafías en el pozo científico de ODP, Hole 977A (Leg 161), utilizados para ajustar los datos de porosidad (ϕ) con los de V_p (en km s^{-1}) y "*gamma-ray*" (en API).

Figure 2. *Logging data from the ODP scientific well Hole 977A (Leg 161) used to fit the in-situ porosity estimates (ϕ) with V_p (km s^{-1}) and gamma-ray (in API units) values.*

Además la curva de subsidencia durante el Plioceno-Cuaternario (post 5,1 Ma) obtenida mediante "*backstripping*" se compara con los valores de subsidencia térmica calculados según el proceso descrito por McKenzie (1978), estimándose finalmente la magnitud del adelgazamiento (expresado según el factor de adelgazamiento, β) asociado a los procesos de "*rifting*".

Fundamentos del "backstripping"

La técnica de descompactación o "*backstripping*" empleada en estos pozos para su sucesión Plioceno-Cuaternaria, sigue el proceso descrito por autores como Watts (2001) y Allen y Allen (2005). Esta técnica se sustenta en el concepto de isostasia local (de tipo Airy) y acomete la descompactación sucesiva de horizontes datados según la ecuación general:

$$Y = S \cdot \left(\frac{\rho_m - \rho_s}{\rho_m - \rho_w} \right) - \Delta_{SL} \cdot \left(\frac{\rho_w}{\rho_m - \rho_w} \right) + \left(W_d - \Delta_{SL} \right) \quad [1]$$

Donde Y es la profundidad corregida (*i.e.* descompactada) de cada horizonte (o subsidencia final o total, a veces denominada "tectónica"), S es el espesor descompactado, ρ_m, ρ_s y ρ_w son las densidades del manto (3,30 x10^3 kg m^{-3}), los sedimentos y el agua (1,03 x10^3 kg m^{-3}) respectivamente, Δ_{SL} es la altura del nivel del mar en relación a su posición actual para un tiempo dado y W_d es la paleobatimetría. En nuestro caso, dada la ausencia de datos sobre algunas de estas variables y el carácter parcialmente restringido de esta cuenca en el periodo analizado, hemos optado por no aplicar las correcciones por paleobatimetría (W_d= 0) y variaciones eustáticas (Δ_{SL}= 0).

El cálculo del espesor descompactado (S) para cada unidad se realiza sobre la reconstrucción de su porosidad inicial (previa a su soterramiento). Para este cálculo hemos estimado en cada caso el mejor ajuste exponencial a los datos de porosidad (ϕ) medidos in-situ en los sondeos de ODP (Leg 161) (*e.g*. Figura 2), según la función general:

$$\phi = \phi_0 \cdot e^{-cz} \quad [2]$$

Donde ϕ_0 es la porosidad inicial y c un coeficiente determinado empíricamente. A partir de esta expresión, la ecuación general de descompactación resulta:

$$y_2' - y_1' = y_2 - y_1 - \frac{\phi_0}{c} \cdot \left[exp(-cy_1) - exp(-cy_2) \right] + \frac{\phi}{c} \cdot \left[exp(-c' y_1) - exp(-c' y_2) \right] \quad [3]$$

Siendo y_i e y'_i las profundidades actuales y descompactadas, respectivamente; por lo que el espesor descompactado ($S = y'_2 - y'_1$) puede reemplazarse en la expresión [1].

Valores de porosidad

Los datos de porosidad inicial (ϕ_0) y del parámetro c para cada una de las secuencias diferenciadas en los pozos de ODP en Alborán (Sites 976 a 979; *e.g*. Figura 2) junto con los valores promedio de densidad (ajustados según los datos medidos también in-situ en estos pozos) se recogen en la tabla 1. Excluyendo los datos del Site 976, las secuencias de edad Cuaternaria poseen valores promedio de ϕ_0, c y ρ_s son de 64, 0,9 (x10^{-4} m^{-1}) y 1,78 (x10^3 kg m^{-3}), respectivamente y en las de edad Plioceno son de 63, 0,8 (x10^{-4} m^{-1}) y 1,98-1,99 (x10^3 kg m^{-3}).

En los pozos comerciales, por el contrario, no existen datos directos de porosidad y se ha buscado una relación empírica que permita estimarla en función de otros parámetros medidos en las diagrafías convencionales (*e.g*., sónico y "*gamma-ray"*). Este tipo de relación está ampliamente documentada en otras cuencas y se ha establecido también en laboratorio para distintas litologías (*e.g*., Magara,

1976; Castagna *et al.*, 1985). Así, por ejemplo, la función polinómica de mejor ajuste a los datos de diagrafías para la sucesión de edad Pliocena (obviando aquellos pozos de ODP en los que existe un hiato amplio en el registro del Plioceno, *i.e.* los Sites 976 y 979), es del tipo:

$$\phi = \frac{100{,}58 - 29{,}83 V_{p(kms^{-1})} - 0{,}43 f_{cl}}{100} \quad [4]$$

Siendo f_{cl} la fracción de arcilla en el sedimento, que según Poupon y Gaymard (1970) se puede obtener a partir de los datos de "*gamma-ray*" (*J*) mediante:

$$f_{cl} = \frac{f_{sh}}{3 - 2 f_{sh}}, \; f_{sh} = \frac{J - Jsd}{J_{sh} - J_{sd}} \quad [5]$$

Siendo J_{sh} y J_{sd} los valores máximos y mínimos de "*gamma-ray*" (en API) en el pozo. Este tipo de aproximación se ha utilizado tentativamente en el pozo Andalucía G1, para aquella porción de la secuencia Pliocena dónde hay datos de diagrafías. Los valores de porosidad obtenidos se exponen también la tabla 1 (ϕ_0= 48 y c= 0,4x10^{-4} m^{-1}) y podrán ser utilizados en ulteriores estudios detallados de subsidencia en el resto de los pozos comerciales del área.

Pozo	ϕ_0 *Porosidad* inicial		c (m^{-1}) Coeficiente determinado empíricamente		ρ_s (x10^3 kg m^{-3}) Densidad del sedimento.	
	Cuaternario	**Plioceno**	**Cuaternario**	**Plioceno**	**Cuaternario**	**Plioceno**
976	63	47	8 x10^{-4}	0,3 x10^{-4}	1,84	1,95
977	65	62	1,1 x10^{-3}	0,7 x10^{-4}	1,78	1,98
978	–	63	–	0,8 x10^{-4}	–	1,98
979	64	66	0,7 x10^{-4}	0,9 x10^{-4}	1,78	1,99
And-G1	–	48	–	0, 4x10^{-4}	–	–

Tabla 1. Parámetros físicos promedio de los sedimentos de edad Plio-Cuaternario utilizados en el análisis de "*backstripping*".

Table 1. *Average physical properties of the Plio-Quaternary sediments used in the backstripping analysis.*

Resultados

Los valores de subsidencia total (*Y*) estimados en los pozos estudiados se muestran en la figura 3. En ella, y para hacer comparables los resultados se ha descontado en cada caso la batimetría actual. Debe tenerse en cuenta también, en la interpretación que sigue de los resultados, que esta reconstrucción de la subsidencia post-Messiniense podrá cambiar ligeramente de forma una vez se complete el análisis con las capas más profundas. No obstante se pueden extraer algunas conclusiones. Así, para el intervalo Plioceno-Cuaternario en todos los pozos estudiados se obtienen valores de subsidencia total muy similares y aproximadamente constantes, con valores netos de subsidencia total, *Y*= 310-355 m, lo que corresponde a una tasa promedio de subsidencia de 0,06-0,07 mm/a. Se comprueba también que las regiones donde se identifica un hiato importante intra-Plioceno (*e.g.*, en el alto de basamento de la Cuenca Oeste de Alborán: Site 976 o en la Cuenca Sur de Alborán: Site

979), la sedimentación durante el Plioceno superior fue especialmente alta (*ca.* 0,14-0,15 mm/a en el Site 979 y 0,25-0,30 mm/a en el Site 976), ralentizándose la subsidencia en el tránsito Plioceno-Cuaternario (< 1,8 Ma; 0,08-0,11 mm/a). La mayor tasa de subsidencia observada en estos pozos hacia el final del Plioceno atestigua la existencia de dos eventos tectónicos de escala regionales en la cuenca. El primero de edad intra-Plioceno, ligado al cual se generaría el hiato mencionado (2,2-5,0 Ma en 976 y 2,8-5,0 Ma. en 979; *e.g*. Comas *et al.*, 1996) y determinaría el ascenso tectónico relativo de regiones como el alto de basamento del Site 976 (Comas y Soto, 1999) o la cresta de Alborán. Y otro hacia el final del Plioceno (2,1-1,8 Ma), produciéndose una disminución general en Alborán de las tasas de subsidencia (*ca.* 0,07-0,11 mm/a) durante el Cuaternario.

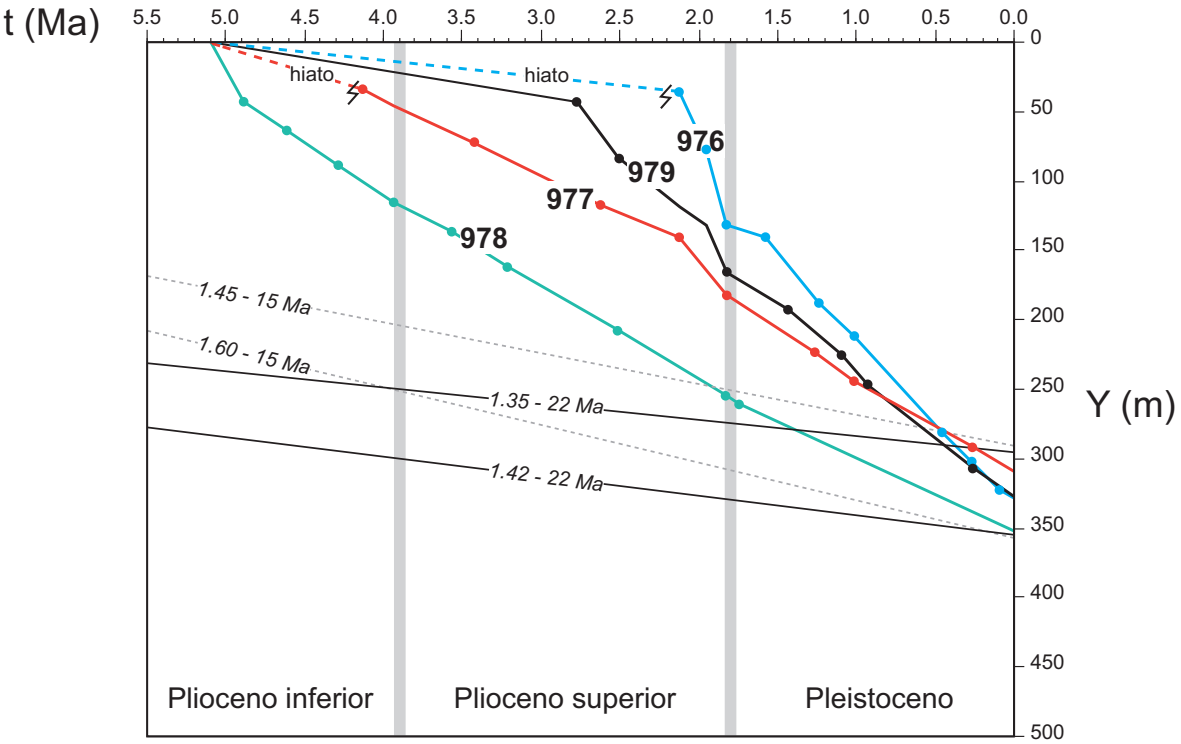

Figura 3. Curvas de subsidencia obtenidas mediante el análisis de "*backstripping*" para las sucesiones de edad Plioceno a Cuaternario en los distintos pozos analizados en el Mar de Alborán (localización en Figura 1).

Figure 3. *Subsidence curves from backstripping analysis for the Plio-Quaternary sequences in the different studied wells in the Alboran Sea (location in Figure 1).*

Se ha valorado también la magnitud de las tasas de adelgazamiento (expresado mediante el factor β) en la cuenca, aproximando las tasas de subsidencia finales (305-350 m en 5,1 Ma) según el procedimiento descrito por McKenzie (1978). Este método requiere asumir varios parámetros cuyo rango de variación puede ser muy grande en esta región, por lo que los resultados deben considerarse tentativos, a falta de un estudio completo de la curva de subsidencia. Los valores de β que ajustan mejor a los resultados se incluyen también en la figura 3. Estas curvas se han calculado tomando como espesores corticales y litosféricos iniciales 32 y 125 km, respectivamente, una densidad promedio de la corteza de 2,8 $x10^3$ kg m^{-3} y los valores habituales de temperatura en la base de la litosfera (1330º C), difusividad térmica (κ= 8 $x10^{-7}$ m^2 s^{-1}) y coeficiente volumétrico de expansión térmica en el manto (α= 3,28 $x10^{-5}$ $ºC^{-1}$) (vse. McKenzie, 1978; Watts, 2001). Atendiendo a la edad de los

sedimentos más antiguos depositados en la cuenca (Burdigaliense y Aquitaniense probable, para la Unidad VI; Comas *et al.*, 1992, 1999; *i.e.* ~24-21 Ma) y considerando las edades obtenidas según la modelización térmica del substrato metamórfico (perteneciente al Dominio de Alborán) de la cuenca (< 27 Ma; Platt *et al.*, 1998), hemos asumido que la edad del "*rifting*" inicial podría ser de 22 Ma. Los resultados de subsidencia se ajustan según valores de β comprendidos entre 1,35 y 1,42. Estas estimaciones resultan comparables, aunque ligeramente inferiores, a las estimadas por otros autores en la región (β= 1,35-1,60), según el estudio de alguno de los pozos comerciales (Docherty y Banda, 1992, 1995; Watts *et al.*, 1993).

Conclusiones

1) En los distintos pozos científicos realizados por ODP (Leg 161) en el Mar de Alborán (Sites 976 a 979) se ha realizado un estudio completo de los registros de diagrafías (V_p y "*gamma-ray*") y de las propiedades físicas medidas in-situ (densidad y porosidad) en la sucesión de edad Plio-Cuaternario. Para las distintas secuencias sedimentarias diferenciadas se han establecido leyes generales que pueden ser extrapoladas a los pozos comerciales, permitiendo estimar la porosidad a partir exclusivamente de las propiedades medidas en diagrafías.

2) Con estos datos se han reconstruido las curvas de subsidencia mediante el método de "*backstripping*", obteniéndose que durante los últimos 5 Ma esta cuenca ha experimentado una subsidencia total aproximadamente constante (*Y*= 310-355 m), equivalente a una razón de subsidencia de 0,06-0,07 mm/a. En algunas regiones, como la cresta de Alborán y el alto de basamento del Site 976 en la Cuenca Oeste de Alborán, existió un evento tectónico intra-Plioceno que condicionó tasas locales de subsidencia mayores (entre 2,2 y 5,0 mm/a para el Plioceno superior), ralentizándose hacia el tránsito con el Cuaternario (0,07-0,11 mm/a). Los datos de subsidencia obtenidos sugieren que el adelgazamiento que dio lugar a la Cuenca del Mar de Alborán pudo ser del orden de β= 1,35-1,42.

Recent submarine slides in the Alboran Ridge (Alboran Sea)

Deslizamientos submarinos recientes en la Cresta de Alborán (Mar de Alborán)

Published in ***Geogaceta*** *(2009), 47, 89-92.*

Pedro Martínez-García[1], Menchu Comas[1], Juan I. Soto[2], Lidia Lonergan[3] and Silvia Pérez-Hernández[1]

[1] Instituto Andaluz de Ciencias de la Tierra (CSIC and University of Granada), Facultad de Ciencias,

[2] Instituto Andaluz de Ciencias de la Tierra (CSIC and University of Granada) and Departamento de Geodinámica, Facultad de Ciencias, Granada, Spain.

[3] Department of Earth Science and Engineering (Imperial College London), South Kensington Campus, London, United Kingdom.

Abstract

From swath bathymetry data and high-resolution acoustic profiles (TOPAS) several slides have been imaged in the Alboran Ridge in the western Mediterranean. This submarine relief is the most prominent morphological feature (> 130 km in length) in the Alboran Sea and its elongated SW-NE shape results from recent convergence between the African and Eurasian plates. The identified gravitational deposits show transparent and chaotic facies, and appear in depths ranging between 640 and 1810 m. Occurrence of slides deposits along fault escarpments affecting the seafloor reveals that submarine instability processes are mainly controlled by tectonics. Mass-transport deposits are generally composed by several overhead lobes of sediments. These observations suggest collectively that instability processes are frequent and may be related with faulting pulses. Instability processes represent therefore a geological risk in the region that should be surveyed and analyzed in the future.

Keywords: slides, instability processes, swath bathymetry, Alboran Sea, active tectonics.

Introducción

Los procesos de inestabilidad gravitatoria condicionan en gran medida la morfología y evolución del fondo marino, siendo de considerable magnitud en los taludes continentales de ámbitos óseanicos. El progresivo desarrollo de técnicas geofísicas y métodos directos para obtener información del fondo marino y su subsuelo somero, ha favorecido el descubrimiento de numerosos deslizamientos submarinos en distintos contextos geológicos y morfológicos (*i.e.*, Casas *et al*., 2003; Sultan *et al*., 2007, entre muchos otros).

En el Mediterráneo Occidental, la Cuenca del Mar de Alborán es bien conocida en aspectos que conciernen a su relleno sedimentario, a su estructura y evolución tectónica, y a sus peculiares características geofísicas (*e.g.*, Comas *et al*., 1992, 1999; Jurado y Comas, 1992; Watts *et al*., 1993; Torné *et al*., 2000). Sin embargo, el origen, procesos y productos de posibles deslizamientos relacionados con los relieves de la Cuenca, han sido objeto de escasa atención específica (*e.g.*, Bárcenas *et al*., 2004; Ballesteros *et al*., 2008).

La denominada Cresta de Alborán es el rasgo fisiográfico más sobresaliente del fondo del Mar de Alborán, destacando entre los numerosos relieves y las depresiones o surcos que los jalonan (Figura 1a). Esta "cordillera submarina", con una morfología marcadamente lineal de dirección SO-NE, destaca como una de las estructuras mayores dentro del Arco de Gibraltar (Figura 1). La Cresta de Alborán delimita las tres cuencas principales conocidas en el Mar de Alborán (Cuencas Oeste, COA; Cuenca Este, CEA y Cuenca Sur, SAB) (Figura 1). Este alto batimétrico tiene unos 130 km de longitud y una elevación máxima de 1000 m sobre el fondo marino. Sus flancos presentan diferencias batimétricas de hasta 700 m y laderas localmente abruptas (pendiente máxima ~30º). Hacia el E, la Cresta pierde altura y su dirección gira a E-O uniéndose con el Escarpe de Yusuf, el otro rasgo fisiográfico de mayor envergadura en Alborán (Figura 1).

En este trabajo presentamos y analizamos algunos casos de procesos de inestabilidad sedimentaria y depósitos relacionados (*Mass Transport Deposits*, MTD) reconocidos en el entorno de la Cresta de Alborán. El trabajo se fundamenta en el análisis de datos batimétricos y sísmicos de alta resolución, describe y cartografía esas estructuras y tiene el propósito de determinar los mecanismos y factores de control que han dado lugar a los deslizamientos submarinos.

Contexto geológico

El Mar de Alborán corresponde a la cuenca marginal de retro-arco del Sistema del Arco Gibraltar (SAG). Este orógeno, que incluye además a las cadenas alpinas Béticas y Rif y al prisma acreción de Gibraltar en el Atlántico (Figura 1), ha evolucionado conjuntamente desde el Neógeno (30 Ma) bajo un régimen cinemático regido por la convergencia N-S de las placas Euroasiática y Africana.

Diversos trabajos establecen que la Cuenca de Alborán se generó a partir del Mioceno inferior por adelgazamiento litosférico y extensión cortical (*e.g.*, Platt and Vissers, 1989; Comas *et al*., 1992, 1999; García-Dueñas *et al*., 1992), y que su evolución estructural conlleva fases extensionales (23-9Ma) seguidas de etapas de tectónica contractiva transcurrente (9-0 Ma) (*e.g.*, Comas *et al*., 1992, 1999; Woodside y Maldonado, 1992; Watts *et al*., 1993; Chalouan *et al*., 1997; Alvarez-Marrón, 1999;

Gràcia *et al*., 2006; Maufrett, *et al*., 2007). La reestructuración post-Messiniense ha condicionado la fisiografía del fondo marino del Mar de Alborán así como su línea de costas.

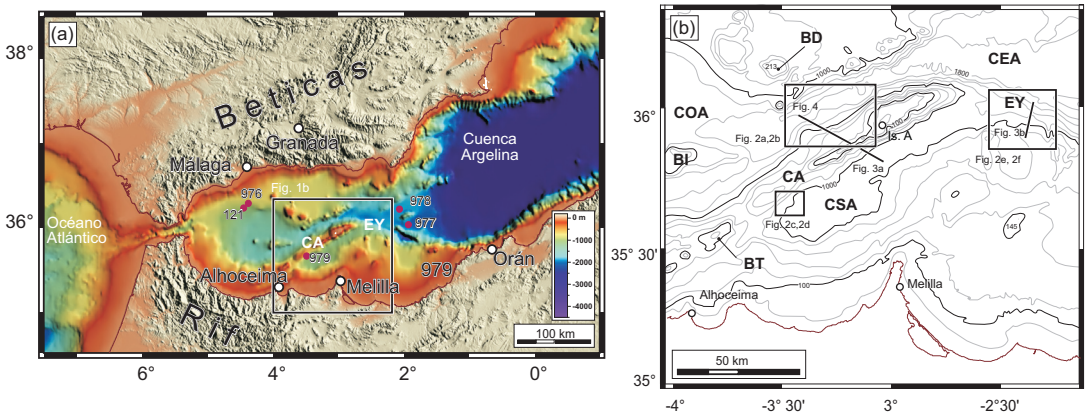

Figura 1. (a) Topografía del Sistema del Arco de Gibraltar construida a partir de la base de datos global SRTM (USGS-NASA) combinada con GEBCO 97 (IOC-IHO). Se indica el área estudiada. **(b)** Ampliación del área de estudio mostrando la localización del resto de las figuras que incluye este trabajo. Contornos batimétricos en metros; equidistancia 200 m. BD, Banco de Djibouti; BI, Banco de Ibn-Batouta; BT, Banco de Tofiño; CA, Cresta de Alborán; CEA, Cuenca Este de Alborán; COA, Cuenca Oste de Alborán; CSA, Cuenca Sur de Alborán; EY, Escarpe de Yusuf; Is. A, Isla de Alborán.

Figure 1. (a) *Topography of the Gibraltar Arc System built on the SRTM (USGS-NASA) global database combined with GEBCO 97 (IOC-IHO). The studied area is indicated.* ***(b)*** *Zoom of the rectangle indicated in Figure 1a with location of other figures included in this work. Bathymetry contours in metres; contour interval is 200 m. BD, Djibouti Bank; BI, Ibn-Batouta Bank; BT, Tofiño Bank; CA, Alboran Ridge; CEA, East Alboran Basin; COA, West Alboran Basin; CSA, South Alboran Basin; EY, Yusuf Escarpment; I. As, Alboran Island.*

La sismicidad registrada en el SAG demuestra que los procesos tectónicos son activos en la región. La deformación actual se encuentra principalmente controlada por dos sistemas de fallas de dirección NE-SO a NNE-SSO (zona de falla de la Cresta de Alborán) y conjugadas NO-SE (zona de falla de Yusuf). Ambos sistemas presentan una importante componente de salto en dirección, de carácter izquierdo y transpresivo para las NE-SO, y dextro y transtensivo para las NO-SE (vse. revisión en Fernández-Ibáñez *et al*., 2007).

El registro sedimentario del Plioceno y Cuaternario en el Mar de Alborán, está determinado a partir de las perforaciones del ODP Leg 161 (Comas *et al*., 1999). Los depósitos del Cuaternario y Holoceno recuperados en los ODP Sites 976, 977 y 979, muestran que esas secuencias contienen comúnmente abundantes intervalos turbidíticos y facies arcillosas redepositadas. Particularmente en el Site 979, situado en el flanco meridional de la Cresta de Alborán, la secuencia del Cuaternario/ Holoceno presenta diversos hiatos y niveles contorsionados (de *slumping*) atribuidos a episodios de inestabilidad sin-sedimentaria causados por el levantamiento coetáneo de la Cresta (Alonso et. al, 1999).

Datos y metodología

Este trabajo se basa en el estudio e interpretación de mapas batimétricos y de perfiles de alta resolución. Los datos utilizados proceden de las campañas de adquisición de geología y geofísica ALBA (1992), TECALB (2000), y MARSIBAL I-06 (2006), realizadas en el Mar de Alborán a bordo del B.I.O. Hespérides. Los datos batimétricos fueron adquiridos mediante la ecosonda multihaz SIMRAD EM12S-120. Además se han utilizado datos complementarios, procedentes de MediMap Group (2008) para elaborar los mosaicos. El análisis morfológico ha sido completado con mapas de pendientes (Figuras 2b, 2d y 2f).

Los deslizamientos identificados en batimetría han sido analizados además sobre perfiles de sísmica multicanal y perfiles acústicos de alta resolución (TOPAS: Topographic Parametric Sonar, penetración máxima de 170-180 m) para conocer la estructura interna de las masas deslizadas.

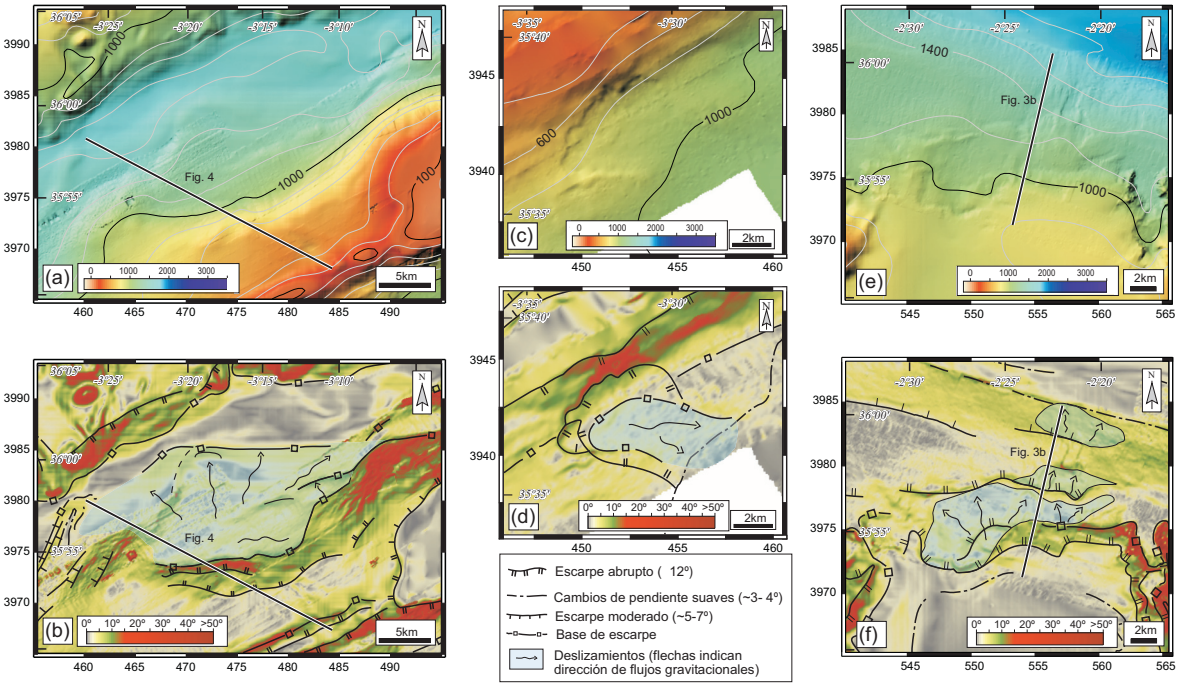

Figura 2. Mosaicos batimétricos y mapas de pendiente mostrando la geometría en planta de los deslizamientos *(slides y scars)* en los sectores estudiados: **(a)** y **(b)** Talud norte de la Cresta de Alborán; **(c)** y **(d)** Talud Sur de la Cresta de Alborán; **(d)** y **(e)** Escarpe de Yusuf. Contornos batimétricos en metros de GEBCO 97 (IOC-IHO); el intervalo de contornos es 200 m. Proyección UTM, unidades en kilómetros (elipsoide WGS 84).

Figure 2. *Bathymetric mosaics and slope maps of different slides showing the geometry in plan view of slides and scars in the different studied sectors:* ***(a)*** *and* ***(b)*** *Northern Slope of the Alboran Ridge;* ***(c)*** *and* ***(d)*** *Southern Slope of the Alboran Ridge;* ***(e)*** *and* ***(f)*** *Yusuf Escarpment. Bathymetry contours in metres from GEBCO 97 (IOC-IHO); contour interval is 200 m. UTM projection, units in kilometres.*

Evidencias de deslizamientos masivos

En el entorno de la Cresta de Alborán se han reconocido numerosos deslizamientos en masa de sedimentos, a profundidades variables entre los -640 y -1810 m. Las cabeceras de los deslizamientos

son escarpes (*scars*) con 10-25º de pendiente, con geometrías cóncavas hacia la base del talud, con depresiones en el frente. Los depósitos correspondientes a estos deslizamientos (Mass Transport Deposits – MTD) forman lóbulos de techo abovedado y están delimitados por cambios de pendiente a su base. Los deslizamientos presentados en este trabajo se localizan en los taludes de la Cresta de Alborán y también en el Escarpe de Yusuf (Figura 1b).

Talud Sur de la Cresta de Alborán

Aquí se ha identificado la cabecera de un deslizamiento localizado entre 35º 36'N - 35º 39`N y 3º34'W-3º28'W, que cubre un área mínima de 19 km^2 y se extiende desde los -640 a -815 m. Las figuras 2c y 2d muestran el *scar* como una cicatriz nítida cóncava hacia el SE con trazado festoneado en detalle y se encuentra en el frente de un escarpe lineal de orientación SO-NE y pendiente variable entre 10º y 25º (Figura 2d). La imagen TOPAS de la figura 3a evidencia la existencia de deslizamientos recientes y subactuales (soterrados). Las facies acústicas transparentes que presentan las masas deslizadas son interpretadas como depósitos caóticos.

Talud Norte de la Cresta de Alborán

Se ha identificado un amplio sector afectado por procesos de inestabilidad sin-sedimentaria, y los deslizamientos resultantes se localizan entre 35º 26'N -36º 0`N y 3º27'W -3º7'W, ubicándose entre los -880 y -1650 m. Este área abarca unos 230 km^2 y se caracteriza por un relieve escalonado, con escarpes estrechos y desnivel de cientos de metros, separados por rellanos. La cicatriz principal tiene una traza festoneada y se instala en cotas altas de la Cresta (Figuras 2a y 2b). En el perfil sísmico de la figura 4 se identifican claramente la arquitectura y facies sísmicas (caóticas y semitransparentes) de tres deslizamientos recientes con despegues gravitacionales en sus bases. Los MTD que localmente conforman depósitos yuxtapuestos, progresan como máximo unos 20 km hacia el N (Figura 2b). Se observan además numerosas fallas de alto ángulo que deforman las secuencias sedimentarias del Plio-Cuaternario; algunas de estas fallas condicionan incluso la morfología del fondo marino, indicando que son actualmente activas.

Escarpe de Yusuf

Existen varias cabeceras de deslizamientos de pequeñas dimensiones marcados por cicatrices de curvatura variable. *Scars* y MTD que ocupan el área comprendida entre 35º26'N-36º0'N y 3º27'W-3º7'W, y se extienden desde -900 a -1810 m (Figuras 2e y 2f). Los depósitos consistentes en lóbulos superpuestos de facies semitransparentes (Figura 3b) son interpretados como MTD. El volumen total de los deslizamientos reconocidos en Yusuf se estima en torno a 1.4 km^3, considerando un área mínima de 70 km^2 (calculada sobre el mosaico batimétrico, Figura 2f) y un espesor promedio de los cuerpos deslizados de 20 m (cálculo sobre perfil TOPAS, Figura 3b).

Discusión y conclusiones: deslizamientos y tectónica activa

Los datos analizados sobre los taludes de la Cresta de Alborán y Escarpe de Yusuf muestran deslizamientos submarinos con depósitos transportados masivamente (MTD). Los depósitos gravitacionales de flujos densos resultan de un transporte a favor de la máxima pendiente en los

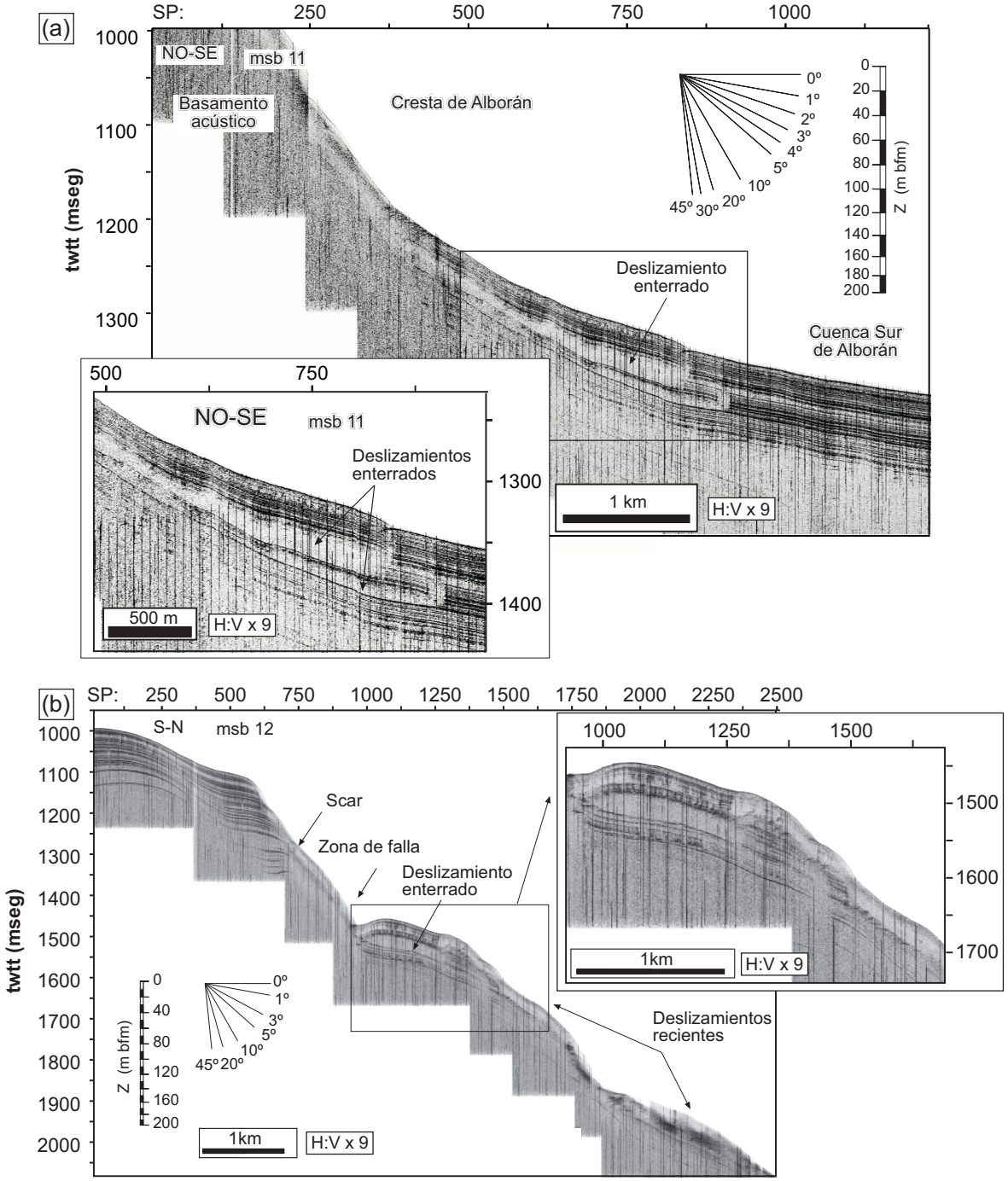

Figura 3. Perfiles de alta resolución TOPAS mostrando la estructura interna de los deslizamientos. Se muestran escala de profundidad estimada y ábaco de buzamientos para comparación. **(a)** Deslizamientos en el talud sur de la Cresta de Alborán; **(b)** deslizamientos en el escarpe de Yusuf. Localización en figura 1.

Figure 3. *TOPAS profiles* showing the internal structure of slides. *Estimated depth scale and calculated dip abacus are shown for comparison.* ***(a)*** *Slides in the South side of the Alboran Ridge;* ***(b)*** *slides in the Yusuf Escarpment. Location in figure 1.*

taludes, perpendicular a la cicatriz de los deslizamientos y a sus frentes lobulados (Figura 2). Con esto, cabe afirmar que las sucesiones de deslizamientos visibles en ambos flancos de la Cresta de Alborán y en el Escarpe de Yusuf han inducido al desmantelamiento y remodelado de esos taludes por

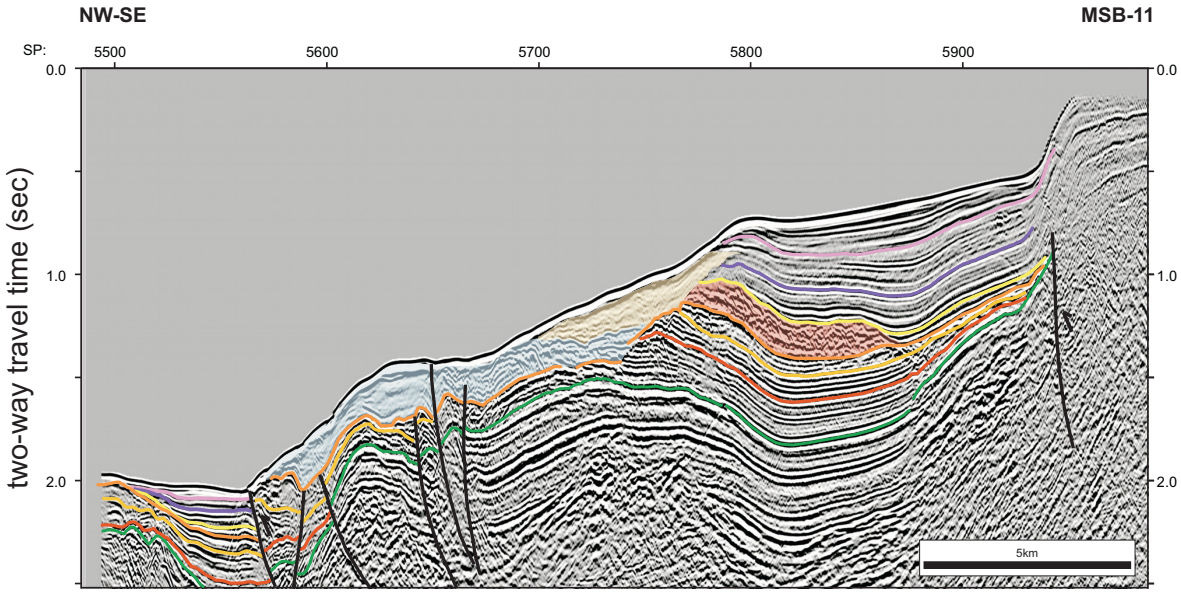

Figura 4. Perfil sísmico de reflexión multicanal mostrando la estructura profunda del talud septentrional de la Cresta de Alborán. Nótese las *slides* determinadas y la intensa deformación que afecta al fondo marino. M: Reflector M, base de secuencias plio-cuaternarias.

Figure 4. *Multichannel seismic reflection profile showing the depth structure of the Northern slope of the Alboran Ridge. Notice determined slides and the intense deformation affecting the seafloor. M: M Reflector, base of the Plio-Quaternary secuences*.

procesos concomitantes de despegues gravitatorios, transporte y acumulación masiva de depósitos alóctonos sobre el fondo marino.

El perfil sísmico de multicanal de la figura 4, correspondiente al flanco septentrional de la Cresta de Alborán (Figura 1), demuestra que los casos de deslizamientos y MTD considerados en este trabajo están generados por procesos de inestabilidad causados por una tectónica activa coetánea. La superposición de las masas deslizadas sugiere una recurrencia de episodios de inestabilidad sedimentaria en la región. El hecho de que el *slide* 2 aparezca plegado y deformado por las fallas, demuestra una tectónica activa posterior a su emplazamiento.

Los deslizamientos estudiados están constituidos por distintos lóbulos superpuestos, y en ocasiones separados por niveles hemipelágicos. Este hecho indica que el acúmulo de MTD sobre los taludes es recurrente en el tiempo y espacio, y denota episodios de acumulación rápida (depósitos caóticos) que alternan con periodos de sedimentación hemipelágica en épocas actuales o muy recientes.

La localización de estos deslizamientos en ámbitos de probada actividad sísmica actual (*e.g.*, Fernández-Ibáñez *et al*., 2007, y referencias incluidas), sugiere que probablemente fueron activados por terremotos. En este sentido, los deslizamientos reconocidos en la Cresta de Alborán y Escarpe de Yusuf pueden estar condicionados por movimientos de fallas sismogénicas activas o recientes. No obstante, para determinar la influencia de otros factores de control en los deslizamientos masivos en esta región (*i.e.*, cambios eustáticos o sobrecarga sedimentaria) sería necesario un estudio de testigos de sedimentos de los deslizamientos de los que por ahora no disponemos.

Finalmente cabe señalar que los procesos actuales de inestabilidad sedimentaría probados en el Mar de Alborán suponen un potencial riesgo geológico de interés por tanto para estudios futuros, dirigidos a cuantificar adecuadamente los volúmenes de los deslizamientos y determinar el riesgo tsunamigénico de esta región.

APPENDIX IV
Contribution to EGU-2007 meeting, Vienna.

Active tectonics related to major fault zones in the Alboran and western Algerian-Balearic basins

Martínez-García, P., Perez-Hernandez, S., Comas, M.C., Roman Alpiste, M.J. and MARSIBAL I-06 Scientific Party

Instituto Andaluz de Ciencias de la Tierra. C.S.I.C. and University of Granada, Campus de Fuentenueva, Faculty of Sciences, University of Granada. 18002 Granada, Spain. e-mail:matez@ugr.es

Geological Setting

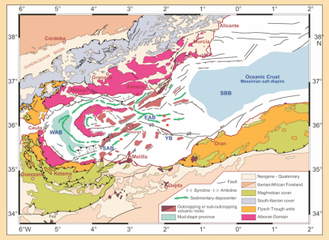

The Alboran Sea is located in the Western Mediterranean, in the inner part of the Betic-Rif Alpine orogen and was formed by sever lithosphere thinning in a plate-convergence setting between African an Eurasian plates. This region is conected to the oceanic Algerian-Balearic basin to the east.

The Alboran sea and Algerian-Balearic basins present a complex seafloor morphology. In this area new data were adquired during the MARSIBAL I-06 cruise conducted onboard the BIO HESPÉRIDES (December 2006).

Situation Map

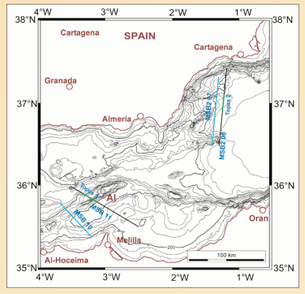

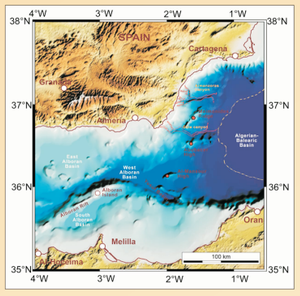

Location map shows the position of several high resolution profiles used in this work: two ultra-high resolution section (Topas) and two high-resolution profiles.

Tectonic Structure and Sediment Acumulation

Alboran Ridge

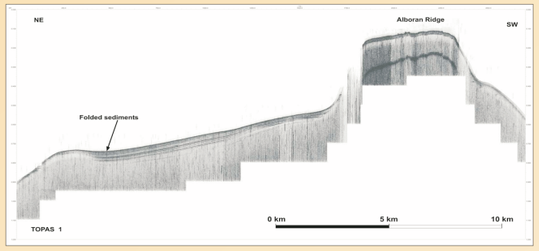

TOPAS profile across the Alboran Ridge. Ultra-high resolution, 50-60m penetration, primary frequency of 16-22kHz.This seamount is one of the major physiographic features on the Alboran sea and controls the oceanographic processes in this area. Active folding is afeccting to the youngest sediments.

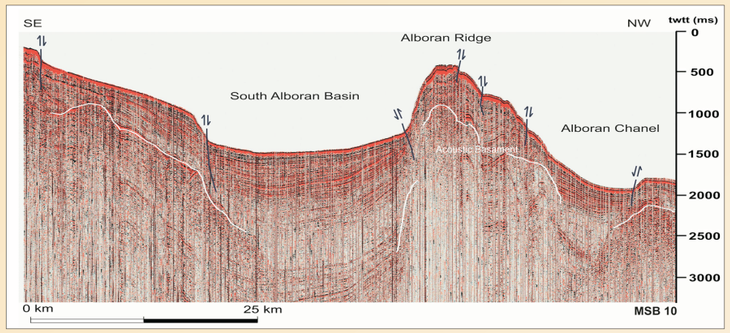

This bathymetric high constitutes a folded structure bounded by two left lateral strike-slip fault zones. Active tectonics occur flanking and bordering the Alboran Ridge anticline. Slumps and slides occur on slopes and escarpments related to faults generated by actual active tectonis.

Palomares Margin

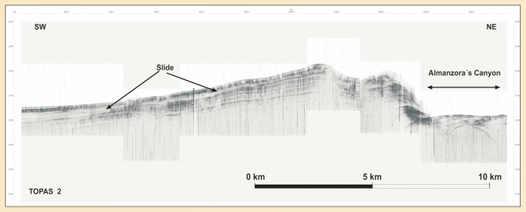

TOPAS profile across the Palomares Margin. Slides and slumps structures are common and may be related to shallow earthquakes.

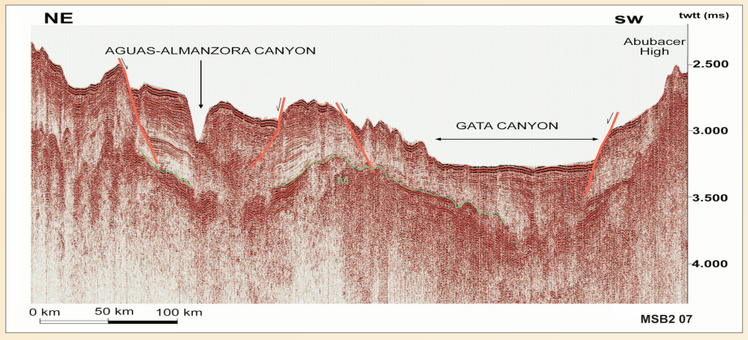

Swath bathymetry (SIMRAD 120 record) of the Gata Canyon. The Palomares Fault Zone controls pathways of this incised and narrow submarine-canyon. Turbidite systems regulate erosion, mass transport and accumulation in this margin segment.

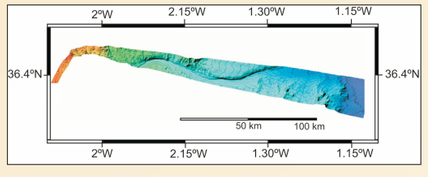

The Palomares margin is a faulted and folded margin-segment of the NW Algerian-Balearic basin and presents strong deformation affecting the seafloor. A large talus with hetereogeneous relief is relatd to Palomares Fault Zone. This profile shows diferences in incision between Aguas-Almanzora and Gata terraced canyons.

Conclusions

The complex seafloor morphology in the Alboran Sea and Algerian-Balearic basins is closer related with shallow faulting.

Slides and slumps structures can be related to earthquakes are features proving the tectonic activity in this region.

Sedimentary processes are controlled by active tectonics.

MARSIBAL I -06 Scientific Party:
N.Babonneau, M. Carmona-Villalba, M.C. Comas, M. Farran, J. Ferreira de Castro, P. Martínez-García, S. Martínez-Loriente, L. Menezes Pinheiro, S. Perez-Hernandez, P. Ruano-Roca

This poster made possible thanks to the partial support from the European Science Foundation (ESF) under the EUROCORES Programme EUROMARGINS, through contact No. ERAS-CT-2003-980409 of the European Commission, DG Research, FP6. Other Contributions from Projects REN 2001-3868-CO3-01 and CTM 2005-08071-CO3-01 (R & D National Plan of the Ministry of Education & Science and FEDER funding, Spain).

Tectonic control on seafloor morphology at the Alboran Ridge and Yusuf lineaments: insights from swath bathymetry and sub-bottom profiling

Martínez-García, P., Comas, M.C. and Soto, J.I.

Instituto Andaluz de Ciencias de la Tierra, CSIC and University of Granada, Campus Fuentenueva, 18002 Granada, Spain. E-mail: matez@ugr.es

LOCATION AND GEOLOGY

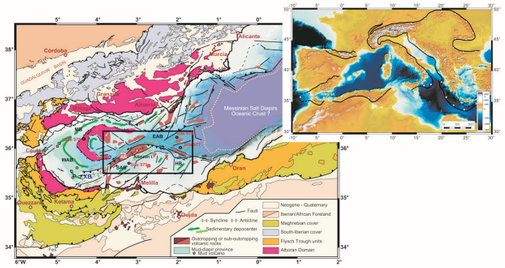

The Alboran Sea is a back-arc Mediterranean basin developed behind the Gibraltar Arc, formed by the Betic and Rif mountain ranges. The basin originated in the Early Miocene from crustal thinning and evolved through extension (Middle and early-Late Miocene) and a subsequent contractive reorganization occurred from the Late Tortonian to Present.

SEAFLOOR TOPOGRAPHY

BATHYMETRY

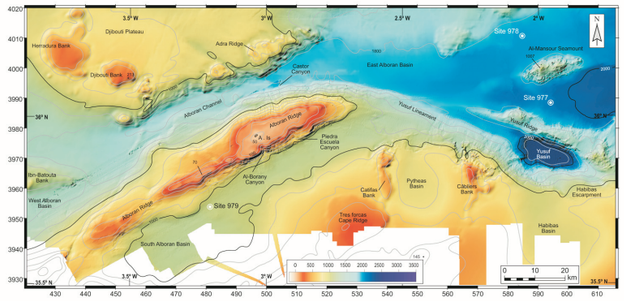

We gathered a bathymetric mosaic covering an area of about 14,400 km^2 in the central sector of the Alboran Sea. The Alboran Ridge is the most prominent relief, SW-NE trending, over 130 km long and rising 1,850 m above the seafloor. Eastwards, this ridge extends to the NW-SE Yusuf Lineament.

SLOPE ANALYSIS

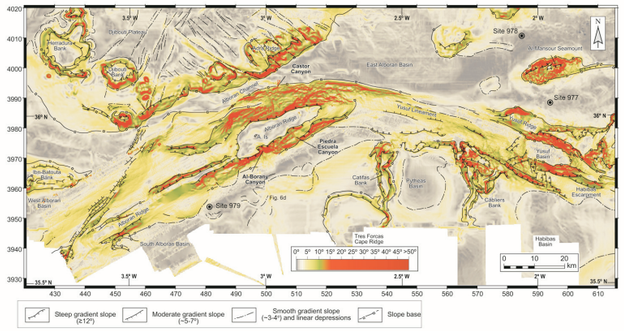

Slope analysis reveals the existence of crests and scarps corresponding with tectonic lineaments. Five physiographic domains have been distinguised: (1) the Alboran Ridge; (2) the Yusuf Lineament, including the associated basin and ridge; (3) the East Alboran Basin; (4) the Alboran Channel, and (5) the Djibouti Plateau.

GEOMORPHOLOGY

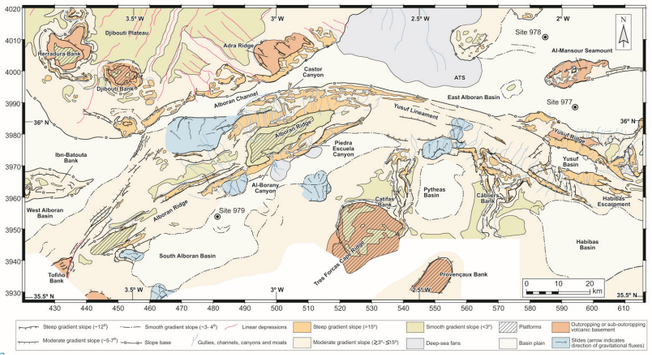

We have carried out a geomorphological study to evaluate the balance between erosive, sedimentary and tectonic processes that have shaped the seafloor.

SHALLOW STRUCTURE

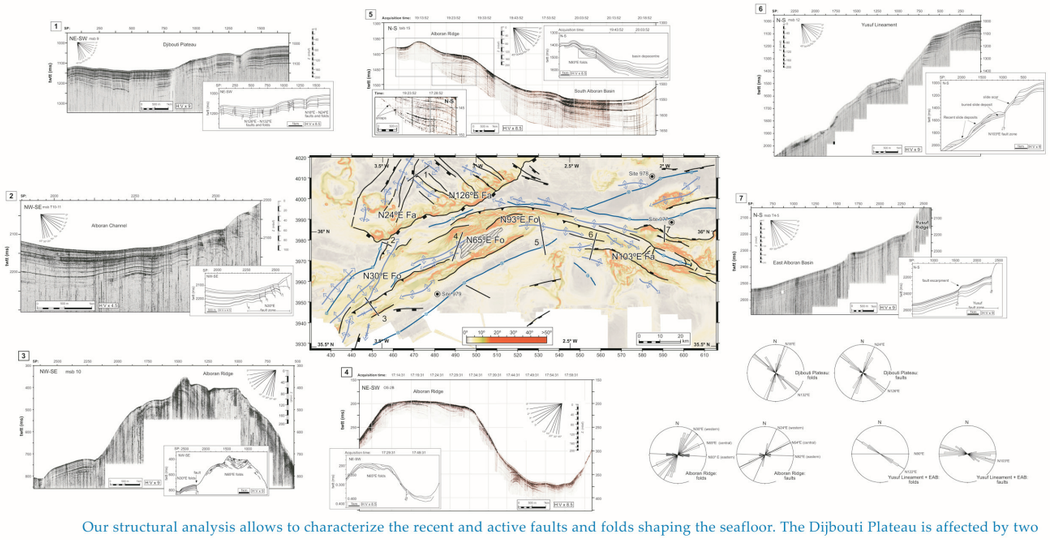

Our structural analysis allows to characterize the recent and active faults and folds shaping the seafloor. The Djibouti Plateau is affected by two conjugate fault-systems with NNE-SSW and NW-SE orientations. Recent uplift and deformation in the Alboran Ridge and Channel has been caused by sub-vertical and reverse fault-zones with associated folding in the sub-seafloor sediments. Their structural directions shifts progressively from SW-NE to WNW-ESE. A narrow N30ºE fault-zone involving folding and reverse faulting cuts across the western end of the Alboran Ridge and Channel. The Yusuf Lineament is proved as a complex fault zone that involves transtensive faulting and subsidence in the Yusuf pull-apart basin.

SEISMICITY AND KINEMATICS

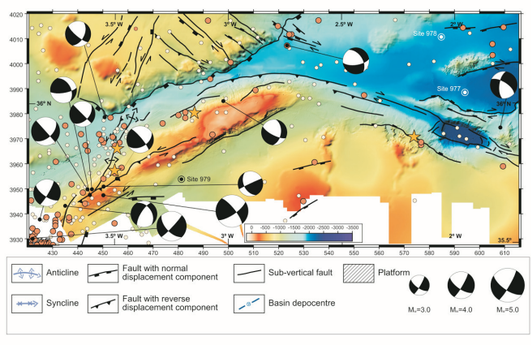

Seismic events at shallow depths (<11 km) were taken from the USGS 1979-2006 seismic catalogue and a set of 13 focal mechanisms were also considered to decipher what faults are nowadays active. Most of the shallow seismicity is concentrated in the western Alboran Ridge, related with the N30ºE fault-zone, where focal mechanisms correspond to left-lateral, strike-slip to reverse faults.

ACTIVE TECTONICS

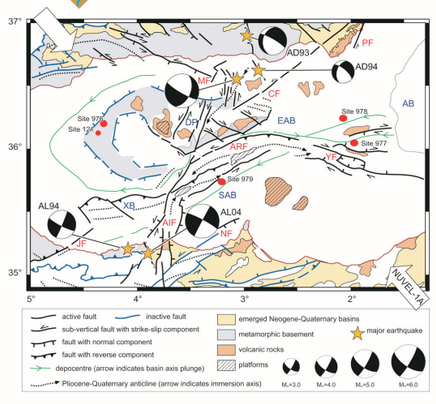

Recent deformation is heterogeneously distributed. The Alboran Ridge and Yusuf Lineament are the morphological expression of a wide zone of deformation (from 8 to 23 km wide) changing in orientation from SW to NW-SE, and including different fault-segments and in-relay folds. The narrow N30ºE fault-zone crosscuts the western Alboran Ridge and extends northwards affecting the Djibouti Plateau. The northeastern and southwestern end of this fault-zone corresponds with both the Adra (36.5ºN/ 3.1ºW) and Al Hoceima (35.3ºN /4ºW) seismic swarms.

CONCLUSIONS

Active-tectonics is the dominant mechanism shaping the Alboran seafloor. Major strike-slip to reverse faults, and in-relay open-folds condition the physiography of its central sector.

Identified structures deform Holocene sequences, control the sediment dispersal via canyon and gullies networks, and cause seafloor instability resulting in submarine slides.

The Alboran Ridge and Yusuf fault-zones are kinematically connected corresponding to a wide zone of deformation with scattered associated seismicity.

The N30ºE seismically-active fault-zone crosscutting the western Alboran Ridge appear as youngest recent structure. It may represent a seismic hazard zone, linking to the South with the Al Hoceima seismic-swarm.

Financed by CTM2009-07715, TOPOMED-CGL2008-03474-E/BT, CONSOLIDER-INGENIO2010-CSD2006-00041, RNM3713 and RNM215 Projects

Submarine instability processes associated with active faulting, eastern Alborán Sea

P. Martínez-García[a,*], J.I. Soto[a,b], M.C. Comas[a], S. Perez-Hernandez [a]

[a] Instituto Andaluz de Ciencias de la Tierra, CSIC and University of Granada, Campus Fuentenueva, 18002 Granada, Spain.
*matez@ugr.es
[b] Departamento de Geodinámica (University of Granada), Facultad de Ciencias, Granada, Spain

1.LOCATION AND GEOLOGICAL SETTING

Figure 1

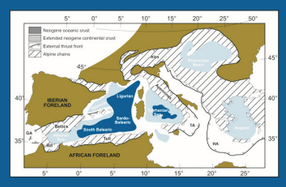

The Alboran Sea Basin, in the Gibraltar Arc, is affected by present-daydeformations as result of the convergence between the African and EurasianPlates. Its eastern sector connecting with the Algerian Basin, exhibits complex seafloor morphology resulting from recent to active tectonic processes

Figure 2

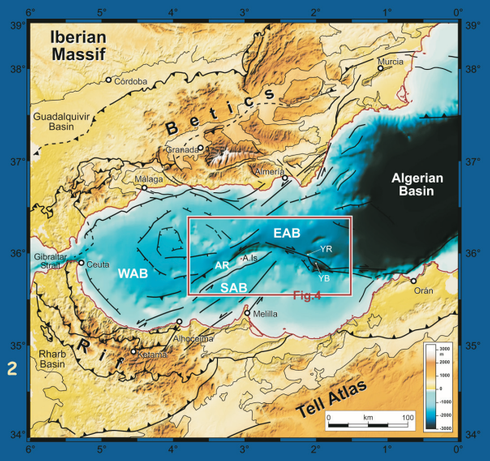

Figure 3

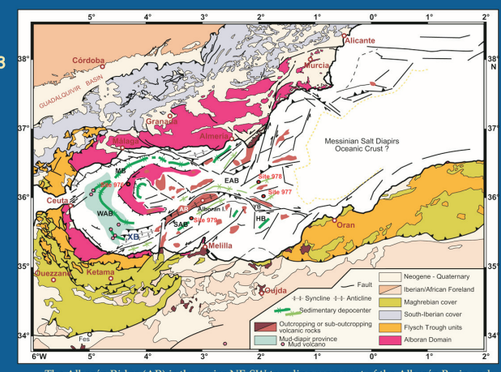

The Alborán Ridge (AR) is the major NE-SW trending seamount of the Alborán Basin and corresponds with a large complex antiform bounded by strike-slip to reverse fault zones. The Yusuf Fault-zone, to the East, is a dextral NE-SW fault system, includes two master normal faults that produce local transtension and form the Yusuf pull-apart Basin (YB). The temporal and spatial relationship between the Alborán-Ridge fault zone and the Yusuf tectonic lineament remain still unclear.

2. SEAFLOOR MORPHOLOGY

Figure 4

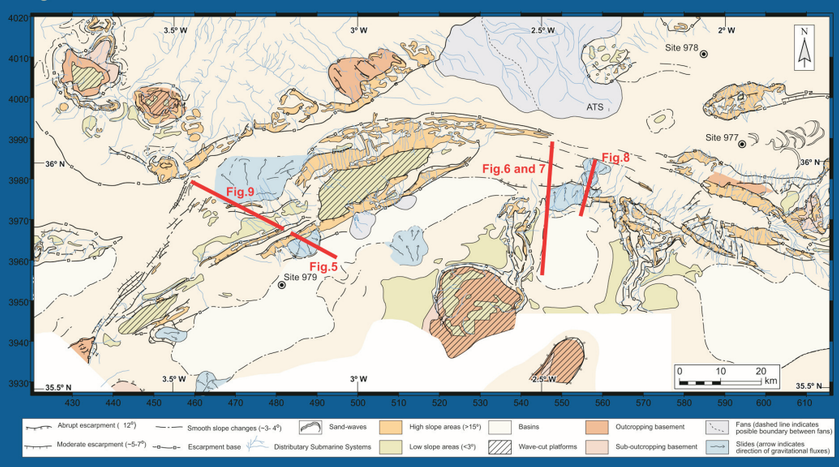

We have compiled high resolution geophysical data including bathymetric mosaics and high resolution seismic profiles in the eastern Alborán Sea. From this dataset we have carried out a detailed geomorphological study characterizing the most recent fault escarpments. Location in Fig.2

Figure 5

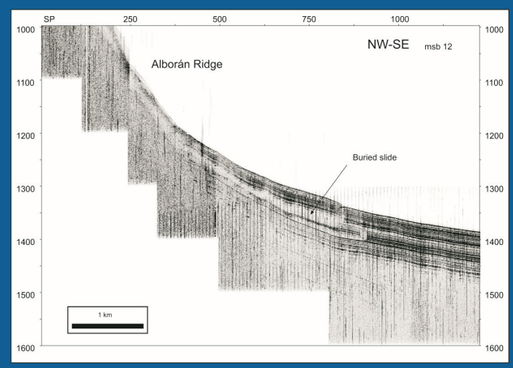

High-resolution TOPAS profile across the South side of the Alborán Ridge showing a recent slide. Location in Fig.4

Figure 8

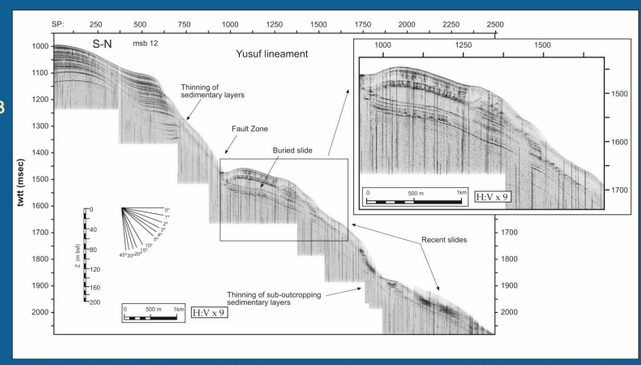

High-resolution TOPAS parametric sub bottom profile showing submarine slides related with faults along the Yusuf Lineament. Location in Fig.4

3.GRAVITATIONAL DEPOSITS AND ACTIVE TECTONICS

Figure 6

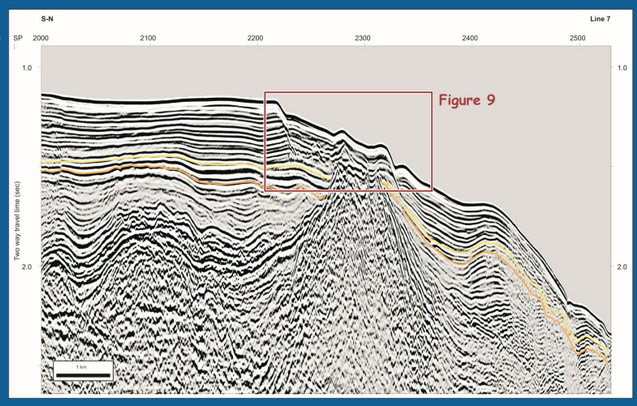

Sismic profile across the Yusuf lineament showing slump structures observable as coherent folded and faulted deposits over non-deformed stratigraphic sequences. Location in Fig.4

Figure 7

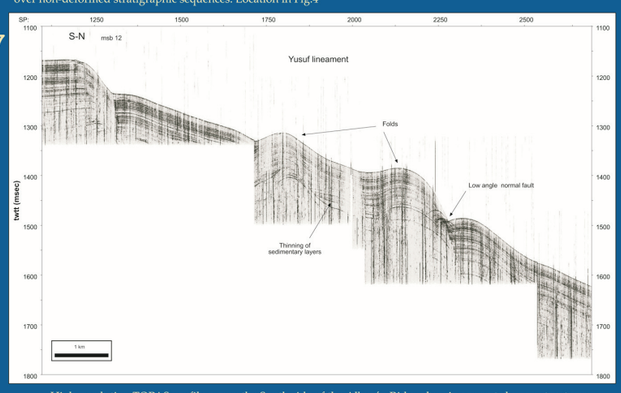

High-resolution TOPAS profile across the South side of the Alborán Ridge showing recent slumps structures (low angle faults and associated folds). Location in Fig.4

Figure 9

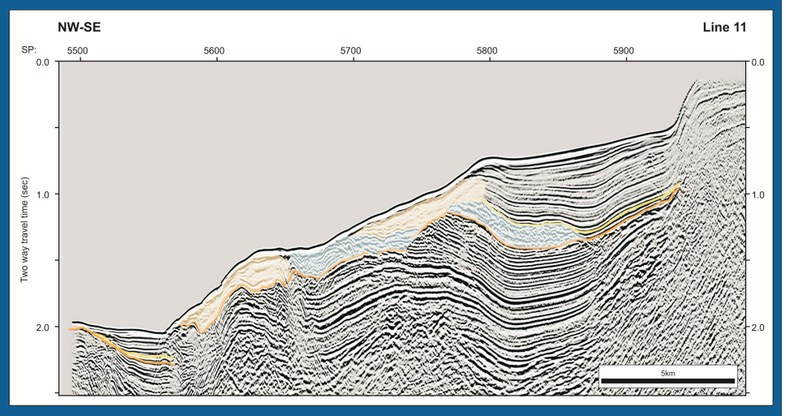

Multichannel seismic section across the North side of the Alborán Ridge showing different generations of slides with characteristic chaotic seismic facies. Sucession of gravitational deposits may be related with reccurent movements along fault escarpments. Location in Fig.4

4. CONCLUSIONS

The present study reveals that seismogenic faults in the Alborán Sea induce submarine instability processes that should be considered as sources of potential tsunami hazard in the western Mediterranean.

Contribution from Projects SAGAS CTM2005-08071-03-01 and TOPO-IBERIA CSD2006-00041 (Funded by R & D National Plan of the Ministry of Science and Technology and FEDER funding, Spain).